Physicochemical Problems of Mineral Processing

Fizykochemiczne Problemy Mineralurgii

Index No. 32213X

ISSN 0137-1282

36

2002

Physicochemical
Problems
of Mineral Processing
36 (2002)

Instructions for preparation of manuscripts

It is recommended that the following guidelines be followed by the authors of the manuscripts:

- Original papers dealing with the principles of mineral processing and papers on technological aspects of mineral processing will be published in the journal which appears once a year.
- The manuscript should be sent to the Editor for reviewing before February 15 each year.
- The manuscript should be written in English. For publishing in other languages on approval of the editor is necessary.
- Contributors whose first language is not the language of the manuscript are urged to have their manuscript competently edited prior to submission.
- The manuscript should not exceed 10 pages.
- Two copies of the manuscript along with an electronic should be submitted for publication before April 15.
- There is a 80 USD fee for printing the paper. No fee is required for the authors participating in the Annual Symposium on Physicochemical Problems on Mineral Processing.
- Manuscripts and all correspondence regarding the symposium and journal should be sent to the editor.

Address of the Editorial Office
Wrocław University of Technology
Wybrzeże Wyspiańskiego 27, 50-370 Wrocław, Poland
Institute of Mining Engineering
Laboratory of Mineral Processing

Location of the Editiorial Office:
Pl. Teatralny 2, Wrocław, Poland
Phone: (071) 320 68 79, (071) 320–68–78
Fax: 3448123, telex: 0712254 pwr.pl
E-mail: Andrzej.Luszczkiewicz@.ig.pwr.wroc.pl
Jan.Drzymala@.ig.pwr.wroc.pl
sadowski@iic.pwr.wroc.pl
http://www.ig.pwr.wroc.pl/conference/conf uk.html

Physicochemical Problems of Mineral Processing 36 (2002)

Z. SADOWSKI and K. MAŁYSA
(EDITORS)

WROCŁAW 2002

The papers published in Physicochemical Problems of: Minercal Processing are abstracted in Chemical Abstracts, Metals Abstracts, Реферативный Журал and other sources

ISSN 0137-1282

OFICYNA WYDAWNICZA POLITECHNIKI WROCŁAWSKIEJ, WYBRZEŻE WYSPIAŃSKIEGO 27, 50-370 WROCLAW
POLAND

CONTENTS

On the occasion of the 80th birthday of Professor Andrzej Pomianowski

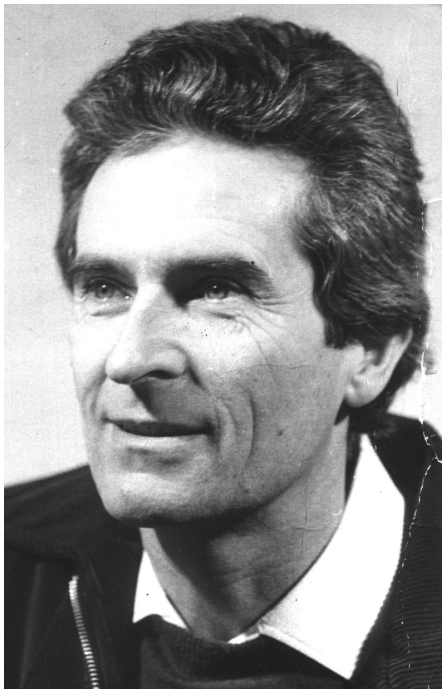

Professor Andrzej Pomianowski will celebrate his 80th birthday in November 2002. This issue of ***the Physicochemical Problems of Mineral Processing*** *annual is dedicated to honor his great achievements and contribution to the development of understanding the chemistry of flotation as well as to present his personality and accomplishments to younger colleagues. Professor Andrzej Pomianowski is an extraordinary man and his life has been also unusual. He had been a university student before he graduated from a high school. He had been a lecturer at the Jagiellonian University while he was still a student of this university. He had become a respected scientist before he got his Ph.D. degree. This was partially due to*

*turbulent period of the Second Word War. In 1939 he had passed the so-called "minor" examination for the secondary school certificate, and continued his education in schools that under German occupation were forced to be only professional schools. However, the education level in the**se** schools and the qualification of their staff were often equivalent to those at renowned universities. No wonder that in 1945, shortly after the war and reopening of the Jagiellonian University he continued his study and soon graduated as a Master of Science in chemistry. As a student Professor Pomianowski was employed by the Department of Physical Chemistry of the Jagiellonian University. He taught physical chemistry since 1952, well before awarding him Ph.D. degree. The doctor degree was conferred on him in 1958 for the thesis on "Electrometric observations of galena flotation". Besides scientific tasks and teaching performed at the Jagiellonian University under the supervision of a famous Polish physicochemist professor Bogdan Kamienski, he conducted research on the determination of the content of certain biologically active substances in plants. He was a director of the laboratory of the Plant Selection Station at Narodowa Górka, and later a part-time expert at the Institute of Forensic Research (IES). Professor Pomianowski was engaged in cooperation with the IES for many years being there a scientific consultant and a member of the Scientific Council of the Institute. Besides his work at the university, he cooperated with the Polish Federation of Engineering Associations (NOT) as well as delivered numerous lectures at meetings and seminars of the Polish Chemical Society (PTCh) and courses organized by and for industry.*

Since 1954 Professor Andrzej Pomianowski had been part-time employed by the Institute of Physical Chemistry in Warsaw. In 1961 he moved from the Jagiellonian University to the Research Laboratories presently Institute of Catalysis and Surface Chemistry of the Polish Academy of Sciences in Kraków, where he has been employed until today as a full-time professor. Since then, Professor Andrzej Pomianowski has become an important pillar of the Institute in which he obtained his doctor of science degree (D.Sc. also called habilitation), and was promoted to an associate professor and finally to a full professor position. For years Professor Andrzej Pomianowski was the vice-director for scientific affairs taking active part in creation of scientific policy of the Institute. Currently, the is a member of the Scientific Council of the Institute. For years Professor Pomianowski has been a consultant to many scientific institutions, for instance to the Institute of Metal Cutting and the Institute of Nonferrous Metals. He had been an active member of the Commission on Physical Chemistry of Surfaces of the Polish Academy of Sciences as well as the Section of the Utilization of Raw Materials of the Committee of Mining of the Polish Academy of Sciences. He had been also a member of two different sections of the Committee on Chemical Sciences of the Polish Academy of Sciences (PAN). During various stages of his fruitful life he had been a member of scientific councils of eight different scientific institutions and universities as well as participated in Polish Central Scientific Programs (CPB). His another important activity had been to chair the Editorial

Board of the Physicochemical Problems of Mineral Processing Conferences and the Annual ***Physicochemical Problems of Mineral Processing****. Presently, he is the honorary chairman of the Editorial Board. Professor Pomianowski has been working and cooperating with the best scientific institutions in the world. He has spent several years at such universities as Cambridge, Edmonton and Vancouver. He had supervised several Ph.D. students and several his co-workers obtained D.Sc. degrees. His recommendations and opinions about Ph.D., D.Sc. candidates for full professor positions are numerous.*

The scientific activity of Professor Andrzej Pomianowski is focused on the chemistry of surfaces, especially all issues dealing with physical chemistry of mineral surfaces and flotation systems. He has been always very reliable person of a critical attitude towards the results obtained and high standards and requirements. He loves to initiate long and stormy scientific discussions, which most of us consider as an excellent lessons on skillful presentation and discussing scientific hypotheses. He has published about 150 scientific works, while the number of presentations and lectures can be counted in hundreds. Some of his scientific works have been presented at more than 30 international conferences and symposia. The fruitful scientific life of Professor, to a great extent, is due to his happy family life. He and his wife Wanda, who passed away, were parents of three daughters.

Ending this note, to avoid leaving the reader with an impression about Professor Pomianowski as a some kind of a "bronze figure", we would like to present some anecdotal facts showing Professor as a colleague and man. He is a very cheerful person, eager to discuss every subject and enjoying jokes, helpful to people in need of an advice. In the scientific community his style of car driving is well known. One of his colleagues says: Professor Andrzej Pomianowski drives his car applying the "zero-and-one system" that is "no-or-full-gas." He does not recognize any intermediate stages. The most unusual and almost unbelievable event in his driver's carrier was the collision with a tractor. During the accident his small car, Fiat 126p, cut into halves a big tractor, but Professor escaped from the accident with small bruises only.

J. Drzymała
A. Łuszczkiewicz
K. Małysa
P. Nowak
Z. Sadowski

Physicochemical Problems of Mineral Processing, 36 (2002) 9-20
Fizykochemiczne Problemy Mineralurgii, 36 (2002) 9-20

Wanda BARZYK[*], Andrzej KOWAL[*], Andrzej POMIANOWSKI[*], Anna RAKOWSKA[**]

SEM/EDX AND AFM STUDY OF GOLD CEMENTATION ON COPPER(I) SULPHIDE

Received March 5, 2002, reviewed, accepted May 15, 2002

This paper is methodological in nature. The results presented here are a preliminary step towards finding an optimal method of sulphide surface preparation for systematic AFM studies of $AuCl_4^-$ cementation products. This technique makes it possible to see surface topography in nanoscale.

Products of $AuCl_4^-$ cementation on synthetic copper (I) sulphide, $Cu_{1.86}S$, were investigated by scanning electron microscopy (SEM/EDX) and atomic force microscopy (AFM). The microstructure of the sulphide surface before and after the reaction with $AuCl_4^-$ was analysed. Changes in the amount and shape of the products formed on polished plates and grains of the same material were compared. The process was performed in a flow-through vessel (on the plates) or in a circulation apparatus (on grain samples), by contacting the sulphide with aqueous solution containing $1.5 \cdot 10^{-4}$ mol/dm^3 $HAuCl_4$ and $1*10^{-1}$ mol/dm^3 HCl. The amount of gold deposited on a grain sample was determined from $AuCl_4^-$ concentration decay. The reaction progress on plates was evaluated from the intensities of the Au_L line of the EDX spectra. The maximum cementation degree was found to be equal to about 80 estimated atomic layers of metallic gold deposited on the sulphide. In SEM images the products were seen as crystallites of different sizes, between 0.1μm (the lowest limit detectable by SEM with a magnification of 5000x) and about 1.5μm, randomly distributed over heterogeneous surfaces of the plates and grains. The AFM technique made it possible to see the shapes of smaller crystallites, with their growth limited to the inside of cavities or cracks formed by polishing. The average density of the crystallites observed by AFM was of the order of 10 per 1μm^2 geometric surface area.

Key words: cuprous sulphide, copper (I) sulphide, sulphide surface preparation, gold deposition/cementation, SEM/EDX and AFM techniques

INTRODUCTION

Polish copper-bearing ores contain economically significant gold admixtures (Piestrzyński i Wodzicki, 2000, Piestrzyński i Sawłowicz, 1999, Kucha et al., 1998). The gold contained in those ores accompanies much larger admixtures of silver, and is much more difficult to recover than the latter (Bortel et al., 1985). Gold recovery losses can reach even 50 percent of the original content, especially when the noble metal is chemically bound with the host mineral crystal lattice (Kucha et al., 1998).

[*]Institute of Catalysis and Surface Chemistry, Niezapominajek 8, 30-239 Cracow, Poland
[**]Institute of Ceramics, Mining Academy, Mickiewicza 30, 30-059 Cracow, Poland

Considering the variety of forms of gold and silver occurrence in copper ores, optimal processing conditions must be selected for each ore lot. To optimize the recovery of metals occurring as accessory minerals, it is necessary to find forms in which they occur in copper-bearing ores, and the changes they undergo during processing (flotation, hydrometallurgical leaching).

In the literature there are no quantitative descriptions of the changes that the gold contained in copper sulphides undergoes. Much more information is available about reactions of silver with copper sulphides. The basic electrochemical property of noble metal ions is their spontaneous deposition (cementation) in the presence of less noble metals. Due to the significant differences in chemical properties of silver and gold (e.g., their reactivity with sulphur), it can be expected that cementation of these metals on copper sulphide will be significantly different, in both the preliminary and secondary stages of the process.

So far, gold cementation processes were mostly investigated on such sulphide minerals as piryte, pyrhotite, galena and sphalerite (Mycroft et al., 1995, Scaini et al., 1997, Becker and Hochella, 1996).

This paper refers to our earlier studies of noble metal (Ag, Au) cementation on non-stoichiometric copper (I) sulphide. Those earlier studies (Barzyk et al., 2002) were done on 60-75μm grains of $Cu_{1.86}S$, which made it possible to determine the rate of the process by measuring the decrease in noble metal concentration as a function of time (Ag^+ - by potentiometry, $AuCl_4^-$ - by UV-Vis spectrophotometry). The sulphide grain samples were also suitable for x-ray diffraction (XRD) studies, thus permitting crystalline phases to be determined in the cementation products (at concentrations greater than 2%, i.e., above the method's detectability). Another advantage of grain samples was that small grain quantities could be collected during the process, to be examined by the electron microscope (SEM/EDX) without altering the process conditions (Barzyk and Pomianowski, 2001). The grains proved, however, not suitable for AFM studies on a larger scale due to the high roughness of the surface. Sharp topographic outlines prevented the AFM tip's access to a significant portion of the surface and often damaged the tip, which significantly reduced the applicability of the AFM microscopy

This paper is methodological in nature. The results presented here are a preliminary step towards finding an optimal method of the copper(I) sulphide surface preparation for systematic AFM studies of topology of products of gold cementation. This technique makes it possible to see surface topography in nanoscale; consequently, structures with dimensions greater than, or comparable to the scanned area, cannot be studied by the AFM microscopy. It should be noted that in order to characterize the topography of the portion of surface that is measurable by AFM technique, a statistical approach is needed, which means that a statistically significant number of images (at least 21) must be analysed. In order to access what proportion of the actual surface is available to AFM microscopy, comparative studies should be done by techniques that can scan larger areas, e.g., electron microscopy (SEM).

It is possible to attain atomic resolution with the AFM technique in high vacuum if the examined surfaces are smooth in atomic scale, i.e., surfaces of monocrystals prepared in a way favouring the formation of atomic terraces (Dakkouri et al., 1999, Warren et. al., 2002). Preparation of monocrystals is costly and in the case of copper (I) sulphide – practically impossible. Also, a monocrystal is too ideal a model of mineral and thus it may lack properties that dominate the course of surface processes in real conditions. These processes are known to depend strongly on the number of defects and admixtures occurring in the mineral crystal lattice (Vaughan, et al., 1997).

Mineral samples are most often prepared in the form of polished plates - particularly suited for electrochemical techniques and solid-state methods (e.g., ESCA). It should be borne in mind that polishing with abrasives may lead to the formation of numerous surface defects – the effect may be much stronger than in the case of comminution. When materials are comminuted they usually break at points of the weakest bonds, i.e., along crystallographic planes with the strongest bonds (and the shortest interatomic distances). This favours the formation of states of lower energy than those in polished surfaces. On the other hand, polishing can lead to the formation of high-energy defects due to very high local stresses applied to microscopic areas. Defects created by polishing can increase the mineral's surface activity and affect its topography. On the other hand, topographic defects, typical of polished surfaces (e.g., scratches made by diamond paste with grain sizes below 3μm) will be outside the scanning capabilities of the AFM technique. Consequently, one should expect that topographic differences in the area "seen" by the AFM shall disappear, i.e., similar images should be obtained for plate and grains samples of the same mineral. The difference in the concentration of defects can, however, markedly affect the distribution of cementation products.

The objective of this study was to compare changes in the surface microstructure of polished plates and grains of the same copper sulphide ($Cu_{1.86}S$) produced by cementation of gold ions ($AuCl_4^-$) in diluted acid solution ($1x10^{-1}$mol/dm^3 HCl). The focus was on whether polishing markedly effects the number and distribution of defects as compared with the surface of grains (more representative of mineral processing).

EXPERIMENTAL

SURFACE ANALYSIS TECHNIQUES

A scanning electron microscope (XL 30) with a conventional secondary electron detector (for SEM) and an energy dispersive x-ray analyser (for EDX) were used to examine the surface microstructure and atomic composition of the surface region (in samples supported on a carbon tape). The electron beam penetrated the sub-surface region with a cross-section area of ca. 1 μm^2 and a depth of 2-4 μm.

The Atomic Force Microscopy (AFM) images were produced by a NanoScope E microscope (Digital Instruments) in the contact mode, with NanoProbes silicon nitride

cantilevers (force constant 0.12 N/m). An x-ray diffractometer (Dron 5) was used to obtain diffraction spectra (XRD) of the sulphide grains dispersed in nujol, using K_α the line of the copper lamp.

MATERIALS AND PROCEDURES

The samples of copper (I) sulphide ($Cu_{1.86}S$) were prepared in the form of grains or plates. The synthesis of $Cu_{1.86}S$, its comminution, classification, and the storage of the grains (class of 60-75 μm) was described earlier (Barzyk et al., 1981). The surface of 1g of the grains was $0.1m^2$, as determined by the BET method.

Plates with dimensions of 7x6x2 mm were used. Their surfaces were polished with abrasive paper (4000) and diamond paste with diamond grain size below 3 μm. After polishing, the plates were washed with CCl_4 and redistilled water. Cementation studies on plates were carried out in a flow-through vessel (Pomianowski and Barzyk, 1987). The solution was introduced to the vessel through a capillary (parallel to the plate) at a flow rate of about 60 ml/min. The solution containing $1.5\cdot 10^{-4}$ mol/dm^3 $HAuCl_4$ in $1*10^{-1}$ mol/dm^3 HCl was in contact with the plate surface, and its concentration did not change throughout the experiment.

In order to study cementation of gold on grain samples, a circulation apparatus was designed, as described elsewhere (Barzyk et al., 2002). The initial concentration of the solution was $1.5*10^{-4}$ mol/dm^3 $HAuCl_4$ in $1*10^{-1}$ mol/dm^3 HCl (380 ml) and the content of gold ions gradually decayed as the reaction with sulphide grains (1g) progressed for less than 10 min. In order to deposit on the sulphide sample the amount of gold well detectable by x-ray diffraction (XRD), i.e., above 2 wt. percent per $Cu_{1.86}S$ grain sample, four portions of $HAuCl_4$ solution (with the above-specified composition) were added. Each subsequent portion was introduced after about 12 hours' equilibration with the oxygen-free electrolyte, circulating through the grain sample. (The step-by-step procedure is discussed in detail elsewhere; Barzyk et al., 2002). The amount of gold deposited on grain samples was determined from $AuCl_4^-$ concentration decay by UV Vis spectrophotometry (cf. Barzyk, 1990). The reaction progress on plates was assessed by comparing the intensities of the Au_L line of the EDX spectra obtained for the grains and plates.

Prior to the experiments, the surface oxidation products were removed from both the plate and grains by washing the mineral's surface with the stream of oxygen-free solution of $1\cdot 10^{-1}$ mol/dm^3 H_2SO_4, according to the procedure described earlier (Pomianowski and Barzyk, 1987).

The solutions were prepared from analytical purity grade H_2SO_4, HCl, $HAuCl_4$, and double distilled water. In the experiments, industrial grade argon was used. The measurements were performed at room temperature, $20\pm3\ ^oC$.

RESULTS AND DISCUSSION

The surface topography and composition of the sulphide, before and after the reaction with $AuCl_4^-$, are compared in Figs. 1-4, for four $Cu_{1.86}S$ samples differing in the extent of the cementation reaction. The results are presented in the form of sets of typical SEM and AFM images, EDX spectra and the corresponding AFM depth profiles. Figs. 1 a-d show the reference sample, i.e., the plate after the same pre-treatment as other plates, but not contacted with $AuCl_4^-$. The reference sample gives AFM images similar to those obtained earlier for grains of pure $Cu_{1.86}S$ (cf. Figs. 6b,c in Barzyk et al., 2002). Hence, the AFM pictures shown in Figs. 1c-d served as reference images for analysing the changes in the sulphide surface topography produced by cementation on both the plate and grain samples.

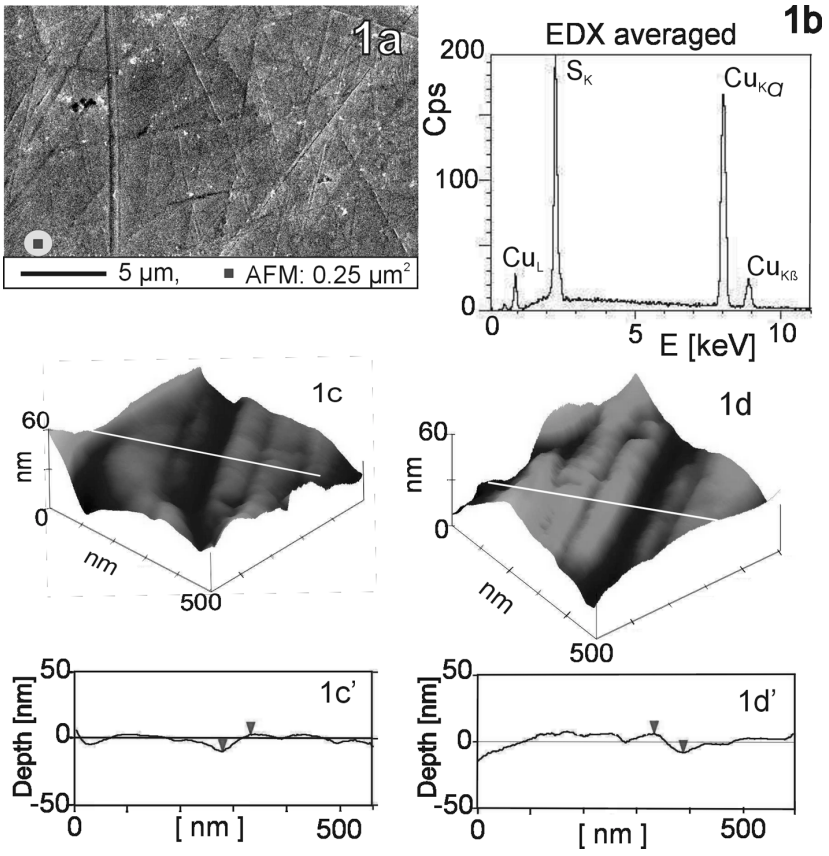

Figs. 1a-1d'. Surface microstructure of a $Cu_{1.86}S$ polished plate, after washing with $1 \cdot 10^{-1}$ mol/dm^3 H_2SO_4 oxygen-free solution for 30 min. (the preliminary stage); Fig. 1a – SEM image, Fig. 1b – averaged EDX spectrum registered along the area shown in the SEM image; Figs. 1c, 1d – AFM images typical of the sample, Figs. 1c-1d' – the AFM depth profiles

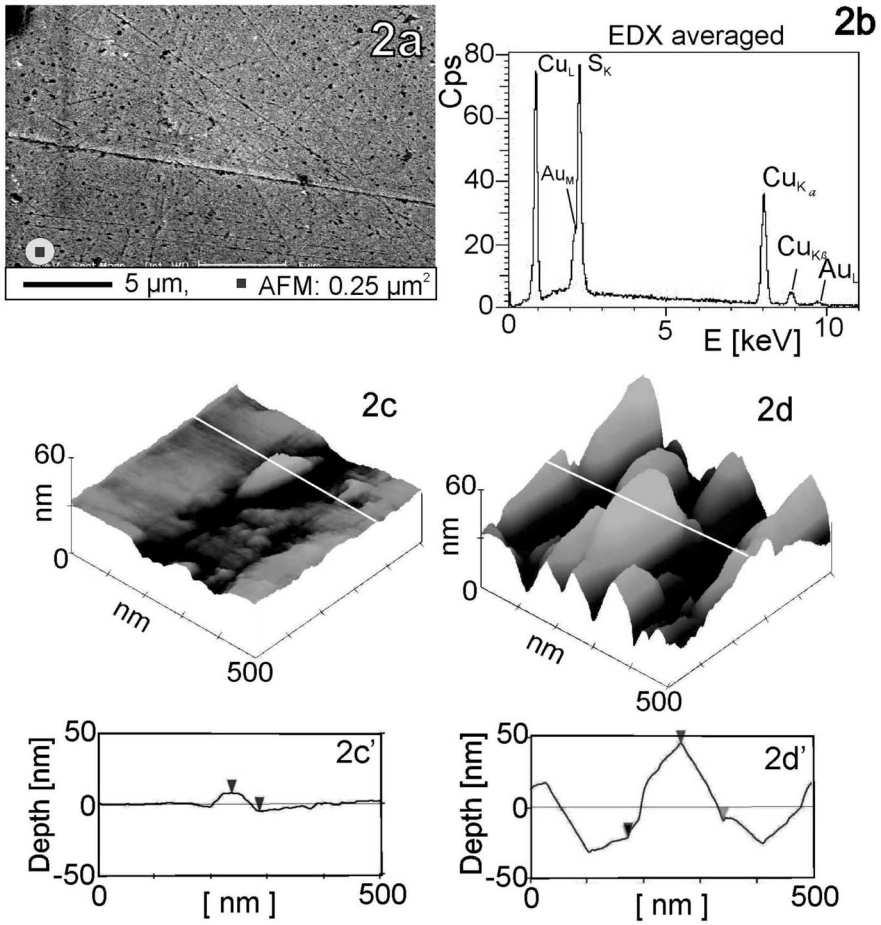

Figs. 2a-2d'. Surface microstructure of $Cu_{1.86}S$ plate after 5 minutes reaction with air-saturated solution of $1.5 \cdot 10^{-4}$ mol/dm^3 $HAuCl_4$ in $1 \cdot 10^{-1}$ mol/dm^3 HCl (the part of the plate where the reaction progress was low due to partial screening of the surface by the capillary tip in the flow-through vessel); Fig. 2a – SEM image, Fig. 2b – averaged EDX spectrum registered along the area shown in the SEM image; Figs. 2c, 2d – typical AFM images; Figs. 2c', 2d' – the AFM depth profiles

Three of the samples discussed here in are in form of plates (Figs. 2-3). They are compared with the grain sample shown in Fig. 4. In the grain sample, the amount of gold deposited as a result of cementation was directly determined from the concentration decay. It corresponded to 3.4 wt. percent of Au per $Cu_{1.86}S$ grain sample. The content of gold in the plates was estimated by comparing the corresponding averaged EDX spectra (i.e., the ratios of Au_L to CuK_β lines, whose energy values are shown in Table I) with the EDX spectrum of the grain sample. The comparisons show that the amounts of gold contained in the region penetrated by the

EDX technique are approximately 0.5 wt. percent (Fig. 2b) and 1 wt. percent (Fig. 3b). The content of gold was expressed in terms of the number of nominal atomic layers of the deposited metal, assuming that the average area occupied by a gold atom (at the BET surface) was 8.0Å^2, as found from the gold density (19.3g/cm^3). The calculated numbers of nominal layers in the samples treated with $AuCl_4^-$ (Figs. 2, 3, and 4) were about 15, 30 and 80, respectively. Note that the $Au_{M\alpha 1}$ line, much more intensive than the $Au_{L\alpha 1}$, could not be used for this quantitative estimation, as it is hidden in the $S_{K\,\alpha 1}$ line (cf. Table I and Figs. 2b, 3b, 4b). The only sample where the $Au_{M\alpha 1}$ line could be identified is presented in Fig. 4.

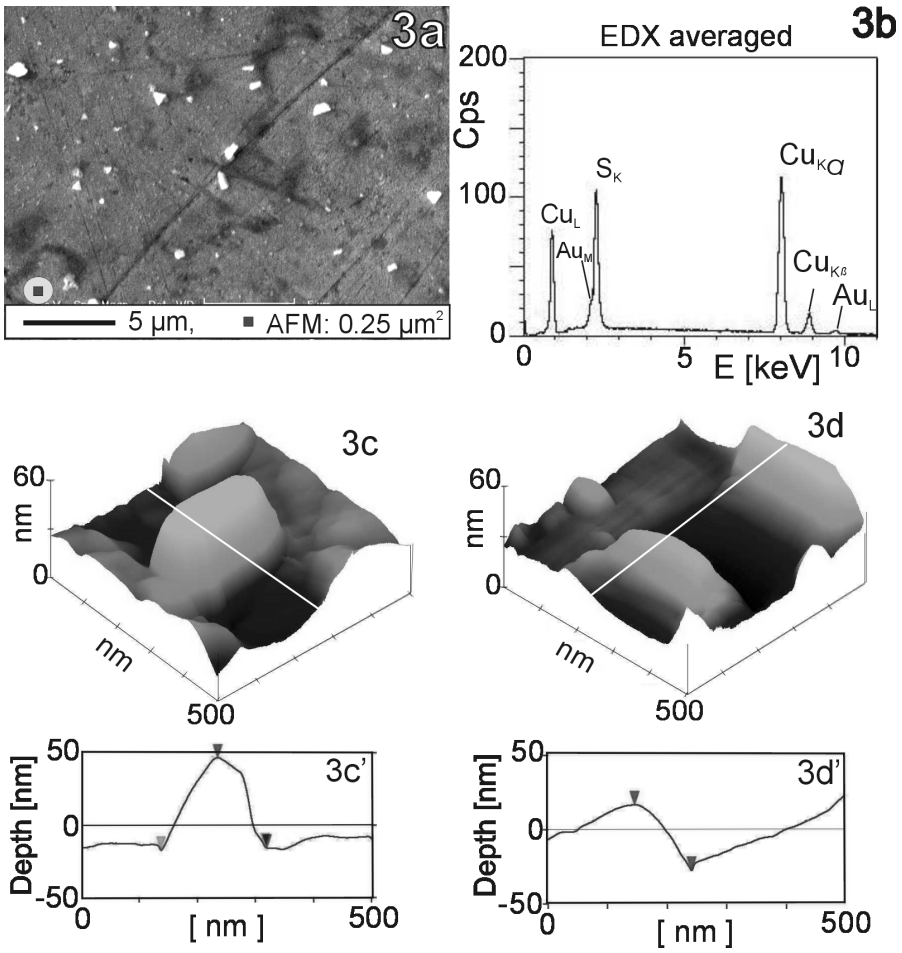

Fig. 3a-3d'. Surface microstructure of the area with a greater reaction progress, on the plate presented in Figs. 2a-d' (i.e., the part of the surface not screened by the capillary); Fig. 3a – typical SEM image, Fig. 3b - averaged EDX spectrum registered along the area shown in the SEM image, Figs. 3c, 3d – typical AFM images; Figs. 3c', 3d' – AFM depth profiles

Table I. The energy and associated wavelength of the strongest K, L, M lines of the elements (Goodhew and Humphreys, 1988)

Element	Energy [keV]			
	$K\alpha_1$	$K_{\beta 1}$	$L\alpha_1$	$M\alpha_1$
S	2.31			
Cu	8.05	8.95	0.93	
Au	68.79		9.71	2.12

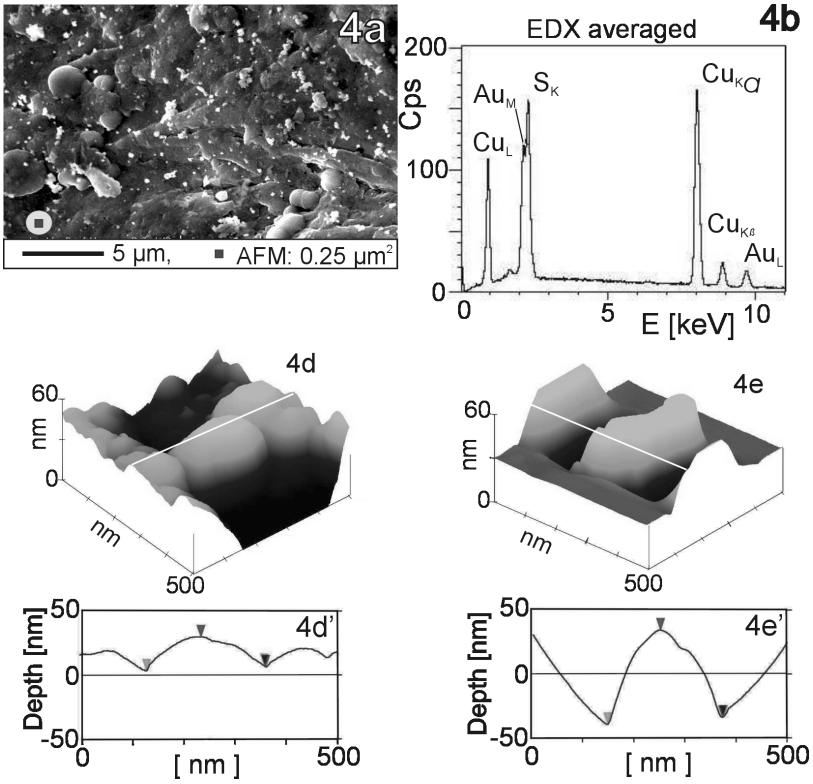

Figs. 4a-4e'. Surface microstructure of $Cu_{1.86}S$ grains containing 4 wt. percent Au (i.e., after reacting with four portions of $1.5 \cdot 10^{-4}$ mol/dm^3 $HAuCl_4$ in $1 \cdot 10^{-1}$ mol/dm^3 HCl); Fig.4a – typical SEM image, Fig. 4b - averaged EDX spectrum registered along the area shown in the SEM image, Figs. 4d, 4e – typical AFM images; Figs. 4d', 4c' – AFM depth profiles

The cementation products can be seen in SEM images as crystallites of different size, i.e., from 0.1µm (which is close to the lower limit detectable in SEM of magnification of 5000x; cf. Fig. 2a) to about 1.5µm (cf. Figs. 3a, 4a). SEM did not reveal any preferential distribution of the product crystallites over the highly heterogeneous surfaces of plates and grains.

It is interesting that for pure sulphide (in the plate and grain samples) a characteristic layered texture is revealed by the AFM technique, i.e., layers with a thickness of about 100nm. The solid material seems to be preferentially split along the texture layers, which could be seen in numerous areas probed by AFM as shown in Figs. 1c-d (cf. also Figs. 6b-c of Barzyk et al., 2002). The layers were significantly disarranged by the cementation reaction, which could be seen as swelling and pitting of the layers, followed by their irregular growth - the effects shown in AFM images of plates and grains were characteristic of lower reaction progress (cf. Figs. 2c, d, and the results of Barzyk et al., 2002).

The degree of disarrangement of the original surface texture increased with the reaction progress, which is shown in the series of AFM images presented in Figs. 1c-d, 2c-d, 3c-d. At higher values of the reaction progress, isolated crystallites were observed in AFM images, on both the plates (Figs. 3c-d) and grains (Figs.4d-e). The smallest, crystallites revealed by the AFM technique are below 0.1μm (cf. Figs. 3c-d and 4d-e). They seem to be preferentially nucleated in textural cavities or cracks (probably formed by comminution) or in scratches formed on plates by polishing. The growth of the crystallites observed by the AFM technique looks to have been stopped by the opposite wall of the crack, or by other crystallite growing in the closest proximity (cf. Figs. 3c-c', 3d-d', 4d-d', 4e-e'). Generally 2-3 crystallites of dimension of 0.1-0.4 μm appeared in areas scanned by AFM (500 x 500nm), suggesting that the average density of nucleation centres is high (of an order of 10 per 1μm^2 geometric surface area).

Crystalline products of the cementation process were identified by examining the grain samples by x-ray diffraction technique (XRD). The minimum content of gold detectable by XRD was of about 2 wt. percent Au per $Cu_{1.86}S$ grain sample, which is slightly lower than the gold content in the sample presented in Fig. 4. The crystalline products identified by the XRD method in the grain sample are mixture of Au^o, Au_2S and Au_2S_3 (cf. Barzyk et al., 2002). It cannot be ruled out that, at a lower gold content in the sulphide, the same products are formed in different ratio, which might be detected by applying a more sensitive method than XRD, e.g., the x-ray synchrotron techniques used by Warren et al., 2002. The occurrence of mixed products suggests a complex mechanism of the cementation process, involving secondary reactions between sulphur present on the surface and the gold deposited in the primary surface reaction. Furthermore, the surface processes may be accompanied by gold dis-proportionation reaction. (Mechanism of the cementation process will be discussed in detail, separately).

The cementation process appears to be accompanied by etching of the sulphide surface. These effects can be seen as pits (craters) with dimensions of about 0.3 μm on the plate containing about 0.5 wt. percent Au in the surface region (Fig. 2a). At the reaction progress corresponding to the content of about 1 wt. percent of Au (or to deposition of about 30 nominal layers of gold), the etching effects can be seen as cavities in the surface, noticeable in the SEM image in Fig. 3a. Pits that appear on

surface as a result of cementation can be attributed to the surface reaction releasing copper ions (I) from the sulphide as a co-product of the primary cementation reaction (initial cementation step). The cementation process involves the reduction of $AuCl_4^-$ ions to Au^o ad-atoms coupled with the oxidation of the sulphide copper to Cu^+ ions. Hence, cuprous ions should be released at the ratio of $AuCl_4^-$: Cu^+= 1:3, however, the ratio is changed by the copper dis-proportionation reaction, $2Cu^+ \rightarrow Cu^0 + Cu^{2+}$, which is inherently accompanying processes at cuprous sulphide. The presence of Cl^- ions and oxygen dissolved in the solution may significantly increase the concentration of copper ions at the sulphide surface, resulting in enhanced etching effects.

CONCLUSIONS

1. The results of the studies employing mineral grains and flat surfaces are complementary. Grain samples permit cementation kinetics to be determined, whereas samples in the form of plates permit determination of the topology of the cementation products formed on the surface.
2. The size and distribution of crystallites formed on $Cu_{1.86}S$ as a result of the reaction with $AuCl_4^-$ were found to be similar for plates and grains.
3. The SEM images do not indicate any preferential distribution of Au cementation products on the copper (I) sulphide surfaces.
4. The AFM results confirm, however, that the smallest crystallites (0.1-0.4μm) are preferentially located within cracks, but this could be due to the limited space, which prevents their growth. The AFM results also suggest high density of the nucleation centres, about 10 per $1\mu m^2$, on both plates and grains.
5. Polished plates of copper sulphide may be used as convenient and representative samples for AFM study of gold cementation.

REFERENCES

BARZYK W., KOWAL A., POMIANOWSKI A., 2002, *Noble Metal (Ag, Au) Cementation on Non-Stoichiometric Cuprous Sulphide Grains*, Colloids and Surfaces, in print.

BARZYK W., POMIANOWSKI A., 2001, *Distribution of Au^0 sub-micro-particles deposited from $AuCl_4^-$ acidic solutions on heterogenous surfaces of Cu_{2-x} S grains – SEI/EDX study*, Poster No50 on Fourth International Symposium: Effects of Surface Heterogeneity in Adsorption and Catalysis on Solids, ISSHAC-4, Cracow, 2001.

BARZYK W., MAŁYSA K., POMIANOWSKI A., 1981, *The influence of surface oxidation of chalcocite on its floatability and ethyl xanthate sorption*, Int. J. Miner. Process., 8, 17-29.

BECKER U., HOCHELLA M.F., JR., VAUGHAN D.J., 1997, *The adsorption of gold to galena surfaces: Calculation of adsorption/reduction energies, reaction mechanisms, XPS spectra and STM images*, Geochim. et Cosmochim. Acta, 61, 3565-3585.

BECKER U., HOCHELLA M.F., JR., 1996, *The calculation of STM images, STS spectra, and XPS peak shifts for galena: New tools for understanding mineral surface chemistry*, Geochim. et Cosmochim. Acta, 60, 2413-2426.

BORTEL R., KUBACZ N., GRZEBIELUCH Z., *Behavior of the metals accompanying the copper ores in the dressing process,* in: Proceedings of Third Symposium on „The State and Perspectives of Development of Processing the Copper Ores in Poland", Institute of Nonferrous Metals, Wisła, Poland, 1985, pp. 75-81 (Polish text).

DAKKOURI A.S. KOLB D.M., 1999, *Reconstruction of gold surfaces*, 151-173, [In:] Więckowski A. (Ed) *Interfacial Electrochemistry – Theory, Experiment, and Applications, Marcel Dekker, Inc., USA.*

GOODHEW P.J., HUMPHREYS F.J., 1988, *Electron microscopy and Analysis*, Taylor & Francis, London, 2nd ed., pp.154-198.

KUCHA H, PLIMER I.R., STUMPFL E.F., 1998, *Geochemistry and mineralogy of gold and PGE's in mesothermal and epithermal deposits and their bearing on the metal recovery*, Physicochem. Probl. Miner. Process., 32: 7-30.

MYCROFT J.R., BANCROFT G.M., MCINTYRE N.S., LORIMER J.W., 1995, *Spontaneous deposition of gold on pyrite from solutions containing Au (III) and Au(I) chlorides. Part I: A surface study*, Geochim. et Cosmochim. Acta, 59, 3351-3365.

PIESTRZYŃSKI A., WODZICKI A., *Origin of the gold deposit in the Polkowice-West Mine, Lubin-Sieroszowice Mining District, Poland*, Miner. Deposita 35 (2000) 37. PIESTRZYŃSKI A., SAWLOWICZ Z., *Exploration for Au and PGE in the Polish*

Zechstein copper deposits (Kupferschiefer), J. Geochem. Explor. 66 (1999) 17.

POMIANOWSKI A., BARZYK W., 1987, *Kinetics of xanthate sorption on clean and weakly oxidized surfaces of synthetic copper sulphide ($C_{1.86}S$) grains*, Bull. Acad. Polon. Sci., Chem., 35, 461-470.

SCAINI M.J., BANCROFT G.M., KNIPE S.W., 1997, *An XPS, AES and SEM study of the interactions of gold and silver chloride species with PbS and FeS_2: comparison to natural samples*, Geochim. et Cosmochim. Acta, 61, 1223-1231.

VAUGHAN D.J., BECKER U., WRIGHT K., 1997, *Sulphide mineral surfaces: theory and experiment*, Int. J. Miner. Process., 51, 1-14.

WARREN S., REITZLE A., KAZIMIROV A., ZIEGLER J.C., BUNK O., CAO L.X., RENNER F.U., KOLB D.M., BEDZYK M.J., ZEGENHAGEN J., 2002, *A structure study of the electroless deposition of Au on Si(111):H,* Surface Science, 496, 287-298.

Barzyk W., Kowal A., Pomianowski A., Rakowska A., *Badania cementacji złota na siarczku miedziawym przy użyciu technik SEM/EDX i AFM,* Fizykochemiczne Problemy Mineralurgii, 36, (2002) 9-20 (w jęz. ang.)

Praca ma cel metodologiczny - optymalizację przygotowania próbek siarczku miedzi (I) do systematycznych badań topologii produktów cementacji jonów $AuCl_4^-$ na powierzchni, techniką AFM. Technika ta daje wgląd w topografię powierzchni w skali nanometrycznej. Badano produkty cementacji jonów $AuCl_4^-$ na syntetycznym siarczku miedzi (I) - $Cu_{1,86}S$, przy użyciu mikroskopii elektronowej (SEM/EDX) oraz mikroskopii sił atomowych (AFM). Porównano kształt oraz ilość produktów utworzonych na ziarnach i wypolerowanych płytkach z tego samego materiału. Proces cementacji prowadzono w naczyniu przepływowym (płytki) oraz w aparacie cyrkulacyjnym (próbki ziarn), przez kontaktowanie próbki w strumieniu roztworu zawierającego w 1 dm^3 wody $1{,}5 \cdot 10^{-4}$ mola $HAuCl_4$ oraz $1 \cdot 10^{-1}$ mola HCl. Ilość złota osadzonego na ziarnach siarczku w wyniku cementacji określono wyznaczając ilość jonów $AuCl_4^-$ ubywających z roztworu w czasie przebiegu procesu. Stopień zaawansowania przebiegu procesu na płytkach oszacowano przez porównanie intensywności linii Au_L widm EDX próbki ziarnowej i płytek. Badana maksymalna ilość produktów cementacji odpowiadała osadzeniu około 80-tu szacunkowych warstw atomowych Au na powierzchni. Produkty cementacji obserwowane na obrazach SEM mają kształt krystalitów o różnej wielkości, od około 0.1µm (dolna granica rozdzielczości SEM przy powiększeniu 5000 razy) do 1.5µm. Obrazy SEM nie wykazały preferencyjnego rozmieszczenia tych krystalitów na niejednorodnej powierzchni płytek lub ziaren.

Technika AFM umożliwiła obserwację kształtu małych krystalitów (0.1μm -0.4 μm), wskazując na ich preferencyjne usytuowanie w rysach lub szczelinach teksturalnych ziaren siarczku. Średnia gęstość krystalitów obserwowanych techniką AFM siarczku jest rzędu 10 na 1 μm^2 powierzchni geometrycznej siarczku.

Physicochemical Problems of Mineral Processing, 36 (2002) 21-38
Fizykochemiczne Problemy Mineralurgii, 36 (2002) 21-38

Gregory A. HOPE*, Ronald WOODS* and Kym WATLING*

SURFACE ENHANCED RAMAN SCATTERING SPECTROELECTROCHEMICAL STUDIES OF MINERAL PROCESSING

Received March 15, 2002, reviewed, accepted May 22, 2002

The application of *in situ* surface enhanced Raman scattering (SERS) spectroscopy to aspects of mineral processing is discussed. In the study of flotation systems, SERS has been used to characterise the species formed on coinage metal surfaces over a range of controlled potentials for ethyl, *i*-propyl, *i*-butyl and *i*-amyl xanthates, for *O*-isopropyl-*N*-ethylthionocarbamate (IPETC), for 2-mercaptobenzothiazole (MBT), and for diisobutyl dithiophosphinate (DIBDTPI). For each collector, adsorption occurs *via* charge transfer to form a metal-sulfur bond and, in situations in which the reversible potential for the formation of the bulk phase is known, at underpotentials. The dissolution of silver in basic solutions containing cyanide has been shown to be inhibited by MBT and by DIBDTPI as a result of the chemisorption of the collector species. In hydrometallurgy, SERS has been applied to the investigation of gold leaching. Changes in the surface species that occur during gold cyanidisation as the potential is varied have been identified from SERS spectra recorded in real time on voltammograms. In electrometallurgy, SERS investigations of copper electrodeposition from sulfuric acid solutions have shown that a transient surface sulfate species is involved in the plating process.

Key words: Spectroelectrochemistry, Raman spectroscopy, collector adsorption, gold leaching, copper electrodeposition.

INTRODUCTION

Froth flotation, oxidative leaching, and electrowinning and refining are important unit processes in the winning of metal values from sulfide mineral ores. All these processes have electrochemical bases and are amenable to study using electrochemical concepts and techniques. Surface species play an important role in determining the efficacy of each of these processes and, whereas electrochemical techniques provide valuable information on the kinetics and mechanisms of processes occurring at the

*School of Science, Griffith University, Nathan, Queensland 4111, Australia

solid/solution interface, they lack the molecular specificity required to give unequivocal identification of species formed at electrode surfaces. For this reason, a number of *in situ*, and *ex situ* spectroscopies have been applied to augment electrochemical approaches and provide information on the elemental and molecular composition, the atomic geometry, and the electronic structure of the interface. The spectroelectrochemical techniques that have been most widely applied to mineral processing systems have involved Fourier transform infrared (FTIR) spectroscopy and X-ray photoelectron spectroscopy (XPS). These methods have provided valuable information on the identity of surface species but each has limitations. XPS is an *ex situ* technique and the surface composition can relax in the time elapsed between removal from potential control in the electrochemical cell and recording of photoelectron spectra (Buckley and Woods, 1996). A similar situation arises with FTIR when it is performed *ex situ*. FTIR can be carried out *in situ*, but the sample has to be in contact with, or within a few microns of the cell window, due to water being a strong absorber of infrared radiation.

Raman spectroscopy is complementary to infrared; both techniques give spectra resulting from transitions between the vibrational energy levels of molecules, but different selection rules apply. Raman has the advantage over infrared techniques that the incident and scattered beams can have wavelengths in the region that is not adsorbed strongly by water and in which glass is transparent. Thus, *in situ* investigations in aqueous media can be carried out using conventional glass cells. In addition, Raman spectroscopy has excellent spectral range (100 to 4000 cm^{-1}) and resolution (1 cm^{-1}) and dynamic response (< ns). On the debit side, it has a lower sensitivity for most systems. In general, only one incident photon in ~10^{10} undergoes Raman scattering; most photons experience Rayleigh scattering in which the incident and scattered photons have the same energy. Nevertheless, the sensitivity of modern Raman spectrometers allows this technique to be applied to a wide range of problems associated with mineral processing. These include the identification of minerals, of reaction products, and of species in aqueous solution and in molten salts.

The phenomenon of surface enhanced Raman scattering (SERS) was first demonstrated by Fleischmann et al in 1973. It is applicable most usefully to adsorption on the coinage metals, copper, silver and gold. It involves a remarkable enhancement of the scattering intensity (by ~ 10^4 to 10^6) of species that are adsorbed on, or are microscopically close to, appropriately roughened surfaces. Silver has the widest spectral region of SERS activity, extending from blue light through to the infrared, while copper and gold are only active when irradiated with red through near infrared light. SERS generally allows surface layers at the sub-monolayer level to be characterized. Roughening electrode surfaces to generate SERS usually involves the application of oxidation-reduction potential cycling (ORC) in chloride or sulfate media. The resulting surface contains features with sizes of up to the wavelength of visible light.

In principle, SERS can also be applied to mineral surfaces by "decorating" the mineral surface with colloidal metal particles. These can be applied by either simply dipping a specimen of the mineral into the colloidal suspension, or applying a small quantity of the suspension to the surface, prior to beginning the experiment.

Raman spectroscopy is a powerful approach that is now included in the armory that metallurgists can apply to elucidating problems. In the present paper, we discuss our recent SERS investigations into flotation, hydrometallurgy and electrometallurgy.

RAMAN SPECTROSCOPY

Griffith University has two Raman spectrometers for spectroelectrochemical and mineralogical studies. One is a System 100 Renishaw Raman Spectrograph (Multi Channel Compact Raman Analyser) that has a rotary encoded grating stage, and an internal two stage Peltier cooled (-70 ºC) CCD detector. The spectral resolution is 5 cm^{-1} and the wavenumber resolution 1 cm^{-1}. The incident radiation is conveyed from the laser to the spectrometer through a fibre optic Raman probe. The other spectrometer is a Renishaw RM2000 Raman spectrometer equipped with a computer controlled stage and a Leica metallurgical microscope incorporating a range of objectives. The FWHM of silicon calibration band at 520 cm^{-1} was 5 cm^{-1} and the wavenumber resolution was 1 cm^{-1}. This instrument has the capability of imaging and mapping surfaces and hence can determine spatial variations in the coverage of surface species. Incident laser radiation is available of 633 nm, 514.5 nm, 442 nm and 325 nm. FT-Raman spectrometers are also accessible for research purposes.

Most spectroelectrochemical studies we have carried out used an electrochemical cell constructed of borosilicate glass with a flat window at one end. For experiments with copper and gold, the working electrode was mounted on an assembly constructed from PTFE and was positioned close to the window. It follows the design devised by Fleischmann et al. (1990). Copper and gold electrodes of 6 mm diameter were prepared from metal of 99.99% purity. With copper, the surface was electrochemically roughened prior to obtaining SERS spectra by oxidation-reduction cycling in 2 mol dm^{-3} H_2SO_4. This procedure involved the application of 4-5 cycles between –0.3 V and 0.7 V with a polarisation period of approximately 30 s before reversing the polarity. With gold, oxidation-reduction cycling was carried out between –0.3 and 1.2 V in 1 mol dm^{-3} KCl acidified with HCl. A cell of similar design was used for silver, but the working electrode was a silver flag attached to a silver wire. This design allowed the electrode to be cleaned by heat treatment. The electrode was heated in a furnace at 450 °C for 16 h to remove any organic species and then roughened by applying oxidation-reduction cycling in 1 mol dm^{-3} KCl acidified with HCl between potentials of –0.2 and 0.6 V after initially reducing at –0.5 V.

In addition to spectra recorded *in situ* under potential control, spectra have been recorded on emersed electrodes and on electrodes *ex situ*. For measurements on emersed electrodes, spectra were recorded after the solution had been drained from the

cell. The removal of solution was carried out under a constant flow of nitrogen to avoid ingress of oxygen from the atmosphere during emersion and the recording of spectra. In the last situation, the electrode was removed from the cell and washed with pure water to remove any cell solution from the electrode surface prior to examination in the spectrometer. This procedure provided information on the tenacity of attachment of species to the electrode surface as well as the identity of adsorbates.

In some experiments, Raman spectra were recorded sequentially on a potential step or scan. With the Renishaw spectrometers, the Grams 32 and 3D software allows sequential spectra to be stored as separate files and viewed as a 'movie' or a 3D image.

FROTH FLOTATION

The key chemical step in the flotation process is the adsorption of the organic collector on selected mineral surfaces and it is now well established that the interaction of thiol collectors with sulfide minerals is electrochemical in nature. It was originally proposed by Nixon (1957) that interaction occurred by an anodic process involving the collector being coupled with a cathodic process which is usually the reduction of oxygen. Professor Andrzej Pomianowski was one of the pioneers of the application of electrochemical techniques to characterizing collector adsorption. He and his co-workers carried out cyclic voltammetric studies of ethyl xanthate on mercury (Pomianowski, 1967), on chalcocite (Kowal and Pomianowski, 1973) and on copper (Szeglowski et al, 1977). The last of these works involved complementary radiochemical studies to confirm the electrochemical findings. The authors concluded that "*flotation phenomena … must be discussed in conjunction with sorption processes, and not, as is common, on the basis of thermodynamic properties of bulk phases only*". Kowal and Pomianowki (1973) concluded that "*the shift in the prepeak potentials towards negative values with respect to the potentials of the bulk reactions underlines the role of electrosorption in the process of collector binding by a mineral surface*". We arrived at similar conclusions (Woods, 1971, 1996) regarding the importance of chemisorbed layers deposited at underpotentials to the development of the metal/collector compound. With a number of co-workers, we have fitted chemisorption coverage data to the Frumkin adsorption isotherm and elucidated the chemisorption process with complementary XPS and FTIR investigations (*see* Woods, 1996). Since chemisorption occurs at underpotentials, it is the thermodynamically favoured process. This process offers the most effective utilization of the collector because a monolayer forms before the nucleation and growth of the bulk phase. The potential at which a finite contact angle is established, and flotation is initiated, has been found to correspond to the chemisorption region (Woods, 1996). Usually, significant flotation recovery is observed at low thiol coverage, about 50% recovery at a fractional coverage of ~0.2, and maximum recovery at a coverage of about half a monolayer.

Buckley et al (1997) applied SERS to verify the integrity of ethyl xanthate chemisorbed on silver and hence to resolve controversy that existed regarding the interpretation of XPS and FTIR data. Woods and Hope (1998) and Woods et al (1998a,b) carried out further studies on the chemisorption of ethyl xanthate on silver and extended these investigations to include copper and gold surfaces. In each case, the SERS spectra confirmed that ethyl xanthate retains its molecular integrity when it is adsorbed on these metals and that chemisorption occurs at underpotentials to the formation of the bulk compound which is the metal xanthates in the case of copper and silver, and dixanthogen for gold. Hope et al (2001a) found that similar behaviour was observed for isopropyl, isobutyl and isoamyl xanthates on silver. In these studies, it was shown that the chemisorption prewave on voltammograms shifted to more negative values by 0.028 V for each additional carbon atom in the alkyl chain. This value is consistent with the data of Kakovsky (1957) for the effect of alkyl chain length on the solubility product of silver xanthates and hence indicates that similar underpotentials for chemisorption apply to each xanthate homologue.

SERS studies on the interaction of *O*-isopropyl-*N*-ethylthionocarbamate (IPETC) with copper surfaces (Woods and Hope, 1999) showed that this collector also chemisorbs at underpotentials to Cu(IPETC) formation. Adsorption involved a charge transfer process in which the sulfur atom in the organic species becomes bonded to a copper atom in the metal surface and the hydrogen is displaced from the nitrogen atom to form a hydrogen ion in solution.

SERS investigations of the interaction of 2-mercaptobenzothiazole (MBT) with silver, gold and copper electrodes in aqueous solutions of pH 4.6 and 9.2 showed that the collector was adsorbed at all potentials studied (Woods et al, 2000). Rest potential measurements did not yield the reversible potentials for the formation of the metal compounds because the systems were electrochemically highly irreversible. Adsorption was shown to occur through a charge transfer process in which MBT becomes bonded to silver atoms in the surface through the exocyclic sulfur atom. Most Raman bands appeared at the same positions as those in the metal compounds, but the band arising from the NCS stretching mode was blue-shifted by ~10 cm^{-1}. This shift was considered to be indicative of chemisorption with the shift being explained in terms of the absence in the monolayer of the intermolecular bonding that occurs in the bulk compound.

Spectroelectrochemical investigations have been made on the suppression of silver dissolution in alkaline cyanide solutions by MBT (Hope et al, 2001b) and by diisobutyl dithiophosphinate (DIBDTPI) (Hope et al, 2001c). The objective of these studies was to determine the extent to which a flotation collector could diminish silver losses in flotation when cyanide is used as a depressant. Voltammograms in the positive-going direction recorded for a silver electrode in solutions of pH 11 containing 10^{-2} mol dm^{-3} CN^- together with different DIBDTPI concentrations following conditioning in the test solution for 10 min or 2 h are presented in Fig. 1.

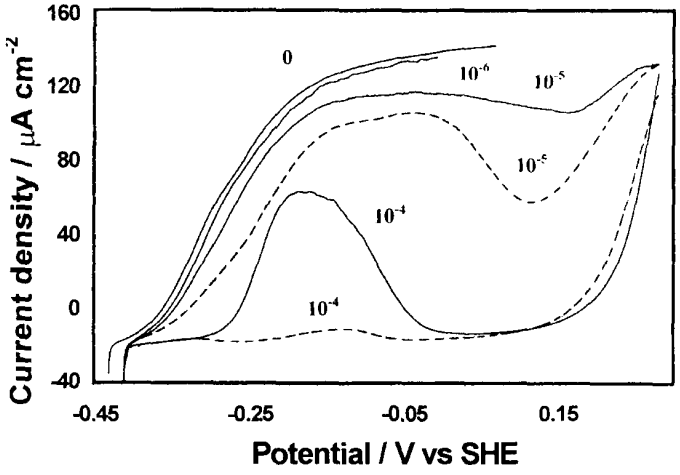

Fig. 1. Polarization curves at 0.5 mV s^{-1} in the positive-going direction for silver in deaerated solutions of the pH 11 buffer containing 10^{-2} mol dm^{-3} CN^- together with 0, 10^{-6}, 10^{-5}, or 10^{-4} mol dm^{-3} DIBDTPI. Silver electrode immersed in a solution of the same composition in equilibrium with air for ——— 10 min and – – – – 2h prior to transfer to the electrochemical cell

In the absence of the collector, the current for dissolution of silver in the cyanide solution increases to a mass transport controlled limiting current. In the presence of DIBDTPI, dissolution is inhibited, the inhibition increasing with increase in DIBDTPI concentration and conditioning time. That the inhibition results from adsorption of DIBDTPI was confirmed by SERS spectra. Figure 2 shows a spectrum from a silver electrode at the corrosion potential compared with a Raman spectrum from AgDIBDTPI.

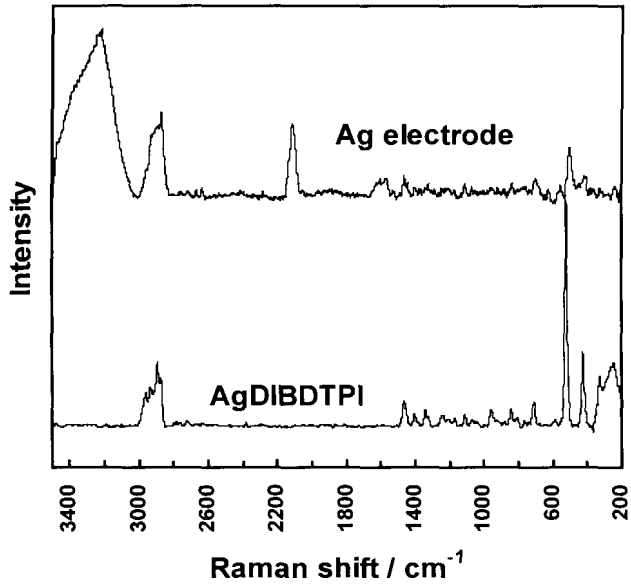

Fig. 2. Raman spectra for AgDIBDTPI and SERS spectrum from a silver electrode in pH 11 solution containing 10^{-2} mol dm^{-3} CN^- together with 10^{-4} mol dm^{-3} DIBDTPI in equilibrium with air at the open circuit potential

The band at 522 cm^{-1} for AgDIBDTPI is assigned to the PS_2 stretching vibration; most of the other bands arise from vibrations within the isobutyl groups. In particular, the bands near 2800 cm^{-1} arise from stretching vibrations of carbon-hydrogen bonds in the hydrocarbon chain. It can be seen from Fig. 2 that the SERS spectrum from the silver electrode displays all the bands exhibited by the silver compound and hence DIBDTPI is bonded to Ag atoms in the silver surface. The spectrum also displays a band at 2114 cm^{-1} which is assigned to the C≡N stretching vibration from cyanide bonded directly to silver atoms in the surface or to adsorbed silver cyano-complexes.

The interaction of DIBDTPI has also been investigated in the absence of cyanide. SERS spectra were observed for a silver electrode in 10^{-4} mol dm^{-3} DIBDTPI at pH 9.2 at all potentials investigated. Spectra were recorded *in situ* at controlled potential, on emersed electrodes, and *ex situ* after washing the electrode surface with pure water. A selection of the spectra is shown in Fig. 3.

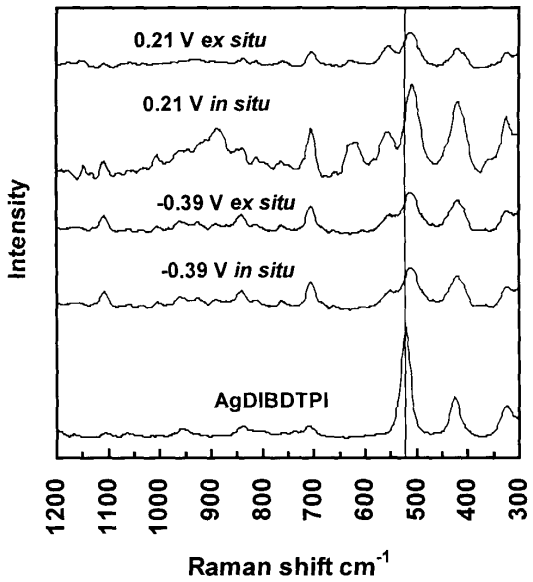

Fig. 3. SERS spectra in the low wavenumber region from a silver electrode in 10^{-4} mol dm^{-3} DIBDTPI solution of pH 9.2 held for 5 min at –0.39 and 0.21 V recorded *in situ* and *ex situ*. Vertical line is the position of the PS_2 band stretch vibration for AgDIBDTPI

For potentials ≥ –1 V, the SERS spectra were the same as the Raman spectrum for AgDIBDTPI except that the band arising from the PS_2 stretching vibration is blue-shifted by ~ 20 cm^{-1}, and an additional band is observed at 556 cm^{-1}. The observed blue shift is consistent with the surface species being chemisorbed. As pointed out above, a similar shift was observed for MBT (Woods et al, 2000). The fact that the SERS spectra were also observed *ex situ* after rinsing the electrode surface confirms that the surface species was chemisorbed and was not present as a specifically adsorbed ion.

In addition, Raman spectra were recorded after polarisation in the region in which voltammetry had shown AgDIBDTPI to develop. After polarisation for 5 min, the PS_2

stretch band appeared at the same wavenumber as it did at lower potentials. On extended polarisation, two bands became apparent, one at the chemisorption position and the other corresponding to that for AgDIBDTPI. Eventually, the latter band became dominant. This is the behaviour expected for the development of a AgDIBDTPI phase covering an initial chemisorbed layer.

No SERS spectra were evident with copper electrodes in the presence of DIBDTPI, but the formation of CuDIBDTPI was confirmed from Raman spectra at potentials at which an anodic current is observed on voltammograms. The absence of a SERS spectrum can not be taken as evidence that DIBDTPI does not chemisorb on copper sulfide minerals since similar results were observed with diethyldithiophosphate (DTP) on copper. It has been established (Woods, 1996) that DTP chemisorbs on chalcocite and this indicates that copper metal does not behave in the same manner as copper sulfide minerals with regard to interaction with thiophosphate collectors. In this regard, thiophosphorous collectors differ from the other collectors studied by Raman spectroelectrochemistry. At potentials at which DIBDTPI oxidizes to $(DIBDTPI)_2$ on gold, Raman spectra were observed from the disulfide and AuDIBDTPI. SERS spectra were also found on gold under laser illumination that were characteristic of the development of layer of sulfur and this is explained in terms of photolysis of DIBDTPI radicals formed as intermediates in the oxidation of DIBDTPI to its disulfide.

HYDROMETALLURGY

Leaching of sulfide minerals is important in both the recovery of metal values from ores and in environmental concerns associated with mining. Passivation of the sulfide surface is important in both these situations. In the former case, avoiding passivation is the key to improving leach performance. Raman spectroscopy has been applied by Wadsworth and co-workers (Zhu et al, 1992; Turcotte et al, 1993; Li et al, 1993; Li and Wadsworth, 1993; Zhu et al, 1997) for the *in situ* identification of elemental sulfur and polysulfides formed on the surface of sulfide minerals. A significant thickness of product is required before normal Raman spectroscopy can detect surface species.

Gold and silver are ideal surfaces for Raman studies since they exhibit surface enhancement. The leaching of these precious metals using cyanide has been carried out since the cyanidation of low-grade ore was commercialised following MacArthur and the Forrest brothers patenting the process in 1887. Gold metal in the ore is oxidised to form the $Au(CN)_2^-$ complex in aqueous solution. This process has been shown to be electrochemical in nature, an anodic gold dissolution process to form the complex ion being coupled to the cathodic reduction of oxygen. Thus, electrochemical techniques provide a means of studying directly the gold dissolution process. The kinetics of the gold-cyanide reaction is critical to the economic leaching of gold ore, and there has been a wide disparity in the results published on the rate of dissolution. Jeffrey and Ritchie (2000) provided convincing evidence that the variation in results is

due to differences in system purity, the presence of lead or silver ions, in particular, enhancing the leaching rate. They postulated that, under conditions of high purity, the gold surface is passivated by a film of a gold cyanide species and, on the basis of electrochemical measurements, argued that the passivating layer must be disrupted by the presence of impurity species.

We are, at present, carrying out Raman spectroelectrochemical studies on the dissolution of gold in different leachants. We have found that recording Raman spectra in real time together with cyclic voltammograms is a useful approach for studying this system and term this procedure CV Raman spectroscopy. A cyclic voltammogram at 10 mV s^{-1} from a gold electrode in a pH 11 buffer solution containing 0.01 mol dm^{-3} sodium cyanide is shown in Fig.4. SERS spectra in the frequency range in which the band for the C≡N stretch appears, recorded during the running of voltammogram, are also presented; spectra recorded on the positive-going scan are shown above the voltammogram, and those recorded on the return scan, below. The SERS spectra are in a 3-dimensional format, with Raman shift being the z-scale and scattering intensity the y-scale. The x-scale is potential and corresponds to that for the voltammogram. CV Raman spectra were also recorded in the lower wavenumber regions where the Au-O, Au-C and Au-N stretching vibrations occur.

It can be seen from Fig. 4 that cyanide is present on the gold surface at the low potential limit. As the potential is scanned in the positive going direction, the intensity of the cyanide band increases. The band position becomes red-shifted by ~35 cm^{-1} per volt between –1.4 and 0 V. This Stark tuning could arise from both chemical and electrostatic effects on the surface bonding, which may be accompanied by alteration of surface binding energetics and preferred binding geometries (Weaver and Wasileski, 2000).

When the potential reaches ~ –0.8 V in Fig. 4, an anodic current is observed on the voltammogram due to dissolution of gold as $Au(CN)_2^-$. At this potential, the appearance of a SERS band was observed in the frequency region in which stretching vibrations of bonds between gold and cyanide are expected. At ~ –0.6 V, the current corresponding to gold dissolution becomes inhibited. It can be seen from Fig. 4 that the intensity of the C≡N stretching band reaches a maximum at this potential. The decrease in intensity as the potential is increased further could result from the formation of a polymeric gold cyanide overlayer as suggested by Jeffrey and Ritchie (2000). The shift in the C≡N stretching band position diminishes above 0 V and becomes close to zero in the region 0.4 to 0.6 V. This indicates that there is no longer a change in the orientation or constitution of the surface cyanide species.

The dissolution current increases again above 0.3 V, but reaches a second maximum at ~ 0.6 V. The C≡N stretching band is diminished at this peak potential and bands become apparent in the region expected for Au-O stretching vibrations. Similar Au-O bands were observed above 0.6 V by CV Raman for gold electrodes in the absence of cyanide and this substantiates identification in terms of the formation of surface oxygen species. It is evident that the surface oxide inhibits gold dissolution.

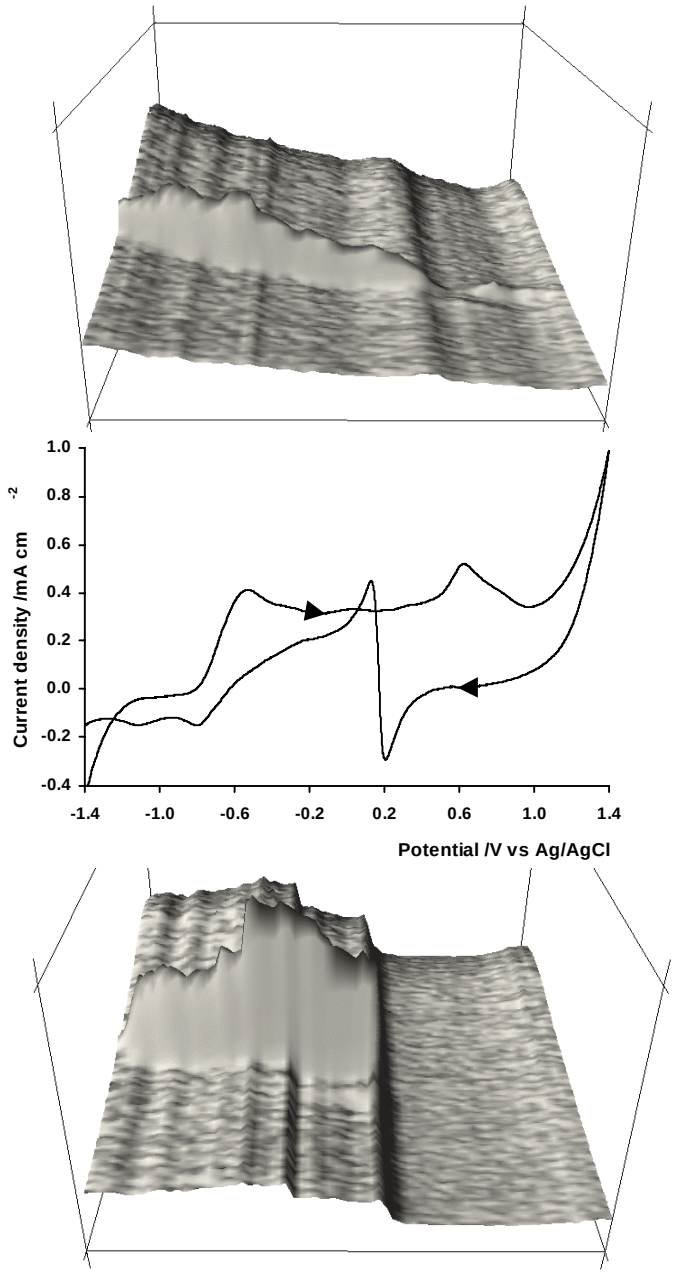

Fig. 4. CV Raman at 10 mV s^{-1} from a gold electrode in 0.01 mol dm^{-3} CN^- at pH 11

On the return scan, a cathodic current resulting from stripping of the oxide commences at ~ 1.2 V and peaks at 0.2 V. There was a corresponding decrease in the intensity of the Au-O SERS band. Just below 0.2 V, the current switches from cathodic to anodic and this is explained by gold dissolution occurring again as the surface oxygen species are removed. The re-appearance of the C≡N stretching band at this potential (Fig. 4) confirms this interpretation. The current diminishes as the scan proceeds and this indicates that the cyanide species responsible for the SERS spectrum is the inhibiting species. This is consistent with the cyanide band position at 0.2 V being the same as that at the corresponding potential on the positive going scan. A corresponding Stark shift is observed on the negative-going scan resulting in the C≡N stretching band returning to the same position at the end of the cycle as it occupied initially. The two small cathodic current peaks that appear at potentials below –0.8 V can be assigned to redeposition of gold from gold cyanide complexes remaining near the electrode surface. It is interesting to note that there are significant changes in the background fluorescence spectrum with change in potential (Fig. 4). These changes provide additional information on the nature of the gold surface during the potential cycle.

ELECTROMETALLURGY

Electrowinning is the most effective method for the large-scale production of pure, marketable metal in hydrometallurgical processes. Electrorefining constitutes the final polishing stage in pyrometallurgical processing. Metals such as zinc, copper and lead, that have low electrodeposition overpotentials, have a propensity to form coarse, rough deposits in such electrodeposition processes. This is due to the slow nucleation rates at low overpotentials, which compels the new metal to grow on few nuclei. To overcome this problem, various additives are included in the solution and adsorb on the metal surface, preferentially at the most active growth sites. Ideally, these additives should not become incorporated into the deposit to any significant extent, since this would diminish product quality.

SERS has been applied by a number of authors (see Buckley et al, 2002 for review) to elucidate the interaction of the additive thiourea with copper and silver surfaces in sulfate-, acid- and halide-containing solutions. In the absence of additives, Brown and Hope (1995) found that sulfate, but not bisulfate, was adsorbed on copper from sulfuric acid solutions, even though bisulfate is the predominant anion in solution.

We have recently revisited the electrodeposition of copper from sulfuric acid media taking advantage of the advances in sensitivity and capability of modern Raman instruments. The improvement in instrument performance allows real-time recording of spectra during potential excursions. The application of modern instrumentation has provided the means for detecting transient adsorption of sulfate during copper electrodeposition.

A Raman spectrum obtained from $CuSO_4.5H_2O$ is shown in Fig. 5. The major feature is a band at 983 cm^{-1} due to the symmetrical stretching vibration of the SO_4^{2-}

group. Bending and antisymmetric stretching vibrations of sulfate give rise to the band at 615 cm^{-1}, and the band at 465 cm^{-1} is assigned to a bending mode. Fig. 5 also presents a Raman spectrum from 1 mol dm^{-3} sulfuric acid; it displays corresponding sulfate bands at 983 cm^{-1} 595 cm^{-1} and 434 cm^{-1} together with bands at 1050 cm^{-1} and 898 cm^{-1} arising from stretching vibrations of the SO_3 group and the OH group components of the bisulfate. It is clear from Fig. 5 that Raman spectroscopy can readily distinguish between sulfate and bisulfate.

A typical spectrum from a copper surface in 1 mol dm^{-3} sulfuric acid at potentials in the region of stability of the metal is also shown in Fig. 5. The spectrum displays bands of low intensity at the same wavenumbers as expected from the 1 mol dm^{-3} sulfuric acid electrolyte itself, and hence involves both sulfate and bisulfate species. This spectrum could have arisen from the solution in the roughened electrode surface or from adsorbed species.

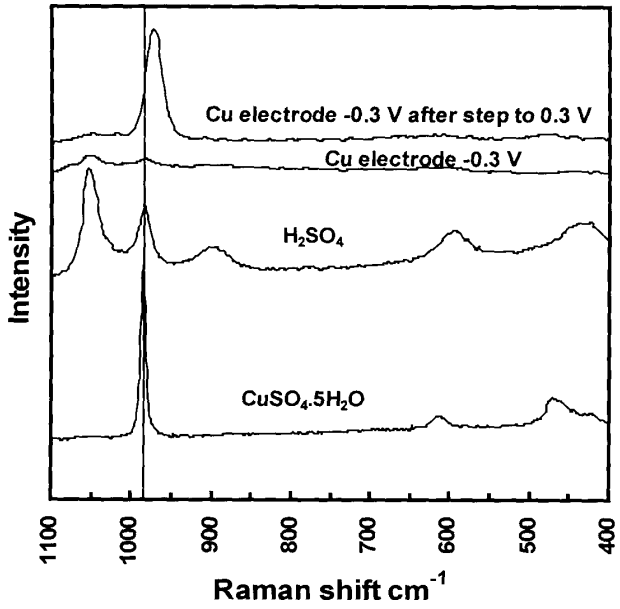

Fig. 5. Raman spectra from $CuSO_4.5H_2O$, 1 mol dm^{-3} H_2SO_4, copper electrode at –0.3 V in 1 mol dm^{-3} H_2SO_4 and a copper electrode at –0.3 V following a potential step to 0.3 V. Vertical line is 983 cm^{-1}, which is the position of the sulfate symmetrical stretch band for $CuSO_4$ and H_2SO_4

When the potential of the copper electrode was taken into the dissolution region and then returned to the region of stability, either on a potential scan or a potential step function, SERS spectra were observed, a typical example of which is shown in Fig. 5. This spectrum has a single band at 972 cm^{-1}, which is assigned to a surface sulfate species.

The adsorbed sulfate spectrum disappeared over a period of a few minutes when the potential was held in the metal stability region. This indicates that the adsorbed sulfate is a transient species associated with copper being deposited. The intensity of the sulfate band decays due to diminution of copper plating as copper(II) ions are depleted in the vicinity of the electrode surface. The decline in intensity is not due to a

change in focus of the Raman probe resulting from copper deposition because the spectrum did not diminish in intensity when copper sulfate was added to the 1 mol dm^{-3} sulfuric acid electrolyte. The sulfate band appeared at all potentials in the Cu^0 stability region following an excursion to dissolution potentials or the addition of copper ions. It displayed only slight Stark tuning, being red-shifted by ~ 5 cm^{-1} V^{-1} between 0.1 V and –0.5 V.

Sulfate ions have also been shown (Watanabe et al, 1995) to co-adsorb in the underpotential deposition (UPD) of copper on platinum and gold and that it is sulfate and not bisulfate that is on the surface (Shi et al, 1994). The structure and composition of copper ad-layers have been extensively studied by a variety of experimental techniques and it is well established that a honeycomb ($\sqrt{3}\times\sqrt{3}$) phase is formed in UPD Cu on Au(111) consisting of 2/3 monolayer of Cu and 1/3 monolayer of SO_4. The copper is considered (Legault et al, 1996) to have a partial positive charge and this induces the adsorption of sulfate anions which themselves become partially discharged.

It is possible that the initial copper deposit formed on copper retains a partial charge analogous to that for UPD copper layers and, similarly, induces the co-adsorption of sulfate ions into the surface. The subsequent discharge of the partially charged copper atoms would complete the electrode reaction and the surface layer would reconstruct to form the stable copper structure. The sulfate ions would then be desorbed.

The SERS spectrum displays only the symmetrical stretching vibration of sulfate; the antisymmetrical vibrations are suppressed. This would indicate that each SO_4 is sited with three oxygen atoms close to surface copper atoms with the fourth vertically above the surface. The symmetrical stretching band is blue-shifted by ~11 cm^{-1} from the corresponding band from H_2SO_4 or hydrated $CuSO_4$. This could arise from bonding between the adsorbed sulfate and surface copper atoms.

The sulfate band did not appear on similar experiments in which the 1 mol dm^{-3} sulfuric acid solution contained 10 ppm chloride. This suggests that the transient adsorbed sulfate ions are replaced by chloride ions in the growing copper electrodeposit.

When thiourea is present in the sulfuric acid solution, SERS spectra from the organic species can readily be characterised. Hope and co-workers (Brown et al, 1995; Brown and Hope 1996; Hope and Brown, 1994) noted that the adsorption of sulfate takes place together with thiourea on copper and concluded that adsorption was a co-operative rather than a competitive process, since the intensity of the sulfate bands as well as those of thiourea, increased with increase in thiourea concentration. Furthermore, the sulfate symmetrical stretch band was found to be significantly shifted from the corresponding band in thiourea-free solution.

Hope and co-workers (Bott et al, 1998) characterized complexes formed between copper(I), thiourea, and anions such as sulfate. They determined the crystal structure of the previously unknown $[Cu_4(tu)_7](SO_4)_2].H_2O$ (where tu is thiourea) and the

vibrational spectra of a range of copper(I) thiourea complexes. The copper atoms were found to lie in a tetrahedral arrangement forming $[Cu_4(tu)_7]^{4+}$ clusters interlinked by sulfate ions, which strongly interact with thiourea ligands through hydrogen bonds. The bond lengths about the thiourea ligands indicated a decrease in the carbon–sulfur double-bond character, consistent with the co-ordination of thiourea with copper being through the sulfur atoms. The Raman bands in the sulfate complexes were found to appear at similar wavenumbers to those of the SERS bands for the species adsorbed on copper. The stretching vibration for Cu-S for these complexes was found to show a strong dependence on the copper coordination environment and the value observed in the SERS indicated that the co-ordination number for the Cu/thiourea species at the metal surface is relatively low. This is what is to be expected for a surface analogue of a copper(I) thiourea sulfate complex.

We have recently confirmed these findings with modern Raman instrumentation. A SERS spectrum from a copper electrode in 5 ppm thiourea, 1 mol dm^{-3} H_2SO_4 recorded at 0 V following a 10 s potential pulse to 0.3 V is shown in Fig. 6;together with Raman spectra from $[Cu_4(tu)_7](SO_4)_2].H_2O$ and from a 1 mol dm^{-3} aqueous thiourea solution.

The thiourea spectrum is characterised by bands arising from skeletal deformation/ C-S stretch at 490 cm^{-1} and C=S stretch at 743 cm^{-1} (Brown et al, 1995). The spectrum from the copper thiourea sulfate crystal displays bands due to sulfate symmetrical stretch (977 cm^{-1}), C-S stretch (712 cm^{-1}), SCN bend (482 cm^{-1}), NCN bend (423 cm^{-1}) and CuS stretch (252 cm^{-1}) (Bott et al, 1998). The C=S vibration observed with thiourea itself is absent in the complex because the sulfur atoms of thiourea are now bonded to copper atoms. The SERS spectrum from the copper electrode shows that the surface species formed on copper is not thiourea itself, but is similar to that for the copper thiourea complex. All the bands observed from the complex appear in the SERS spectrum, but some are blue-shifted by ~ 10 cm^{-1}. There is also a bisulfate band at 1055 cm^{-1} apparent in the SERS spectrum in Fig. 6, and this indicates that bisulfate as well as sulfate can be involved in complex formation at the copper surface. Brown et al (1995) found that the relative intensity of the bisulfate band to the other bands decreased with increase in thiourea concentration, whereas that from sulfate increased.

Brown and Hope (1996) applied *in situ* SERS spectroscopy to investigate the influence of chloride ion on the co-adsorption of thiourea and sulfate ions in sulfuric acid solution at the concentration levels used in the electrorefining of copper. They found chloride also to co-adsorb and that adsorption of the halide was favoured at low negative potentials. The presence of the chloride in solution at low concentrations was also found to result in enhancement of the adsorption of thiourea and sulfate. Furthermore, the adsorption of chloride at the copper electrode altered the molecular structure of the interface due to an interaction with co-adsorbed thiourea and sulfate species at the electrode surface.

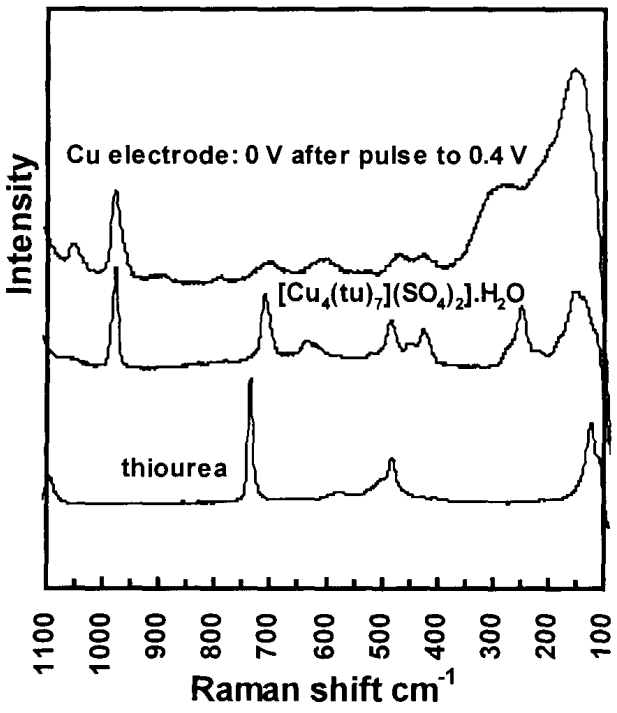

Fig. 6. Raman spectra from thiourea and from $[Cu_4(tu)_7](SO_4)_2].H_2O$ and a SERS spectrum from a copper electrode at 0V after a 10 s potential pulse to 0.3 V

Brown and Hope (1996) considered that the chloride interacts with the nitrogen containing groups of the thiourea molecule adsorbed at the electrode surface as evidenced by changes in band shape and intensity for the NH_2 torsion and C-N stretching vibrational modes. In this manner, the adsorption of chloride results in a rearrangement or alteration of the molecular structure at the electrode surface that is observed by changes in signal intensity for the various vibrational bands associated with the adsorption of thiourea, sulfate and chloride at the electrode surface. These finding are consistent with adsorption of the organic molecule on the copper electrode occurring by co-ordination with the sulfur atom.

ACKNOWLEDGEMENTS

This project was supported by the Australian Research Grants Scheme. Flotation collectors were generously provided by Cytec Industries Inc.

REFERENCES

BOTT, R C., BOWMAKER, G.A., DAVIS, C.A., HOPE, G.A. and JONES, B.E. (1998), *Crystal structure of $[Cu_4tu_7](SO_4)_2.H_20$ and vibrational spectroscopic studies of some copper (i) thiourea complexes*, Inorganic Chemistry, Vol. 37, 651-657.

BROWN G.M. and HOPE, G.A. (1995) *In-situ spectroscopic evidence for the adsorption of SO_4^{2-} ions at a copper electrode in sulfuric acid solution***,** J. Electroanal. Chem., Vol. 382, 179-182.

BROWN G.M. and HOPE, G.A. (1996), *Confirmation of thiourea/chloride ion co-adsorption at a copper electrode by in situ SERS spectroscopy*, J. Electroanal. Chem., 413 (1996) 153-160.

BROWN, G.M., HOPE, G.A., SCHWEINSBERG D.P. and FREDERICKS, P.M. (1995), *SERS study of the interaction of thiourea with a copper electrode in sulphuric acid solution*, J. Electroanal. Chem., 380 (1995) 161-166.

BUCKLEY A.N. and WOODS, R. (1996), *Relaxation of the lead-deficient sulfide surface layer on oxidized galena*, J. Appl. Electrochem., Vol. 26, 899 - 907.

BUCKLEY, A.N., HOPE, G.A. and WOODS, R. (2002), *Metals from sulfide minerals: the role of adsorption of organic reagents in processing technologies*, Solid-Liquid Interfaces Macroscopic Phenomena - Microscopic Understanding (K. Wandelt and S. Thurgate, Eds) Topics in Applied Physics, Vol. 85, Springer; Germany, pp. 59-94.

BUCKLEY, A.N., PARKS, T.J., VASSALLO, A.M. and WOODS, R. (1997), *Verification by surface enhanced Raman spectroscopy of the integrity of xanthate chemisorbed on silver*, Int. J. Miner. Process., Vol. 51 303-313.

FLEISCHMANN, M.; HENDRA, P. J. and McQUILLAN, A. J. (1974), *Raman spectra of pyridine adsorbed at a silver electrode.*, Chem. Phys.Lett. , **26**, 163-166.

FLEISCHMANN, M., SOCKALINGUM, D. and MUSIANI, M.M. (1990), *The use of near infrared Fourier Transform techniques in the study of surface enhanced Raman spectra*, Spectrochim. Acta, Vol. A46, 285-294.

HOPE, G.A. and BROWN, G.A. (1994) *In-situ additive monitoring during copper deposition in acid sulfate electrolyte*, Proc. Int. Symp. Electrochemistry in Mineral and Metal Processing, (R. Woods, F.M. Doyle and P. Richardson, Eds.), PV 96-6, Electrochem. Soc., Pennington, NJ., pp. 429-438

HOPE, G.A., WATLING, K. and WOODS, R. (2001a), *A SERS spectroelectrochemical investigation of the interaction of isopropyl, isobutyl and isoamyl xanthates with silver*, Colloids and Surfaces A, Vol. 178 157-166.

HOPE, G.A., WATLING, K. and WOODS, R. (2001b), *An electrochemical investigation of the suppression of silver dissolution in aqueous cyanide by 2-mercaptobenzothiazole*, J. Appl. Electrochem. , Vol. 31, 703-709.

HOPE, G.A., WOODS, R. and WATLING, K. (2001c), *A spectroelectrochemical investigation of the influence of sodium diisobutyldithiophosphinate on silver dissolution in aqueous cyanide*, J. Appl. Electrochem. Vol. 31, 1285-1291.

JEFFREY, M.I. and RITCHIE, I.M. (2000), *The leaching of gold in cyanide solution in the presence of impurities I. The effect of lead*, J. Electrochem. Soc., Vol. 147 3257-3262.

KAKOVSKY, I.A. (1957), *Physicochemical properties of some flotation reagents and their salts with ions of heavy non-ferrous metals*, Proc. 2nd Int. Congr. Surface Activity, Vol. IV, (J.H. Schulman, Ed.), Butterworth, London, pp. 225-237.

KOWAL, A. and POMIANOWSKI, A. (1973), *Cyclic voltammetry of ethyl xanthate on a natural copper sulphide electrode*, J. Electroanal. Chem., Vol. 46, 411-420.

LEGAULT, M., BLUM L. and HUCKABY, D.A. (1996), *An extended hexagon model for Cu underpotential deposition on Au(III)*, J. Electronal. Chem., Vol. 409, 79-86.

LI, J., ZHU, X. and WADSWORTH, M.E. (1993), *Raman spectroscopy of natural and oxidized metal sulfides*, EPD Congress, (J.P. Hager, Ed.) MME/AIME, Warrendale PA, pp.229-243.

LI, J. and WADSWORTH, M.E. (1993), *Raman spectroscopy of electrochemically oxidized pyrite and optimum conditions for sulfur formation*, Hydrometallurgy: Fundamentals, Technology and Innovation, (J.B. Hiskey and G.W. Warren, Eds.) SME/AIME, Littleton, CO, pp.127-141.

NIXON, J.C. (1957), *Discussion*, Proc. 2nd Int. Congr. Surface Activity, Butterworth, London, Vol. 3, p.369.

POMIANOWSKI, A. (1967), *Cyclic voltammetry in dilute solutions of potassium ethyl xanthate*, Roczniki Chem., Vol. 41, 1125-1129.

SHI, Z. and LIPKOWSKI, J. (1994), *Coadsorption of Cu^{2+} and SO_4^{2-} at the Au(111) electrode***,** J. Electroanal. Chem., Vol 365, 303-309.

SZEGLOWSKI, Z., CZARNECKI, J., KOWAL, A. and POMIANOWSKI, A. (1977), *Adsorption of potassium ethyl xanthate on a copper electrode surface*, Trans. IMM, Vol. 86, C115-118.

TURCOTTE, S.B., BENNER, R.E., RILEY, A.M., LI,J., WADSWORTH M.E. and BODILY, D.M. (1993), *Surface analysis of electrochemically oxidized metal sulfides using Raman spectroscopy*, J. Electroanal. Chem., Vol. 347, 195-205.

WATANABE, M. UCHIDA H. and IKEDA, N. (1995), *Electrochemical quartz crystal microbalance study of copper ad-atoms on gold and platinum electrodes Part I. Adsorption of anions in sulfuric acid*, J. Electroanal. Chem., Vol. 380, 255-260.

WEAVER, M.J. and WASILESKI, S.A. (2000) *Electrochemical Surface Spectroscopy*, The Electrochemical Society Interface. pp.34-36.

WOODS, R. (1971) *The oxidation of ethyl xanthate on platinum, gold, copper, and galena electrodes: relation to the mechanism of mineral flotation*, J. Phys. Chem., Vol. 75, 354-362.

WOODS, R. (1996) *Chemisorption of thiols on metal and metal sulfides*, Modern Aspects of Electrochemistry, No. 29, (Eds., J.O'M. Bockris, B.E. Conway and R.E. White), Plenum Press, NY, pp. 401-453.

WOODS, R. and HOPE, G.A. (1998), *Spectroelectrochemical investigations of the interaction of ethyl xanthate with copper, silver and gold: I. FT-Raman and NMR spectra of xanthate compounds*, Colloids and Surfaces A, Vol. 137, 319-328.

WOODS, R. and HOPE, G.A. (1999), *A SERS spectroelectrochemical investigation of the interaction of O-isopropyl-N-ethylthionocarbamate with copper surfaces*, Colloids and Surfaces A, Vol. 146, 63-74.

WOODS, R., HOPE, G.A. and BROWN, G.M. (1998a), *Spectroelectrochemical investigations of the interaction of ethyl xanthate with copper, silver and gold: II. SERS of xanthate adsorbed on silver and copper surfaces*, Colloids and Surfaces A, Vol. 137, 329-337.

WOODS, R., HOPE, G.A. and BROWN, G.M. (1998b), *Spectroelectrochemical investigations of the interaction of ethyl xanthate with copper, silver and gold: III. SERS of xanthate adsorbed on gold surfaces*, Colloids and Surfaces A, Vol. 137, 339-344.

WOODS, R., HOPE, G.A. and WATLING, K. (2000), *A SERS spectroelectrochemical investigation of the interaction of 2-mercaptobenzothiazole with copper, silver and gold surfaces*, J. Appl. Electrochem., Vol. 30, 1209-1222.

ZHU, X.; LI, J.; BODILY, D.M.; WADSWORTH, M.E. (1992), *Tranpassive oxidation of pyrite*, Proc. Int. Symp. Electrochemistry in Mineral and Metal Processing III, PV 92-17, (R. Woods and P.E. Richardson Eds.), Electrochem.Soc., Pennington, NJ., pp.391- 409.

ZHU, X.; WADSWORTH, M.E.;. WOODS, R. (1997), *Electrochemical kinetics of the anodic dissolution of nickel matte and synthetic Ni_3S_2*, Nickel-Cobalt 97, Volume I: Hydrometallurgy and Refining of Nickel and Cobalt (W.C. Cooper and I. Mihaylov, Eds.) CIM, Canada, pp. 153-167.

Hope G.A., Woods R., K. Watling K., *Badania spektrochemiczne SERS w przeróbce kopalin***,** Fizykochemiczne Problemy Mineralurgii, 36, (2002) 21-38 (w jęz. ang.)

W pracy przedyskutowano zastosowania spektroskopii rozproszenia ramanowskiego (ze wzmocnieniem sygnału wskutek odbicia promieniowania od powierzchni - SERS) w badaniach związanych z procesami przeróbki minerałów w których widmo wykonywane jest *in situ*. W układach flotacyjnych zastosowano SERS do charakterystyki pokryć na metalach z grupy miedzi, powstających w wyniku oddziaływania na te metale w warunkach kontrolowanego potencjału roztworów ksantogenianów: etylowego, izopropylowego, izobutylowego i izoamylowego, a także o-izopropylo-N-etylotionocarbaminianu, 2-merkaptobenzotiazolu oraz dwuizobutylo dwutiofosfonianu. W przypadku wszystkich kolektorów adsorpcja następuje w wyniku przeniesienia ładunku z wytworzeniem wiązania metal-siarka, a jeśli znany jest odwracalny potencjał tworzenia fazy objętościowej to można stwierdzić,

że wiązanie z powierzchnią następuje przy potencjale niższym niż dla reakcji w fazie objętościowej. Zaobserwowano, że roztwarzanie srebra w zasadowych roztworach cyjankowych jest silnie spowalniane w wyniku chemisorbcji 2-merkaptobenzotiazolu i dwuizobutylo dwutiofosfonianu. W zakresie hydrometalurgii zastosowano SERS do badania ługowania złota. Stosując rejestrację widm SERS w trakcie wykonywania woltamperogramów przy zmieniającym się potencjale obserwowano zmiany w składzie warstw powierzchniowych na złocie w wyniku traktowania powierzchni złota cyjankami przy różnych potencjałach. SERS zastosowano również do badania procesów elektrometalurgicznych, stwierdzając że w procesach osadzania miedzi z kwaśnych roztworów siarczanowych bierze udział przejściowy produkt zawierający grupę siarczanową.

Physicochemical Problems of Mineral Processing, 36 (2002) 39-49
Fizykochemiczne Problemy Mineralurgii, 36 (2002) 39-49

Piotr WARSZYŃSKI[*], Barbara JACHIMSKA[*]

CONFORMATIONS OF HYDROPHOBIC CHAINS AT LIQUID/GAS INTERFACE AND THEIR IMPLICATIONS ON SURFACTANT ADSORPTION[#]

Received March 5, 2002, reviewed, accepted May 17, 2002

We present a simple model of single chain, non-ionic surfactant adsorption at gas/liquid interface. Our model takes explicitly into account the effect of conformations the surfactant hydrocarbon chains can assume at the interface. We applied our model for the description of a dependence of surface tension on solution concentration of homologous series of n-alkanols. Aliphatic alcohols with the chain length from four to ten carbon atoms were studied. We found that our model correctly describes experimental data and predicts a distribution of chain conformation at the interface for all n-alkanols studied. We detected small but distinct even-odd effect in the distribution of conformations.

Key words: s*urfactants, adsorption, hydrocarbon chains, conformationsk*

INTRODUCTION

Modification of interfacial properties of various interfaces is a key issue for mineral processing. For instance in the process of flotation a decrease of surface tension and increase of surface elasticity of air/water interface favors bubble production of the desired size and enhance foamability. Due to their amphiphatic molecular structure surfactants, when present at low concentration in solution, have the property of adsorbing onto surfaces or interfaces of the system and altering to a significant degree their interfacial properties. In order to optimize the choice of surfactant for a specific application, the fundamental information concerning its equilibrium and dynamic adsorption properties have to be known. This properties are obviously controlled by the structure of surfactant molecule itself. Water soluble surfactants typically consist of the hydrophilic ionic, non-ionic or zwitterionic head-

[*]Institute of Catalysis and Surface Chemistry, Polish Academy of Sciences, ul. Niezapominajek 8, 30-239, Cracow, Poland, e-mail: ncwarszy@cyf-kr.edu.pl
[#]Paper dedicated to Professor Andrzej Pomianowski on the occasion of his 80th birthday.

group and hydrophobic part, which for simple surfactants is a single hydrocarbon chain. For the same head-group, length of the chain, i.e. the position of a given surfactant in a homologous series, decides on its surface activity. The unrestricted hydrocarbon chain is quite flexible and therefore, can assume many conformation when exposed into gas phase at aqueous solution/air interface. When adsorption progresses and the interface becomes crowded with surfactant, less area is accessible for a single chain. Therefore, some conformations with the highest area are strongly restricted. This decrease of the conformational freedom should lead to decrease of the free energy of adsorption, therefore, should be reflected in the adsorption equilibrium isotherm and also in the adsorption kinetics.

In our paper we propose a simple model to describe the effect of conformations of hydrophobic chains at interface on adsorption. We verify the implications of our model on the experimental data concerning the dependence of surface tension on concentration of the homologous series of the simplest surface active species – n-alkanols.

THEORETICAL BACKGROUND

Consider adsorption equilibrium between surfactant in bulk and interface. Formally we can write the criterion of the equilibrium in terms of chemical potentials in bulk μ_b and surface phase μ_s:

$$\mu_{\mathrm{b}} = \mu_0^{\mathrm{b}} + \mathrm{kT}\ln(\gamma \mathrm{c})$$
$$\mu_{\mathrm{s}} = \mu_0^{\mathrm{s}} + \mathrm{kT}\ln(\gamma_{\mathrm{s}} \Gamma) \qquad (1)$$

where: μ_0^b and μ_0^s is the standard chemical potential of the surfactant in bulk and at interface respectively, c is surfactant concentration in solution, Γ is its surface concentration, γ and γ_s are respective surfactant activity coefficients in bulk and at interface. For dilute solutions $\gamma \approx 1$. In the equilibrium the chemical potentials are equal and that leads to a general adsorption isotherm in a form:

$$\gamma_{\mathrm{s}} \Gamma = \gamma \mathrm{c} \exp\left(-\frac{\Delta\mu_0}{\mathrm{kT}}\right) \qquad (2)$$

where: $\Delta\mu_0$ - the standard free energy of adsorption (per one molecule) i.e. energy of transfer of molecule from the bulk of the solution to empty interface. Surfactant activity coefficient at the interface can be expressed in terms of free energy of interactions with solvent and other surfactant molecules:

$$\gamma_s = exp\left(-\frac{\Delta\mu_{int}}{kT}\right) \qquad (3)$$

We assume that this free energy consists of several additive terms (Ben Shaul et al., 1985, Warszyński and Lunkenheimer, 1999):

$$\Delta\mu_{\mathrm{int}}(\Gamma) = \Delta\mu_{\mathrm{hg-hg}} + \Delta\mu_{\mathrm{hg-ch}} + \Delta\mu_{\mathrm{ch-ch}} + \Delta\mu_{\mathrm{conf}} \tag{3}$$

Here, $\Delta\mu_{hg\text{-}hg}$ - is the head-group interaction free energy which originates mainly from the excluded volume interactions between head-groups, $\Delta\mu_{hg\text{-}ch}$ - is the free energy of other head-group\head-group or head-group\chain interactions, $\Delta\mu_{ch\text{-}ch}$ - is free energy of the van der Waals cohesive interaction between hydrocarbon chains, $\Delta\mu_{conf}$ - is conformational free energy of surfactant tails involving all possible chain conformations resulting from the intrachain C-C bonds rotations and rotations of entire surfactant molecule at the interface.

For example, if we assume that the head-group interaction free energy can be expressed as (Nagarayan and Ruckenstein, 1977):

$$\Delta\mu_{\mathrm{hg-hg}} = -\,\mathrm{k\,T}\ln\left(1 - \frac{\mathrm{A_{hg}}}{\mathrm{A}}\right) = -\,\mathrm{k\,T}\ln(1-\theta) \tag{4}$$

where: $\mathrm{A_{hg}}$ is the cross-sectional area of the headgroup, $\mathrm{A} = \dfrac{1}{\mathrm{N_a}\,\Gamma}$ is the area per molecule adsorbed, $\theta = \dfrac{\mathrm{A_{hg}}}{\mathrm{A}} = \dfrac{\Gamma}{\Gamma_\infty}$ is the surface coverage and Γ_∞ is the limiting surface concentration corresponding to the closely packed monolayer. Additionaly, we express second and third component in the Eq. (4) in terms of mean field approximation (Rowlinson and Widom, 1989):

$$\Delta\mu_{\mathrm{hg-ch}} + \Delta\mu_{\mathrm{ch-ch}} = -\,2\,\mathrm{H}\,\Gamma \tag{5}$$

where H is a mean field parameter, and if we neglect the conformational contribution, we arrive at Frumkin isotherm:

$$\frac{\mathrm{c}}{\mathrm{a}} = \frac{\theta}{1-\theta}\exp\left(-\frac{2\mathrm{H_s}}{\mathrm{k\,T}}\theta\right) \tag{6}$$

which is commonly used for the description of surfactants' adsorption. Here, a is the surface activity parameter or the bulk-surface distribution coefficient and $\mathrm{H_s} = \dfrac{\mathrm{H}}{\mathrm{A_{hg}}}$ is the Frumkin interaction parameter assuming positive values for attractive interactions favoring adsorption.

The hydrocarbon chain is quite flexible due to low energy difference (~ 1.2 kT) between trans (t) and gauche (g^+, g^-) conformation of four consecutive carbon atoms in the chain (dihedral angles) (Flory, 1971). Therefore, for long chains it exists a considerable amount of conformations which are energetically accessible. Figure 1. presents an example of such conformations for n-hexanol. The number of conformations of surfactant at the interface is restricted because a surfactant molecule is anchored to it by the head-group and penetration of solution sublayer by surfactant tail is limited.

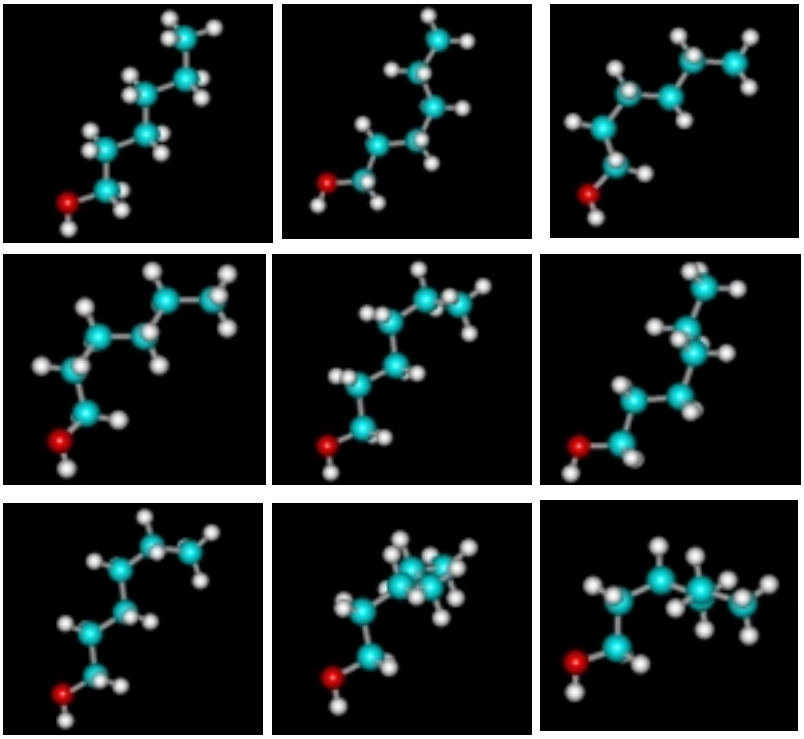

Fig. 1. Examples of conformations of n-hexanol molecule

Conformational free energy of surfactant has to be evaluated from (Ben Shaul et al., 1985):

$$\Delta \mu_{conf} = - k T \ln z_{conf} \tag{7}$$

where: z_{conf} is the effective partition function (configurational sum) of a single surfactant tail at the interface :

$$z_{conf} = \sum_{\{a_i\}} \exp\left(- \frac{\varepsilon(a_i)}{k T} \right) \tag{8}$$

where: $\{a_i\}$ is a set of all possible tail conformations, i.e. all possible sequences of trans and gauche conformations of dihedral angles in a hydrocarbon chain and all possible orientations of the entire chain at the interface, $\varepsilon(a_i)$ the energy of the chain in conformation a_i consisting of bonds bending energies, torsional energies of C-C bonds' rotations, the van der Waals and hard core interactions between distant (separated by more than four C-C bonds) CH_2 and/or CH_3 groups of the same chain.As it was demonstrated by Vold (Vold 1984) with the procedure of exhaustive enumeration one can determine the cumulative distribution of surfactant conformations in terms of effective area occupied by a given conformation at interface, A_c. Taking into account the interaction of the surfactant tail with water subphase (which was not done by Vold), this distribution can be approximated with gamma function:

$$f_{conf}(A_c(a_i)) \approx (A_c(a_i) - A_{CH_2})^{\alpha} \exp\left(-\frac{A_c(a_i) - A_{CH_2}}{\beta} \right) \tag{9}$$

where two parameters α and β describe shape of the distribution and A_{CH_2} is the limiting effective cross-sectional area of the chain in all trans-conformation, 0.20 nm^2 (see the top left picture in Fig.1.). Knowing the distribution of the chain conformations, one can determine the dependence of the single chain conformational partition function on surfactant surface concentration using a very simple model. At the low coverage surfactant chains does not contact with each other and all conformations possible to attain at the interface are available. Thus, replacing the sum over conformations by integration over the distribution of effective areas of a chain in Eq.(9) we obtain:

$$z_{conf}(\infty) = \int_{A_{CH_2}}^{\infty} f'_{conf}(A_c)\, dA_c \tag{10}$$

When the interface is partially covered with surfactant at the surface concentration equal to Γ we assume that all conformations with the effective area less than A per two surfactant chains are equally possible, whereas conformations with the effective area higher than A are prohibited by the excluded volume interactions with the neighboring chains. Thus,

$$z_{conf}(A) = \int_{A_{CH_2}}^{A} f'_{conf}(A_c)\, dA_c \tag{11}$$

where: $f'_{conf}(A_c(a_i)) = \left(\frac{A_c(a_i) - A_{CH_2}}{2} \right)^{\alpha} \exp\left(-\frac{A_c(a_i) - A_{CH_2}}{2\beta} \right)$

The difference of the conformational free energy per one molecule adsorbed at partially covered and empty interface is then given by:

$$\Delta\mu_{conf} = - k T \ln \frac{z_{conf}(A)}{z_{conf}(\infty)} \tag{12}$$

Combining Eqs. (2) – (6) with Eq, (13) we obtain modified Frumkin isotherm which explicitly takes into account the surfactant chain conformations:

$$\frac{c}{a} = \frac{\theta}{(1-\theta)} \exp\left(-\frac{2H_s}{kT}\theta\right) \exp\left(\frac{\Delta\mu_{conf}}{k T}\right) \tag{13}$$

More details of the model are given elsewhwere (Warszyński and Lunkenheimer 1999).

To compare predictions of the model with experimental data for the dependence of surface tension, σ, of surfactant solution on its concentration, c_b, we integrate the Gibbs adsorption equation:

$$\sigma(c_b) = \sigma_0 - k T \int_0^{c_b} \Gamma \, d \ln c = \sigma_0 - k T \, \Gamma_\infty \int_0^{\theta(c_b)} \frac{\theta}{c} \frac{d c}{d \theta} d\theta \tag{14}$$

where σ_0 is the surface tension of water, using adsorption isotherms given by Eq.(14) and assuming that surface concentration is approximately equal to surface excess concentration in the sense of Gibbs.

RESULTS AND DISCUSSION

Figure 2. presents a dependence of the surface tension on the concentration of aqueous solution of n-alkanols with the carbon number ranging from four (n-butanol) to ten (n-decanol). Surface tension was determined using Lauda tensiometer with du Noüy ring. All necessary corrections for measurements in soluble systems (Lunkenheimer and Wantke, 1981) were applied. The experimental error of a single measurement was 0.2 mN/m.

Aliphatic alcohols: n-butanol (Merck), n-pentanol, n-hexanol, n-heptanol, n-octanol and n-nonanol (Sigma) of analytical purity grade were used as received. Results for n-decanol presented in Fig. 2. were obtained using the same technique (Warszyński et al. 2002). The n-alkanols have been chosen because the size of hydroxyl headgroup is smaller than cross-section of the hydrocarbon chain. Therefore, the effect of conformational changes should be considerable, unscreened by the excluded volume headgroup-headgroup interactions. In Fig. 2. symbols represent experimental data while lines show fits to the theoretical model. Best fit parameters are presented in Table 1. The quality of the fit was evaluated according to the condition that the mean square fitting

error:

$$s = \sqrt{\sum_{i=1}^{m} \frac{(\sigma_{ex}(c_i) - \sigma_{ev}(c_i))^2}{f_g}} \tag{15}$$

where $\sigma_{ex}(c_i)$ is the measured surface tension at a given concentration, $\sigma_{ev}(c_i)$ is the surface tension calculated according to the model adsorption isotherm, m is the number of experimental points, $f_g = n - m - 1$ is the number of the degree of freedom and n is the number of fitted parameters.

Table I. Values of the best fit parameters for homologous series of n-alkanols. $\Gamma_\infty = 8.5 \cdot 10^{-10}$ mol/cm^2, common for all n-alkanols was selected to reflect the limiting area per one molecule attained for insoluble aliphatic alcohols in Langmuir monolayer at maximal compression (Lunkenheimer and Miller, 1986)

n-alkanol	a [mol/dm^3]	H_s [kJ/mol]	<A> [nm^2]	σ_A [nm^2]	s [mN/m]
n–butanol (C4)	$8.2 \cdot 10^{-2} \pm 2 \cdot 10^{-3}$	0.6±0.2	0.27±0.01	0.052±0.005	0.11
n-pentanol (C5)	$3.5 \cdot 10^{-2} \pm 2 \cdot 10^{-3}$	2.2±0.3	0.30±0.02	0.07±0.007	0.26
n-hexanol (C6))	$1.1 \cdot 10^{-2} \pm 5 \cdot 10^{-4}$	3.3±0.2	0.31±0.01	0.075±0.007	0.21
n-heptanol (C7)	$3.5 \cdot 10^{-3} \pm 1 \cdot 10^{-4}$	4.5±0.2	0.33±0.02	0.085±0.008	0.29
n-octanol (C8)	$1.6 \cdot 10^{-3} \pm 2 \cdot 10^{-5}$	6.1±0.4	0.34±0.02	0.1±0.008	0.32
n-nonanol (C9)	$5.5 \cdot 10^{-4} \pm 6 \cdot 10^{-6}$	7.4±0.2	0.37±0.01	0.117±0.005	0.19
n-decanol (C10)	$2.4 \cdot 10^{-4} \pm 5 \cdot 10^{-6}$	8.2±0.2	0.38±0.02	0.118±0.008	0.29

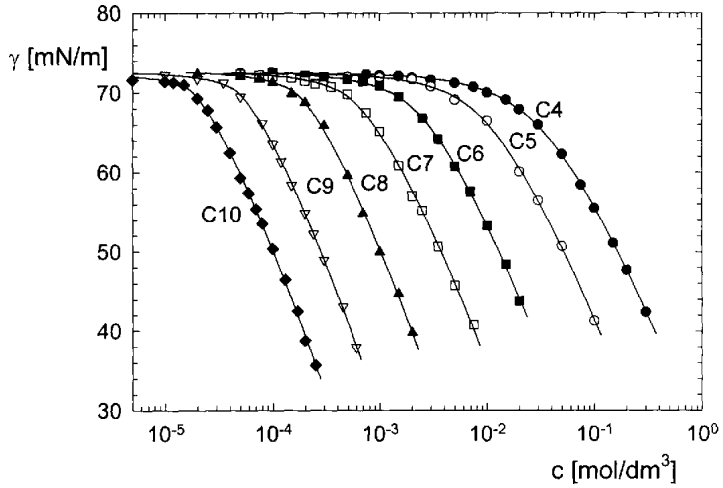

Fig. 2. Dependence of surface tension on concentration of solutions of homologous series of n-alkanols

Surface activity of n-alkanols ranges from $5 \cdot 10^{-5}$ for n-decanol to 10^{-1} mol/dm^3 for the shortest n-butanol. As the results presented in Fig. 2. suggest the description of the experimental data in terms of the model presented above for all n-alkanols in the

homologous series is very good. Basing on the best fit values of parameters of the model we determined the distribution of cross-sectional area taken by hydrocarbon chain conformations at interface for all members of homologous series. Results are presented in Figure 3.

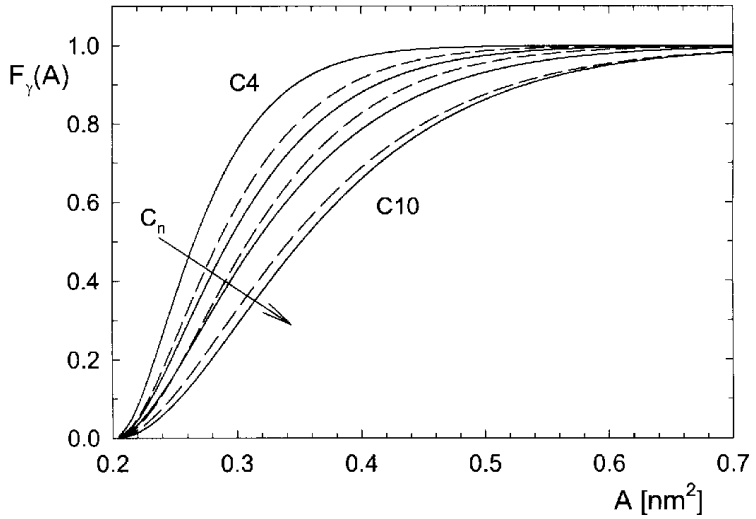

Fig. 3. Distribution of the effective cross-sectional area of hydrocarbon chain conformations for n-alkanols obtained from the best fit of Eq. (14) to the experimental data shown in Fig. 2. Distributions for chains containing odd number of carbons are shown as dashed lines.

As it is illustrated in Fig. 3. the effective size of n-butanol conformations at air/solution interface ranges from 0.20 nm^2 for the chain in trans conformation to ca. 0.35 nm^2 which correspond to tilted gauche conformation. On the other hand, the range of effective size of n-decanol conformations is much broader. The chain containing n carbon atoms can assume 3^{n-3} conformations of dihedral angles. Some of these conformation are energetically unfavorable (e.g. containing of g^+g^- sequence (Flory, 1971)), some are restricted due to the presence of the interface but there is still a considerable number of them which can be assumed by the chain. Moreover, longer chain poses more rotational freedom at the interface and both this factors are reflected in broad distribution of effective sizes. The results shown in Fig. 3. suggest noticeable even-odd effect in the distribution of conformations. Hydrocarbon chains consisting of odd number of carbon atoms tend to assume at the interface on the average more expanded conformations than chains with even number of carbons. It is also illustrated in Figure 4. where the dependence of the mean effective cross-sectional area of the hydrocarbon chain for the homologous series of n-alkanols is plotted as a function of the number of carbon atoms in the chain.

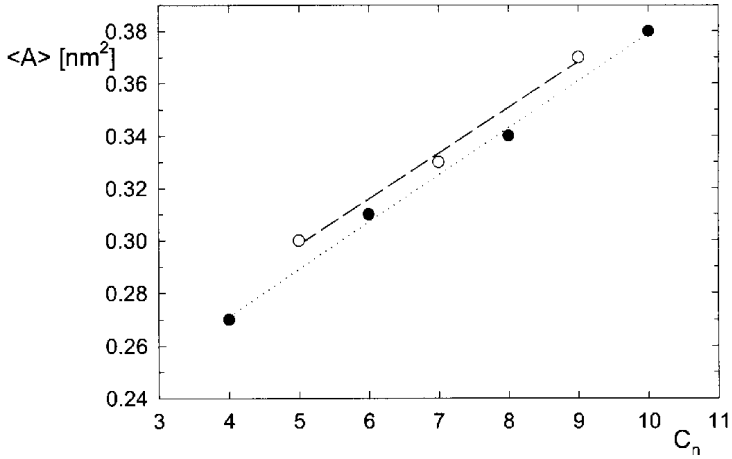

Fig. 4. Dependence of the average effective cross-sectional area of the hydrocarbon chain at interface on the number of carbon atoms

As it can be seen the average effective cross-sectional area of the hydrocarbon chain for even and odd members of the homologous series of n-alkanols can be arranged along two distinct lines. Similar effect was observed in liquid crystals, where chains with even number of carbon atoms were able to pack more effectively (Marcelja, 1974).

CONCLUSIONS

We presented a simple model of single chain, non-ionic surfactant adsorption which explicitly takes into account the distribution of the chain conformations. Every conformation has an effective cross-sectional area at the interface. When adsorption progresses and the interface becomes crowded with surfactant, conformations which occupy large space are restricted. That leads to a decrease of the chain conformational freedom and consequently to a decrease of free energy of adsorption. We checked the implications of our model by applying it for the description of dependence of surface tension on concentration of solutions of homologous series of n-alkanols. It occurred that our model adequately describes experimental data and predicts the variation of effective cross-sectional area determined by a distribution of conformations of chains for all studied n-alkanols. We detected small but distinct even-odd effect in the distribution of conformations.

Acknowledgements

Authors would like to thank Eng. Marta Barańska for her skillful help.

REFERENCES

BEN-SHAUL A., SZLEIFER I., GELBART W. M. 1985, *Chain Organization and Thermodynamics in Micelles and Bilayers. I. Theory*, J. Chem. Phys., 83 (7), 3597-3611.

FLORY P. J. 1971, *Principles of Polymer Chemistry*, Russian Edition, MIR, Moskwa.

LUNKENHEIMER K., MILLER R. 1985, *Properties of Homologous Series of Surface-chemically Pure Surfactants at the Water-air Interface*, VI Int. Congress Surface Active Substances, Bad Stuer, pp 113-122; Abh. Akad. Wiss. DDR 1N, Akademie Verlag Berlin 1987.

LUNKENHEIMER K., WANTKE K.D., 1981, *Determination of the Surface Tension of Surfactant Solutions Applying the Method of Lecomte du Nouy (ring tensiometer)*, Colloids & Polymer Sci., 259, 354-366.

NAGARAYAN R., RUCKENSTEIN E., 1977, *Critical Micelle Concentration: A Transition Point for Micellar Size Distribution. A Statistical Thermodynamical Approach*, *J. Colloid Interface Sci.*, 60, 221-233.

ROWLINSON J. S., WIDOM B., *Molecular Theory of Capillarity*, Clarendon Press, Oxford 1989.

VOLD M. J., 1984, *The Packing of n-alkyl Chains in Gibbs Monolayers*, J. Colloid Interface Sci., 100, 224-232.

WARSZYŃSKI P., LUNKENHEIMER K. 1999, *Influence of Conformational Free Energy of Hydrocarbon Chains on Adsorption of Nonionic Surfactants at the Air/Solution Interface*, J. Phys. Chem. B., (21) 103, 4404-4411.

WARSZYŃSKI P., LUNKENHEIMER K., CZICHOCKI G., 2002, *Effect of Counterions on the Adsorption of Ionic Surfactants at Fluid-Fluid Interfaces*, Langmuir (Web Edition).

SYMBOL LIST

$\{a_i\}$ - a set of all possible tail conformations a_i,

c, c_b – surfactant concentration in solution,

f_g - number of the degree of freedom,

m - the number of experimental points,

n - number of fitted parameters of the isotherm.

z_{conf} - is the effective partition function of a single surfactant tail at the interface,

A - the area per molecule adsorbed,

A_{hg} is the cross-sectional area of the headgroup,

A_{CH_2} - the limiting effective cross-sectional area of the chain in all trans- conformation,

H – mean field interaction parameter,

H_s – Frumkin interaction parameter,

α - parameter of Gamma function,

β - parameter of Gamma function,

γ - surfactant activity coefficients in bulk,

γ_s - surfactant activity coefficients at interface,

$\varepsilon(a_i)$ the energy of the chain in conformation a_i,

μ_0^b - the standard chemical potential of the surfactant in bulk,

μ_0^s - the standard chemical potential of the surfactant at interface,

σ - surface tension of a solution,

σ_0 – surface tension of water,

$\sigma_{ex}(c_i)$ - the measured surface tension at a given concentration,

$\sigma_{ev}(c_i)$ - the surface tension calculated according to the model adsorption isotherm,

θ - surfactant surface coverage,

$\Delta\mu_0$ - the standard free energy of adsorption (per one molecule),

$\Delta\mu_{hg\text{-}hg}$ - the head-group excluded volume interaction free energy,
$\Delta\mu_{hg\text{-}ch}$ - the free energy of other head-group\head-group or head-group\chain interactions, $\Delta\mu_{ch\text{-}ch}$ - is free energy of the van der Waals cohesive interaction between hydrocarbon chains,
$\Delta\mu_{conf}$ - is conformational free energy of surfactant tails,
Γ - surfactant surface concentration,
Γ_{∞} - the limiting surfactant surface concentration,

Warszyński P., Jachimska B., *Wpływ konformacji hydrofobowych łańcuchów na powierzchni roztwór/gaz na adsorpcję prostych substancji powierzchniowoczynnych*, Fizykochemiczne Problemy Mineralurgii, 36, (2002) 38-49 (w jęz. ang.)

Zaprezentowano prosty model adsorpcji na swobodnej powierzchni roztworu dla niejonowych surfaktantów o pojedynczym łańcuchu węglowodorowym. Model ten bezpośrednio uwzględnia efekt swobody konformacyjnej łańcuchów na powierzchni. Został oparty na założeniu, że izolowany łańcuch na powierzchni może przyjmować wszystkie energetycznie dozwolone konformacje związane obrotem wokół wiązań C-C w obrębie łańcucha, jak i jego rotacji jako całości. Wraz ze wzrostem adsorpcji konformacje o dużym efektywnym polu powierzchni są wzbronione co prowadzi do spadku entropii a w konsekwencji do spadku swobodnej energii adsorpcji. Model został zastosowany do opisu zależności napięcia powierzchniowego wodnych roztworów szeregu homologicznego alkoholi alifatycznych o długościach łańcucha od czterech do dziesięciu atomów węgla. Stwierdzono, że model dobrze opisuje wyniki doświadczalne i pozwala przewidzieć rozkłady efektywnego pola zajmowanego przez łańcuchy węglowodorowe w różnych konformacjach na powierzchni. Rozkłady te silnie zależą od długości łańcucha - liczby atomów węgla - jak również w pewnym stopniu od tego czy w łańcuchu znajduje się ich nieparzysta bądź parzysta ilość.

Physicochemical Problems of Mineral Processing, 36 (2002) 51-64
Fizykochemiczne Problemy Mineralurgii, 36 (2002) 51-64

Adam SOKOLOWSKI[*], Kazimiera A. WILK[*], Urszula KOMOREK[*],
Bartłomiej RUTKOWSKI[*], Ludwik SYPER[**]

AGGREGATION PROPERTIES OF CATIONIC GEMINI SURFACTANTS IN AQUEOUS SOLUTION[#]

Received March 5, 2002, reviewed, accepted May 15, 2002

New cationic gemini surfactants bearing two hydrogen methanesulphonate groups and two long-chain alkyl groups (octyl, dodecyl or hexadecyl) were prepared in good yields by the reaction of N,N'-bis-alkyl,N,N'-bis(3-aminopropyl)ethylenediamine with methanesulphonic acid. All of these gemini salts showed good water solubility. Their aggregation ability in water has been determined by steady-state fluorescence spectroscopy. Furthermore, the micellar properties for the concentration near above the cmc have been characterized by the aggregation number, N_{agg}. The presence of the dimeric segments in the surfactant molecule is found to be in charge of their unusual physicochemical behavior. They are very efficient at adsorbing at the free surface and at forming micelles in water. Accordingly, both the micelle-forming property, and the ability to lower the surface tension increased with the increase in the length of the hydrophobic chain. The studied surfactants were found to form stable and reproducible n-tetradecane emulsions, for which the multimodal size distribution, effective diameter and zeta potential in the system: n-tetradecane/water/surfactant IVa-c have been determined.

Key words: dimeric surfactants, emulsions, surface activity, micelle aggregation number, steady-state fluorescence, PCS

INTRODUCTION

Surfactants with two hydrophilic and two hydrophobic groups in the molecule, called „gemini" surfactants (or „dimeric"), have evoked considerable interest (Menger et. al 2000, Oliviero et. al 2002, Zana et. al 1993, Rosen 1993, Mathias et. al 2001, Diamant et. al 1994, Camesano et. al 2000, Karaboni et. al 1994, Song et. al 1996) since it became evident that these surfactants appear to be superior to the corresponding conventional monomeric surfactants (i.e., with one hydrophilic and one hydrophobic group in the structure). Dimeric surfactants with a great variety of structures and differing in the nature of the head groups and spacer have been reported

[*] Institute of Organic and Polymer Technology, Wrocław University of Technology, Wybrzeże St. Wyśpiańskiego 27, 50-370 Wrocław, Poland
[**] Institute of Organic Chemistry, Biochemistry and Biotechnology, Wrocław University of Technology, Wybrzeże St. Wyspiańskiego 27, 50-370 Wrocław, Poland
[#]This paper is dedicated to prof. A. Pomianowski on the occasion of his 80th birthday

(Menger et.al 2000, Oliviero et. al 2002, Diamant et. al 1994, Tatsumi et. al 2001, Manne et. al 1997, Knaebel et. al 2000, Wilk et. al in press, Paddon-Jones 2001). They reveal a greater tendency to absorb at the surface relative to their tendency to form micelles (Wilk et. al in press, Rosen et. al 1986). In the present contribution we describe first the interfacial and aggregation properties of a new series of cationic gemini surfactants which structures and the preparation route are shown in Table 1. In the second step of our studies we have examined the stability and formation of emulsions by surfactants IV a-c and n-tetradecane, used as the oil phase. Using the ZetaPlus instrument the effective diameter of microdroplets, sign and magnitude of zeta potential were acquired.

EXPERIMENTAL PROCEDURES

MATERIALS

The cationic gemini surfactants IV a-c were synthesized by the reaction of N,N'-bis-alkyl,N,N'-bis(3-aminopropyl)ethylenediamine (III) with methane-sulphonic acid (MsOH) in methanol. Preparation of III was carried out according to the method previously developed for the gemini sugar surfactants (Wilk et. al in press) and shown in Table 1, in which further intermediate compounds are indicated i.e.,N,N'-bis(3-nitropropyl)ethylenediamine(I),N,N'-bisalkyl(3-nitropropyl)ethylene-diamine(II).
Purification of IVa-c was performed by a repeated crystallization from methanol/acetonitrile mixtures. Their purity and established structure were ascertained by electrospray ionization (ESI) mass spectrometry and elemental CHN analyses (Table 2). The ESI spectra were obtained with a Finnigan TSQ-700 mass spectrometer and the latter – a Perkin-Elmer CHN Analyser. 6-Propionyl-2-(dimethyl-amino)naphthalene (PRODAN) was purchased from Molecular Probes, Inc. (Eubene, Or 97402), tris(2,2`bipirydyl)rythenium(II) chloride hexahydrate ($Ru(bpy)_3^{2+}$) and 9,10-dimethylanthracene (9,10-diMeA) – from Aldrich Chemical Co. (Milwaukee, WI).Water of specific resistance at least 18.2 MΩcm was obtained by passing doubly distilled water through Millipore-MilliQ purification system.

METHODS

Air-water solution tension were measured with an accuracy of 0.01 mNm^{-1} at 25 ^oC ($\pm 0.1^oC$) by the duNuoy method using a Kruss K12 processor tensiometer. The absence in the γ=f(log c) curved minimum near the critical micelle concentration (cmc) is direct evidence for the purity of the studied surfactants. The cmc was taken as the concentration at the point of intersection of the two linear portions of the γ=f(log c) plots (Figure 1). The steady-state emission fluorescence spectra were recorded on an IBH 5000U spectrometer, used as a single-photon sensitive steady-state fluorimeter by means of an additional Model 5000U-06 steady-state accessory with xenon lamp. Emission and excitation slits were fixed at 16 nm. Measurements were performed in a

thermostated cuvette holder at 25±0.5 °C. The cmc values of IVa-c were determined by means of the method previously described by Wong et al. (1999).

Table. 1. Structures and the preparation of cationic gemini surfactants

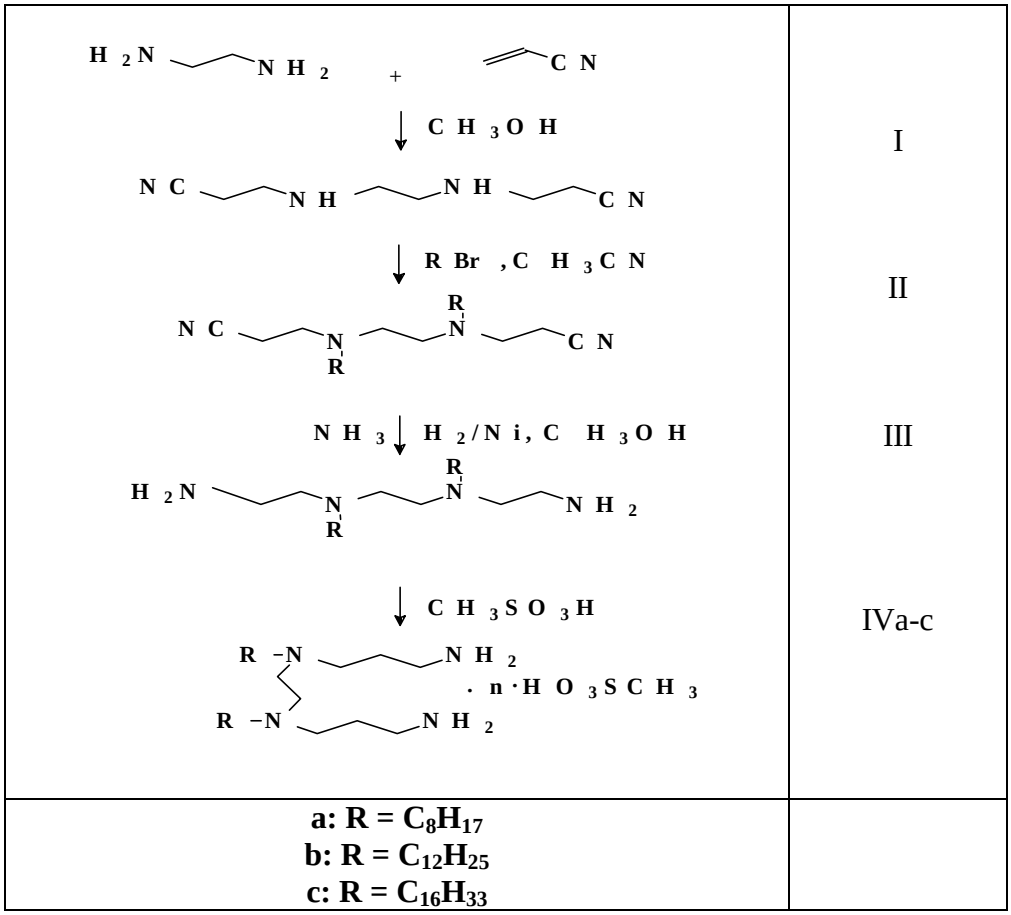

Table 2. Physicochemical properties of the studied cationic gemini surfactants IV a-c

Surfact	R	Formula	m.p. °C	Elemental Analysis, found (calc.) C(%)	H(%)	N(%)	ESI-M [a] m/z (E+)
IVa	C_8H_{17}	$C_{26}H_{62}O_6S_2$	167.6-8.9	52.93 (52.84)	11.05 (10.58)	9.40 (9.48)	590.9
IVb	$C_{12}H_{25}$	$C_{34}H_{78}O_6S_2$	167.8-9.5	58.15 (58.08)	11.22 (11.18)	7.90 (7.97)	703.2
IVc	$C_{16}H_{33}$	$C_{42}H_{94}O_6S_2$	162.0-4.0	61.96 (61.87)	11.69 (11.62)	6.80 (6.87)	815.4

[a] Electrospray ionization (ESI) mass spectrometry (Finningan TSQ-700 mass spectrometer)

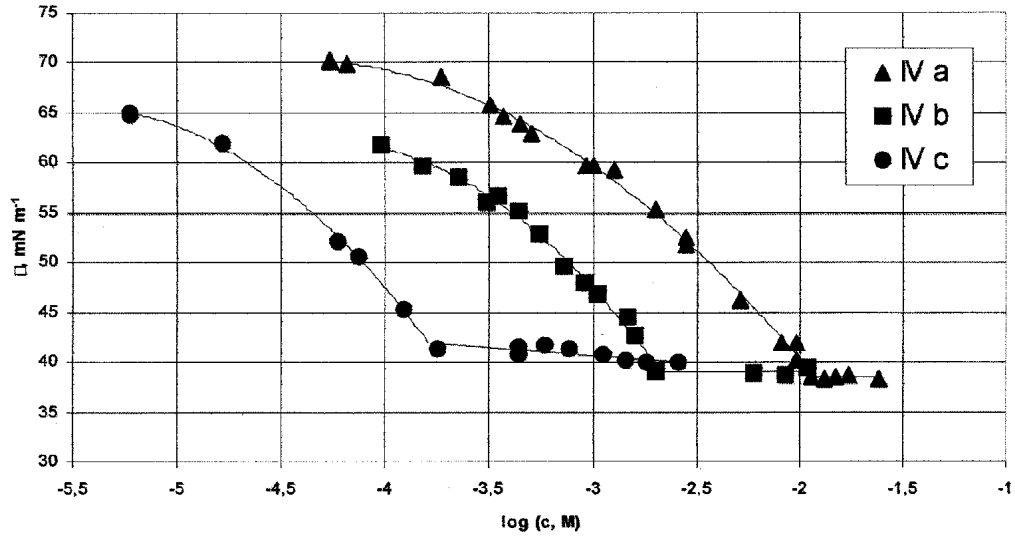

Fig. 1. The surface tension (γ) vs. logarithm of molar concentration (log c) of gemini surfactants IVa-c at 25°C

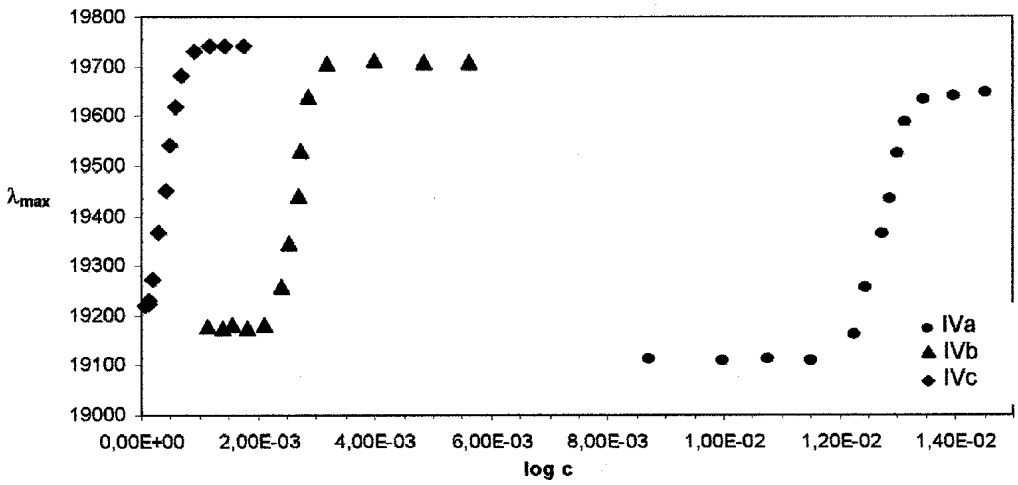

Fig. 2. The wavelength for maximum PRODAN fluorescence intensity as a function of the concentration of IVa-c at 25°C

Accordingly, the fluorescence peak shift in the emission spectra of 6-propionyl-2-(dimethylamino)naphthalene (PRODAN) (λ_{ex} = 360nm) was measured with variation of the given surfactant concentration. The content of the probe was 1.6×10^{-6}M in all cases. The maximum were calculated from the fit of a Gaussian function to the fluorescence spectrum as in (Wong et al. 1999). The plots of the wavelength for

maximum PRODAN fluorescence intensity as a function of the concentration of IVa-c at 25°C are shown in the Figure 2. The micelle aggregation numbers, N_{agg}, were obtained by means of the steady-state fluorescence quenching (SSFQ) technique according to (Zana at. al 1997), using $Ru(bpy)_3^{2+}$ as the fluorescence probe and 9,10-diMeA as the fluorescence quencher. Excitation of the probe of a constant concentration (1.0×10^{-6}M) was performed at 415.5nm and the emission was monitored at 638nm (Almgren et. al 1981). Changing the quencher concentration ([Q]) from 0.00 to 5×10^{-4}M a straight line was obtained with a linear relationship between $\ln[I_0/I_q]$ and [Q] (Figure 3).

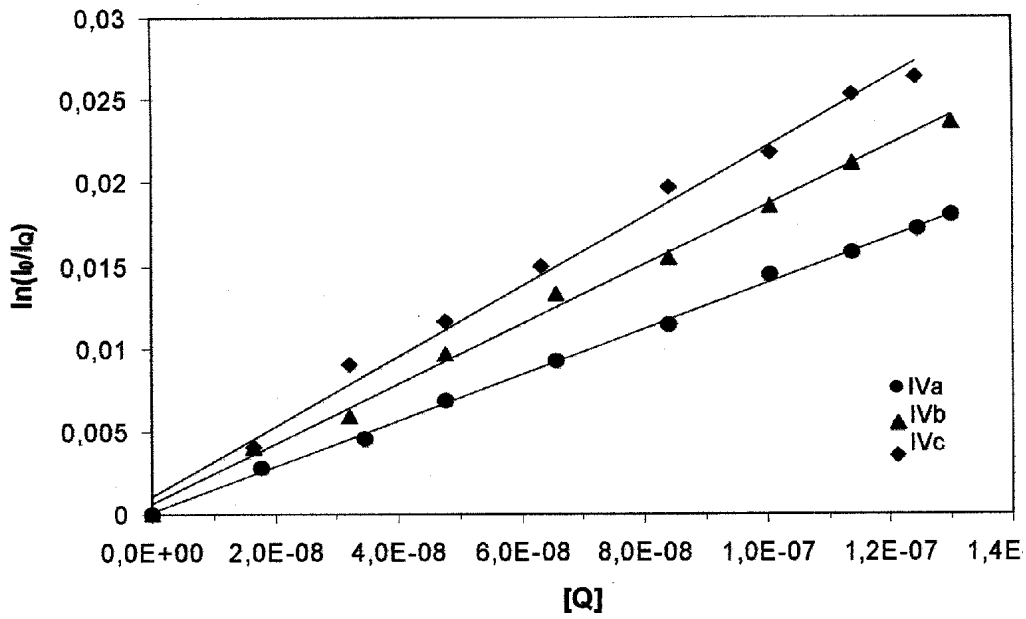

Fig. 3. The luminescence quenching of $Ru(bpy)_3^{2+}$ vs. quencher concentration for aqueous solution of IVa-c at the concentration of surfactants equal to $2.5\times cmc_i$ (i – given compoud) at 25°C.he peak current (diffusion and capacity current), Δi_p , vs. surfactant concentration. at 25°C

PCS measurements of micellar properties of IVb-IVc were made on a Zetasizer 3000HS at a temperature of 25°C. The micelle samples were prepared using Fasenius water (this is a pharmaceutical grade water used for irrigation and is extremelly clean and ideal for PCS use). The 0,5% w/v samples were sonicated in a bath sonicater for 5 minutes to aid dispersion of the powder to form micelles. Then, the samples were filtered through an Anotop® l00 nm pore size filter remove unwanted larger particles so that measurement of the micelles was possible. Count rates of approximately 87kcps (kilo counts per second) were obtained with a pinhole of 400 μm, for IVc surfactant and 30kcps for IVb. The emulsion parameters, i.e., the multimodal size distribution and effective diameter of the microdroplets in the system: n-tetradecane/water/surfactant IVa-c (0.005 wt.-%) as a function of oil

concentration and time were studied by means of the ZetaPlus (Brookhaven Instrument Co., NY, USA) apparatus, which operates in dynamic scattering mode. The emulsions were prepared in an ultrasonic bath and their effective diameter was measured after 5, 15, 30, 60 120 min, and 1 day of preparation. Following the size distribution, the zeta potential was also calculated. The experiments were all carried out at 25 ^{o}C.

RESULTS AND DISCUSSION

ADSORPTION AT THE SOLUTION-AIR INTERFACE

The plots of surface tension (γ) vs. log c (bulk phase concentration) of aqueous solutions of the studied surfactants IV a-c at 25^{o}C are shown in Figure 1. The surface activity of the dimeric compounds increases with the increase of the alkyl chain length R. The surface tension data provided possibilities to calculate the maximum surface excess concentration Γ_{max} of surfactants at the aqueous solution-air interface from the maximum slope in each case by the use of the relationship (Chattoraj 1966):

$$\Gamma_{max} = [d\Pi / d(\ln c + \ln y_{\pm})] / f\,RT \qquad (1)$$

where R is the gas constant at the absolute temperature T, π is the surface pressure in N m^{-1} ($\pi=\gamma_o - \gamma$, where γ_o is the surface tension of water at 25 ^{o}C), f=1+1/(1+r), r is the ratio between the molar concentration of added salt and the molar concentration of surfactant in the solution, and $y\pm$ is the mean activity coefficient evaluated from the Debye-Huckel limiting law equation valid for 1:1 electrolytes (Eq.2) (Horvath 1985):

$$\log y_{\pm} = (\log y_{+} + \log y_{-}) / 2 = - 0.509\,(I)^{1/2} \qquad (2)$$

where I is the ionic strength.

The Π minimum surface area per molecule at the aqueous solution-air interface, A (m^2/molecule), is then calculated from

$$A_{min}=1/(N_A\Gamma_{max}) \qquad (3)$$

where N_A is Avogadro's number.

The values of effectiveness in surface tension reduction π_{cmc}, surface excess concentration, Γ_{cmc}, surface area demand per molecule A_{min} for the studied surfactants IV a-c are listed in Table 3. The effectiveness of surface tension reduction for IV increases with increasing hydrophobic alkyl chain length R. The cross-sectional area (A_{min}) of IV are not constant across the homologous series but decrease with increasing chain length due to an increasing van der Waals interaction.

MICELLAR AGGREGATION

The studied gemini surfactants IV aggregate in water. Their solutions are clear and nonviscoelastic under the studied conditions. In Table 3 we summarize the cmc values determined for IV by means of the surface tension (Figure 1) and the steady-state fluorescence technique. In case of the latter the cmc values were determined from plots of the wavelength for maximum PRODAN fluorescence intensity vs. IVa-c concentration (Figure 2). Each of the studied surfactants, according to present isotherms in Figure 3, has a well-defined cmc_0 marking the onset of the formation of premicellar aggregates.

Table 3. Parameters of adsorption and micelle formation of the cationic gemini surfactants Iva-c

Surfactant	R	cmc mM	$-\Delta G^o_{cmc}$ kJ mol^{-1}	γ_{cmc} mN m^{-1}	$10^{20}A_{min}$ m^2	Fluorescence	
						cmc,mM	N_{agg}
IVa	C_8H_{17}	11.5	52.7[b]	38.4	80	12.1	24[f] 42[g]
IVb	$C_{12}H_{25}$	2.0	65.7[b]	39.1	82	2.1	30[f] 48[g]
IVc	$C_{16}H_{33}$	0.11	87.1[b]	40.8	86	0.12	36[f] 54[g]
$RN^+(CH_3)_3Br^-$	$C_{10}H_{21}$	67[a]	13[c]	40[d]	-		
$RN^+(CH_3)_3Br^-$	$C_{12}H_{25}$	15[a]	21[c]	39[d]	52[e]		
$RN^+(CH_3)_3Br^-$	$C_{14}H_{29}$	4[a]	27[c]	38[d]	52[e]		
$RN^+(CH_3)_3Br^-$	$C_{16}H_{33}$	1[a]	34[c]	40[d]	49[e]		

a) From Ref. (van Os et. al 1993).
b) From Eq. (4) for Q = 4, ν = 3.
c) From Eq. (4) for Q = 1, ν = 2.
d) From Ref. (Dam et. al 1996).
e) Surface tension (plate) method, from Ref. (Sokołowski 1995)
f) Determined for [surfactant] = 25 x cmc.
g) Determined for [surfactant] = 25 x cmc.

The cmc value provides a measure for the Gibbs energy of transfer (ΔG^o) of a surfactant from aqueous phase to the micellized state. Dam et al. (1996) have shown that if we assume ideal solution bahavior, aggregation number N is larger then 30, and that the micelles have zero electric charge (α=1), ΔG^o for micelle formation of surface active ionic salt $\nu_+AM^{z+}\nu_-X^{z-}$ is equal to:

$$\Delta G^o_{cmc} = \nu RT \ln(Q\, x_{cmc}) \tag{4}$$

$$\nu = \nu_+ + \nu_- \tag{5}$$

$$Q = (\nu_+)^{\nu+} (\nu_-)^{\nu-} \tag{6}$$

where ν_+ is the number of moles of cation produced upon complete dissociation of one mole of surfactant, ν_- is the number of moles of anions produced upon complete dissociation of one mole of surfactant, z^+ is the charge number for the cation, z^- is the charge number for the anion, and α is the ionization degree. For the studied gemini

surfactants $\nu = 3$, $\nu_+ = 1$ and $\nu_- = 2$ and hence $Q = 4$. Values of ΔG^o for the studied surfactants IV a-c and the conventional cationic surfactants are listed in Table 3.

The aggregation numbers, N_{agg}, of studied IVa-c micelles have been obtained from steady-state fluorescence quenching measurements. As can be seen in Table 3, the N_{agg} values for the micellar solutions of the tested cationic gemini compounds are found to be slightly depending upon the alkyl chain length. It is generally known that the micelle aggregation numbers for dimeric surfactants are larger than for the corresponding monomers, reflecting a much stronger tendency to micelle growth to elongeted and threadlike aggregates (Zana 1995, Danino 1995). However, under the experimental conditions the obtained N_{agg} for studied gemini surfactants correspond to the values expected for the spherical micelle (Alami 1993). For example, at low surfactant concentration ($c=2.5\times cmc$) used in present study, the N_{agg} achieve the values in the range of 24-36 and increase to 42-54 for the ten fold higher concentration. Such a concentration-dependent change in IVa-c micelle size requires further investigations using other techniques, i.e., time-resolved fluorescence quenching and small-angle neutron scattering.

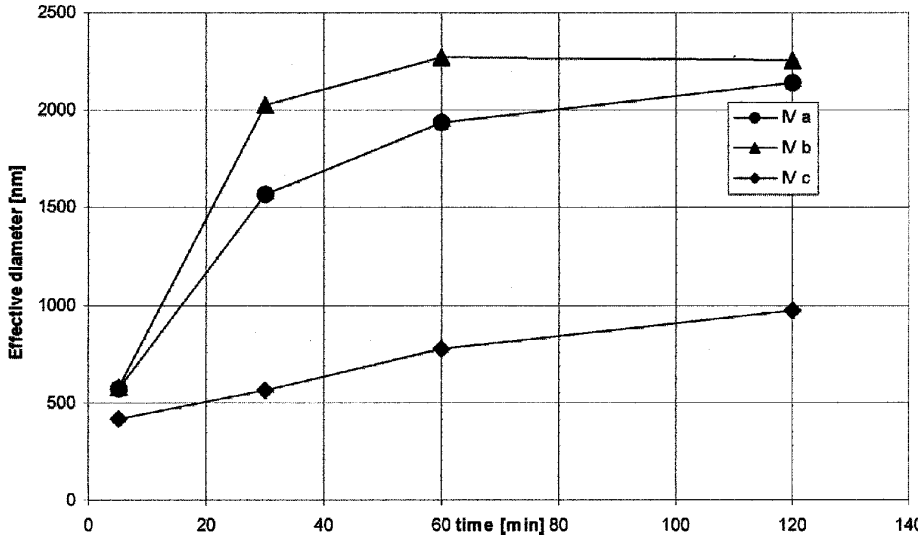

Fig. 4. The effective diameter of n-tetradecane/water/surfactant IVa-c emulsion vs. time

EMULSION SYSTEMS

In this part of studies we have performed experiments describing stability of o/w emulsions: n-tetradecane/water/surfactants IV a-c, as the function of oil concentration and time. The effective diameter (Figure 4) and zeta potential (Figure 5) of n-tetradecane droplets in the studied systems containing 0.005 wt-% of gemini surfactants oscillate from 22 to 2300 nm and from –6 to +15 mV, respectively.

The changes of zeta potentials in all studied emulsions are not monotonic and does not influence the effective diameter of the oil droplets. Generally, zeta potential increases from negative (ca.-5mV) to positive (+14 mV) values vs. time. The effective diameter as a function of oil concentration is presented in Figure 6. The most stable n-tetradecane/water/IVa emulsions were obtained for system containing 10 wt-% of oil. After 30 min, a bimodal distributions is evident due to the coalescence. Bigger droplets than 3000nm move up to the surface where they are not visible for laser beam of instrument.

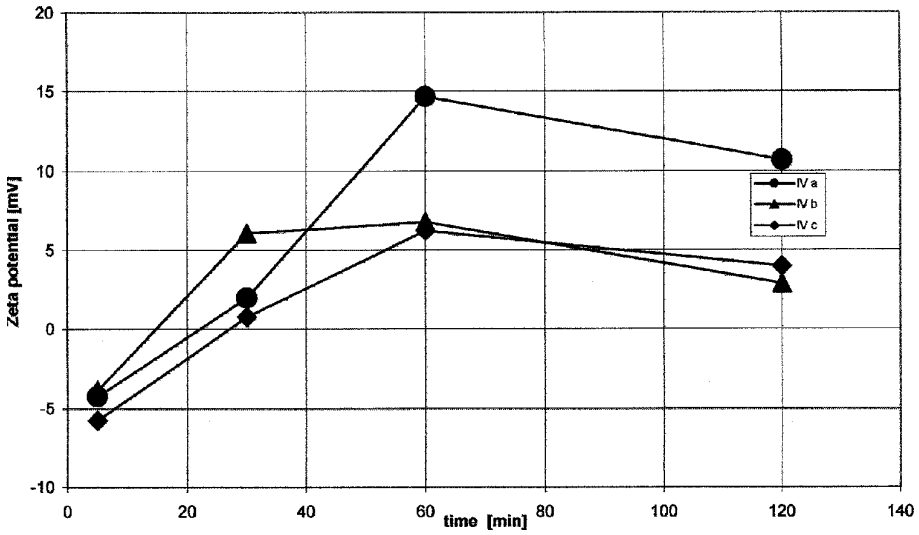

Fig. 5. The zeta potential of n-tetradecane/water/surfactant IVa-c emulsion vs. time

PCS MEASUREMENTS

Table 4 shows the results obtained from 4 repeated measurements at 25°C. The count rates, z-average diameters and polydispersities are all very repeatable indicating that the sample is stable between measurements. The z-average diameters and polydispersity values were obtained using the cumulants analysis according to ISO 13321 Part 8 1996 (International Standard on Determination of Particle Size Distributions by PCS). The size distributions displayed are intensity distributions and were obtained from the correlation functions by analysis with the CONTIN algorithm. Passes were obtained with the Result Quality Factor for all four measurements (see later for details about the Result Quality Factor). The intensity distributions are bimodal consisting of a large peak (approximately 98% of the population) with a mean at 2.7nm and a second, much smaller peak (2% of the population) at 102nm. The mode of these two peaks are at approximately 3 and 80nm respectively. The second, smaller peak is probably due to the continued presence of poorly dispersed surfactant. Zetasizer reports for each measurement are provided together with an overplot of the four measurement.

Table 4: IVc 0.5% w/v Zetasizer 3000HS using 400 µm pinhole

Run Number	Count Rate (kcps)	z-average diameter (nm)	Poly-dispersity	Intensity Mean Peak l(nm)	%of distr.	Intensity Mean Peak 2 (ran)	%of distr.
1	87.2	4.5	0.582	2.7	98.5	102.4	1.5
2	87.0	4.5	0.587	2.7	98.1	82.5	1.9
3	86.7	4.4	0.588	2.6	98.2	91.1	1.8
4	86.9	4.5	0.593	2.7	98.5	102.7	1.5
Mean	86.9	4.5	0.587	2.7	98.3	94.7	1.7
	0.2	0.1	0.005	0.05	0.21	9.7	0.21

Table 5: IVb 0.5% w/v Zetasizer 3000HS using 400 µm pinhole

Run Number	Count Rate (kcps)	z-average diameter (nm)	Poly-dispersity	Intensity Mean Peak l(nm)	%of distr.	Intensity Mean Peak 2 (ran)	%of distr.
1	30.5	4.5	0.541	4.9	100	-	-
2	30.4	4.6	0.522	4.4	100	-	-
3	30.4	4.6	0.515	4.1	100	-	-
4	30.4	4.6	0.526	3.9	99.6	199.7	0.4
Mean	30.4	4.6	0.526	4.3	99.9	-	-
	0.1	0.1	0.011	0.4	0.2	-	-

PCS measurements for IVc

Run	Angle	KCps.	Zave	Poly	Fit	Time
1	90	87.2	4.5	0.582	0.001622	11:39:47
2	90	87	4.5	0.587	0.000977	11:48:12
3	90	86.7	4.4	0.598	0.001411	12:05:03
4	90	86.9	4.5	0.593	0.001979	12:22:03
Avarage		86.9	4.5	0.587		
+/-		0.2	0.1	0.005		

PCS measurements for Ivb

Run	Angle	KCps.	Zave	Poly	Fit	Time
1	90	30.5	4.5	0.541	0.00283	13:29:33
2	90	30.4	4.6	0.522	0.001775	14:00:23
3	90	30.4	4.6	0.515	0.002234	14:15:56
4	90	30.4	4.7	0.526	0.001678	15:02:38
Avarage		30.4	4.6	0.526		
+/-		0.1	0.1	0.011		

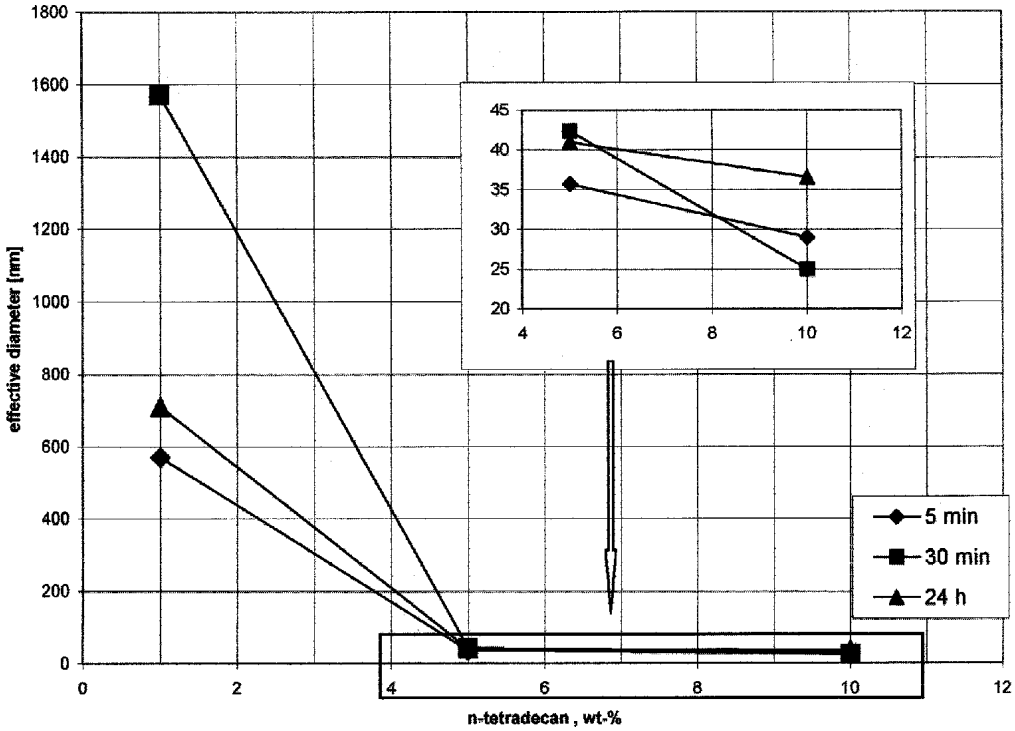

Fig. 6. The effective diameter of tetradecane/water/surfactant IVa emulsion vs. oil concentration

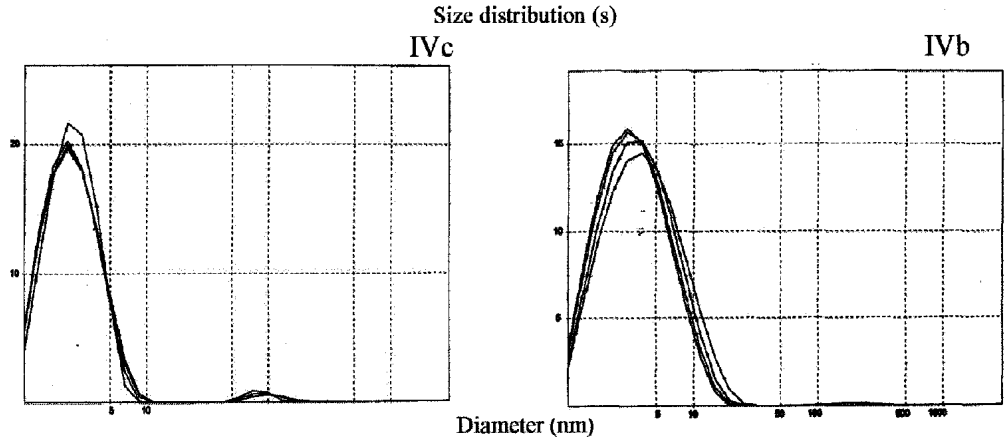

Fig. 7. PCS measurements

Table 5 shows the results obtained from four repeat measurements at 25°C. The count rates, z-average diameters and polydispersities are all very repeatable indicating that the sample is stable between measurements. The size distributions (Figure 7) displayed are intensity distributions and have been obtained from the correlation functions by analysis again with the CONTIN algorithm. Passes were obtained with the Result Quality Factor for all four measurements (see later for details about the Result Quality Factor).The intensity distributions are monomodal apart from the 4th measurement which has a very small peak at around 200nm (however this consists of less than 1% of the distribution). Zetasizer reports for each measurement are provided together with an overplot of the four measurements. Information about the numbers quoted on the reports is provided later in this document.

CONCLUSION

The studied cationic surfactants show moderate tendency to form micelles. Influence of the hydrophobic alkyl chain length upon the cmc and emulsification ability is not as effective as in the case of conventional cationics.

REFERENCES

ALAMI, E.; VAN OS, N.M.; RUPERT, L.A.M.; DE JONG, B.; KERKHOF, F.J.M.; ZANA, R. (1993), *Aggregation Behavior of Hexaoxyethyleneglycol Myristate and Hexaoxyethyleneglycol Mono(1-methyltridecane) Ether and Dynamics of Their Micelles in Aqueous Solution*, J. Colloid Interface Sci., 160, 205-208.

ALMGREN, M.; LÖFROTH, J.-E. (1981), *Determination of Micelle Aggregation Numbers and Micelle Fluidities from Time-Resolved Fluorescence Quenching Studies*, J. Colloid Interface Sci., 81, 486-499.

CAMESANO, T.A.; NAGARAJAN, R. (2000), *Micelle formation and CMC of gemini surfactants: a thermodynamic model*, Colloids Surfaces A: 167, 165-177.

CHATTORAJ, D.K. J., (1966), Phys. Chem., *Gibbs Equation for the Adsorption of organic Jons in Presence and Absence of Neutral salt*, 70, 2687.

DAM, TH.; ENGBERTS, J.B.F.N.; KARTHÄUSER, J.; KARABONI, S.; VAN OS, N.M. (1996), *Synthesis, surface properties and oil solubilisation capacity of cationic gemini surfactants*, Colloids Surfaces A:, 118, 41-49.

DANINO, D.; TALMON, Y.; ZANA, R. (1995), *Alkanediyl-,-bis(dimethylalkylammonium bromide) Surfactants (Dimeric Surfactants). 5. Aggregation and Microstructure in Aqueous Solutions*, Langmuir, 11, 1448-1456.

DIAMANT, H.; ANDELMAN, D. (1994), *Dimeric Surfactants: Spacer Chain Conformation and Specific Area at the Air/Water Interface*, Langmuir, 10, 2910-2916.

HORVATH, A.L. (1985), "*Handbook of Aqueous Electrolyte Solutions*", Kemp, T.J., Ed.; Ellis Horwood, Chichester, p.206.

KARABONI, S.; ESSELINK, K.; HILBERS, P.A.J.; SMIT, B.; KARTHÄUSER, J.; VAN OS, N.M.; ZANA, R. (1994), *Simulating the Self-Assembly of Gemini (Dimeric) Surfactants*, Science, 266, 254-256.

KNAEBEL A.; ODA R.; MENDES E.; CANDAU S.J., (2000), *Lamerall Structure aqueous solutions of a dimeric surfactant*, Langmuir, 16, 2489-2494.

MANNE S.; SCHAFFER T.E.; HUO Q.; HANSMA P.K.; MORSE D.E; STUCKU G.D.; AXAY I.A., (1997), *Gemini Surfactants At Solid-Liquid Interfaces: Control Of Interfacial Aggregate Geometry* Langmuir 13, 6382-6387

MATHIAS, J.H.; ROSEN, M.J.; DAVENPORT, L. (2001), *Fluorescence Study of Premicellar Aggregation in Cationic Gemini Surfactants*, Langmuir, 17, 6148-6154.

MENGER, F.M.; KEIPER, J.S. (2000), *Gemini Surfactants*, Angew. Chem. Int. Ed., 39, 1906-1920.

OLIVIERO, C.; COPPOLA, L.; LA MESA, C.; RAMIERI, G.A.; TERENZI, M. (2002), Colloids Surfaces A. *Gemini surfactant – water mixtures: some physical-chemical properties* 201, 247.

PADDON-JONES, G.; REGISMOND, S.; KWETKAT, K.; ZANA, R. (2001), *Micellization of Nonionic Surfactant Dimers and of the Corresponding Surfactants Monomers in Aqueous Solution*, J. Colloid Interface Sci., 243, 496-502.

ROSEN, M.J.; LIU, L. J. AM. OIL CHEM. SOC., (1986), *Surface activity and Premicellar Aggregation of some Novel Dignaterancy Gemini Surfactants*, 73, 885-890.

ROSEN, M.J. (1993), *Geminis: A new generation of surfactants*, CHEMTECH, 23, 30-33.

SOKOŁOWSKI, A.; BIENIECKI, A.; WILK, K.A.; BURCZYK, B. Colloids Surfaces A:, (1995), *Surface Activity and Micelle Formattion of Chemodegradable Caiotnic Surfactants containing the 1,3-dioksolane moiety*, 98,

SONG, L.D.; ROSEN, M.J. (1996), *Surface Properties, Micellization, and Premicellar Aggregation of Gemini Surfactants with Rigid and Flexible Spacers*, Langmuir, 12, 1149-1153.

TATSUMI, T.; ZHANG, W.; NAKATSUJI, Y.; MIYAKE, K.; MATSUSHIMA, K.; TANAKA, M.; FURUTA, T.; IKEDA, J. (2001), *Preparation, Surface-Active Properties, and Antimicrobial Activities of Bis(alkylammonium) Dichlorides Having a Butylene Spacer*, J. Surf. Deterg., 4, 271-277.

VAN OS, N.M.; HAAK, J.R.; RUPERT, L.A.M., (1993) *Physicochemical Properties of Selected Anionic, Cationic and Nonionic Surfactants*, Elsevier, Amsterdam,

WILK, K.A.; SYPER, L.; DOMAGALSKA, B.W.; KOMOREK, U.; MALISZEWSKA, I.; GANCARZ, R. (in press.), *Aldonamide-Type Gemini Surfactants: Synthesis, Structural Analysis and Biological Properties*, J. Surf. Deterg.

WONG, J.E.; DUCHSCHERER, T.M.; PIETRARU, G.; CRAMB, D.T. (1999), *Novel Fluorescence Spectral Deconvolution Method for Determination of Critical Micelle Concentrations Using the Fluorescence Probe PRODAN*, Langmuir, 15, 6181-6186.

ZANA, R.; TALMON, Y. (1993) *Dependence of aggregate morphology on structure of dimeric surfactants*, Nature, 362, 228-230.

ZANA, R.; LEVY, H.; PAPOUTSI, D.; BEINERT, G. (1995), *Micellization of Two Triquaternary Ammonium Surfactants in Aqueous Solution*, Langmuir, 11, 3694-3698.

ZANA, R.; LEVY, H.; DANINO, D.; TALMON, Y; KWETKAT, K. (1997) *Mixed Micellization of Cetyltrimethylammonium Bromide and an Anionic Dimeric (Gemini) Surfactant in Aqueous Solution*, Langmuir, 13, 402-408.

Sokołowski A., Wilk K.A. , Komorek U., Rutkowski B., Syper L., *Agregacyjne właściwości kationowych surfaktantów typu gemini w roztworze wodnym*, Fizykochemiczne Problemy Mineralurgii, 36, (2002), 51-64 (w jęz. ang.)

Nowe kationowe surfaktanty gemini zbudowane z dwóch grup metylosulfonowych oraz z dwóch długich łańcuchów alkilowych (oktylowy, dodecylowy, lub hexadecylowy) zostały zsyntetyzowane z dobrą wydajnością w reakcji N,N'-bis-alkilo-N,N'-bis(3-aminopropylo)etylenodiaminy z kwasem metylosulfonowym. Wszystkie sole "gemini" wykazały dobrą rozpuszczalność w wodzie. Ich zdolność agregacyjną w wodzie oznaczono metodą SSFS. Ich micelarne właściwości powyżej cmc scharakteryzowano przez oznaczenie liczby agregacji $N_{agg.}$ Obecność podwójnych segmentów w cząsteczce surfaktantów odpowiada za ich niezwykłe właściwości fizykochemiczne. Surfaktanty są bardzo efektywne w procesie adsorpcji powierzchniowej jak również przy tworzeniu miceli w wodzie.

Zarówno zdolność do tworzenia miceli jak również do obniżania napięcia powierzchniowego wzrasta wraz ze wzrostem długości łańcucha hydrofobowego. Badane surfaktanty stanowią wielki krok do otrzymywania stabilnych oraz powtarzalnych form emulsji n-tetradekanu. Do określenia najbardziej stabilnych form tychże surfaktantów posłużono się pomiarami potencjału zeta, średnicy efektywnej oraz dimodalnej metody rozrzutu w układzie n-tetradekan/woda/surfaktant.

Physicochemical Problems of Mineral Processing, 36 (2002) 65-76
Fizykochemiczne Problemy Mineralurgii, 36 (2002) 65-76

Marcel KRZAN*, Kazimierz. MALYSA*

INFLUENCE OF FROTHER CONCENTRATION ON BUBBLE DIMENSIONS AND RISING VELOCITIES[#]

Received March 5, 2002, reviewed, accepted May 15, 2002

Influence of α-terpineol concentration on local and terminal velocities of bubbles, their dimensions and shapes was studied within solution concentration range $1\cdot 10^{-5}$ to $1\cdot 10^{-3}$ mole/dm^3. Bubble behaviour was monitored using CCD camera with stroboscopic illumination and high speed camera Speedcam 512. Variations of the bubble local velocity and its deformation were determined as a function of distance from the capillary orifice and analysed in terms of adsorption coverage at interface of the departing bubble. Two kinds of dependencies of the bubbles local velocities on distance were observed. At low α-terpineol concentrations the profiles of the bubble local velocity showed maximum at distances ca. 5-20 mm from the capillary orifice, prior to reaching a value of the terminal velocity. No maximum was observed at distilled water and α-terpineol concentrations c>0.0001 mole/dm^3. It was found that α-terpineol adsorption coverage of ca. 6% was the minimum needed to assure the full immobilization of the bubble surface and the lowering of bubble terminal velocity by ca. 60% as result of it.

Key words: bubble, rising velocity, frother, α-terpineol, adsorption, surface coverage

INTRODUCTION

Frother is one of the main reagents applied in flotation processes and its essential task is to modify properties of the solution/gas interface and assure formation of a foam layer. According to Leja frother is also important in elementary act of flotation, i.e. in formation of the bubble-grain aggregates (Leja, 1956/57; Leja, 1982*)*. Interactions between frother and collector molecules, during collisions in flotation cell of bubbles and grains, facilitate formation of stable bubble-grain aggregates. Importance of a proper choice of the frother and existence of the collector-frother interaction was later also discussed and documented in (Lekki and Laskowski, 1971; Laskowski, 1998; Bansal and Biswas, 1975; Malysa at al., 1981) amongst others.

*Institute of Catalysis and Surface Chemistry Polish Academy of Sciences,
ul. Niezapominajek, 30-239 Krakow, Poland
[#] This paper is dedicated to prof. A. Pomianowski on the occasion of his 80th birthday

In flotation bubbles act as carriers transporting grains of useful ore component(s) to froth layer. Probability of collision, $P_{k,}$ of bubbles and grains depends on their dimensions (Laskowski, 1974; Reay and Ratckliff, 1973; Weber and Paddock, 1983; Yoon and Lutrell, 1989; Schimmoler at al. 1993) as:

$$P_k = A\,(R_g / R_b)^n \tag{1}$$

where R_b and R_g are the bubble and grain radius, respectively, A and *n* are parameters that vary with Reynolds' number of bubbles. For conditions representative for flotation n=2 is generally assumed. As a result of frother adsorption the dimensions of bubbles formed during gas dispersing and their rising velocity can be changed. Degree of adsorption coverage at interface of the bubble formed depends mainly on velocity of creation of fresh gas/liquid interface and kinetics of frother adsorption. When the bubble formed starts to rise up its motion causes disequilibration of the adsorption coverage along the bubble interface and a gradient of the frother surface concentration is induced (Levich, 1962; Dukhin and Deryaguin, 1961). This gradient of the surface concentration (surface tension) reduces mobility of the bubble interface and consequently the bubble velocity is lowered. Lower bubble velocity means a longer time of contact with colliding grains.

The paper presents results of studies on influence of α-terpineol concentration on local and terminal velocities of bubbles, their dimensions and shapes. Profiles of the local velocities of bubbles in clean water and α-terpineol solutions were determined as a function of distance from the capillary orifice on which the bubbles were formed. Variations of the bubble velocity and dimensions are analysed in a function of solution concentration and adsorption coverage at interface of the departing bubble, as well.

EXPERIMENTAL

Figure 1 presents schematically the set-up used in the experiments. Bubbles were formed at the capillary orifice of inner diameter 0.07mm using the Cole-Parmer syringe pump enabling high precision control of the gas flow. To avoid optical distortions a square glass column (40x40 mm) was used to monitor velocity and dimensions of the bubbles departing from the capillary. Bubble motion was monitored and recorded over ca. 350mm distance from the capillary orifice. Sony XC-73CE CCD camera (with Cosmicar objective and rings for magnification) coupled with TV monitor and JVC BR-S800U professional video recorder (with Editing Control Unit RM-86U) were used to monitor and record the bubbles motion. To determine local velocity of the bubble at various distances from the capillary orifice a stroboscope (Drelloscope) illumination with 100-200 flashes per second was applied. In such manner 4-8 images of the bubble positions were obtained on each frame of the videotape. To get absolute dimensions an image of the nylon sphere of 7.85mm diameter was recorded after each experiment.

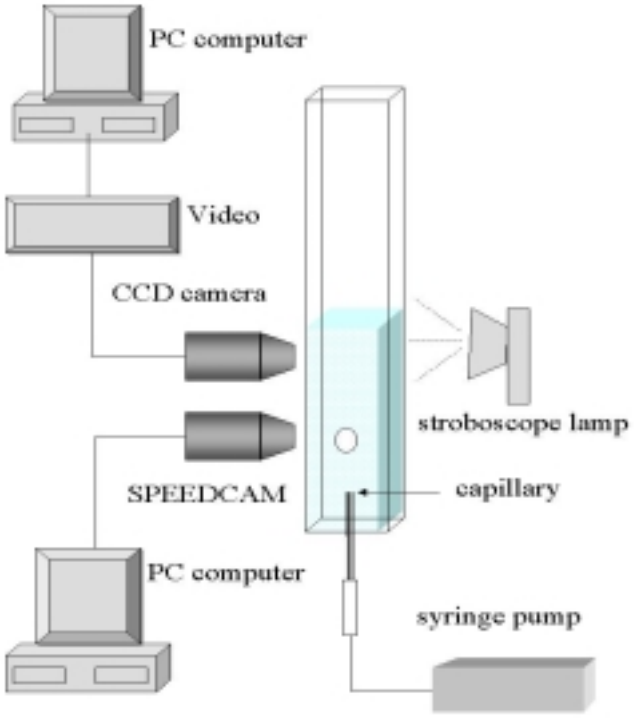

Fig.1. Schematic of the experimental set-up

Sequences of frames of the video recordings were digitalized using frame grabber and analyzed using a PC with SigmaScanPro Image Analysis Software. Distances between subsequent positions of the bubble on the frame and its vertical and horizontal diameters were measured as a function of distance from the capillary. Every measurement was performed at least 3 times and mean values were calculated.

High speed camera Speedcam 512+ was used to determine bubble behavior during acceleration, immediately after departing from the capillary, and at the stage of "collision" with free surface, i.e. at the bubble arrival at solution surface. The camera maximum speed is 1182 frames per second, i.e. it makes possible recording of phenomena occurring in time scale shorter than 1 msec (ca. every 850 microseconds).

Surface tension of α-terpineol solutions was measured using the du Nouy ring method (Lauda tensiometer model TD 1), taking into account the necessary correction factors (du Nouy and Lectome, 1919; Lunkenheimer, 1982). The accuracy of the measurements was 0.1mN/m.

Four-times distilled water and commercial α-terpineol was used for the solutions preparation. The experiments were carried out in room temperature (20±1^{o}C).

RESULTS AND DISCUSSION

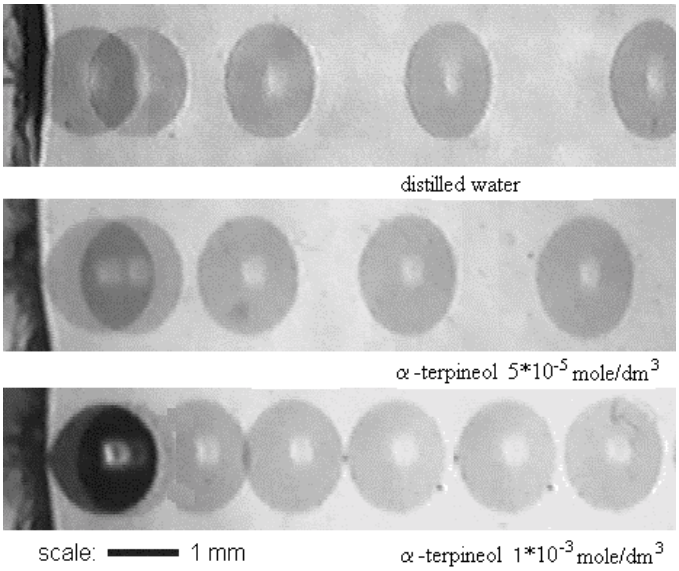

Fig.2. Images of bubbles departing from the capillary orifice at distilled water and α-terpineol solutions of concentrations $5\cdot 10^{-5}$ and $1\cdot 10^{-3}$ mole/dm^3.

Figure 2 presents the images of bubbles departing from the capillary orifice at distilled water and α-terpineol solutions of concentrations $5\cdot 10^{-5}$ and $1\cdot 10^{-3}$ mole/dm^3. A few important features can be noted immediately from these pictures. With increasing α-terpineol concentration: i) the distances between consecutive images, ii) dimensions, and iii) deformations of the bubbles are decreasing. As these experiments were carried out under identical stroboscopic illumination (100 flashes/sec) it shows that the bubbles velocity was decreasing with increasing α-terpineol concentration. It is seen also that the bubbles, which were spherical at the capillary orifice, underwent deformation immediately after departure and the deformation was the largest in clean water.

Variations of local velocities of bubbles with the distance, L, from the capillary orifice are presented in Fig. 3 for distilled water and α-terpineol solutions of different concentrations. Local velocity, U, of the bubble was calculated from position of subsequent images of the bubble as:

$$U = \frac{\sqrt{(x_2 - x_1)^2 + (y_2 - y_1)^2}}{\Delta t} \qquad (2)$$

where (x_2, y_2) and (x_1, y_1) are coordinates of the bubble positions, and Δt is the time interval between flashes of the stroboscopic lamp. Fig. 3A shows the velocity profiles in close neighbourhood of the capillary, i.e. for L<40 mm, while Fig. 3B for the distances up to 350mm. Immediately after departure the bubble velocity in distilled

water and α-terpineol solutions increases rapidly. Next, at distances ca. 5-20 mm either a plateau value is attained or a maximum is observed. As seen in Fig. 3 at low α-terpineol concentrations three stages can be distinguished on the U=f(L) dependences: i) a rapid acceleration of the bubble immediately after departure, ii) attainment a maximum value followed by a monotonic decreasing of the velocity, and iii) a constant value of velocity, which did not change with distance.

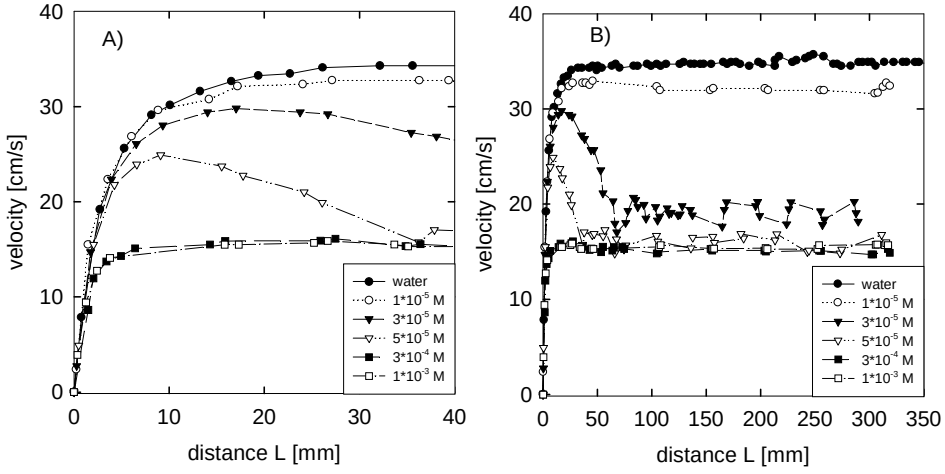

Fig. 3. Variations of local velocities of bubbles with the distance, L, from the capillary orifice. Part A - in the proximity of the capillary (L≤ 40 mm), part B – for the distance L up to 350mm

This constant value of the bubble velocity is called the terminal velocity. With increasing α-terpineol concentration the maximum height was diminishing and its position was shifted towards shorter distances L. In high concentrations of α-terpineol solutions and in distilled water no maximum was observed and after period of rapid acceleration the bubbles attained the terminal velocity. The bubble terminal velocity was decreasing steadily with increasing α-terpineol concentration, from 34.8±0.3 cm/s in distilled water down to 15.4±0.03 cm/s in 0.001 mole/dm^3 α-terpineol solution.

Influence of α-terpineol concentration on size of the bubbles formed at the capillary orifice is illustrated in Fig. 4. There are presented the bubble sizes determined experimentally and calculated. As was discussed above (see Fig. 2) the bubbles were not spherical and therefore the equivalent diameter (d_{eq}), i.e. diameter of sphere having identical volume as the distorted bubble, was determined on a basis of measurements of the bubble vertical (d_v) and horizontal (d_h) diameters as:

$$d_{eq} = (d_v\, d_h^2)^{1/3} \tag{3}$$

Simultaneously the bubble diameters were measured at the capillary orifice, immediately before their departure. Line in Fig. 4 presents values of bubble diameters as calculated from the classical Tate's Law (a balance of the buoyancy and surface tension forces acting on the bubble) the bubble diameter is given as:

$$d_t = [6\, d_o\, \sigma / (\Delta\rho\, g)]^{1/3} \quad (4)$$

where d_o is the inner capillary diameter, σ is the solution surface tension, $\Delta\rho$ is the density difference and g is the gravity acceleration. As seen in Fig. 4 with increasing solution concentration the bubbles diameters were decreasing, but the changes were relatively small (ca. 10%), from 1.48±0.03 mm in distilled water to 1.38±0.03 mm in 0.001 mole/dm^3 α-terpineol solution.

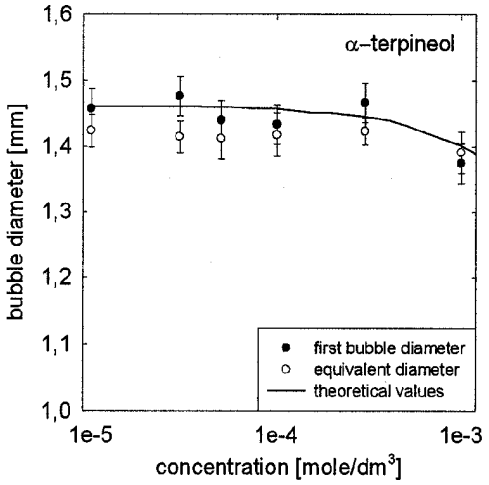

Fig. 4. Variations of the bubble diameter with α-terpineol concentration

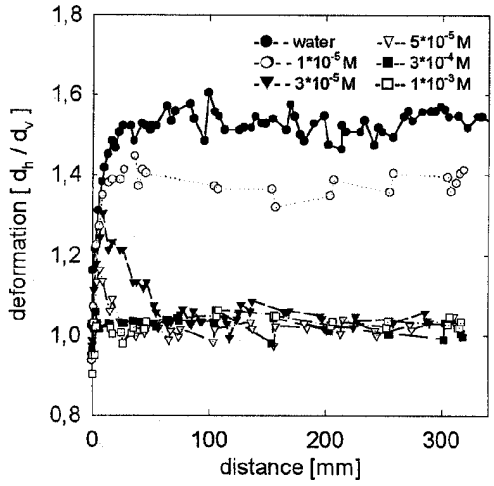

Fig 5. Variations of the bubble deformation with the distance, L, from the capillary orifice

Variations of the bubble shape deformation with distance L are showed in Fig. 5 for different α-terpineol concentrations. Deformation from the spherical shape was determined from measurements of the horizontal and vertical diameters as a ratio of these diameters. As seen the bubbles, spherical on the capillary orifice, deformed almost immediately after departing. The maximum deformation was observed in a clean water. With increasing α-terpineol concentration the deformations were decreasing, At high concentrations ($c \geq 3 \cdot 10^{-4}$ mole/dm^3) the deformations were very small, of an order ca. 5% only. Comparing data presented in Figs. 5 and 3 a correlation between variations of the bubble local velocities and its deformation can be noted. Maxima were observed for the same solution concentrations (lowest α-terpineol

concentrations) and at similar distances from the capillary. Reasons of these phenomena will be discussed further.

To get information about degree of adsorption coverages the surface tension of α-terpineol solutions was measured and values of the surface excess (surface concentration), Γ, were calculated. Fig. 6A presents the dependences of the surface tension, σ, and the Γ values on α-terpineol concentration. Equation of state derived from the Frumkin isotherm:

$$\sigma = \sigma_o + RT\,\Gamma_\infty[\,\ln(1-\theta) + \frac{H_S}{RT}\theta^2\,] \tag{5}$$

where σ_0 - is the surface tension of water, $\theta = \Gamma/\Gamma_\infty$, Γ_∞ the maximum surface concentration and H_s is the Frumkin interaction parameter, was fitted to the dependencies of surface tension on concentration of the n-alkanols solutions studied The obtained parameters of the Frumkin isotherm are as follows: $\Gamma_\infty = 4.15*10^{-10}$ mole/cm^2, $a_i = 1.21*10^{-3}$ mole/dm^{-3}, Hs = 1.75 kJ/mole. Points in Fig. 6A show the measured surface tension data, while line is the fitted dependence.

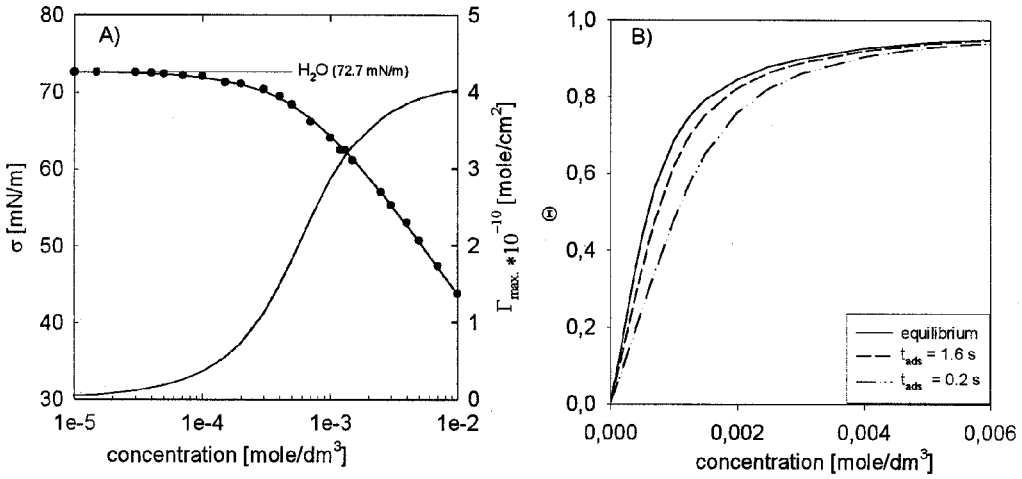

Fig. 6. A - Dependences of the surface tension, σ, and the surface excess, Γ, on α-terpineol concentration. B - Values of the equilibrium adsorption coverage, θ, and the adsorption coverage over surface of the departing bubbles for $t_{ads.}$=1.6 and 0.2 sec as a function of α-terpineol concentration

To determine adsorption coverage at the interface of the bubble detaching from capillary orifice in α-terpineol solution the convective-diffusion model elaborated in (Warszynski at al., 1998) for the bubble detaching from capillary described in details in (Jachimska at al., 2001) was applied. In our experiments the time of rapid expansion of the bubble surface was 1.6 sec. It means that degree of adsorption

coverage over surface of the departing bubble was determined by amount of α-terpineol adsorbed at the bubble interface during this time. Figure 6B presents values of the adsorption coverages over surface of the departing bubbles, θ_{dep}, as a function of α-terpineol concentration. For sake of comparison there are also presented the equilibrium adsorption coverages. As seen the adsorption coverages at interface of the departing bubble (t_{ads}=1.6 s) were lower than the equilibrium ones (t_{ads}= ∞). However, these deviations were not large – of an order 20-30% (maximum). Certainly, when the bubble formation time is shorter then the differences could be very significant. This is illustrated also in 6B (see data for $t_{ads.}$ = 0.2s).

In Fig. 7 the experimentally determined values of the bubble terminal velocities are compared to that ones predicted from the models available in the literature. Solid points show the terminal velocity values, while empty points refer to the maximum local velocities in α-terpineol solutions. The dashed lines present values of the bubble terminal velocity in clean water as calculated from the Moore (1965) theory and the Clift at al. (1973) model. In the Moore theory the terminal velocity is calculated from a drag coefficient C_D of an oblate spheroid:

$$C_D = \frac{48G(\chi)}{Re}\left(1+\frac{H(\chi)}{Re^{\frac{1}{2}}}+...\right) \tag{6}$$

where Re is a Reynolds number and G and H are functions of the aspect ratio χ defined as the ratio of the major and minor diameters of bubble).

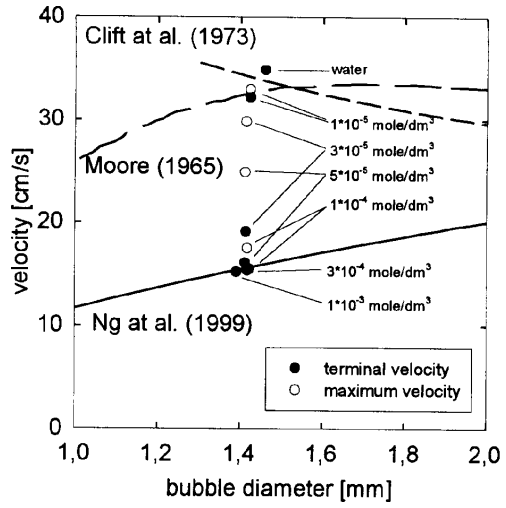

Fig.7. Comparisons of the experimental values, of the terminal (solid symbols) and maximum (empty symbols) velocities of bubbles in distilled water and α-terpineol solutions, to predictions of the models

The terminal velocity U_t of bubble is calculated by an iteration procedure from the relation:

$$U_t\,(1+\frac{H(\chi)}{Re^{\frac{1}{2}}}) = \frac{r^2 g}{9\nu\, G(\chi)} \tag{7}$$

where r, g, and ν and a bubble radius, a gravitation acceleration and viscosity, respectively. According to Clift at al. for bubbles of diameters d_e > 1.3 mm their terminal velocity can be approximated line as:

$$U = [(2.14\,\sigma / \rho\, d_e) + 0.505\, g\, d_e]^{1/2} \tag{8}$$

The solid line shows velocity values as calculated from the equation:

$$\mathrm{U} = 5450\Delta\rho \mathrm{d}^2(\frac{7}{6}\mathrm{Re}^{0.15} + 0.02\,\mathrm{Re})^{-1} \tag{9}$$

(Ng at al., 1999) describing motion of a "contaminated" bubble, i.e. in a presence of surfactant.

A few important features can be noticed in Fig. 7. First, the bubble velocity measured in clean water was even a bit higher than that predicted by Moore (Eq. 7) and Clift at al. (Eq. 8) models describing bubble motion in clean liquids, what indicates that our water was really clean. Next, at high α-terpineol concentrations the experimentally determined velocity values are in a good agreement with the „contaminated" model (Eq. 9) predictions. However, at low α-terpineol concentrations ($c < 0.0001$ mole/dm^3) the experimental data are between the values predicted by the models for „clean" and „contaminated" bubbles. Models for motion of „clean" bubbles assume full fluidity of the bubble interface, while the „contaminated" ones assume that the bubble interface is fully immobilized („solidified") as a result of surfactant adsorption. Results presented in Fig. 7 clearly show that there is needed a critical (minimum) degree of adsorption coverage to immobilize fully the bubble surface. In the case of α-terpineol this minimum adsorption coverage needed is ca. 6%. When adsorption coverage is not high enough to retard motion at the bubble surface then its rising velocity can be very significantly higher (even 2 times). Empty points in Fig. 7 present values of the local velocity of bubbles at their maximum (see Fig. 3). In our opinion higher velocity of the bubbles having identical dimensions and rising in the same solution can be caused only by differences in the degree of immobilization of the bubble surface. It indicates also that at low solution concentration there is needed some time to develop a steady state distribution of the adsorbed surfactant, i.e. steady state surface tension gradients immobilizing interface of the accelerating bubble. This is confirmed by data presented in Fig. 5, which shows pulsations of the bubbles shape and are in a good correlation with variations of the bubble rising velocity with distance (see Fig. 3). When local values of surface tension over the bubble surface are changing the bubble shape is expected to pulsate.

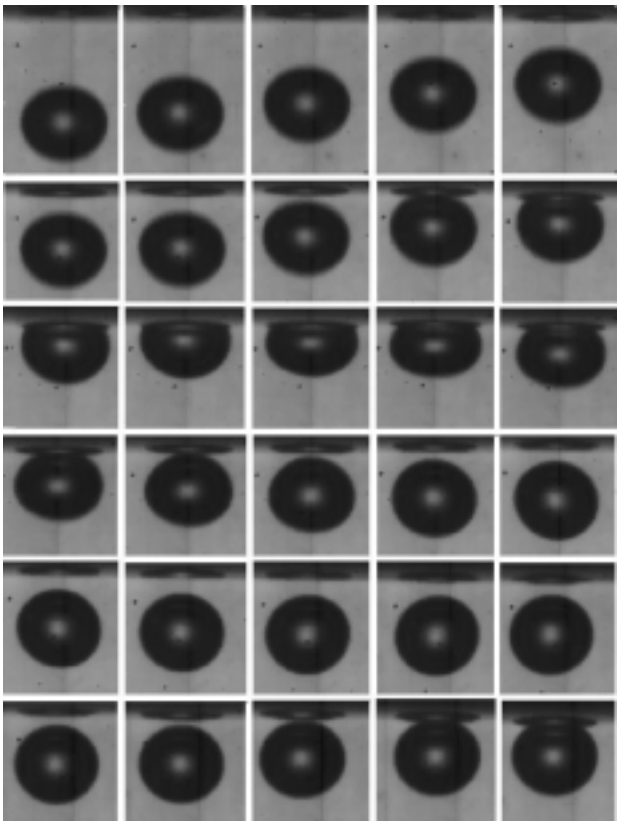

Fig. 8. Images of the bubble bouncing back to the solution from a liquid-gas interface. Time delay between the subsequent frames is 846 μs

To illustrate how rapid are phenomena related to bubble motion and collisions a sequence of pictures of the bubble approaching surface of $3 \cdot 10^{-5}$ mole/dm^3 α-terpineol solution is presented in Fig. 8. Each subsequent picture shows the bubble position and its shape after a time interval of 0.845 ms. It is clearly seen that bubble approaching solution surface neither ruptures immediately nor „stays" at the surface. Velocity of the bubble approaching free surface didn't decrease till the surface started to be deformed. After forming a "dome" the bubble started to move backward, i.e. opposite to the direction of buoyancy force, within time period ca. 2-4 ms. Simultaneously, the bubble shape started to pulsate very rapidly, changing its shape during time intervals shorter than 0.845 ms. Number of these „bouncing" from solution surface and its distance varied with solution concentration.

These data show clearly, in our opinion, the importance of dynamic effects and non-equilibrium adsorption coverages in bubble motion, bubble collisions with grains and formation of the flotation aggregates.

CONCLUSIONS

Adsorption of α-terpineol at bubble surface causes significant decreasing of the bubble rising velocity. Even such low α-terpineol concentration as $3 \cdot 10^{-5}$ mole/dm^3 lowered the bubble terminal velocity by ca. 40%, from 34.8 to 19.1 cm/s. Depending on α-terpineol concentration the bubbles showed 2 kinds of variations of the local velocity with distance from a point of their formation. At lowest α-terpineol concentrations three stages; acceleration, deceleration and finally steady state (terminal velocity) were detected. At high concentrations only the first and last stage were observed, i.e. there was no maximum on the U_{local}=f(distance) dependencies. It was showed that degree of adsorption coverage of the bubble surface by α-terpineol molecules is the most important factor affecting bubble local velocity profiles and shape pulsations. It was found that adsorption coverage of ca. 6% was the minimum needed to assure a full immobilization of the bubble surface and as result of it the lowering of bubble terminal velocity by ca. 60%.

It was demonstrated that phenomena related to bubble motion, such as shape pulsations and collisions are very rapid (time scale of microseconds). It indicates that dynamic effects and lack of equilibrium adsorption coverages should always be taken into consideration in description of the bubble-grain collisions, formation of the flotation aggregates and their transport to froth layer.

ACKNOWLEDGMENTS

Partial financial support from grant of State Committee for Scientific Research (KBN 4 T09A 058 22) is gratefully acknowledged. The authors thank Dr. P. Warszynski for program for calculations of the adsorption coverages and Eng. M. Baranska for her help in surface tension measurements.

REFERENCES

BANSAL V.K. AND BISWAS A.K., Trans. IMM. Sect. C, 84 (1975) 131-135. Clift R., Grace J.R. and Weber M.E., Academic Press New York San Francisco London 1978

DUKHIN S.S., DERYAGUIN B.V., *Zh. Fiz. Khim*., 35, (1961) 1246-1453.

JACHIMSKA B., WARSZYnSKI P., MALYSA K., *Colloids & Surfaces* A:, 192 (2001) 177.

LASKOWSKI J.S., in "*Frothing in Flotation II*" (Laskowski J.S. and Woodburn E.T.- Editors), Gordon and Breach Science Publishers, 1998, chap. 1, p. 1.

LASKOWSKI J., *Miner. Sci. Eng*., 6 (4), 223 (1974)

LEJA J., Trans. IMM., 66 (1956/57) 425-437.

LEJA J., *Surface Chemistry of Froth Flotation.* Plenum Press, New York and London, 1982, chap. 9, p. 549.

LEKKI J. and Laskowski J.S., *Trans. IMM*. Sect. C, 80 (1971) 174-180.

LEVICH V.G., *Physico Chemical Hydrodynamics*, Prentice Hall., (1962)

LUNKENHEIMER K., *Tenside Detergents*, 19 (1982) 272-281.

MALYSA K., BARZYK W. AND POMIANOWSKI A., *Int. J. Mineral P*rocess., 8 (1981) 329-343.

MOORE D.W., J. *Fluid Mechanics*, 23 (1965) 749-766

NG S., WARSZYŃSKI P., ZEMBALA M., MALYSA K., *Physicochemical Problems of Mineral Processing*, 33(1999) 143-161

du NOUY, P. LECOMTE, *J.Gen. Physiol*., 1 (1919) 521.

REAY D., RATCKLIFF G.A., *Can. J. Chem. Eng.* 52, 178 (1973)
SCHIMMOLER B.K., LUTRELL G.H., Yoon R.-H., Proc. XVIII *Intern. Miner. Process. Congress*, Sydney, 23-28 May, Vol. 3, 263 (1993)
WARSZYNSKI P., WANTKE K.-D., FRUHNER H., *Colloids & Surfaces* A:, 139 (1998) 137.
WEBER M.E., PADDOCK D., *J. Coll. Interface Sci.*, 94 (2), (1983)
YOON R-H., G.H. LUTRELL G.H. (1989), *Mineral Process. Extractive Metall. Review*, **5**, 101.

Krzan M., Małysa K., *Wpływ stężenia odczynnika pianotwórczego na rozmiary i prędkości lokalne banieczek gazu,* Fizykochemiczne Problemy Mineralurgii, 36, (2002) 65-76 (w jęz. ang.)

Badano wpływ stężenia α-terpineolu na prędkości lokalne i graniczne baniek, ich rozmiar oraz deformacje kształtu. Wyznaczono profile prędkości lokalnych baniek i kształtów w funkcji odległości od kapilary (φ=0.07mm) na której wytwarzano bańki przy pomocy precyzyjnej pompy strzykawkowej. Pomiary wykonano dla roztworów α-terpineolu w zakresie stężeń od $1*10^{-5}$ do $1*10^{-3}$ mole/dm^3. Ruch baniek był monitorowany za pomocą dwóch kamer, zbierających informacje o położeniu i kształcie z częstotliwościami 100 i 1182 Hz. Stwierdzono występowanie kilku różnych etapów w ruchu baniek wypływających w roztworach α-terpineolu. Bańki bezpośrednio po oderwaniu od kapilary przyspieszają, po czym w zależności od badanego stężenia ich prędkości osiągają stałą wartość graniczną (woda i roztwory α-terpineolu o dużym stężeniu) lub też obserwowane jest przejście przez maksimum i stopniowe spowolnienie prędkości do innej, często znacznie mniejszej niż maksymalna, wartości prędkości granicznej (stężenia mniejsze od 0.0001 mol/dm^3). W przypadkach niskich stężeni równocześnie ze zmianami profili prędkości lokalnych są obserwowane dynamiczne zmiany kształtu baniek. Wartości prędkości granicznych unoszących się baniek spadają wraz ze wzrostem stężenia α-terpineolu od 34.8±0.03 cm/s w wodzie destylowanej do 15.4±0.03 cm/s w roztworze α-terpineolu o stężeniu 0.001 mol/dm^3.

Stwierdzono, że stopień pokrycia adsorpcyjnego na powierzchni bańki jest czynnikiem decydującym o profilach prędkości lokalnych baniek, jak i ich deformacjach. Największe zmiany występują w obszarze niskich stężeń α-terpineolu, przy których stopień pokrycia adsorpcyjnego zmienia się w zakresie 0-10%. Pokrycie adsorpcyjne α-terpineolem Θ=6% jest minimalnym pokryciem niezbędnym dla całkowitego unieruchomienia powierzchni bańki w wyniku którego graniczna prędkość baniek ulega znacznemu zmniejszeniu.

Physicochemical Problems of Mineral Processing, 36 (2002) 77-88
Fizykochemiczne Problemy Mineralurgii, 36 (2002) 77-88

Paweł NOWAK*, Barbara KOZIOŁ**

ON THE REST POTENTIAL OF PYRITE ELECTRODE IN OXYGEN-FREE SOLUTIONS OF IRON (II) SULFATE[1]

Received March 15, 2002; reviewed and accepted May 15, 2002

The exchange current density (ECD) for the reaction: $Fe_{1+y}S_2 = Fe_{1+y-x}S_2 + xFe^{2+} + 2xe^-$ was estimated measuring the impedance of pyrite electrodes in the solutions of iron (II) sulfate. For five different pyrite electrodes, 0.5 mol dm^{-3} $FeSO_4$ solution and potentials close to the potential of the reaction $FeS_2 = Fe^{2+} + 2S^0 + 2e^-$ the ECD was found to be between 8 and 15 μA cm^2. Low value of the ECD causes that the potential of pyrite electrode in solutions of iron (II) sulfate does not attain the equilibrium value (i.e. the value within the range of pyrite thermodynamic stability) except the most concentrated and very well deoxidized solutions. For the concentrations of $FeSO_4$ solution lower than 0.5 mol dm^{-3} pyrite electrode shows the rest potential outside the limits of thermodynamic stability, which means that the measured potential is a mixed (corrosion), not equilibrium potential.

Key words: pyrite, pyrite electrochemistry, impedance spectroscopy

INTRODUCTION

Pyrite is undoubtedly the most abundant sulfide mineral in the earth crust. Pyrite accompanies almost all other sulfides and many non-sulfide minerals (including coal) and the separation of pyrite from other minerals (especially from coal) by flotation is a process of extreme importance (Tao et al., 1993). In hydrometallurgy the presence of pyrite in the raw material being processed influences strongly the process because the oxidation of pyrite generates sulfuric acid and iron (III) ion, the later being a strong oxidant (Dutrizac and MacDonald, 1974). In oxidizing environment pyrite exhibits

*Polish Academy of Sciences, Institute of Catalysis and Surface Chemistry, ul. Niezapominajek 8, 30239, Kraków, Poland
**Undergraduate student, Jagiellonian University, Faculty of Chemistry
[1]Presented material is a part of the MSc thesis prepared by B.K.

high rest potential, usually higher than other sulfide minerals, inducing galvanic effects both in flotation as well as in hydrometallurgy (Nowak et al., 1984).

A lot of pyrite may be found in the environment either as natural constituent of the rocks or as a waste product, left at the disposal places. The oxidation of those pyrite liberates sulfuric acid and toxic metal ions, creating problems in the environment protection (Jambor et al., 2000). So, it is not surprising that the literature on the pyrite oxidation is very rich (Peters, 1977, Hiskey and Schlitt, 1982, Lowson, 1982, Williamson and Rimstidt, 1994). Despite the vast body of literature on the subject there are many problems, connected with pyrite oxidation which require further elucidation. One of such problems is the path of the sulfide sulfur oxidation. Some authors (see Wei, 1997, and references cited therein) think that the formation of sulfates and elemental sulfur are two independent processes, proceeding through intermediate lower-valence sulfur species. The other authors (Hamilton and Woods, 1981) proposed that elemental sulfur is the primary product of pyrite oxidation. According to Buckley and Woods (1987) and Buckley and Walker (1988) the oxidation of pyrite (and other sulfides) begins with the creation of metal-depleted sulfide which eventually rearranges further to elemental sulfur and stable sulfide phase. Such mechanism of sulfur formation during oxidation of copper sulfides was proposed by Filmer et al. (1979). Therefore, the initial stage of a metal sulfide anodic dissolution may be described by the equation:

$$Me_{1+y}S = Me_{1+y-x}S + xMe^{2+} + 2xe^{-} \tag{1}$$

Most of sulfide minerals are pure electronic or mixed ionic-electronic conductors and show the tendency to non-stoichiometry (Shuey, 1975). Binary compounds of pure ionic conductivity (silver halides, for example) together with the parent metal of the binary compound form the second type electrodes of electrode potentials quite stable in the solutions containing the ions of either metal or nonmetal constituting the binary compound. Contrary, the potential of a metal sulfide electrode in the solution of either metal or sulfide ions shows usually variability. Sato (1966) discussed the problem long time ago. For the binary sulfide of the composition $Me_{1+y}S$ the potential of a sulfide electrode in the solution of either metal or sulfide ions may be described, according to Sato, by the equation:

$$E_{MS} = E^{0}_{MS} + \frac{RT}{4F} ln \frac{a_{M^{2+}_{aq}} a_{S_{MS}}}{a_{S^{2-}_{aq}} a_{MS}} \tag{2}$$

where $a_{M^{2+}_{aq}} (a_{S^{2-}_{aq}})$ is the activity of a metal (sulfide) ion in the solution and $a_{M_{MS}} (a_{S_{MS}})$ is the activity metal (sulfur) in the sulfide phase, and

$E^0_{MS} = \frac{E^0_{M,M^{2+}} + E^0_{S^{2-},S}}{2}$, where $E^0_{M,M^{2+}}$ is the standard potential of the metal in the solution of metal ions and $E^0_{S^{2-},S}$ is the standard potential of sulfur in the solution of sulfide ions. So, the potential of a metal sulfide electrode in the solution containing either metal or sulfide ions of fixed concentration (note that if one of the concentrations is given, the activity of the other ion is fixed by the solubility product relation) may attain the value within two limits. The lower limit is determined by the condition: $a_{M_{MS}} = 1$ (metal-rich sulfide or sulfide in equilibrium with the other sulfide phase of higher metal content). The higher limit is determined by the relation: $a_{S_{MS}} = 1$ (sulfur-rich sulfide or sulfide in equilibrium with the other sulfide phase of higher sulfur content).

Pyrite is a special case because it is a disulfide and the equilibrium is established with S_2^{2-} ions, not with S^{2-} ions, but the situation should be similar. Considering the possible reactions, the potential of a pyrite electrode in the solution of Fe^{2+} ions should attain the value between the potential of the reaction:

$$FeS_2 = Fe^{2+} + 2S^0 + 2e^- \tag{3}$$

and the potential of the reaction:

$$FeS_2 + Fe^{2+} + 2e^- = 2FeS \tag{4}$$

depending on the exact composition of the mineral surface. Between those two limits the only electrochemical reaction which can carry the electrical charge through the interface (unless other redox couples are present either in the solution or at the surface) is the reaction:

$$Fe_{1+y}S_2 = Fe_{1+y-x}S_2 + xFe^{2+} + 2xe^- \tag{5}$$

The exchange current density for the reaction (5) might be measured which would allow the estimation of the rate of this reaction. An ideal method for this purpose seems to be electrochemical impedance spectroscopy (EIS) since this method allows one to measure the rate of an electrochemical reaction at the equilibrium potential without extensive polarization of the interface. Note that when reaction (5) proceeds the composition of the surface changes continuously and, hence, the rate constant of the reaction may also change gradually. Therefore, the methods in which rather high charge is flowing through the surface, like linear polarization method, cannot be applied in that case.

EXPERIMENTAL

The impedance spectra and the voltammograms have been measured using 1250 Frequency Response Analyzer and 1286 Electrochemical Interface (Schlumberger-Solartron). The impedance data were subsequently processed by fitting the parameters of a proper electrical equivalent circuit (EEC) to experimental data using the MINUIT program (James and Roos, 1975). Five pyrite samples, all museum grade manocrystals, were used in the experiments. One of the pyrite samples was from the ore deposits in Huanzala, Peru, supplied by Wards Sci. Establishment, the other samples were also mineral pyrites from ore deposits in Ural mountains, from ore deposits in Elba (Italy) and in Rio Tinto (Spain). One sample was a coal-pyrite sample from the coal deposits in Poland (Halemba coal mine). The crystals were cut with a diamond saw to dimensions approximately 0.5x0.5x0.5 cm^3 and cubic shape and embedded at the end of a glass tube with an epoxy resin. Before the measurements the exposed surface of the crystal was polished on SiC emery papers ending with the 4000 grade. Because the extensive polishing may significantly influence the surface properties of the mineral (Libowitzky, 1994, Mendiratta et al., 1996) the polishing was performed very gently. Water purified by catalytic pyrodistillation (Conway et al., 1973) was used for preparation of the solutions. Solutions were bubbled with argon before the measurements to remove oxygen. All reagents used were of analytical reagent purity grade.

Typical electrochemical cell in three electrode configuration with saturated calomel electrode as a reference electrode and platinum wire as a counter electrode was used. Some pyrite samples exhibited high resistance and rectifying properties. In that case the potentiostat was operated in a four-electrode mode with the "Reference 2" electrode connected to a potentiometric contact on the side surface of the pyrite sample (Peters, 1977).

The iron (II) sulfate, used in the experiments was recrystallized just before the start of experiments and kept tightly covered. The salts of divalent iron contain always traces of trivalent iron, which may oxidize the surface of pyrite electrode. So, the experiments were performed in the following manner. Iron (II) sulfate was dissolved in the 0.5 mol dm^{-3} solution of sodium sulfate of the pH of 1.85. The Na_2SO_4 solution was deoxidized previously by bubbling with argon. pH was chosen not too low to prevent the spontaneous dissolution of pyrite and not too high to prevent the formation of oxides at the surface (Sato, 1992).

In a separate beaker a portion of metallic iron powder (about 0.5 g) was washed with deoxidized 0.5 mol dm^{-3} sulfuric acid solution to remove oxides from the surface. Iron powder was finally washed with a portion of methanol (to remove water), dried and introduced to the cell with the solution of iron (II) sulfate. The powder in the cell was agitated with the magnetic stirrer and the value of the redox potential (measured with the Pt electrode) was continuously registered. The pyrite electrode was not introduced to the solution before the attainment of the redox potential lower than the

potential of the redox couple H^+/H_2. The lowest registered potentials were about –0.15 V. Note that the standard potential of the Fe^{2+}/Fe^{3+} redox couple is very high (+0.771 V, according to Heusler, 1985), so at the registered potential the concentration of trivalent iron would be negligibly small.

After the introduction of the pyrite electrode to the solution the rest potential of this electrode was registered for some time, until it stabilized. Then impedance spectrum at the rest potential was measured (usually three spectra one after the other were measured to check the stability of the system). All potentials in that work are quoted versus standard hydrogen electrode – when converting the potentials to SHE the potential of 0.242 for SCE was assumed. All measurements were performed at the constant temperature (25°C) box serving at the same time as a Faraday cage, in the dark to prevent the influence of light on the behavior of pyrite electrodes.

RESULTS AND DISCUSSION

Most of the experiments were performed in the solution of the pH 1.85 and the concentration of the Fe^{2+} ions of 0.5 mol dm^{-3}.

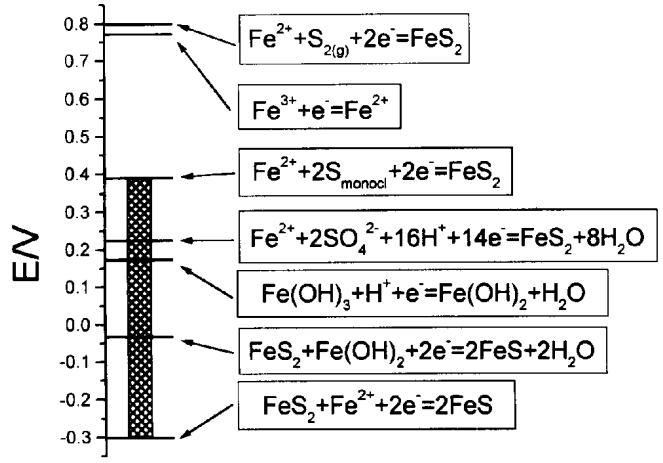

Species	ΔG/kJmol^{-3}
Fe_{aq}^{2+}	-84.9
Fe_{aq}^{3+}	-10.5
$Fe(OH)_2$	-486.6
$Fe(OH)_3$	-696.6
FeS_2	-166.9
FeS	-100.4
$S_{monoclinic}$	0.19
$S_{2(gas)}$	+79.33
$SO_4^{2-}{}_{aq}$	-744.6
H_2O	-237.18

Figure 1. The potentials of different reactions, which may occur at the pyrite surface in the solution of iron (II), sulfate at the concentration of 0.5 mol dm^{-3} and pH 1.85. Table shows the values of free energy of formation for the species participating in the reaction

The equilibrium potentials of the reactions that may occur at the pyrite surface in that solution are collected in figure 1. It is to be seen that between the potential of the most probable reaction of pyrite dissolution (reaction 3) and the reaction of pyrite reduction to pyrrhotite (reaction 4) there is about 0.7 V difference. However, if iron hydroxides (or hydrated oxides) are present at the surface they may react in that potential range. Indeed, if freshly polished electrode was cycled in pure base

electrolyte solution, voltammetric maxima were observed in that range of potentials (Fig. 2), in accordance with the literature (Conway et al., 1980, Hamilton and Woods, 1981, Mishra and Osseo-Asare, 1988, Ramprakash at al., 1991). Note that the potentials of mentioned reactions do not depend on the presence of Fe^{2+} in solution - see Fig.1. However, when the electrode was introduced to the solution of $FeSO_4$ and kept there for several hours the shape of the voltammogram changed (see Fig. 3).

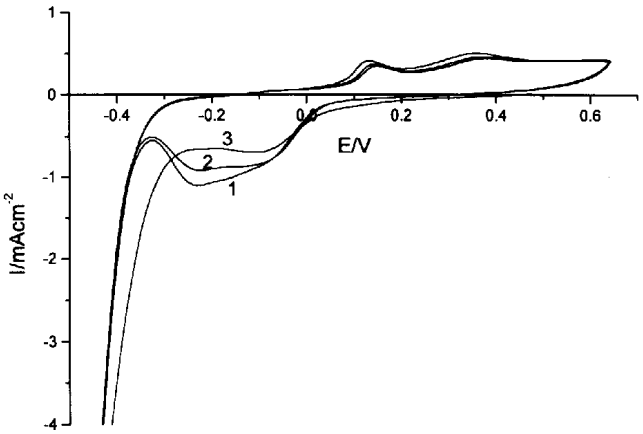

Figure 2. Cyclic voltammogram (first three consecutive cycles) for the Huanzala pyrite in 0.5 mol dm^{-3} Na_2SO_4 solution of pH 1.85. Potential sweep rate 50 mV s^{-1}

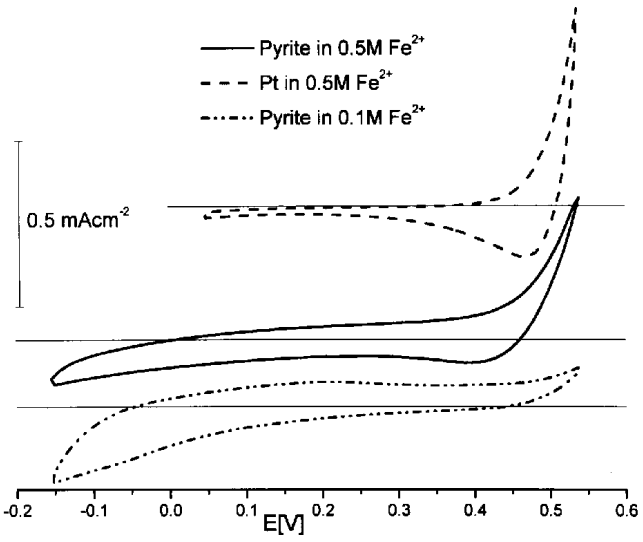

Figure 3. Cyclic voltammograms of the Huanzala pyrite in the solution of 0.5 mol dm^3 and 0.1 mol dm^{-3} $FeSO_4$ solution (0.5 mol dm^{-3} Na_2SO_4 solution of pH 1.85 as a base electrolyte) and of Pt electrode in 0.5 mol dm^{-3} $FeSO_4$ solution (0.5 mol dm^{-3} Na_2SO_4 solution of pH=1.85 as a base electrolyte). Potential sweep rate 50 mV s^{-1}

The voltammetric maxima, which were ascribed to the redox transformations of surface hydroxides, disappeared (note however that the pyrite electrode in the 0.1 mol dm^{-3} solution still shows weak peaks in that region). Similar effect was observed by Bungs and Tributsch (1997) after etching of the pyrite electrode in sulfuric acid and

ascribed to the removal of the surface hydroxides. However only in the case of 0.5 mol dm^{-3} $FeSO_4$ solution the potential stabilized close to the potential expected for the reaction of pyrite decomposition to elemental sulfur. For six experiments with six different electrodes potential stabilized between +0.19 and +0.37 V. It is to be seen in the figure 3 that the reaction of the oxidation of divalent iron in solution starts at the potential far from the equilibrium potential of the reaction $Fe^{2+} = Fe^{3+} + e^-$. This is the consequence of the relatively high exchange current density (ECD) for that reaction. Thus, the proper estimation of the ECD for reaction 5 might be made only if the measurement is performed at the potential sufficiently far from the equilibrium potential of the reaction $Fe^{2+} = Fe^{3+} + e^-$ and if trivalent iron is very carefully removed from the solution.

For a series of 10 experiments on 6 different pyrite electrodes with 0.1 mol dm^{-3} $FeSO_4$ solution the potential stabilized in the range of 0.35 – 0.5 V i.e. higher than expected for reaction (3) and higher than in the case of 0.5 mol dm^{-3} $FeSO_4$ solution.

Note further that due to the inaccuracy of the data on free energy of formation of the considered species the equilibrium potential of any of the reactions may be known with only limited confidence. For the E^0 of the reaction $Fe^{2+} + 2e^- = Fe^0$ Heusler (1985) gives the value of -0.44 ±0.04. Similar range of confidence may be expected for any reaction in which Fe^{2+} ions participate.

Taking into account that the thermodynamic data for pyrite and sulfur may be also charged with some error, the potentials attained by pyrite electrodes in the 0.5 mol dm^{-3} $FeSO_4$ solution may be close to the equilibrium potential of reaction 3. The potentials observed in the case of 0.1 mol dm^3 $FeSO_4$ solutions were evidently too high (potential in 0.1 mol dm^3 solution should be lower than the potential in 0.5 mol dm^{-3} solution) if the composition of the mineral surface is the same. In one experiment performed in 0.5 mol dm^{-3} $FeSO_4$ solution, after the stabilization of the potential and acquisition of the impedance spectrum the electrode was polarized in anodic direction to +0.44, +0.54, +0.64 and +0.74 V consecutinely, for 100 s each time. Note that due to the presence of 0.5 mol dm^{-3} $FeSO_4$ most of the charge was consumed in the reaction $Fe^{2+} = Fe^{3+} + e^-$, but some elemental sulfur might be formed at the surface too.

After each polarization the change of the rest potential in time was observed. The stabilization of the rest potential after the polarization to +0.74 V is presented in figure 4. It may be seen that there was no arrest on the curve at the potential of the reaction (3). It must however be remembered, that the freshly deposited sulfur is very reactive and as long as metallic iron is present in the system the elemental sulfur may recombine with iron according to the reaction $Fe^0 + S^0 = FeS$ which is thermodynamically favorable. Naturally there must be a soluble redox mediator in the solution. Note also that the solution was all the time saturated with hydrogen (due to slow evolution of hydrogen on iron), that hydrogen may also reduce sulfur to

hydrogen sulfide. If no sulfur is present at the surface of the electrode, the pyrite electrode potential may attain practically any value within the range between the potential of reaction 3 and 4, depending on the exact stoichiometry of the surface.

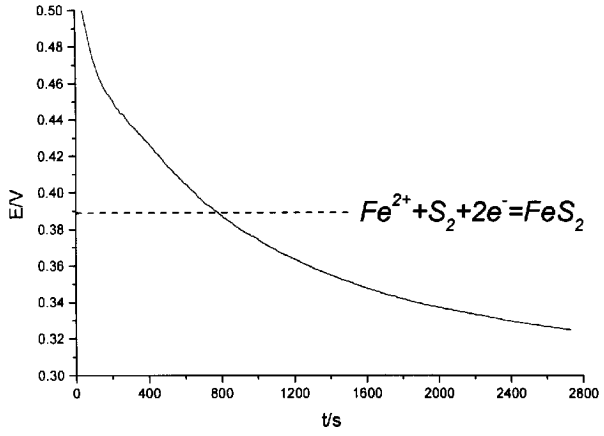

Figure 4. The change of the potential of the Huanzala pyrite electrode in the solution of 0.5 mol dm^{-3} $FeSO_4$ (0.5 mol dm^{-3} Na_2SO_4 solution of pH 1.85 as a base electrolyte), after the polarization to +0.74 V

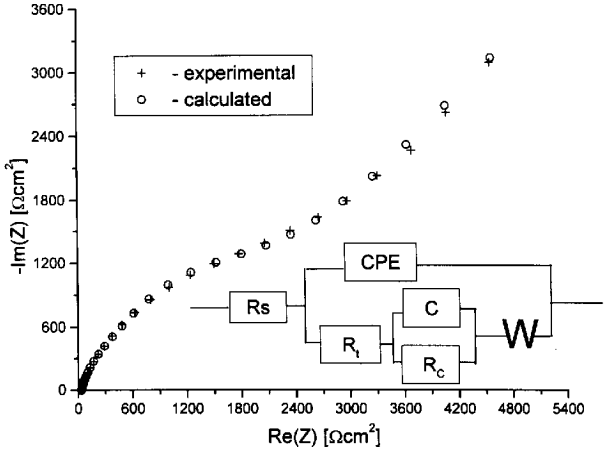

Figure 5. Impedance spectrum measured on Huanzala pyrite electrode in the solution of 0.5 mol dm^{-3} $FeSO_4$ solution (0.5 mol dm^{-3} Na_2SO_4 solution of pH 1.85 as a base electrolyte). + - measured points. o – impedance values for the EEC showed in figure and the parameters of EEC obtained by least-square fitting

The example of the impedance spectrum measured in the 0.5 mol dm^{-3} $FeSO_4$ solution at the rest potential is presented in Figure 5. Similar spectra were obtained in other experiments with the pyrite electrodes in the solutions of iron (II) sulfate. The key step in the interpretation of the impedance data is the selection of the proper EEC. The EEC shown in Fig.5 was assumed in the calculations. In that EEC Rs is the resistance of the electrode and the electrolyte, R_t is the charge-transfer resistance of the Faradaic reaction occurring at the surface, CPE (constant phase element) stands for the impedance of the electrical double layer at the interface pyrite/solution, C and R_C are connected with the capacitance of the surface states and W represent the diffusion (Warburg) impedance. The detailed discussion of the EEC for the phase boundary

semiconductor – electrolyte is out of scope of this paper so only the parameters influencing the dynamics of the exchange of Fe^{2+} ions between the surface and the solution will be discussed. Exhaustive discussion of the EECs of the boundary pyrite/solution may be found, for example, in the paper of Pang (1990).

Charge transfer resistance R_t may be associated with reaction (5). For the samples investigated in 0.5 mol dm^{-3} $FeSO_4$ solution the measured R_t values ranged between 950 and 1500 Ω cm^2, except one sample for which the value of 350 Ω cm^2 was obtained, but in that case the fit of the EEC parameters to the measured data was much worse than in the other cases. The exchange current density for reaction (5) calculated from the formula:

$$i = \frac{RT}{2F}\frac{1}{R_t} \tag{6}$$

was between 8 and 15 μA cm^{-2} (except the lastly mentioned electrode). It means that every Fe^{2+} ion in the surface of pyrite exchanges place with a Fe^{2+} ion from the solution approximately one time per 5 seconds. This exchange current density was rather low. For non-stoichiometric cuprous sulfide electrode two of the present authors (Nowak and Pomianowski, 1985) estimated the ECD in 1 mol dm^{-3} $CuSO_4$ solution to be about 100 mA cm^{-2}. Warburg constants for the measured pyrite samples ranged between 300 and 3900 Ω $s^{-1/2}$ cm^2 which gives the diffusion coefficient for iron in pyrite (the diffusion of Fe^{2+} ions in solution was orders of magnitudes faster) between $2 \cdot 10^{-14}$ and $1 \cdot 10^{-16}$ cm^2 s^{-1}, assuming that every Fe atom in pyrite participates in the diffusion process. There is practically no data on diffusion in solids at room temperature, but this value seems to be too high. On the other hand there might be so-called accelerated diffusion paths in the solid body, which usually allow relatively fast diffusion to take place, even at the room temperature.

The capacitance of the electrical double layer at the surface of pyrite electrodes in 0.5 mol dm^{-3} $FeSO_4$ solution was calculated to be between 10 and 25 μFcm^{-2} (this value comprises mainly the capacitance of the space charge layer in semiconducting pyrite). Taking into account very rough surface, polished on emery papers, (and hence the relatively high surface roughness factor) this values seems to be reliable. Also the value of capacitance connected with the surface states was obtained in quite good agreement with the prediction of Bronold et al. (1994), based on theoretical calculations. That increases the confidence to the correctness of the choice of the EEC for the investigated interface.

As was already stated ten experiments were performed on 0.1 mol dm^{-3} $FeSO_4$ solution. Only in one case the potential of pyrite electrode was below the potential of reaction (3). Evidently, it means that the measured potential was a mixed (corrosion), not equilibrium potential and the measured current was not the exchange current but rather the corrosion current. Indeed, for some electrodes the R_t values much lower than in the case of 0.5 mol dm^{-3} solution (of the order of 800 Ωcm^2) were observed.

Note the potential attained by these electrodes is situated in the range where divalent iron starts to be oxidized. Further, the traces of the surface oxides were discernible on the voltammograms; these surface oxides may produce parasitic currents due to the reactions of their redox transformations.

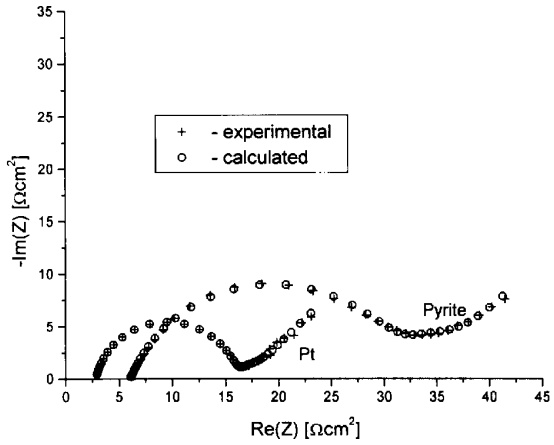

Figure 6. Impedance spectra of pyrite and platinum electrodes in the solution of the composition: 0.5 mol dm^{-3} $FeSO_4$ + 0.25 mol dm^{-3} $Fe_2(SO_4)_3$, 0.5 mol dm^{-3} Na_2SO_4 solution of pH=1.85 as a base electrolyte

It should be stated that it was not the low free carriers concentration within the semiconductor pyrite which caused that so low current flew in the experiments in $FeSO_4$ solutions. When a redox couple, able to exchange the electrons with the electrode was present in the solution, quite high current flew through the electrode surface. Figure 6 presents the comparison of the impedance spectra made on platinum and pyrite electrodes (Ural pyrite) in the same solution (0.5 mol dm^{-3} $FeSO_4$ + 0.25 mol dm^{-3} $Fe_2(SO_4)_3$, 0.5 mol dm^{-3} Na_2SO_4 solution of pH 1.85 as a base electrolyte). It is to be seen that the pyrite electrode shows R_t for the reaction $Fe^{3+} + e^- = Fe^{2+}$ only about 2 times higher than Pt electrode (which may be estimated from the diameters of the activation semicircles in both cases). It means that the ECD for pyrite electrode is only about two times lower than for platinum, which is known to be the best electrode material. This is in accordance with the electronic structure of the pyrite surface proposed by Bronold et al. (1994). These authors state that due to specific electronic situation there is a very high density of surface states (about $5.5x10^{14}$ cm^{-2}) at the pyrite surface. Due to this situation the Fermi level is pinned at a specific position at the surface and the pyrite electrode shows the behavior similar to metal electrodes.

CONCLUSIONS

Despite the fact that both iron(III) as well as iron(II) sulfates are well soluble in water, the surface of the pyrite electrode always contain some hydrated iron oxides at the surface even in acidic solutions. Surface iron oxides govern the behavior of pyrite electrode at moderately cathodic potentials and moderately anodic potentials. These

oxides may be removed from the surface by equilibration of the electrode with the solution of iron (II) sulfate of high concentration, being in turns in contact with metallic iron. Only in the $FeSO_4$ solutions of the highest concentration used (practically close to saturation) it was possible to measure the exchange current density for the reaction $Fe_{1+y}S_2 = Fe_{1+y-x}S_2 + xFe^{2+} + 2xe^-$ in the case of natural pyrite electrodes.

In the solutions of the lower concentration rather the corrosion currents were measured. The measured ECD was of the order of 10 μAcm^{-2}, orders of magnitude lower than, for example, in the case of cuprous sulfide electrode. Even this value may be overestimated, because for any electrode there are always some parasitic currents flowing through the electrode surface (due to, for example, impurities present in the solution). So, it may be stated that the ECD for the above written reaction is very low. It means that when assessing the mechanism for pyrite oxidation in aqueous solution the non-electrochemical path must be taken into account. This non-electrochemical path might be either the direct attack of the oxidant on the surface or the so-called dissolution-precipitation mechanism. In the later case sulfide first dissolve, than the components of the sulfide undergo the oxidation.

REFERENCES

M. BRONOLD, Y. TOMM and W. JAEGERMANN, (1994), *Surface states on cubic d-band semiconductor pyrite (FeS_2)*, Surface Science, 314, L931.

A.N. BUCKLEY and G.W. WALKEr, (1988), *Sulfur Enrichment at Sulfide Mineral Surfaces*, XVI International Mineral Processing Congress, E. Forssberg (editor), Elsevier, Amsterdam, p.589.

M. BUNGS and H. TRIBUTSCH, (1997), *Electrochemical and Photoelectrochemical Insertion and Transport of Hydrogen in Pyrite*, Ber. Bunsenges. Phys. Chem., 101,1844.

B.E. CONWAY, H. ANGERSTEIN-KOZLOWSKA, B.E. SHARP and E.E. CRIDDLE, (1973), *Ultrapurification of water for electrochemical and surface chemical work by catalytic pyrodistillation*, Anal. Chem., 45, 1331.

B.E. CONWAY, J.C.H. KU and F.C. H, (1980), *The electrochemical Surface Reactivity of Iron Sulfide, FeS_2*, J. Colloid Interface Sci., 75, 357.

J.E. DUTRIZAC and R.J.C. MACDONALD, (1974), *Ferric Ion as a Leaching Agent*, Minerals Sci. Eng, 6, 59.

A.O. FILMER, J.D. MCLEOD and A.J. PARKEr, (1979), *Oxidation of copper sulfides in aqueous ammonia. I. Formation of sulfur*, Australian J. of Chemistry, 32, 961.

I.C. HAMILTON and R. WOODS, (1981), *An Investigation of Surface Oxidation of Pyrite and Pyrrhotite by Linear Potential Sweep Voltammetry*, J. Electroanal. Chem., 118, 327.

K.E. HEUSLER, (1985), *Iron, Ruthenium, and Osmium*, in: *Standard Potentials in Aqueous Solution*, A.J. Bard, R. Parsons and J. Jordan (editors), Marcel Dekker, New York, p 391.

J.B. HISKEY and W.J. SCHLITT, (1982), *Aqueous Oxidation of Pyrite*, Interfacing Technologies in Solution Minning, Proc. SME-SPE Int. Solution Min. Symp., 2nd, p.55.

F. JAMES and M. ROOS, (1975), *Minuit – a system for function minimization and analysis of the parameter errors and correlations*, Computer Phys. Commun., 10,343.

J.L. JAMBOR, D.W. BLOWES, C.J. PTACEK, (2000), *Mineralogy of mine wastes and strategies for remediation*, in: *Environmental Mineralogy* (Vol. 2), G. D.J. Vaughan, R.A. Wogelius (editors), Eövös University Press, Budapest, (2000), p.255.

E. LIBOWITZKY, (1994), *Anisotropic Pyrite: A Polishing Effect*, Phys. Chem. Minerals, 21, 97.

R.T. LOWSON, (1982), *Aqueous Oxidation of Pyrite by Molecular Oxygen*, Chemical Reviews, 82, 461.
N.K. MEDIRATTA, R.-H. YOON and P.E. RICHARDSON, (1996), *Electrochemical Impedance Spectroscopy of Freshly Fractured and Polished Pyrite Electrodes*, Proceedings of the Fourth International Symposium on Electrochemistry in Mineral and Metal Processing, R. Woods, F.M. Doyle and P. Richardson (editors), The Electrochemical Society, Pennington, p. 155.
F.M. DOYLE, P. RICHARDSON (editors), The Electrochemical Society, Pennington, p. 155.
K.K. MISHRA and K. OSSEO-ASARE, (1988), *Electrodeposition of H^+ on Oxide Layers at Pyrite (FeS_2) Surface*, J. Electrochem. Soc., 135,1898.
P. NOWAK, E. KRAUS and A. POMIANOWSKI, (1984), *The electrochemical characteristics of the galvanic corrosion of sulfide minerals in short-circuited model galvanic cells*, Hydrometallurgy, 12, 95.
P. NOWAK and A. POMIANOWSKI, (1985), *The electrochemical characteristics of the non-stoichiometric copper(I) sulfide electrode in solutions of copper (II) ions*, ION-SELECTIVE ELECTRODES, 4, "Analytical Chemistry Symposia Series", vol.22, E. Pungor and I. Buzsas (editors), Akademiai Kiado, Budapest, p. 591.
J. PANG, A. A. BRICENO and S. CHANDER, (1990), *A study of pyrite/solution interface by impedance spectroscopy*, J. Electrochem. Soc., 137, 3447.
E. PETERS, *Electrochemistry of sulfide* minerals, in: Trends in Electrochemistry (J.O'M Bockris, D.A.J. Rand, B.J. Welch – editors), Plenum Press, New York (1977), p. 267
Y. RAMPARAKRASH, D.A.F. KOCH and R. WOODS, *The interaction of iron species with pyrite surfaces*, J. Appl. Electrochem., 21, 531.
M. SATO, (1966), *Half-cell potentials of semiconductive simple binary sulfides in aqueous solution*, Electrochimica Acta, 11, 361.
M. SATO, (1992), *Persistency-field Eh-pH diagrams for sulfides and their application to supergene oxidation and enrichement of sulfide ore bodies*, Geochimica et Cosmochimica Acta, 56, 3133.
R.T. SHUEY, (1975), *Semiconducting Ore Minerals*, Elsevier, New York
D.P. TAO, P.E. RICHARDSON, G.H. LUTTREL and R.-H. YOON, (1993), *An Electrochemical Investigation of Surface Reactions of Coal- and Mineral- Pyrite in Aqueous Solutions,* Processing and Utilization of High-Sulfur Coals V, B.K. Parekh and J.G. Groppo (editors), Elsevier, p. 219.
D. WEI and K. OSSEO-ASARE, (1997), *Semiconductor Electrochemistry of Particulate Pyrite*, J. Electrochem. Soc., 144, 546.
M.A. WILLIAMSON, D. RIMSTIDT, (1994), The kinetics and electrochemical rate-determining step of aqueous pyrite oxidation, Geochimica et Cosmochimica Acta, 58, 5443.

Nowak P., Kozioł B., *Potencjał spoczynkowy elektrody pirytowej w odtlenionym roztworze siarczanu żelaza(II)*, Fizykochemiczne Problemy Mineralurgii, 36, (2002) 77-88 (w jęz. ang.)

Na podstawie pomiarów impedancji elektrod pirytowych w roztworach sirczanu żeleza (II) oceniono wartość gęstości prądu wymiany dla reakcji: $Fe_{1+y}S_2 = Fe_{1+y-x}S_2 + xFe^{2+} + 2xe^-$. Dla pięciu elektrod pirytowych w roztworze siarczanu żelaza (II) o stężeniu 0,5 mol dm^{-3}, przy potencjale zbliżonym do potencjału równowagowego reakcji: $FeS_2 = Fe^{2+} + 2S^0 + 2e^-$, wyznaczono prąd wymiany pomiędzy 8 i 15 μA cm^2. Niska wartość prądu wymiany powoduje, że elektroda pirytowa w roztworach siarczanu żelaza (II) nie osiąga warości równowagowych, to znaczy wartości w obszarze termodynamicznej stabilności elektrody, z wyjątkiem najbardziej stężonych i dobrze odtlenionych roztworów. W przypadku roztworów siarczanu żelaza (II) o stężeniu mniejszym niż 0,5 mol dm^{-3} potencjał spoczynkowy elektrody przyjmuje wartości poza zakresem termodynamicznej stabilności, co oznacza że mierzony potencjał jest potencjałem korozyjnym (mieszanym) a nie potencjałem równowagowym.

Physicochemical Problems of Mineral Processing, 36 (2002) 89-99
Fizykochemiczne Problemy Mineralurgii, 36 (2002) 89-99

Janina GRODZKA*, Andrzej KRYSZTAFKIEWICZ*, Teofil JESIONOWSKI*

CARBONATE-SILICATE FILLERS MODIFIED WITH TWO TYPES OF PROADHESIVE COMPOUNDS

Received March 5, 2002, reviewed, accepted May 23, 2002

Surface modification of precipitated carbonate-silicate fillers was performed. For this purpose silane coupling agents and stearic acid were used. The modification was performed employing two agents: silane, with affinity to silicate silanol groups, and stearic acid, adsorbing on the carbonate surface. The unmodified and the modified carbonate-silicate fillers were subjected to physicochemical analysis. Studies were also performed which aimed at determining dispersion and particle morphology using SEM and DLS techniques. Moreover, calorimetry permitted to establish the extent of hydrophobization of carbonate-silicate filler surface following the modification. The extent of hydrophobization of filler surface clearly correlated with the uniform character of particles formed in the course of surface modification.

Key words: carbonate-silicate fillers, silane coupling agents, stearic derivatives

INTRODUCTION

Activity of carbonate-silicate fillers depends to a significant extent upon chemical structure of their surface (Iler, 1979). Properties of carbonate-silicate fillers can be modified using various chemical reactions (Grodzka, 2001). Numerous studies have been published on reactions of silicate surface silanol groups with silane proadhesive compounds (Grodzka, 2000, Jesionowski, 2000; Jesionowski, 2001) as well as with acrylic and stearic derivatives (Domka, 1995). The principal aim of the efforts involved a decrease or removal of silicate hydrophilic properties as well as introduction to their surface of new organofunctional groups. Due to the gradual substitution of bound silanol groups by organic radicals, an interaction of carbonate-silicate fillers with silanes or acrylic and stearic derivatives results in organophilic properties of the filler surface.

* Poznan University of Technology, Institute of Chemical Technology and Engineering, Pl. M. Sklodowskiej-Curie 2, 60-965 Poznan, Poland, E-mail: Teofil.Jesionowski@put.poznan.pl

Modified and unmodified silicates and carbonates represent very good fillers of elastomers: butadiene-styrene rubbers and polyurethanes. The fillers provide vulcanizates with higher strength parameters and augment their chemical resistance (Krysztafkiewicz, 1997). Moreover, silicates can serve as carriers, adsorbing organic pigments on their surface (Binkowski, 2001).

The principal aim of the performed studies was definition of modifier effect on agglomeration and particle surface morphology in a carbonate-silicate filler. For this purpose we decided to modify in parallel the filler surface with one agent which showed affinity to silicates (e.g., silane coupling agent) and with another agent, showing affinity to carbonates (e.g., stearic acid).

EXPERIMENTAL

MATERIALS

For production of carbonate-silicate fillers, the following substrates were used:

- Sodium metasilicate (10 wt% solution of M=3.3 modulus),
- Calcium hydroxide (10 wt% solution),
- Carbon dioxide (gaseous),

For surface modification of carbonate –silicate fillers the following compounds were used:

- Stearic acid,
- Silane coupling agents:
  - N-2-(aminoethyl)- 3- aminopropyltrimethoxysilane (U-15D),
  - n-octyltrimethoxysilane (U-222).

METHODS

Carbonate-silicate fillers were precipitated using 10 wt% solution of calcium hydroxide, 10 wt% solution of sodium metasilicate, the modulus of SiO_2/Na_2O=3.3 and gaseous CO_2 with the flow rate equal 300 cm^3/min. On the other hand, modification of carbonate-silicate filler surface was performed by the „dry" technique (Grodzka, 2001). The carbonate-silicate filler, precipitated from solutions of sodium metasilicate and calcium hydroxide in the presence of gaseous CO_2 (Na_2SiO_3: $Ca(OH)_2$=2:1 (v/v), the temperature of precipitation: 60^oC), was placed in a mixer, adding appropriate amounts of the modifier. The mixing was conducted for 1h.

The carbonate-silicate filler with two types of proadhesion compounds was modified. In this aim selected modifiers were used – one which could react with the silicate surface silanol groups and the other one, with affinity to adsorption on the carbonate surface. The silanes were added at 1 to 5 weight parts per 100 weight parts of the filler and stearic acid at 1 to 5 weight parts per 100 weight parts of the filler. The carbonate-silicate filler at the first was modified with one proadhesion compound, and then, with the second agent. The changes of the physicochemical properties of modified fillers were observed.

Selected samples of modified fillers were subjected to microscopic analysis, mainly in order to characterize the surface morphology of respective particles and their tertiary butanol, application of the suspension on the microscope table and 10 min coating with gold atoms on an ionisation plate.

Particle size distribution was also examined using a Zeta Plus apparatus (Brookhaven Instruments Co, USA). The particle size was measured using, the dynamic light scattering (DLS) technique. The prepared sample was placed in a cuvette and size distribution of carbonate-silicate particles was then measured. Polydispersity represented a measure of heterogeneity of particle size distribution in the studied system.

Heats of immersion of the surface in water (H_i^W) and in benzene (H_i^B) for the unmodified and modified carbonate-silicate fillers were established using a calorimetric technique (Krysztafkiewicz, 1996). A KRM- type calorimeter permitted the detection of even slight thermal effect by a dynamic technique, under conditions approaching adiabatic. The extent of surface modification or hydrophobization was calculated using the following equation:

$$N = \frac{(H^{B}{}_{i})_m - (H^{B}{}_{i})_n}{(H^{B}{}_{i})_m} \cdot 100\% \qquad (1)$$

where $(H_i^B)_m$ is the heat of immersion of the modified filler surface in benzene and $(H_i^B)_n$ that of the unmodified filler surface in benzene, both in J/g.

RESULTS AND DISCUSSION

The samples of carbonate-silicate fillers precipitated from sodium metasilicate and calcium hydroxide solutions using gaseous CO_2 at various temperatures, are listed in Table 1.

Carbonate-silicate filler of best parameters was obtained at 60^{o}C. The product showed the lowest bulk density, the highest paraffin oil and dibutyl phthalate absorbing capacities and a high value of flow-off point. Particle size distribution and electron micrograph of the unmodified carbonate-silicate filler are presented in Figs.1a and 1b, respectively.

Table 1. Physicochemical properties of carbonate-silicate fillers precipitated with calcium hydroxide and sodium metasilicate solutions as well as gaseous carbon (Na_2SiO_3:$Ca(OH)_2$ =2:1)

Temperature (^{o}C)	Bulk density (g/dm^3)	Flow-off point (cm^3/10g)	Dibutyl phthalate absorbing capacity (cm^3/100g)	Paraffin oil absorbing capacity (cm^3/100g)	Water absorbing capacity (cm^3/100g)
40	243	26.5	300	400	250
60	235	26.5	300	450	200
80	282	23.0	250	300	200

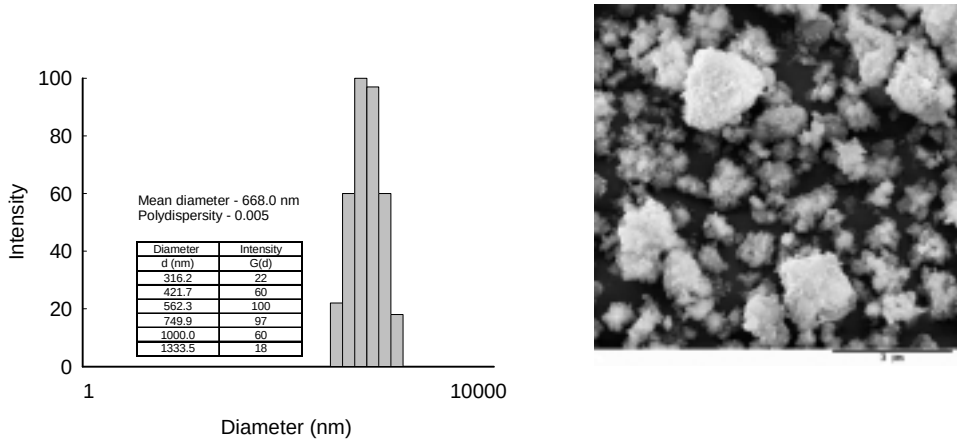

a) b)

Fig.1. a) Multimodal particle size distribution and b) SEM of unmodified carbonate-silicate filler

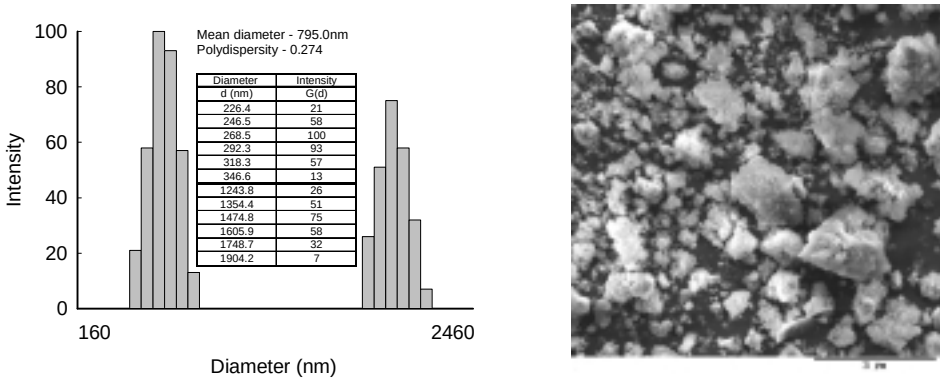

a) b)

Fig. 2. a) Multimodal particle size distribution and b) SEM of modified carbonate-silicate filler with 5 w/w of U-222 silane

As evident from the particle size distribution, the precipitated filler manifested the presence of relatively large particles with strong tendency to form agglomerates. The broad band in Fig.1a fitted the range of 316.2-1.333.5 nm (maximum intensity of 100 corresponded to the particle diameter of 562.3 nm). Mean particle diameter of the unmodified filler was 688.0 nm. This was corroborated by respective electron micrograph (Fig.1b), which documented presence of large particles of the carbonate-silicate filler and and their non-uniform character.

Following modification with 5 weight parts of octylsilane U-222, the carbonate-silicate filler demonstrated strong tendency to form agglomerates. The particle size distribution (Fig.2a) manifested two bands of a different intensity. The high intensity band corresponded to particles which formed primary agglomerates (aggregates) in the range of lower diameters. The band occupied the range of 226.4-346.6. nm (maximum intensity of 75 corresponded to the agglomerate diameter of 1,474.8 nm). Mean diameter of the agglomerates was 795.0 nm. The SEM electron micrograph (Fig. 2b) confirmed the pronounced non-uniform character of the sample: two types of agglomerates, primary and secondary ones, were present.

Following modification of carbonate-silicate filler with 2 weight parts of stearic acid also certain non-uniformity of the sample could be noted (Fig. 3).

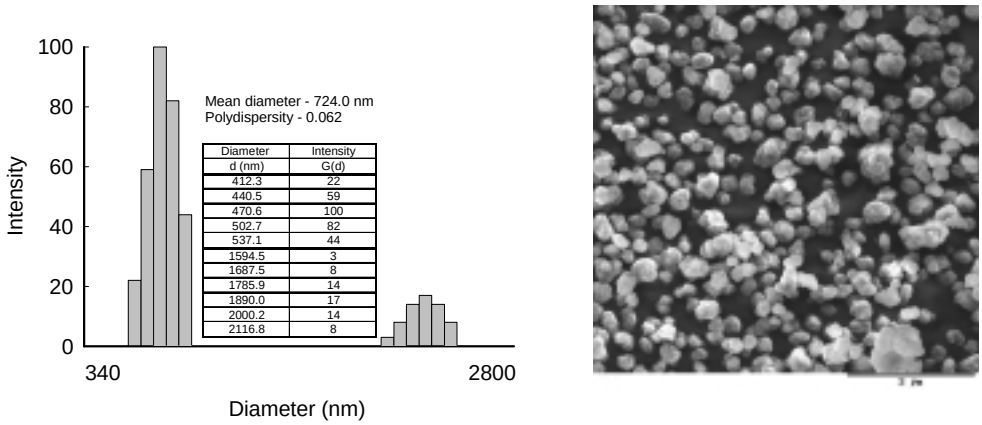

a) b)

Fig. 3. a) Multimodal particle size distribution and b) SEM of modified carbonate-silicate filler with 2 w/w of stearic acid.

In the particle size distribution (Fig. 3a), two bands of different intensity could be noted. The more intense band corresponded to particles of 412.3-537.1 nm in diameter (maximum intensity of 100 corresponded to particles of 470.6 in diameter). The low intensity band documented the presence of secondary agglomerates within the range of 1,594.5-2,116.8 nm in diameter (maximum intensity of 17 corresponded to agglomerates of 1,890.0 in diameter). Mean size of agglomerate particles was 724.0 nm. The electron micrograph fully confirmed the presence of small amounts of secondary agglomerates, which comprised a very low fraction of all particles.

A significantly improved uniformity of carbonate-silicate filler particles was expected following the modification with two different coupling agents. The compounds were selected so that the carbonate and the silicate portion of the studied filler could be modified in parallel. The performed studies proved that application of

two modifying agents significantly improved the uniform character of carbonate-silicate filler particles.

The carbonate-silicate filler modified at first with 2 weight parts of stearic acid and, then, with 2 weight parts of octylsilane U-222 exhibited a very highly uniform character, as documented in Fig.4.

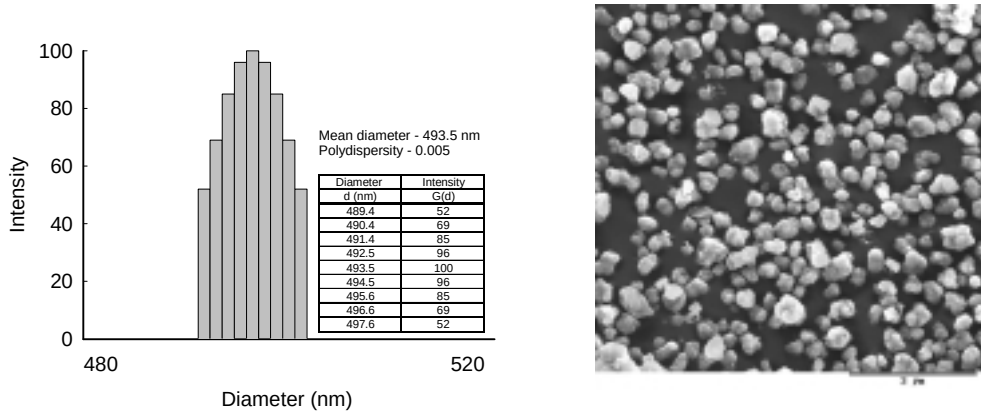

a) b)

Fig. 4. a) Multimodal particle size distribution and b) SEM of modified carbonate-silicate filler with 2 w/w of stearic acid and subsequently with 2 w/w octylsilane

As shown in Fig. 4a, the particle size distribution manifested a very narrow range of particles of the so modified filler, 489.4-497.6 nm (maximum intensity of 100 corresponded to particles of 493.5 nm in diameter). The mean particle size was 493.5 nm. The particle size distribution was corroborated by SEM micrograph (Fig. 4b), which documented the presence of highly uniform shape and diameter of the particles. Following modification of the carbonate-silicate filler with higher amounts of the same modifiers (5 weigth parts of stearic acid and 5 weight parts of octylsilane) the particles remained uniform but their minimum diameter increased. The mean particle diameter increased to 606.4 nm.

The altered sequence of applying the two coupling agents during modification of carbonate-silicate filler (octylsilane first, followed by stearic acid) also resulted in highly uniform samples. Particle size distribution for the carbonate-silicate filler modified first with 2 weight parts of octylsilane and, then, with 2 weight parts of stearic acid is presented in Fig. 5a. Only one band was noted, within the range of 370.2-376.4 nm (maximum intensity of 100 corresponded to particles of 373.3 nm in diameter). The mean particle size was also 373.3. nm.

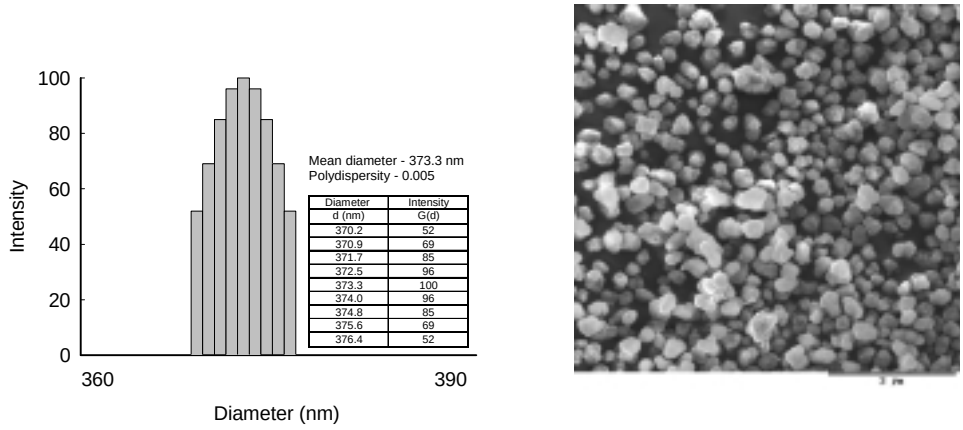

Fig. 5a) Multimodal particle size distribution and b.) SEM of modified carbonate-silicate filler with 2 w/w of octylsilane and subsequently with 2 w/w of stearic acid.

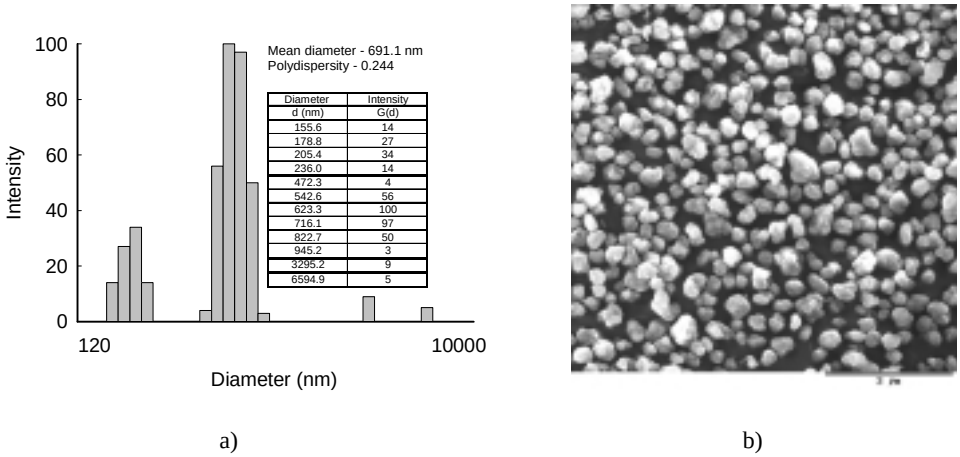

Fig. 6. a) Multimodal particle size distribution and b.) SEM of modified carbonate-silicate filler with 2 w/w of stearic acid and subsequently with 2 w/w of aminosilane.

The particle size distribution manifested two bands of different intensity. The band of lower intensity corresponded to particles of very low diameters: 155.6-236.0 nm (maximum intensity of 34 corresponded to particles of 205.4 nm in diameter). The more intense band represented particles of particles with slightly higher diameters, 472.3-945.2 nm (maximum intensity of 100 corresponded to particles of 623.3. nm in diameter). The mean particle diameter was 691.0 nm. The electron micrograph (Fig. 6b) corroborated the data obtained using the DLS technique.

Increase in amounts of the applied modifiers (to 5 weight parts of stearic acid and 5 weight parts of aminosilane) was accompanied by certain deterioration of particle uniformity and by increase in particle diameters (Figs. 7a and b).

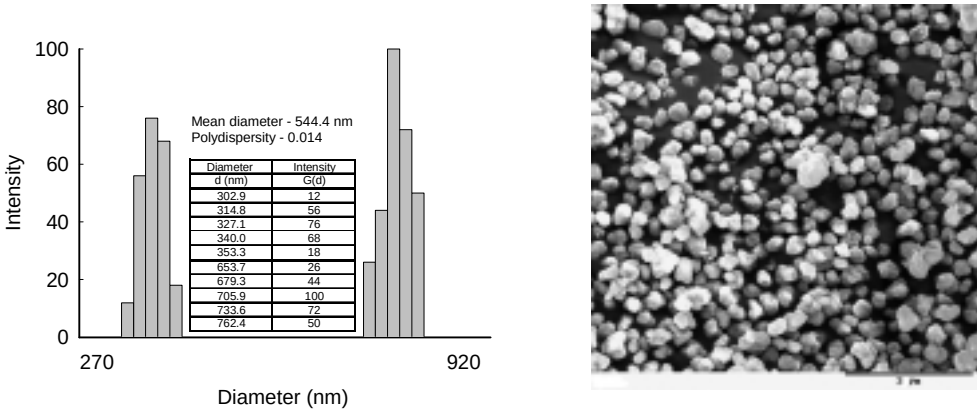

a) b)

Fig. 7. a) Multimodal particle size distribution and b) SEM of modified carbonate-silicate filler with 5 w/w of stearic acid and subsequently with 5 w/w of aminosilane.

In the particle size distribution (Fig. 7a) two particle bands of different intensity were observed. The less intense band represented the smaller particles and occupied the range of 302.9-353.3 nm (maximum intensity of 76 corresponded to particles of 327.1 nm in diameter). The more intense band fitted the range of 653.7-762.4 nm (maximum intensity of 100 corresponded to particles of 705.9 nm in diameter). Mean diameter of the filler particles was 544.4 nm.

Modification using the reciprocal sequence of proadhesive compounds (aminosilane first, followed by stearic acid) again improved the uniformity of the carbonate-silicate filler.

The particle size distribution and SEM micrograph of carbonate-silicate filler modified with 2 weight parts of aminosilane and, then, with 2 weight parts of stearic acid is presented in Fig. 8. Clearly uniformity of the sample improved, as shown in Fig. 8.

In the particle size distribution (Fig. 8a) a single band was noted, within the range of 719.8-737.5 nm (maximum intensity of 100 corresponded to the particle diameter of 728.6 nm). The electron micrograph (Fig. 8b) fully confirmed the uniform character of the so modified filler.

Results of studies on heats of immersion of carbonate-silicate fillers in water or benzene, before and after modification, are shown in Table 2. In the Table, the calculated extent of surface hydrophobization is also given.

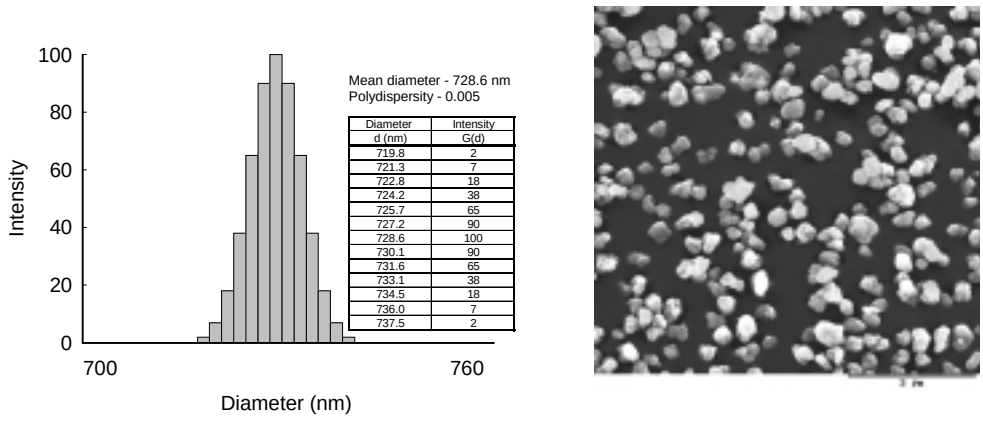

Diameter d (nm)	Intensity G(d)
719.8	2
721.3	7
722.8	18
724.2	38
725.7	65
727.2	90
728.6	100
730.1	90
731.6	65
733.1	38
734.5	18
736.0	7
737.5	2

a) b)

Fig. 8. a) Multimodal particle size distribution and b.) SEM of modified carbonate-silicate filler with 2 w/w of aminosilane and subsequently with 2 w/w of stearic acid.

As evident from data of Table 2, the modification of carbonate-silicate filler surface with proadhesive compounds was followed by an evident decrease in the heat of surface immersion in water while the heat of immersion in benzene showed increased values. The modification exerted particularly marked augmenting effect on the extent of surface hydrophobization and increased amounts of the applied modifying compounds clearly increased the effect. The extent of hydrophobization of carbonate-silicate fillers increased particularly following the modification with stearic acid and with octylsilane and the effect was most pronounced when the modification employed first 5 weight parts of stearic acid and, then, 5 weight parts of octylsilane U-222. A much lower extent of hydrophobization was observed when the modification involved the application of stearic acid and aminosilane U-15D. The changes in the hydrophobization extent might explain the increase in uniform character of the fillers following modification with the two types of proadhesive compounds.

Table 2. Heats of immersion of carbonate-silicate filler surface and extent of surface hydrophobization before and after modification with selected proadhesive compounds

Amount of modifying compound (w/w)	Heat of immersion in water H_i^W (J/g)	Heat of immersion in benzene H_i^B (J/g)	Extent of hydrophobization N (%)
Unmodified carbonate-silicate filler			
-	22.5	23.1	-
Carbonate silicate filler modified with U-222 silane			
2	20.2	25.0	7.6
3	18.7	26.3	12.2
5	17.2	28.9	20.1
Carbonate silicate filler modified with stearic acid			
2	20.7	24.2	4.6
5	18.5	27.6	16.3
Carbonate silicate filler modified with stearic acid and then with U-222 silane			
2/2	18.9	26.1	11.5
3/3	16.8	27.7	16.6
5/5	15.4	29.5	21.7
Carbonate silicate filler modified with U-222 silane and then with stearic acid			
2/2	19.1	25.7	10.1
3/3	17.2	27.1	14.8
5/5	15.7	28.9	20.1
Carbonate silicate filler modified with stearic acid and then with U-15D silane			
2/2	20.2	24.8	6.1
3/3	18.8	26.0	11.2
5/5	17.3	27.1	14.8
Carbonate silicate filler modified with U-15D silane and then with stearic acid			
2/2	19.3	25.5	9.4
3/3	17.7	27.0	14.4
5/5	16.9	28.4	18.7

CONCLUSIONS

- Carbonate-silicate filler modified at first with 2 weight parts of stearic acid and, then, with 2 weight parts of octylsilane exhibited the most uniform character and showed no tendency to form agglomerate structures.
- The extent of hydrophobization of carbonate-silicate filler surface increased in particular following the modification with two agents: stearic acid and octylsilane.
- The changes in hydrophobization extent of carbonate-silicate filler surface might explain the more pronounced uniform character of fillers following modification with the two types of proadhesive compounds.

REFERENCES

BINKOWSKI S., KRYSZTAFKIEWICZ A., JESIONOWSKI T. and ŻURAWSKA J., 2001, *Fizykochemiczne właściwości ekologicznych pigmentów nieorganicznych,* Chemia i Inżynieria Ekologiczna, 8, 1025.

DOMKA L., 1995, *Wpływ parametrów na właściwości fizykochemiczne węglanu wapnia otrzymywanego z kredy naturalnej,* Fizykochemiczne Problemy Mineralurgii, 29,109.

GRODZKA J., KRYSZTAFKIEWICZ A., JESIONOWSKI T., 2000, *Influence of silane coupling agents on properties of carbonate-silicate fillers,* Physicochemical Problems of Mineral Processing, 34,95.

GRODZKA J., KRYSZTAFKIEWICZ A., JESIONOWSKI T., 2001, *Comparison of carbonate-silicate fillers modified with various proadhesion compounds,* Physicochemical Problems of Mineral Processing, 35,73.

ILER R. K., 1979, *The Chemistry of Silica*, John Wiley and Sons, New York.

JESIONOWSKI T., KRYSZTAFKIEWICZ A., 2000, *Comparison of the techniques used to modify amorphous hydrated silicas*, J. Non-Crystalline Solids, 277, 45.

JESIONOWSKI T., KRYSZTAFKIEWICZ A., 2001, *Influence of silane coupling agents on surface properties of precipitated silicas,* Appl. Surf. Sci., 172, 18.

KRYSZTAFKIEWICZ A., RAGER B., MAIK M., WALKOWIAK J., 1996, *Modified sodium aluminum silicate- a highly dispersed polymer filler and a pigment,* Colloids Surf. A, 113, 203.

KRYSZTAFKIEWICZ A., JESIONOWSKI T., RAGER B., 1997, *Reinforcing of synthetic rubber with waste cement dust modified by coupling agents,* J. Adhesion Sci. Technol., 11, 507.

ACKNOWLEDGEMENTS

This work was supported by the PUT Research Grant DS No. 32/008/2002.

Grodzka J, Krysztafkiewicz A., Jesionowski T., *Napełniacze węglanowo-krzemianowe modyfikowane dwoma rodzajami związków proadhezyjnych,* Fizykochemiczne Problemy Mineralurgii, 36, (2002) 89-99 (w jęz. ang.)

Przeprowadzono modyfikację powierzchni strącanych napełniaczy węglanowo-krzemianowych. W tym celu wykorzystano silanowe związki wiążące oraz kwas stearynowy. Modyfikację przeprowadzono przy użyciu dwóch związków - silanu o powinowactwie do grup silanolowych krzemianu i kwasu stearynowego adsorbującego się na powierzchni węglanowej.

Niemodyfikowane i modyfikowane napełniacze węglanowo-krzemianowe poddano analizie fizykochemicznej. Przeprowadzono również badania mające na celu określenie dyspersji i morfologii cząstek za pomocą techniki SEM i DLS. Ponadto metodą kalorymetrczną określono stopień hydrofobizacji powierzchni napełniaczy węglanowo-krzemianowych po modyfikacji. Zauważono wyraźną korelację pomiędzy wzrostem stopnia hydrofobizacji powierzchni napełniaczy, a jednorodnością cząstek kształtowanych w trakcie powierzchniowej modyfikacji.

Physicochemical Problems of Mineral Processing, 36 (2002) 101-113
Fizykochemiczne Problemy Mineralurgii, 36 (2002) 101-113

Maciej TÓRZ, Krzysztof ALEJSKI, Jan SZYMANOWSKI*

RECOVERY OF ZINC(II) FROM MODEL HYDROCHLORIC ACID SOLUTIONS IN HOLLOW FIBER MODULES

Received March 5, 2002, reviewed, accepted May 10, 2002

The recovery of zinc(II) from model hydrochloric acid solutions in hollow fiber modules was studied. It was found that zinc(II) could be removed from these model solutions by 80% tributyl phosphate in kerosene. The efficiency of extraction was limited by low values of zinc(II) distribution coefficients. Two types of experiments were carried out: the extraction in one module and the extraction-stripping process in a set of two modules. Simplified models of mass transfer based on the solute concentration changes in the aqueous phases were formulated and verified.

Key words: hollow fiber module, extraction, stripping, hot-dip galvanizing, modelling

INTRODUCTION

Hot-dip zinc coating method has been introduced on an industrial scale by Sorel in 1836. It is nowadays one of the most commonly used method of protecting steel from corrosion. The method generates problems of spent pickling solution, which has recently become increasingly important due to tightening of environmental regulations. The pickling of steel goods is usually carried out with 20% HCl at room temperature, and the process is stopped when the concentration of hydrochloric acid achieves 10%. Such a solution can be successfully used for depleting the bad quality zinc protective layers, and the concentration of free hydrochloric acid decreases then near 1%. During the pickling the rust is dissolved and accumulation of iron, mainly iron(II), in the hydrochloric solution occurs. When pickled goods are housed on recycled hooks, i.e. covered in previous process with zinc, an accumulation of zinc(II) in the pickling solution is also observed. If waste pickling solution is additionally used

*****Poznan University of Technology, Institute of Chemical Technology and Engineering
Pl. M. Sklodowskiej-Curie 2, 60-965 Poznan, Poland, e-mail: jan.szymanowski@put.poznan.pl

to deplete the wrongly deposited zinc layer, then zinc(II) concentration in the spent pickling solution may increase to a few tens g/dm^3. Thus, the spent pickling solution may contain: Zn(II) (10 – 130 g/dm^3), Fe(II) (25 - 75 g/dm^3), Fe(III) (10 - 20 g/dm^3) ions and Cl^- (approx. 5 mol/dm^3) anions. The most economically justified method of recovery of the metal ions is solvent extraction. Many popular extractants have been tested in last years (Cierpiszewski et al., 2002, Regel et al. 2001, Kirschling et al., 2001). Tributyl phosphate (TBP) has been chosen as the only extractant allowing efficient and selective extraction and stripping of zinc after reduction of Fe(III) to Fe(II).

Tributyl phosphate is a week extractant of zinc(II). It has to be used as a concentrated solution (above 80%) in kerosene. The use of undiluted extractant is inconvenient because of relatively high mutual solubility of TBP and water. Additionally, a third phase consisted of TBP, water and HCl may be formed in the system. Another constraint results from very small difference of water and TBP densities. This often causes problems with phases separation due to emulsification.

All the aforementioned problems could be avoided when the extraction-stripping process was carried out in the supported liquid membrane systems. Due to the immobilizing of organic phase in the pores of membrane the difference of densities as well as interfacial tension can be very small (de Gyves and de San Miguel, 1999).

The hollow fiber liquid membrane modules have been increasingly explored since 1980's as they provide large area of phases' contact. In the presented work single extraction as well as extraction-stripping processes were carried out in one and two parallel hollow fiber modules, respectively. The research was limited to zinc(II) extraction because it was shown previously (Regel et al., 2001) that Fe(II) ions do not deteriorate zinc(II) extraction as they are not transported by TBP. The aim of work was checking of the possibility of using TBP in membrane process of removing zinc(II) ions from model solutions as well as simplified mathematical modeling of such a process.

EXPERIMENTAL

The composition of model aqueous solution was as follows: [Zn(II)]=20 g/dm^3, $[H^+]$=0.54 mol/dm^3, $[Cl^-]$=5 mol/dm^3 (adjusted with NaCl). All materials ($ZnCl_2$, NaCl and HCl from P.O.Ch. Gliwice) were of pure grade. Deionised water from reverse osmosis was used. The original purity of tributyl phosphate (Fluka) was 97%. TBP was mixed with kerosene (Deutsche Exxon Chemical GmbH) in ratio 8:2 in order to avoid forming of a third phase (TBP + water + HCl) during experiments. Dispersion-free extraction-stripping experiments were carried out on a set-up depicted in Fig. 1. Commercial cross-flow Liqui-Cel® Extra-Flow 2.5×8" X30 membranes (Table 1) were used. In all experiments the aqueous feed phase flowed through the tube side and the organic phase through the shell side. Flows were always countercurrent in closed circulations. The total volume of organic phase was equal to about 500 ml. The total

initial volumes of aqueous feed and stripping phases were equal to 850 and 780 ml, respectively. In case of extraction experiments a set-up of one module and two tanks was used.

Table 1. Geometrical parameters for the Liqui-Cel® Extra-Flow 2.5''×8'' X30 modules studied.

Fiber internal diameter	240 μm
Fiber wall thickness	30 μm
Effective pores size	0.03 μm
Porosity	40 %
Effective fiber length	15 cm
Effective surface area	1.4 m^2
Tubeside volume	145 ml
Shellside volume	195 ml
Fiber potting material	Polyethylene

During each experiment ten 15-mililitre samples of water phases were taken and the losses were not replenished with fresh solutions. This fact influenced the process and was taken into account in calculations.

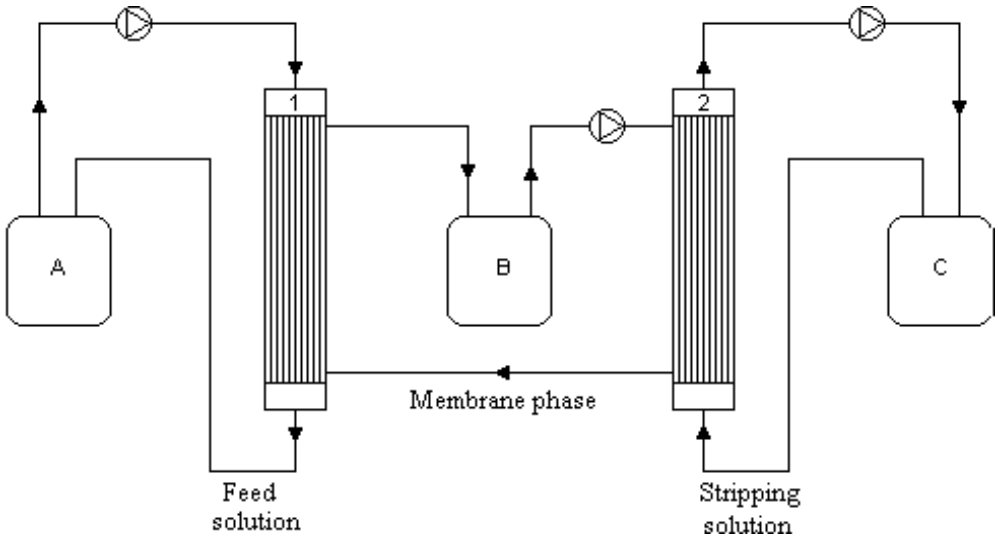

Fig. 1. Experimental two-module extraction-stripping system (A, B, C - tanks; 1 – extraction module, 2 – stripping module). In case of extraction experiments the system consisted of the module 1 and the tanks A and B

Since the fibers were made of polypropylene the pores in membrane's wall were more easily filled with less polar organic phase (Prasad and Sirkar, 1988). In order to avoid forming of dispersion 0.5-bar overpressure was attached on the aqueous phase sides. The concentration of zinc(II) in the aqueous phases was determined by titrating with EDTA.

RESULTS AND DISCUSSION

The distribution coefficients (m_{Zn}) calculated from consecutive experiments carried out in one hollow fiber module decrease in the first four experiments (Table 2). The organic phase was not exchanged during about 2-month research; the only method of its regeneration was washing it with distilled water for two hours after each experiment. Thus, some properties of the membrane phase were changing within the time of research. This assumption was supported by study carried out by Kertes and Halpern (1961) who reported that TBP, being an ester, was slowly hydrolysed in the presence of hydrochloric acid solutions giving di- and monoesters of ortophosphoric acid. In addition, it could not be excluded that some impurities always present in aqueous solutions gathered in the organic phase gradually deteriorating its extractive abilities. Another reason for the problem might be caused by impurities present originally in TBP. Commercial TBP of 97% purity could contain pirophosphoranes which exhibited superior ability to extract metal ions than TBP. However, they were much more susceptible to hydrolysis than TBP. Thus, aging of the membrane phase could directly affect the distribution coefficient of solute.

Table 2. Distribution coefficients of zinc(II) in one-module extraction system

No	Volumetric flow of the feed phase [dm^3/min]	Volumetric flow of the membrane phase [dm^3/min]	Final zinc(II) concentration in the feed phase* [mol/dm^3]	Final zinc(II) concentration in the membrane phase* [mol/dm^3]	Distribution coefficient m_{Zn}
1	1.6	0.46	0.17	0.20	1.18
2	2.4	0.46	0.18	0.21	1.17
3	3.2	0.46	0.19	0.18	0.95
4	4.0	0.46	0.19	0.17	0.90
5	2.4	0.57	0.18	0.18	1.00
6	2.4	0.97	0.18	0.16	0.89
7	2.4	1.60	0.18	0.18	1.00

*determined from the plateau of the relationship zinc(II) concentration versus time.

For the case of extraction-stripping process carried out in two parallel hollow fiber modules two distribution coefficients of zinc(II) were calculated, $m_{Zn,1}$ and $m_{Zn,2}$ for the extraction and stripping processes, respectively:

$$m_{Zn,1} = \frac{C^*_{Zn(o)}}{C^*_{Zn}} \qquad m_{Zn,2} = \frac{C^*_{Zn(o)}}{C^*_{Zn(R)}}$$

where C^*_{Zn} , $C^*_{Zn(o)}$ and $C^*_{Zn(R)}$ denote the equilibrium zinc(II) concentration in the feed, organic and stripping phases, respectively. They amounted: $m_{Zn,1} = 0.98$ and $m_{Zn,2} = 0.16$.

Typical profiles of zinc(II) concentration in the aqueous phases versus time are shown in Figs. 2 and 5a. The concentration of solute in the feed phase in extraction system decreased abruptly in the first period of experiments and after about 45 minutes reached approximately constant value. The situation was analogous in two-module system. However, the concentration of zinc(II) in the organic phase achieved a maximum value and then slowly decreased, whilst it reached maximum constant value in the extraction system. The extraction-stripping system achieved equilibrium after a longer period of time compared to one-module system.

Similar concentration profiles were obtained for HCl transfer, although the species was stronger accumulated in the membrane phase. In all experiments the molar ratio of HCl to zinc(II) removed from the feed phase was equal to about 1.2:1.

MODELS OF MASS TRANSFER

In the presented work simplified mathematical models of mass transfer were applied. The models described the solute concentration changes regarding all phases independently.

The models of mass transfer in hollow fiber modules were rarely presented in literature (Escalante et al.,1996). They were based on macroscopic mass balance of solute and took into consideration the solute concentration changes in feed and stripping phase volumes with time.

In case of one-module extraction experiments the model equation was:

$$-\frac{dC_{Zn}}{dt} = K_E \cdot \left(C_{Zn} - C^f_{Zn}\right) \tag{1}$$

where C^f_{Zn} was the final concentration of zinc in the feed phase, obtained from the plateau of concentration profile versus time.

After integration including the initial condition $C_{Zn} = C_{Zn,i}$ for t = 0 the following equation was obtained:

$$C_{Zn} = C^f_{Zn} + \left(C_{Zn,i} - C^f_{Zn}\right) \cdot \exp\left(-K_E \cdot t\right) \tag{2}$$

The values of apparent mass transfer coefficient K_E were collected in table 3. In most experiments the simple model equation did not reflect properly the solute concentration changes at the initial period of extraction process (see Fig. 2) when the solute concentration decreased abruptly. The discrepancies disappeared when the curves reached plateau.

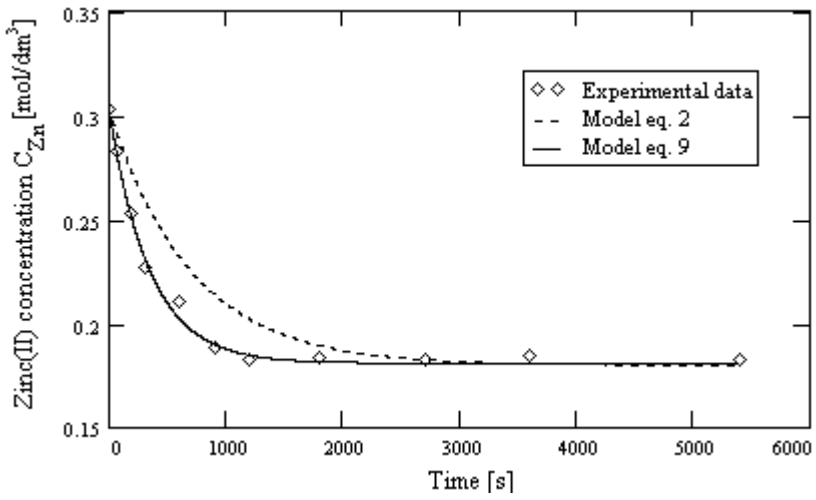

Fig. 2. Exemplary data of zinc(II) concentration changes with time in extraction system (experiment No. 7 - see Table 2) and the results of fitting model equations

The probable reason for observed discrepancies was the decrease of feed phase volume caused by sampling. The volume of each of 10 samples taken for analysis was equal to 13-15 ml. This resulted in the total loss of feed phase of 15-18% during whole experiments. At the same time the volume of organic phase remained unchanged.

To improve the model equation the volume changes were included into the C^f_{Zn} parameter:

$$C^f_{Zn,N} = \frac{C_{Zn,i} \cdot V_{w,i} - \sum_{j=1}^{N} C_{Zn,j} \cdot V_{w,j}}{V_{w,i} + V_o \cdot m_{Zn} - \sum_{j=1}^{N} V_{w,j}} \tag{3}$$

where $C_{Zn,i}$ is the initial concentration of zinc(II) in the feed phase, $C_{Zn,j}$ – the concentration of zinc(II) in the sample j, $V_{w,i}$ – the initial volume of the feed phase, $V_{w,j}$ – the volume of sample j taken for analysis and V_o – the volume of organic phase.

The above equation was correct unless the distribution coefficient varied within the range of experimental concentration changes. When the driving force expressed as the

difference of actual and final concentrations of zinc(II) in the feed phase reached zero the sampling did not change the value of C_{Zn}^{f} any more.

To include the variation of the final solute concentration into model equation it was necessary to express it as a function of time (Fig. 3). The points represented the consecutive values of C_{Zn}^{f} after sampling. The correlation could be approximated by the following equation:

$$C_{Zn}^{f}(t) = C_{Zn,N}^{f} + \left(C_{Zn,0}^{f} - C_{Zn,N}^{f}\right) \cdot \exp(-\alpha \cdot t) \tag{4}$$

where $C_{Zn,0}^{f}$ - the final zinc(II) concentration reached in the system if no samples were taken, $C_{Zn,N}^{f}$ - the final zinc(II) concentration reached after taking all samples.

The constant α had to be found by means of regression. Then, the model equation became as follows :

$$-\frac{dC_{Zn}}{dt} = K_E^{'} \cdot \{C_{Zn} - \left[C_{Zn}^{f} + \left(C_{Zn,0}^{f} - C_{Zn,N}^{f}\right) \cdot \exp(-\alpha \cdot t)\right]\} \tag{5}$$

After integrating by means of the method of variation of parameters the resultant equation was found to be:

$$C_{Zn} = C_{Zn,N}^{f} + \frac{K_E^{©}}{K_E^{©} - \alpha} \cdot \left(C_{Zn,0}^{f} - C_{Zn,N}^{f}\right) \cdot \exp(-\alpha \cdot t) +$$
$$+ \left[C_{Zn,i} - C_{Zn,N}^{f} - \frac{K_E^{©}}{K_E^{©} - \alpha} \cdot \left(C_{Zn,0}^{f} - C_{Zn,N}^{f}\right)\right] \cdot \exp\left(-K_E^{©} \cdot t\right) \tag{6}$$

The apparent mass transfer coefficients calculated by the least squares method were collected in Table 3. The model equation (6) fitted experimental data very well (see Fig. 2).

Table 3. Apparent mass transfer coefficients for one-module extraction system

No	Apparent mass transfer coefficient $K_E \cdot 10^4$ [s^{-1}]	Parameter $\alpha \cdot 10^3$ [s^{-1}]	Apparent mass transfer coefficient $K_E^{©} \cdot 10^4$ [s^{-1}]
1	10.09	2.03	11.54
2	11.91	2.11	12.18
3	8.17	1.94	7.41
4	13.78	2.23	18.94
5	10.44	1.49	17.92
6	17.57	2.41	27.72
7	14.23	2.14	28.94

A disadvantage of equation (6) was the necessity of calculating two constant parameters, i.e. $K_E^{'}$ and α while the equation (1) contained only one parameter, K_E.

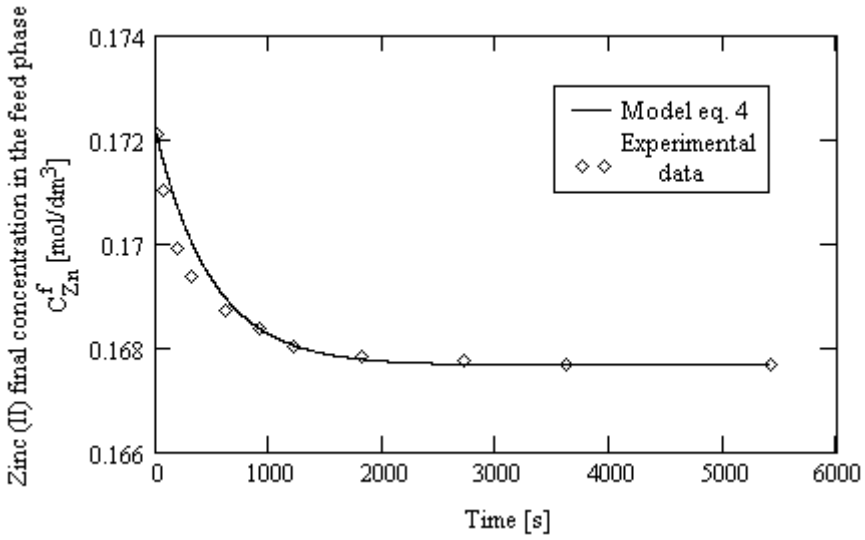

Fig. 3. The variation of zinc(II) final concentration in the feed phase with time (Experiment No. 1 – see Table 2)

Table 4. Apparent mass transfer coefficients for two-module extraction-stripping system (volumetric flow of the membrane phase Q_o = 0.25 dm^3/min).

No	Volumetric flow of the feed phase [dm^3/min]	Volumetric flow of the stripping phase [dm^3/min]	Apparent mass transfer coefficient $K_E \cdot 10^4$ [s^{-1}]	Apparent mass transfer coefficient $K_R \cdot 10^4$ [s^{-1}]
8	1.6	1.6	6.28	3.65
9	1.7	1.7	6.05	3.70

No	Time t_f [s]	Apparent mass transfer coefficient $K_{R1} \cdot 10^4$ [s^{-1}]	Apparent mass transfer coefficient $K_{R2} \cdot 10^4$ [s^{-1}]
8	256	0.93	15.83
9	332	2.40	17.02

For extraction-stripping process a set of two equations was proposed for describing solute concentration changes (Escalante et al., 1996). For the presented system they were:

$$-\frac{dC_{Zn}}{dt} = K_E \cdot \left(C_{Zn} - C_{Zn}^f\right) \tag{7}$$

$$\frac{dC_{Zn(R)}}{dt} = K_R \cdot \left(C_{Zn(R)}^f - C_{Zn(R)}\right) \tag{8}$$

After integrating, taking K_E and K_R as constants and assuming $C_{Zn} = C_{Zn,i}$ and $C_{Zn(R)} = 0$ when t = 0 one could obtain:

$$C_{Zn} = C_{Zn}^f + \left(C_{Zn,i} - C_{Zn}^f\right) \cdot \exp\left(-K_E \cdot t\right) \tag{9}$$

$$C_{Zn(R)} = C_{Zn(R)}^f \cdot \left[1 - \exp\left(-K_R \cdot t\right)\right] \tag{10}$$

The apparent mass transfer coefficients could be calculated by simple regression. Due to similar conditions in both carried experiments respective values were approximately equal (Table 4).

The fitting to experimental data was satisfactory only in the case of extraction process (see Fig. 5). The model equation (10) exhibited significant discrepancies with experimental points. They were especially strong for the initial period of experiments; the solute concentration appeared to increase much slower than predicting from equation (10).

The model correlation (10) did not reflect the real nature of solute transfer. In most extraction-stripping processes the solute was temporary accumulated in the membrane phase (Fig. 4). In order to derive a model correlation that would properly describe the observed solute concentration changes in stripping phase a mass balance of membrane phase was introduced. The solute concentration changes in organic phase were expressed by the difference between actual and final solute concentrations. Two equations were obtained:

$$V_o \cdot \frac{dC_{Zn(o)}}{dt} = K_E \cdot V_w \cdot \left(C_{Zn} - C_{Zn}^f\right) - K_{R1} \cdot V_R \cdot \left(C_{Zn(o)}^f - C_{Zn(o)}\right)$$

$$\text{for } C_{Zn(o)} < C_{Zn(o)}^f \tag{11}$$

$$V_o \cdot \frac{dC_{Zn(o)}}{dt} = K_E \cdot V_w \cdot \left(C_{Zn} - C_{Zn}^f\right) - K_{R2} \cdot V_R \cdot \left(C_{Zn(o)} - C_{Zn(o)}^f\right)$$

$$\text{for } C_{Zn(o)} \geq C_{Zn(o)}^f \tag{12}$$

where V_w, V_o and V_R denote the volume of the feed, organic and stripping phases, respectively.

Equation (11) described the variation of solute concentration changes from the initial time $t = 0$ until the moment $t = t_f$ when the actual solute concentration for the first time reached its final value (see Fig. 4). After that the driving force expressed as $(C^f_{Zn(o)} - C_{Zn(o)})$ became negative and the process was thereafter described by equation (12). Combining equations (11) and (12) with (9) two differential equations were obtained. They could be solved by the method of variation of parameters.

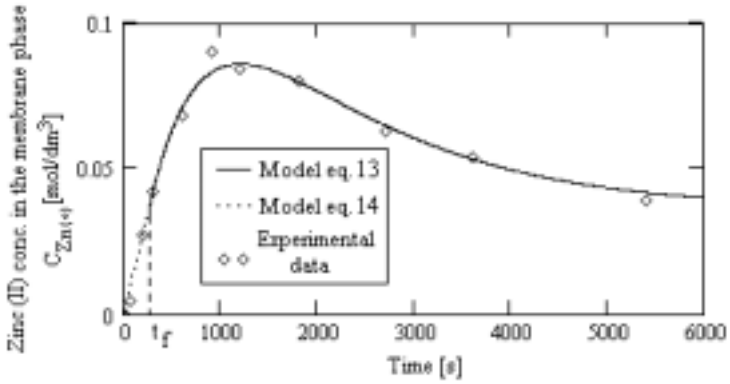

Fig. 4. Zinc(II) concentration profile in the membrane phase in two-module extraction-stripping process (Experiment No. 8 – see Table 4)

For the initial conditions $t = 0 \quad C_{Zn(o)} = 0$ and $t = t_f \quad C_{Zn(o)} = C^f_{Zn(o)}$ the solutions were as follows:

$$C_{Zn(o)} = \frac{V_w \cdot K_E \cdot \left(C_{Zn,i} - C^f_{Zn}\right)}{K_E \cdot V_o + V_R \cdot K_{R1}} \cdot \left[\exp\left(\frac{V_R \cdot K_{R1}}{V_o}\right) - \exp\left(-K_E \cdot t\right)\right] + C^f_{Zn(o)} \cdot \left[1 - \exp\left(\frac{V_R \cdot K_{R1}}{V_o}\right)\right] \quad \text{for} \quad t < t_f \tag{13}$$

$$C_{Zn(o)} = \frac{V_w \cdot K_E \cdot \left(C_{Zn,i} - C^f_{Zn}\right)}{K_{R2} \cdot V_R + V_o \cdot K_E} \cdot \left\{\exp\left[-K_E \cdot t\right] + -\exp\left[\left(\frac{V_R \cdot K_{R2}}{V_o} - K_E\right) \cdot t_f - \frac{V_R \cdot K_{R2}}{V_o} \cdot t\right]\right\} + C^f_{Zn(o)} \quad \text{for} \quad t \geq t_f \tag{14}$$

Introducing a mass balance for the stripping phase:

$$V_R \cdot C_{Zn(R)} = V_w \cdot C_{Zn,i} - V_w \cdot C_{Zn} - V_o \cdot C_{Zn(o)} \tag{15}$$

and combining equations (13) and (14) with (15) one could obtain:

$$C_{Zn(R)} = \frac{V_w \cdot C_{Zn,i} - V_w \cdot \left[C_{Zn}^f + \left(C_{Zn,i} - C_{Zn}^f\right) \cdot \exp\left(-K_E \cdot t\right)\right]}{V_R} + \\ + \left\{ - \frac{V_o \cdot V_w \cdot K_E \cdot \left[C_{Zn,i} - C_{Zn}^f\right]}{V_R \cdot \left[V_o \cdot K_E + V_R \cdot K_{R1}\right]} \cdot \left[\exp\left(\frac{V_R \cdot K_{R1}}{V_o} \right) - \exp\left(-K_E \cdot t\right) \right] - \right. \\ \left. - \frac{V_o \cdot C_{Zn(o)}^f}{V_R} \cdot \left[1 - \exp\left(\frac{V_R \cdot K_{R1}}{V_o} \right) \right] \right\} \\ \text{for} \qquad t < t_f \tag{16}$$

$$C_{Zn(R)} = \frac{V_w \cdot C_{Zn,i} - V_w \cdot \left[C_{Zn}^f + \left(C_{Zn,i} - C_{Zn}^f\right) \cdot \exp\left(-K_E \cdot t\right)\right]}{V_R} + \\ + \frac{V_o}{V_R} \cdot \left\{ - \frac{V_w \cdot K_E \cdot \left[C_{Zn,i} - C_{Zn}^f\right]}{V_R \cdot K_{R2} - V_o \cdot K_E} \cdot \left[\exp\left(-K_E \cdot t\right) + \right. \right. \\ \left. \left. - \exp\left(\frac{V_R \cdot K_{R2} \cdot \left(t_f - t\right)}{V_o} - K_E \cdot t_f \right) \right] - C_{Zn(o)}^f \right\} \\ \text{for} \qquad t \geq t_f \tag{17}$$

The apparent mass transfer coefficients could be calculated by means of the least squares method (Table 4). The results of fitting of the equations (16) and (17) were presented in Fig. 5.

When deriving of the model equations for extraction-stripping process the variation of phase volumes caused by sampling was neglected. This did not introduce a significant error because the same volumes of both aqueous phases were removed at the same time. Thus, the influence of sampling was much smaller than in the case of extraction process.

In the models presented above the driving force of the process was defined as the difference between the actual and the final concentrations in the appropriate phase. Future discussion must consider models with the driving force expressed as the difference between the actual solute concentration in one phase and the equilibrium concentration in the other phase.

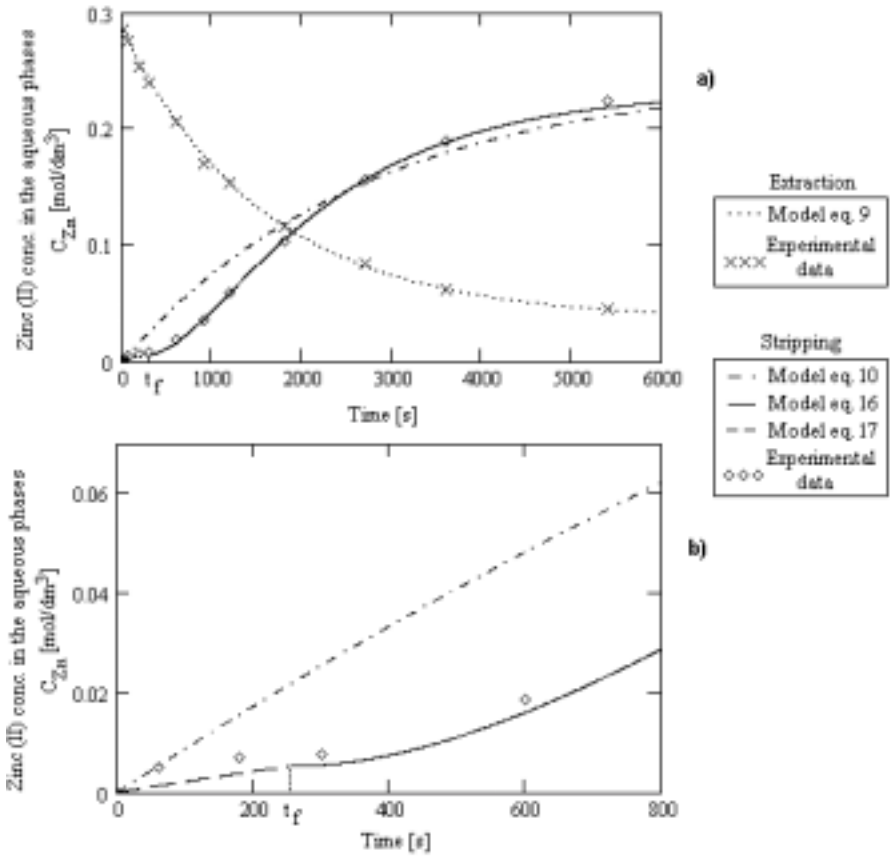

Fig. 5. The variation of the zinc(II) concentration in the feed and stripping phases with time (Experiment No. 8 – see Table 4): a) full range of the concentration changes; b) first period of experiment involving the model equation 17

CONCLUSIONS

The experimental results presented and discussed in the work suggested that zinc(II) could be effectively removed from model acidic chloride solutions. However, the final efficiency of the process was limited by relatively small values of the distribution coefficient of zinc(II) between TBP and aqueous solution. This fact implied that at least several modules should be used to achieve a sufficiently low level of zinc(II) in waste water.

In the presented work simplified mass transfer models in hollow fiber modules were explored. In these models the mass transfer coefficients were found by fitting to experimental data. The driving force was defined as the actual and final solute

concentration difference. The presented models properly described the extraction system. In case of two-module system, however, the equation describing the solute concentration variation in the stripping phase showed significant discrepancies with experimental data. The simple model did not include temporary accumulation of solute in the membrane phase. The suggested improved model described the observed phenomena much better. However, it was quite complicated.

The influence of sampling on the extraction process was found to be significant. This was caused by the fact that the volumes of samples were large and the loss of feed phase was not replenished with fresh solution. The loss of feed phase influenced the final solute concentration and thus the driving force was changed.

REFERENCES

CIERPISZEWSKI R., MIESIĄC I., REGEL-ROSOCKA M., SASTRE A. M., SZYMANOWSKI J., 2002, *Removal of Zinc(II) from Spent Hydrochloric Acid Solutions from Zinc Hot Galvanizing Plants*, Ind. Chem. Eng. Res., Vol. 41, pp. 598-603.

ESCALANTE H., ALONSO A. I., ORTIZ I., IRABIEN A., 1998, *Modelling of Liquid-Liquid Non-dispersive Extraction Processes in Hollow Fiber Modules*, Liquid-Liquid Two Phase Flow and Transport Phenomena, Marn D. M. (Ed.), Begell House Inc., New York, pp. 155-164.

DE GYVES J., DE SAN MIGUEL E. R., 1999, *Metal Ions Separations by Supported Liquid Membranes*, Ind. Eng. Chem. Res., Vol. 38, pp. 2182-2202.

KERTES A. S., HALPERN M., 1961, *Hydrochloric Acid Promoted Hydrolysis of Tri-n-butyl Phosphate*, J. Inorg. Nucl. Chem., Vol. 20, pp. 117-126.

KIRSCHLING P., NOWAK K., MIESIĄC I., NITSCH W., SZYMANOWSKI J., 2001, *Membrane Extraction-Stripping Process for Zinc(II) Recovery from HCl Solutions*, Solvent Extr. Dev., Jpn, Vol. 8, pp. 135-143.

PRASAD R., SIRKAR K. K., 1988, *Dispersion-free Solvent Extraction with Microporous Hollow-Fiber Modules*, AIChE J., Vol. 34, pp. 177-188.

REGEL M., SASTRE A. M., SZYMANOWSKI J., 2001, *Recovery of Zinc(II) from HCl Spent Pickling Solutions by Solvent Extraction*, Environ. Sci. Technol., Vol. 35, pp. 630-635.

ACKNOWLEDGEMENTS

The work was supported by NATO Science for Peace grant No. 972398.

Tórz M., Alejski K., Szymanowski J, *Odzysk jonów cynku(ii) z modelowych roztworów kwasu solnego w modułach z włóknami kapilarnymi,* Fizykochemiczne Problemy Mineralurgii, 36, (2002) 101-113 (w jęz. ang.)

W pracy przedstawiono wyniki badań ekstrakcji i reekstrakcji jonów cynku(II) w modułach z włóknami kapilarnymi z modelowych roztworów kwasu solnego o składzie zbliżonym do roztworów potrawiennych pochodzących z ocynkowni stosujących metodę cynkowania ogniowego. Stosowanym ekstrahentem był fosforan tributylu, fazą odbierającą natomiast woda. Wykazano, że cynk(II) może być usuwany z roztworów modelowych w modułach z włóknami wydrążonymi, przy czym o wydajności procesu decydował niski współczynnik podziału cynku(II) między fazę organiczną i wodną. Sformułowano oraz pozytywnie zweryfikowano uproszczony model matematyczny procesu, bazujący na bilansie masowym jonów cynku w fazach wodnych.

Physicochemical Problems of Mineral Processing, 36 (2002), 115-122
Fizykochemiczne Problemy Mineralurgii, 36 (2002) 115-122

Cezary KOZŁOWSKI*, Wiesław APOSTOLUK**, Władysław WALKOWIAK**, Andrzej KITA***

REMOVAL OF Cr(VI), Zn(II) AND Cd(II) IONS BY TRANSPORT ACROSS POLYMER INCLUSION MEMBRANES WITH BASIC ION CARRIERS

Received March 5, 2002, reviewed, accepted May 15, 2002

An experimental investigation of chromium(VI), zinc(II), and cadmium(II) ions removal from acidic chloride aqueous solutions by polymer inclusion membrane (PIM) transport with basic ion carriers, *i.e*. 4-(1'-*n*-tridecyl)pyridine *N*-oxide (TDPNO) and tri-n-octylamine (TOA) is presented. The initial fluxes of all metal ions are higher for the less basic carrier, i.e. TDPNO. On the other hand, the more basic carrier, i.e. TOA gives higher Cr(VI)/Cd(II) and Cr(VI)/Zn(II) selectivity coefficients. Also the application of PIM transport process for removal of 99% chromium(VI) from galvanic waste waters is shown.

Key words: polymer inclusion membranes, separation, chromium(VI), zinc(II), cadmium(II)

INTRODUCTION

Chromium is regarded as a toxic element in the environment. Toxicity of chromium compounds depends on its oxidation states, *i.e.* chromium(III) and chromium(VI), which are regulated in different ways (Kimbrough et al., 1999). Chromium(VI) was recognized to be much more toxic than chromium(III). Chromium(VI) compounds were found to be toxic for bacteria, plants, animals and people. Human toxicity includes lung cancer, as well as kidney, liver and gastric damage. Chromium(VI) is one of major toxic elements present in environmental samples. For this reason, the application of liquid membranes for Cr(VI) removal from aqueous solutions was evaluated.

*Institute of Chemistry and Environment Protection, Pedagogical University of Częstochowa, 42-200 Częstochowa, Armii Krajowej 13 Street, Poland, e-mail: c.kozlowski@wsp.czest.pl
**Institute of Inorganic Chemistry and Metallurgy of Rare Elements, Wrocław University of Technology, 50-370 Wrocław, Wybrzeże Wyspiańskiego 27 Street, Poland
e-mail: Apostoluk@ichn.ch.pwr.wroc.pl, Walkowiak@ichn.ch.pwr.wroc.pl
***Silesian University, Department of Analytical Chemistry, ul. Szkolna 9, 40-006 Katowice, Poland

Batch solvent extraction was used widely for chromium(VI) removal from aqueous solutions. As extractants were used tri-n-octylamine (Horn et al., 1994; Chilukuri et al., 1998), tri-iso-octylamine (Huang et al., 1991), trioctylmethylammonium salts such as Aliquat 336 (Lo and Shiue, 1998). Another option of chromium(VI) removal from aqueous solutions is the application of tertiary amines and quaternary ammonium salts as carriers in the membrane transport in microporous hollow-fiber modules (Yun et al., 1993; Yang et al., 1996; Alonso et al., 1996; Ortiz et al., 1996). The process, called also nondispersive solvent extraction (NDSX), offers a very large interfacial area per unit equipment volume without any dispersion. Recent years have seen a remarkable increase in the applications of liquid membranes in separation processes. These membranes include bulk liquid membranes (BLMs), emulsion liquid membranes (ELMs) and supported liquid membranes (SLMs). Ho and Sirkar (Ho and Sirkar, 1992) provide a good overview of membrane processes.

The applications of SLMs with tertiary amines and/or quaternary ammonium salts as ion carriers used for chromium(VI) concentration and separation have been shown in several papers (e.g.. Chiarizia, 1991; Chaudry et al., 1997; Wang et al., 1998). A common problem for SLMs is the loss of membrane solvent and/or carrier to the both aqueous phases. As a result, SLM-based process have not been exploited industrially owing their poor durability.

An alternate approach to the problem of SLM stability has been related with the organic liquid phase immobilized within a porous structure. Recently, a novel type of liquid membranes systems, called polymer inclusion membranes (PIMs) has been developed. The PIMs are formed by casting as a support cellulose triacetate (CTA) from an organic solution to form a thin, stable film. This solution also contains an ion carrier and a membrane plasticizer (mostly o-nitrophenyl alkyl ethers). The resultant membrane does not contain organic solvent but is able to maintain the transport of ionic species through and may be used to separate source and receiving phases in PIM systems.

CTA membranes were used for carrier mediated transport of Cr(VI) ions from an aqueous source phase into an aqueous receiving phase. Walkowiak et al. have studied the competitive transport of zinc(II), cadmium(II), chromium(III) and chromium(VI) across PIMs using tertiary amines-based carriers (Walkowiak et al., 2000). The chromium(VI) extraction and transport with 4-(1'-*n*-tridecyl)pyridine N-oxide across the CTA-based polymer inclusion membrane system were found to be strongly dependent upon the concentration of sulphuric acid in the aqueous and/or source phase, respectively (Wionczyk et al., 2001).

Present work deals with the transport of chromium(VI) from chloride aqueous solutions by polymer inclusion membranes with tertiary amine and N-oxide pyridine alkyl derivative as ion carriers. The effect of plasticizer content on chromium(VI) transport across PIMs and separating properties of PIMs with tri-n-octylamine and 4-(1'-*n*-tridecyl)pyridine N-oxide for chromium(VI), zinc(II) and cadmium(II) transport have been studied.

EXPERIMENTAL PART

CHEMICALS

The 4-(1'-*n*-tridecyl)pyridine *N*-oxide (TDPNO) with formula weight 277.45 is a white, crystalline powder which was synthesised by Golubski (Golubski, 1998). The melting point of TDPNO purified by crystallisation from hexane solution is $61 \div 63^0$C. The organic compounds, *i.e.* tri-n-octylamine (TOA), dichloromethane, o-nitrophenyl pentyl ether (ONPPE) and cellulose triacetate (CTA) were purchased from Fluka and used without further purfication. The aqueous solutions of inorganic compounds, *i.e.* potasium dichromate, zinc chloride, cadmium chloride, sodium hydroxide, sodium acetate and hydrochloric acid, were prepared from analytical grade reagents (POCh, Gliwice, Poland).

POLYMER INCLUSION MEMBRANE PREPARATION

Cellulose triacetate, an ion carrier and a plasticizer were dissolved in dichloromethane. A portion of this solution was poured into a membrane mold comprised of a 9.0 cm glass ring attached to a glass plate with CTA - dichloromethane glue. Dichloromethane was allowed to evaporate overnight and the resultant membrane was separated from the glass plate by immersion in cold water. The membrane was soaked in aqueous solution of 0.1 M HCl for 12 hours and stored in distilled water.

TRANSPORT STUDIES

Transport experiments through PIMs were carried out in a permeation cell in which the membrane film was tightly clamped between two cell compartments (Fig. 1). The average CTA membrane thickness was 28 μm (measured by digital ultrametr of A 2002M type from Inco-Veritas with 0.1 μm standard deviation over four readings). The effective membrane area exposed to both phases was 6.0 cm^2. Both, the source and receiving aqueous phases (45 cm^3 each) were stirred at 600 rpm with synchronous motors. The permeation of chromium(VI) was monitored by periodically sampling the source phase, and chromium, zinc, and cadmium was analyzed after appropriate dilution by an atomic absorption Perkin Elmer spectrophotometer.

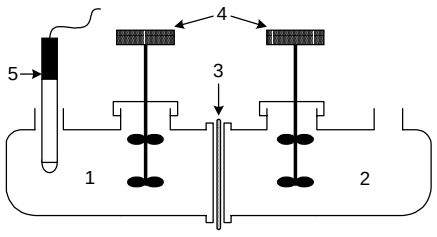

Fig. 1. Diagram of the transport cell: 1 - source phase, 2 - receiving phase, 3 - membrane, 4 - mechanical stirrers, 5 - pH electrode

Kinetics of PIM transport can be described by a first-order reaction in metal ion concentration:

$$\ln\left(\frac{c}{c_i}\right) = -kt \tag{1}$$

were c is the metal ion concentration (M) in the source phase at some given time, c_i stands for the initial metal ion concentration in the source phase, k denotes the rate constant (s^{-1}), and t is the elapsed time (s) of transport.

To calculate the value of k , a plot of $\ln(c/c_i)$ versus time was prepared. The values of rate constant for the duplicate transport experiments were averaged and standard deviation was calculated. The straight line relationships of $\ln(c/c_i)$ vs. time with high values of determination coefficient (r^2), i.e., from 0.9699 to 0.9918, were obtained.

The initial flux (J_i) was determined as equal to:

$$J_i = \frac{V}{A} \cdot k \cdot c_i \,. \tag{2}$$

where V is volume of the aqueous source phase, and A is an area of effective membrane.

The selectivity coefficient, S, was defined as the ratio of initial fluxes for M1 and M2 metal ions, respectively.

$$S = J_{i,M1} / J_{i,M2} \tag{3}$$

The removal (R) of metal ions from the source phase into receiving phase was calculated as:

$$R = \frac{c_i - c}{c_i} \cdot 100\% \tag{5}$$

where c_i – the initial concentration of metal in the source phase.

RESULTS AND DISCUSSION

EFFECT OF PLASTICIZER CONTENT ON THE TRANSPORT Cr(VI) ACROSS PIM WITH TOA AND TDPNO

Initially, transport of chromium(VI) ions through PIMs containing TOA or TDPNO as ionic carriers and various plasticizer content was studied. Blank experiments, in the absence of carrier, yielded no significant flux across PIM containing only the support and plasticizer. To understand the influence of plasticizer on chromate ions transport through PIM, membranes with different content of o-nitrophenyl pentyl ether were prepared and tested at temperature 25 ^{0}C.

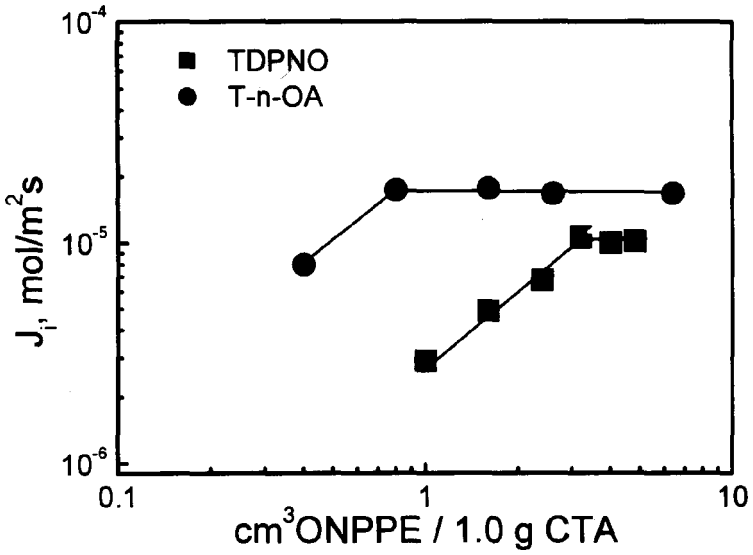

Fig. 2. Relationship between initial fluxes and plasticizer content in membrane support for chromium(VI) transport with TOA or TDPNO as ion carriers

SEPARATION OF Cr(VI), Zn(II) AND Cd(II) FROM HCl SOLUTION THROUGH PIM USING TOA AND TDPNO

The selectivity of chromium(VI), cadmium(II), and zinc(II) transport from aqueous chloride solutions by polymer inclusion membrane with 1.0 M TOA or TDPNO as a ion carriers, 0.80 cm^3 and 4.0 cm^3 ONPPE / 1.0 g CTA, respectively, depends on the basicity of carriers used (Table 1).

Table 1. The values initial fluxes and selectivity orders with selectivity coefficients for competitive transport of chromium(VI), cadmium(II), and zinc(II) through PIM. Source phase: 1.0· 10^{-3} M each metal ions in 0.50 M HCl; Receiving phase: 0.50 M CH_3COONa (pH=8.0); Membrane: 0.80 cm^3 ONPPE / 1.0 g CTA, 1.0 M TOA; Membrane: 4.0 cm^3 ONPPE / 1.0 g CTA, 1.0 M TDPNO.

Carrier	Metal ions	Initial flux, J_i (μmol/m^{2}s)	Selectivity orders and selectivity coefficients
TOA	Cr(VI)	6.62	Cr(VI) > Cd(II) > Zn(II) 15 106
	Cd(II)	0.449	
	Zn(II)	0.062	
TDPNO	Cr(VI)	16.01	Cr(VI) > Cd(II) > Zn(II) 5 16
	Cd(II)	3.16	
	Zn(II)	1.01	

As can be seen from Table 1, the initial fluxes of Cr(VI), Cd(II), and Zn(II) are higher for TPNO than for TOA. This is caused by differences of those carriers basicities – the basicity constant of TOA ($pK_b = 5.8$) is much stronger in comparison with TDPNO ($pK_b = 12.9$) (Chmurzyński, 1996; Martell and Smith, 1974). On the other hand, the selectivity coefficients of chromium(VI)/cadmium(II) and chromium(VI)/zinc(II) are higher for TOA than for TDPNO.

APPLICABILITY OF POLYMER INCLUSION MEMBRANES IN ENVIRONMENTAL PROTECTION – UTILIZED OF TOXIC EFFLUENTS

As the costs of wastewater disposal increase, more emphasis is being placed upon the recovery and recycling of valuable chemicals contained within these streams. In the chrome-electroplating industry, rinsing of finished products generates toxic waste water containing chromium(VI) compounds. These waste waters decisive of a significant disposal problem. However, chromium, zinc, and cadmium compounds always present in such waste waters could be regarded as a valuable components which can be effectively removed and separated. The example illustrating such recycling of chromium compounds is presented below. The experiments were carried with the acidic waste water from electroplating plant. The volume source phase of 50 cm^3 industrial solution of acidified sodium chromate (pH 1.0, 250 ppm Cr(VI)) was placed in one compartment, and 50 cm^3 of dilute NaOH aqueous solution (pH 12) was placed in the other compartment. As can be noticed from Figure 3 the maximum removal of Cr(VI) after 30 hours of transport reaches 99%.

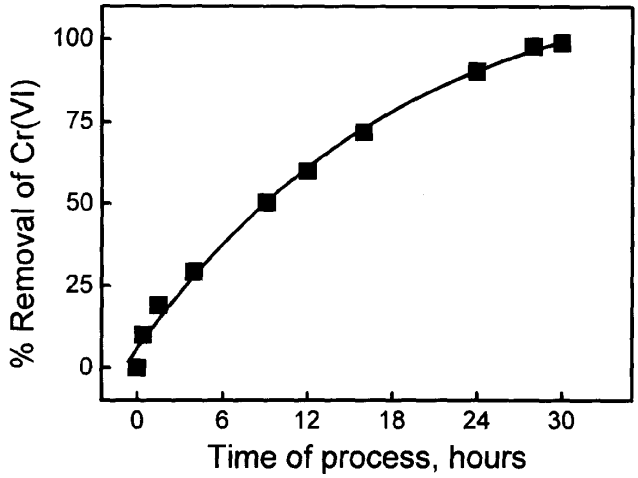

Fig. 3. Removal (%) of Cr(VI) ions from waste water by PIM transport. Membrane: 0.80 cm^3 ONPPE / 1.0 g CTA, 1.28 M TOA

CONCLUSIONS

The polymer inclusion membrane transport of chromium(VI), cadmium(II), and zinc(II) from acidic aqueous solutions using basic ion carriers is an effective method of selective removal of metal ions studied. The used ion carriers, i.e. 4-(1'-*n*-tridecyl)pyridine *N*-oxide and tri-n-octylamine allow to separate metal ions; the selectivity orders were found as follows: Zn(II) < Cd(II) < Cr(VI). The initial fluxes of chromium(VI), cadmium(II), and zinc(II) for TOA and TDPNO were as follows 6.62, 0.449, 0.062, and 16.01, 3.16, 1.01, respectively. These results were discussed in terms of the basicity of ion carriers. Also the application of effective chromium(VI) removal (99 %) from galvanic waste waters using transport through PIM with TOA is shown.

ACKNOWLEDGMENT

Financial support of this work was provided by Polish Science Foundation Grants: 4T09B 10722 (W.A. and W.W.) and 4T09C 04522 (C.K.).

REFERENCES

ALONSO A.I., PANTELIDES C.C. (1996), *Modelling and simulation of integrated membrane processes for Cr(VI) with Aliquat 336*, J. Membr. Sci. 110, 151.

CHAUDRY M.A., AHMAD S., MALIK M.T. (1997), *Supported liquid membrane technique application for removal of chromium from tannery wastes*, Waste Management 17, 211.

CHIARIZIA R. (1991), *Application of supported liquid membranes for removal of nitrate, technetium(VII) and chromium(VI) from groundwater*, J. Membr. Sci. 55, 39.

CHILUKURI R., YANG Z.-F., SIRKAR K.K. (1998), *Batch extraction studies of cationic and anionic heavy metallic species by a mixed solvent extraction system.* Sep. Sci. Technol., 33, 2559.

CHMURZYŃSKI L. (1996), *Studies of correlation of acid-base properties of substituted pyridine N-oxides in solution*. Anal. Chim. Acta, 334, 155.

GOLUBSKI Z. (1998), *The method of preparation of N-oxides of 4-alkylpyridines*. The project P 326 848 registered in Polish Patent Office, 15 June.

HO W.S.W., SIRKAR K.K. (1992), *Membrane Handbook*, Van Nostrand Reinhold, New York.

HORN M.W., FRASER B.G., PRITZKER M.D., LEGGE R.L. (1994), *Chemistry of Cr(VI) solvent extraction using tri-n-octylamine*, Sep. Sci. Technol., 29, 535.

HUANG Y.-H., CHEN C.-Y., KUO J.-F. (1991), *Chromium(VI) complexation with triisooctylamine in organic solvents*, Bull. Chem. Soc. Jpn. 64, 3059.

KIMBROUGH D.E., COHEN Y., WINER A.M., CREELMAN L., Mabuni C. (1999), *A critical assessment of chromium in the environment*, Critical Reviews in Environmental Science and Technology, 29, 1.

LO S.L., SHIUE S.F. (1998), *Recovery of Cr(VI) by quaternary ammonium compounds*, Wat. Res. 32, 174.

MARTELL A.E., SMITH R.M. (1974), *Critical Stability Constants. Vol. 2, Amines*, New York: Plenum Press.

ORTIZ I., GALAN B., IRABIEN A. (1996), *Kinetic analysis of the simultaneous nondispersive extraction and back-extraction of chromium(VI)*, Ind. Eng. Chem. Res. 35. 1369.

WALKOWIAK W., BARTSCH R.A., KOZŁOWSKI C., GĘGA J., CHAREWICZ W.A., AMIRI-ELIASI B. (2000), *Separation and removal of metal ionic species by polymeric inclusion membranes*, Journal of Radioanalitycal & Nuclear Chemistry 246, 643.

WANG Y., THIO Y.S., DOYLE F.M. (1998), *Formation of semi-permeable polyamide skin layers on the surface of supported liquid membranes*, J. Membr. Sci. 147, 109.

WIOŃCZYK B., APOSTOLUK W., PROCHASKA K., KOZŁOWSKI C. (2001), *The properties of 4-1'-n-tricecyl)piridine N-oxide in the extraction and polymer inclusion membranes transport of Cr(VI)*, Analytica Chimica Acta 428, 89.

YANG Z., GUHA A.K., SIRKAR K.K. (1996), *Simultaneous and synergistic extraction of cationic and anionic heavy metallic species by a mixed solvent extraction system and a novel contained liquid membrane device*, Ind. Eng. Chem. Res. 35, 4214.

YUN C.H., PRASAD R., GHUA A.K., SIRKAR K.K. (1993), *Hallow fiber solvent extraction removal of toxic heavy metals from aqueous waste stream*, Ind. Eng. Chem. Res. 32, 1186.

Kozłowski C., Apostoluk W., Walkowiak W., *Wydzielanie jonów chromu(VI), cynku(II) i kadmu(II) za pomocą polimerowych membrany inkluzyjnych zawierających zasadowe przenośniki*, Fizykochemiczne Problemy Mineralurgii, 36, (2002) 115-122 (w jęz. ang.)

W pracy przedstawiono wyniki badań transportu jonów chromu(VI), kadmu(II) i cynku(II) przy użyciu polimerowych membran inkluzyjnych z trioctanu celulozy (CTA) zawierających jako przenośniki jonów n-tlenek 4-(1'-n-tridecylo)pirydyny (TDPNO) lub tri-n-oktyloaminę (TOA). W celu określenia najkorzystniejszego składu polimerowych membran inkluzyjnych zbadano wpływ ilości plastyfikatora w membranie na transport jonów chromu(VI). Maksymalną szybkości transportu Cr(VI) osiągnięto używając membrany z TDPNO zawierające więcej plastyfikatora w porównaniu z TOA, ze względu na dobre właściwości plastyfikujące amin. W przypadku transportu jonów Cr(VI), Cd(II) i Zn(II) za pomocą w/w zasadowych przenośników selektywność procesów malała w szeregu: Zn(II) < Cd(II) < Cr(VI). Membrany inkluzyjne z trójoctanu celulozy zawierające TOA zastosowane do wydzielania jonów chromu(VI) z roztworów przemysłowych (ścieki z galwanizerni) pozwoliły na 99 % wydzielenie tego metalu po 30 godzinach procesu transportu.

Physicochemical Problems of Mineral Processing, 36 (2002) 123-134
Fizykochemiczne Problemy Mineralurgii, 36 (2002) 123-134

A.M AMER*

PROCESSING OF COPPER ANODE-SLIMES FOR EXTRACTION OF METAL VALUES

Received March 5, 2002, reviewed, accepted May 28, 2002

Processing of anodic slimes from an Egyptian copper electrorefining plant, exhibiting high contents of copper, lead, tin and silver has been presented. The proposed hydrometallurgical process consists of two leaching stages for extraction of copper with $H_2SO_4 – O_2$ and silver with thiourea – Fe^{3+}. Pyrometallurgical treatment of the leaching solid residue for production of Pb-Sn soldering alloy was proposed. Parameters affecting both the leaching and smelting stages were studied.

Key words: anode slimes, leaching, copper, silver

INTRODUCTION

Considering the depleting reserves of primary mineral resources for the extraction of metal values, every effort should be made to process secondary sources such as slag, slimes etc. Electrolytic refining of copper is carried out in Jumbo-cells where a series of cathodes, which are made of pure copper and insoluble lead anodes rest in a steel tanks. Metallic copper is deposited at the cathodes, while the water molecules are decomposed at the anode to produce oxygen. Sulphuric acid is regenerated in the solution which is used to leach copper again (Landsberg, 1977; Subbaiah et al., 1986; Mahadavi and Ditze, 1996). The electrolysis of copper may be described by the following equations:

$$CuSO_4 \Leftrightarrow Cu^{2+} + SO_4^{2-} \quad (1)$$

$$\text{At the anode: } H_2O = 0.5\ O_2 + 2H^+ + 2e^- \quad (2)$$

$$\text{At the cathode: } Cu^{2+} + 2e^- = Cu \quad (3)$$

$$CuSO_4 + H_2O = Cu + H_2SO_4 + ½\ O_2 \quad (4)$$

*Environmental Science Dept., Faculty of Science, Moharrem Bey, Alexandria, Alexandria University – Egypt, e-mail: ashraf-amer@37.com

Anode slimes are collected from the bottom of the electrolytic cells during the refining of copper. There are two different kinds of slimes depending on the sources from which they are obtained. The first one produced during the processing of copper concentrate which exhibits a relatively high gold, silver, tellurium and selenium content, and the second one produced during the processing of recycled scrap has a higher lead, copper, tin and silver content. This work focuses on processing of anodic slimes obtained from an Egyptian copper electrorefining plant which is characterized by a high content of copper, lead, tin and silver.

Several methods have been attempted for recovery of copper from slags and anodic slimes. These methods can be differentiated into: a) pyrometallurgical processing which includes roasting in the presence of oxidizing agent, suflate-roasting and soda-ash process (Ying, 1983; Swayn et al., 1993; Hughes, 2000, Filipov et al., 2000), b) hydrometallurgical processing of anode slimes were carried out using different leachants. Chlorination, nitric acid and sulphuric acid (Gill, 1980; Holmes, 1981; Everett, 1994; Petrov, 1999) are used most frequently.

Among the methods of the processing of copper anode-slimes, two of them have been successful on an industrial scale, namely roasting and pressure leaching (Gaylarde and Videla, 1995).

The by-production of sulphuric acid is the troublesome aspect of roasting process because the economic marketing of sulphuric acid depends strongly on site location. Furthermore, even though the gas emission regulation are respected, harmful SO_2 may be released. The advantages of the roasting process are: simplicity, low costs when compared to other processes, and also the fact that know-how is available worldwide. On the other hand, pressure leaching results generally in high degree of extraction which together with the fact that wastes can be confined as stable solids. Hydrometallurgical processing of copper anode slimes has the following advantages: capital costs are relatively low when compared to those for a smelter, process may be applied to small and large operations, air pollution by sulfur dioxide is eliminated, equipment may be designed and installed in modules.

In this investigation sulphuric acid pressure leaching was chosen from various hydrometallurgical methods to process the copper-anode slimes for extraction of copper. The decopperized slimes are then enriched in lead, tin, and silver.

Many hydrometallurgical processes were reported for extraction of noble metals, among them, cyanide (Hoffmann, 1991; McClincy, 1990) and thiourea leaching (Schulze, 1984). The later seems to be effective for silver extraction due to its high complexing ability. Thiourea leaching has been performed in hydrochloric sulfuric and nitric acid media. Dissolution of gold and silver up to 97% was reported in a solution containing 20 g/dm^3 HCl, 0.20 g/dm^3 H_2O_2, and 100 g/dm^3 thiourea.

Some researchers (Kusnierov et al., 1993; Kucha and Cichowska, 2001) have reported that, thiourea is very effective in the recovery of noble metals from copper concentrates which are especially refractory to cyanidation. An industrial application of thiourea leaching has been reported in New South Wales (Deschenes and Ghali,

1988), where thiourea leaching shows a good potential application to treat sulphide concentrates.

A low toxicity of thiourea compared to cyanide is always mentioned as one of the motivations for developing the research in the field.

MATERIAL

Anode slime samples were collected from the bottom of the electrolytic cells during the electro-refining of copper. These samples were sieved through a 2.0 mm sieve to remove large inclusions of copper and other foreign material present in the slime.

A representative sample of the feed slime was analysed for Cu, Pb, Sn, Zn, Ni, Fe, As, Sb, SiO_2, MgO, and Ag using atomic absorption, spectrophotometer. The chemical analysis is given in Table 1.

Table 1. Chemical analysis of representative sample of studied anode-slime

Chemical constituents	Weight percent (%)
Cu	18.57
Pb	15.3
Sn	9.8
Ag	0.46
Ni	0.94
Fe	1.72
Sb	1.30
As	0.49
Zn	0.74
S	9.22
SiO_2	8.51
CaO	1.54
MgO	0.82

EXPERIMENTAL

A schematic diagram of the experimental apparatus shows the one-dm^3 glass reactor with baffles used for the leaching tests. The cover of the reactor had four ground-glass parts, which contained a Friedrich's condenser, sampling device, oxygen dispersion tube and glass impeller. The impeller was inserted through the center part by means of a Chesapeake stirrer connection and was driven by a Fisher mixer. The entire reactor assembly was clamped into place in water bath which was heated with a temperature controller and held to within ±0.1 ^oC of the desired temperature.

In each test a 100 g sample of the ground anodic slime (-0.075 mm) was leached with 1 dm^3 solution of sulfuric acid of known concentration. The leaching tests were

conducted at different temperatures for various leaching time and with the admission of variable rates of oxygen as oxidizing agent for copper dissolution. Samples of 5 cm^3 liquor were taken for subsequent analysis using atomic absorption technique to determinate the dissolved copper concentration.

At the end of the leaching experiment the slurry was then filtered using water suction pump, through A-No-42 Whatman filter paper and washed thoroughly with hot distilled water, dried at 110 ^oC, and then ground to minus 0.075 mm. The decopperised slime has been analysed for Pb, Sn, and Ag.

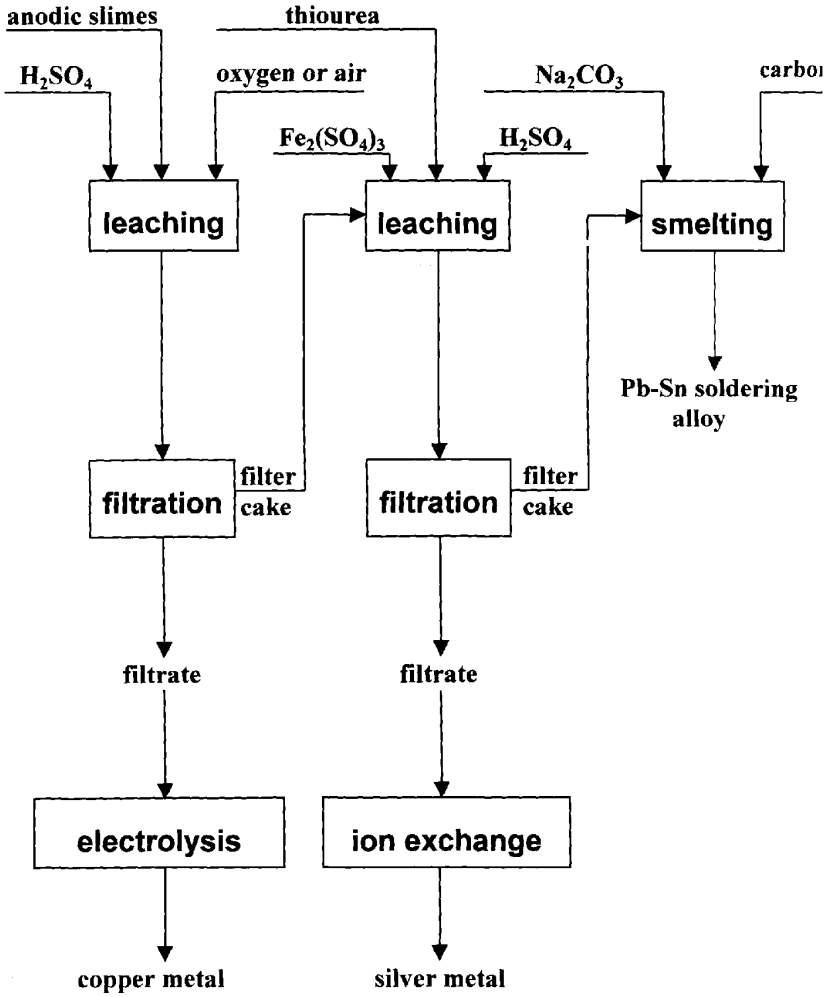

Fig. 1. The flowsheet of the process of utilization of anodic slime for production of Cu, Ag and Pb-Sn soldering alloy

Forty-gram samples of the decopperised slime were leached with 1 dm^3 of solution containing different amounts of acidified thiourea and ferric ion as oxidant. The slurry was agitated with a magnetic stirrer at various agitation speeds. Various factors such as temperature, leaching time, and thiourea concentration were examined to determine the optimum operating conditions for silver dissolution.

Liquid samples were analysed using atomic absorption for determination of dissolved silver. The decopperised-silver free residue enriched in lead and tin could be a feed for the production of Pb-Sn soldering alloys.

Fifty-gram samples of decopperised, silver-free residue was mixed in proper proportions of sodium carbonate and carbon and smelted in a graphite crucible at different temperatures and time for production Pb-Sn soldering alloy.

The aim of this investigation according to the flow-sheet illustrated in Fig. 1, is to investigate and optimize the parameters influencing the dissolution of both copper and silver as well as those affecting the production of soldering alloys.

RESULTS AND DISCUSSION

EXTRACTION OF COPPER

EFFECT OF TEMPERATURE

Figure 2 shows that the copper extraction rate increased with the increase of temperature in the range 65-85°C. Further increase in temperature had a little effect on copper extraction.

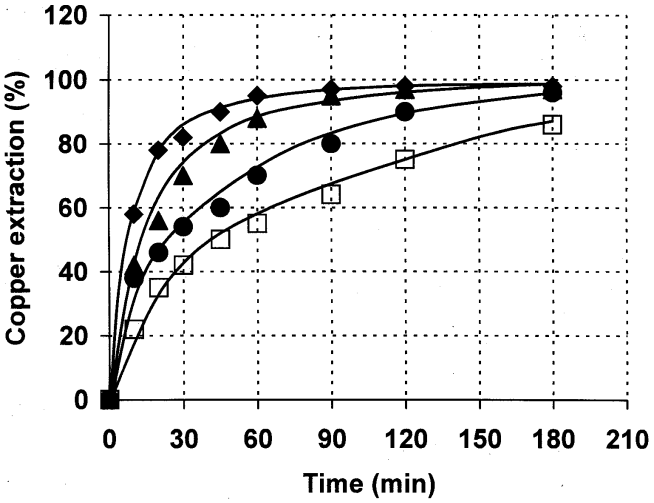

Fig. 2. The effect of temperature on the leaching rate of copper from anode slime by oxygenated 0.5 M H_2SO_4, particle size -75 μm

Applying the following equation:

$$1-(1-\alpha)^{1/3} = -kt \quad (5)$$

where α= fraction reacted, k= a constant for the reaction rate and t= leaching time. Figure 3 shows that the plot of $1-(1-\alpha)^{1/3}$ versus t over the studied temperature range consist of a series of straight lines indicating that the sulphuric acid leaching of anode slimes is chemically rate-limited.

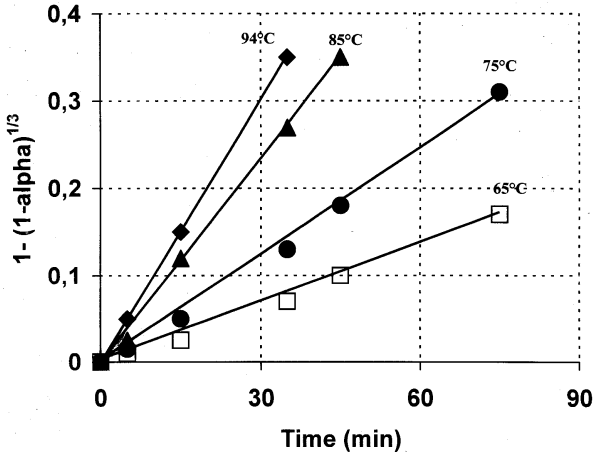

Fig. 3. Kinetic analysis of experimental data of copper leaching (as in Fig. 2).

From the slopes of linearised isotherms in Fig. 3, plot rate constants were determined at given temperatures. The activation energy E_A is determined from Arrhenius plot given in Fig. 4.

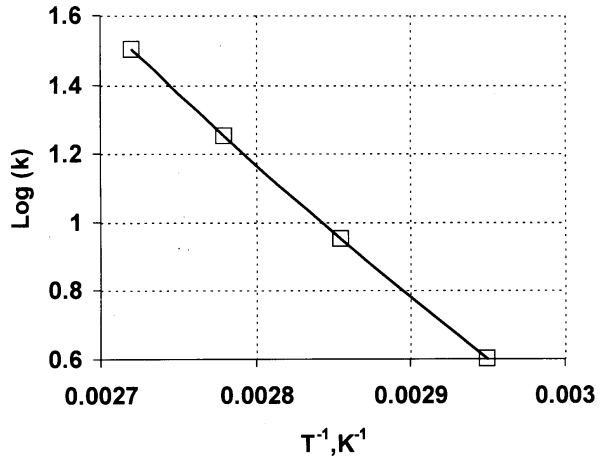

Fig. 4. Arrhenius plot for the copper leaching with oxygenated H_2SO_4. Parameters as in Fig. 2.

$$\text{Slope} = -E_A/RT \qquad (7)$$

The value calculated for the activation energy is 69 kJ/mol which indicates surface chemical control.

EFFECT OF ACID CONCENTRATION

Figure 5 shows that copper extraction increases when the acid concentration increases from 0.02 M to 0.5 M. A further increase in the acid concentration resulted in practically no increase of copper extraction which may be due to the fact that the solubility of oxygen at high acid concentration is low in comparison with its solubility at low acid concentration. Figure 6 illustrates the relation of pH of the leach solution and extraction which indicates that the percentage of the metal uptake increases with increasing pH up to pH 4-5 and thereafter it is more or less constant in the pH range investigated.

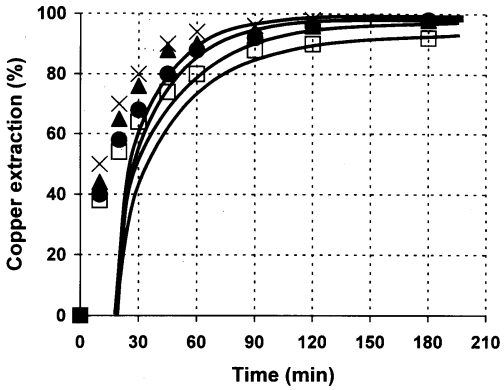

Fig. 5. The effect of H_2SO_4 concentration on the leaching rate of copper with oxygenated solution at 85°C. Particle size 75µm

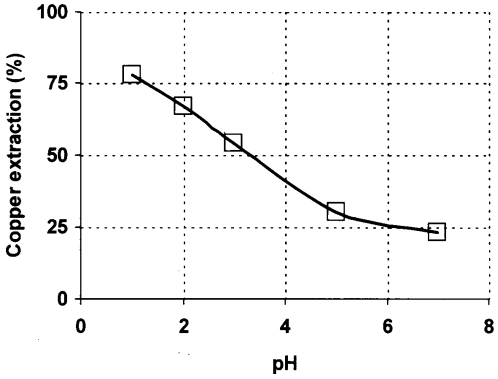

Fig. 6. The effect of pH on the copper extraction at 85°C. Particle size 75µm

EFFECT OF OXYGEN FLOW RATE

Figure 7 shows the results of leaching 75 µm diameter anode slime in 0.5 M H_2SO_4 under various oxygen flow rate. It is concluded that under the experimental conditions used the higher the oxygen flow rate, the higher extraction of copper.

It was determined that the leaching of anodic slime in sulphuric acid under oxygen pressure led to extraction of copper (97%) under the following leaching conditions: temperature: 85 °C, sulphuric acid concentration: 0.5 M, oxygen flow rate: 1 bar, leaching time: 90 min, and particle size: -75 µm.

EXTRACTION OF SILVER

This section represents the experiments conducted for the silver extraction from decopperized slime residue. The variables influencing the potential of acidified thiourea solution as leaching agent are: thiourea concentration, temperature, leaching time, Fe^{3+} concentration as oxidant. The previously decopperized slime residue is ground to -0.075 mm and then leached by acidified thiourea solution.

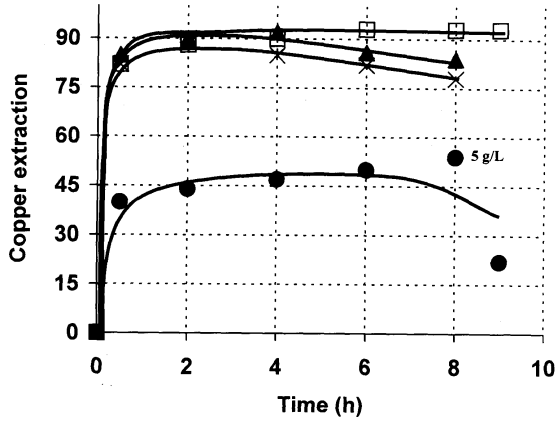

Fig. 7. The effect of thiourea case concentration on the leaching rate of Ag. Temperature 25°C, solid/liquid ratio equal to 0.1. Fe^{3+} concentration 5g/dm^3

EFFECT OF THIOUREA CONCENTRATION

In an acidic solution of thiourea, the dissolution of silver proceeds according to the following reaction:

$$Ag + 2\ CS(NH_2)_2 \Leftrightarrow Ag[CS(NH_2)_2]_2^+ + e \quad (8)$$

This is a reversible reaction with an electrode potential of 0.352 V at 25 °C on a fresh silver surface and 0.41 V on a passivated surface. According to Fig. 7, the silver extraction increases with the increase of the thiourea concentration and reaches its maximum recovery (90%) at 10 g/dm^3 thiourea concentration. The increase of the thiourea concentration up to 10 g/dm^3, produces an increase in the silver extraction, especially in the initial leaching period (0.5 h). There is however, a decrease in silver extraction with the increase of thiourea >20 g/dm^3. It may be due to that the thiourea is less stable at higher concentrations and decomposes.

EFFECT OF TEMPERATURE

Table (2) presents the effect of temperature using 10 g/dm^3 thiourea and 5.0 g/dm^3 ferric ion. Extraction of more than 90% silver is reached at both 40°C and 60°C after leaching time of 30 minutes. The silver extraction is improved with the increase of temperature to 40°C where it reaches 93.5% after 4 hrs of leaching.

Table 2. Effect of temperature on silver extraction (S/L = 10%, thiourea. 10 g/dm^3, F^{3+}= 5 g/dm^3, pH 1-0)

Temperature	Silver extraction		
	30 min	4h	8h
25	80.4	87.3	93.4
40	80.7	93.5	93.4
60	92.2	94.0	92.5

EFFECT OF FERRIC ION

The oxidating effect of ferric ion in the presence of thiourea can be illustrated in the following reaction.

$$Fe^{3+} = CS(NH_2)_2^{2-} \Leftrightarrow [Fe\ (CS(NH)_2)_2]^+ \quad (9)$$

In contact with oxidants such as Fe^{+3}, thiourea may be oxidized in successive stages to form several products. The first is the formation of formamidine disulphide [Schulze, 1984).

$$2CS(NH_2)_2 \Leftrightarrow [(NH_2)(NH)CSSC(NH)(NH_2) + 2H^+ + 2e;\ E^o = 0.42\ V \quad (10)$$

In a second irreversible reaction the formamide disulphide yields thiourea and unidentified sulphinic compound which then decompose to yield cyanomide and elemental sulphur. The elemental sulphur created at the end of this decomposition has a detrimental effect by passivating the leachable silver surface and precipitating some silver from solution.

The study of the effect of oxidizing agent shows that there is an equilibrium between thiourea and formamidine disulfide. The leaching efficiency of silver depends on this equilibrium. It indicates that the optimum extraction of silver was 93% using 10 g/dm^3 thiourea and 5.0 g/dm^3 Fe^{3+} in one leach of 4 hrs.

As seen in Fig. 8, an addition of 2 g/dm^3 of Fe^{+3} slightly improves the initial leaching kinetics but results in no real improvement in silver extraction.

Further increase in Fe^{3+} concentration to 5.0 g/dm^3 results in increase of the leaching rate and also increases the extraction of silver to 93.4% for 7 hrs of leaching. It is seen that, the rate of silver dissolution is very rapid in the first 30 min of leaching. For the 5.0 g/dm^3 concentration of the oxidant, 80% of silver was leached in this period. Adding 8.0 g/dm^3 Fe^{3+} in solution caused a significant decrease in silver extraction. When the amount of oxidant is too large, there is oxidation of thiourea and the remaining amount of leachant is less effective for extraction of silver.

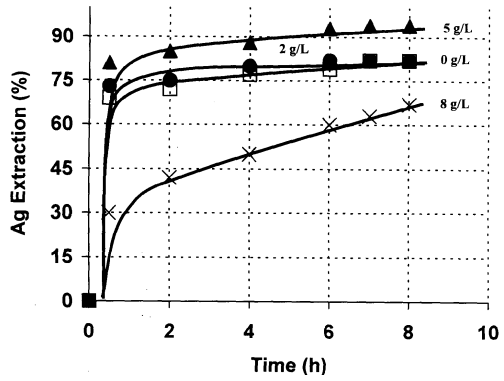

Fig. 8. Effect of Fe^{3+} concentration on the leaching rate of Ag with thiourea

PRODUCTION OF LEAD-TIN SOLDERING ALLOY

After the removal of the copper and silver the slime was then enriched in lead (41.6%) and tin (29.0%). Residues were dried and ground to <0.075 mm and then mixed with different proportions of sodium carbonate and carbon. There were smelted in graphite crucibles at different temperatures and various time intervals. The effects of the following parameters were studied: carbon as reducing agent, sodium carbonate as flux, temperature, and reduction time.

The effects of these variables are illustrated in Tables 3–6. The optimum operating conditions can be summarized as follows: carbon added: 30% by weight of slime added, sodium carbonate: 40% by weight of slime added, temperature: 1100^{o}C, and reducing time: 1-0 hr. Under the above mentioned operating conditions, the led and tin contents are 53.0% and 33.0%, respectively.

However, a wide range of lead-tin soldering alloys is known to depend on the lead-tin ratio.

Table 3. Effect of carbon as reducing agent. Temp. 1100^{o}C, Na_2CO_3 40%, reducing time 1 hr

% of carbon	Chemical composition								
	Pb	Sn	Cu	Ni	Zn	Sb	As	Al	Ag
10	82.42	2.2	4.2	5.5	0.5	3.3	0.25	0.09	0.32
15	82.30	3.9	1.2	3.9	0.4	6.2	0.5	0.1	0.17
20	80.90	4.0	2.1	4.2	1.0	6.7	0.5	0.1	0.2
30	55.0	31.6	1.5	2.0	0.4	6.8	2.0	0.07	0.15
40	52.7	31.5	1.5	2.5	0.98	7.3	2.0	0.2	0.15

Table 4. Effect of sodium carbonate as flux. Temp. 1100^{o}C, carbon: 40%, reducing time 1hr

Na_2CO_3 %	Chemical composition								
	Pb	Sn	Cu	Ni	Zn	Sb	As	Al	Ag
20	55.0	31.0	1.5	2.0	0.4	6.8	2.0	0.07	0.15
30	53.0	32.5	1.3	2.3	1.1	6.4	2.0	0.09	0.10
40	52.88	33.62	1.5	2.0	0.6	0.6	2.0	0.07	0.10

Table 5. Effect of temperature. Carbon 40%, Na_2CO_3 40%, reducing time 1hr

Temp. ^{o}C	Chemical composition								
	Pb	Sn	Cu	Ni	Zn	Sb	As	Al	Ag
900	44.0	34	1.0	1.7	0.8	0.2	1.7	0.08	0.04
1100	52.8	33.6	1.5	2.0	0.6	0.6	2.0	0.07	0.1
1300	59.0	23.23	1.7	3.3	0.5	9.0	2.1	0.05	0.51

Table 6. Effect of reducing time. Temp. 1100°C, C 40%, Na_2CO_3 40%

Reduction time	Chemical composition								
	Pb	Sn	Cu	Ni	Zn	Sb	As	Al	Ag
1.0	53	33.24	1.4	2.1	1.3	5.8	1.9	0.03	0.12
2.0	52.8	33.62	1.5	2.0	0.6	0.6	2.0	0.07	0.1
3.0	53.8	32.7	1.2	2.1	0.8	6.3	1.8	0.06	0.12

CONCLUSIONS

About 90% of copper initially present in the anodic slimes with 75 μm in diameter particles dissolved in 0.25 M H_2SO_4 solutions at 85°C under 1 bar oxygen pressure within 90 min. leaching time. The apparent activation energy of 69.0 kJ/mole is characteristic for systems under chemical reaction control.

Thiourea leaching of silver shows a good potential application to treat slimes bearing silver to recover silver where the low toxicity of thiourea compared to cyanide is always mentioned as one of the motivations for developing the research in this field. Almost 93% of silver is extracted using concentration of thiourea of 10 g/dm^3, under temperature 60°C in 30 min leaching time.

Smelting of the slimes after leaching of copper and silver at 1100°C in the presence of sodium carbonate 40% and carbon 30% for one hour lead to production of Pb-Sn soldering alloy (Pb: 53.0% - Sn: 33%).

REFERENCES

DESCHENES, G and GHALI, E. (1988*), Leaching of gold from chalcopyrite concentrates by thiourea*, Hydrometallurgy, 20, 179-202.

EVERETT, P.K. (1994*), Development of intec copper process by an international consortium*, Proceeding of Hydrometallurgy 94 Sci, England.

FILIPOV, JU.A.; ANISIMOVA, N.N.; KOTUCHOVA, A.K.; TER-OGANESJANE, A.K. and TICHOV, I.V. (2000), *Rokonstruktion der anodenschlammverabeitung.* Cventnye metally 75, Nr. 6., S. 61-63.

GAYLARDE, C.C. and VIDELA, H.A. (1995), *Bioextraction and biodeterioration of metals.* Cambridge Univ. Press, pp. 51-55.

GILL, C.B. (1980), *Non ferrous extractive metall*urgy, Wiley-Interscience Publication. John Wiley and Sons, Inc.

HOFFMANN, J.E. (1991), *Advances in the extractive metallurgy of selected rare and precious metals*, JOM, April, pp. 18-23.

HOLMES, J.A. (1981), *Recent experience in the application of hydrometallurgical techniques proceedings of Hydrometallurgy 81*, England.

HUGHES, S. (2000), *Applying ausmelt technology to recover Cu, Ni and Co from slags (overview)*, JOM, August, pp. 30-33.

KUCHA, H. and CICHOWSKA, K. (2001), *Precious metals in copper smelting products.* Physicochemical Problems of Mineral Processing Journal 35, pp. 91-101.

KUSNIEROV, M.; SEPELK, V. and BRIANCEN, J. (1993), *Effects of biodegradation and mechanical activation on gold recovery by thiourea leaching.* JOM, Dec., pp. 54-56.

LANDSBERG, R. (1977), *Elektrochemische Reaktionen und Prozesse.* VEB Deutscher Verlag der Wissenschaften, Berlin.

MAHDAVI, M. and DITZE, A. (1996) *Basic investigations of the dissolution of copper and the formation of anode slime during copper electrolysis with pure copper-oxygen anodes.* Erzmetall 49, Nr. 6, p. 358-65.

MCCLINCY, R.J. (1990), *Unlocking refractory gold ores and concentrates*. JOM, Sept., pp. 10-11.

PETROV, G.V.; PLEKHANOV, K.A.; KOZLOVSKOYA, A.E. GREIVER, T.N. (1999), *Hydrometallurgische Technologie zur verarbeitung von kupferelektroly seschlammen*. Sventnye metally 74, Nr.1, S. 43-45.

SCHULZE, R.G. (1984), New aspects in thiourea leaching of precious metals. Int. Precious metals Symposium Los-Angeles. Feb. 27-29.

SUBBAIAH, T.; DAS, S.C. and DAS, R.P. (1986), *Electrowinning of copper under forced convection*. Erzmetall 34, Nr. 10, pp. 501-6.

SWAYN, G.P.; ROBILLIARD, K.R. and FLOYD, J.M. (1993), *Applying ausmelt processing to complex copper smelter dusts*, JOM, August, pp. 35-38.

YING, C.H. (1983), *Copper refinery anode slime.* Proceeding of the Third Int. Symp. Of Hydrometallurgy. Annual Meeting. Atlanta, Georgia, March 6-10.

Amer A.M., *Przeróbka miedziowych szlamów anodowych w celu wydzieleniu z nich wartościowych metali*, Fizykochemiczne Problemy Mineralurgii, 36, (2002) 123-134 (w jęz. ang.)

Opisano przeróbkę szlamów anodowych pochodzących z egipskiego zakładu elektrorafinacji szlamów. Szlamy te posiadają wysoką zawartość miedzi, ołowiu, cyny i srebra. Zaproponowano proces hydrometalurgiczny składający się z dwóch etapów ługowania, czyli ekstrakcji miedzi za pomocą H_2SO_4–O_2 oraz srebra w układzie z tiomocznikiem i Fe^{+3}. Zaproponowano także pirometalurgiczny przerób pozostałości po ługowanie w celu otrzymania stopu Pb-Sn. Przebadano parametry wpływające na procesy ługowania i wytopu.

Physicochemical Problems of Mineral Processing, 36 (2002) 135-146
Fizykochemiczne Problemy Mineralurgii, 36 (2002) 135-146

Kazimierz St. SZTABA*

EVALUATION OF NON-SEPARATION OPERATIONS OF MINERAL ENGINEERING

Received March 5, 2002, reviewed, accepted May 17, 2002

The vast majority of technological operations in mineral engineering involves separation operations in which two or more products are obtained differing in the value of a particular property that constitutes the separation characteristic. They include all enrichment, classification and dewatering operations. The determination and evaluation of the technological efficiency of such processes is the subject-matter of numerous theoretical, and particularly methodical studies, as well as control procedures that are commonly applied in industry and experimental investigations. Apart from these operations there are others that (as a rule) aim at the change of the material form without the separation of elements having common properties. Such operations include first of all comminution and inversely agglomeration (as well as briquetting and pelletizing), but also division into smaller portions (or parts) – its specific kind is sampling. These operations have crucial, though variable in importance, significance for the processing while the evaluation issue of their efficiency is practically non-existent in professional literature and in wider practical applications. The aim of this paper is to present the idea of determining the technological efficiency of such operations. Alternative principles of defining the efficiency and methods for obtaining quantitative results as well as their selection for the assumed control targets and the required evaluation accuracy are presented.

Key words: *technological operations of mineral engineering, non-separation operations, and technological efficiency*

SEPARATION AND NON-SEPARATION OPERATIONS

In the entire, large and very differentiated, set of types of technological operations of mineral engineering, one can separate two groups which differ significantly with respect to the general characteristics of their results. The review of the discussed operations indicates that a vast majority of them are used for obtaining several products, mutually differentiated, from the initial material, i.e. the feed, which is either

* Professor emeritus – University of Mining and Metallurgy in Cracow, Faculty of Mining, Department of Mineral Processing, Environmental Protection and Waste Utilization, Al. Mickiewicza 30,30-059 Kraków.

raw mineral or, quite often, a secondary material (intermediate product or waste products of other processing processes) of several products of mutually differentiated properties. These are such operations as:

- enrichment the aim of which is to reach the differentiation of the content of the feed component which is considered to be useful. In such an operation at least two separate products are obtained. These usually are: the concentrate of high content of the useful component and the waste of possibility low content of it;
- grain classification the products of which differ by grain distribution and are as a rule separate (all feed grains of a certain size, most often determined in ranges, should be only in one product);
- dewatering[1] which contributes to the fact that one of the products of the feed, which is a two-phase mixture of water and solid parts, contains mainly solid parts whereas the other one mainly water (here is also water clearing the product of which is cleaned water and not dewatered solid material as in classical dewatering).

Such operations are classified as **separation operations**. They constitute the basic technological set of mineral engineering, particularly mineral processing, and in the majority of practical tasks, in the specially constructed technological systems, they are the "main" operations, determining the final result of the technological task.

The second group of operation, much smaller, is used to modify the feed material properties, generally[2] without separating it into several products. In technological processes they usually are preparatory operations, only in some cases as main operations, although they are certainly necessary in such systems and cannot be neglected in any case. Here there are only operations which change the form of the material:

- comminution – the aim of which is to decrease the grain sizes, in practice it is the elementary part of the task of changing the grain composition of the feed material, i.e. decreasing the grain size distribution; sometimes this task is accompanied by the implementation of requirements concerning grains shapes, practically reaching a significant content of grains of assumed shapes in the product,
- lumping – of the tasks opposite to crushing, assuming the increase of the material grain size distribution by means of consolidation of fine grains into larger permanent aggregates, it includes pelletizing, briquetting (together with "compacting") and agglomeration (sintering); in majority of cases, despite agglomeration, the products of certain grain shapes are obtained, especially in case of briquetting which fulfills the role of the main operation, giving a completed commercial product. Other operations are usually used to make intermediate products to be further processed (e.g. agglomeration or lumping of

[1] Analogical assumptions occur in mixtures of the solid and gaseous phases (gas suspensions, aerosols), for their separation dust removal is applied

[2] this concerns the division operations

fine-grained iron-ore concentrates to be used as blast-furnace charge) or to be refined (e.g. making crude lumps from clays, transformed later into lightweight aggregates),

- division – separation of the feed into parts, occurring mainly as a preparatory operation in sampling and sample preparation as well as in the division of the material stream is large plants into several parallel streams, processed in separate machine lines of mutually similar operation characteristics, the lack of differentiation of qualitative characteristics of the obtained products is the basic qualitative requirement,
- averaging – homogenization of qualitative properties of the material in the entire range in which it is included (this may be the range determined statically, only by means of geometrical features, or dynamically – when the characteristics of material stream movements are considered on the geometrically track – closed or open).

These operations belong to the group of **non-separation processes**.[3]

Formal differentiation of separation and non-separation processes result from the characteristics of their product though the number of products is an additional criterion for most non-separation products: only one product occurs exclusively in case of non-separation products.

The criteria which qualify the technological operations into separation or non-separation groups can be presented as follows.

Let an operation be given in the result of which N products of qualitative characteristics sets $\{K_j\}$ – j = 1, 2, ..., N are obtained from the feed material of the $\{K_0\}$ qualitative characteristics set. In such a product k exists ($1 \leq k \leq N$) when $\{K_k\} \neq \{K_{j\neq k}\}$ at least for one $j \neq k$, the operation is a **separation** one[4];
In the opposite case the operation is non-separation, then, additionally, if N > 1, then $\{K_k\} = \{K_0\}$ for every j (division operation)[5].

TECHNOLOGICAL EFFICIENCY OF OPERATIONS

Every technological process must have its goal. The determination of its technological efficiency is used to evaluate how much of this goal has been reached. For the basic group of mineral engineering processes it was assumed to determine the efficiency as a numerically balanced relation of really obtained process results to the results assumed, forecast or theoretically possible. The latter variant is generally assumed in general methods of efficiency calculations. The general definition of efficiency is as follows:

---

[3] it may appear amazing to include the division into non-separation processes but it results from the quoted condition of not differentiating the obtained products among themselves

[4] then most often $\{K_j\} \neq \{K_0\}$ at least for some values

[5] all these names concern elementary operations, many operations, especially the non-separation ones, occur simultaneously with others, when it is not taken into account at identification, mistakes may appear,

$$S = \frac{W_r}{W_0} \tag{1}$$

where:
W_r – the obtained result,
W_0 – the expected result (or more rarely, theoretically possible[6]).

Equation (1) is a general definition of efficiency. In technological applications only such cases are considered in which W_r and W_0 assume the strictly determined numerical values. In practice, multiplying the fraction in expression (1) by 100, the efficiency value, calculated in this way, is assumed to be a percentage evaluation of success in aiming at reaching the value W_0.

The position of separation operations, privileged in mineral engineering, (cf. Chapter 1) caused that so far the notion of technological efficiency (in abbreviation "efficiency") had been practically considered exclusively in relation to these operations. Various detailed requirements, concerning both shaping the process reevaluation, caused the origin of very many methods and useful means of such an evaluation. The literature contains literally hundreds of various proposals of formulas to calculate the efficiency of these operations in various variants of conditions and detailed requirements in relation to the performed evaluations (Verchovskij 1949, Barskij, Plaksin 1967; Barskij, Rubinštejn 1970; Sztaba 1983-2001, Stępiński 1961, Sztaba 2000a, 2000b, 2001, 2002 and the others). Depending on the basic evaluation criterion, these methods were formally ordered into a few basic groups:

- technological,
- statistical,
- economic,

but also:

- power engineering,
- thermodynamic,

and separating the approaches:

- statical and
- kinetic.

No such considerations have been made in relation to non-separation operations. This work is the first public presentation of an attempt to determine the method of evaluation of the efficiency of such operations. Only a part of them was presented during the lectures held by the author (Sztaba 1983-2001).

[6] considerations of assuming one or another level of reference – of a precise definition of the W_0 value – are not included in this paper

THE CONCEPTS OF EVALUATION OF EFFICIENCY OF A NON-SEPARATION OPERATION IN CRUSHING

Comminution (crushing and grinding) is a non-separation operation that occurs practically in all technological systems. Its general aim is, as it was said before, to decrease the grain sizes of the feed.

Additional detailed requirements can concern (in the order of increasing the requirements and the rate of complication).

- decreasing[7] the maximum grain size d_m[8] to the fixed value,
- transforming a certain part of the feed (exactly or limitingly: "at least" / "utmost") (of the yield γ) to the class of assumed grain size distribution – $d_1 \div d_2$ ($d_1 < d_2$),
- obtaining the comminution product of an assumed value of the average grain size[9] (D),
- obtaining the product of the fixed grain composition described by the grain composition function, for example the $\Phi(d)$ increasing function,
- obtaining the product of the fixed specific area (P),
- obtaining the product of the fixed grain shape, expressed by the dimensionless shape coefficient, for example the spherical coefficient (k_g)[10] (Sztaba 1983-2001).

Figure 1 represents the example of a draft of grain composition curves of comminution products:

- with t index – the planned ("theoretical") product,
- with r index – the real product, obtained as a result of the performed operation, which clearly go in different direction (strongly exaggerated on purpose).

Such curves, as it is known, fully characterize the grain composition of the grained material and allow us to read the data necessary for investigating this composition and for calculating the derivate values, such as specific area (in approximation depending on grain shapes) and others, depending on the grain size distribution (Sztaba 1983-2001).

The values read from the curves in Fig.1 will be used to present simple formulas for calculating the formerly given variants of determining the comminution efficiency.

It should be noted that comparing the values characterizing grain compositions has been the basic of description of comminution results by means of "comminution rates" for a long time (Budryk, Stępiński 1954) and these values are also obtained from the grain composition curves, in this case describing the grain size distribution of the feed

---

[7] all grain sizes are linear (mm), specific area m^{-1} (m^2/m^3)

[8] this value can be also determined as the grain size below which not 100 % material occurs but less, for example 80 % (then we speak about the eighty-percent grain – d_{80}) or, similarly, in general $d_{\%}$, (so-and-so) percent grain

[9] determined according to the method chosen from numerous possibilities (Sztaba 1983-2001)

[10] requirements concerning the grain shapes of the comminution product can be additionally developed and detailed similarly as those concerning the grain size distribution.

and operation product. Therefore the majority of formulas used to calculate the effectiveness are of the form similar to the formula for comminution rates. The simplicity of these approaches and forms of formulas allows us to see these analogies without an additional commentary.

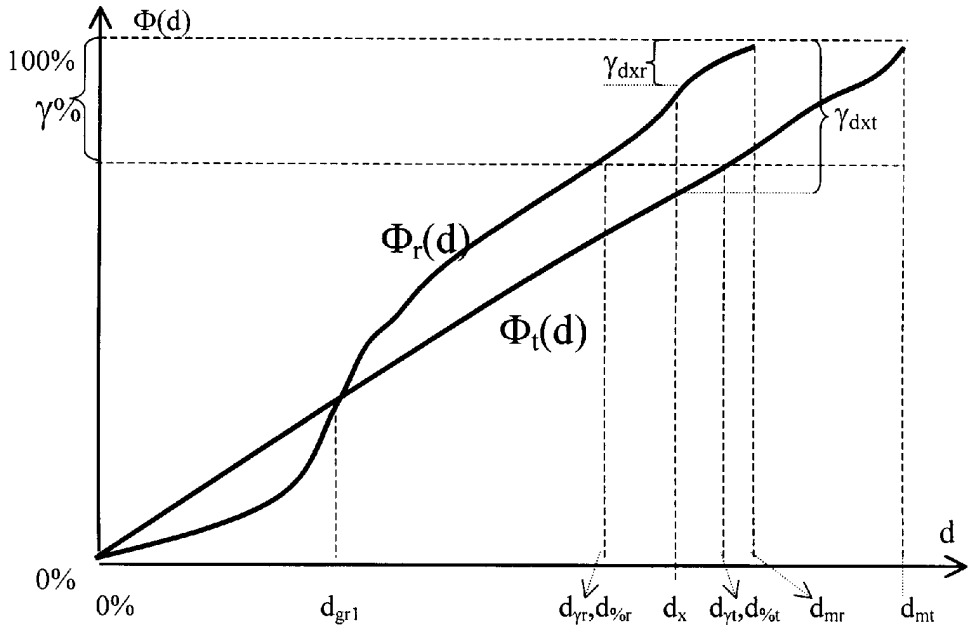

Fig. 1.

a) in case of requiring the fixed value of maximum grain or percent gran:

$$S_m = \frac{d_{mr}}{d_{mt}} \cdot (100\%) \tag{2.1}$$

$$S_{\%} = \frac{d_{\%r}}{d_{\%t}} \cdot (100\%) \tag{2.2}$$

Whereas it is also possible to use class limits of a selected yield γ ($d_{\gamma r}$ and $d_{\gamma t}$), they overlap with $d_{\%r}$ and $d_{\%t}$ on the graph.

b) in case of requiring the fixed content in the product of grains of the determined grain class, here, as an example, the classes of grain size distribution > d_x ($d_x < d \leq d_m$)[11]

[11] Assuming the markings < and ≤ results from the way of defining the grain class limits, cf. for instance (Sztaba 1961, 1983-2001)

$$S_{\gamma} = \frac{\gamma_{d_x r}}{\gamma_{d_x t}} \cdot (100\%) \tag{3}$$

c) in case of requiring the fixed value of specific area of the comminution product (most often in case of grinding):

$$S_P = \frac{P_r}{P_t} \cdot (100\%) \tag{4}$$

d) analogically in the case of the assumed average grain size in the product:

$$S_D = \frac{D_r}{D_t} \cdot (100\%) \tag{5}$$

e) if the requirements concern the full characteristics of the grain size distribution (obtaining a product of the assumed course of the function of grain composition ($\Phi(d)$), the effectiveness, i.e. the rate of compability of the obtained composition with the assumed one, can be estimated, for example, according to the average distance of the grain composition curves in question (its value will be expressed in the units of the Y-axis scale – the $\Phi(d)$ axis:

$$S_{\Phi} = \frac{1}{d_{mt}} \cdot \int_0^{d_{mt}} \left| \Phi_r(z) - \Phi_t(z) \right| \cdot dz \tag{6.1}$$

if the analogical forms the Φ (d) function are known , or

$$S_{\Phi} = \frac{1}{d_{mt}} \cdot \sum_{i=1}^{n} \left| \Phi_r(d_i) - \Phi_t(d_i) \right| \cdot (d_{i2} - d_{i1}) \tag{6.2}$$

if at disposal there are only data of the grain composition in the table or graphic form.

In this case d_1 and d_2 are the boundaries – upper and lower – of the summed classes (grain size ranges) of the representative grain size d_i, whereas n – is the number of the selected ranges of summing while it is their current numeration. It can be observed that the more precise the result will be, the denser are the points d_i selected. High accuracy can be provided[12] by a direct measurement of the surface area contained between the $\Phi_r(d)$ and $\Phi_t(d)$ curves which are determined by the integral in equation (6.1) or the sum in equation (6.2). The measurement, of course, should be executed by fragments determined by the points of intersection of both curves, limiting the fragments of the discussed area , in the graph there is, for instance, one

[12] depending, of course, on the assumed method of measurement and the way of its execution

"boundary" point d_{gr1}, or along the sections of both curves, constituting the envelope of measured surface, and not in the continuous way, along both lines respectively (absolute value of this area is needed).

THE BASES OF DETERMINING THE EFFECTIVENESS OF OTHER NON-SEPARATION OPERATIONS

EFFECTIVENESS OF LUMPING

The aim of lumping is as a rule to obtain a product which is not only caked (and in the case of agglomerations and some applications of pelletizing, also over-reacted to a certain degree), but also included in the fixed grain class. Briquetting in the full-matrix presses (roll and punch ones) corresponds best this requirement, most difficult it is in agglomeration whose raw product, sinter, is subjected to crushing. Assuming that quantitively the operation goes correctly (possible mistakes may occur only in agglomerating), the yield of the required product grain class can be treated as lumping effectiveness:

$$S_{kaw} = \gamma_{prod} \tag{7.1}$$

while the yield of the required class – γ_{prod} – is usually given in percent values. If the production plan predicts making a few classes, for instance provided for different aims (different grain classes of lightweight aggregates, etc., the γ_{prod} value is the sum of planned and obtained[13] production of all such classes. A simple recording of formula (7.1) assumes that the entire bulk (100%) of the material is the W_0 value (formula (1)). This can be only assumed, for instance, in case of briquetting. For other processes it is known in general what are the real boundary quantitative possibilities of obtaining a "good" product from the processed feed ($W_{gran} < 100\%$). In these cases it is plansible to calculate the effectiveness:

$$S_{kaw} = \frac{\gamma_{prod}}{W_{gran}} \cdot (100\%) \tag{7.2}$$

It can be easily noticed that assuming the W_{gran} value has the same logical represcutation as the assumption of the meaning of the expected value instead of the theoretically obtainable value, as it was shown when discussing formula (1) in chapter 2.

[13] this formulation means that it c be counted as a "successful" operation of the formed surpluses of one of classes providing it can be subject to another application, or, for instance, additional

EFFECTIVENESS OF DIVISION AND AVERAGING

For both operations it is assumed that the obtained products will not differ qualitatively from the input product (feed), nor among themselves ($\{K_{0,1,2,...,N}\}$ = const), while:

- in the division operation we obtain physically separated products which must additionally meet other requirements:
  - in case of division into, for example, parallel technological streams, a similar value of yields of these streams ($\gamma_{1,2,...N}$=const=γ_0 (100%/N))[14] is an additional requirement,
  - in case of sampling, the requirement {K} = const can be limited if the samples are collected only to test one or several material features, not sufficing its full characteristics (including technological) requirement concerns then only the material properties taken into consideration in the test; it cannot be limited when taking a general sample whose characteristics of the tested material – general population (Poradnik 1976; Sztaba 1983-2001, 1988),
  - in the averaging operation no physically separated products are obtained; effectiveness is determined under the same assumption as the one at the beginning of this subchapter; jointly for division and averaging, but the material is subareas into which the entire area (tank, dump, means of transport), occupied by the considered material can be divided in assumed to constitute conventional "products". Separating these subareas, and practically the representative testing spots of interesting properties, occurs most often together with the assumption of regular grid of points of sampling, treated as representative for these areas (Sztaba 1983-2001, 2000a and others). Similarly as in sampling, in averaging limited ranges of properties {K} can be assumed, which are considered execution of the operation and determining its effectiveness, depending on the fixed detailed goals of this operation (resulting from market demands, conditioning of respective technological operations, etc.).

In all the cases of subchapter 4.2. the effectiveness is determined according to obtained homogeneity of property sets {K} (at the division, additionally the homogeneity of sets of division product yields). This enables the well-known dispersion dimensions to be applied to estimate this effectiveness, most often:

- average deviation

[14] practically, it is not possible to obtain the yields of product streams of exactly equal values, a certain permissible level of tolerance of deviations should be assumed, for instance analogically to the determination of representativeness of samples (Poradnik 1976, Sztaba 1983-2001)

$$S_s = \frac{\sum_i |x_i - E(x)|}{n} \tag{8}$$

– standard deviation

$$S_d = \sigma = \sqrt{\frac{\sum_i (x_i - E(x))^2}{n-1}} \tag{9}$$

[15]

or others,
where:
x – value which is the evaluation basis
E(x) – average value of value x,
meanings of symbols "i" and "n" were assumed as in formula (6.2) with the appropriate change of action objects.

The large practical significance of the averaging operations, sampling sample preparation contributed to the origin of large basis works, methodological works and directly utilisation papers, concerning these operations. The remarks in chapter 4.2 can be treated only as an outline of initial assumptions which are made in these works and a broader discussion of these problems here would not be purposeful. Nevertheless, mentioning their effectiveness as the operations clearly belonging to the non-separation group as it is meant in chapter 1 seemed to be necessary to stress the consistency of the set of general features of such operations despite their differentiated specifications and various practical applications. Due to it we can talk about the grounds of a general system of determining the effectiveness of such operations, adapting the general rule of effectiveness evaluation to their characteristics formulated according to formula (1) and its discussion.

The paper was written in 2001 in the confines of the research of Department of Mineral Processing, Environment Protection and Waste Utilisation of UMM in Cracow, contract no 10.10.100.660 and the implementation in 2001 of a part of the project no 9 T12A 032 19, *Elaborating the systems of identification and evaluation of properties of mineral raw materials and their processing with special respect paid to the conditions of complex utilisation*, financed by the Polish Committee of Scientific Research.

[15] as it is known, when the value n is sufficiently large, n-1 can be replaced by n in the denominator

REFERENCES

Л. А. БАРСКИЙ, И. Н. ПЛАКСИН (1967) *Критерии оптимизации разделительных процессов* (Criteria of Optimization of Separation Processes), Москва, „Наука" 1967.

БАРСКИЙ, Л. А., РУБИНШТЕЙН Ю. Б. (1970), *Кибернетические методы в обогащении полезных ископаемых* (Cybernetic Methods in Mineral Processing)– Москва, „Недра".

BUDRYK, W., STĘPIŃSKI, W. (1954), *Teoria przeróbki mechanicznej kopalin cz. 1 (Theory of Mechanical Processing of Minerals part 1)* – Akademia Górniczo-Hutnicza w Krakowie – PWN, Skrypty dla szkół wyższych – Kraków.

Poradnik Górnika, Wyd. 2., t. 5 (Miner's Manual, 2nd iss., 5th vol.) (1976), Wydawnictwo „Śląsk", Katowice.

STĘPIŃSKI, W. (1961), *Ekonomika procesów wzbogacania rud i węgli (Economics of Ores and Coals Enrichment Processes)* – Wydawnictwo Górniczo-Hutnicze, Katowice.

SZTABA, K. (1961), *Przyczynek do zagadnienia określania wielkości ziarna mineralnego (Contribution to the Problem of Determining the Size of a Mineral Grain)* – Przegląd Naukowo-Techniczny AGH nr 9, seria „G" z.6., s.63-73.

SZTABA, K (1983-2001), *Kontrola procesów technologicznych; działy*: *pobieranie próbek* oraz *ocena skuteczności procesów technologicznych* (Controlling of Technological Processes, parts: S*ampling* and *Evaluation of Efficiency of Technological Processes*) – wykłady dla studentów Wydziału Górniczego AGH – specjalności „przeróbka kopalin stałych", Kraków – nie publikowane.

SZTABA, K. (1988), *Określenie własności technologicznych kopaliny jako ważny element dokumentacji złoża i podstawa wyodrębniania typów surowca (Determining the Technological Properties of a Mineral as an Important Element of Deposit Documentation and Basis of Selection of Mineral Types) - Materiały* Seminarium „Metodyka rozpoznawania i dokumentowania złóż kopalin stałych" - Bierutowice 1988, AGH IHiGI - Zakład Geologii Górniczej - Przedsiębiorstwo Geologiczne we Wrocławiu - Zakład Podstaw Gospodarki Surowcami Mineralnymi i Energią PAN - Komisja Zasobów Kopalin, Wydawnictwo AGH, Kraków, s.42-53.

SZTABA, K. S. (2000a), *Evaluation of the Effectiveness of Separation Processes according to the Obtained Feed-Segregation Rate* – Proceedings of the XXI International Mineral Processing Congress, Rome, Italy July 23-27, 2000, Elsevier Science B.V. Amsterdam, Vol.A, s.A7-1-7.

SZTABA, K. St. (2000b) – *Описание и оценка многопродуктовых технологических операций в технологии минералов* (Description and Evaluation of Multi-product Technological Operations in Mineral Technology) **–** *Тезисы докладов юбилейных „Плаксинских Чтений"*: „Развитие идей И. Н. Плаксина в области обогащения полезных ископаемых и гидрометаллургии", Москва 10-14 октября 2000 г. s.103.

SZTABA, K. S. (2001) – *Koncepcje oceny wieloproduktowych procesów rozdzielczych* (Concepts of Evaluation of Multi-product Separation Processes) **–** VI Międzynarodowa Konferencja Przeróbki Rud Metali Nieżelaznych (ICNOP '2001), Instytut Metali Nieżelaznych – Gliwice, KGHM „Polska Miedź" S.A., CBPM „Cuprum" Sp. z o. o., Szklarska Poręba 16-18.05.2001 r., *Streszczenia*: s.1-2, pełny tekst: *Materiały konferencyjne*: s.1-19.

SZTABA, K. S. (2002), *Concepts of the Evaluation of Multi-product Separation Processes of Mineral Engineering* – Archives of Mining Sciences (Archiwum Górnictwa) PAN, r. 47, z.1, str.51-67

ВЕРХОВСКИЙ, М. (1949), *Основы проектирования и оценки процессов обогащения полезных ископаемых* (Principles of Designing and Estimation of Mineral Processing) – Углетехиздат, Москва.

Sztaba K.St., *Skuteczność procesów nierozdzielczych w inżynierii mineralnej*, Fizykochemiczne Problemy Mineralurgii, 36, (2002) 135-146 (w jęz. ang.)

Zdecydowaną większość operacji technologicznych inżynierii mineralnej (w szczególności przeróbki surowców mineralnych) stanowią operacje rozdzielcze, w których otrzymuje się dwa lub więcej produktów, różniących się wartością określonej właściwości, będącej cechą rozdziału. Należą do nich wszystkie operacje wzbogacania, klasyfikacji ziarnowej, odwadniania itp. Określanie i ocena skuteczności (efektywności) technologicznej takich procesów są przedmiotem bardzo licznych zwłaszcza metodycznych opracowań procedur kontrolnych oraz są powszechnie stosowane w przemyśle i doświadczalnictwie. Poza takimi operacjami istnieją jeszcze takie, których zadaniem jest (z reguły) zmiana postaci rzadziej innych właściwości materiału, bez wydzielania z niego określonych części o wyróżnionych właściwościach. Należą do nich: przede wszystkim rozdrabnianie, a także kawałkowanie oraz dzielenie, którego specyficznym rodzajem jest pobieranie próbek. Operacje te mają istotne, aczkolwiek wzajemnie nieporównywalne co do rangi, znaczenie dla procesów przeróbki. Tymczasem problem oceny ich skuteczności właściwie nie istnieje w literaturze przedmiotu, ani w szerszych zastosowaniach praktycznych. Zarys tej problematyki był jedynie treścią fragmentu wykładów z przedmiotu *kontrola procesów technologicznych*, prowadzonych przez autora od kilkudziesięciu lat dla studentów specjalności Przeróbka Kopalin Stałych na Wydziale Górniczym AGH w Krakowie. Celem niniejszego opracowania jest przedstawienie koncepcji określania tytułowej skuteczności technologicznej takich operacji. Przedstawia się różne warianty zasad jej definiowania i metod otrzymywania wyników ilościowych, a także ich doboru do założonych celów kontrolnych.

Physicochemical Problems of Mineral Processing, 36 (2002) 147-157
Fizykochemiczne Problemy Mineralurgii, 36 (2002) 147-157

Tomasz DYR, Piotr WODZIŃSKI*

MODEL PARTICLE VELOCITY ON A VIBRATING SURFACE

Received March 15, 2002; reviewed and accepted May 28, 2002

In mechanical processing of granular materials the basic process is screening, hence it is extremely important to have a well designed screen. A correctly determined real velocity at which material moves along the screen surface is a prerequisite of designing a screen. The authors made an attempt to develop a new method for determination of the velocity of a granular layer moving on the vibrating surfaces of sieves or oscillating conveyors. The method is based on an analytical description of phases of the model particle movement, and next on an empirical correction made for the layer. The particle velocity is determined on the edges of subsequent phases of the movement, hence the name "a phase method". The authors present preliminary results of investigations whose aim was to verify the existing models and to determine an empirical correction with respect to the impact of process variables.

Key words: particle material, screening, sieve, undersize, vibrating sieve, phase method

NOMENCLATURE

d - mean particle diameter [m],
g - acceleration of gravity [m/s^2],
H_p - initial height of the layer [m],
m - mass [g],
n - frequency of vibrations [1/s],
r - radius of the crank of the screen driving gear [m],
A_0 - amplitude of sieve vibrations [m],
t - time [s],
T - screen operating period [s],
K - dynamic factor [-],
u_m - mean velocity of material [m/s],
w - moisture content [%],

* Łódź Technical University, Faculty of Process and Environmental Engineering, Department of Process Equipment, ul. Stefanowskiego 12/16, 90-924 Łódź

α - angle of sieve inclination between the sieve plane and horizontal plane [1°],
β - angle of sieve trajectory between tangent of the initial sieve movement and sieve plane [1°],
φ - angle of crank rotation calculated from conventional position 0 [1°],
φ_0 - angle of crank rotation at which particles fall onto the sieve [1°],
μ_s - coefficient of static friction of particles against the sieve [-],
μ_z - coefficient of static friction of particle against a particle [-],
ω - angular frequency of the drive [1/s],
l - mesh size [m].

INTRODUCTION

Screening is the main process in granular material processing. The most frequent screening method is to feed material onto the sieve, and then to transport it along the sieve surface during which the feed is segregated into the oversize and undersize class.

The authors decided to investigate the movement of a granular layer moving along the screen surface, and the movement of the trough of an oscillating conveyor, because also here the mechanisms of material transport are the same. A basis for a description of the granular layer movement on the vibrating surface is a phase diagram of model particle movement. Such diagrams were proposed by several researchers, e.g. Dietrych (1962), Czubak (1964) and Olewski (1955) (cf. Fig. 1). When analysing diagrams presented in Fig. 1 we can observe some differences in particular phases of the movement. These differences were also noted by Błasiński and Wodziński who decided to verify experimentally which of the proposed diagrams were most accurate. The investigations were carried out using a multi-speed camera at 3000 frames/s. A screen with linear horizontal movement and a sieve inclined to the level were used. The screen reached the dynamic factor $K_{max} = 6$, and the investigations were carried out for the dynamic factor ranging from 1 to 4. A particle was a metal ball whose movement was filmed. From analysis of the image obtained it was concluded that the most realistic diagram appeared to be the one proposed by Dietrych. On this basis the velocity of model particle movement was determined for one cycle of screen operation. It was determined as a weighted average from mean velocities in subsequent phases of the particle movement, hence the name of this method is the "phase method".

Because so far the investigations had been carried out with a metal ball used as a model particle, the authors decided to repeat the experiments using balls produced from a different material as model particles and to analyse results again. An important element of almost all solutions is the assumption that particles fall onto the sieve surface in an inelastic way. So, it follows that a particle which is a model of a layer, should behave as a layer. During the fall of the layer onto the vibrating surface the energy transmitted by the surface to the layer is dispersed in the bed, so the layer does not rebound from the surface. This means that the coefficient of layer restitution is 0

and the coefficient of restitution of particles should be also equal to 0. The restitution coefficient of a metal ball is different than 0, hence it is not a reliable model of the layer. In our investigations either plasticine balls or a sand bag was used. It should be borne in mind that in real industrial conditions, the role of particles is played by the whole layer on the sieve which has the above mentioned properties.

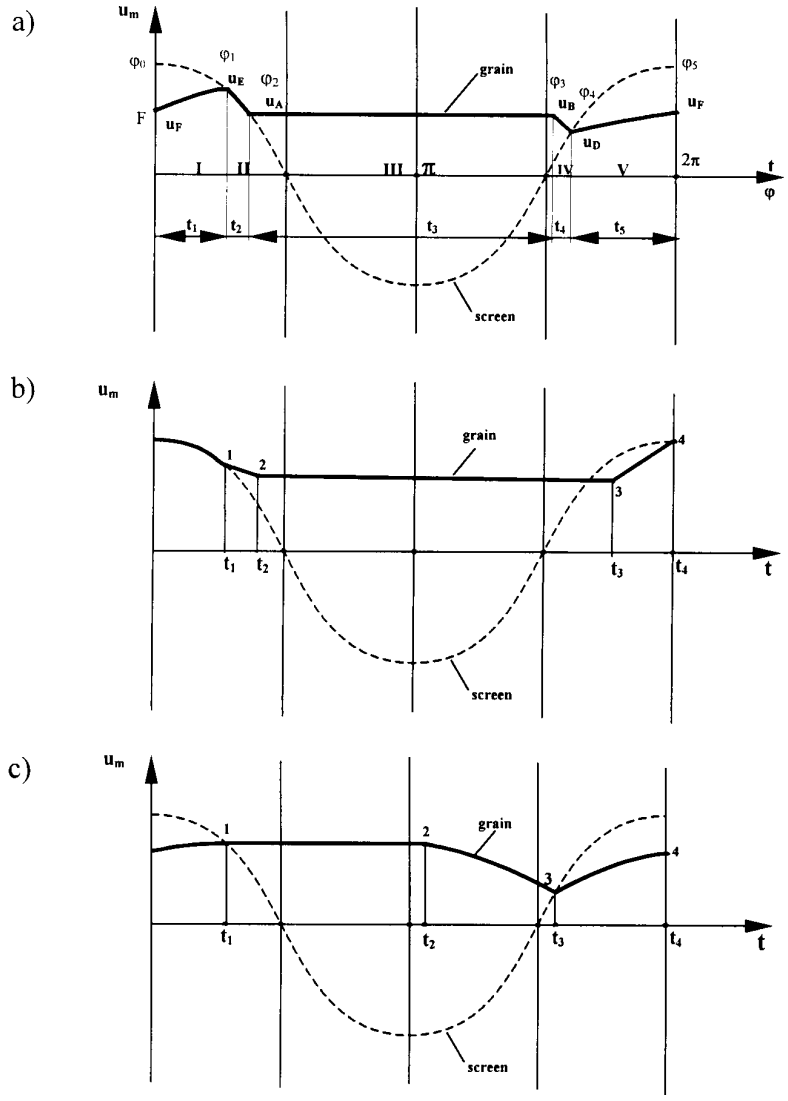

Fig. 1. Dependence of particle and sieve velocity on time
a) according to Dietrych, b) according to Czubak; c) according to Olewski

THE PHASE METHOD FOR DETERMINATION OF FEED VELOCITY ALONG THE SIEVE

A condition which must be satisfied to make the process of screening proceed, is the motion of particles against the sieve. This motion is induced by inertia forces from the machine drive which act on the layer (particles). Depending on the motion of a riddle, material on the sieve may slide on the surface, fly over it or move at a velocity equal to that of the surface, i.e. rest on it. The present screen designs force a resultant motion of the layer, i.e. such a motion where all mentioned types of motion occur.

As it has been mentioned already, many researchers (Dietrych, Czubak, Olewski) tried to describe the motion of a granular layer on a vibrating surface. Diagrams which they proposed (Fig. 1) illustrate particle motion describing all phases of the resultant motion, however equations proposed by them (equations (1), (2) and (3)) describe only the phase of flying.

Dietrych formula:

$$u_m = \frac{g \cdot cos(\beta - \alpha)}{\omega \cdot sin\,\beta} \sqrt{\frac{K-1}{2}(K^2 - 1)} \tag{1}$$

where K is the dynamic factor determined by the equation:

$$K = \frac{A_0 \cdot \omega^2 \cdot sin\,\beta}{g \cdot cos\,\alpha} \tag{2}$$

Czubak formula:

$$u_m = \xi \cdot \frac{g \cdot k \cdot m}{p \cdot n \cdot 2} \cdot (cos\,\alpha \cdot ctg\,\beta - sin\,\alpha) \tag{3}$$

where ξ – refers to the effect of such phenomena as different velocity of a material on different depths of the layer; k is the ratio of the time of particle free flight to the trough vibration period; p is the prime integer greater than or equal to k, when the latter is an integer.

Olewski formula

$$u_m = K_\sigma \cdot N \cdot \frac{n^2 \cdot r}{g} \cdot \left(1 + 22 \cdot tg^{3/2}\,\alpha\right) \cdot \left(\frac{\alpha}{18°}\right) \tag{4}$$

In 1979 Błasiński and Wodziński developed a new method for determination of particle velocity on the sieve, which referred to all phases of motion. As it has been mentioned already, the investigations carried out by these researchers led to the conclusion that among the proposed diagrams which describe particle motion, the most realistic is the diagram proposed by Dietrych (Fig. 1. a). Five phases can be

distinguished. A velocity in each phase of the motion is a logarithmic mean from two velocities at the extremes of each phase (formulae (5) through (8)).

$$u_F = u_D + \left(\frac{2 \cdot \pi \cdot g}{\omega} - \frac{\varphi_4 \cdot g}{\omega} \right) \cdot (\mu_s \cdot cos\,\alpha - sin\,\alpha) - (\mu_s \cdot sin\,\beta + cos\,\beta) \cdot r \cdot sin\,\varphi_4 \tag{5}$$

$$u_E = \frac{\omega \cdot r \cdot sin\,\varphi_1 \cdot cos\,\beta}{cos\,\alpha} \tag{6}$$

$$u_A = u_B = A_0 \cdot \omega \cdot \sqrt{1 - \frac{1}{K^2}} \tag{7}$$

$$u_D = \omega \cdot r \cdot cos\,\varphi_4 \cdot cos\,\beta \cdot cos\,\alpha \tag{8}$$

Having the mean velocities and duration of each phase, one can determine the mean particle velocity on a sieve as a weighted mean of these velocities; the weight is here the duration of each phase, formula (9):

$$u_m = \frac{\frac{u_E - u_F}{ln(u_E / u_F)} \cdot t_1 + \frac{u_E - u_A}{ln(u_E / u_A)} \cdot t_2 + u_B \cdot t_3 + \frac{u_A - u_D}{ln(u_A / u_D)} \cdot t_4 + \frac{u_D - u_F}{ln(u_D / u_F)} \cdot t_5}{T} \tag{9}$$

where:

$$T = t_1 + t_2 + t_3 + t_4 + t_5 \tag{10}$$

is the screen operation period.

The phase method of velocity determination was developed on the basis of the movement of a single model particle which in this case was a metal ball. The authors are of the opinion that the application of metal balls as model particles is dubious, so they decided to approach the subject again after some years using model particles prepared from a different material, whose restitution coefficient would be close to zero. Next part of this paper will refer to the experimental set-up and results obtained by the authors recently.

EXPERIMENTAL SET-UP AND METHOD

Experiments were carried out on a linearly vibrating screen (Fig. 2) with an electromagnetic vibrator of the frequency of vibrations equal to 50 Hz and smoothly adjustable amplitude in the range from 0 to 2 mm. It was possible to adjust the angle of inclination of the screen to the level from 0° to 20° (the investigations were carried out in the range from 0° to 10°) and to control the inclination of the sieve in the range from 0° to 40° in relation to the riddle (the investigations were carried out in the range from 0° to 15°). The screen can attain the dynamic factor $K_{max} = 20$ (experiments were made at K = 8 to 15). The main elements of the screen are as follows:

1. – screen base,
2. – spring suspension,
3. – supporting structure,
4. – tested sieve,
5. – electromagnetic vibrator,
6. – charging hopper,
7. – flow control valve,
8. – vessel for oversize fraction,
9. – vessel for undersize fraction.

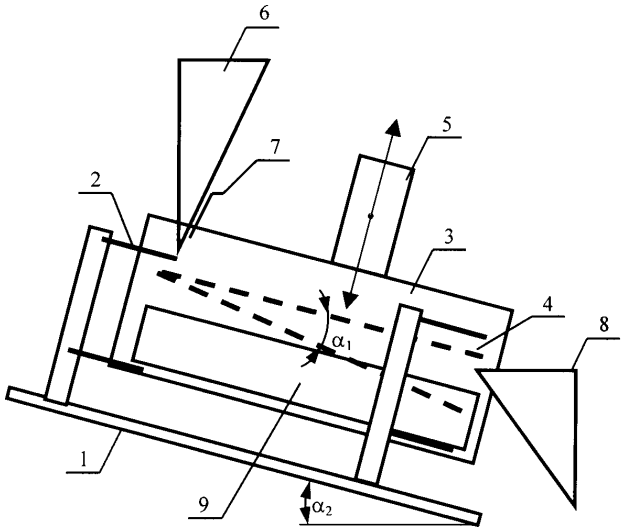

Fig. 2. Schematic diagram of the experimental screen

The model particles of spherical shape, 5 mm in diameter, were made from coloured plasticine. The choice of material was determined by material properties during rebound. It was justified to use a material with possibly small restitution coefficient because such particles as a model of the layer, should have the restitution coefficient equal to 0.

To record particle motion, a digital multi-speed camera with a PCI card and software supplied by Redlake Imaging Corporation was used. The camera made colour photos at the speed of 500 frames/s, shutter time 1/1500 s. The recorded image had the resolution 320×280 pixels. The investigation consisted in filming a fragment of the vibrating surface with particles moving on it. A schematic diagram of the experimental set-up is shown in Fig. 3.

Particles were supplied to the vibrating surface about 200 mm before the region of filming, which was 250 mm. Particles moved against the riddle edge with the scale 10 × 10 mm (cf. Fig. 4). Additionally, on the riddle frame two points at a distance of 178 mm from one another were marked.

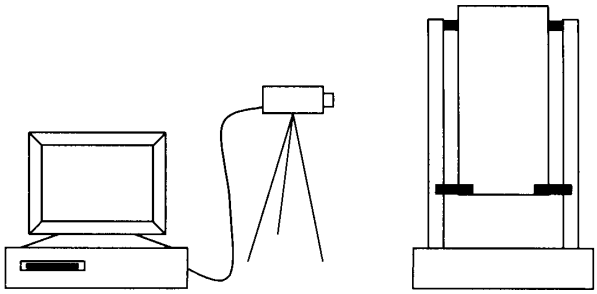

Fig. 3. Schematic diagram of the experimental set-up

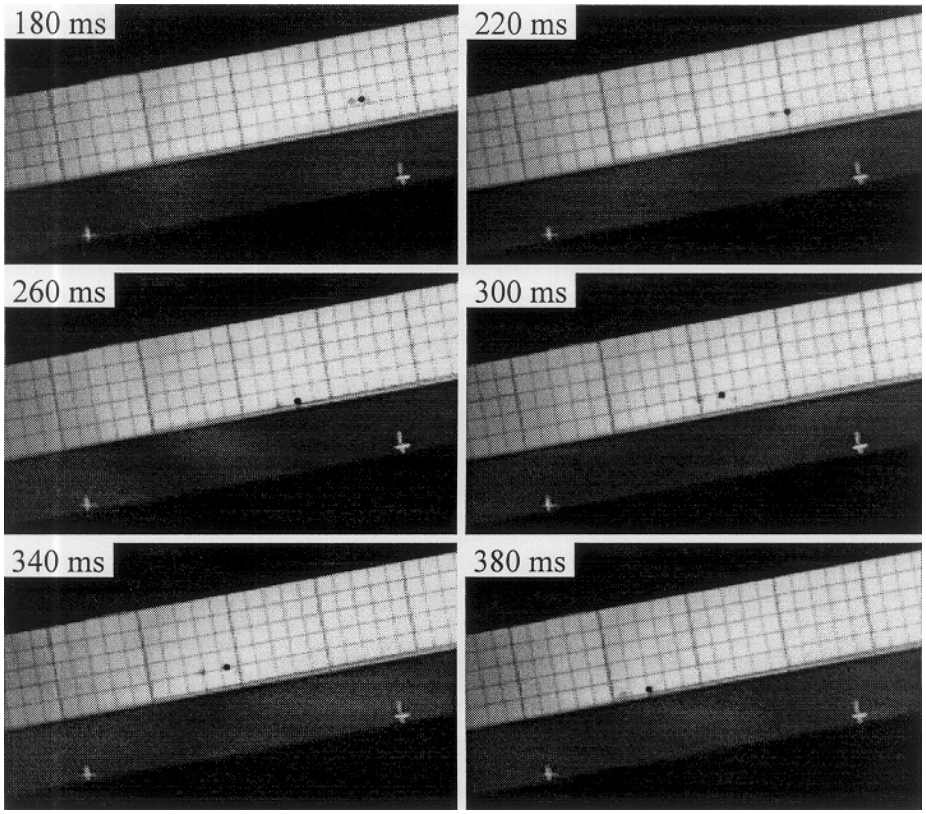

Fig. 4. Examples of the frames representing the system set-up:
$\alpha_1 = 10°$; $\alpha_2 = 0°$; A = 1.15 mm

After having filmed the particle motion, the image was analysed using a special software provided along with the camera. Data concerning the position, transfer and velocity were read to a file and then analysed by generally available programs. Results are presented in a graphical form.

RESULTS AND DISCUSSION

When considering the process, the authors drew a conclusion that the most appropriate reference system would be such one in which the axis of abscissae would be in the plane of the vibrating surface and would be directed towards the layer motion, while the axis of ordinates would be perpendicular to the surface (cf. Fig. 5). The proposed reference system reflects material motion against the vibrating surface.

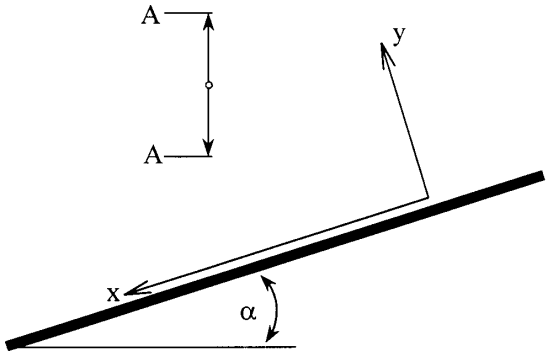

Fig. 5. Schematic diagram of the location of coordinate system vs. vibrating surface

Results presented in this study provide examples of a system with the following parameters: $\alpha_1 = 10°$, $\alpha_2 = 0°$, A = 1.15 mm (Figs. 6 and 7) at the dynamic factor K = 12.

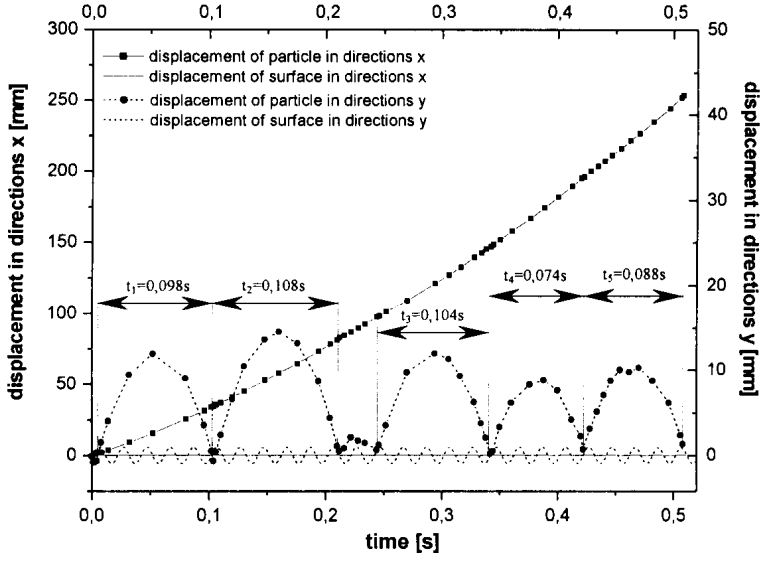

Fig. 6. Displacement of particles parallel to (x) and perpendicular to (y)

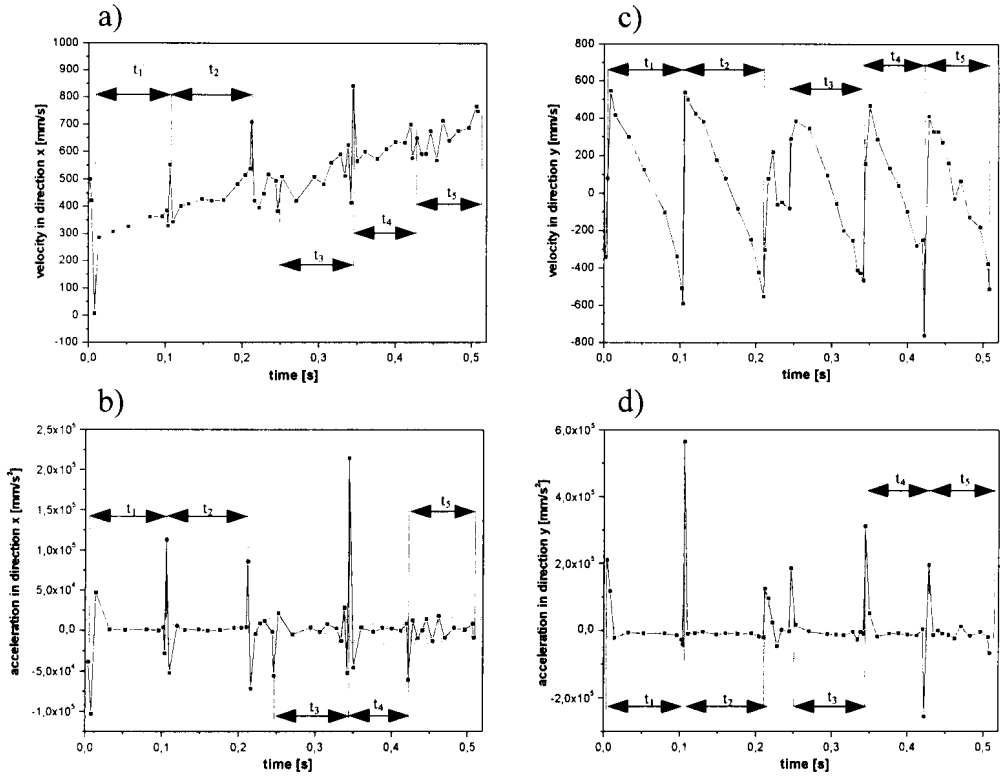

Fig. 7. Dependence of particle and surface velocity and acceleration parallel to (a, b) and perpendicular to (c, d)

Figure 6 shows a diagram of the displacement of particles and the surface in directions x and y. To better illustrate the particle trajectory in particular phases, both displacement compounds are mapped on one diagram. As the amplitude of the system vibrations in direction x is very small (in the example presented it is A_x= 0.17 mm) it is not possible to show in one diagram the dislocations of particles and the surface, so the dislocation of the surface in direction x is represented by a straight line in the diagram.

When analysing the diagrams of dislocation velocity, the authors observed some regularities:

– in the moment when particles collided with the surface, in many cases the acceleration decreased below 0 (braking occurred);
– the peak of acceleration corresponded to the point of particle detachment in the displacement diagram;
– next, the acceleration decreased to zero and was maintained so until the next contact with the surface.

It can be concluded from the above that despite elasticity of the particle rebound, there are elements of phase motion which were discussed above.

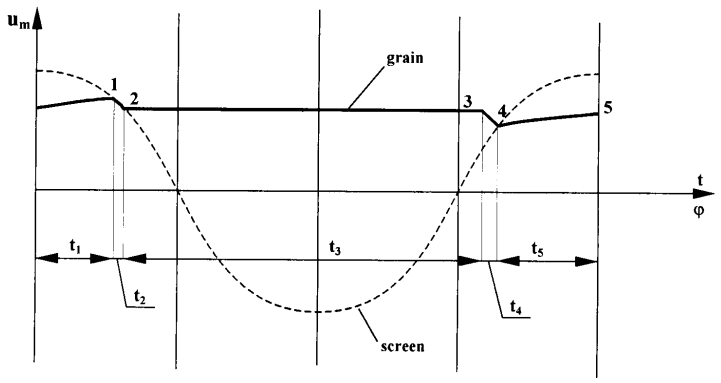

Fig. 8. Proposed diagram of particle motion along a vibrating surface

Figure 8 shows a diagram proposed by the authors to describe the particle trajectory during one of the periods of screen operation. This occurs when the screen works at a low value of the dynamic factor, i.e. K = 3 to 4.

The proposed diagram is based on the research carried out so far. It resembles a diagram proposed by Dietrych (Fig. 1a), however, the authors are of the opinion that the time of contact between the particles (t_2 and t_4 in Fig. 8) with the screen surface is much shorter than that proposed by Dietrych.

CONCLUSIONS

Results presented in this paper are an introduction to a research whose aim is to develop a new method for calculation of material velocity on a sieve – a phase method. The authors realise that model particles do not satisfy the assumption of non-elastic rebound and they will make experiments with particles of other materials.

It is true that the tested model particles are not characterised by a dynamic factor equal to 0 and the fall to the vibrating surface is elastic. However, such properties are characteristic of the particles of real granular materials which are screened in industry. Only thick granular beds encountered in thick-layer screening specific for fine- and very fine granular materials, can approach ideal conditions because only in such conditions the rebound does not occur.

Experiments will be also carried out with other configurations of the screen described in this paper, and on a circular motion screen. Results of investigation of model particle motion will be verified using the coefficients obtained in the course of process investigations performed on the same screens and for the same process conditions using different types of aggregates.

REFERENCES

БЕЛЕЦКИЙ В.А. (1949), *Теория и расчет просеивателей с прямолинейными качаниями*, Заготидат, Москва

BŁASIŃSKI H., WODZIŃSKI P.: *Metoda korekcyjna wyznaczania prędkości średniej materiałów ziarnistych na sitach przesiewaczy o ruchu liniowym*. Z.N. P.Ł., Inż. Chem., No 10/1979.

BUDRYK W. (1974), *Przeróbka mechaniczna użytecznych ciał kopalnych*, Kraków.

CZUBAK A. (1964), *Przenośniki wibracyjne*, Śląsk, Katowice.

DIETRYCH J. (1962) *Teoria i budowa przesiewaczy*, WGH. Katowice.

KLOCKKHAUS H. (1952), *Fördergeschwindigkeiten von Schwingrinnen*, Erdöl und Kohler, No. 8.

ОЛЕВСКИЙ Б.А. (1955), *Конструции и расчеты грозотов*, Металлургиздат, Москва

Dyr T., Wodziński T., *Prędkość ziarna modelowego na powierzchni drgającej*, Fizykochemiczne Problemy Mineralurgii, 36, (2002) 147-157 (w jęz. ang.*)*

W mechanicznym przerobie materiałów ziarnistych podstawowym procesem obróbki jest przesiewanie, zatem niezwykle ważne jest aby przesiewacz na którym odbywa się proces był poprawnie zaprojektowany. Właściwe określenie rzeczywistej prędkości z jaką porusza się materiał na powierzchni sitowej jest koniecznym warunkiem do zaprojektowania przesiewacza. Autorzy niniejszej pracy podjęli próbę opracowania nowej metody wyznaczania prędkości poruszającej się warstwy ziarnistej na powierzchni drgającej przesiewaczy lub przenośników wibracyjnych. Metoda ta opiera się na analitycznym opisie faz ruchu modelowego ziarna, a następnie empirycznej korekcji dla warstwy. Prędkość ziarna będzie wyznaczana na krańcach poszczególnych przedziałów (faz) ruchu, stąd nazwa „metoda fazowa". Omawiana praca prezentuje pierwsze wyniki badań mających na celu weryfikacje istniejących modeli i określenie empirycznej korekty uwzględniającej wpływ zmiennych procesu.

Physicochemical Problems of Mineral Processing, 36 (2002) 159-172
Fizykochemiczne Problemy Mineralurgii, 36 (2002) 159-172

Stefaan SIMONS, Damiano ROSSETTI, Michael SPYRIDOPOULOS,
Xavier PEPIN*

MICRO-STUDIES OF MINERAL PROCESSING FUNDAMENTALS

Received March 15, 2002; reviewed, accepted May 29, 2002

Since many mineral processes rely on the manipulation of interfacial properties, such as hydrophobocity, surface tension and wettability, there is a great deal of interest in being able to relate the micro-scale properties of the solid/fluid species to the macro-scale behaviour of the processes themselves. In order to develop this understanding, it is necessary to be able to directly measure and observe such properties, a task which can be non-trivial due to the conditions that can be encountered on the plant scale. Over several years, a range of unique devices, collectively known as Micro-Force Balances (MFBs), have been designed and constructed in the author's laboratory, which can measure and observe micro-scale interactions between solid particles in both gaseous and liquid media, at ambient and high temperatures. Mineral processing applications such as granulation, flotation and spherical agglomeration have been the subjects of studies to date. This paper presents an overview of the MFB designs and the significant findings in relation to these applications.

Key words: micro-manipulation, flotation, granulation, spherical agglomeration, separation

INTRODUCTION

Mineral processing general involves the separation and/or collection of solid particles of different species, either suspended in liquids or agitated in gaseous media. The design and operation of such multi-tonne processes have changed little over the last few decades. Dwindling mineral resources and high energy costs have focussed attention on improvements in process efficiency and the recovery of much finer mineral grades. There is a growing realisation that significant advances can be made in process design and operation by developing understanding, on a fundamental basis, of the interactions between the solid particles and the surrounding medium, be it gas or liquid.

The fundamental understanding of particulate and surface interactions requires sensitive instrumentation to provide direct measurements and observations. Atomic

*Colloid & Surface Engineering Group, Department of Chemical Engineering, University College London, Torrington Place, London WC1E 7JE, UK. Email: stefaan.simons@ucl.ac.uk

Force Microscopy can be used to measure surface properties arising from molecular-scale interactions, such as electrostatic forces and surface asperities. However it can prove difficult to use such devices to monitor directly the behaviour between particulate species in suspension, particularly at high temperatures. It is for this reason that a novel device, termed a Micro-Force Balance, was developed at UCL in order to measure and observe the interaction between particles held together by liquid binder bridges. These studies were in relation to granulation and spherical agglomeration processes (Simons and Fairbrother 2000; Pepin et al 2000a,b; Pepin et al. 2001; Rossetti and Simons 2002). Subsequently, three further devices have been constructed, using state-of-the-art technology and with higher force-displacement resolution than the prototype version, to study particulate interactions in flotation froths (Spyridopoulos and Simons 2002), high temperature fluidisation (Pagliai and Simons 2002) and crystallisation (Pratola et al. 2001). In this paper, the experimental set-ups and main findings of the granulation, flotation and spherical agglomeration work will be discussed.

GRANULATION STUDIES

Despite the wide spread use of granulation in minerals processing, pharmaceuticals, detergents, fertilisers and foodstuffs, the fundamental mechanisms governing granule growth and subsequent strength are not fully understood. Hence, mineral processors have taken an empirical approach to the operation of granulators, whilst pharmaceutical companies have taken a product formulation approach. Over the last ten years this has started to change and currently there is a large amount of research being carried out on granulation which can be considered to be divided into two areas; (i) relating particle and formulation properties such as binder viscosity and interfacial energy, particle size distributions, friction and plasticity, to the bulk agglomeration behaviour, and (ii) the incorporation of these relationships into process scale simulations. The work reported here investigated microlevel phenomena in relation to particle and binder properties with the overall aim of improving the understanding and control of macroscopic granulation processes.

MEASURING LIQUID BRIDGE PROPERTIES

The objective of the work was to develop the fundamental understanding of the role of the liquid and solid properties in the growth, consolidation and strength of granules, from the initial contact between the liquid and particles to the resultant multi-particle bodies. The strength of liquid bridges was measured using a novel Micro-Force Balance (MFB) described in detail elsewhere (Simons and Fairbrother 2000). In brief, a pair of micro-pipettes holds the particles in position, of which one is highly flexible (see Fig.1). Once a drop of binding liquid has been administered between them (using a third pipette), the movement of the pipette base as the particles

are pulled apart is monitored by sensitive position transducers, providing a direct measure of the applied force. A unique optical follower with a resolution of order 1nm monitors the much smaller movement of the pipette tip. The pipette tips can be submerged in an optically clear dish so that the surface effects in liquid media can be investigated (see below).

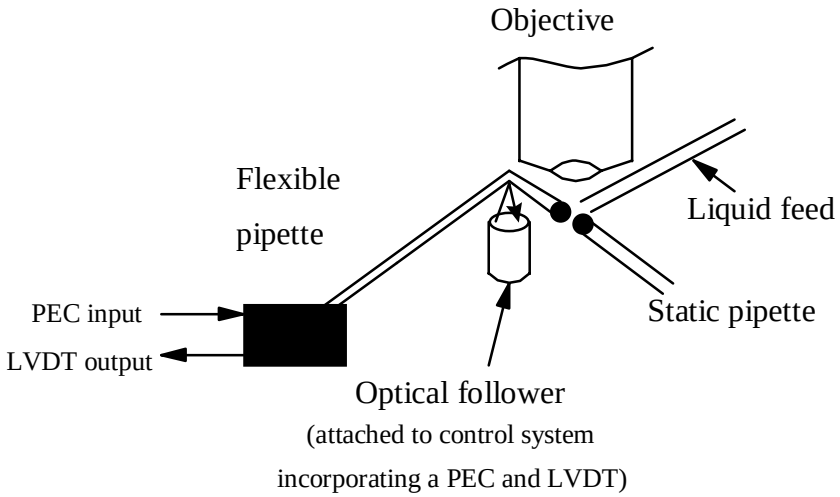

Fig. 1. Schematic of the micro-manipulation stage

The entire apparatus is PC controlled and, coupled with image analysis software, leads to accurate determination of liquid bridge dimensions and forces. For dynamic measurements, events separated in time by 0.1ms can be distinguished. In addition, the particles can be brought together, then separated, under (computer) controlled rates, by varying the voltage sent to the piezoelectric crystals in the position transducers. In this way, the dynamic nature of agglomeration processes can be studied.

In the work reported here, images of liquid bridges were sampled from a video recording of the rupture sequence. From the images, interparticle forces, separation velocity and interparticle distances were measured. When applicable, liquid volumes and liquid surfaces were also calculated from the 2D images using the parabolic approximations of the liquid bridge profiles (Pepin et al. 2000a,b). Such calculations are only valid for spherical particles.

GRANULE STRENGTH

Pellets of 18 mm diameter and 17 mm length were made from various spherical and non-spherical powders and moistened with silicon oils of increasing viscosity. The powders were: Sugar beads, Suglets 30-35 (SB1) and Suglets 250-355 (SB2), used as

a comparison to granules made of glass ballotini (GB) reported in (Iveson et al. 2001), a lactose DCL11 (L1), separated in three fractions (L1A), (L1B), (L1C), with 90 and 180-µm-mesh sieves, a lactose EFK sieved into coarse (L2) and fine (L3) fractions with a 100-µm-mesh sieve and a lactose 150 mesh (L4) (Pepin et al. 2001). Finally, a crystalline drug powder (DP) and Magnesium stearate NF-VG-1-726 (MGST), which exhibits low interparticle friction were also used. The liquid binders were: Silicone oils of increasing viscosity 9, 96, 971, 996 and 97920 mPa.s, water, a 0.2% w/w sodium dodecyl sulphate aqueous solution and aqueous solutions of hydroxypropylmethylcellulose and polyvinylpyrrolidone of increasing viscosity and varying surface tension.

The pellets were carefully retrieved from the die on a pre-tared microscope slide, weighed and then deformed radial to the cylinder axis between the two flat punches of an TAXt2® texture analyser (Stable Micro Systems). The upper punch was lowered onto the pellets at speeds of between 0.1 mm/s and 10 mm/s. From the weight of the pellet and a knowledge of its composition, the pellet solid and liquid volume fractions and porosity could be calculated. The slope of the force versus contact area curve was taken as the mass hardness.

RELATING LIQUID BRIDGE PROPERTIES TO GRANULE STRENGTH

The first step was to provide a more rigorous understanding of the effect of the liquid and solid properties on the shape of the liquid bridges and, hence, the strength. Liquid bridges were created on glass spheres and lactose using the silicone oils.

As is reported in (Pepin et al. 2000a), the investigations have shown that the rupture of liquid bridges occurs spontaneously at a certain interparticle distance and that two cases exist: One where the volume of liquid is fixed, that is when the three-phase contact line is observable on the particle surfaces during elongation, the second where there is no observable three-phase contact line and liquid covers the entire particle surfaces and the surrounding objects, creating liquid reservoirs outside the particles. The second case is observed when the bridging liquid perfectly wets the solid particles (advancing contact angle, θ_a = receding contact angle, $\theta_r = 0$). In this case, depending on the bridge elongation speed and viscosity of liquid binder, some liquid can move from the liquid reservoirs to the inter-particle gap and the liquid volume of the bridge can increase. In the former case, there is generally a noticeable contact angle hysteresis and the shape the bridge adopts depends on the wetting behaviour and the value of the three-phase contact angles (Pepin et al. 2000b). In Figure 2, two examples are shown. In Fig. 2(a), the liquid does not de-wet the particle surfaces during bridge elongation, the three-phase contact line is fixed. The shape then adjusts as the contact angles change with separation (in order for the constant volume condition to be met and $\theta_a > \theta > \theta_r$). In Fig. 2(b), the liquid de-wets the silanised particle and the contact angle on this particle remains relatively constant during separation ($\theta = \theta_a = \theta_r$) whereas the contact angle on the unsilanised particle, which

has a fixed three-phase contact line, does change ($\theta_a > \theta > \theta_r$). In the case where there is no observable three-phase contact line, the liquid perfectly wets the solid and the bridge shape remains torroidal throughout separation.

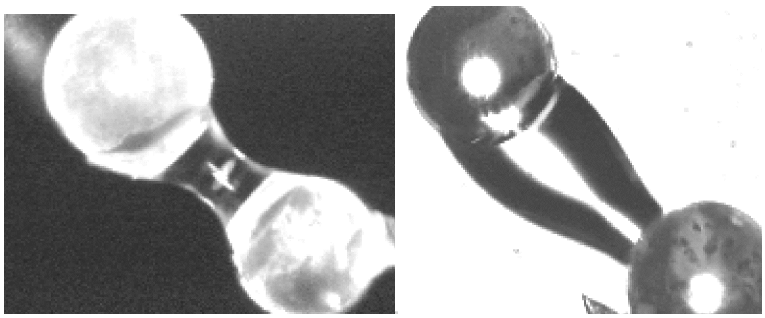

Fig. 2. Glycerol liquid bridges showing three-phase contact lines with glass spheres; (a) two non-silanised spheres (left, 126μm; right, 111μm), (b) left, unsilanised (118μm), right, silanised (125μm)

A parabolic model has been developed that predicts well the evolution of bridge shape with separation distance (Pepin et al. 2000a,b). The separation distance where rupture occurs can then be predicted by assuming that this occurs through the bridge's thinnest neck, y_{min}. This gives rise to an empirical expression for the bridge volume and the reduced hyrostatic pressure in the bridge caused by the bridge curvature. A three-term equation can then be derived for liquid bridge forces from contact through to rupture. With the assumption of glass spheres hard enough to sustain the surface tension and pressure forces of the liquid bridge, the normal force can be expressed as:

$$F_N = 2\pi y_{min}\gamma_{LV} + \Delta P_{neck}\pi y_{min}^2 + \frac{3\pi\eta v_i \bar{R}^2}{2H} \tag{1}$$

The first term is the capillary contribution, the second is that due to the reduced hydrostatic pressure, whilst the third is due to interparticle friction. H is the separation distance between the particles of average radius $\bar{R}$, v_i, the particle separation velocity, and η, the dynamic viscosity of the bridge liquid. This expression was shown to provide accurate predictions of the force when compared to those measured directly by the MFB, for both quasi-static and dynamic separations. The viscosity term becomes more dominant as the separation speed increases.

From the individual bridge strength model, an expression was derived, relating the hardness of granules to their porosity and liquid content (Simons et al. 2003):

$$\Omega_{calc} = \frac{1}{2}\left[\left(3\pi\bar{d}\eta v_i \times \frac{\varepsilon}{\phi_L}\right)\times\left(\frac{1}{\bar{v}}\right)^{2/3} + \left(2\pi y_{min}\gamma_{LV} + \gamma_{LV}(\cos\theta+1)\times\frac{A_{ab}}{H}\right)\times\left(\frac{c}{\bar{v}}\right)^{2/3}\right] \tag{2}$$

where $\bar{v}$ is the average particle volume, A_{AB} is the average solid-solid contact area between two solid particles in the wet agglomerate, ϕ_L is the liquid volume fraction, c is the co-ordination number (for spheres) and ε is the agglomerate voidage. The calculated hardness was plotted against the hardness measured for granules made up of the range of solid particles and liquids indicated above. From figure 3, it can be seen that agglomerates made from L1, L2, L3, L4, SB1, SB2, and DP exhibit measured hardness which can be predicted from the above equation. The hardness of agglomerates made from glass beads (Iveson et al. 2001) are also well predicted below 10^5 N.m^{-2}. Above this limit, which corresponds to capillary numbers (a measure of the strain rate suffered by the agglomerate) which exceed $7x10^{-2}$, the mass hardness is over estimated. Further work is required to address this anomaly, probably caused by the fact that dynamic forces are transmitted between layers throughout the agglomerate and, hence, liquid bridges cannot be considered in isolation.

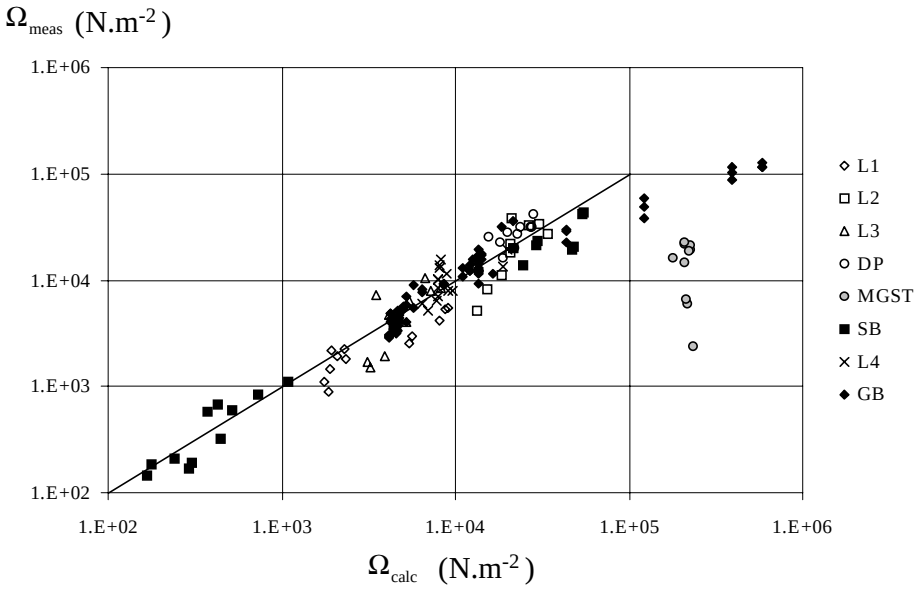

Fig.3. Measured versus calculated mass hardness (Simons et al. 2003)

The hardness of agglomerates made with magnesium stearate (MGST) is over estimated. The wet masses made from magnesium stearate had a low porosity and the liquid saturation of the pores created by the solid particles was close to 80%. These granules were therefore actually in the funicular saturation state, with the particles not in contact, but rather suspended in liquid with some air present. Hence, the model is not applicable. Further investigations on the measured mass hardness can be made by individually neglecting the capillary, friction and viscous elements of the three-term equation (Pepin et al. 2001).

SPHERICAL AGGLOMERATION STUDIES

Spherical agglomeration is an industrial process traditionally used to separate or recover fine solids dispersed in a liquid suspension through the addition of a second immiscible liquid (binder) which presents an affinity for the solids and is capable of forming small liquid bridges that hold the particles together. Under appropriate physicochemical conditions the desired particles can be selectively agglomerated and removed from the slurry.

More recently, the spherical agglomeration technique has been used for the manufacture of high value products, such as crystalline pharmaceutical drugs, and is attracting increasing attention in the bioprocessing area. However, spherical agglomeration has yet to reach widespread commercialisation beyond the minerals industry. This is despite the simplicity of the process, the low cost of installation required and the possibility of agglomerating particles down to a few microns in size and is probably due to the lack in understanding of the controlling mechanisms involved. Even in the minerals industry, there is scope for improvement in understanding of the process, particularly as the requirement to recover very fine particles increases due to economic considerations. Viewing the process as a production, rather than separation, technique may also hold new opportunities for minerals applications.

In the work reported here, a micro-scale approach has been taken to investigate the mechanisms that lead to spherical agglomeration. The geometry and the strength of liquid bridges formed between pairs of particles with diameters in the range 70 to 130 μm, submerged in a second liquid, have been analysed and compared with values predicted by theory. The effects of different surface properties, created by the addition of surfactants and electrolyte, on the bridge behaviour and the forces developed between the particles, have also been investigated.

LIQUID PHASE MEASUREMENT OF BRIDGE PROPERTIES

For measurements of liquid bridge forces between particles suspended in liquid media, the pipette shapes shown previously must be adapted so that their tips can be submerged in an optically clear dish under the view of a water objective (Fig.4). For such cases, it was not possible to monitor the movement of the bend using the optical follower. Hence, a manual technique, taking the distance measurements directly from the image sequences, was used for the liquid phase work. Next generation MFBs, have done away with the optical follower and instead measure the amount of bend of a pre-calibrated flexible strip using a linear variable differential transducer of much higher resolution (Pratola et al. 2001) (see below).

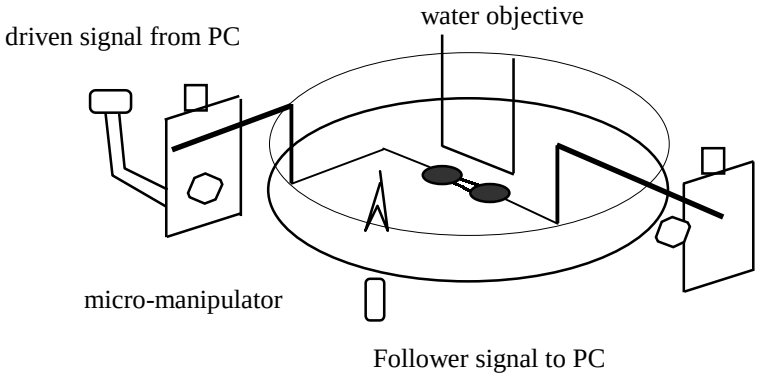

Fig.4. Schematic of the set up used to form a liquid bridge in a second immiscible liquid

LIQUID BRIDGE STRENGTH IN SPHERICAL AGGLOMERATES

Experiments were conducted to determine the effects on bridge geometry and strength caused by having a liquid phase continuous medium under a range of physico-chemical conditions. Glass ballotini spheres of diameter in the range of 70-130 μm were used as the solid particles, with silicon oil 100cSt (BDH) and water ("Analar" BDH) as the bridging and suspending liquid respectively. One electrolyte (NaCl -AnalaR) and two surfactants (sodium dodecyl sulphate, SDS-specially pure, cetyltrimethilammonium, CTAB-biochemical grade) were used to modify zeta potentials and interfacial energies. The pH was adjusted with either KOH or HCl (0.1M), both supplied by Fisher Scientific.

A rupture sequence of a silicon oil bridge in water is shown in Figure 5. From such images the advancing and receding contact angles can be measured and the liquid bridge profiles determined using the geometrical approximation developed during the gas phase work. It was observed that the variation in contact angle hysteresis between aqueous solutions at different pH, electrolyte and surfactanct concenctration was directly related to the zeta potential on both the glass and oil droplet surfaces and, hence, the double layer interaction between the two (Rossetti and Simons 2001). For instance, at pH ~3, the potentials of glass and silicon oil have opposite signs, leading to attraction and, hence, a more stable glass-oil interface. This is reflected in a lower value of the receding contact angle corresponding to a higher degree of hydrophobicity of the glass. As the pH of the solution is increased, both the glass and the oil potential drop to negative values with an increase of the receding angle and a diminution of the hydrophobicity.

To validate this postulation, a hybrid Atomic Force Microscope (AFM), formerly used to measure interactions between ink particles and air bubbles in liquids in relation to paper pulp flotation (Berg et al. 1998), was adapted to provide quantitative

data on the double layer interaction. Measurements were made between a glass sphere attached to the tip of the cantilever and an oil droplet formed on a glass slide submerged in various aqueous solutions. This device has a higher force and distance resolution than the MFB. This work is currently being analysed and has not yet been published, but current indications are that the postulation is correct.

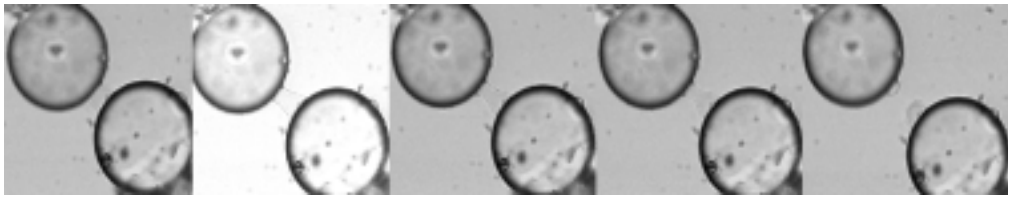

Fig.5. Rupture sequence of a 100cSt silicon oil bridge between two glass spheres, 43 μm (left) and 45 μm (right) diameter, separated at 1μm/s. The volume of the bridge is ~ 5500 μm³

Force measurements obtained using the MFB indicate the importance of selecting the appropriate conditions for successful agglomeration (Fig. 6). The geometrical model was seen to hold for the liquid phase experiments. Optimum conditions for agglomerating glass spheres with silicon oil rely on high interfacial tension between the particle and the suspending medium coupled with low zeta potential on the glass surface (e.g. by using CTAB as the surfactant).

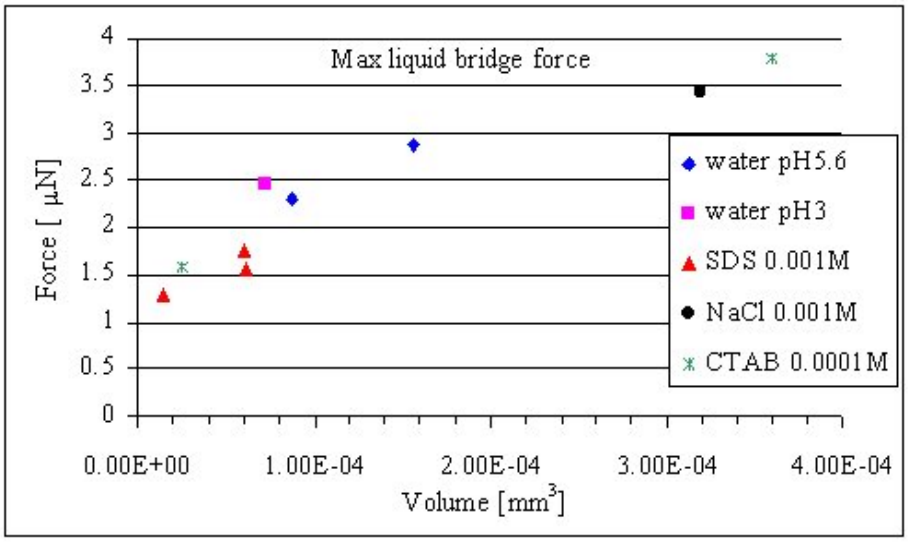

Fig.6. Max. liquid bridge force versus volume for a 100 cS silicon oil bridge in an aqueous solution

FLOTATION STUDIES

Flotation processes utilise air bubbles to capture solid particles from the bulk liquid gangue and subsequently rise to the surface, where they form a froth layer. The froth is then removed, either to recover or discharge the solid matter. A great deal of work has been published attempting to establish the influence of various parameters on froth formation and stability, such as the characteristics of the surfactants, electrolytes and solid particles. As interest increases on the application of dissolved air flotation (DAF) to the recovery of fine mineral particles, a fundamental understanding of the effect of various operational conditions on both froth formation and stability is vital for process optimisation and control, since the efficiency of the process depends heavily on these phenomena.

MEASUREMENT OF BUBBLE-PARTICLE INTERACTIONS

A novel apparatus has been developed to execute a wide range of interparticulate interactions, such as bubble-bubble and bubble-solid particle interactions. It is based on the earlier device described above and comprises the MFB where the interparticulate interactions take place, a sophisticated visual system, and a computer to control the electronic components of the set-up.

The MFB is shown in Fig.7 (Spyridopoulos and Simons 2002). At its centre is an optical-clear glass cell, which contains the liquid in which the interactions take place. A 3-axis micromanipulator is located above the cell, used either to hold directly the upper micropipette, at the tip of which either a bubble or particle is held, or the force measurement device. On the right of the cell, there is a piezo-driven branch, which holds a second micropipette. The piezo-driven branch can move the micropipette in very small steps, down to 0.05 μm. A visual system monitors and records the interactions in the cell.

The force-measurement device consists of two stainless-steel sheets connected vertically to rigid blocks. Any force between the particulates is transferred to the left-hand micropipette, which moves the lower block of the flexure-strip assembly. The latter carries the armature of an LVDT, which measures the displacement (resolution better than 0.1 μm), caused by the bending of the sheets. This depends on the force constant of the sheets which, for a 50 μm thickness is about 20 N/m. Lower force constants can be achieved, either by employing thinner strips, or by making holes at the centre of the sheets.

The visual system is comprised of two cameras and their respective displays; a high-speed camera capable of recording images between 30 and 3000 frames per second (fps) and a CCD camera placed at right angles to the high-speed camera. Each camera is coupled to a single-tube microscope fitted with a plan achromatic objective lens. The mechanism of the microscope permits the movement of the cameras in two dimensions.

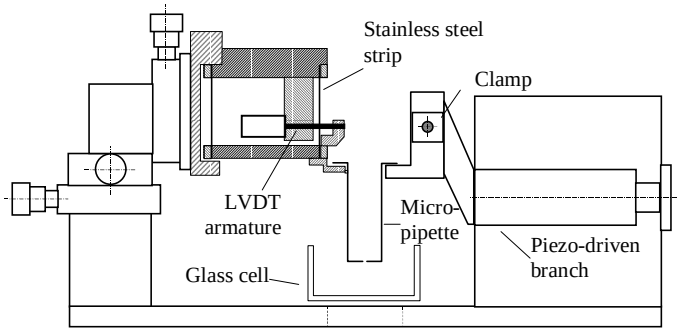

Fig.7. Schematic diagram of the MFB

The positioning of either two bubbles or a bubble and particle is achieved by using the 3-axis micromanipulator. The separation between the two bubbles is controlled by two means. Either a coarse adjustment can be made using the micromanipulator, or fine separation control can be obtained by moving the branch attached to the piezoelectric tube. Due to the inherent hysteresis of piezo tubes, a displacement sensor, LVDT, mounted in parallel with the piezo tube, follows and records the exact displacement. Instrument control and data acquisition is carried out via a computer.

BUBBLE COALESCENCE IN FLOTATION FROTHS

The effect of naturally occurring surfactants, known as humic substances (HS), on DAF froth formation and stability have been investigated by conducting bubble coalescence experiments. Bubbles of typical diameter 250 μm and 500 μm were grown on opposing nozzles inside the glass cell which was filled with an aquatic solution. The bubbles were brought together by the expansion of the piezoelectric tube. The rate of expansion and the resulting collisions were controlled by software, which controls the frequency and the value of the signals sent to a micromanipulator. The conditions under which the bubbles coalesce, e.g. coalescence frequency, type and concentration of HS in solution, and bubble size, have been observed. For the cases where coalescence did occur, the time elapsed for coalescence was measured using the high-speed video. After the formation of the bubbles, their vertical alignment and their positioning to a separation distance of about 10μm, the piezoelectric crystal was expanded at a rate of 10 μm/s and the event recorded using the high-speed camera. The event ended either with the coalescence of the bubbles, or when the piezoelectric tube had reached its maximum expansion, 100μm. In the latter case, the bubbles were squeezed but did not coalesce. At least 10 repetitions were conducted for each case (bubble size, HS concentration and type). All the experiments and measurements took place at room temperature, 21-23 °C.

Two samples of HS were tested: (a) a model polymaleic acid of molecular weight <500 Da, and (b) NOM taken from a sitka Spruce stand at Rumster in Caithness, UK.

Both of the samples were supplied from Thames Water Plc, UK, one of the major water companies in England and collaborators in this project.

HS solutions were prepared by dissolving a specific quantity of the sample in AnalaR-grade water (BDH, Dorset, UK). The pH of the aquatic solutions was in the acidic region (3.5-4.0) and a few drops of NaOH 1N (BDH, Dorset, UK) were required to adjust it to 5.25-5.5, the pH usually encountered in drinking-water treatment. The non-soluble matter was removed by passing the solutions through a filter paper with pore size of 0.2 μm.

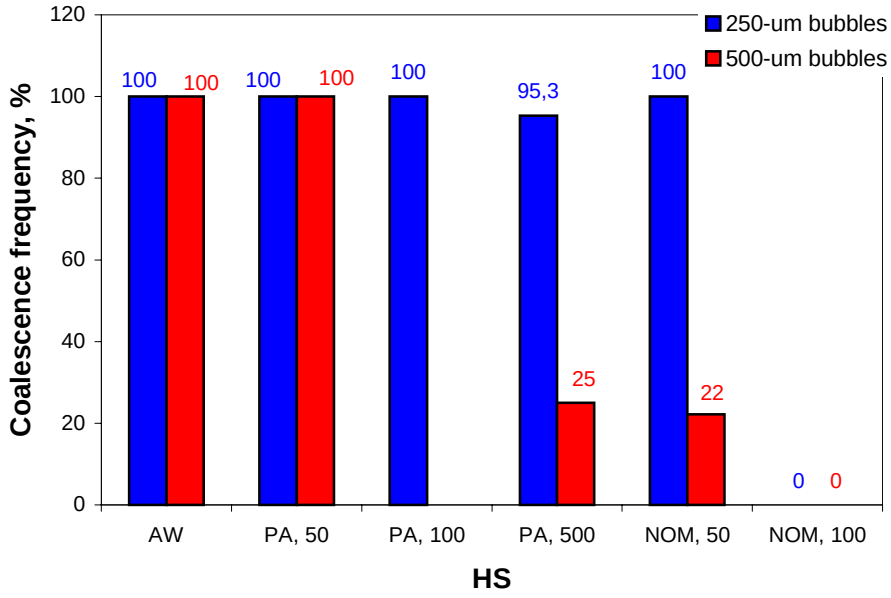

Fig.8. Coalescence frequency in HS solutions. AW: AnalaR water, PA: Polymaleic acid (MW <500 Da), NOM: Natural organic matter from Rumster – The numbers after commas denote the concentration in mg/l (Spyridopoulos and Simons 2002)

The results for the coalescence frequency versus HS concentration are shown in Figure 8. As was expected, there was always bubble coalescence in AnalaR water. The two HS tested in this work, however, showed different effects. The NOM reduced the coalescence frequency to 25%, even at the concentration of 50 mg/l. When its concentration was 100 mg/l, it inhibited the coalescence of bubbles completely. On the other hand, the polymaleic acid reduced the coalescence frequency only when its concentration was 500 mg/l. At lower concentrations, the coalescence frequency was 100%. These observations seem to be in accordance with the measurements of the surface tension of these HS, where the NOM appeared to be more surface-active than the polymaleic acid. From the same figure, also, it can be seen that the presence of HS affected the bubbles of 500 μm more than those of 250 μm.

The effect of the presence of solid particles on bubble coalescence has also been investigated. The experimental method and results have been reported elsewhere (Spyridopoulos and Simons 2001). In brief, coalescence depends not only on particle size, but also on the degree of hydrophobicity exhibited by the particle, measured through the 3-phase contact angle. High contact angles reduce coalescence.

CONCLUSIONS

A range of novel devices, known as Micro-Force Balances, have been developed that can be used to elucidate the fundamental mechanisms behind micro-scale interactions in mineral separation processes. It has been shown that direct measurement and observation of interactions between solid particles in the presence of liquids and bubbles is leading to important developments in understanding and modelling that, in turn, will lead to improvements in process design and operation. Further work is now underway in using such results to develop, for instance, computer simulations of flotation froths (Spyridopoulos et al. 2003).

ACKNOWLEDGEMENTS

The work reported in this paper was funded in part by the Engineering & Physical Sciences Research Council of the UK, under grant numbers GR/L77720 and GR/M98647, and Rhone Poulenc Industrialisation (now Aventis).

REFERENCES

BERG, S.R., HASSLER, J.C., BOUSFIELD, D.W. and THOMPSON, E.V. (1998). *Tappi 1998 Recycling Symposium Proceedings*, TAPPI PRESS, Atlanta, .315-326.

IVESON, S.M., PAGE, N.W. and LITSTER, J.D. (2001) *The importance of wet-powder dynamic mechanical properties in understanding granulation*, Proc. 7th Int. Symp. Agglom., 29th-31st May, vol. 2, 541-547.

PAGLIAI, P. and SIMONS, S.J.R. (2002). Defluidisation at high temperatures: Direct measurement of interparticle forces. World Congress on Particle Technology 4, 21st-26th July, Sydney, Australia.

PEPIN, X., ROSSETTI, D., IVESON, S.M. and SIMONS, S.J.R. (2000a). *Modeling the evolution and rupture of pendular liquid bridges in the presence of large wetting hysteresis.* J. Coll. Int. Sci., 232, 289-297.

PEPIN, X., ROSSETTI and SIMONS, S.J.R. (2000b*). Modeling pendular liquid bridges with a reducing solid-liquid interface.* J. Coll. Int. Sci., 232, 298-302.

PEPIN, X, SIMONS, S.J.R., BLANCHON, S., ROSSETTI, D. and COUARRAZE, G. (2001). *Hardness of moist agglomerates in relation to interparticle friction, granule liquid content and nature.* Powder Tech., 117, 123-138.

PRATOLA, F., SIMONS, S.J.R. and JONES, A.G. (2001). *A novel experimental device for measurements of agglomerative crystallization forces. Submitted* to Trans. IChemE.

ROSSETTI, D. and SIMONS, S.J.R. (2001). *Investigation of Liquid Bridges and Particle Surface Properties in Spherical Agglomeration Processes.* Proc. 6th World Congress Chem. Eng., Melbourne, Australia, 23rd-27th Sept.

ROSSETTI, D. and SIMONS, S.J.R. (2002). *A micro-scale investigation of liquid bridges in the spherical agglomeration process. Special Issue,* Powder Tech. on selected papers form *7th Int. Symp. Agglom.*, Albi, France, 29th-31st May.

SIMONS, S.J.R. and FAIRBROTHER, R.J. (2000). *Direct observations of liquid binder- particle interactions: the role of wetting behaviour in agglomerate growth.* Powder Tech., 110, 44-58.
SIMONS, S.J.R., PEPIN, X. and ROSSETTI, D. (2003). Submitted to Int. J. Min. Proc. for publication in 2003 (special issue on granulation to honour Prof. D. Fuerstenau).
SPYRIDOPOULOS, M. and SIMONS, S.J.R. (2001*). Mechanisms of bubble coalescence in water treatment flotation froths: A micro-mechanistic approach to determine the influence of solid particles*. Proc. 6th World Congress Chem. Eng., Melbourne, Australia, 23rd-27th Sept.
SPYRIDOPOULOS, M. and SIMONS, S.J.R. (2002). *Bubble coalescence in aquatic solutions of humic substances***.** World Congress on Particle Technology 4, 21st-26th July, Sydney, Australia.
SPYRIDOPOULOS, M., SIMONS, S.J.R., NEETHLING, S. and CILLIERS, J.J. (2003). Proc. Int. Conf. Min. Process. XXII, Cape Town, South Africa.

Simons S., Rossetti D., Spyridopoulos M., Pepin X., *Podstawy procesów przeróbczych w badaniach w skali mikro,* Fizykochemiczne Problemy Mineralurgii, 36, (2002) 159-172 (w jęz. ang.)

W szeregu procesach przeróbczych wykorzystuje się właściwości międzyfazowe takie jak hydrofobowość, napięcie powierzchniowe lub zwilżalność dla osiągnięcia zamierzonego celu. Jest interesujące znalezienie korelacji między właściwościami granic międzyfazowych w skali mikro, a realizacją procesów przeróbczych w skali makro. W celu lepszego poznania i zrozumienia tych zależności, konieczny jest bezpośredni pomiar oraz obserwacja tych właściwości. Szereg lat doświadczeń doprowadziły nas do zaprojektowania i budowy szeregu unikalnych aparatów o wspólnej nazwie Micro-Force Balance (MFB). Dzięki tym aparatom możemy mierzyć i obserwować oddziaływania między cząstkami ciała stałego w fazie gazowej i ciekłej, w temperaturze pokojowej oraz w podwyższonej. Przedmiotem badań z wykorzystaniem tych aparatów były takie procesy przeróbcze jak granulacja, flotacja, aglomeracja sferyczna. Przedstawiona praca zawiera opis działania aparatów oraz znaczące odkrycia dokonane w trakcie badań wyżej wzmiankowanych procesów.

Physicochemical Problems of Mineral Processing, 36 (2002) 173-183
Fizykochemiczne Problemy Mineralurgii, 36 (2002) 173-183

S.S. IBRAHIM, H.A. MOHAMED, T.R. BOULOS*

DRY MAGNETIC SEPARATION OF NEPHELINE SYENITE ORES

Received March 5, 2002; reviewed and accepted May 15, 2002

Different types of dry high intensity magnetic separators are applied to remove the iron bearing contaminants from two nepheline syenite samples. Ding's cross belt separator was applied in this study as a "pick up" separator, while "Carpco" induced roll was employed as a free fall kind of separator, that is widely used with dry sand size materials. Magnaroll magnetic separator, the latest design by Boxmag Rapid that uses rare earth permanent magnets for high intensity magnetic separation, was also applied. The main parameters affecting the separation efficiency of these machines were studied. It was found that Magnaroll separator was of high performance, as compared with the other separators. It was possible to produce clean concentrates containing 0.24% and 0.28% iron oxide from original samples containing 6.0% and 5.3% Fe_2O_3, respectively. These products are acceptable as glass grade materials in amber glass and fiberglass industries, as well as for ceramic purposes.

Kay words: magnetic separation, Magnaroll separator, iron oxide concentrate, glass, ceramic

INTRODUCTION

Feldspathic minerals are intermediate igneous techto-silicate rocks, having general compositional formula of Na,K,Ca aluminum silicate. They are indispensable raw materials in glass, ceramics and filler industries. However, nepheline is the most common (Guillet 1994). Due to its high alkali and alumina content per unit weight, it has been a formidable competition to feldspar.The low fusion point of nepheline syenite lowers the melting temperature, promoting faster melting, higher productivity and fuel savings in glass industry. In ceramic industry, the high fluxing capacity of nepheline allows it to act as a good vitrifying agent and permits a lower flux content in the ceramic body, lower firing temperature and faster firing schedules. In plastics, nepheline syenite is used as an inert, low cost filler in PVC, epoxy and polyester resin

* CMRDI, P.O.Box 87, Helwan, Cairo, Egypt

systems. Because it exhibits a low resin demand, high filler loading are possible, permitting reduced requirements for more expensive components. In PVC resins, it exhibits a low tinting strength, has a refractive index close to that of vinyl resin and has a very low optical dispersion (Guillet 1994). Finely ground nepheline syenite is especially employed as an inert filler in paints, both latex and alkalid type, for use in high traffic areas, as metal primers, wood stains, etc. It contributes a high dry brightness, high bulking value, easy wetting and dispersion in paint formulations**.**

In Egypt, the presence of nepheline syenite is confined to the ring complexes which are circular igneous structures formed after magma solidification. These structures are located in the southern sector of the Eastern Desert, south Edfu-Marsa Alam road in a square limited by the longitudes 33^{o} and 36^{o} and latitudes 22^{o} and 24^{o} (Dardir et al., 1994). Reserve estimation of these deposits are exceeding 90 million tons (El-Ramely et al., 1971).

Research and development projects in Egypt, were not able to conform the techno-economic feasibility of the Red Sea nepheline syenite in production of alumina and portland cement (Ismail 1976). Nevertheless, direct utilization of the beneficiated rock as filler in plastics industry or/and in glass and ceramic production might be another option for making the most of 90 million tons of ore reserves in the Eastern Desert, (Bolger 1995, Harben 1995). Since it would be most unusual to find a nepheline syenite ore that could be used commercially for glass and ceramics purposes without beneficiation, and due to the arid nature of the Egyptian ore deposits, it is important to study the amenability of this ore to dry beneficiation. Nevertheless, the dry processing is to be preferable than wet one from the point of view of the cost.

The effective capture of fine particles using dry high intensity magnetic separation depends mainly on the magnetic attractive force as well as the other competing forces including centrifugal and gravitational forces. The magnetic attractive force acting on a particle is the product of the particle magnetization and the magnetic filed gradient. The competing forces vary as the mode of separation varies (Cohen 1973, Mathieuand Sirois 1988). Dry high intensity separators typically consists of a grooved or laminated magnetized roll that generates high magnetic field gradients. The rotor is magnetized by using an external electromagnetic circuit or by using rare earth permanent magnets in the construction of the rotor. Separation occurs when the paramagnetic minerals are magnetically deflected from the non-magnetic stream (Arvidson 1995).

The aim of this paper is to study the amenability of dry beneficiation of two nepheline syenite samples from Gabel Abu-Khrug and Gabel El-Khafa localities in the Eastern Desert of Egypt to overcome typical problem of no water resources, as well as to reducethe operating cost of the beneficiation process. Application of the final products specifications for various industrial applications was considered.

EXPERIMENTAL

SAMPLES CHARACTERIZATION

Two nepheline syenite repesentative samples were supplied from the Gabel Abu-Khrug and El-Kahfa localities, Eastern Desert of Egypt. The complete chemical analysis of the original samples are shown in Table 1.

Table 1.Complete chemical analysis of nepheline syenite samples (in %)

Constituent	Gabal Abu Khrug	El-Kahfa
SiO_2	59.50	57.82
Al_2O_3	18.42	17.08
Fe_2O_3	6.00	5.30
CaO	0.37	0.87
MgO	0.40	0.20
Na_2O	7.70	9.18
K_2O	4.60	5.46
TiO_2	0.42	0.13
P_2O_5	0.02	0.01
S	0.07	0.02
Cl	0.06	0.05
CO_2	0.26	0.15
Humidity	0.86	0.48
L.O.I.	0.88	0.53

Table 2. Size analysis of Abu-Khrug (I) and El-Kahfa (II) crushed samples

Size, mm	Cumulative Wt. % Passing		Fe_2O_3, %		Al_2O_3, %	
	I	II	I	II	I	II
+6.68	100	100	5.84	5.28	17.99	17.31
-6.68+4.67	96.06	95.07	5.87	5.18	17.68	17.26
-4.67+2.40	88.52	88.02	6.03	5.27	18.61	17.27
-2.40+1.67	57.18	59.13	5.89	5.3	18.29	16.86
-1.67+0.85	45.35	46.14	5.95	5.23	18.24	16.96
-0.85+0.58	28.74	29.19	5.97	5.21	18.73	17.28
-0.58+0.40	22.76	22.36	5.81	5.26	18.06	16.86
-0.40+0.20	17.22	15.82	5.77	5.28	18.48	16.79
-0.20+0.106	9.80	10.54	5.82	5.43	18.46	16.96
-0.106+0.074	4.56	6.31	5.75	5.86	17.02	16.89
-0.074	6.54	4.49	5. 91	6.20	17.97	16.86
Calculated			5.93	5.42	18.35	17.36
Head			5.30	6.00	18.42	17.08

Results indicate that both samples are of low grade according to the market specifications for glass and ceramic production as well as bulk filler grade requirements (Harben 1995). Their alumina content is between 17.1 % and 18.4% as compared with at least 23% for glass manufacture. Similarly, their alkali content ranges between 12.3% and 14.6%, slightly lower or on the border line of the market specification which is 14%. Both samples have high iron content, that is 5–6 % Fe_2O_3.

The samples were primary crushed in a Denver pilot jaw crusher followed by Wedag roller to less than 3.36mm. Chemical analysis of different size fractions of the secondary crushed samples shows nearly even distribution of alumina and iron oxide, indicating no differential friability of components (Table 2).

Microscopic examination and x-ray diffraction of the samples show that they costitute mainly of perthitic orthoclase and albite with minor amounts of various iron bearing minerals, for example augite, biotite and hornblend.

LIBERATION STUDY OF THE SAMPLES USING FRANTZ ISODYNAMIC TESTER

Frantz isodynamic laboratory separator was used as a dry tool to study the liberation characters of the samples. Ferromagnetic particles were first separated from the feed samples by hand magnet and the reminder was subjected to magnetic separation under various field strength at constant angle of inclination (15^o forward, and 5^o degree side angle of inclination). Different magnetic and non-magnetic fractions were collected, weighed and analyzed. Results shown in Tables 2 and 3 indicate that it might be possible to obtain an ambre glass nepheline syenite products from Abu-Khrug sample (0.24%Fe_2O_3 and 25% Al_2O_3) and ceramic grade product from El-Kahfa sample (0.1% Fe_2O_3, 25.1% Al_2O_3) by fine grinding to less than 0.053mm.

Table 3. Effect of “Dings” beltspeed on the separation efficiency

Belt speed m/min	Product	Wt. %	Fe_2O_3	
			Assay Wt.%	Dist.Wt.%
2	Conc.	87.6	2.89	45.61
	Tail	12.4	24.34	54.39
4	Conc.	88.1	2.93	46.2
	Tail	11.9	25.28	53.8
6	Conc.	90.8	3.72	60.6
	Tail	9.2	24.09	39.4
8	Conc.	93.8	4.3	72.03
	Tail	6.2	25.27	27.97

FEED PREPARATION FOR BENEFICIATION

A Wedag rod mill was used for feed preparation for concentration process to minimize slimes production and to get a narrow sized material. The mill is operated in a locked cycle regime with duration time of 15 min./cycle, fed with 1kg sample of the –3.36mm ore and operated in a closed circuit with a 0.25 mm screen or 0.125mm one.

After each grinding period the mill was discharged and the ground product was screened to remove the under size from the circuit. The mill was then compensated with an amount of a feed equivalent to the removed fraction. 9 grinding rods and 15min grinding time were applied to prepare 100% -0.25mm or –0.125mm feed for the beneficiation process. On the other hand preparation of finer feed samples was conducted dry in planetary porcelain mill. Calculations of the Work Index Wi, required for dry grinding of both nepheline synite samples indicate the high hardness of the ores, reaching about 26-30 kWh/Mg (Bond 1985).

DRY HIGH INTENSITY MAGNETIC SEPARATION OF THE GROUND SAMPLES

Different types of dry magnetic separators that vary in the field intensity and the mode of separation were carried out. “Dings” cross-belt separator was applied as a dry pick up separator with an auxiliary permanent magnet for the separation of ferromagnetic material ahead of the electromagnet. Optimization of the main parameters affecting separation efficiency including applied magnetic field, feed size and rate were studied.

”Carpco” induced roll magnetic separator was employed in this investigation as a free fall kind of separator that it is widely used with dry sand size materials. Higher capacities are attained by such equipment compared with the pick-up type separators. However, “Carpco” induced roll used in this investigation model MIH (13) (111-5) is characterized by its capability of processing granular material up to 90 kg/h , variable magnetic field intensity up to 0.96T(tesla) and 127mm diameterX 50.8mm length laminated roll with variable speed 0–100 rpm. Optimization of the separation process including, roll speed, magnetic field intensity and both rate andsize offeeding material, was carried out.

“Magnaroll” magnetic separator used in this study is the latest design introduced by “Boxmag Rapid” that features the incorporation of rare earth permanent magnets in high intensity magnetic separation. It is considered as a dry HIMS. This particular type of magnetic pulley separator model MR 1.125 attains a magnetic field intensity up to 1.45T. Belt speed, feed rate and feeding material grain size were studied as the main woking parameters.

RESULTSAND DISCUSSIONS

The effect of changing the main belt speed of “Dings” separator, which determines the residence time of the particles in the magnetic field, is shown in Table 3. This was carried out using Abu-Khrug sample under one particle layer feed, feed size – 0.25 mm, magnetic field of 1.0T and a minimum air gap of 3 mm..

The results indicate that at a belt speed of 2 m/min, it was possible to obtain a concentrate with Fe_2O_3 of 2.89% from a head sample containing 5.5% F_2O_3 i.e with about 54.39% Fe_2O_3 operational removal. Changing the number of feed layers on the

belt at its optimum speed and under the same operating conditions resulted in deterioration of the separation process due to the shielding effect. This has a major effect on the quality of the concentrate and the capacity of separator as well. Results shown in Table 4 indicate that at a four-particle layer feed, a non magnetic concentrate having 4.61 % Fe_2O_3 was obtained from a feed assaying 5.5% Fe_2O_3 i.e. only 16.2% removal of iron bearing impurities was achieved. By increasing the magnetic field strength to its maximum of 1.3,T under the predetermined optimum conditions, relative improvement in the quality of the concentrate was achieved and its iron content was decreased to 1.96% Fe_2O_3 i.e. about 69.9% removal of magnetic impurities was achieved (Table 5).

Table 4. Effect of "Dings"cross belt feeding rate on the separation efficiency

Feed rate, kg/h	Product	Wt. %	Fe_2O_3	
			Assay %	Dist. Wt. %
12	Conc.	87.6	2.89	45.61
	Tail	12.4	24.34	54.394
24	Conc.	89.6	3.10	49.8
	Tail	10.4	26.94	50.2
36	Conc.	92.01	3.86	63.3
	Tail	7.99	25.8	51.1
48	Conc.	94.2	4.61	77.14
	Tail	5.8	22.19	22.86

Table 5. Separation of Abu-Khrug sample at maximum magnetic field strength

Feed size, mm	Product	Wt.%	Fe_2O_3	
			Assay %	Dist. Wt..%
-0.25mm	Conc.	85.0	1.96	30.1
	Tail	15	25.8	69.9
	Total	100	5.53	100
	Head	93.8	5.5	88.34

However better result was obtained by fractionating of the -0.25 mm feed into two size cuts, - 0.25 + 0.106mm and – 0.106 mm. A corresponding decrease in the iron content of the final concentrate to 1.4% Fe_2O_3 was obtained with 74.5% removal of the iron content. This confirms the shielding effect of coarse particles and necessitates using very closed size feeds with this kind of separator. Using a finer feed i.e.– 0.125mm, under a monolayer feed rate (about 12 kg/h), belt speed of 4 m/min, and maximum field strength of 1.3T resulted in an appreciale decrease in the iron content of the concentrate to 1.3% Fe_2O_3,(Table 6).

On the other hand, when El-Kahfa sample was subjected to separation using the cross belt dry magnetic separator under the predetermined optimum conditions, better results were achieved. A non magnetic concentrate having 0.98% Fe_2O_3 was obtained with the – 0.25mm feed, and decreased to 0.58% Fe_2O_3 with the – 0.125 mm feed, (Table 7).

Table 6. Effect of feed fractionation prior to separation

Fraction size, mm	product	Wt. %	Fe_2O_3	
			Assay %	Dist. Wt.%
-0.25+0.106	Conc. Tail	83.1 16.9	1.46 24.3	22.80 77.20
-0.106+0.045	Conc. Tail	81.6 18.4	1.25 27.6	16.72 83.27
-0.125+0.045	Conc. Tail	80.6 19.4	1.3 21.66	19.96 80.04

Table7. Separation of El-Kahfa sample at "Dings"optimum working conditions

Feed size, mm	Product	Wt.%	Fe_2O_3	
			Assay %	Dist. Wt. %
-0.25+0.045	Conc. Tail	72.46 27.54	0.98 16.27	13.68 86.32
-0.125+0.045	Conc. Tail	73.69 26.31	0.58 17.76	8.38 91.620

One can conclude that, within the afore mentioned limits of experimentation on these samples, that it was not possible to produce high quality nepheline syenite concentrates by this type of magnetic separators only.

Although the magnetic flux intensity of "Carpco" separator is relatively less than that of the "Dings" cross-belt (0.96T as compared with 1.3T), yet it can handle sandy – sized feeds at a much higher capacity than the latter one. In the mean time, having a roll of diameters 88.9mm D X 50.8mm L with a variable speed controller from 0 to 100 rpm, the generated centrifugal force with the free fall of the feed create much more favorable conditions for separation, as compared with the "shielding" effect of belt separators. That might result in producing concentrates with better grades.

Table 8. Effect of changing"Carpco"feeding rate on the separation effeciency

Feed rate, kg/h	Product	Wt. %	Fe_2O_3	
			Assay %	Dist. Wt. %
12	Conc. Tail	70.98 29.02	1.74 15.21	21.97 78.13
24	Conc. Tail	74.86 25.14	1.76 16.99	23.57 76.43
36	Conc. Tail.	76.2 23.8	1.96 17.59	26.3 73.7
48	Conc. Tail	73.86 26.14	2.38 14.77	31.28 66.72

By applying the separation of Abu Khrug sample at various drum speeds a pronounced decrease in the iron oxide content of the product was recorded up a roll speed of 60 rpm. A product with a weight recovery of 75% with an assay of 1.76% Fe_2O_3 was obtained. By elevating the drum speed over this value , a remarkable drop

in the product grade was noticed. The increasing in the feed rate to 48 kg/h at this optimum roll speed i.e. 60rpm, keeping all other parameters constant, a corresponding grade deterioration occurred (Table 8). An appreciable improvement in the concentrate quality was achieved by increasing the applied magnetic field to the maximum (0.96T) at optimum feed rate of 24 kg/h (Table 9). A concentrate assaying 1.4% Fe_2O_3 was reached as compared with 1.96% Fe_2O_3 with the"Dings" cross-belt separator at its maximum magnetic field strength. Separation of – 0.125 mm feed under these optimum conditions resulted in a remarkable decrease in the iron content of the concentrate to 0.72% Fe_2O_3, (Table 9).

Table 9.Magnetic separation of sample I at "Carpco" maximum magnetic field

Feed Size, mm	Product	Wt. %	Fe_2O_3	
			Assay %	Dist. Wt.%
-0.25+0.045	Conc. Tail	73.5 26.5	1.4 18.04	17.71 82.29
-0.125+0.045	Conc. Tail	70.22 29.78	0.72 15.53	9.72 90.28

Table 10. El-Kahfa separation at " Carpco" optimum conditions

Feed size, mm	Product	Wt.%	Fe_2O_3	
			Assay %	Dist. Wt.%
-0.25+0.045	Conc. Tail	70.86 29.14	1.03 15.2	14.14 85.86
-0.125+0.045	Conc. Tail	71.68 28.32	0.61 16.92	8.36 91.64

Table 11. "Magnaroll" belt speed effect in the separation of Abu-Khruq sample

Belt speed, m/min	Product	Wt. %	Fe_2O_3	
			Assay %	Dist. Wt. %
2	conc. Tail	53.9 46.1	0.24 11.216	2.44 97.56
4	conc. Tail	57.2 42.8	0.24 12.06	2.59 97.41
6	conc. Tail	59.5 40.5	0.45 12.43	5.05 94.95
10	conc. Tail	64.3 35.7	0.62 13.73	7.52 92.48

Magnetic separation of El-Kahfa sample, under the predetermined optimum conditions, gave relatively better results. Non magnetic concentrates assaying 1.03 and 0.61% Fe_2O_3 were obtained with the – 0.25mm feed and the – 0.125mm feed, respectively (Table 10). Regardless of the improved results obtained with the induced roll magnetic separator, the nepheline syenite concentrate did not satisfy the requirements for glass and ceramics production. Although the magnetic flux intensity of "Carpco"separator is relatively less than that of the "Dings" cross-belt (0.96T as

compared with 1.3T), yet it can handle sandy – sized feeds at a much higher capacity than the latter one. In the mean time, having a 88.9mm D X50.8mm L roll with variable speed 0–100 rpm, the generated centrifugal force with the free fall of the feed create much more favorable conditions for separation, as compared with the "shielding" effect of belt separators. That might result in producing concentrates with better grades.

Table 11 indicates that at the "Magnaroll" belt speed of 4 m/min and feed rate of 12 kg/h a non magnetic concentrate assaying 0.27% Fe_2O_3 was obtained by separating the – 0.125mm feed, which is the most clean concentrate obtained as compared with the other separators. A magnetic flux intensity as high as 1.45T incorporated by the rare earth permanent magnets of this separator, leads to increasing the separation efficiency of paramagnetic particles, beside lowering the operating cost of the process, where no power is required to generate the magnetic field during the operation.

Table 12. "Magnaroll" feed rate effect on separation of Abu-Khruq sample

Feed rate, kg/h	Product	Wt.%	Fe_2O_3	
			Assay %	Dist. Wt. %
6	Conc. Tail	57.2 42.8	0.24 12.06	2.59 97.41
12	Conc. Tail	59.6 40.4	0.27 12.56	3.07 96.93
18	Conc. Tail	61.3 38.7	0.58 13.06	6.57 93.43
24	Conc. Tail.	65.1 34.9	0.64 13.99	7.86 92.14
30	Conc. Tail	68.3 31.7	0.81 15.16	10.32 89.68

Table 13. Separation of El-Kahfa at "Magnaroll"optimum working conditions

Feed size, mm	Product	Wt.%	Fe_2O_3	
			Assay %	Dist. Wt.%
-0.25+0.045	Conc. Tail Total Head	74.38 25.62 100 94.2	0.77 18.45 5.30 5.25	10.81 89.19
-0.125+0.045	Conc. Tail Total Head	68.6 31.4 100 87.7	0.28 15.69 5.12 5.25	3.75 96.25

Increasing the feed rate of "Magnaroll" to more than 12 kg/h at an optimum belt speed of 4 m/min led to over crowding in the separation zone and, hence a corresponding deterioration in the quality of the concentrate took place, (Table 12). Separation of sample 2 under the predetermined optimum conditions yielded nepheline syenite concentrate assaying 0.48% Fe_2O_3 and 0.28% Fe_2O_3 for both the –

0.25mm and the – 0.125mm feeds, respectively (Table 13). These concentrates could be intentionally acceptable as glass grade products in amber glass and fiberglass industries, as well as ceramic purposes. Microscopic studies of the nepheline syenite concentrates shows a brownish tinge of iron-bearing minerals which can be a surface coating or disseminated fine grains in a matrix of syenite. This might explain the difficulty of obtaining higher quality products. Some additional improvement may be possible by further size reduction of the feeding materials by applying wet process with special"Carpco" or "Jones" magnetic separators, or by flotation, but it will be at the expense of higher losses and additional cost.

CONCLUSIONS

Characterization of two nepheline syenite samples from Gabel Abu-Khrug and El-Kahfa localities in the Eastern Desert of Egypt, indicated that both samples are low in grade with 17.1% - 18.4% Al_2O_3, 12.3 – 14.6% $Na_2O + K_2O$ and high in iron content 5.3 – 6% Fe_2O_3. Granulometric analysis of the secondary crushed samples showed a unimodal trend with respect to both alumina and iron oxide contents. Liberation study of the ground samples using Frantz isodynamic laboratory separator, implied fine grinding, some times to less than 0.053 mm, to achieve a reasonable degree of liberation of minerals. Applying the dry high intensity magnetic separation of the ground samples using "Ding's" cross belt separator at a maximum magnetic field intensity of 1.3T, and feed size 0.125 + 0.045 mm gave nepheline concentrates having 1.3% and 0.58% Fe_2O_3 for Abu-Khrug and El-Kahfa samples, respectively.

Using "Carpco" induced roll magnetic separator, as a free fall technique, showed better separation with doubling the feeding rate (24 kg/h) andat nearly the same magnetic field strength, concentrates having 0.72% and 0.61% Fe_2O_3 were obtained with the – 0.125 + 0.045 mm feed of both samples, respectively.

Application of "Magnaroll" rare earth permanent magnetic separator, with a field intensity of 1.45T at a feed rate of 12 kg/h and belt speed of 4 m/min resulted concentrates with a substantial decrease in the iron content, reaching 0.24% and 0.28% for Abu-Khrug and El-Kahfa samples, respectively. These concentrates satisfy the international specifications for amber glass and fiberglass production as well as local ceramics industries**.**

REFERENCES

ARVIDSON, B.R., (1995), *New Rare Earth Magnetic Roll Separator Developments*, Proc. of the X Ind. Min. Proc. Congress, Berlin, pp.98.

BOLGER R., (1995), *Feldspar and Nepheline Syenite: Magnetic Separation and Flotation*, Raw Materials for Pigments Fillers and Extenders, 2nd Edition, M.J. O'Driscoll, Metal Bulletin.

BOND, F.C., (1985), *General Aspects of Comminution: Testing and Calculations*, SME Mineral Processing Handbook.

COHEN,H.H., (1973*), Proceedings of the High GradientMagnetic Separation Symposium*, MJT., Mass.

DARDIR, A.A AND ABU-ZEID,K.M. AMIN, H.M., (1994), *Ceramics, Glass and Refractories Ores in Egypt from the Economic Conception*, Cairo, Egypt.
EL-RAMELY, M.F; BUDAROUV, V.I AND HUSSIEN, A.A., (1971), *Alkaline Rocks of South Eastern Desert*, Geol. Surv. Cairo, Egypt.
GUILLET, R.G, (1994), *Nepheline Syenite Benificiation for Different Industrial Applications*, Industrial Minerals and Rocks, 6th Edition, Senior Editor Carr D.D. Society of Mining,Metallurgy & Exploration.Inc.
HARBEN, P.W.,(1995), *The Industrial Minerals Handbook*, Second Edition, Metal Bulletin, London.
ISMAIL, A. K., (1976), *A Contribution to Extractive Metallurgy of Local Nepheline Syenite Deposits for Alumina Production*, Ph.D.Thesis, Cairo Univ., Egypt.
JONES, J. H.,(1967), *Magnetic Separators*, US Patent 3, 346, 116.
MATHIEU, G.L. AND SIROIS, L.L., (1988), *Advances in Technology of Magnetic Separation*, Proceedings of XVI Int. Min. Proc. Congress, Stockholm.

Ibrahim S.S., Mohamed H.A., Boulos T.R., *Separacja magnetyczna na sucho rud nefelinowo-sjenitowych*, Fizykochemiczne Problemy Mineralurgii, 36, (2002) 173-183 (w jęz. ang.)

Stosowano różne, działające na sucho, separatory magnetyczne o dużej intensywności pola magnetycznego do usuwania minerałów żelazonośnych z dwóch rud nefelinowo-sjenitowych. Do separacji wstępnej użyto separatora typu Dingo o skrzyżowanych taśmach. Jako separator właściwy zastosowano separator indukcyjny bębnowy typu Carpco, który jest szeroko stosowany do przeróbki piasków na sucho. Użyto także separator magnetyczny typu Magnaroll, najnowszy model separatorafirmy Boxmag – Rapid, który posiada stałe magnesy wykonane z pierwiastków ziem rzadkich. Badano wpływ głównych parametrów na proces separacji magnetycznej. Stwierdzono, że najlepsze wyniki uzyskuje się stosując separator Magnaroll. Wytworzono koncentraty zawierające 0,24% i 0,28% tlenków żelaza z nadawy zawierającej odpowiednio 6,0 i 5,3% Fe_2O_3. Uzyskane produkty mogą być stosowane do produkcji szkła miodowego oraz włókna szklanego oraz ceramiki.

Physicochemical Problems of Mineral Processing, 36 (2002) 185-195
Fizykochemiczne Problemy Mineralurgii, 36 (2002) 185-195

T.N. KHMELEVA, W. SKINNER, D.A. BEATTIE and T.V. GEORGIEV*

THE EFFECT OF SULPHITE ON THE XANTHATE-INDUCED FLOTATION OF COPPER-ACTIVATED PYRITE

Received March 15, 2002; reviewed and accepted May 15, 2002

The effect of sulphite ions on the xanthate-induced flotation of copper-activated pyrite has been studied. Various techniques have been used to identify the plausible mechanisms of interaction of sulphite with both collector and pyrite surface. It was found that sulphite depressed the xanthate-induced flotation of copper-activated pyrite with nitrogen or air purging at pH 7. However, the depression effect was greater when air was used. Solution and spectroscopic studies indicated that sodium bisulphite interacted with the pyrite surface, as well as with isobutyl xanthate in solution and its adsorbed state. Based on the results obtained, a combination of possible mechanisms has been proposed to explain the depressing effect of sulphite on copper-activated pyrite. It was suggested that both the decomposition of the xanthate in solution via perxanthate formation and dixanthogen desorption from the pyrite surface were responsible for the pyrite depression. Furthermore, iron hydroxy species were formed on the pyrite surface, rendering it hydrophilic, thus preventing the formation of bubble-pyrite particle aggregates.

Key words: pyrite, flotation, sulphite, depressants

INTRODUCTION

Froth flotation is widely used for separating sulphide minerals in complex ores. Typical examples in sequential separation of sulphides include sphalerite and pyrite depression during galena and/or chalcopyrite flotation. A common problem for copper-zinc-iron mineral selectivity is related to the unintentional activation of pyrite and sphalerite by copper ions. Cyanide addition is usually employed in industrial practice for complexing and removing copper ions from unwanted sulphides in the selective flotation of minerals. However, the use of cyanide causes environmental and

* Ian Wark Research Institute, University of South Australia, Mawson Lakes Campus, Mawson Lakes, South Australia 5095, Australia.

safety problems. Sulphur-oxy species, such as sulphite (SO_3^{2-}), bisulphite (HSO_3^-), metabisulphite ($S_2O_5^{2-}$) or sulphur dioxide (SO_2), have been used in some mineral processing operations as depressants instead of cyanide.

Different mechanisms have been proposed to explain the effect of sulphite on the selective depression of sulphide minerals. In general, these mechanisms can be divided into two main categories. The first category involves interaction of sulphite ions with the mineral surface. Misra et. al (1985) suggested two mechanisms of depression including the formation of a metal sulphite hydrophilic surface layer and consumption of copper ions in solution by sulphite. As a result of this interaction, some insoluble copper sulphite precipitates are formed rendering the mineral surface hydrophilic (Misra et. al 1985). Also, it has been shown that adsorbed sulphite species interact with mineral sulphur species and this may decrease the surface hydrophobicity (Li et. al 1995). The second category includes the interaction of sulphite with collector either in solution or its adsorbed state. Yamamoto (1980) found that sulphite ions decomposed the xanthate collector in solution via perxanthate formation. Miller (1970) reported desorption of pre-adsorbed collector species such as dixanthogen by sulphite ions. Illyuvieva et. al (1984) proposed a mechanism involving the consumption of dissolved oxygen by sulphite. In this particular case, the Eh of the solution might be reduced because of sulphite oxidation to sulphate. Due to the lack of oxygen in solution, the formation of dixanthogen and collector adsorption may also be minimised (Illyuvieva et. al 1984).

Still, the action and mechanisms of sulphur-oxy reagents are not well understood, particularly when applied to copper-activated pyrite. The aim of this current work is to study the effect of sulphite on the xanthate-induced flotation of copper-activated pyrite and identify the mechanisms, which are involved in the interaction of sulphite both with the pyrite surface and collector (xanthate) species.

EXPERIMENTAL

MATERIALS AND REAGENTS

The pyrite sample was obtained from the Huanzala Mine, Peru. The elemental composition of pyrite analysed by ICP-MS (Inductively Coupled Plasma - Mass Spectroscopy) is shown in Table 1.

Table 1. Chemical assay of the pyrite sample

Mineral	Chemical elements present (Wt.%)								
	Fe	S	Ca	Mg	Mn	Si	Pb	Cu	Zn
Pyrite	44.93	53.51	0.45	0.08	0.02	0.69	0.02	0.13	0.18

All chemicals were of analytical grade. Cupric nitrate ($Cu(NO_3)_2 \cdot 3H_2O$) was used to introduce copper ions during the conditioning time. Sodium isobutyl xanthate ($C_4H_9OCSSNa$, abbreviated as SIBX) and polypropylene oxide methanol (Dowfroth 250) were added in the experiments as a flotation collector and frother, respectively. The sulphite reagent used in the current studies as a depressant was sodium bisulphite ($NaHSO_3$). The slurry pH values of 7 and 9 were controlled using HCl solutions and a carbonate/bicarbonate buffer, respectively. Deionised water was used throughout the experimental work.

MINERAL GRINGING, CONDITIONING AND FLOTATION EXPERIMENTS

A known mass (50 grams) of pyrite was wet ground at 30% solids in a Fritsch ball centrifuge mill (200 ml volume) for 7 minutes. The d_{80} of the ground mineral was around 38 microns. After grinding, the slurry was washed from the mill into a 500 ml Gliwice flotation cell. The pulp was conditioned in 5 stages and four concentrates and the final tail were collected. The total time of flotation was 8 minutes. Wet and dry weights were measured for all flotation products. The pulp pH was kept constant during the flotation batch tests. Nitrogen (or air) purging was used throughout the study. The pulp Eh was measured using an Hg/Hg_2Cl_2 electrode. A summary of the experimental procedure is schematically shown in Figure 1.

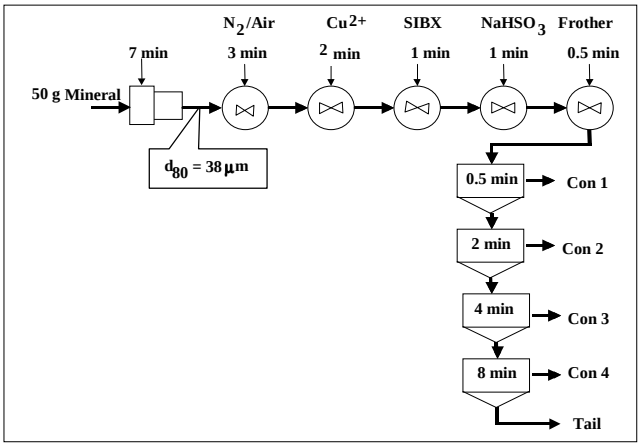

Fig. 1. Schematic presentation of the flotation procedure

FOURIER TRANSFORM INFRARED SPECTROSCOPY (FTIR)

Fourier Transform Infrared spectra were obtained using a Nicolet Magna 750 spectrometer. The pyrite samples for FTIR analysis were prepared in a similar manner to the flotation experiments. The pulp pH was kept constant at around 7, while the

slurry was nitrogen purged. After conditioning and filtration, the pyrite sample was placed in the cup of a Spectra Tech diffuse reflectance accessory apparatus. The contribution from pyrite was subtracted from all infrared spectra and the respective subtraction factors were close to 1.

UV-VISIBLE SPECTROSCOPY

A Varian CARY 5E spectrometer was used to determine the concentration of the xanthate remaining in solution before and after the addition of sodium bisulphite. Isobutyl xanthate was added to a 100 ml conditioning vessel containing deionised water that had been pre-purged with nitrogen prior to collector addition. The pH was adjusted to 7. The spectrum of xanthate was recorded within the range from 200 to 400 nm. Sodium bisulphite was then added and the absorption spectra were recorded as a function of time.

ION CHROMATOGRAPHY

A Water 431 conductivity detector was employed to determine sulphite stability and any adsorption onto pyrite in the presence and absence of adsorbed copper. Sulphur-oxy species in solution, i.e., sulphate (SO_4^{2-}) and sulphite (SO_3^{2-}), were measured using Waters Ion Chromatography Method with an IC-Pak A HC column. UV adsorption at 220 nm was used for the IC measurements. The pyrite samples were prepared in a similar way as in the flotation experiments shown in Figure 1. The pulp pH was kept constant at 9 using a carbonate/bicarbonate buffer and the slurry was nitrogen purged. After conditioning, the suspension was filtered to remove the solids and the amount of residual sulphite species was determined as a function of time.

RESULTS

FLOTATION STUDY

Figures 2 and 3 show the effect of sodium bisulphite on the flotation recovery of copper-activated pyrite pre-treated with isobutyl xanthate at pH 7 and 9, respectively. Table 2 presents the flotation data that have been analysed using the following first order kinetic equation (Lynch et. al 1981):

$$R = R_{max}\,(1 - e^{-kt}) \tag{1}$$

where R is the percent of pyrite recovered at time t, R_{max} is the maximum flotation recovery at infinite time and k is the flotation rate constant (min^{-1}).

Under the experimental conditions studied (at pH 7 and 9), the effect of sodium bisulphite on the xanthate-induced flotation of copper-activated pyrite with nitrogen purging was found to be similar. In the presence of sulphite, the recovery of pyrite was reduced from 69.7% to 53.2% at pH 7 and from 69.3% to 57.7% at pH 9. During all flotation tests, a decrease in Eh of 40 mV was observed after sodium sulphite addition, which suggested a possible consumption of dissolved oxygen by sulphite ions.

Table 2. Maximum flotation recovery (R_{max}) and rate constant (k) of pyrite as a function of pulp pH

Experiment description	pH 7		pH 9	
	R_{max}	k	R_{max}	k
Pyrite only	15.2	0.30	18.0	0.30
Pyrite + Cu^{2+}	20.4	0.50	19.5	0.50
Pyrite + Cu^{2+} + SIBX	69.7	0.86	69.3	0.88
Pyrite + Cu^{2+} + SIBX + $NaHSO_3$	53.2	0.90	57.7	0.85

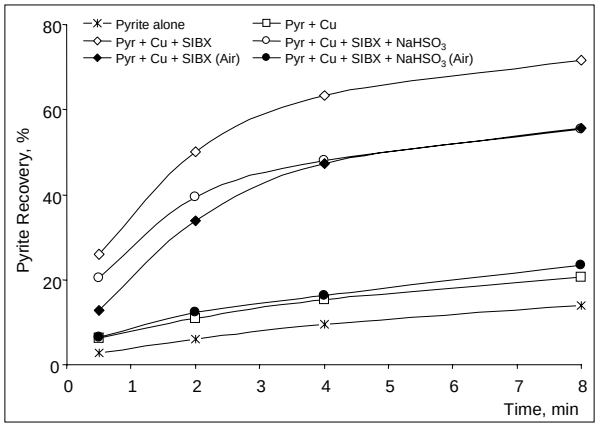

Fig. 2. Effect of sodium bisulphite on the flotation recovery of copper-activated pyrite pre-treated with isobutyl xanthate. All tests at pH 7, in nitrogen (empty symbols) and with air purging (filled symbols).

$[Cu(NO_3)_2] = 2.6 \times 10^{-4}$ mol dm^{-3};
$[SIBX] = 1.1 \times 10^{-4}$ mol dm^{-3};
$[NaHSO_3] = 1.9 \times 10^{-3}$ mol dm^{-3}

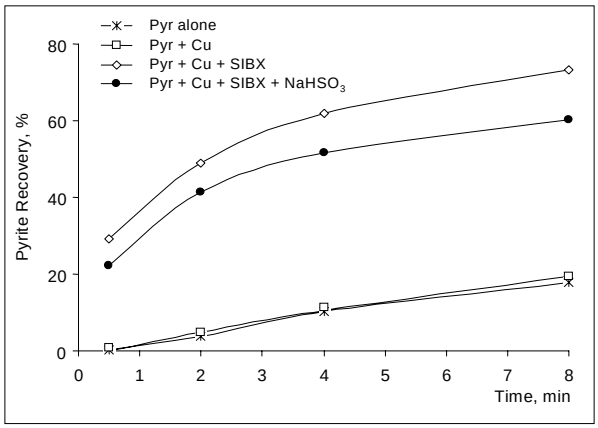

Fig. 3. Effect of sodium bisulphite on the flotation recovery of copper-activated pyrite pre-treated with isobutyl xanthate. All tests at pH 9, in nitrogen.

$[Cu(NO_3)_2] = 2.6 \times 10^{-4}$ mol dm^{-3};
$[SIBX] = 1.1 \times 10^{-4}$ mol dm^{-3};
$[NaHSO_3] = 1.9 \times 10^{-3}$ mol dm^{-3}

Additional flotation experiments were carried out with air purging to identify the effect of air on the xanthate-induced flotation of copper-activated pyrite either in the presence or absence of sodium bisulphite (at pH 7). In this case, the xanthate-induced flotation of copper-activated pyrite in an air atmosphere was lower compared to the same experiment with nitrogen purging. Recovery of pyrite was 71.8% in nitrogen and 55.6% in air. The combination of sodium bisulphite and air purging decreased the recovery of pyrite even further, from 55.6% to 32% (Figure 2).

Unless otherwise stated, pH 7 was chosen for additional spectroscopic studies conducted to identify the depression effects of sodium bisulphite on the xanthate-induced flotation of copper-activated pyrite.

FTIR STUDY

Figure 4 shows DRIFT FTIR spectra of adsorbed isobutyl xanthate on the surface of copper-activated pyrite at pH 7 with nitrogen purging in the absence and presence of sodium bisulphite.

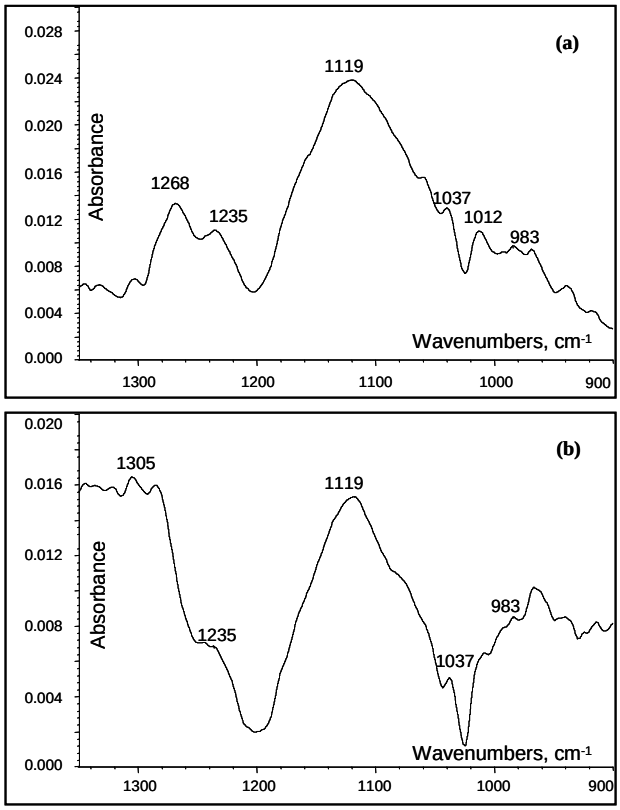

Fig. 4. Infrared spectra of isobutyl xanthate adsorbed on copper-activated pyrite conditioned at pH 7, in nitrogen: (a) in the absence of sodium bisulphite, (b) in the presence of $NaHSO_3$

$[Cu(NO_3)_2] = 1.0 \times 10^{-3}$ mol dm^{-3};
$[SIBX] = 1.1 \times 10^{-3}$ mol dm^{-3};
$[NaHSO_3] = 1.0 \times 10^{-2}$ mol dm^{-3}

The infrared bands observed in Figure 4a at 1230 - 1270 cm^{-1} are characteristic of dixanthogen (Poling 1961; Leppinen et. al 1988, 1989; Prestidge et. al 1993). The broad peak at 1120 cm^{-1} is due to incomplete subtraction of pyrite. In the presence of sodium bisulphite, the bands owing to isobutyl dixanthogen disappeared with loss of structure within the 1000 - 1100 cm^{-1} region (Figure 4b).

UV-VISIBLE STUDY

The adsorption spectra for the interaction of isobutyl xanthate with sodium bisulphite in solution have been recorded as a function of time at pH 7, as shown in Figures 5. It is clear that the initial xanthate concentration (peak at 301 nm) decreased with time, while at the same time, an adsorption band at 347 nm appeared (Figure 5). This suggested that an intermediate product of the xanthate decomposition, known as perxanthate, was formed (Yamamoto 1980). In approximately 15 minutes, xanthate was completely decomposed and virtually no xanthate or perxanthate were detected, as shown in Figure 6.

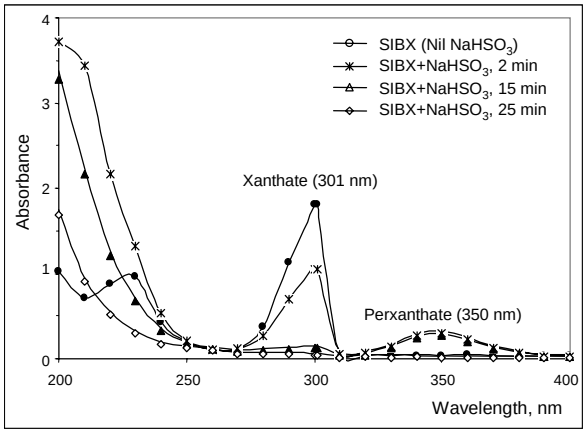

Fig. 5. UV spectra of isobutyl xanthate solution in the presence of sodium bisulphite as a function of time

All tests in the presence of 1.9×10^{-3} mol dm^{-3} $NaHSO_3$ added after pyrite conditioning with 1.1×10^{-4} mol dm^{-3} [SIBX], pH 7, in nitrogen

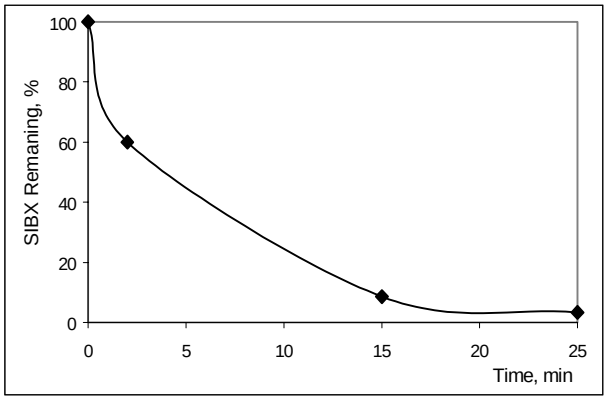

Fig. 6. Decomposition of sodium isobutyl xanthate (measured at 301 nm) in the presence of 1.9×10^{-3} mol dm^{-3} sodium bisulphite as a function of time, pH 7, in nitrogen

[SIBX] = 1.1×10^{-4} mol dm^{-3};
[$NaHSO_3$] = 1.9×10^{-3} mol dm^{-3}

ION CHROMATOGRAPHY STUDY

Figure 7 shows the stability of sulphite and adsorption onto pyrite in the presence and absence of copper ions at pH 9. The results are presented as sulphite (SO_3^{2-}) and sulphate (SO_4^{2-}) residual concentrations in solution versus time. In both cases, compared to their initial concentrations, the amount of sulphite remaining in solution decreases, while the amount of sulphate increases after 25 minutes of conditioning. However, in the presence of copper ions, less sulphite is detected in solution and the formation of sulphate is more rapid.

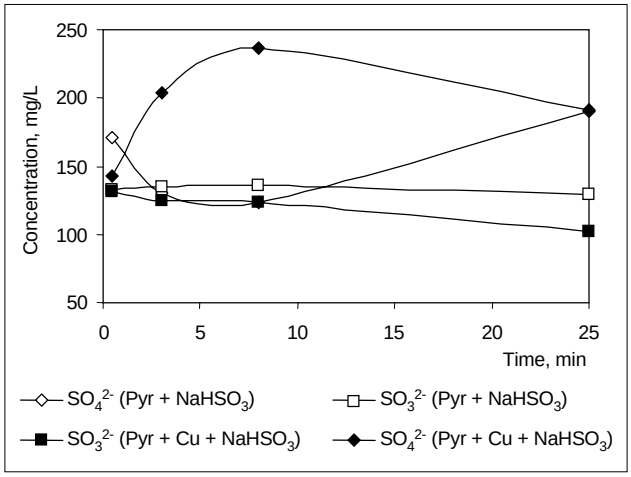

Fig. 7. Sulphite stability and adsorption onto pyrite measured by IC in the presence and absence of copper ions, at pH 9 (nitrogen purging)

$[Cu(NO_3)_2] = 2.6 \times 10^{-4}$ mol dm^{-3};
$[NaHSO_3] = 1.9 \times 10^{-3}$ mol dm^{-3}

DISCUSSION

Flotation data have shown that at pH 7 and 9 sodium bisulphite acts as a depressant for the xanthate-induced flotation of copper-activated pyrite with nitrogen or air purging. However, the depression effect of sulphite with air purging was found to be greater. It is possible that more oxidation products were formed on the pyrite surface with air purging, rendering it more hydrophilic (Figures 2). The depression of pyrite by sulphite may be explained by the results obtained from the spectroscopic and solution studies.

Infrared analysis has indicated that under the experimental conditions tested, isobutyl xanthate adsorbed on the surface of copper-activated pyrite in the form of dixanthogen. The addition of sodium bisulphite resulted in dixanthogen desorption (Figure 4). Since dixanthogen is the collector species responsible for pyrite flotation (Fuerstenau et. al 1968; Majima and Takeda 1968; Huiatt 1969; Huang and Miller 1978; Montalti 1994), desorption of dixanthogen from the surface can lead to the

pyrite depression. Moreover, it was noticed that the introduction of sulphite decreased the pulp redox potential by 40 mV. Consequently, sulphite addition may also reduce the xanthate adsorption due to the lack of oxygen in solution, thus limiting dixanthogen formation (Miller 1970; Shen et. al 2001).

The results from UV-visible spectroscopy may further explain the decrease in the recovery of pyrite. It has been demonstrated that sulphite decomposed the xanthate ions in solution, as well as these present at the pyrite surface (Figures 5 and 6). Perxanthate was formed (at 350 nm) during the xanthate decomposition. A similar mechanism was proposed by Yamamoto (1980), who identified the products of the ethyl xanthate decomposition by sulphite as ethanol, thiosulphate and carbon dioxide.

Furthermore, the ion chromatography study has illustrated that less sulphite and more sulphate ions were found in solution when both sodium bisulphite and copper ions were present. It is likely that copper ions promoted the sulphite oxidation to sulphate. Sulphite ions also promoted the surface oxidation of copper-activated pyrite rendering it hydrophilic, thus reducing the floatability of pyrite particles (Figure 7). It was hence suggested that the consumption of sulphite from solution could be due to the sulphite adsorption on the mineral surface, sulphite oxidation to sulphate and surface precipitation of sulphite. Moreover, some additional sulphate in solution can be due to the direct oxidation of the pyrite surface (Hoyack at. al 1987).

Based on the results obtained in the current work, a compound effect of sulphite on the pyrite flotation has been suggested. It was found that under the studied experimental conditions, a combination of four mechanisms was responsible for the depression of the xanthate-induced flotation of copper-activated pyrite by sulphite, namely:

i) Xanthate decomposition in solution via perxanthate formation (Yamamoto 1980):

$$ROCSS^- + HSO_3^- + SO_3^{2-} + O_2 \rightarrow ROCSSO^- \rightarrow ROH + 2S_2O_3^{2-} + CO_2$$

ii) Desorption of dixanthogen from the pyrite surface (Miller 1970):

$$Fe(C_4H_9OCSS)_2 + HSO_3^- \rightarrow 2C_4H_9OCSS^- + FeSO_3 + H^+$$

iii) Consumption of dissolved oxygen by sulphite ions, accompanied by a drop of the pulp redox potential (Illyuvieva et. al 1984):

$$HSO_3^- + 1/2O_{2(aq)} \rightarrow SO_4^{2-} + H^+$$

iv) Pyrite oxidation by sulphite ions, rendering the mineral surface hydrophilic (accompanied by an oxidation of thiosulphate to sulphate):

$$FeS_2 \rightarrow FeS + S^0 \text{ (Abramov and Avdohin 1997)}$$

$$S^0 + HSO_3^- \rightarrow S_2O_3^{2-} + H^+ \text{ (Li et. al 1995)}$$

CONCLUSION

Sulphite depressed the xanthate-induced flotation of copper-activated pyrite at pH 7 and 9. The depressant effect of sulphite ions can be improved using air purging instead of nitrogen. Spectroscopic and solution studies revealed that depression of the pyrite flotation was due to the sulphite interaction with the isobutyl xanthate in solution and its adsorbed state, as well as with the pyrite surface itself.

The specific effect of sulphite ions on the surface chemistry of copper-activated pyrite pre-treated with isobutyl xanthate will be further determined using XPS and ToF-SIMS analyses. These spectroscopic techniques will allow identifying the type and exposure of the surface species that may be responsible for the pyrite depression. This study is ongoing and the results obtained will be discussed in a future work.

REFERENCES

ABRAMOV A.A. and AVDOHIN V.M. (1997), *Oxidation of sulphide minerals in beneficiation processes.* Gordon and Breach Science Publisher.

FUERSTENAU M.C., KUHN M.C., ELIGILLANI D.A. (1968), *The role of dixanthogen in the flotation of pyrite*. Trans. SME/AIME, 241, 148.

HOYACK M.E., RAGHAVAN S. (1987), *Interaction of aqueous sodium sulphite with pyrite and sphalerite*. Trans. Inst. Min. Metall. (Sect. C) 96, 173-178.

HUANG H.H. AND MILLER J.D. (1978), *Kinetics and thermochemistry of amyl xanthate adsorption by pyrite and marcasite*. Int. J. Miner. Process., 5, 241.

HUIATT J.L. (1969), *A study of the oxidation of the flotation collectors KETX and ammonium diethyl dithiophosphate*. M.Sc.Thesis, University of Utah.

ILLYUVIEVA G.V., GORSHTEIN A.E., TOROPOVA M.N. (1984), *Role of sulphite and thiosulphate ions in the copper-nickel sulphide ore flotation process*. Chem. Abs., 101: 175164n.

LEPPINEN J.O., BASILIO C.I., YOON R.H. (1988), In: Proc. 2nd Int. Symp. on Electrochemistry in Mineral and Metal Processing, P.E. Richardson and R. Woods (Editors), Atlanta, Georgia. The Electrochemical Society, Pennington, NJ, pp. 49-65.

LEPPINEN J.O., BASILIO C.I., YOON R.H. (1989), *In-situ FTIR studies of ethyl xanthate adsorption on sulphide minerals under conditions of controlled potential*. Int. J. Miner. Process., 26, 259-274.

LI J., MILLER J.D., WANG R.Y., LE VIER M. (1995), *The ammoniacal thiosulfate system for precious metal recovery*. In: Proceedings XIX Int. Mineral Processing Congress, SME, Littleton, Colorado, USA, vol. 4, pp. 37-42.

LYNCH A.J., JOHNSON N.W., MANLAPIG E.V., THORNE C.G. (1981), *Mathematical models of flotation. In: Mineral and Coal Flotation Circuits. Their Simulation and Control*. Developments in Mineral Processing, Elsevier, Amsterdam, pp. 57-96.

MAJIMA H. AND TAKEDA M. (1968), *Electrochemical studies of the xanthate-dixanthogen system of pyrite*. Trans. AIME., 241, 431.

MILLER J.D. (1970), *Pyrite depression by reduction of solution potential. Report to EPA Water Quality Office*, Grant No. 12010 DIM.

MISRA M., MILLER J.D., SONG Q.Y. (1985), *The effect of SO_2 in the flotation of sphalerite and chalcopyrite*. In: Flotation of sulphide minerals, Forssberg, K.S.E. (Ed.), Developments in Mineral Processing. Elsevier, Amsterdam, pp. 175-196.

MONTALTI M. (1993), *The interaction of ethyl xanthate with pyrite and pyrrhotite surfaces. Ph.D. Thesis*, Univ. S.A., Adelaide, Australia.

POLING G.W. (1961), *Infrared spectroscopy of xanthate compounds in the solid, solution and the adsorbed state*, M.Sc. thesis, University of Alberta, Edmonton, Canada.

PRESTIDGE C.A., RALSTON J., SMART R.ST.C. (1993), *The competitive adsorption of cyanide and ethyl xanthate on pyrite and pyrrhotite surfaces*. Int. J. Miner. Process., 38, 205-233.

SHEN W.Z., FORNASIERO D., RALSTON J. (2001), *Flotation of sphalerite and pyrite in the presence of sodium sulfite*. Int. J. Miner. Process., 63 (1), 17-28

YAMAMOTO T. (1980), *Mechanism of depression of Pyrite and sphalerite by sulphite*. In: Complex Sulphide Ores, Jones, M.J., (Ed), Inst. Miner. Metall., London, pp. 71-78.

Khmeleva T.N., Skinner W., Beattie D.A., Georgiev T.V., *Wpływ siarczynu sodu na flotację pirytu aktywowanego miedzią z udziałem ksantogenianu,* Fizykochemiczne Problemy Mineralurgii, 36, (2002) 185-195 (jęz. ang.)

Do badania wpływu siarczynu sodowego na proces flotacji pirytu aktywowanego miedzią użuto szeregu technik badawczych. Ich zadaniem było wyjaśnienie mechanizmu oddziaływania siarczynu sodowego z kolektorem (ksantogenianem izobutylowym) oraz z powierzchnią pirytu. Odkryto, że siarczyn depresuje flotację pirytu aktywowanego miedzią przy udziale ksantogenianu w warunkach pH 7, przy przepływie azotu lub powietrza. Depresujący efekt był większy, gdy powietrze zostało użyte. Badania spektroskopowe wskazują, że siarczyn sodu reaguje z powierzchnią pirytu a także z izobutylowym ksantogenianem i to zarówno w roztworze jak i na powierzchni ciała stałego. Na tej podstawie zaproponowano mechanizm depresji aktywowanego pirytu przez siarczyn sodu. Wyniki badań sugerują, że zarówno dekompozycja ksantogenianu jak i desorpcja dwuksantogenu z powierzchni pirytu są czynnikami odpowiedzialnymi za depresowanie pirytu. Dodatkowo zaobserwowano powstawanie na powierzchni pirytu grup hydroksylowych, które dodatkowo depresowały piryt, powodując hydrofilizacje jego powierzchni i brak możliwości utworzenia trwałego agregatu z banieczką powietrza.

Physicochemical Problems of Mineral Processing, 36 (2002) 197-208
Fizykochemiczne Problemy Mineralurgii, 36 (2002) 197-208

Hidayet CEYLAN*, Cahit HİÇYILMAZ**,Taki GÜLER**

COLLECTORLESS FLOTATION OF LEAD AND ZINC SULPHIDE FROM DEREKÖY ORE DEPOSITE

Received March 5, 2002; reviewed and accepted May 15, 2002

A study on collectorless flotation of lead and zinc sulphide present in the Derekoy ore in the presence of sodium sulphide was performed. The parameters of the process and influence of sodium sulphide, zinc sulphide, conditioning time, pH and cleaning of concentrate were investigated. The results were compared with collector added flotation using several types of collectors.

Kay words: flotation, galena , zinc sulphide, conditioning time, pH

INTRODUCTION

Sulphide minerals are readily amenable to flotation, but in most cases after a proper surface treatment. Thiol type collectors are most widely used to render selected constituents of a sulphide ore hydrophobic. However, at the Tsumeb concentrator in South Africa, galena and sphalerite are floated selectively from chalcopyrite without using any collector in the first 8 cells of each rougher bank (Boyce et al., 1970). Lepetic (1974) has also shown that chalcopyrite can be floated successfully by using frother alone after a dry autogenous grinding. These reports on collectorless flotation have rekindled an old controversy as to whether or not the sulphide minerals are naturally hydrophobic (Stewart and Finkelstein, 1973; Finkelstein et al., 1975; Fuerstenau, 1975; Heyes and Trahar, 1977; Gardner and Woods, 1979).

Over the years, experimental evidences have suggested that hydrophobicity of sulphide minerals varies from none to that of sulfur. Gaudin (1932), Ravitz and Porter (1933), Fuerstenau (1975), Yoon (1981), Luttrell and Yoon (1984), Hayes and Ralston (1988), Matabishi et al. (2000) showed that collectorless flotation of sulphide minerals

*Municipality of Çankaya, Ankara, Turkey
**Middle East Technical University, Ankara, Turkey

are possible under proper conditions. The proper conditions have been discussed by authors with different explanations. Yoon (1981) suggested the collectorless flotation was possible with the addition of sodium sulphide (Na_2S) to the pulp. The sulphide ions were thought to displace the hydrophilic surface oxidation products such as SO_4^{-2}, $S_2O_3^{-2}$, etc., due to difference in the fresh, unoxidised sulphide surface.

Luttrell and Yoon (1984) suggested that under the light of the thermodynamic instability of elemental sulphur in alkaline solution, polysulphide (i.e. S_x^{-2}; $2<x<8$) rather than elemental sulphur (S^o) causes the collectorless flotation. They also suggested that the increased floatability at low pH is due to a greater stability of elemental sulphur which has greater hydrophobicity compared to polysulphide.

Miller (1988) also stated that sulphide minerals are thermodynamically unstable and sufficient oxygen remains in the system to cause oxidation, presumably leading to the formation of elemental sulphur. This hypothesis originally proposed by Wark (1938). Plaksin (1949) stated that adsorbed oxygen decreases surface hydration, thereby, rendering hydrophobicity to mineral. On the other hand, formation of metal deficient surface was proposed by Buckley et al. (1985) as the key species for self-induced floatability.

Luttrell and Yoon (1982, 1983) stated the importance of pulp potential (Eh) which is a critical factor in the collectorless flotation. Typically, when sodium sulphide was added to the pulp, the potential immediately dropped and no flotation was possible. Only after approximately 15 minutes of conditioning time, when potential become positive, the flotation was possible. Several researchers suggested that sulphide minerals can be floated under mild to modest oxidising condition.

It was shown that the collectorless floatability of each sulphide studied was directly linked to its ease of oxidation as well as to the stability of the hydrophobic surface state which was produced. The hydrophobic surface species might be elemental sulphur or polysulphide or a sulphur-rich metal-deficient surface.

EXPERIMENTAL

Lead and zinc sulphide ore from Şebinkarahisar - Giresun in Turkey was tried to float without collector. The mineralogical analysis of the specimens showed that main ore minerals were sphalerite, galena, pyrite, chalcopyrite, fahlerz (tennantite and tetrahedrite), cerussite-anglesite, quartz (~ 40-45 %), limonite and other siliceous minerals. Sphalerite, having more massive appearance, had sometimes chalcopyrite inclusions in it. The size of the inclusions was sometimes as low as 5 microns. Chalcopyrite was also found as free grains in galena and sphalerite together with fahlerz. Liberation size of minerals was around 150 microns. The sample contained 3.34 % Pb, 11,68 % Zn, 0.20 % Cu, 11.3 % S and 0.36 % Al.

The ore was ground to –1 mm and stored in a double nylon bags with a weight of 300 gram to prevent possible surface oxidation. Flotation experiments were carried out with Denver Sub-A flotation machine having 1.1 dcm^3 cell after the grinding of ore to

100 % passing 150 µm (80 % -69 µm). Rotational speed of the impeller was 1500 rpm and aeration rate was 2.75 dcm^3/min throughout the experiments. The frother (MIBC) dosage was kept constant in all tests as 90 g/Mg.

Figure 1 shows the general flowsheet for collectorless flotation. In this research, effect of sodium sulphide, zinc sulphide, conditioning time, pH and cleaning of concentrates were investigated. Optimum result was compared with that of a conventional flotation using different types of collector.

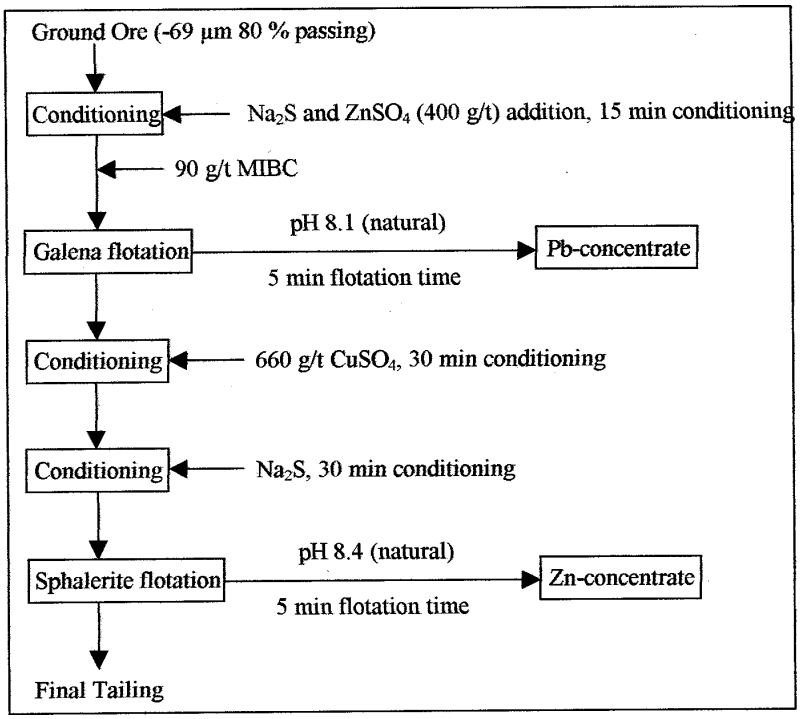

Fig 1. General flowsheet of collectorless flotation with initial values of parameters

RESULTS AND DISCUSSIONS

COLLECTOR ADDED FLOTATION EXPERIMENTS

To see the flotation characteristics of the ore, experiments were initiated with collector addition. A comparison of the results obtained with collector addition and without collector will helps to measure the success of idea of collectorless flotation of the lead and zinc minerals in the ore. The galena and sphalerite were floated selectively a sulphydryl type collectors. 100 g/Mg collector was used and conditioned for 5 minutes throughout the experiments. Sodium sulphide was not used in collector added flotation experiments. The results are given in Table 1.

Table 1. Effect of different collectors on galena and sphalerite flotation

		Grade		Recovery		Type of collector
Product	Weight, %	Zn, %	Pb, %	R_{Zn}, %	R_{Pb}, %	
Pb-Conc	28.42	21.60	10.76	52.56	91.56	CyanamidAero 3051
Zn-Conc	10.34	44.50	1.70	39.14	5.29	
Tailing	61.19	1.50	0.26	8.30	3.15	
Pb-Conc	17.33	17.32	17.70	27.07	89.90	CyanamidAero 238
Zn-Conc	17.14	41.11	0.52	63.54	2.61	
Tailing	65.53	1.59	0.39	9.39	7.49	
Pb-Conc	1909	18.80	16.70	30.13	89.27	CyanamidAero 3477
Zn-Conc	21.21	35.00	0.56	62.33	3.32	
Tailing	54.70	1.50	0.44	7.54	7.11	
Pb-Conc	20.56	20.50	14.46	36.62	89.28	CyanamidAero 343
Zn-Conc	15.94	40.60	1.20	56.23	5.74	
Tailing	63.50	1.30	0.26	7.15	4.98	
Pb-Conc	10.76	14.00	27.14	13.41	86.82	CyanamidAero 208
Zn-Conc	24.83	35.00	0.80	77.39	5.91	
Tailing	64.41	1.60	0.38	9.20	7.27	
Pb-Conc	20.62	19.10	15.00	38.88	89.39	CyanamidAero 325
Zn-Conc	14.95	34.10	0.86	50.34	3.72	
Tailing	64.43	1.70	0.37	10.78	6.89	
Pb-Conc	13.40	21.60	24.60	25.21	90.81	CyanamidAerophine 3418 A
Zn-Conc	20.29	38.40	0.34	67.87	1.90	
Tailing	66.31	1.20	0.40	6.92	7.29	
Pb-Conc	20.46	20.20	16.30	36.29	90.13	Cyanamid Aerofloat 33
Zn-Conc	15.99	40.60	0.70	57.00	3.03	
Tailing	63.55	1.20	0.10	6.71	6.84	
Pb-Conc	27.83	20.10	11.70	49.24	91.21	Cyanamid Aerofloat 25
Zn-Conc	13.73	36.90	1.00	44.60	3.85	
Tailing	58.44	1.20	0.30	16.16	4.97	
Pb-Conc	16.38	17.80	18.90	26.27	87.70	Hoechst Hostafloat LSB
Zn-Conc	18.36	40.30	0.50	66.66	2.60	
Tailing	65.26	1.20	0.52	7.07	9.70	
Pb-Conc	16.52	15.91	18.72	22.43	91.66	CyanamidAero 4037
Zn-Conc	20.41	36.08	0.47	63.05	2.87	
Tailing	63.07	2.68	0.29	14.52	5.53	

COLLECTORLESS FLOTATION EXPERIMENTS

Sodium Sulphide

Sodium sulphide (Na_2S $9H_2O$) was used to clean the surface oxides of sulphide minerals as sulphidising agent. The amount of sodium sulphide added in zinc circuit was kept constant as 150 g/Mg of ore while it was changed from 0 to 300 g/Mg in lead circuit. The experimental conditions and results are shown in Figure 2.

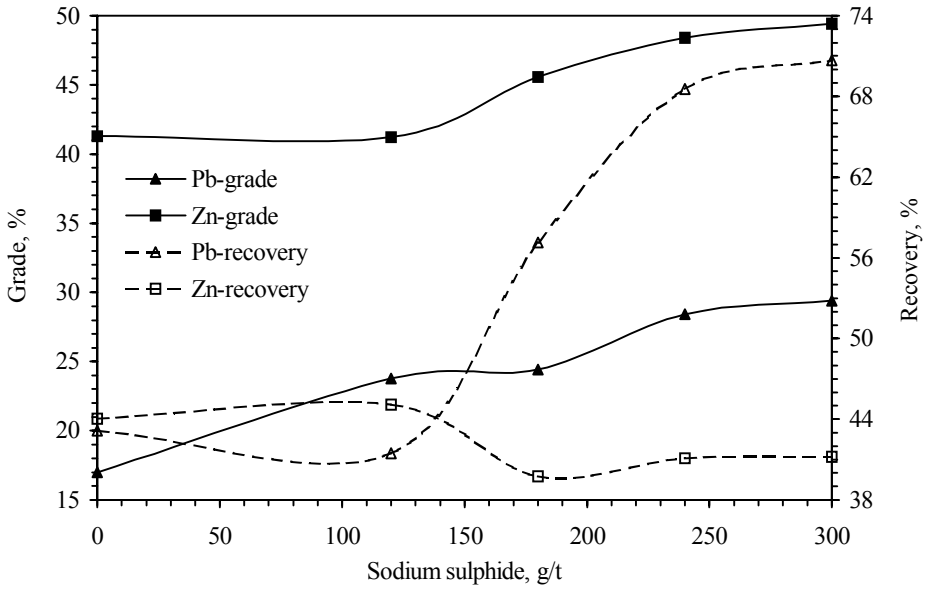

Fig. 2. Effect of sodium sulphide added in Pb-circuit on Pb and Zn grade and recoveries in their corresponding concentrates (pH 8.1 in Pb-circuit, and pH 8.4 and 660 g/Mg $CuSO_4$ addition in Zn-circuit)

The Pb grade as well as the recovery and Zn grade increased with Na_2S addition up to 240 g/Mg Na_2S concentration. As it was mentioned above, Na_2S can be used either as sulphidising agent for oxidised minerals or a reducing agent for sulphide depression. Then, it may be concluded that the iron-oxyhydroxides, possibly coming from steel-mill grinding and pyrite, a component of the ore, and Pb and Zn-oxyhydroxides would cover mineral surfaces. So, the increasing of the Pb and Zn grade would be attributed to the removal of these interfering metal-oxyhydroxides and concomitant exposure of the sulphur-rich sub-layer (Cases et al., 1997; Grano et al., 1997). 240 g/Mg sodium sulphide gave a reasonable results by considering both Pb and Zn grades and recoveries of their corresponding concentrates. Since sodium sulphide is a strong reducing agent, it was not preferred to use more than 240 g/Mg in the lead circuit due to possibility of an adverse effect in the zinc circuit (Herrera-Urbina, 1999)

Figure 3 shows the experiment conditions and results of effect of sodium sulphide in the Zn-circuit. Results showed that Zn-recovery sharply increased up to 60 g/Mg Na_2S, and then gradually decreased. This would be originated from the removal of hydrophilic oxyhydroxide compounds from the sphalerite surface as pointed out above. Or, it may also be proposed that formation of a metal-deficient sulphur-rich surface (Buckley et al., 1985), adsorption of polysulphides (Luttrell and Yoon, 1984) or the presence of elemental sulphur (Gardner and Woods, 1979; Hayes and Ralston, 1988) probably contributed to hydrophobicity of the Cu-activated sphalerite surface. More than 60 g/t of sodium sulphide did not improve the zinc grade and recovery. Instead, it results in a small decrease, since Na_2S is a depressing agent for unoxidised sulphide minerals due to decrease in pulp potential. Therefore, this gradual decrease would be attributed to the depression of sphalerite due to reducing pulp potential values.

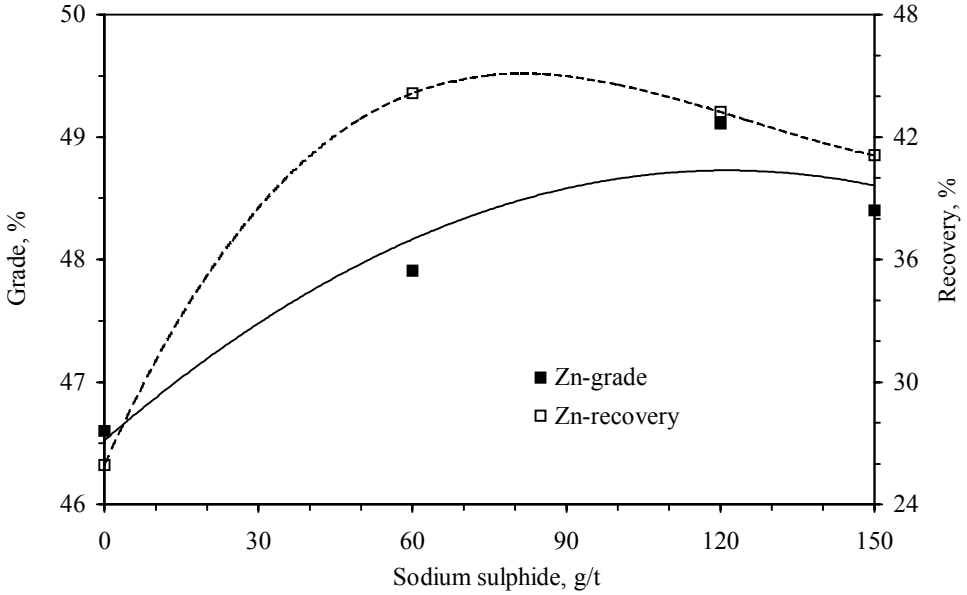

Fig. 3. Effect of sodium sulphide added in zinc-circuit on Zn-grade and recovery (pH 8.1 in Pb-circuit, and pH 8.4 and 660 g/Mg $CuSO_4$ addition in Zn-circuit)

Zinc Sulphide

Zinc sulphate dosage was varied from 20 g/Mg to 830 g/Mg. Zinc sulphate decreases the possible activation of sphalerite by Pb^{+2} ions coming from galena, and so the loss of sphalerite in the Pb-circuit (Figure 4). However, large amounts of it made the flotation of sphalerite difficult in the zinc circuit (Figure 5), which caused the zinc losses in final tailing. In addition, its adverse effect was also observed in Pb grade and recovery of galena concentrate (Figure 4) possibly due to $Zn(OH)_2$ precipitation on

mineral surface (Laskowski et al., 1997; Trahar et al., 1997; El-Shal et al., 2000). Also, it results in the increase in Pb recovery in Zn-circuit possibly due to Cu-activation (Figure 5). Since, in the zinc-circuit copper sulphate was added to activate sphalerite and to eliminate the depressing effect of zinc sulphate. 100 g/Mg of zinc sulphate was the optimum value as seen from Figures 4 and 5.

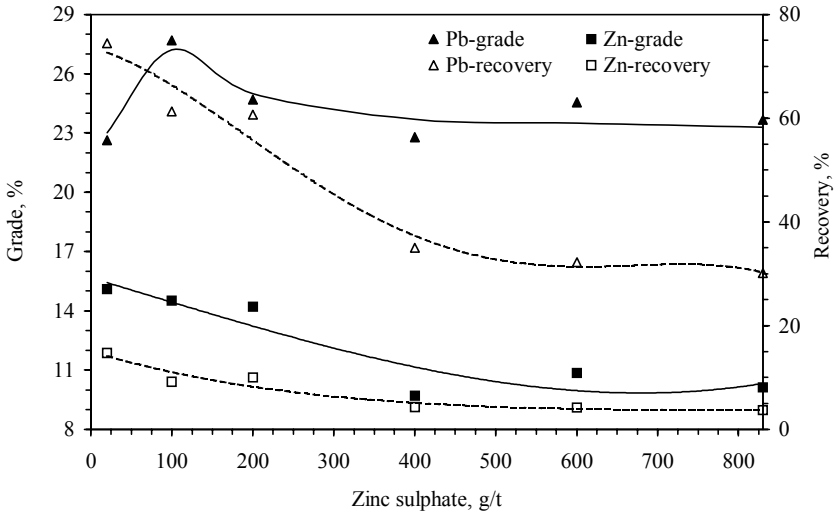

Fig. 4. Effect of zinc sulphate on Pb and Zn grades and recoveries in Pb-concentrates (pH 8.1 in Pb-circuit)

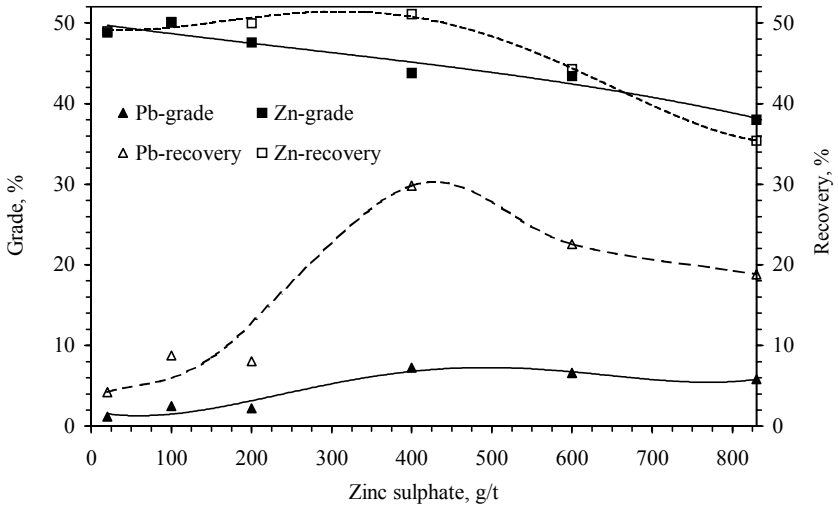

Fig. 5. Effect of zinc sulphate on Pb and Zn grades and recoveries in Zn-concentrates (pH 8.1 in Pb-circuit and, pH 10.3 and 660 g/t $CuSO_4$ addition in Zn-circuit)

Conditioning Time

The conditioning period for sodium sulphide reaction on sulphide surface is an important parameter. This is not only for covering of sulphide surfaces with elemental sulphur and polysulphide ions but also important for the oxidation potential of pulp. Sodium sulphide, as it is mentioned before, is a strong reducing agent and, therefore, time is necessary for increasing the pulp potential. Also, iron coming from steel mill was a high oxygen consumer and, hence, decreased the rate of sulphide oxidation, which in turn diminished the hydrophobisation with sodium sulphide. So, conditioning time was increased to maintain oxygen and then to reduce the adverse effect of iron ions coming from the mill.

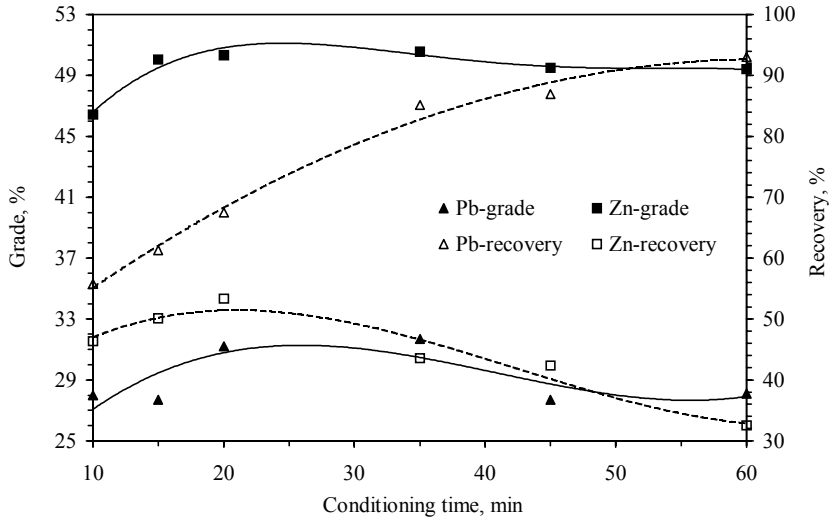

Fig. 6. Effect of conditioning time in lead circuit on both Pb and Zn grades and recoveries in their corresponding concentrates (pH 8.1 and 100g/Mg $ZnSO_4$ in Pb-circuit and pH 10.3 and 660 g/Mg $CuSO_4$ in Zn-circuit)

The conditioning time was changed from 10 to 60 minutes in the lead circuit while it was kept constant as 30 minutes in the zinc circuit. Figure 6 shows the experimental conditions and results. The results support the findings of Luttrell and Yoon (1983) that a relatively fresh surface made by sodium sulphide is needed to an oxidising environment for collectorless flotation.

pH

pH of the medium is an important factor that influences flotation. To investigate the optimum values for both circuits, pH was varied from 5 to 9 in the Pb-circuit while it was kept constant at pH 8 in Zn-circuit. After the determination of optimum pH in lead circuit, it was varied from 5 to 11 in zinc circuit. Figure 7 shows the experimental conditions and results.

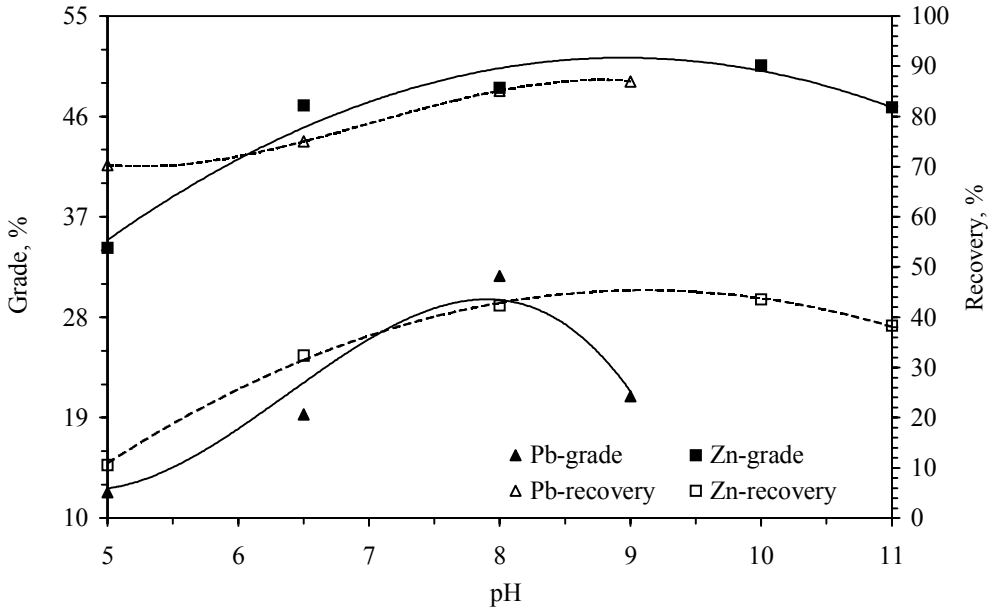

Fig. 7. Effect of pH on Pb grade and recovery in Pb-circuit and on Zn grade and recovery in Zn-circuit (100g/t $ZnSO_4$ in Pb-circuit and, 660 g/t $CuSO_4$ in Zn-circuit)

Galena showed good flotation at pH 8 and similar results has been found by Matabishi et al. (2000). At very high pH values, iron hydroxides possibly coming from the steel mill and pyrite content of ore and metal-oxyhydroxides made the surface hydrophilic, thereby reducing floatability (Laskowski et al., 1997; Zhang et al., 1997). On the other hand, higher pH values (pH 10) were suitable for Cu-activated sphalerite flotation with high grade and recovery. Hukki et al. (1952) suggested that copper hydroxy species or hydroxide adsorbs rapidly on sphalerite but, because of the high solubility of $Cu(OH)_2$, the adsorbed precipitate would be converted to less soluble copper sulphide in basic solution. Ralston and Healy (1980a, b) and Laskowski et al. (1997) suggested that the hydroxide slowly releases Cu^{+2} ions into solution, which in turn form a flotation active product such as (Zn,Cu)S.

Cleaning of Lead and Zinc Concentrates

Most of the sulphide concentrates can be upgraded by cleaning steps. To upgrade the rougher concentrate, an experiment with cleaning stage was performed. The flowsheet with its conditions and results are shown in Figure 8.

As shown in Figure 8, a galena concentrate assaying 43.08 % Pb with a recovery of 72.49 %, and a sphalerite concentrate assaying 59.79 % Zn with a recovery of 46.99 % were obtained by one stage cleaning. However, zinc grade in lead concentrate was

also high. More or less the same results were obtained with collector added flotation experiments. Almost about 20 % zinc grade in lead concentrate may cause penalty in lead smelter. It might be due to chalcopyrite inclusion to sphalerite mineralogically and lead activation of sphalerite during flotation.

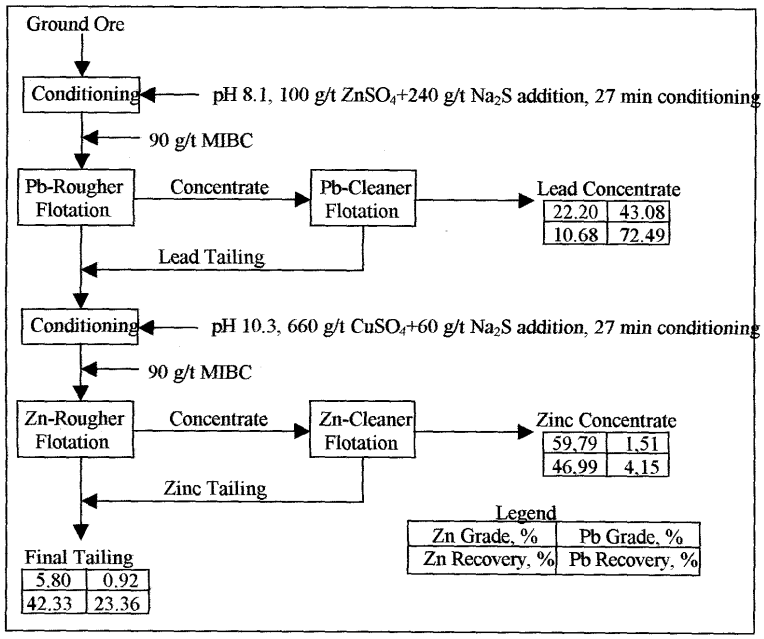

Fig. 8. Cleaning of lead and zinc concentrates

CONCLUSIONS

Collectorless flotation of lead and zinc sulphide from ores is possible after selective rougher concentrates were obtained. The lead concentrate contained 31.70 % Pb with 85.13 % recovery and the Zn concentrate assayed 50.59 % Zn assay with 43.58 % recovery. It was able to challenge with collector added flotation results. Collector added flotation had higher recovery for both lead and zinc in their corresponding concentrates. The cleaning of concentrates obtained by collectorless flotation increased the lead and zinc grades. The final lead concentrate contained 43.08 % Pb with 72.49 % recovery and the final zinc concentrate contained 59.79 % Zn with 46.99 % recovery.

The losses of Pb and Zn in tailing can not be ignored. The tailing should be reground to recover the lead and zinc values. The loss of zinc was higher than the loss of lead in tailing. It can be explained with the size distribution of the minerals. Since the hardness of galena is less than sphalerite, it was finer during flotation, which decreased the loss of lead in tailing.

REFERENCES

BOYCE, J.R., VENTER, W.J. and ADAM, J., (1970*). Beneficiation of particle at the Tsumeb Concentrator,* World Symposium on Mining and Metallurgy of Lead and Zinc, Raush, D.O. and Mariacher, B.C. (Eds.), AIME, New York, N.Y., V.1, pp.542-570.

BUCKLEY, A.N., HAMILTON I.C. and WOODS, R., (1985). *Investigation of The Surface Oxidation of Sulphide Minerals by Linear Potential Sweep Voltammetry and X-Ray Photoelectron Spectroscopy,* Flotation of Sulphide Minerals, Forssberg, K.S.E. (Ed.), Elsevier, Amsterdam, pp.41-60.

CASES, J.M., MIELCZARSKI, J.A., de DONATO, P., MIELCZARSKI, E., KONGOLO, M., BARRJS, O., ALNOT, M. and EHRHARDT, J.J., (1997). *Relationship between Surface Composition and Flotation Behaviour of Chalcopyrite Prepared under Different Conditions*, Proceedings of the XX International Mineral Processing Congress, Aachen, 21-26 September, pp. 477-489.

EL-SHALL, H.E., ELGILLANI, D.A. and ABDEL-KHALEK, N.A., (2000). *Role of zinc sulfate in depression of lead-activated sphalerite, Int. J. Miner. Process.*, V.58, pp.67-75.

FINKELSTEIN, N.P., ALLISON, S.A., LOVELL, V.M. and STEWARt, B.V., (1975). *Natural and induced hydrophobicity of sulphide mineral system*, Advances in Interfacial Phenomena os Particulate/Solution/Gas Systems: Application to Flotation Research, Somasundaran, P. and Grieves, R.G. (Eds.), Am. Ins. Chem. Eng., Symosium Series No. 150, V.71, pp.159-160.

FUERSTENAU, M.C., (1975). Future Trends in Mineral Processing Research, Special Lecture at Mc Gill University, Montreal, Que.

GARDNER, J.R. and WOODS, R., (1979. "An Electrochemical Investigation of the Natural Floatability of Chalcopyrite", *Int. J. Miner. Process.*, Vol. 6, pp. 1-16.

GAUDIN, A.M., 1932. Flotation, 1st Edition, McGraw-Hill, New York, 552 p.

GRANO, S.R., SOLLAART, M., SKINNER, W., PRESTIDGE, C.A. and RALSTON, J., (1997). *Surface modifications in the chalcopyrite-sulphite ion system. I. Collectorless flotation, XPS and dissolution study, Int. J. Miner. Process.*, V.50, pp.1-26.

HAYES and RALSTON, (1988). *The Collectorless Flotation and Separation of Sulphide Minerals by Eh Control, Int. J. Miner. Process.*, Vol. 23, pp. 55-84.

HERRERA-URBINA, R., SOTILLO, F.J. and FUERSTENAU, D.W., (1999). *Effect of sodium sulphide additions on the pulp potential and amyl xanthate flotation of cerussite and galena, Int. J. Miner. Process.*, V.55, pp.157-170.

HEYES, G.W. and TRAHAR, (1977). *Natural Floatability of Chalcopyrite, Int. J. Miner. Process.*, Vol. 4, pp. 317-344

HUKKI, R.T., PALOMAKI, A. and ORIVUORI, E., (1952). *Electrophoretic investigation of the activation of sphalerite by copper sulphide in flotation, Suom. Kemistil.*, B 52, pp.42-49.

LASKOWSKI, J.S., LUI, Q. and ZHAN, Y., (1997). *Sphalerite activation: Flotation and electrokinetic studies, Minerals Eng.*, V.10, No.8, pp.787-802.

LEPETIC, V.M., (1974). *Flotation of Chalcopyrite without Collector after Dry, Autogenous Grinding, CIM Bulletin*, pp.71-77.

LUTTRELL, G.H. and YOON, R.-H., (1982). *The collectorless flotation of sulphide ores,* 111th AIME Annual Meeting, February 14-18, Dallas, Texas.

LUTTRELL, G.H. and YOON, R.-H., (1983). *ESCA and mass spectrometric studies of the collectorless flotation of chalcopyrite,* 111th AIME Annual Meeting, March 6-10, Atlanta, Georgia.

LUTTRELL, G.H. and YOON, R.-H., (1984). *The collectorless flotation of chalcopyrite ores using sodium sulphide*, Int. J. Miner. Process., Vol. 13, pp.271-283.

MATABISHI, M.K., HANDFIELD-JONES, R. and AKDOĞAN, G., (2000). *Effect of Electrochemical Environment on Collectorless Flotation of Some Sulphide Minerals,* Mineral Processing on the Verge of the 21st Century, Proceedings of the 8th International Mineral Processing Symposium, Özbayoğlu, G., Hoşten, Ç., Atalay, M.Ü., HIÇYILMAZ, C. and AROL, A.İ. (Eds.), 16-18 October, Antalya/Turkey, pp. 211-214.

MILLER, J.D., (1988). *The significance of electrochemistry in the analysis of mineral processing phenomena*, 7th Australian Electrochemistry Conference, Sydney, Australia.

PLAKSIN, I.N., (1949). *Inherent hydrophobicity of sulphide minerals under flotation conditions*, Doklayd Akad. Nauk. SSSR, V.66, pp.91-93.
RALSTON, J. and HEALY, T.W., (1980a). *Activation of zinc sulphide with Cu(II), Cd(II) and Pb(II) I: Activation in weakly acid media, Int. J. Miner. Process.* V.7, pp.175-201.
RALSTON, J. and HEALY, T.W., (1980b). *Activation of zinc sulphide with Cu(II), Cd(II) and Pb(II) I: Activation in neutral and alkaline media, Int. J. Miner. Process.*, V.7, pp.203-217.
RAVITZ, S.F. and PORTER, R.R., (1933). *Oxygen Free Flotation I: Flotation of Galena in Absence of Oxygen*, AIME Technical Publication, No: 513, USA, 17 p.
STEWART, B.V. and FINKELSTEIN, N.P., (1973*). A preliminary investigation of the flotation of copper activated sphalerite without the use of collectors*, National Institute of Metallurgy, Johannesburg. Report No. 1587.
TRAHAR, W.J., SENIOR, G.D., HEYES, G.W. and CREED, M.D., (1997). *The activation of sphalerite by lead: A flotation perspective, Int. J. Miner. Process.*, V.49, pp.121-148.
WARK, I.W., (1938). *Principles of Flotation,* Australasian Institute of Mining and Metallurgy, Melbourne, 346 p.
YOON, R.-H., (1981). *Collectorless Flotation of Chalcopyrite and Sphalerite Ores Using Sodium Sulphide*, Int. J. Miner. Process., Vol. 8, pp. 31-48.
ZHANG, Q., XU, Z., BOZKURT, V. and FINCH, J.A., (1997). *Pyrite Flotation in the Presence of Metal Ions and Sphalerite,* Int. J. Miner. Process., V.52, pp.187-201.

Ceylan H., Hicyilmaz C., Guler T., *Flotacja bez użycia kolektora rudy ołowiu i cynku z pokładu Derekoy (Turcja)*, Fizykochemiczne Problemy Mineralurgii, 36, (2002) 197-208 (w jęz. ang.)

Przeprowadzono badania procesu flotacji bez użycia kolektora siarczkowej rudy ołowiu i cynku, stosując siarczek sodu. Badano wpływ stężenia siarczku sodu, czasu kondycjonowania oraz pH zawiesiny flotacyjnej na parametry wzbogacania cynku i ołowiu. Określono także wpływ czyszczenia koncentratu na proces wzbogacania. Otrzymane wyniki z flotacji bez użycia kolektora porównano z wynikami, jakie uzyskano stosując szereg znanych kolektorów.

Physicochemical Problems of Mineral Processing, 36 (2002) 209-216
Fizykochemiczne Problemy Mineralurgii, 36 (2002) 209-216

Krystyna SEIFERT*, Agnieszka MOSKA*, Florian DOMKA*

THE EFFECT OF WASTE PHOSPHOGYPSUM ON THE DENITRIFICATION AND DESULFURICATION PROCESSES

Received March 15, 2002; reviewed and accepted May 15, 2002

The effect of waste phosphogypsum obtained after phosphoric acid production from apatites and phosphorites, on the processes of denitrification and desulfurication taking place with the use of bacteria from the genera *Bacillus* and *Desulfotomaculum*, have been investigated.

It has been shown that the phosphogypsum concentrations used in the experiments were can serve as a sulphate source for the *Desulfotomaculum* bacteria. The phosphogypsum is not toxic towards the bacteria. The phosphogypsum has also been found to play the role of an electron acceptor in the processes of oxidation of simple organic substrates in the processes of bioreduction of nitrates or sulphates. In the optimum conditions of desulfurication in a medium containing the phosphogypsum, organic substrate and *Desulfotomaculum ruminis* bacteria, the degree of conversion is close to 90%, and a decrease of TOC reaches about 50%.

Key words: phosphogypsum, denitrification, desulfurication, sulphate reducing bacteria (SRB)

INTRODUCTION

Phosphogypsum is a waste product of the process in obtaining phosphoric acid from apatites and phosphorites by extraction with sulphuric acid. It is characterised by strongly acidic pH, and apart from calcium sulphate (~95%) it contains some amount of adsorbed phosphoric acid, organic contaminants and a small admixture of rare earth metals (mainly lanthanides) (Praca zbiorowa, 1958). In Poland there are almost 40 mln tons of this waste, aggressive towards the natural environment, at dumping grounds near Boleslawiec (Wizow), Gdansk and Police (Kowalski et al.).

Because of high and increasing demand for phosphoric acid and its derivatives (fertilisers and detergents), the amounts of this waste are expected to increase. In the chemical plant Police, the dumping grounds are filled with about 20 mln tons of this waste and this amount is expected to increase each year by about 2 mln tons. The hitherto used methods of utilisation of this waste, including conversion into cement,

* Adam Mickiewicz University, Faculty of Chemistry, 60-780 Poznan, Grunwaldzka 6

construction materials or sulphuric acid have been uneconomic, as required high investment costs. An interesting alternative are the microbiological methods based on phosphogypsum biodegradation and simultaneously utilising the organic matter e.g. from the wastes from agricultural and food industry (Gąsiorek et al. 1986).

Under anaerobic conditions sulphate reducing bacteria (SRB) cause phosphogypsum biotransformation to hydrogen sulphide, whereas the organic matter is oxidised to CO_2 or simple organic acids (Przytocka-Jusiak et al. 1995). Because of the possibility of biodegradation of many different organic substances in the presence of sulphate, SRB have been successfully used for reduction of ChZT in wastes (Domagała et al 1991, Domka et al. 2000, Barton 1995). The sulphides formed in the process of SO_4^{2-} - reduction may be subjected to oxidation by sulphur bacteria *Thiobacillus ferrooxidans* and *Thiobacillus thiooxidans*. In this process sulphur and sulphuric acid are formed ((Gąsiorek et al. 1983).

The methods of detoxication and biodegradation of all kinds of wastes have recently gained recognition because of the need to tackle chemical contamination of the waste dumping grounds threatening ecological equilibrium. This paper presents effect of the concentration of phosphogypsum being a waste product from processing of apatites and phosphorites from Morocco in the Police Chemical Plant, on the processes of denitrification and microbiological reduction of sulphates with the use of bacteria from the genera *Bacillus* and *Desulfotomaculum*.

MATERIALS AND METHODS

MICROORGANISMS

Bacteria from the genus *Bacillus* were isolated and identified according to the earlier given procedure ((Waligórska et al. 1992). The sulphate reducing bacteria from the genus *Desulfotomaculum* were isolated in a modified Starkey medium, according to the earlier described procedures (Domagała et al. 1992). The phosphogypsum studied was the waste from the Police Chemical Plant (sample collected on June 20th, 2000) processing raw materials from Morocco. Prior to the introduction into bioreactors, the samples were grounded and sieved (mesh size 0.315 mm).

KINETIC STUDY

The process of denitrification was conducted at 37^{o}C in closed and sterilised glass reactors of 90 cm^3 capacity, filled with a portion of 50 cm^3 of the medium supplemented with phosphogypsum tested. After pH adjustment to 7.5, the contents of the reactor was inoculated with 4% inoculum of pure bacteria culture collected at the logarithmic phase of growth. The medium was sterilised under the conditions: p = 0.5 MPa, T = 120^{o}C for 20 minutes. Because of acidity production in the reaction environment, every two hours pH was corrected to 7.5 value. Samples taken at certain time intervals were subjected to determination of nitrate (V) and nitrate (III) concentrations.

The results analysed and interpreted were mean values obtained from three measurements of NO_3^- (nitrate) and NO_2^- (nitrite) concentrations. They were referred to the results obtained for the reference samples without phosphogypsum.

MICROBIOLOGICAL DESULFURICATION

The process was conducted at 37°C under anaerobic conditions (helium) at pH 6.8 – 7.2, in tightly closed glass reactors filled with 50 cm^3 of the modified sulphate-free Starkey medium containing [g/dm^3]: $MgCl_2 \times 6H_2O$ = 1.65, NH_4Cl = 1.00, K_2HPO_4 = 5.00, $CaCl_2$ = 0.13, $Fe(NO_3)_3 \times 9H_2O$ = 0.515, sodium lactate 10.16. After addition of appropriate amount of phosphogypsum, the medium was deoxidised and inoculated with 4% volume of inoculum collected from culture being in the logarithmic phase of growth (after 24h). The reaction rate was determined as the degree of sulphate conversion to sulphide measured at certain time intervals. To measure the degree of this conversion, the system was blown with helium and the H_2S released was collected in absorber containing 0.1N cadmium acetate. The equipment used in the study and the media were sterilised for 20 minutes at 120°C.

Parallel experiments were conducted under the same conditions, but using the standard Starkey medium (without phosphogypsum) for obtaining reference samples. The results are averages of at least 3 measurements. TOC (total organic carbon) – the index describing the content of organic substance, was determined by the dichromate titration before and after the experiment (Standard Methods, 1992).

CHEMICAL ANALYSES

Concentrations of sulphates were determined by the weight method (Pol. Kom. Normalizacji i Miar), calcium – by the complexometric method (Standard Methods, 1992), phosphates - by the spectrophotometric method (Williams 1985), total iron and magnesium - by ASA (ELA Unicam SP 90A spectrophotometer).

Concentration of nitrates (V) were measured using the ion-selective electrode Detector, and concentration of nitrates (III) – using the spectrophotometric method (Beckman DU-640 spectrometer, wavelength λ = 520 nm).

Concentration of sulphides was determined by the iodometric method after precipitation of CdS (Williams 1985).

RESULTS AND DISCUSSION

The chemical composition of the phosphogypsum studied is given in Table 1. Knowing this composition we could choose the correct proportion between sulphate ions and organic carbon in the reaction mixture. The impact of phosphogypsum on the environment was studied on the example of two well-known processes of microbiological conversion involved in the cycles of nitrogen and sulphur. Fig. 1 illustrates the effect of the concentration of the phosphogypsum on the process of denitrification by genus *Bacillus.*

Table 1. Chemical composition of Morocco phosphogypsum

Component	Content [% w/w]
SO_4^{2-}	60.25
Ca^{2+}	22.39
PO_4^{3-}	1.60
Mg^{2+}	0.06
Fe total	0.04
Insoluble matter	0.70

Phosphogypsum solubility at 25°C = 2.81 g/dm^3

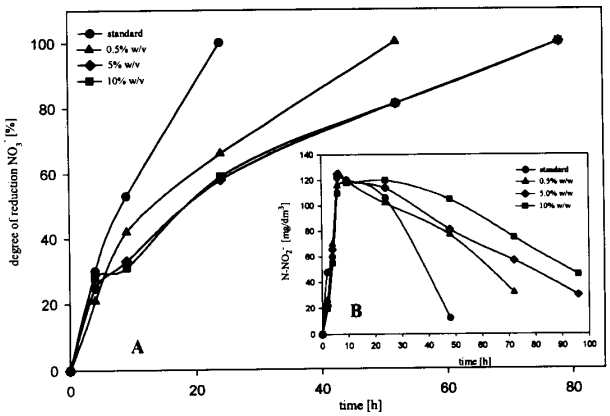

Fig. 1. The influence of the Marocco phosphogypsum concentration on efficiency of nitrates(V) reduction (A) and concentration of nitrates(III) (B) carried out in the presence of *Bacillus licheniforms* bacteria (pH = 7.5, T = 37°C, C/N = 2.28)

The kinetic curves of the process, obtained for three different concentrations of phosphogypsum in the medium and for the reference sample were similar, which indicated a similar mechanism of the process. No induction period of the reaction was observed. The presence of phosphogypsum causes only an extension of the time of the process. As the denitrification process studied involves the following intermediate compounds according to the scheme (Domka et al. 2000):

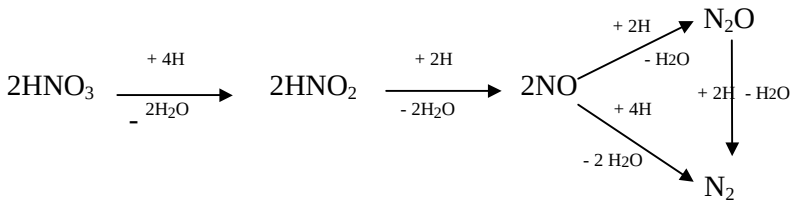

controlled the changes in the concentration of nitrates (III). As follows from the measurements of changes in NO_2^- concentration (Fig. 1b), the concentration of nitrates (III) at first strongly increases to a value of 120 mg/dm^3, irrespectively of the

concentration of phosphogypsum in the medium, and then it smoothly drops to a level below 10 mg/dm^3 – also in the reference sample. The presence of phosphogypsum only extends the time needed for its decomposition (Kornaros et al. 1996)..

The process of denitrification is of great importance in agriculture (soil deficiency in biologically useful nitrogen), in this context the results of the study indicate that the use of phosphogypsum for field cultivation should not disturb the cycle of nitrogen conversions in the soil. Similarly, the presence of phosphogypsum in water reservoirs will not cause an over-accumulation of difficult to remove nitrates (V) and nitrates (III).

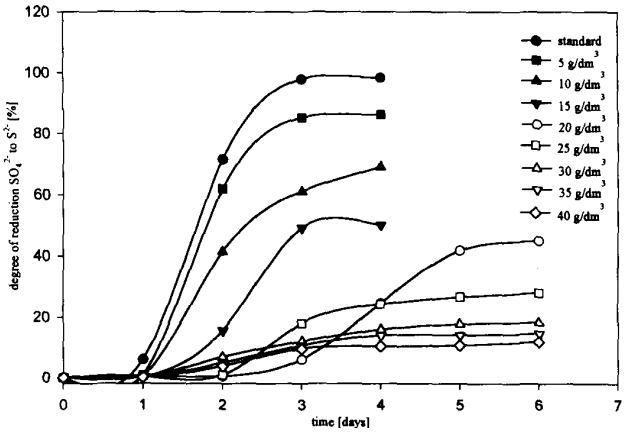

Fig. 2. The influence of the concentration of phosphogypsum on the dissimilatory sulphates reduction proces carried out with *Desulfotomaculum ruminis* bacteria (pH = 7.0, 37^{o}C, C/S = 3.2)

Fig. 2 presents results of a study on the effect of the concentration of phosphogypsum on desulfurication taking place in the medium in the presence of *Desulfotomaculum ruminis* bacteria. This species is the best known mezophilous bacteria living at a neutral pH and capable of using many different organic compounds in the process of reduction of sulphates and for this reason often used in studies on utilisation of wastes and purification of sewage (Szulczynski et al. 1987, Waligórska et al. 2000, Walenciak et al. 1999).

The kinetic curves of biotransformation of phosphogypsum used at concentrations up to 15 g/dm^3 in a lactate medium have a similar shape corresponding to typical phases of micro-organisms multiplication, that is to the induction period, phase of logarithmic growth, equilibrium phase and stabilisation of the process. In this range of concentrations the induction period is more or less the same and takes about 24h. With increasing concentration of phosphogypsum, from 5 to 15 g/dm^3, the degree sulphate reduction systematically decreases reaching 45% in the medium containing 15 g phosphogypsum per dm^3. A further increase of its concentration causes a pronounced inhibition of the process of sulphate reduction reaching a level of 10% in a medium containing 40 g phosphogypsum per dm^3, Fig. 2.

Thus, it has been shown that the phosphogypsum tested (from Police Chemical Plant) can be used as a substrate for sulphates reducing bacteria. In a medium

containing up to 15 g/dm^3 of the phosphogypsum, in the presence of lactate at a C/S ratio of 3.2, it can be suggested that the phosphogypsum is decomposed into, among others, calcium carbonate and hydrogen sulphide. This process might be described as follows:

$$\underset{\text{(phosphogypsum)}}{CaSO_4 \cdot 2H_2O} + \underset{\text{(organic compound)}}{2(CH_2O)} \xrightarrow{BRS} Ca^{2+} + CO_2 + H_2O + \uparrow H_2S$$

The hydrogen sulphide released precipitates the metal ions contaminating the phosphogypsum and neutralised the pathogens which could occur in the medium. Moreover, the produced metal sulphides and hydrogen sulphide can be subjected to biological oxidation with the use of the genus *Thiobacillus* bacteria, according to the scheme [8]:

$$2MeS_2 + 2H_2O + 7O_2 \xrightarrow{Thiobacillus} 2MeSO_4 + 2H_2SO_4.$$

Therefore, as has been shown, biotransformation of the waste phosphogypsum can be a double blessing: it enables a decomposition of a harmful waste and oxidation of organic contaminants introduced into the reaction medium. The evidence presented allows us to claim that there is a real possibility of realisation of the above process of utilisation of the phosphogypsum and oxidation of the organic substrate present in e.g. agricultural waste.

Table 2**.** TOC reduction and degree of dissimilatory sulphates reduction in the medium containing different amounts of Morocco phosphogypsum with *Desulfotomaculum ruminis* bacteria (T = 37^{o}C, C/S = 3.2)

Concentration of Morocco phosphogypsum in the medium [g/dm^3]	Proces duration [days]	Degree of SO_4^{2-} reduction [%]	TOC decrease [%]
0.0	3	100	-
5.0	3	91	47.5
10.0	4	76	56.2
15.0	4	55	64.8
20.0	6	49	72.7
25.0	6	35	76.2
30.0	6	26	76.2
35.0	7	22	76.2
40.0	7	19	76.2

Table 2 gives the results of the study on the decrease of TOC at a certain degree of conversion of sulphates from the phosphogypsum. As follows from the data, at the phosphogypsum concentrations up to 5g/dm^3, the degree of conversion is close to

90%, and the corresponding TOC decrease is close to 50%. For a series of experiments conducted at higher concentrations of the phosphogypsum - up to 40 g/dm^3, TOC decrease reaches over 76%.

CONCLUSIONS

The above presented results of the preliminary study have shown that the phosphogypsum tested (Police Chemical Plant) is not toxic towards the bacteria *Bacillus licheniformis* and can be used as a substrate for *Desulfotomaculum ruminis*. The phosphogypsum can act as electron acceptor in the processes of oxidation of simple organic substances and thus can be used for purification of reservoirs with water characterised by excess amounts of organic carbon. In all series of the experiments, desulfurication in media containing up to 10 g/dm^3 of the phosphogypsum at the C/S ratio if 3.2, the degree of conversion was 80-90%, and TOC decreased by 47-57%. The laboratory tests conducted in the optimum conditions have proved that after 10 days the reduction of the phosphogypsum gives about 2g of sulphide sulphur in 1 dm^3 of the medium containing lactate (Juszczak et al.) . All the results indicate a real possibility of biotransformation of this waste on a large scale. The project would require low investment cost and would bring additional profit of sewage waste purification - a decrease of TOC, especially the waste of agricultural origin. The phosphogypsum tested should not be used directly in agriculture because of strongly acidic pH and the content of metal ions, which could be harmful for cultivation.

REFERENCES

DOMAGAŁA Z., DOMKA F. (1991), *Estimation of effect of Desulfotomaculum ruminis bacteria on the process of degradation of simple organic substrates*. Envir. Prot. Eng., 17, 83.

DOMAGAŁA Z., DOMKA F. (1992), *Kinetic model of dissimilatory sulfate reduction*. Envir. Prot. Eng., 18(1-2), 100.

DOMKA F., JUSZCZAK A. (2000), *Wykorzystanie mikrobiologicznych przemian nieorganicznych związków azotu i siarki w biotechnologii środowiskowej*. Na Pograniczu Chemii i Biologii, Praca zbiorowa, Wyd. Nauk. UAM, tom IV, 461-481.

GĄSIOREK J. KOSIŃSKA K., ŁANOWY T., OLESZKIEWICZ J., KLEMM A., DOMKA F., GOŁĘBIOWSKA J. (1986), *Sposób biologicznego oczyszczania ścieków zwłaszcza z przemysłowego tuczu trzody chlewnej*. Pat. PRL Nr 211710.

GĄSIOREK J., DOMKA F. (1983), *Mikrobiologiczna korozja betonowych składowisk w przemyśle siarkowym*. Cement, Wapno, Gips, 9, 241.

JUSZCZAK A., WALIGÓRSKA M., SEIFERT K., MELLER A., HABRYCH M., DOMKA F. (w druku), *The effect of phosphogypsum on the activity of Desulfotomaculum ruminis bacteria in lactate medium*. Pol. J. Environ. Stud.

KORNAROS M., ZAFIRI C., LYBERATOS G. (1996), *Kinetics of denitrification by Pseudomonas denitrificans under growth condition limited by carbon and/or nitrate and nitrite*. Wat. Envir. Res., 68, 934.

KOWALSKI W., PRZYTOCKA-JUSIAK M., WOLICKA D., HOŁUB W. (1999), *Biotransformacja fosfogipsu w podłożach zawierających związki organiczne stanowiące główne zanieczyszczenia różnych płynnych odpadów organicznych*. Biotechnologia Środowiskowa, 213-220.

Polski Komitet Normalizacji i Miar. Woda i Ścieki – badanie zawartości siarki i jej związków – oznaczanie siarczanów metodą wagową.

PRZYTOCKA-JUSIAK M., KOWALSKI W., RZECZYCKA M., BŁASZCZYK M., MYCIELSKI R. (1995), *Produkty mikrobiologicznej transformacji fosfogipsów w beztlenowych hodowlach bakterii termofilnych*. Biotechnologia, 2(29), 102-112.

Standard Methods for the Examination of Water and Wastewater (1992), PPHA, AWWA, WPCF, Washington DC, 5220 A,C.

Sulfate Reducing Bacteria, ed. by Larry L. Barton (1995), Plenum Press, New York and London.

SZULCZYŃSKI M., GĄSIOREK J., DOMKA F. (1987), *Niektóre aspekty skutecznego oczyszczania ścieków z równoczesnym przetwarzaniem siarczanowych odpadów przemysłowych.* Gaz, Woda i Technika Sanit., 3(III), 65-69.

Technologia związków fosforowych. Praca zbiorowa, PWT, Warszawa 1958, s. 194.

WALENCIAK M., DOMKA F., SZYMAŃSKA K., GŁOGOWSKA L. (1999), *Biological reduction of sulphates in purification of wastes from the alcohol industry.* Pol. J. Environ. Stud., 8(1), 51-54.

WALIGÓRSKA M., DOMKA F. (1992), *Kinetic model of denitrification by Bacillus bacteria*. Envir. Prot. Eng., 18(1-2), 117.

WALIGÓRSKA M., DOMKA F., CHERMUŁA K. (2000), *The use of molasses in the process of desulfurication*. Pol. J. Environ. Stud., 9(6), 463.

WILLIAMS JOHN W. (1985), *Oznaczanie anionów*. PWN, Warszawa, 971-973.

K. Seifert, A. Moska, F. Domka, *Wpływ odpadowego fosfogipsu na proces denitryfikacji i redukcji siarczanów*, Fizykochemiczne Problemy Mineralurgii, 36, (2002), 209-216 (w jęz. ang.)

Badano wpływ odpadowego fosfogipsu, powstającego podczas produkcji kwasu fosforowego z apatytów i fosforytów, na procesy denitryfikacji oraz dysymilacyjnej redukcji siarczanów, zachodzące z wykorzystaniem bakterii z rodzaju *Bacillus* oraz *Desulfotomaculum.*

Wykazano, że w określonym zakresie stężeń testowany fosfogips nie działa toksycznie na proces namnażania bakterii i stanowi źródło siarczanów dla bakterii *Desulfotomaculum.* Ponadto stwierdzono, że może on pełnić rolę akceptora elektronów w procesach utleniania prostych substratów organicznych w procesie bioredukcji azotanów lub siarczanów. W optymalnych warunkach dysymilacyjnej redukcji siarczanów, zachodzącej w podłożu zawierającym fosfogips, substrat organiczny oraz bakterie *Desulfotomaculum ruminis*, stopień przemiany kształtuje się na poziomie 90%, a ubytek ChZT wynosi około 50%.

Physicochemical Problems of Mineral Processing, 36 (2002) 217-224
Fizykochemiczne Problemy Mineralurgii, 36 (2002) 217-224

Magdalena BARTKOWSKA, Magdalena REGEL-ROSOCKA, Jan SZYMANOWSKI*

EXTRACTION OF ZINC(II), IRON(III) AND IRON(II) WITH BINARY MIXTURES CONTAINING TRIBUTYL PHOSPHATE AND DI(2-ETHYLHEXYL)PHOSPHORIC ACID OR CYANEX 302

Received March 15, 2002; reviewed and accepted May 15, 2002

The extraction of zinc(II), iron(III) and iron(II) with TBP and its binary mixtures with DEHPA and CYANEX 302 from hydrochloric acid solutions was studied. It was found that the extraction ability of zinc(II) chlorocomplexes from hydrochloric acid solutions decreased in the order: TBP > TBP:HL=3:1 vol/vol > TBP:HL=1:1 vol/vol. Iron(III) was strongly extracted by TBP and its binary mixtures with DEHPA and CYANEX 302, and the extraction fell in the order: binary mixtures with DEHPA or CYANEX 302> TBP> DEHPA >> CYANEX 302. Iron(II) was not extracted by the considered extractants. Zinc(II) could not be selectively extracted in the presence of iron(III). Contrary, iron(III) could be selectively extracted, especially with the binary 1:1 vol/vol mixtures of TBP with DEHPA or CYANEX 302. The stripping of zinc(II) could be accomplished in three successive stages using water and 0.1 M H_2SO_4. Iron(III) could be stripped in three stages with 0.1 M H_2SO_4.

Key words: extraction, zinc(II), iron(III), iron(II), tributyl phosphate, di(2ethylhexyl)phosphoric acid, CYANEX 302.

INTRODUCTION

Metallic coating (mainly with zinc) is nowadays a principal technique used to improve the corrosion resistance of various types of steel. Typically more than 50% of common automobile body sheets are metallically coated today.

Hot-dip galvanizing in 96.5-99% purity zinc, carried out at 445-465°C (Maass, 1998), needs the pure surface of iron goods. The rust is removed by the pickling with 20% HCl carried out at room temperature. As a result, the concentration of

*****Poznan University of Technology, Institute of Chemical Technology and Engineering
Pl. M. Sklodowskiej-Curie 2, 60-965 Poznan, Poland, e-mail: jan.szymanowski@put.poznan.pl

hydrochloric acid decreases and accumulation of iron ions (90% as Fe(II)) occurs. When pickled goods are housed on recycled hooks, i.e., covered in previous process with zinc, an accumulation of zinc(II) in the pickling solution is also observed.

The presence of zinc(II) causes technological problems in the Ruthner process (OSKO, Austria) used to regenerate the spent pickling solutions (Winkel, 1986). Metallic zinc evaporates and glues to the walls of installation at high temperatures used in the process (800°C).

We found in our recent work (Regel et al. 2001, Wojtaszak et al. 2000, Kirschling et al. 2001, Cierpiszewski et al. 2002, Regel-Rosocka et al. 2002) that zinc(II) can be recovered by extraction with various solvating and basic extractants, including tributyl phosphate (TBP), trialkylphosphine oxides and alkylamines. However, the effective stripping was only possible when TBP was used.

The main drawback of the extraction with TBP is the strong extraction of iron(III). The aim of this work was to study the effect of acidic extractants (di(2-ethylhexyl)phosphoric acid – DEHPA and bis(2, 4, 4-trimethylpentyl)monotio-phosphinic acid – CYANEX 302) on extraction of zinc(II) from 10% HCl with TBP. Both these acidic extractants are used for zinc(II) recovery from acidic sulfate solutions (Bart, 2000, Alguacil et al. 1992). CYANEX 302 shows good selectivity of zinc(II) extraction with respect to iron(III) at pH below 1. However, it is impossible to predict a priori the extraction of zinc(II) from hydrochloric acid solutions with binary mixtures containing TBP and DEHPA or CYANEX 302.

EXPERIMENTAL

Tributyl phosphate (Merck, Germany), di(2-ethylhexyl)phosphoric acid (Merck, Germany) and CYANEX 302 (Cytec, Canada) were used as extractants. All these reagents were used as delivered without any purification and without dilution with any solvent. Undiluted TBP and binary mixtures of TBP with DEHPA or CYANEX 302 (3:1 or 1:1 vol/vol) were used.

Extraction was carried out in a small scale using 10 ml volumes of phases at the volume ratio equal to 1. Phases were mechanically shaken for 10 minutes and left for phase separation. The aqueous feed used for the determination of extraction isotherms contained 56.88 g/L Zn(II), or 50 g/L Fe(II) or 30 g/L Fe(III) and 3.26 M (10%) HCl. The chloride concentration adjusted with NaCl (POCh, Poland) was equal to 5 M in the initial aqueous feed. The separated aqueous phase (raffinate) was extracted with a new portion of extractants, always at the volume ratio equal to 1. The extractions were repeated several times.

Concentrations of zinc(II) in the aqueous phase were determined by titration with 0.05 M EDTA using PAN as an indicator. Iron concentrations were determined by titration with 0.1 M K_2CrO_7 in the presence of diphenylamine-4-sulphonic acid.

RESULTS AND DISCUSSION

In the considered system of high chloride concentration, metal ions were mainly in the form of chlorocomplexes:

$$M^{n+} + i\ Cl^{-} = MCl_i^{n-i} \quad (1)$$

where i = 1, 2, 3 and 4. Knowing the chlorocomplex formation constants, it was possible to calculate the content of each species present in the aqueous phase. However, β values were very sensitive for ionic strength and the constants were mainly determined for diluted solutions of relatively low ionic strength.

The computer program Medusa (Puigdomenech) was used to estimate roughly the distribution of various chlorocomplexes. The computing showed that in the initial aqueous feed iron(II) was present in comparable amounts in the form of Fe^{2+} and $FeCl^{+}$ (Table 1). Iron(III) was distributed between $FeCl_2^{+}$, $FeCl_3$, $FeCl^{2+}$ and Fe^{3+} given in the order of decreasing content. However, in spectra of aqueous ferric chloride solutions in hydrochloric acid, the absorption at 335 nm appears in 2-4 M HCl, and then the absorption bands at 245, 316 and 364 nm appear gradually with increasing acid concentration. These absorptions are due to $FeCl_4^{-}$ (Cotton and Wilkins, 1988, Sato et al 2002.). Over 80% of zinc was in the form of $ZnCl_4^{2-}$, and only few percents existed as $ZnCl_3^{-}$. However, the concentration of chloride ions and ionic strength were lower in each successive extraction step, especially in extraction of Zn(II) and Fe(III). Thus, the equilibrium was shifted towards lower chlorocomplexes.

Table 1. Estimated distribution of metal species in the aqueous phase

$[M^{n+}]$ M	$[Cl^{-}]$ M	Ionic strength M	Mole fraction				
Zn(II)			Zn^{2+}	$ZnCl^{+}$	$ZnCl_2$	$ZnCl_3^{-}$	$ZnCl_4^{2-}$
0.84	5	5.84	0.03	-	0.05	0.09	0.81
0.65	4	4.69	0.06	0.03	0.06	0.11	0.73
0.40	3	3.40	0.11	0.07	0.05	0.13	0.64
0.15	2	2.00	0.19	0.09	0.08	0.14	0.49
Fe(III)			Fe^{3+}	$FeCl^{2+}$	$FeCl_2^{+}$	$FeCl_3$	$FeCl_4^{-}$
0.54	5	6.72	0.06	0.20	0.46	0.27	-
0.39	4	5.21	0.1	0.27	0.42	0.16	-
0.24	3.3	4.01	0.13	0.31	0.45	0.10	-
0.09	2.5	2.76	0.17	0.36	0.41	0.06	-
Fe(II)			Fe^{2+}	$FeCl^{+}$	-	-	-
0.90	5	5.93	0.56	0.44			

It was impossible to predict precisely the composition of the successive aqueous phases because the composition of the extracted complexes could change. If zinc(II)

and iron(III) were extracted with TBP (S) according to the following equations (Morris and Short, 1962):

$$2H^+_w + ZnCl_4^{2-}{}_w + 2S_o = H_2ZnCl_4 \cdot 2S_o \quad (2)$$

$$H^+_w + Cl^-_w + FeCl_{3w} + 2S_o = HFeCl_4 \cdot 2S_o \quad (3)$$

then the total recovery of zinc(II) or iron(III) would give a decrease of chloride concentration equal to 3.36 and 2.16 M, respectively. The extraction of hydrochloric acid was relatively low and the concentration of hydrochloric acid in the organic phase did not exceed 0.1 M. The total decrease of HCl concentration would be 2.2 and 1 M for the extraction of zinc(II) and iron(III), respectively (e.g. 1.68 M with $H_2ZnCl_4 \cdot 2S$ and 0.5 M of free HCl in 5 successive extraction steps).

All these meant that in extraction with extractant binary mixtures (S and HL) the role of the acidic extractant (DEHPA and CYANEX 302) could increase in each successive step. Both these acidic reagents extracted cations of zinc according to the reaction (Alguacil et al. 1992):

$$(2+n)\,(HL)_{2\,o} + 2Zn^{2+}{}_w = (ZnL_2)_2 \,.n(HL)_{2\,o} + 4H^+_w \quad (4)$$

where n=1 or 2.

When mixtures of two extractants were used then the mixed complexes could be formed. As a result, the ability and selectivity of extraction could be changed.

The isotherms of zinc(II) extraction presented in Fig. 1 indicated that an addition of acidic extractants to TBP decreased the extraction of zinc(II), especially strongly in the first four extraction steps in which the concentration of chloride in the aqueous feeds was high. The extraction ability decreased in the order: TBP > TBP:HL=3:1 vol/vol > TBP:HL=1:1 vol/vol. Both acidic extractants had similar effects and there was no statistical difference when 1:1 vol/vol mixtures of DEHPA or CYANEX 302 with TBP were used. A better performance of DEHPA was observed when the mixture of TBP:DEHPA=3:1 was used.

Iron(III) (Fig. 2) was better extracted than zinc(II). The isotherms were very steep and the concentration of iron(III) in the organic phase increased rapidly in the region of low equilibrium concentrations in the aqueous phase. An addition of acidic extractants to TBP had a significant effect on extraction of iron(III). The extraction ability of extractants changed in the order: binary mixtures with DEHPA or CYANEX 302> TBP> DEHPA >> CYANEX 302. The high extraction of iron(III) with acidic extractants, especially DEHPA, was in a good agreement with the computing results (Table 1) demonstrating high molar contribution of iron(III) cationic species extracted by the acidic extractants.

It is worth to mention here that the shapes of extraction isotherms given in this work (Figs. 1 and 2) were different in comparison to those presented in our previous works (Regel et al. 2001, Wojtaszak et al. 2000). The shape of isotherms depended upon the concentrations of Cl^- and HCl in aqueous feeds. In previous works these

concentrations were kept constant, while in this work they changed in each successive step. The approach used in this work is more justified in design of the multistage counter-current process in which the concentrations also decrease in each successive step.

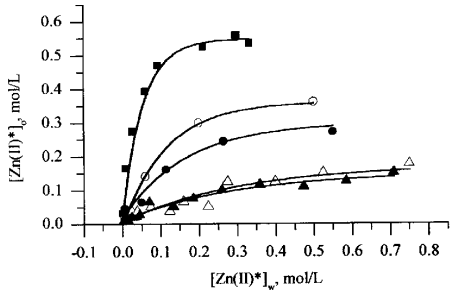

Fig. 1. Isotherms of zinc(II) extraction (■ – TBP; ○ – TBP:DEHPA=3:1 vol/vol; ● - TBP:Cyanex 302=3:1 vol/vol; Δ - TBP:DEHPA=1:1 vol/vol and ▲ - TBP:Cyanex 302=1:1 vol/vol).

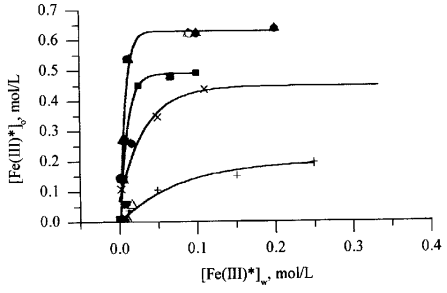

Fig. 2. Isotherms of iron(III) extraction (■ – TBP; ○ – TBP:DEHPA=3:1 vol/vol; ● - TBP:Cyanex 302=3:1 vol/vol; Δ - TBP:DEHPA=1:1 vol/vol; ▲ - TBP:Cyanex 302=1:1 vol/vol – each mixture gives approximately the same extraction of iron(III); x – DEHPA and + - Cyanex 302).

Iron(II) was only slightly extracted (Table 2). The concentration of iron(II) in the organic phase was below 0.6 g/L with the distribution coefficient equal to 0.01-0.03. The comparison of the distribution coefficients given in Table 2 could be only quantitative because they were determined at different locations on the extraction isotherms. However, it was obvious that iron(II) did not disturb the extraction of zinc(II). Thus, prior to extraction iron(III) must be reduced to iron(II). Selectivity of extraction can be characterized by the ratio of distribution coefficients:

$$S_{Zn(II)/Fe(III)} = \frac{D_{Zn(II)}}{D_{Fe(III)}} \tag{5}$$

Extraction isotherms were not linear and the distribution ratios depended upon the loading of the organic phase or the equilibrium concentrations of metal ions in the aqueous phase. Thus, the selectivity $S_{Zn(II)/Fe(III)}$ depended also on the equilibrium contents of metal species (Fig. 3). The obtained results indicated that $S_{Zn(II)/Fe(III)}$ decreased in the same order as the extraction of zinc(II). Iron(III) could be extracted with the binary mixtures of extractants from solutions containing similar molar concentrations of zinc(II) and iron(III). The use of 1:1 vol/vol mixture was preferred.

The separation of iron(III) could be quantitative with an excess of the aqueous feed due to the crowd effect, i.e. when the organic phase was saturated with metal species and weaker complexes were replaced by the stronger ones. This selective extraction of iron(III) could be explained by the formation of mixed complexes composed from iron(III) di(2-ethylhexyl)phosphates solvated with TBP molecules.

Table 2. Distribution coefficients (56.88 g/L Zn(II), 50 g/L Fe(II) or 30 g/L Fe(III), 3.26 M HCl (10%) and $[Cl^-]$=5 M in the aqueous feed)

Extractant	$D_{Zn(II)}$	$D_{Fe(II)}$	$D_{Fe(III)}$
TBP	2.65	0.029	2.45
TBP:DEHPA = 3:1 vol/vol	1.50	0.014	3.16
TBP:DEHPA = 1:1 vol/vol	0.43	0.016	3.16
TBP:Cyanex 302 = 3:1 vol/vol	1.08	0.015	3.16
TBP:Cyanex 302 = 1:1 vol/vol	0.38	0.009	3.16

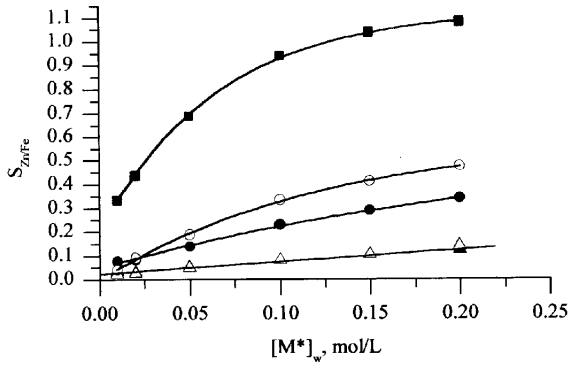

Fig. 3. Selectivity of extraction for various equilibrium concentrations of metal ions (equimolar quantities of zinc(II) and iron(III)) in the aqueous phase (■ – TBP; ○ – TBP:DEHPA=3:1 vol/vol; ● - TBP:Cyanex 302=3:1 vol/vol; Δ - TBP:DEHPA=1:1 vol/vol and ▲ - TBP:Cyanex 302=1:1 vol/vol)

Although iron(II) was not extracted, its presence in the aqueous feed caused a positive increase of zinc(II) extraction with TBP and TBP-DEHPA mixtures (Table 3). The effect could be explained by an increase of the ionic strength. Such a positive effect was not observed for TBP-CYANEX 302 mixture.

TBP formed easily complexes with water, especially in the presence of HCl (Kertes and Halpern 1961). As a result, a significant transfer of water to TBP phase (4-6%) was observed. An addition of acidic extractants caused a decrease of water in the extractant phase to about 3% and 1-3% for TBP-DEHPA and TBP-CYANEX 302 mixtures, respectively.

Table 3. Effect of iron(II) presence upon zinc(II) extraction. Aqueous feed: FI – 5 g/L Zn(II), 10% HCl, $[Cl^-]$=5 M or FII – 5 g/L Zn(II), 50 g/L Fe(II), 10% HCl, $[Cl^-]$=5 M

Extractant	FI			FII		
	Ionic strength [M]	%	$D_{Zn(II)}$	Ionic strength [M]	%	$D_{Zn(II)}$
TBP	5.08	96.3	23.7	6.17	97.9	39.5
TBP:DEHPA = 3:1 vol/vol	5.08	68.8	2.21	6.17	81.3	4.34
TBP:DEHPA = 1:1 vol/vol	5.08	20.0	0.25	6.17	31.2	0.45
TBP:Cyanex 302 = 3:1 vol/vol	5.08	80.0	4.00	6.17	75.2	3.03
TBP:Cyanex 302 = 1:1 vol/vol	5.08	37.5	0.60	6.17	30.6	0.44

Table 4. Percentage of zinc(II) and iron(III) stripping from loaded TBP:DEHPA = 3:1 vol/vol with different stripping phases in three successive steps (Aqueous feed: 10% HCl, $[Cl^-]$ = 5 M and 5 g/L Zn(II) or 30 g/L Fe(III), o/w = 1:1 vol/vol)

Stripping phase	$\%S_{Zn(II)}$	$\%S_{Fe(III)}$
H_2O	71.7	37.7
0.1 M H_2SO_4	100.0	59.2
0.1 M H_2SO_4	100.0	60.8
H_2O	71.1	37.2
H_2O	77.0	55.5
H_2O	83.9	55.5
0.1 M H_2SO_4	75.2	41.4
0.1 M H_2SO_4	83.7	79.2
0.1 M H_2SO_4	83.7	100.0

Water could strip only zinc(II) and iron(III) from complexes with TBP. Zinc(II) was better stripped than iron(III), and about 71 and 38% of zinc(II) and iron(III) could be stripped in one stage (Table 4). Additional stripping with water caused an increase of the stripped metal ions to about 84 and 55% for zinc(II) and iron(III), respectively. The total stripping of zinc(II) was obtained when the stripping with water was followed by the stripping with sulphuric acid. The total stripping of iron(III) was achieved in three stages using 0.1 M H_2SO_4. The necessity of using two different stripping solutions had to be considered as an important technological disadvantage.

CONCLUSIONS

The extraction ability of zinc(II) chlorocomplexes from hydrochloric acid solutions decreased in the order: TBP > TBP:HL=3:1 vol/vol > TBP:HL=1:1 vol/vol. Iron(III) was strongly extracted by TBP and its binary mixtures with DEHPA and CYANEX 302, and the extraction fell in the order: binary mixtures with DEHPA or CYANEX 302> TBP> DEHPA >> CYANEX 302. Iron(II) was not extracted by the considered extractants.

Zinc(II) could not be selectively extracted in the presence of iron(III). Contrary, iron(III) could be selectively extracted especially with the binary 1:1 vol/vol mixtures of TBP with DEHPA or CYANEX 302.

The stripping of zinc(II) could be accomplished in three successive stages using water and 0.1 M H_2SO_4. Iron(III) could be stripped in three stages with 0.1 M H_2SO_4.

REFERENCES

ALGUACIL F. J., COBO A., CARAVACA C. 1992, *Study of the Extraction of Zinc(II) in Aqueous Chloride Media by Cyanex 302*, Hydrometallurgy, Vol. 31, pp.163-174.

BART H. J. 2000, *Reactive Extraction*, Springer, Berlin.

CIERPISZEWSKI R., MIESIĄC I., REGEL-ROSOCKA M., SASTRE A. M., SZYMANOWSKI J. 2002, *Removal of Zinc(II) from Spent Hydrochloric Acid Solutions from Zinc Hot Galvanizing Plants*, Ind. Chem. Eng. Res., Vol. 41, pp. 598-603.

COTTON F.A., WILKINSON G., 1988, *Advanced Inorganic Chemistry*, John Wiley & Sons, New York, pp. 717.

KERTES A. S., HALPERN M. 1961, *Hydrochloric Acid Promoted Hydrolysis of Tri-n-butyl Phosphate*, J. Inorg. Nucl. Chem., Vol. 20, pp. 117-126.

KIRSCHLING P., NOWAK K., MIESIĄC I., NITSCH W., SZYMANOWSKI J. 2001, *Membrane Extraction-Stripping Process for Zinc(II) Recovery from HCl Solution*, Solvent Extr. Res. Dev., Jpn, Vol. 8, pp. 135-143.

MAASS P., PEISSKER P. 1998, *Cynkowanie Ogniowe*, Agencja Wydawnicza Placet, Warszawa.

MORRIS D. C. F., SHORT E. L. 1962, *Zinc Chloride and Zinc Bromide Complexes. Part II. Solvent-Extraction Studies with Zinc-65 as Tracer*, J. Chem. Soc., pp. 2662-2671.

PUIGDOMENECH I., *Medusa*, Royal Institute of Technology, Sweden.

REGEL M., SASTRE A. M., SZYMANOWSKI J. 2001, *Recovery of Zinc(II) from HCl Spent Pickling Solutions by Solvent Extraction*, Environ. Sci. Technol., Vol. 35, pp. 630-635.

REGEL-ROSOCKA M., MIESIĄC I., SASTRE A. M., SZYMANOWSKI J., *Screening of Reagents for Recovery of Zinc(II) from Hydrochloric Acid Spent Pickling Solutions*, Proceed. ISEC 2002 (in press).

SATO T., ISHIKAWA I., SATO K., NOGUCHI Y., 2002 *Solvent Extraction of Iron(III) from Hydrochloric Acid Solutions by Dihexyl Sulphoxide*, Proc. ISEC'2002, pp.366-370.

WINKEL P. 1986, *Wasser und Abwasser*, Leuze Verlag, Saulgau, p. 117.

WOJTASZAK A., MIESIĄC I., SZYMANOWSKI J. 2000, *Extraction of zinc(II), iron(II) and iron(III) from hydrochloric acid solutions*, Fizykochem. Probl. Mineralurgii, Prace Naukowe Instytutu Górnictwa Politechniki Wrocławskiej, Konferencje, Nr 25, pp. 31-37.

ACKNOWLEDGEMENTS

The work was supported by the grant of State Committee for Scientific Research No. 1473/T09/2001/2.

Bartkowska M, Regel-Rosocka M., Szymanowski J., *Ekstrakcja cynku(ii), żelaza(iii) i żelaza(ii) za pomocą mieszanin dwuskładnikowych zawierających fosforan tributylu i kwas di(2-etyloheksylo)fosforowy lub cyanex 302*, Fizykochemiczne Problemy Mineralurgii, 36 (2002), 217-224, (w jęz. ang.)

Badano ekstrakcję cynku(II), żelaza(III) oraz żelaza(II) za pomocą fosforanu tributylu (TBP) i jego mieszanin dwuskładnikowych z kwasem di(2-etyloheksylo)fosforowym (DEHPA) oraz tlenkiem trialkilofosfiny (CYANEX 302) z roztworów kwasu solnego. W wyniku przeprowadzonych badań stwierdzono, że zdolność ekstrakcji chlorokompleksów cynku z roztworów kwasu solnego maleje w następującej kolejności: TBP > TBP:HL=3:1 vol/vol > TBP:HL=1:1 vol/vol. Żelazo(III) jest silnie ekstrahowane przez TBP i jego mieszaniny dwuskładnikowe z DEHPA i CYANEX 302. Zdolność ekstrakcyjna maleje w kolejności: mieszaniny dwuskładnikowe TBP:DEHPA lub TBP:CYANEX 302> TBP> DEHPA >> CYANEX 302. Żelazo(II) nie jest ekstrahowane przez badane reagenty organiczne.Cynku(II) nie można selektywnie wyekstrahować w obecności żelaza(III). Natomiast żelazo(III) można wyekstrahować przy użyciu mieszaniny dwuskładnikowej TBP:DEHPA=1:1 vol/vol lub TBP:CYANEX 302=1:1 vol/vol.Przebadano również reekstrakcję cynku(II) i żelaza(III) z naładowanej fazy organicznej TBP:DEHPA = 3:1 vol/vol. Uzyskane wyniki wskazują na to, że cynk można całkowicie wydzielić prowadząc trzystopniową reekstrakcję w pierwszym etapie wodą, a następnie 0.1 M H_2SO_4. Najskuteczniej można zreekstrahować żelazo(III) za pomocą trzystopniowej reekstrakcji 0.1 M H_2SO_4.

Physicochemical Problems of Mineral Processing, 36 (2002) 225-232
Fizykochemiczne Problemy Mineralurgii, 36 (2002) 225-232

Małgorzata ULEWICZ*, Władysław WALKOWIAK**

FLOTATION OF ZINC(II) AND CADMIUM(II) IONS FROM DILUTE AQUEOUS SOLUTIONS IN THE PRESENCES OF INORGANIC LIGANDS

Received March 15, 2002; reviewed and accepted May 15, 2002

An experimental investigation is presented on competitive flotation of zinc(II) and cadmium(II) ions from dilute aqueous solutions with sodium dodecylbenzenesulfonate (DBSNa) as the anionic surfactant and hexadecylpyridinium chloride (CPCl) as the cationic surfactant. The effect of inorganic ligands, i.e. cyanides, thiocyanides, sulfates, thiosulfates, nitrates, and perchlorates on the selectivity of cadmium(II) over zinc(II) is established. Separation of Cd(II) and Zn(II) ions by DBSNa is not occurred. The separation of Cd(II)/Zn(II) by CPCl in presence of inorganic ligands at concentration range from 0.01 M to 1.0 M increases in the sequence: $CN^- \leq SCN^- < SO_4^{2-} < S_2O_3^{2-}$.

Key words: zinc(II), cadmium(II), inorganic ligands, ion flotation

INTRODUCTION

Zinc(II) and cadmium(II) ions are removed from dilute aqueous solutions applying physicochemical methods such as solvent extraction, ion flotation, sorption, liquid membranes and ionic exchange. Ion flotation is an effective and simple process of metal ions concentration and separation from dilute aqueous solutions ($c_{Me} \leq 1.0 \cdot 10^{-4}$M), which involves the use of the ionic surfactant (collector) and the subsequent passage of gas bubbles through the aqueous solution.

The ion flotation selectivity for metal ions has been presented in several papers. Foam separation of Cd(II) ions by sodium dodecylsulfate and sodium dodecanoate from aqueous solutions was investigated by Jurkiewicz (1984-85). The presence of electrolytes in the solutions have a negative influence on cadmium(II) foam removal. Jurkiewicz (1985) also investigated separation of thiocyanate and iodide complexes of

* Department of Chemistry, Technical University of Czestochowa, 42-200 Czestochowa, Armii Krajowej 19 Street, e-mail: ulewicz@mim.pcz.czest.pl
** Institute of Inorganic Chemistry and Metallurgy of Rare Elements, Wroclaw University of Technology, 50-370 Wroclaw, Wybrzeze Wyspianskiego 27 Street, e-mail: Walkowiak@ichn.ch.pwr.wroc.pl

cadmium(II) from acidic aqueous solutions using hexadecyltrimethylamonium bromide (CTMABr). In the presence of acids, the zinc thiocyanate complex removal increases in the presence of following acids: perchloric < iodidc < nitric < sulfuric < phosphoric < acetic. Jurkiewicz (1990) conducted the separation of zinc(II) and cadmium(II) ions with CTMABr in the presence of chloride, bromide, iodide and thiocyanate ions. For anionic surfactants (sodium dodecylbenzenesulfonate and sodium dodecylsulfonate) Walkowiak (1991) found the following foam separation selectivity sequences toward cations: $Mn^{2+} < Zn^{2+} < Co^{2+} < Fe^{3+} < Cr^{3+}$, and $Ag^{+} < Cd^{2+} < In^{3+}$. The good correlation between selectivity sequences of studied metal ions with anionic surfactant and the ionic potentials of those cations was discovered. The flotation selective of zinc(II), cadmium(II), mercury(II), and gold(III) ions using hexadecyltrimethylamonium chloride in the presence of chlorides and cyanides was also investigated by Walkowiak et al. (1976, 1979, 1992). Selectivity order of foam fractionation was as follows: $Au(CN)_4^- > Hg(CN)_4^{2-} > Cd(CN)_4^{2-} > Zn(CN)_4^{2-}$ (Walkowiak and Grieves 1976). The effect of inorganic ligands, i.e. thiosulfates, thiocyanates, and cyanides on the selectivity of ion flotation of Zn(II) and Ag(I) was investigated by Charewicz et al. (1999). The influence of zinc(II) and cadmium(II) ions concentrations on the effectiveness of flotation removal with potassium oleate was studied by Sinkova (1998). Zinc(II) and cadmium(II) ions are removed effectively from aqueous solution using this surfactant. Also, Scorcelli et al. (1999) was studied the removal of cadmium(II) using sodium dodecylsulfate as a collector. The best removal (99 %) was achieved for the concentration ratio of a metal cations to collector equal to 1:3. Preliminary research of cadmium(II) over zinc(II) ions separation by hexadecyltrimethylamonium chloride was conducted by Kozłowski et al. (2000). Recently Ulewicz et al. (2001) investigated separation of cadmium(II) over zinc(II) ions by hexadecyltrimethylamonium chloride in the presence of halides in the aqueous solutions. In the presence of halides in the aqueous solutions the separation of Cd(II) over Zn(II) ions by DBSNa was not occurred, whereas selective separation of Cd(II)/Zn(II) by CPCl in presence of halides at concentration range of 0.001 M to 1.0 M increases in the sequence: $F^- < Cl^- < Br^- < I^-$.

This paper concerns the selective removal of zinc(II) and cadmium(II) ions from dilute aqueous solutions ($c_{Me} = 1.0 \cdot 10^{-5}$ M) in competitive ion flotation in the presence of inorganic ligands such as cyanides, thiocyanides, sulfates, thiosulfates, nitrates, and perchlorates. The Zn(II) and Cd(II) flotation for anionic complexes from aqueous solutions by hexadecylpyridinium chloride as a cationic surfactant was applied. The competitive ion flotation of Zn^{2+} and Cd^{2+} by sodium dodecylbenzenesulfonate was also studied.

EXPERIMENTAL

The apparatus and procedure were as described in recently published paper (Ulewicz et al., 2001). Experiments were performed at an ambient temperature (20 ± 2 ^{o}C) and at a constant gas (nitrogen) flow rate of 12 ml/minute through a sintered

glass sparger of 20-30 μm, nominal porosity. The concentration of zinc(II) and cadmium(II) was $1.0 \cdot 10^{-5}$M. All ligands, i.e. CN^-, SCN^-, SO_4^{2-}, $S_2O_3^{2-}$, NO_3^-, and ClO_4, were investigated in range of the concentrations of $5.0 \cdot 10^{-5} \div 1.0$ M. Reagent grade inorganic chemicals, i.e. NaCN, NaSCN, $NaNO_3$, $NaClO_4$, Na_2SO_4, $Na_2S_2O_3$, $ZnSO_4$, $CdSO_4$, NaOH and H_2SO_4 were obtained from POCh (Gliwice, Poland). Typical ionic surfactants were applied, i.e. sodium dodecylbenzenesulfonate (DBSNa, BHD reagent) as an anionic surfactant, and hexadecylpyridinium chloride (CPCl, Loba-Chemie reagent) as a cationic surfactant. Both surfactants were purified by recrystalization from ethanol. The concentration of surfactants in the aqueous solutions was $2.0 \cdot 10^{-4}$ M. The gamma radioactive isotopes used, i.e., Zn-65 and Cd-115m, were from the Atomic Energy Institute „POLATOM" (Świerk, Poland). They were of sufficiently high specific activity to neglect the effect of carrier concentration (9.2 MBq/mg for Zn-65 and 2.26 MBq/mg for Cd-115m).

The efficiency and rate of flotation, i.e. the flotation degree ($M = 1-c_r/c_i$) and the first order rate constant (k, min^{-1}) were calculated from experimental curves of c/c_i vs. time (where c_i, c, and c_r are the initial, actual, and final concentration of floated ion). The selectivity coefficient (S) was also used such as in previous paper (Ulewicz et al., 2001).

Table 1. Stability constants of zinc(II) and cadmium(II) for complexes with inorganic ligands (Stability constants, 1982). Ionic strength I = 0.1 M

System		$\log\beta_1$	$\log\beta_2$	$\log\beta_3$	$\log\beta_4$
$S_2O_3^{2-}$	Zn(II)	0.96	1.94	3.30	-
	Cd(II)	2.74	4.65	6.95	7.12
SO_4^{2-}	Zn(II)	0.89	1.23	1.66	1.67
	Cd(II)	0.95	1.55	1.76	2.30
SCN^-	Zn(II)	0.71	1.00	1.20	1.50
	Cd(II)	1.16	1.49	1.63	1.65
CN^-	Zn(II)	-	10.64	15.74	19.98
$pK_a = 9.21$	Cd(II)	5.62	10.80	15.70	19.20
NO_3^-	Zn(II)	-0.20	-0.64	-	-
	Cd(II)	-0.05	-0.80	-	-
ClO_4^-	Zn(II)	1.70	-	-	-
	Cd(II)	-	-	-	-

The total concentration of metal in aqueous solutions can be described by an equation (1), whereas the ratio of formed metal complexes was calculated by an equation (2). In Table 1 are given values of the stability constants of inorganic complexes for Zn(II) and Cd(II).

$$c_M = [M] + [ML] + [ML_2] + ... + [ML_n] \quad (1)$$

$$\alpha_n = \frac{\beta_n [L]^n}{1 + \beta_1 [L] + \beta_2 [L]^2 + ... + \beta_n [L]^n} \quad (2)$$

where [L] - concentration of ligand which is not complexed by a metal,
β_n - overall stability constants of metal complex.

RESULTS AND DISCUSSION

The flotations of zinc(II) and cadmium(II) ions with sodium dodecylbenzenesulfonate from aqueous solutions containing single metal ions at the concentrations of metals equal to $1.0 \cdot 10^{-5}$ and $2.0 \cdot 10^{-5}$ M were described in previous papers (Ulewicz et. al 2001). The flotation removal and rate of Zn^{2+} and Cd^{2+} cations with DBSNa as the anionic surfactant was comparable. Also the removal of Zn^{2+} and Cd^{2+} cations with DBSNa in the presence of halides was comparable. The differences in the removal of Zn(II) and Cd(II) ions from solutions containing halides with CPCl were observed. In the this paper the influence of inorganic ligands, i.e. CN^-, SCN^-, SO_4^{2-}, $S_2O_3^{2-}$, NO_3^-, and ClO_4^- on the separation of zinc(II) and cadmium(II) ions was examined.

It was found that the removal of zinc(II) and cadmium(II) ions decreases with increasing of ligands concentration in aqueous solutions using anionic collector, i.e. DBSNa (Fig.1).

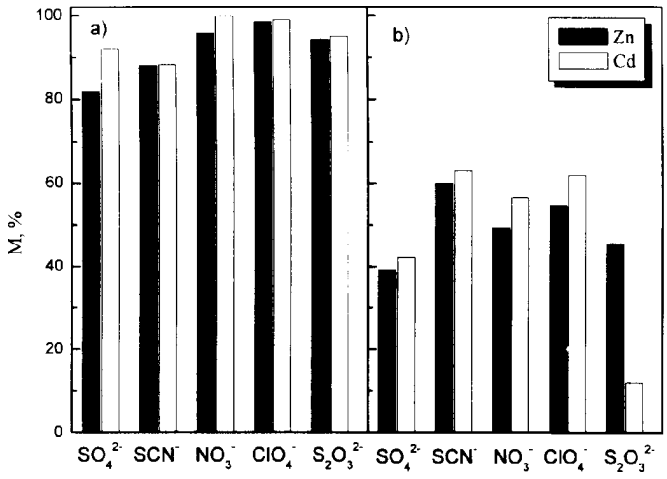

Fig. 1. The flotation degree of Zn(II) and Cd(II) ions from aqueous solutions in the presence of the inorganic ligands at concentration of $1.0 \cdot 10^{-4}$ M (a) and $1.0 \cdot 10^{-2}$ M (b) by $2.0 \cdot 10^{-4}$ M DBSNa

The separation of Zn(II) and Cd(II) in thiocyanides, sulfates, nitrates, and perchlorates media aqueous solution with DBSNa does not occurred, since the removal of both metals was comparable. Only in the presence of thiosulfates at higher concentration (0.01 M) of $S_2O_3^{2-}$ ions, the removal of Zn(II) was observed as much

higher than Cd(II) ions. The selectivity coefficients of Zn(II)/Cd(II) for concentration of $S_2O_3^{2-}$ equal to 0.001, 0.01, and 0.1 M were: 2.5; 3.8 and 9.7, respectively. In the presence of CN^- removal of Zn(II) and Cd(II) ions is not occurred.

The partial separation of studied metals occurs when a cationic collector, i.e. CPCl, was applied. Flotation kinetics curves of Zn(II) and Cd(II) for competitive ion flotation of those metals from 0.1 M (a) and 1.0 M (b) $S_2O_3^{2-}$ aqueous solutions with CPCl is presented in Fig. 2. As can be seen from this figure cadmium(II) is floated much higher than zinc(II) ions. The removal of Zn(II) and Cd(II) ions increases with increase of thiosulfates ions concentration. The selectivity coefficients of Cd(II)/Zn(II) for concentration of $S_2O_3^{2-}$ equal to 0.10 and 1.0 M were 1.4 and 4.2, respectively.

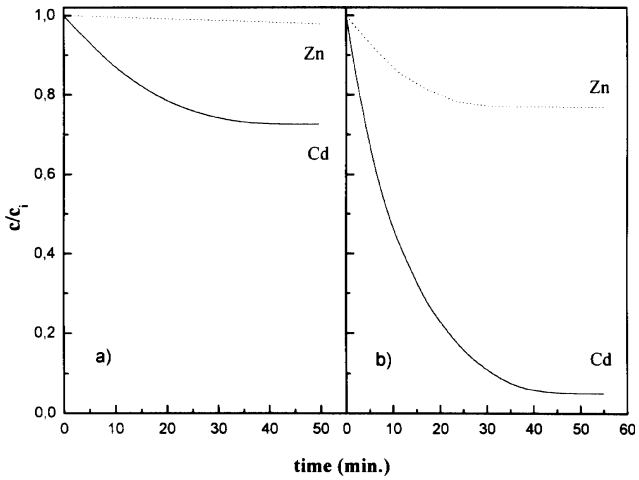

Fig. 2. Kinetic curves of the Zn(II) and Cd(II) ions from aqueous solutions containing 0.10 M (a) and 1.0 M (b) $S_2O_3^{2-}$ by CPCl, $[Zn^{2+}] = [Cd^{2+}] = 1.0 \cdot 10^{-5}$ M, $[CPCl] = 2.0 \cdot 10^{-4}$ M, pH = 4.0

Floatation of Zn(II) and Cd(II) ions from aqueous solutions containing NO_3^-, or ClO_4^- with cationic collector does not occur. The maximal percent removal of Zn(II) and Cd(II) ions in presence of cyanides, thiocyanides, sulfate, and thiosulfates ions are shown in Fig. 3. In this figure, the calculated formation percent of metal complexes for cyanides, thiocyanides, sulfate, thiosulfates, is also shown. Using this collector it is possible to remove Zn(II) and Cd(II), which are existing as anionic forms in aqueous solutions. The differences of predomination range for anionic forms of Zn(II) and Cd(II) allow to separate cadmium(II) over zinc(II). With the increase of ligand concentration, the removal of Cd(II) and Zn(II) ions increase. The flotation degree of Cd(II) and Zn(II) is comparable for the inorganic complex anions of the investigated metals.

The selectivity coefficients of cadmium(II) over zinc(II) in presence of investigated ligands are shown in Fig. 4. The selectivity coefficients for Cd/Zn by CPCl in inorganic media aqueous solutions at the concentration range from 0.01 to 1.0 M increase in the following sequence: $CN^- \leq SCN^- < SO_4^{2-} < S_2O_3^{2-}$, respectively.

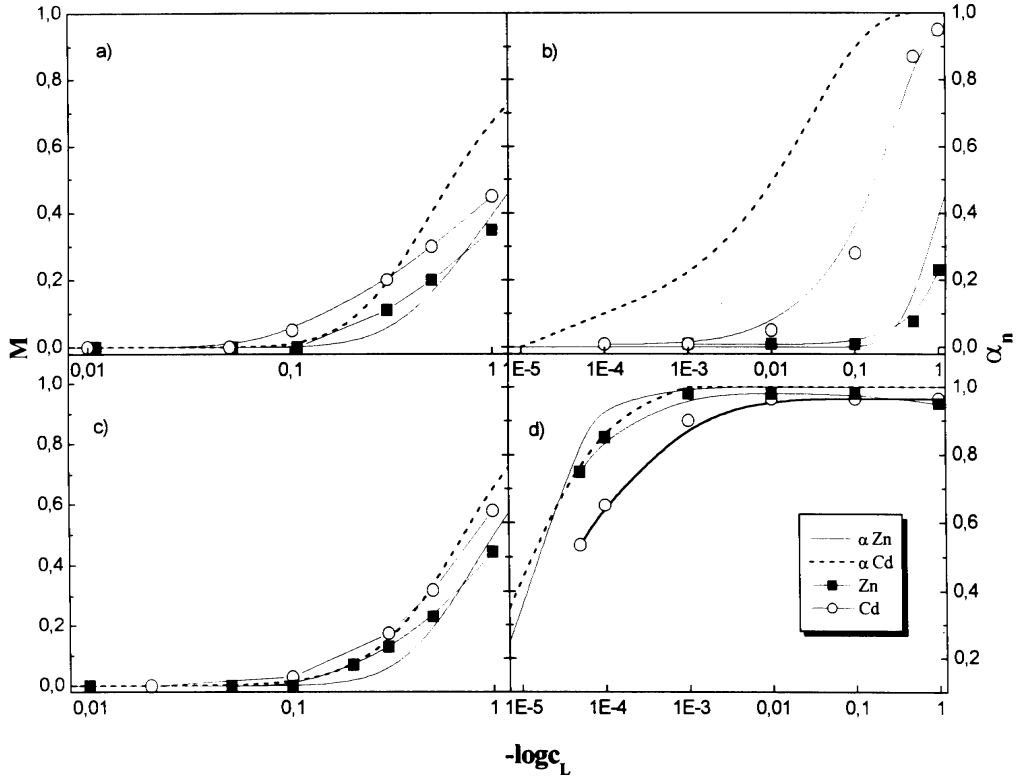

Fig. 3. Influence of analytical concentration of sulfates (a), thiosulfates (b), thiocyanates (c), and cyanides (d) on removal of Zn(II) and Cd(II) ions with CPCl , and molar fractions of anionic metal complexes, pH = 4.0 (for CN^- pH=11.0)

Separation of Cd(II) and Zn(II) ions with CPCl is the best in the presence of thiosulfates (Table 2). As can be seen from this table the kinetic rate constants for cadmium(II) are higher than for zinc(II). The rate constant ratios of Cd(II)/Zn(II) for SO_4^{2-}, SCN^-, and $S_2O_3^{2-}$ are equal: 1.2; 1.1 and 5.3, respectively.

Table 2. Rate constant of Zn(II) and Cd(II) by CPCl in presence of inorganic ligands at concentration of 0.5 M

Lignads	k [min^{-1}] Zn(II)	r^2 determination coefficients	k [min^{-1}] Cd(II)	r^2 determination coefficients
SO_4^{2-}	0.137	0.9916	0.168	0.9909
$S_2O_3^{2-}$	0.069	0.9941	0.369	0.9875
SCN^-	0.172	0.9829	0.184	0.9934

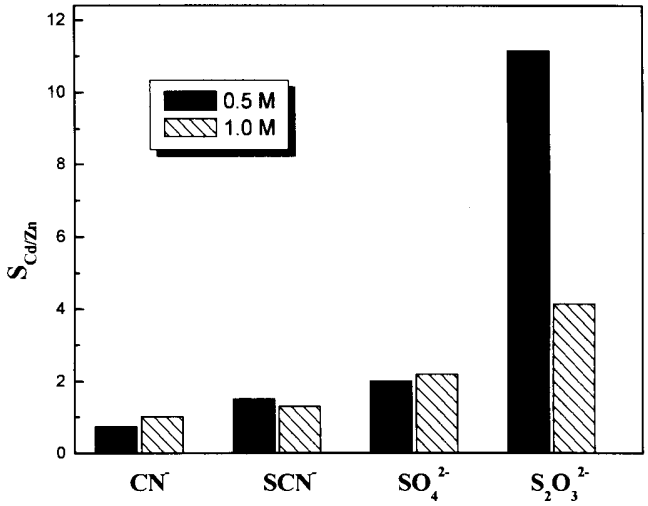

Fig. 4. Selectivity coefficients ($S_{Cd/Zn}$) vs. concentration of ligands, [CPCl] =2.0· 10^{-4} M, $[Zn^{2+}] = [Cd^{2+}] = 1.0 \cdot 10^{-5}$ M, pH = 4.0 (for CN^- pH=11.0)

CONCLUSIONS

Separation of Cd(II) and Zn(II) ions using anionic collector, i.e. DBSNa from aqueous solutions in the presence of inorganic ligands at the concentrations range of $5.0 \cdot 10^{-5} \div 1.0$ M with the exception of $S_2O_3^{2-}$, was not observed since the removal of both metals is comparable. This is caused by the fact, that zinc(II) and cadmium(II) form cation complexes which possess comparable values of stability constants. In the presence of thiosulfates the removal of Zn(II) is much higher than Cd(II) ions by DBSNa. The high selectivity coefficient of Zn(II)/Cd(II), i.e. 9.7, was obtained for concentration of $S_2O_3^{2-}$ equal 0.1 M.

The cadmium(II) over zinc(II) selectivity was observed in the presence of thiosulfates ligands when cationic surfactant, i.e. hexadecylpyridinium chloride, was applied. The selectivity coefficients for Cd(II)/Zn(II) increase in the following order of ligands: $CN^- \leq SCN^- < SO_4^{2-} < S_2O_3^{2-}$. The values of Cd(II)/Zn(II) selectivity coefficients at $S_2O_3^{2-}$ concentration equal to 0.10, 0.05, and 1.0 M were 1.4, 11.2, and 4.2, respectively.

ACKNOWLEGMENT

Financial support of this work was provided by Polish Science Foundation Grants 4 T09B 107 22.

REFERENCES

CHAREWICZ W. A., HOLOWIECKA B. A., WALKOWIAK W., (1999), *Selective flotation of zinc(II) and silver (I) ions from dilute aqueous solutions,* Sep. Sci. Technol., Vol. 34, No 12, 2447-2460.

CHAREWICZ W., NIEMIEC J., (1969), *Flotation of anions using cationic surfactants, I. Flotation of molibdates,* Nukleonika, Vol. 14, 17-27.

GRIVES R. B., WALKOWIAK W., BHATTACHARYYA D., (1979), *Foam fractionation selectivity sequence of quaternary ammonium surfactant for simple and complex anions:* A review, In: *Recent development in Separation Science, CRC Press Inc.*, Florida, 5, 55-65.

JURKIEWICZ K. (1984-85), *Study on the separation of Cd from solutions by foam separation. I. Foam separation of cadmium cations*, Sep. Sci. Technol., Vol. 19, 1039-1050.
JURKIEWICZ K. (1985), *Study on the separation of Cd from solutions by foam separation. III. Foam separation of complex cadmium anions*, Sep. Sci. Technol., Vol. 20, 179 –192.
JURKIEWICZ K. (1990), *The removal of zinc from solutions by foam separation. I. Foam separation of complex zinc anions*, Int. J. Miner. Process., Vol. 28, 173 – 187.
KOZŁOWSKI C., ULEWICZ M., WALKOWIAK W., (2000), *Separation of zinc and cadmium ions from chlorides by ion flotation and liquid membranes*, Physicochemical Problems of Mineral Processing, No. 34, 141-151.
SCORZELLI I. B., FRAGOMENI A. L., TOREM M. L., (1999), *Removal of cadmium from a liquid effluent by ion flotation*, Minerals Engineering, Vol. 12, 905-917.
SINKOVA L. A. (1998), *Influence of zinc and cadmium ions concentration on effectiveness of flotation removal from aqueous solutions with potassium oleate*, Ukr. Kim. Zhrn. Vol. 64 , 94-99.
Stability Constants of Metal-Ion Complex; Part A: Inorganic Ligands, Pergamon Press, New York, 1982.
ULEWICZ M., WALKOWIAK W., KOZŁOWSKI C (2001), *Selective flotation of zinc(II) and cadmium(II) ions from aqueous solutions in the presence of halides*, Physicochemical Problems of Mineral Processing, 35, 21-29.
ULEWICZ M., (2001), *Flotation of ions from aqueous solutions in hydrometallurgical process of removal and separation of cadmium and zinc*, Doctoral dissertation, Technical University of Częstochowa.
WALKOWIAK W. (1991), Mechanism *of selective ion flotation. 1. Selective flotation of transmission metal cations.* Sep. Sci. Technol., Vol. 26, 559 – 568.
WALKOWIAK W., (1992), *Mechanism of selective ion flotation technology", In: Innovation in flotation technology*, Edited by P. Mavros, K. A. Matis, *NATO ASI Series, Kluwer Academic Publishers, London*, Vol. 208, 455-473.
WALKOWIAK W., BHATTACHARYYA D., GRIEVES R. B., (1976), *Selective foam fractionation of chloride complex of Zn(II), Cd(II), Hg(II), and Au(III)*, Anal. Chem., Vol. 48, 975-979.
WALKOWIAK W., GRIEVES R. B. (1976), *Foam fractionation of cyanide complex of zinc(II), cadmium(II), mercury(II), and gold(III)*, J. Inorg. Nucl. Chem., Vol. 38, 1351-1356.
WALKOWIAK W., ULEWICZ M., (1999), *Kinetics studies of ions flotation*, Physicochemical Problems of Mineral Processing, No. 33, 201-214.

Ulewicz M., Walkowiak W., *Flotacja jonów Zn(II) i Cd(II) z rozcieńczonych roztworów wodnych w obecności ligandów nieorganicznych*, Fizykochemiczne Problemy Mineralurgii, 36, (2002) 225-232 (w jęz. ang.)

Przy użyciu kolektora kationowego – chlorku heksylopirydyniowego (CPCl) oraz kolektora anionowego - dodecylobenzenosulfonianu sodu (DBSNa) wydzielano oraz rozdzielano jony cynku(II) i kadmu(II) odpowiednio w postaci kationowych i anionowych form kompleksowych z wybranymi ligandami nieorganicznymi z roztworów wodnych zawierających równomolową mieszaninę obu metali. Rozdzielenie jonów Zn(II) i Cd(II) przy użyciu kolektora anionowego w obecności jonów SCN^-, SO_4^{2-}, NO_3^- i ClO_4^- nie jest możliwe ponieważ cynk(II) i kadm(II) tworzą kationowe formy kompleksowe o podobnych wartościach stałych trwałości. Przy użyciu tego kolektora jedynie w obecności $S_2O_3^{2-}$ obserwowano separację jonów Zn(II)/Cd(II). Współczynniki selektywności Zn(II)/Cd(II) przy stężeniu $S_2O_3^{2-}$ równym 0,001; 0,01 i 0,1 M wynoszą odpowiednio: 2,5; 3,8 i 9,7. Natomiast przy użyciu kolektora kationowego, tj. chlorku heksylopirydyniowego, obserwowano separację jonów kadmu(II) od cynku(II). Separacja badanych jonów metali przy użyciu CPCl w obecności ligandów nieorganicznych w zakresie ich stężeń 0,1 ÷ 1,0 M wzrasta w szeregu: $CN^- \leq SCN^- < SO_4^{2-} < S_2O_3^{2-}$. Współczynniki selektywności Cd(II)/Zn(II) przy stężeniu $S_2O_3^{2-}$ równym 0,1; 0,5 i 1,0 M wynoszą odpowiednio: 1,4; 11,2 i 4,2.

Physicochemical Problems of Mineral Processing, 36 (2002) 233-242
Fizykochemiczne Problemy Mineralurgii, 36 (2002) 233-242

Tadeusz GLUBA*

THE EFFECT OF WETTING CONDITIONS ON THE STRENGTH OF GRANULES

Received March 15, 2002; reviewed and accepted May 15, 2002

Results of investigations of the effect of the size of wetting liquid droplets and particle size distribution of a fine-grained raw material on the mechanical strength of granules formed during wet drum granulation were discussed. The process of granulation was carried out batch-wise in a drum granulator 0.5 m in diameter and 0.4 m long at rotational speed $0.33s^{-1}$ and constant volumetric drum filling degree $\varphi = 0.1$. On the bed tumbling in the drum the wetting liquid (distilled water) was supplied at a constant flow rate $Q_w = 12 \cdot 10^{-3}$ m^3/h. The size of wetting droplets was changed using various air flow rates through pneumatic spray nozzles in the range Q_a=1.0 to 3.0 m^3/h and applying a sprinkler which supplied /drop-wise/ the liquid uniformly along the entire drum length. In the whole experimental cycle constant mean saturation degree of the feed equal to S = 0.293 was used. The effect of wetting droplet size and particle size distribution of the raw material on the breaking force and corresponding breaking stress was discussed.

Key words: granulation, agglomeration, size distributions, strength of agglomerates

INTRODUCTION

In wet granulation the main role is played by phenomena which take place at the liquid-solid-gas interface that depend on the properties of media involved in the process and also on process conditions. For these reasons the choice of wetting conditions for a fine-grained bed of specified physical properties constitutes one of main problems of every granulation process.

One of the often applied agglomeration methods is pressure-free granulation carried out in rotary drums. During the tumbling of a wetted fine-grained bed, solid particles interact with liquid droplets and air. The size and type of forces acting on single material particles and their agglomerates strictly depend on the properties of particular media, their relationships and in particular on the particle size distribution of

* Technical University of Łodz, Department of Process Equipment
90-924 Łodz, Stefanowskiego 12/16, Poland

the raw material, the shape of particles and extent of spraying of the wetting liquid. The effect of the quantity and properties of wetting liquid on the mechanisms of agglomerate growth and their properties was studied by many researchers (Kapur and Fuerstenau 1969, Sastry and Fuerstenau 1973, Gluba et al. 1990, Iveson and Litster 1998). These studies carried out for various solid-wetting liquid systems, confirmed a significant impact of the amount and properties of the liquid on growth kinetics of agglomerates and their physico-mechanical properties. There are a few references in the literature to the influence of the wetting liquid droplet size on granulation effects.

Mechanical strength of agglomerates is one of the main features determining their further applicability or processing. There are many methods of defining and measuring the strength. Depending on needs, impact, wear, compression, bend and tensile tests are used (Błasiński and Gluba 1981, Schubert 1975, Kristensen et al. 1985, Gluba and Antkowiak 1988) In all these cases strength is determined by means of testing machines, so the theory and transfer of results of these measurements to other stresses are more or less hampered. Strength tests are, however, a significant source of information on the quality and structure of granulated product.

Production of a granular material with defined properties (mechanical strength) from a fine-grained raw material requires an appropriate method of granulation and selection of proper process parameters. One of little known problems is the determination of the effect of wetting liquid droplet size and physical properties of the material being granulated, and particle size distribution in particular, on the strength of granules being formed. This paper tries to explain the above mentioned relations.

AIM OF THE STUDY

The aim of the study was to determine the effect of the size of wetting liquid droplets and particle size distribution of a fine-grained raw material on the mechanical strength of granules formed during wet drum granulation.

EXPERIMENTAL

MATERIALS

Fine-grained dolomite flour was used in the experiments. Raw materials for testing were composed of five size fractions of the dolomite flour with particle size ranging to 10 μm, to 15 μm, to 60 μm, to 100 μm and to 250 μm. Particle size distribution of each fraction was determined using a laser particle size analyser "Analysette 22". The particle size distribution was described by the statistical moments: mean particle size d_m, variance of dimensions s^2, asymmetry coefficient γ_1 and concentration coefficient γ_2. On the basis of data obtained from the laser analyser particle size distributions of raw materials to be granulated were calculated numerically (by mixing input fractions) assuming that they were geometrically similar. In the calculations the following were assumed constant: variation coefficient: $s/d_m = 1.07$ and asymmetry coefficient $\gamma_1 =$

2.00 for different values of mean particle size d_m ranging from 10.6 to 28 μm. Grain-size compositions of mixtures obtained (denoted by symbols D1 to D5), which are raw materials for the granulation process, are shown in Fig. 1. Such a selection of particle size distributions enables an evaluation of the impact of mean particle diameter on the granulation process and the mechanical strength of granules.

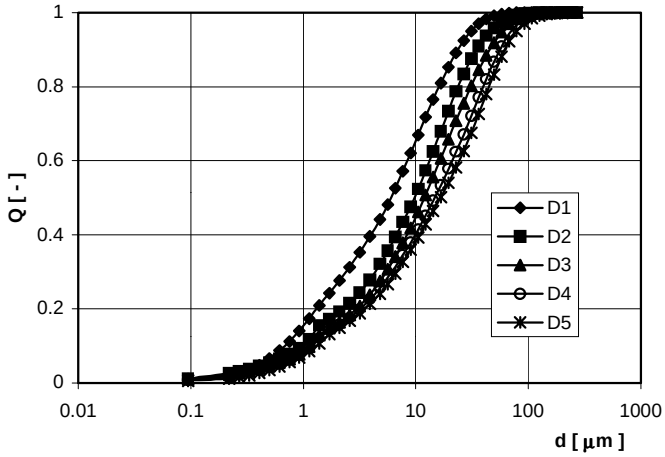

Fig. 1. Comparison of particle size distributions of raw materials

EXPERIMENTAL RIG AND METHODS

The process of granulation was carried out batch-wise in a drum granulator 0.5 m in diameter and 0.4 m long at rotational speed $0.33s^{-1}$ and constant volumetric drum filling degree $\varphi = 0.1$. The feed volume was determined each time on the basis of mean bulk density of particular raw materials. On the bed tumbling in the drum the wetting liquid (distilled water) was supplied at a constant flow rate $Q_w = 12 \cdot 10^{-3}$ m^3/h. The size of wetting droplets was changed using various air flow rates through pneumatic spray nozzles in the range Q_a=1.0 to 3.0 m^3/h and applying a sprinkler which supplied (drop-wise) the liquid uniformly along the entire drum length.

The size distribution of wetting liquid droplets supplied by a pneumatic nozzle was determined by a DANTEC laser analyser. The droplet size distribution was analysed at a distance of 100 mm from the nozzle outlet along the radius of dispersed liquid stream every 2.5 mm from the nozzle axis. A comparison of averaged droplet size distributions for the whole stream at specified nozzle operating parameters (q) is shown in Fig. 2, while the relation of mean droplet size d_{dm} in the stream and distribution range s/d_{dm} is illustrated in Fig. 3. From Fig. 3 it follows that with an increase of the liquid atomisation $q=Q_w/Q_a$ the mean droplet size in the stream increases, while the coefficient of distribution variability s/d_{dm} decreases which means that the stream becomes more homogeneous.

During drop-wise wetting the bed was wetted with droplets of the same size equal to about 3 mm. In the whole experimental cycle constant wetting was used which was determined by the mean saturation degree of the feed equal to S = 0.293.

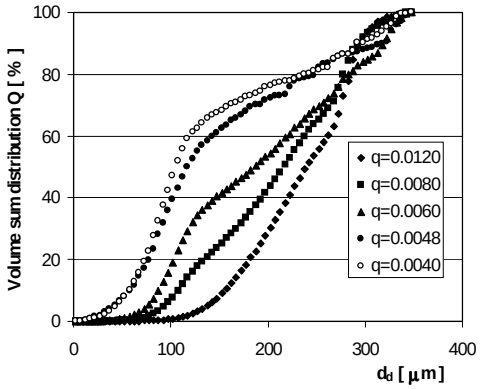

Fig. 2. Size distributions of wetting liquid

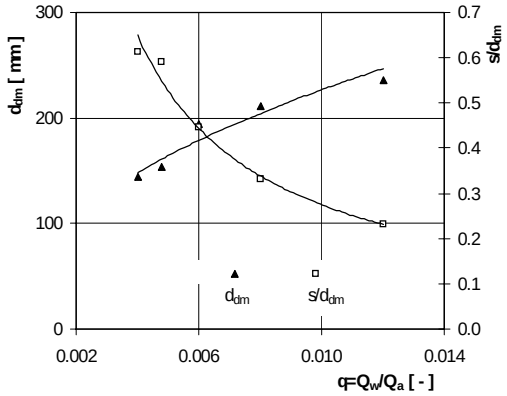

Fig. 3. Dependence of mean droplet size d_{dm} and droplets coefficient s/d_{dm} on the liquid dispersion q

After completing the wetting, the process of granulation was continued until the moment when the granulated material started to stick to the drum walls because water had been pressed off. In determined time intervals, samples representative of the whole feed were taken. On this basis properties of the product obtained were specified. The first sample was taken immediately after wetting (granulation time t = 0) and the last one in the moment when water pressed out to the granule surface made them stick to the inner surface of the drum.

In order to determine the compression resistance, a single dry granule from a size fraction (of given dimensions) was placed between two parallel plates of the strength testing machine, where it was loaded with an increasing compressive force until the sample was damaged. Schematic diagram of the equipment used for compressive strength tests is shown in Fig. 4.

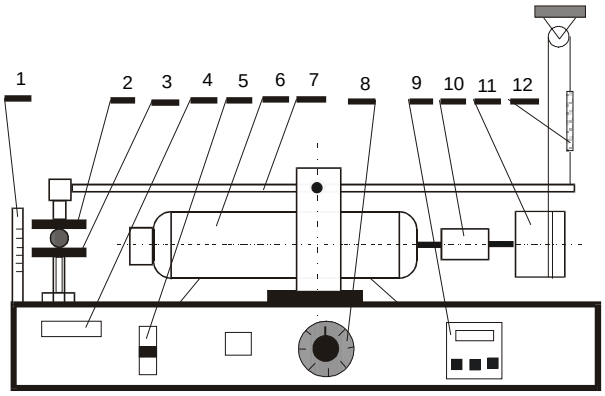

Fig. 4. Schematic diagram of the equipment for compressive strength tests: (1) scale, (2, 3) compressing plates, (4) feed control, (5) direction switch, (6) engine with a reducer, (7) double-arm lever, (8) potentiometer, (9) torque meter, (10) torque sensor, (11) winding reel, (12) spring

The compressive force was generated as a result of tension of the spring caused by winding of the flexible connector onto the reel, which rotated at a given rotational velocity. Constant rotational velocity of the drum was applied, which gave a constant growth rate of the loading force ΔN=0.245 N/s.

RESULTS

The value of breaking force was calculated according to eq. (1) on the basis of twisting moment on the reel shaft, recorded at the instant when the sample was destroyed:

$$P = \frac{M_s}{D/2} \tag{1}$$

The breaking force for granules from a given size fraction was assumed to be the arithmetic mean from values obtained for 10 single samples. Breaking compressive stresses were determined on the basis of mean value of breaking force and granule size according to the formula:

$$\sigma = \frac{4P}{\pi d_g^{\,2}} \tag{2}$$

Figure 5a shows an example of the dependence of breaking force and Fig. 5b the effect of breaking stresses on the diameter of granules obtained from one material (D3) for different granulation times at determined mean wetting liquid droplet size (d_{dm}=0.144mm).

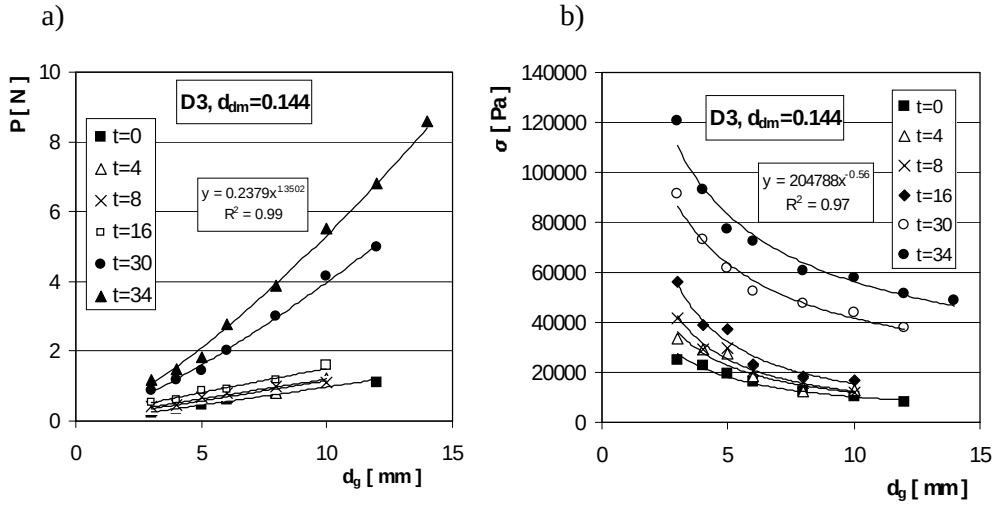

Fig. 5a, b. Dependence of breaking force (P) and breaking stresses (σ) on granule size

For all tested materials relations similar to those shown in Figs. 5a, b were obtained. In every case the growth of granulation time results in a stepwise increase of granule strength. The dependence of breaking force on granule diameter is approximated with high accuracy by the power function:

$$P = A \cdot d_g^{\,B} \tag{3}$$

while breaking stresses are determined by a function in the following form:

$$\sigma = A_1 \cdot d_g^{\,-B_1} \tag{4}$$

In order to estimate the effect of wetting liquid droplet size on strength of the produced dried granulated material, a comparison was made of curves $P = f(d_g)$ and $\sigma = f(d_g)$ obtained for a given raw material at the same granulation time. A character of the relations obtained for the granulated product shortly after completion of the wetting (t=1) is illustrated in Fig. 6a, b.

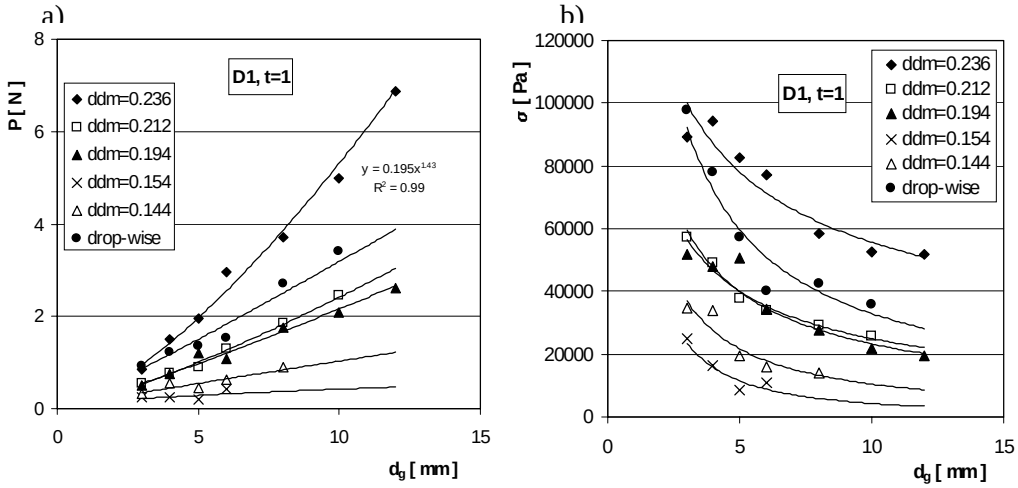

Fig. 6a, b. Dependence of breaking force (P) and breaking stresses (σ) on granule size

It is clear that the strength of product particles obtained in the initial period of granulation depends significantly on the wetting liquid droplet size. The highest strength have the granules formed when the wetting was carried out by a pneumatic nozzle at the smallest possible breaking of the liquid stream (the largest droplets). With an increase of the liquid distribution degree (a reduction of the droplet size) the compressive strength of granules gradually decreases. The strength of granules formed during the drop-wise wetting (droplets about 3 mm in diameter), in this initial granulation period is smaller than the values obtained for wetting with a nozzle using the largest droplets. It can be presumed that the size of droplets of the liquid supplied

to the bed during the wetting affects the mechanisms of agglomerate formation, in particular the forces which bind material particles. Larger liquid droplets supplied to the fine-granular bed provide a possibility of occurrence of stronger liquid bridges which causes that the particles are closer to each other. Such a relation found for a determined, tested range of the wetting liquid droplet size cannot be probably extended onto arbitrary droplet sizes. At droplet sizes much exceeding the feed particle dimensions as used during the drop-wise wetting there are other mechanisms of agglomerate formation and growth. A large droplet, when falling down onto the fine-granular bed, spreads in the vicinity and forms a large nucleus, in which liquid occupies significant part of the interparticle space. What determines the position of particles in such a nucleus is the capillary negative pressure. The total number of droplets supplied to the bed during the drop-wise wetting is many times smaller than the number of liquid droplets during the wetting with a pneumatic nozzle and the droplets are of the same size. After completing the wetting process a more homogeneous product of larger granules is obtained. During further granulation, in the tumbling bed complex mechanisms are observed whose result is both the growth of agglomerates and a systematic concentration of their structure. As a consequence, water is pressed onto the agglomerate surface which causes an abrupt growth of the agglomerates due to combining of granules that earlier were separate, and in a very short time hamper significantly the further process because of an intensive sticking to the drum walls. The rate of these phenomena depends greatly on the liquid droplet size during wetting.

The strength of final product particles (corresponding to the surface overwetting) for particular raw materials also depends on the size of wetting liquid droplets. Examples of the relations $\sigma = f(d_g)$ for the final product obtained from one of the raw materials at different sizes of the wetting liquid droplets are shown in Fig. 7.

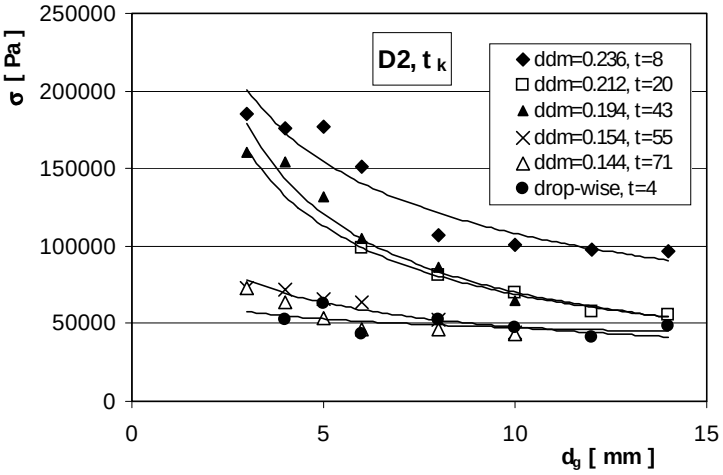

Fig. 7. Dependence of breaking stresses on granule size

Despite a relatively short time of granulation, of the highest strength are the agglomerates produced during wetting with the largest droplets supplied by the pneumatic nozzles. The lowest compressive strength is characteristic for the agglomerates obtained during the drop-wise wetting, for which the time necessary to reach the state of surface overwetting is also the shortest. This means that in this case the state of granule inner structure formed after the wetting changes slightly during further granulation. Hence, also an increase of strength as compared to the wetting with sprayed liquid is insignificant.

To evaluate the effect of particle size distribution of a raw material on product particle strength, the curves $P = f(d_g)$ and $\sigma = f(d_g)$ were compared for granulated material produced from different raw materials (with different average particle diameters) at a steady size of the wetting liquid droplets and granulation time. Example of diagrams of these relations are shown in Fig. 8. The effect of the particle size distribution is most distinct in the initial period of granulation. In the tested range of particle size distribution, the compressive strength of granules decreases with an increase of the mean material particle size. With an increase of the granulation time differences in the strength of granules made of particular raw materials become smaller. The least distinct differences in the strength of granulated product obtained from raw materials with different particle size distributions were obtained during the drop-wise wetting. For the product obtained after several minutes of granulation these differences are practically negligible.

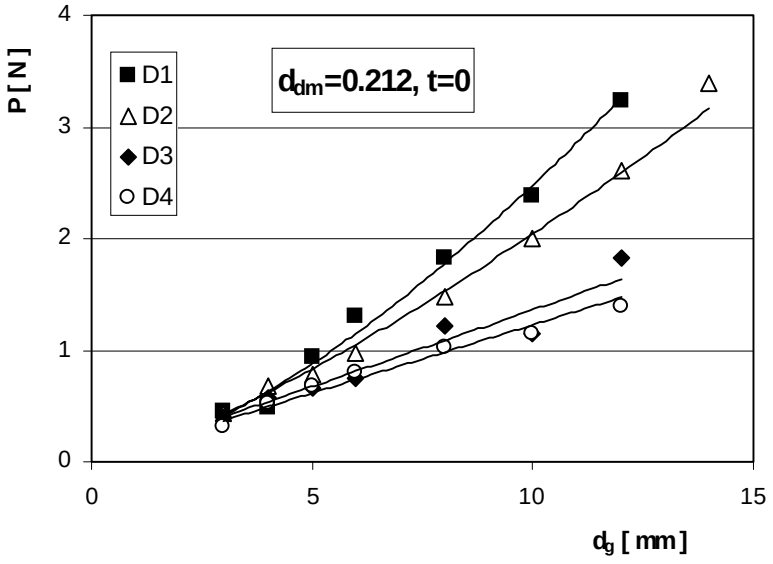

Fig. 8. Dependence of breaking force on granule size

CONCLUSIONS

On the basis of the obtained results the following conclusions were drawn:

1. Compressive strength of granules obtained during wet drum granulation depends strongly on the bed wetting parameters.
2. The size of droplets of the wetting liquid supplied to the bed during wetting has an influence on the granulation process, and as a result on the product properties including its mechanical strength.
3. An increase of the size of droplets supplied by pneumatic nozzles (in the tested range) leads to a product of higher strength.
4. During wetting with large droplets (the drop-wise wetting) the agglomerates grow very quickly, however, the obtained product is characterised by lower mechanical strength.
5. At the same size of the wetting liquid droplets a more resistant granulated product is obtained from the raw material with smaller mean particle diameters.
6. With an increase of the granulation time, there is a systematic increase of the strength of the obtained product particles.

ACKNOWLEDGMENT

The work was carried out under research project no. 4 T09C 023 22. financed by The Polish State Committee for Scientific Research for the years 2002-2005

REFERENCES

BŁASIŃSKI H., GLUBA T., (1981), *Metody i aparaty do pomiaru wytrzymałości aglomeratów*, Inż. i Aparat. Chem., 4, 29-33

GLUBA T., ANTKOWIAK W., (1988), *Effect of wetting on granule abrasion resistance.* Aufbereitungs-Technik, 2, 76-80.

GLUBA T., HEIM A., KOCHANSKI B., (1990), *Application of the theory of moments in the estimation of powder granulation of different wettabilities,* Powder handling & processing, 2, 323-326.

IVESON S. M., LITSTER J. D., (1998), *Fundamental studies of granule consolidation. Part 2: Quantifying the effects of particle and binder properties,* Powder Technol., 99, 243-250.

KAPUR P.C., FUERSTENAU D.W., (1969), *A coalescence model for granulation,* I&EC Process Design and Development, 8, 56-62.

KRISTENSEN H. G., HOLM P., SCHAEFER T., (1985), *Mechanical Properties of Moist Agglomerates in Relation to Granulation Mechanisms*, Powder Technology, 44, 227-237

SASTRY K.V.S., FUERSTENAU D.W., (1973), *Mechanisms of Agglomerate Growth in Green Pelletization*, Powder Technology, 7, 97-105.

SCHUBERT H., (1975), *Tensile strength of agglomerates*, Powder Technology, 11, 107-119

NOMENCLATURE

d	-particle size of the raw material, μm,
D –	-winding reel diameter, m
d_g –	-granule diameter, mm
d_{gm}	-mean particle size of the granulated product, mm
d_d	-droplet size, mm
d_{dm}	-mean droplet size, mm
M_s –	-twisting moment during sample destruction, Nm
P –	-force causing granule breaking, N
$q=Q_w/Q_a$	-liquid dispersion
Q	-volume sum distribution
t	-granulation time after wetting, min,
σ –	-breaking stress, Pa

Gluba T., *Wpływ warunków nawilżania na wytrzymałość granulek*, Fizykochemiczne Problemy Mineralurgii 36, (2002) 233-242 (w jęz. ang.)

W pracy przedstawiono analizę wpływu stopnia rozbicia strumienia cieczy zwilżającej (wielkości kropel) oraz czasu prowadzenia procesu mokrej granulacji bębnowej na wytrzymałość mechaniczną wytworzonych cząstek granulatu ocenianą w stanie wysuszonym, przy użyciu testu na ściskanie. Jako materiał badawczy zastosowano mączkę dolomitową o zmiennym składzie ziarnowym. Skład granulometryczny surowca obliczano numerycznie przy założeniu stałości dwóch parametrów: współczynnika zmienności s/d_m = 1.07 oraz współczynnika asymetrii γ_1 = 2.00, dla pięciu wartości średniego wymiaru ziaren d_m w zakresie 10.6 do 28 μm. Proces granulacji prowadzono w sposób okresowy w granulatorze bębnowym o średnicy 0.5m i długości 0.4m przy stałej prędkości obrotowej 0,33 1/s i stałym objętościowym współczynniku wypełnienia bębna φ = 0.1. Na cyrkulujące w bębnie złoże podawano ciecz zwilżającą (wodę destylowaną) za pomocą dwóch dysz pneumatycznych przy stałym objętościowym natężeniu przepływu $Q_w = 12 \cdot 10^{-3}$ m^3/h. Wielkość kropel cieczy zmieniano stosując zmienne natężenia przepływu powietrza przez dysze w zakresie Q_a=1.0 do 3.0 m^3/h, oraz stosując zraszacz kroplowy, który podawał równomiernie na całej długości bębna ciecz w postaci kropel o wielkości ok. 3 mm. W całym cyklu badań stosowano stały współczynnik saturacji złoża to S = 0.293. Po zakończeniu nawilżania proces granulacji prowadzono do chwili gdy przewilżone na powierzchni granulki zaczęły przywierać do ścianek granulatora uniemożliwiając dalszy proces. Na podstawie próbek pobranych w określonych przedziałach czasowych określano właściwości wytrzymałościowe cząstek produktu.. Stwierdzono, że wielkość kropel cieczy zwilżającej istotnie wpływa na przebieg procesu granulacji, wielkość cząstek otrzymanego produktu i ich właściwości wytrzymałościowe. Stwierdzono również, że na wytrzymałość wytworzonych aglomeratów ma również wpływ skład ziarnowy granulowanego surowca.

Physicochemical Problems of Mineral Processing, 36 (2002) 243-252
Fizykochemiczne Problemy Mineralurgii, 36 (2002) 243-252

Teofil JESIONOWSKI*

INFLUENCE OF N-2-(AMINOETHYL)-3-AMINOPROPYLTRIMETHOXYSILANE ON PHYSICOCHEMICAL AND MORPHOLOGICAL PROPERTIES OF SILICAS OBTAINED IN AN EMULSION SYSTEM

Received March 15, 2002; reviewed and accepted May 15, 2002

Synthesis of monodisperse silica was performed in a precipitation reaction from aqueous solution of sodium metasilicate using hydrochloric acid in an emulsion system. Effect of N-2-(aminoethyl)-3-aminopropylotrimethoxysilane was studied on surface and morphological properties of the precipitated silica. Particle size and polydispersity were measured using the technique of dynamic light scatter (DLS) and scanning electron microscopy (SEM). The extent of surface modification and its type were evaluated using FTIR spectroscopy. Moreover, adsorptive properties were characterised by estimation of specific surface area (BET) and of macroporosity. The XPS technique permitted to quantify the amount of modifier deposited on silica surface. Alterations in surface charge were studies by estimation of isoelectric point by direct testing of electrophoretic mobility and, indirectly, by calculating zeta potential. Aminosilane modification of SiO_2, formed in emulsion medium, results in extensive changes in surface character and in morphology of the particles. Already at the time of silica preparation surface silanol groups become markedly reduced and, in addition, aminosilane chemisorption results in augmented hydrophobicity. Increased particle homogeneity has also been obtained and a decreased value of polydispersity due to aminosilane interactions with the surface of examined silica.

Key words: spherical silica particles, surface modification, SEM, DLS, ELS, XPS

INTRODUCTION

Silicas represent a very valuable research material in several scientific centers of the world (Iler, 1979; Bergna, 1994; Legrand, 1998). Numerous methods of obtaining silicas are known. The most important include flame hydrolysis (Barthel, 1995). Products of the technology exhibit a strictly defined dispersive character but they encounter application restrictions in adsorption processes.

***** Poznan University of Technology, Institute of Chemical Technology and Engineering
Pl. M. Sklodowskiej-Curie 2, 60-965 Poznan, Poland
E-mail: Teofil.Jesionowski@put.poznan.pl, phone:+48(61)6653720, fax:+48(61)6653649

Silicas obtained in the form of a gel represent a vast group of products (Faramway et al., 1997; Goworek et al., 1997). On the other hand, the technique of Stöber allows to obtain silicas in reactions of alkoxysilane hydrolysis and condensation in acidic or alkaline medium (Buining, 1996). Formation of silicas in an emulsion medium represents a new, alternate way of producing monodisperse silica particles, frequently of a nanometric size (Gan et al., 1996; Esquena et al., 1997; Jesionowski, 2001; 2001).

Due to their specific surface structure, reflecting the presence of sinalol (≡SiOH) groups, almost all types of silica exhibit hydrophilic character. The character can be modified mainly by adsorption of surfactants (Suhara et al., 1995) or by chemisorption of alkoxysilanes (Van der Voort et al., 1996; Jesionowski et al, 2000; 2001).

The studies aimed at obtaining silicas of a strictly defined particle size, spherical shape and exhibiting a stable dispersive character. Alteration of the surface character, i.e., restriction of its hydrophilicity was performed by aminosilane modification of surface hydroxyl (silanol) groups. The so obtained and modified silicas should exhibit high reactivity, in particular with organic dyes and thermoplastic polyolefines, due to their specific surface structure (presence of =NH and $-NH_2$ groups).

EXPERIMENTAL DETAILS

MATERIALS

Aqueous solution of sodium metasilicate, silicate modulus of 3.3 (Na_2O=8.50 wt%; SiO_2=27.18 wt%, density = 1.39 g/dm^3) represented the principal raw material for production of the silica. The precipitating agent involved 5 wt% HCl solution. The organic phase was formed by cyclohexane and the non-ionic surfactant from the group of oxyethylenated fatty alcohols ($RO(CH_2CH_2O)_n$, R=$C_{16\text{-}22}$, and $n_{mean}\cong 7$), produced by Chemical Works 'Rokita' S.A., Poland, served as an emulsifier. For silica surface modification, N-2-(aminoethyl)-3-aminopropyltrimethoxysilane, technical grade (Witco Co., USA), was used.

EMULSION AND SILICA PREPARATION

Two emulsions were prepared. The 'alkaline' one (E_1) contained 100 cm^3 5 wt% Na_2SiO_3 solution and 110 cm^3 cyclohexane, supplemented with an emulsifier. The 'acidic' emulsion (E_2) consisted of 33 cm^3 5 wt% of HCI and 35 cm^3 of cyclohexane, supplemented with an emulsifier of the same composition as in E_1 but in appropriately lower amount. The pre-dissolved emulsifiers were diluted in cyclohexane. The aqueous phase (for E_l 5 wt% solution of Na_2SiO_3, for E_2 5 wt% solution of HCI) was dosed in few portions and the mixture was homogenised at 19,000 rpm for 5 min. The so prepared emulsions were used in precipitation reactions.

The precipitation was conducted in the reactive vessel of 0.5 dm^3 capacity. Mixing took place in a homogeniser of ULTRA TURRAX T25 basic type (IKA LABORTECHNIK, Germany) at 19,000 rpm. The E_2 emulsion was placed in the

reactive vessel and subjected to intense mixing. Emulsion E_1 was dosed to emulsion E_2 at a constant rate, using peristaltic pump. As a result of the reaction taking place in the reactive vessel a silica-containing emulsion was obtained. The emulsion was heated to 80°C in order to destabilise it. Subsequently, cyclohexane was separated from it by distillation. The subsequent stage involved filtration of the remaining mixture under a lowered pressure. In this way, the obtained sample was washed with hot water and, then, with acetone in order to wash out the remaining surfactants. Acetone was separated by distillation. Subsequently, the sample was subjected to drying for 48 hours in a stationary drier at 105°C.

PHYSICOCHEMICAL EVALUATION

Following the precipitation, the silicas were subjected to physicochemical tests, bulk densities as well as water, dibutyl phthalate and paraffin oil absorbing capacities were estimated.

Examinations of particle shape and morphology were conducted using scanning electron microscopy (SEM). The observations were performed in the Phillips SEM 515 microscope.

Laser Doppler electrophoretic light scattering determinations were performed with a ZetaPlus instrument (Brookhaven Instruments Inc., USA), in the reference beam mode at the wavelength of laser light source of 635 nm, sampling time 256 its, modular frequency 250 Hz and the scattering angle 15°. The zeta potentials were obtained by averaging 10 runs. Each examination were performed in a stable ionic strength (solution of 10^{-3}mol NaCl).

The technique of dynamic light scattering (DLS), applied also in the ZetaPlus apparatus, permitted to obtain multimodal particle size distribution pattern on the basis of autocorrelative functions of laser light beam (670 nm) scatter. The most important parameters obtained using the technique included polydispersity and a mean particle diameter. Polydispersity represented a measure of heterogeneity of particle size distribution in the studied system.

Specific surface areas of silica powders were determined by N_2 adsorption (BET method) using ASAP 2010 instrument (Micrometrics Instrument Corporation). Moreover, the volume and size of pores of precipitated materials were examined. Samples were heated at 120°C for 2 hours prior to measurements.

The chemical composition of the obtained silicas was measured with X-ray photoelectron spectroscopy (XPS) on a SPECS ESCA system with Phoibos 100 energy analyser. The spectra were taken with a non-monochromated MgKα X-ray source. The survey scans were recorded using a pass energy of 30 eV and X-ray energy of 100 W, the high resolution spectra were recorded using 5 eV pass energy and 200 W. Charging of the sample surface was neutralised with flood gun with calibrating at 284.6 eV for C 1s peak.

The extent of modification and the character of the reaction between silane coupling agent and the silica were established in the FTIR EQUINOX (Bruker) equipment. In this aim, tablets of KBr with the studied silica were prepared.

RESULTS AND DISCUSSION

Principal physicochemical parameters of the obtained silica and of the silica following aminosilane modification are presented in Table 1.

Table 1. Basic physicochemical properties of examined silicas.

Sample	Bulk density (g/dm^3)	Water absorbing capacity ($cm^3/100g$)	Paraffin oil absorbing capacity ($cm^3/100g$)	Dibutyl phthalate absorbing capacity ($cm^3/100g$)
SiO_2				
A	283	250	300	225
SiO_2 + 3 w/w of U-15D silane				
B	261	250	350	250
SiO_2 + 5 w/w of U-15D silane				
C	221	150	350	275

The silica obtained in the process of precipitation exhibited a relatively high bulk density and high water absorbing capacity. Following modification, the silica altered its physicochemical properties: its bulk density and water basorbing capacity decreased while its paraffin oil absorbing capacity increased. The results have demonstrated increase in hydrophobicity of the silica surface. The increase has depended to a significant extent upon the amount of silane used for the modification.

Particle size distribution and electron micrograph of the unmodified silica are shown in Fig.1. Mean particle diameter amounted to 792.0 nm and the polydispersity was 0.059. The latter value has demonstrated a relatively highly uniform character of silica particles. In the particle size distribution (Fig.1a) two bands could be noted. The more intense band reflected presence of silica particles of smaller diameter and fitted the range of 391.6 to 684.6 nm (maximum intensity of 100 corresponded to the particle diameter of 489.6 nm). The other band within the range of 3,658.7 to 5,905.8 nm was related to particles of much higher diameters and to the formed aggregates and was definitely much less intense (maximum intensity of 5 corresponded to particles with diameters in the range of 4,431.0-5,366.4 nm). SEM micrograph (Fig.1b) confirmed presence of almost absolutely spherical particles of low diameters, which formed larger groups (the so called agglomerates) and the latter represented an undesirable development.

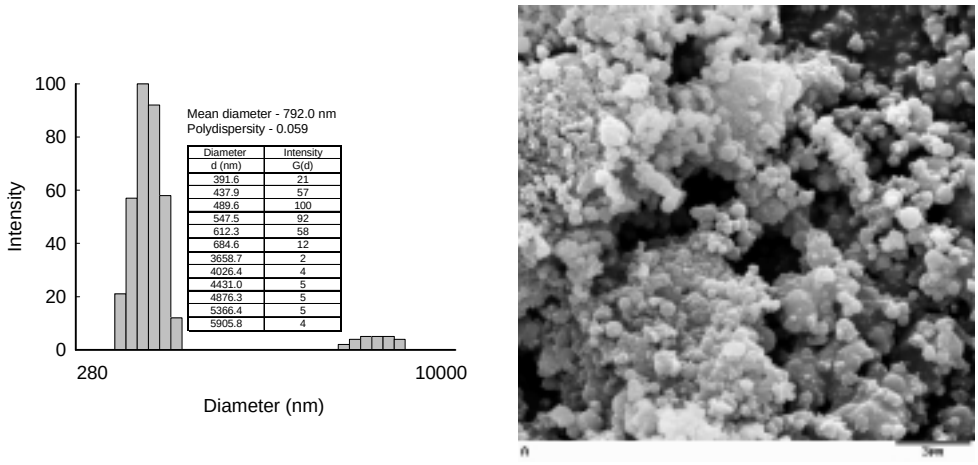

a) b)

Fig.1. a) Multimodal particle size distribution and b) SEM of unmodified silica.

Particle size distribution and SEM micrograph of silica modified with 3 weight parts of N-2-(aminoethyl)-3-aminopropylotrimethoxysilane are shown in Fig.2. Mean particle size in the silicas was 507.3 nm, while polydispersity was as low as 0.005. This pointed to a most advantageous effect of U-15D silane on silica dispersion. The particle size distribution (Fig.2a) also demonstrated presence of two bands, which have been ascribed to particles of, respectively, smaller and of significantly larger diameters. The more intense band reflected presence of particles of lower diameters (315.9-471.6 nm) and maximum intensity of 100 corresponded to particle diameter of 370.8 nm. Silica modified with 3 weight parts of aminosilane manifested presence of particles within the lower range of diameters as compared to the unmodified silica. The band within the range of 2104.6-2571.3 nm reflected presence of particles of larger diameters and of agglomerates and was decissively less intense (maximum intensity of 7 corresponded to particle diameter of 2249.9 nm). Presence of spherical particles and the highly uniform character of the so modified silica was verified by the microphotogram presented in Fig.2b. Particles of the silica presented much more fine, spherical grains and the system became more uniform.

Silica modified with 5 weight parts of aminosilane also exhibited a highly uniform character of particles (Fig.3). In this case, mean particle diameter was 442.2 nm and its polydispersity was 0.005. The particle size distribution (Fig.3a) demonstrated only one typical band within the diameter range of 438.5-444.3 nm. Maximum intensity of 100 corresponded to particles of 442.6 nm in diameter. The pronounced homogeneity of particles could also be confirmed by SEM micrograph (Fig.3b).

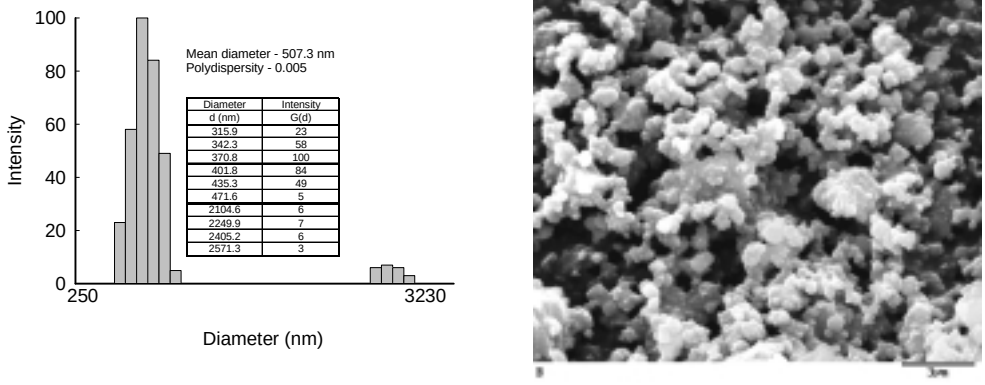

a) b)

Fig.2. a) Multimodal particle size distribution and b) SEM of silica modified with 3 w/w aminosilane

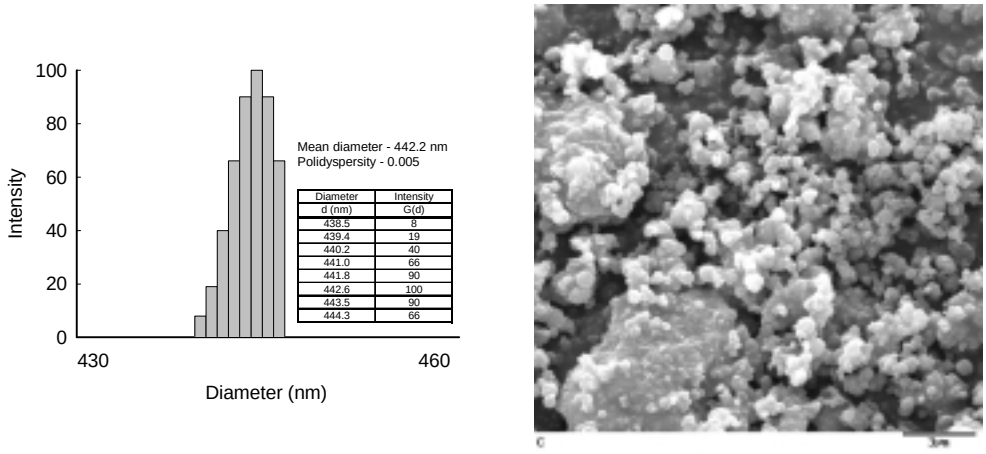

a) b)

Fig.3. a) Multimodal particle size distribution and b) SEM of silica modified with 5 w/w aminosilane

Results of studies on specific surface area (BET) and on the volume and diameter of pores are shown in Table 2.

As evident in the Table 2, the unmodified silica exhibited a relatively extensive development of specific surface area, amounting to 182 m^2/g. Folowing modification with 3 weight parts of aminosilane BET area decreased to 119 m^2/g, which was confirmed by the data of Fig.2b, documenting absence of large groups, the so called agglomerates. Increased amount of the modifier (sample C) resulted in enhanced tendencies for particle-particle interactions and this was accompanied by a pronounced

increase in the area, which reached the value of 208 m^2/g. The alterations in specific surface area were accompanied by altered desorptive-adsorptive properties, expressed by the volume and size of pores.

Table 2. Specific surface area, volume and average size of pores of obtained silicas.

Sample No.	Specific surface area BET (m^2/g)	Total pores volume (cm^3/g)	Pores volume 17 do 30000Å (cm^3/g)		Average size of pores* (Å)
			from adsorption curve	from desorption curve	
A	182	0.45	0.4987	0.4996	99.24
B	119	0.34	0.3907	0.3913	114.16
C	208	0.39	0.4534	0.4525	74.95

* calculated from BET equation (4V/A)

Dependence of zeta potential on pH (the so called isoelectric point) was demonstrated both for the unmodified and the modified silicas (Fig.4). Numerous studies (Kosmulski et al., 2000; Spange et al., 2000) demonstrated that altered protonisation in the reaction of:

$$\equiv Si\text{-}OH \longrightarrow \equiv Si\text{-}O^- + H^+ \ (pH>3) \text{ or } \equiv Si\text{-}OH + H^+ \longrightarrow \equiv Si\text{-}OH_2^+ \ (pH<3)$$

induced alterations in zeta potential and, indirectly, also in the isoelectric point. In this study effect of aminosilane protonisation was analysed on the course of electrokinetic curves and, thus, on values of isoelectric point. In the acidic range of pH, evident differences in surface charge can be noted between silicas modified with aminosilane and the unmodified silica (Fig.4). Almost within the entire acidic range of pH zeta potential manifested positive values and the highest stability was reached at pH ranging between 2 and 6. A completely distinct surface character could be ascribed to the unmodified silica, in which the range of pH = 2 to 6 determined a negative charge of zeta potential. In the range of pH = 8 to 9.5 the studied silicas manifested similar values of the potential. Moreover, the modified silica manifested a definitely higher value of the isoelectric point as compared to the unmodified silica. The value amounted to 1.5 in sample A, 6.2 in sample B, 6.7 in sample C.

The studies performed by XPS technique demonstrated to which extent silane modification affected the atomic composition (%) of the silica (Table 3). Modification with 3 weight parts of silane introduced 1% nitrogen, and the nitrogen content increased to 2% following modification with 5 weight parts of the silane. The nitrogen originated from =NH and $–NH_2$ groups of the applied aminosilane.

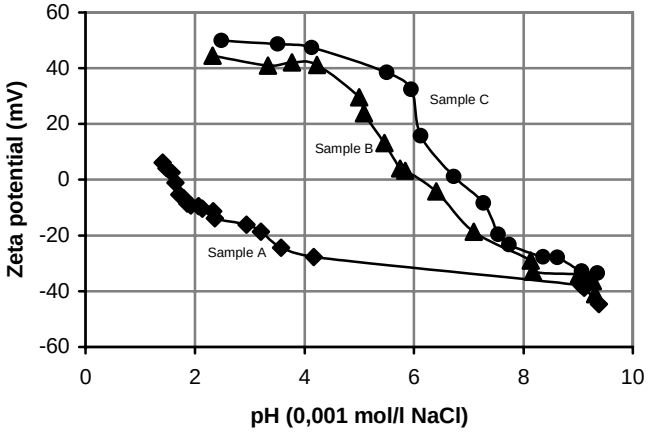

Fig. 4. Zeta potential as a function of pH for unmodified silica and amino-silane modified silicas

Table 3. Surface elemental composition from XPS analysis.

Sample	Surface composition (at%)	
A	C	22.3
	O	55.0
	Si	22.6
	N	0.0
B	C	33.4
	N	1.0
	O	46.7
	Si	18.9
C	C	17.8
	N	2.0
	O	56.4
	Si	23.9

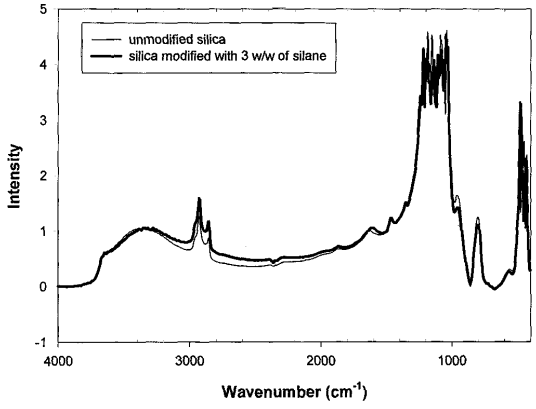

Fig. 5. FTIR spectra for unmodified and 3 w/w of U-15D silane modified silica

Character of the modification was evaluated by FTIR spectroscopy. As can be noted in Fig.5, the studied silicas exhibited no intense 3,748 cm^{-1} band, responsible for the presence of isolated silanol groups. Traces of the band could only be noted. Most probably, thus resulted from blocking of silanol groups by organic emulsion components in the course of silica precipitation. On the other hand, the band in the range of 2,965-2,850 cm^{-1} corresponding to distracting oscillations could be clearly noted. Its presence reflected production of the silica in an organic medium (in the case of the unmodified silica) and modification of the silica with silane coupling agent. Therefore, intensity of the band was higher in aminosilane-modified silica.

CONCLUSIONS

Following modification with aminosilane extensive changes were noted in silica surface hydrophilicity (e.g., the decrease in water absorbing capacity from 250 cm^3/100g to 150 cm^3/100g). Moreover, the studied silicas demonstrated a highly monodisperse character, which was confirmed by SEM microphotographs and particle size distributions. Silica surface modification, particularly with 3 weight parts of aminosilane, induced a pronounced increase in particle homogeneity. On the other hand, spectroscopic studies and laser light scattering provided evidence for the chemical character of N-2-(aminoethyl)-3-aminopropyltrimethoxysilane with the silica surface. Chemical interaction of silane with silica surface induced evident changes in isoelectric point and in the surface composition.

REFERENCES

BARTHEL H., 1995, *Surface interactions of dimethylsiloxy group-modified fumed silica*, Colloids Surf. A 101, 217.

BERGNA H.E., 1994, *The Colloid Chemistry of Silica*, ACS: Advences in chemistry series 234, Washington, pp. 1-47.

BUINING P.A., LIZ-MARZAN L.M. and PHILIPSE A.P., 1996, *A simple preparation of small, smooth silica spheres in a seed alcosol for Stöber synthesis*, J. Colloid Interf. Sci.179, 318.

ESQUENA J., PONS R., AZEMAR N., CAELLES J. and SOLANS C., 1997, *Preparation of monodisperse silica particles in emulsion media*, Colloids Surf. A 123-124, 575.

FARAMAWY S., EL-FADLY A.M. and EL-NAGGAR A.Y., YOUSSEF A.M., 1997, *Surface-modified silica gels as solid stationary phases in gas chromatography*, Surf. Coat. Technol. 90, 53.

GAN L.M., ZHANG K. and CHEW C.H., 1996, *Preparation of silica nanoparticles from sodium orthosilicate in inverse microemulsion*, Colloids Surf. A 110, 199.

GOWORKEK J., NIERADKA A. and DĄBROWSKI A., 1997, *Adsorption from ternary liquid mixtures on silica gel of different mesoporosity*, Fluid Phase Equalibria 136, 333.

ILER R.K., 1979, *The Chemistry of Silica*, John Wiley & Sons, New York, pp. 622-714.

JESIONOWSKI T. and KRYSZTAFKIEWICZ A., 2000, *Comparison of the techniques used to modify amorphous hydrated silicas*, J. Non-Crystalline Solids 277, 45.

JESIONOWSKI T. and KRYSZTAFKIEWICZ A., 2001, *Influence of silane coupling agents on surface properties of precipitated silica*, Appl. Surf. Sci. 172, 18.

JESIONOWSKI T., 2001, *Preparation of colloidal silica from sodium metasilicate solution and sulphuric acid in emulsion medium*, Colloids Surf. A 190, 153.

JESIONOWSKI T., 2001, *Preparation of silica particles in emulsion systems,* J. Dispersion Sci. Technol. 22, 363.
KOSMULSKI M., ERIKSSON P., BRANCEWICZ CH. and ROSENHOLM J.B., 2000, *Zeta potential of monodispersed, spherical silica particles mixed solvent as a function of cesium chloride concentration,* Colloids Surf. A 162, 37.
LEGRAND A.P., 1998, *The Surface Properties of Silicas,* John Wiley & Sons, New York, pp. 313-361.
SPANGE S., REUTER A., PRAUSE S. and BELLMANN C., 2000, *Electrokinetic and solvatochromic studies of functionalized silica particles,* J.Adhesion Sci. Technol. 14, 399.
SUHARA T., KANEMARU T., FUKUI H. and YAMAGUCHI M., 1995, *Fine silica powder modified with quartenary ammonium groups: rectivity and characteristics,* Colloids Surf. A 95, 1.
VAN DER VOORT P. and VANSANT E.F., 1996, *Silylation of the silica surface a review,* J. Liq. Rel. Technol. 19, 2723.

ACKNOWLEDGEMENTS

This work was supported by the PUT Research Grant DS No. 32/008/2002.

Jesionowski T., *Wpływ n-2-(aminoetylo)-3-aminopropylotrimetoksysilanu na właściwosci fizyko-chemiczne i morfologiczne krzemionek otrzymywanych w układzie emulsyjnym***,** Fizykochemiczne Problemy Mineralurgii, 36, (2002) 243-252 (w jęz. ang.)

Przeprowadzono syntezę monodyspersyjnej krzemionki w reakcji strącania z wodnego roztworu metakrzemianu sodu kwasem solnym w środowisku emulsji. Badano wpływ N-2-(aminoetylo)-3-aminopropylotrimetoksysilanu na właściwości powierzchniowe i morfologiczne strącanej krzemionki. Wielkość cząstek i polidyspersyjność mierzono stosując technikę dynamicznego rozpraszania światła (DLS) oraz skaningową mikroskopię elektronową (SEM). Stopień powierzchniowej modyfikacji oraz jej charakter oceniano wykorzystując spektroskopię w podczerwieni. Ponadto charakteryzowano właściwości adsorpcyjne przez wyznaczenie powierzchni właściwej (BET) i makroporowatości. Technika XPS umożliwiła wyznaczenie ilościowe obecnego modyfikatora na powierzchni krzemionki. Zmiany ładunku powierzchniowego badano wyznaczając dla poszczególnych krzemionek punkt izoelektryczny przez bezpośredni pomiar ruchliwości elektroforetycznej, a pośrednio przez wyliczenie potencjału zeta. Modyfikacja SiO_2 formowanej w środowisku emulsji aminosilanem powoduje duże zmiany charakteru powierzchniowego i morfologicznego. Następuje wyraźne ograniczenie grup silanolowych na powierzchni już w chwili preparatyki krzemionki, a dodatkowo zwiększenie hydrofobowości na skutek chemisorpcji aminosilanu. Uzyskano również wzrost homogeniczności cząstek i zmniejszenie wartości polidyspersyjności na skutek oddziaływań aminosilanu z powierzchnią badanej krzemionki.

Physicochemical Problems of Mineral Processing, 36 (2002) 253-272
Fizykochemiczne Problemy Mineralurgii, 36 (2002) 253-272

Jakub NALASKOWSKI*, Anh V. NGUYEN**, Jan HUPKA***, Jan D. MILLER*

STUDY OF PARTICLE – BUBBLE INTERACTION USING ATOMIC FORCE MICROSCOPY – CURRENT POSSIBILITIES AND CHALLENGES

Received March 15, 2002; reviewed and accepted May 15, 2002

Study of interaction forces between mineral particles and air bubbles is a key to understanding flotation processes. Measurement of such interaction forces has only recently been made possible with the introduction of the atomic force microscope (AFM) and the colloidal probe technique. Using AFM, interactions between a single particle attached to the AFM cantilever and an air bubble placed on a flat hydrophobic surface are measured in an aqueous environment. Interaction forces prior to rupture of the interfacial water film as a function of the hydrophobic surface state can be established, as shown in the present study. Additionally, the effect of the hydrodynamic force between approaching air bubble and particle is quantified. Despite the great potential of the AFM colloidal probe technique for studying particle – bubble interactions, several challenges pertaining to the AFM design, experimental procedure, and data analysis have to be addressed due to deformation of the air-water interface. For example, such issues as the range of the piezoelectric translator and cantilever deflection, determination of the bubble spring constant, and identification of the point of contact between bubble and particle are now under consideration.

Key words: particle – bubble interaction, Atomic Force Microscopy (AFM), hydrophobic force, contact angle, hydrodynamic force

INTRODUCTION

Flotation is an important separation process used for the recovery of billions of tons of valuable minerals (Fuerstenau and Herrera-Urbina, 1989), for the recycling of paper and plastic (Drelich and Miller, 2001; Shen et al., 2002) and for the treatment of

* Department of Metallurgical Engineering, University of Utah, 135 South 1460 East, Room 412, Salt Lake City, Utah 84112-0114, USA. Corresponding author: phone: (801) 581-6814; fax: (801) 581-4937; email: kubn@mines.utah.edu.
** Department of Chemical Engineering, The University of Newcastle, University Drive, Callaghan NSW 2308, AUSTRALIA
*** Department of Chemical Technology, Technical University of Gdansk, Narutowicza 11/12, 80-952 Gdansk, POLAND

wastewater (Ramirez and Johnson, 1980; Odegaard, 2001). This complex process includes many physicochemical and hydrodynamic phenomena in a dynamic system composed from solid particles, air bubbles, and aqueous solutions of various chemicals. Although many of these phenomena have been successfully studied in the past and significant practical as well as fundamental knowledge has been gained, a complete understanding is still not developed. The particle – bubble interactions, leading to attachment are a key to flotation and have received much attention (Lekki and Laskowski, 1976; Chiang, 1983; Alekseev, 1991; Luttrell and Yoon, 1992; Yoon, 1992). It has been realized that these interactions are composed from DLVO forces, non-DLVO interactions and a hydrodynamic component. (Yoon, 1992; Skvarla and Kmet, 1993; Yoon and Mao, 1996; Yoon, 2000). In this view, a significant effort has been made to characterize such interaction forces by establishing Hamaker constants for mineral particles (Lins et al., 1995), and zeta potentials for both air bubbles (Laskowski et al., 1989) and mineral particles (Drzymala and Laskowski, 1980). However, in order to account for all the components in the system the direct measurement of the interaction force between a particle and an air bubble is necessary.

Although the direct force measurements have been possible for some time using the Surface Force Apparatus (SFA) (Israelachvili and Tabor, 1972; Derjaguin et al., 1978), only development of the Atomic Force Microscope (AFM) (Binnig et al., 1986) and the colloidal probe technique (Ducker et al., 1991) has made it possible to study interaction forces between a single particle of choice and a selected surface.

Using this method a single particle with diameter from 1 to 100 μm is attached to the AFM cantilever and is moved toward the surface using a piezoelectric translator. During this movement the deflection of the cantilever is recorded by means of a reflected laser beam which serves as an optical lever. Using this data the profile of interaction force as a function of distance between the particle and the surface is obtained. Additionally, after contact, during retraction of the cantilever from the surface, the adhesion force between particle and surface can be measured.

This setup has been successfully used in the study of interaction forces between particles and solid surfaces, particularly in systems closely related to mineral processing (Rabinovich and Yoon, 1994; Biggs and Proud, 1997; Pazhianur and Yoon, 1997; Yoon et al., 1997; Toikka et al., 1998; Yoon and Pazhianur, 1998), and many important findings pertaining to the role of hydrophobic interactions, system stability, coagulation, influence of surfactants and flocculants, etc. were established. A significant number of these research initiatives pertain to flotation. Unfortunately experimental and theoretical difficulties of measurement involving the deformable air-water interface have forced researchers to consider model, solid hydrophobic particles to represent the air bubble. Different materials have been used as a model air bubbles including silanated glass (Pazhianur and Yoon, 1997) and polyethylene (Nalaskowski et al., 1998; Drelich et al., 2000). However, this approach although giving applicable results, is far from reality. Deformation of the air-water interface during particle approach and subsequent changes in charge density and surfactant adsorption density

cannot be reproduced with the use of solid hydrophobic particles as representation of air bubbles. Also, formation of the three-phase contact line (TPL) and the relaxation of air-water interface after attachment can only be observed when a real air-water interface is used during the experiment.

Fortunately, during the last few years significant progress has been made in this area, both with respect to instrumentation and experimental procedure. Further, advances in the theoretical analysis have been made as well. Several researchers have successfully conducted interaction force measurements between an air bubble and a solid particle using commercially available AFM systems (Ducker et al., 1994; Fielden et al., 1996), and specially designed, home-built instruments, closely related to the AFM design ((Butt, 1994; Preuss and Butt, 1998a; Preuss and Butt, 1999). Unfortunately, despite numerous significant contributions to the theoretical analysis of interaction forces between the solid particle and the deformable interface and the deformation of this interface during particle approach (Miklavcic et al., 1995; Miklavcic, 1998; Nguyen and Stechemesser, 1998; Ralston and Dukhin, 1999; Ralston et al., 1999; Nguyen et al., 2001; Nguyen and Evans, 2002), the geometry of the interface during approach must be considered during calculation of these interfacial forces. Despite some limitations, it has to be stated here, that significant progress has been made and AFM measurements can significantly contribute to the analysis of particle-bubble interactions in mineral processing science.

In this paper, examples of experimental data from the authors' research will be shown. Possibilities for the use of AFM for different studies as well as limitations of the technique will be discussed.

EXPERIMENTAL SECTION

MATERIALS

Glass spherical particles (Polysciences, Inc.) were carefully cleaned by subsequent sonication in acetone, methanol and RCA SC-1 cleaning solution composed of 5 vol. H_2O, 1 vol. 29% NH_{3aq}, and 1 vol. 30% H_2O_2 at 80 ^oC (Kern and Puotiene, 1970), rinsed with deionized water and dried. The glass spheres, which were not cleaned with this procedure, were hydrophobic and had an estimated contact angle around 10 degrees. The liquid film between these particles and a bubble was unstable, leading to its rupture.

Spherical polyethylene (PE) particles were obtained using a procedure, which involves suspending a powder of polymeric thermoplastic materials, such as PE, in glycerol, heating the suspension above the melting point of the polymer, and then solidification of the dispersed polymeric droplets at a reduced temperature. After appropriate filtration and drying, this procedure was found not to change the surface properties of PE particles, which retained a high degree of hydrophobicity. These particles had a relatively smooth surface and were particularly useful for investigating

interaction forces using the AFM colloidal probe technique (Nalaskowski et al., 1999a).

Other materials include: highly ordered pyrolytic graphite (HOPG – Digital Instruments, Inc.), KCl (Malinckrodt, Inc.) and deionized water (Milli-Q Millipore system).

METHODS

The prepared spherical particles were glued to the AFM cantilever with a small amount of epoxy resin using a procedure described elsewhere (Ducker et al., 1991). Tipless triangular silicon nitride cantilevers having a spring constant of 0.12 N/m (Digital Instruments, Inc.) were used. The cantilever was placed under the CCD camera fitted with long distance lens giving a 500× magnification. A small amount of resin was transferred on the tip of the cantilever using a 50 μm diameter tungsten wire attached to a micromanipulator. After that, a selected sphere was picked up using a new tungsten wire and carefully placed on the cantilever using the micromanipulator. Cantilevers were ready for measurements after at least 24 hours of drying. Using this procedure, spherical particles with a diameter down to 1 μm could be precisely glued to the end of AFM cantilever, see Fig. 1.

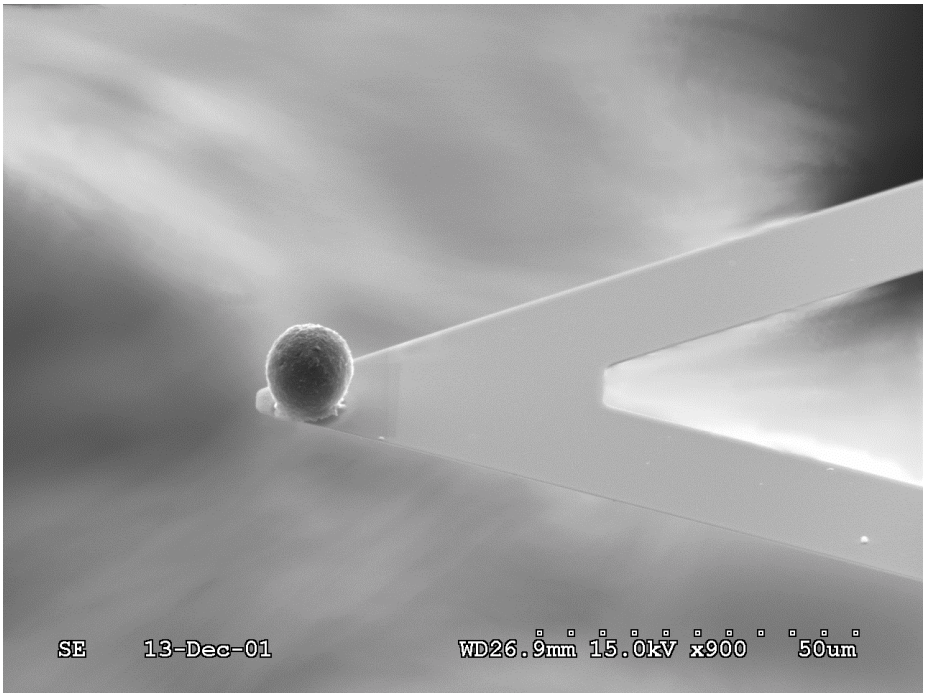

Fig. 1. SEM photograph of a spherical particle (14 μm diameter) glued to the end of AFM cantilever

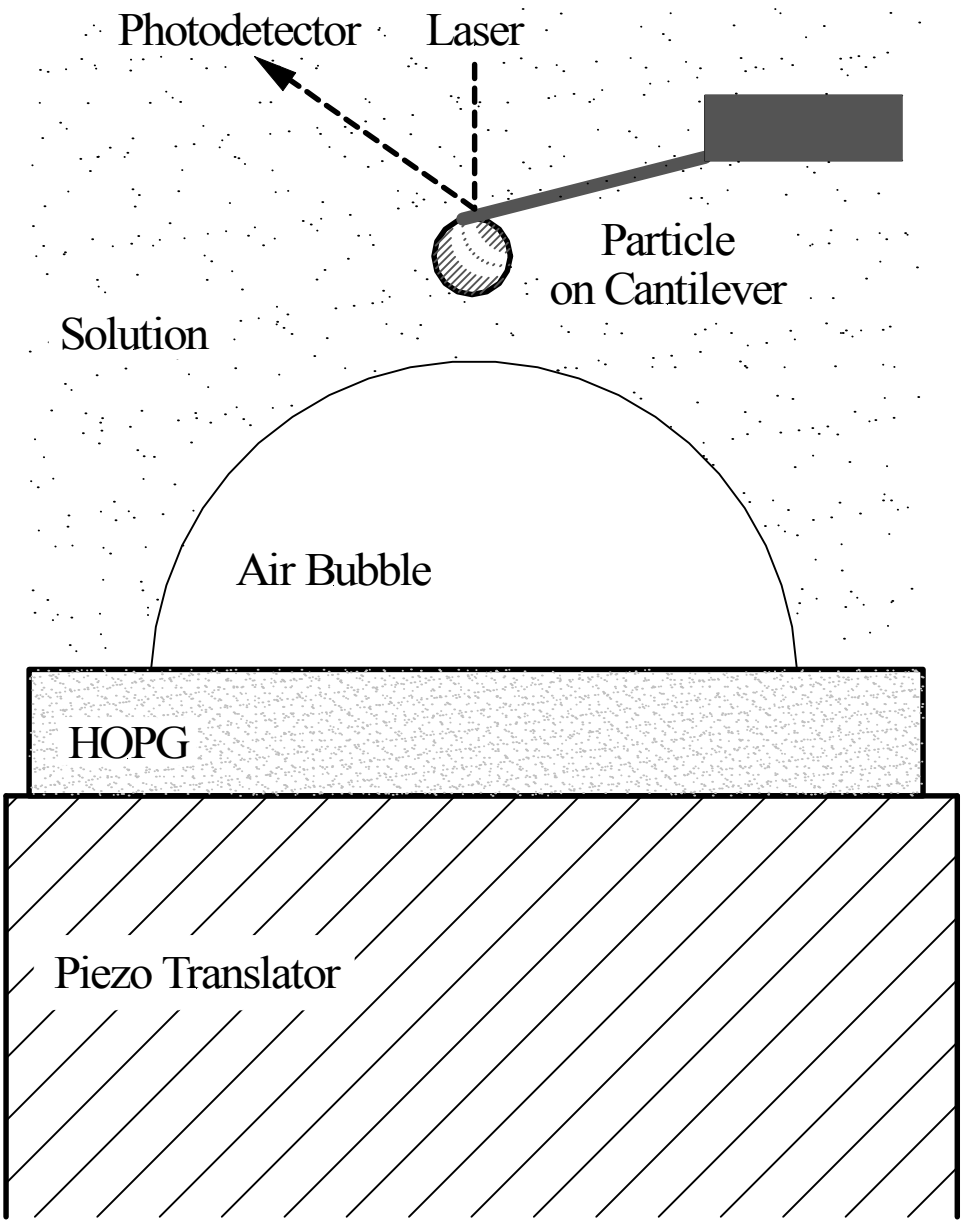

Fig. 2. Schematic of the AFM setup used for particle-bubble interaction force measurement

A Nanoscope IIIa atomic force microscope (Digital Instruments, Inc.) equipped with a fluid cell was used for the measurements. As shown in, a laser light is focused on the back of the cantilever to detect the cantilever's deflection as it interacts with the surface beneath it. The reflected light is directed onto a split photodiode detector, which produces a voltage signal proportional to the cantilever deflection. If the spring constant is known, the deflection of the spring can be converted to force using Hooke's law. Using such a setup the force acting on the cantilever can be determined with sensitivity greater than 0.1 nN. The sample beneath cantilever is moved using a piezoelectric transducer. In the force measurements, motion in the *x* and *y* directions is disabled and the piezoelectric tube is used to move the surface in the *z* direction and the cantilever deflection is continuously measured. The approach velocity of the surface can be accurately controlled and varied over three orders of magnitude.

A silicone o-ring was placed on the surface of the HOPG and filled with 1 mM KCl solution or deionized water. A hemispherical air bubble with a diameter from 400 to 600 μm was formed on the graphite surface using a microsyringe. The air bubble attached to the hydrophobic graphite surface was stable for many hours. Such prepared sample was mounted on the top of the piezoelectric transducer of the AFM system and the prepared cantilever with attached particle in the quartz fluid cell holder was mounted above.

The particle on the cantilever was initially positioned, under optical microscope control, on the center of air bubble and roughly one micrometer above the bubble surface. Different speeds of approach were obtained by changing the scan rate of the piezoelectric translator and the cantilever deflection versus piezoelectric transducer displacement was recorded. At least 5 measurements were taken for each speed of approach. Subsequently, deflection was recalculated into force normalized with respect to particle diameter and separation distance was obtained based on constant compliance region.

RESULTS AND DISCUSSION

Using the experimental setup previously described, many interesting and important properties of the particle-bubble system can be studied. Several possibilities are discussed below.

PARTICLE CONTACT ANGLE AND MICROSPHERE TENSIOMETRY

Wetting properties of micrometer-size particles are important in many industrial applications including paint, plastic, pharmaceutical and mineral processing industries. Measurement of the contact angle of small particles, which is the most common way to describe wetting characteristics, is unfortunately by no means an easy task. Usually different variations of the capillary rise method are employed (Bartell and Osterhof, 1927; Diggins and Ralston, 1993; Siebold et al., 1997). In these methods particles are packed into a tube, closed at the bottom by a porous plug. The bottom of the tube is

immersed into the studied solution and capillary rise of the liquid through the packed bed of particles is observed. Contact angle can be obtained from the speed of the capillary rise or from the pressure necessary to stop the rise. Unfortunately this method is strongly depandant on the packing of the particle bed and it is not easy to compare results when different procedures for particle bed preparation are employed. Additionally models of the capillary rise used for the contact angle measurements are not yet clear (Siebold et al., 2000). Finally, it has to be emphasized that only the average contact angle for the whole population of particles is obtained.

AFM can be easily used for measurement of the contact angle of single particles if their geometry is close to spherical. In such a measurement the particle is glued to the cantilever and the deflection of the cantilever due to the force acting between the particle and the air bubble is recorded in function of piezo translator displacement. An example of such force curves is given on Fig 3.

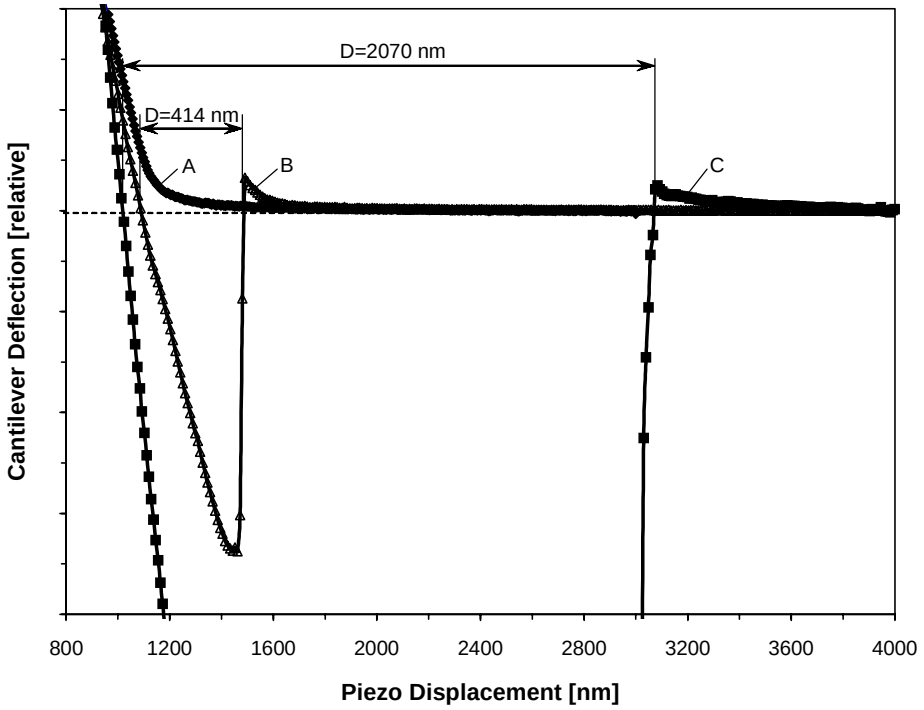

Fig. 3. Cantilever deflection versus piezo displacement for three different particles interacting with an air bubble in water. (A) - hydrophilic glass particle, (B) - slightly hydrophobic glass particle, (C) - highly hydrophobic PE particle. (D) denotes the distance at which particle penetrates the air bubble under the zero force

Three curves for three different particles with varying wettability are shown. The curve (A) is typical for a completely hydrophilic glass particle. In this case the interfacial water film between particle and bubble is thermodynamically stable and no attachment is observed as is evident by only repulsive interactions which are a net effect of repulsive electrostatic, van der Waals and hydrodynamic forces. The curves (B) and (C) are recorded for a slightly hydrophobic glass particle (B) and strongly hydrophobic PE particle (C). In the case of these particles the water film between the interfaces is unstable and jump to contact and formation of TPL occurs. At a certain point after attachment, during the continuous approach of particle there is a point where the force curve crosses zero. At this point no force is acting on the particle. The distance D (shown on Fig. 3) is a distance of particle penetration into the air bubble.

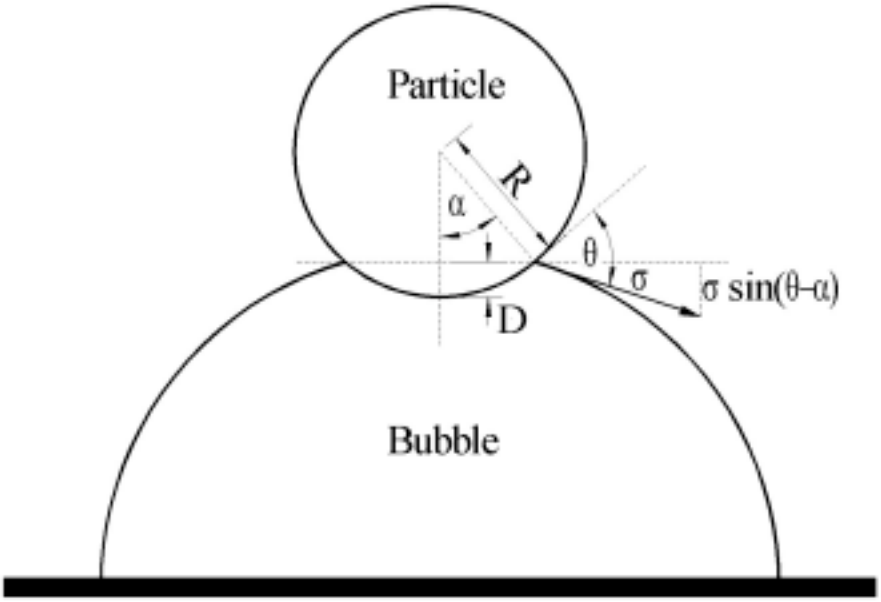

Fig. 4.The equilibrium state of a spherical particle at the air-water interface. (R) – particle radius, (D) – distance of penetration into air bubble, (σ) – surface tension, (α) – central angle, and (θ) – contact angle

The equilibrium state of the particle at the air-water interface is shown on Fig. 4. The gravitational force acting on micrometer-size particle can be neglected and the interaction between the air bubble and particle after the jump to contact is dominated by a capillary force. For a spherical particle this force is given by: Eq. 1 (Scheludko et al., 1976)

$$F_C = 2\pi R\sigma \sin\alpha \sin(\theta_R - \alpha) \quad (1)$$

where *R* – radius of the particle, σ – air-water interfacial tension, α – central angle and θ_R is the receding contact angle, since the particle is moving into the air bubble and the liquid recedes on the particle surface. By resolving the (1 with respect to the vertical component D one can obtain:

$$\cos\grave{e}_R = \frac{R - D}{R} \qquad \text{Eq. (2)}$$

Using Eg. 2 then θ_R can be easily obtained by measuring the distance D and knowing the radius of the particle. Although the interpretation of force/radius versus separation distance is complicated and still not a satisfactorily resolved issue for measurements between a particle and a deformable surface, it is not necessary to take all these problems into account for contact angle measurements. There is even no necessity of converting the obtained deflection versus piezo displacement curves which means that even knowledge of the spring constant for the system in not necessary.

The calculated receding contact angle θ_R for the glass particle of radius 27 μm (curve B) was 10^O, while the θ_R for the PE particle of radius 9 μm (curve C) was 39^O. The measured value for the PE particle is smaller than θ_R measured for similarly treated planar PE surface which was equal 67^O (Nalaskowski et al., 1999a). This difference can be explained by considering additional work required for formation of TPL which is known as a line tension. If work is required for an increase of TPL it will result in a decrease in the contact angle (Preuss and Butt, 1998b).

In a similar way the advancing contact angle θ_A can be measured using a water drop instead of an air bubble (Ecke et al., 1999). Although the θ_A can also be obtained with an air bubble by measuring the pull-off force during the retracting of particle from air-water interface (Preuss and Butt, 1998b) it is usually possible only with specially designed instruments – commercial AFM systems are not able to fully record cantilever deflection during the retraction of hydrophobic particle from the bubble. By measuring the pull-off force of a spherical particle with known contact angle air-water interfacial tension can be also obtained.

HYDROPHOBIC INTERACTIONS

The understanding of interaction forces between mineral particle and an air bubble is crucial for the understanding of the flotation process. It is widely accepted that the attachment of a particle to the bubble cannot be explained based on DLVO theory. This is because in most cases the electrostatic component is repulsive (air-water interface is negatively charged (Collins et al., 1978; Saulnier et al., 1996; Graciaa et al., 2000)) and the van der Waals interaction between particle and bubble is also repulsive (Hough and White, 1980; Nguyen et al., 2001). It is evident that an additional attractive non-DLVO force is involved. This so called long range

hydrophobic force existing between hydrophobic surfaces has been an object of extensive study for the last 20 years (Christenson and Claesson, 2001; Skvarla, 2001). The origin and nature of these interactions is not completely clear but it is accepted that they are related to the formation of submicroscopic bubble cavities between hydrophobic surfaces an the subsequent rupture of the water film (Christenson and Claesson, 1988; Parker et al., 1994; Nalaskowski et al., 1999b; Attard, 2000; Tyrrell and Attard, 2002). Since previous research was limited only to solid surfaces it was unclear how these long range attractive forces are manifested in particle-bubble interactions. Recently such measurements has been conducted for different particles in various surfactant solutions by several researchers (Ducker et al., 1994; Preuss and Butt, 1998a). They have showed that a long-range jump to contact between particle and the bubble exists, which is a manifestation of the long-range hydrophobic forces. This jump-to-contact distance is dependent on the hydrophobicity of the particle and the presence of adsorbed surfactants at the air-water interface as well.

Unfortunately, in comparison with solid-solid interactions, the theoretical approach to the measurement involving a deformable surface is difficult and still unclear. Several important matters should be taken into consideration.

The first important difference is that since we deal with a very “soft”, deformable surface of an air bubble the spring constant of the system, k, is no longer equal to the cantilever spring constant, k_C, but also constitutes the spring constant of the bubble, k_B, which acts as a second spring during the interactions. The total spring constant is given by (3:

$$\frac{1}{k} = \frac{1}{k_C} + \frac{1}{k_B} \tag{3}$$

The spring constant, k, can be obtained from the slope of constant compliance region of force curve – the linear part of the force curve after contact (assuming the calibration of photodetector response versus deflection of the cantilever has been performed and the deflection of cantilever is known). When the spring constant of the cantilever is measured using one of the known methods (Cleveland et al., 1993; Sader et al., 1995; Maeda and Senden, 2000) the bubble spring constant can be determined from (3. The spring constant of an air bubble of diameter 500 μm in water was found to be k_B = 0.065 N/m (Ducker et al., 1994). It has to be noted that this value is smaller than many of the commercially available cantilevers which means that the air bubble will deflect more than the cantilever itself. Additionally this spring constant is dependent on bubble size (smaller bubble – larger k_B) and on the adsorption of surfactants on the air-water interface. Moreover, the assumption is usually made that k_B is constant during the approach and is not dependent on the interaction forces exerted at the interface due to the presence of the particle in the vicinity. The validity of this assumption is by no means obvious.

The second important difference between bubble-particle measurements and particle-solid surface measurements is the uncertainty of the real separation distance between the particle and bubble. This is related to the low spring constant of the bubble and contribution of the bubble to the deflection. Such a problem can be relatively easily addressed in the case of fully hydrophilic particles as shown in Fig. 5.

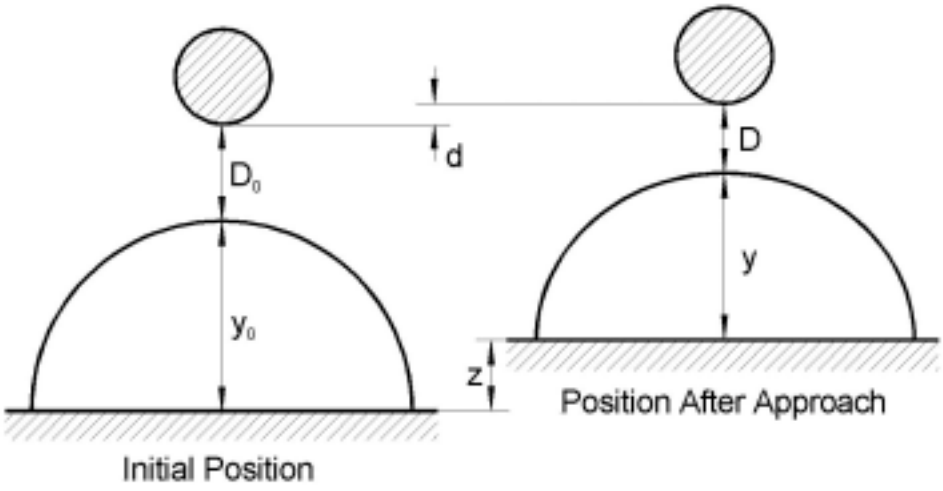

Fig. 5. Schematic of the relative positions of a particle and a bubble with surface deformation. (D_O, D) – initial and real separation distance, (y_O, y) – initial and real height of the air bubble, (z) – piezo displacement, (d) – cantilever deflection

The deflection of the cantilever, d, can be converted to force using Hooke's law:

$$F = k_C d \tag{4}$$

If the bubble behaves like a linear spring with a spring constant k_B , we can also obtain:

$$F = k_B (y_O - y) \tag{5}$$

where y_O and y are the initial and actual heights of the bubble surface at the apex.

Solving (4 and Eq. 5 gives:

$$y_O - y = d\frac{k_C}{k_B} \tag{6}$$

The distance balance yields:

$$D + y + z = D_O + y_O + d \tag{7}$$

In this equation, z is the position of the piezoelectric stage, which is experimentally determined from the applied voltage independently of the cantilever deflection, d, and the actual deformation, y, of the gas-liquid interface, the relative value of which is described by (6. The solution to (6 and (7 for the actual separation distance, D, gives:

$$D = d\left(1 + \frac{k_C}{k_B}\right) - z + D_O \tag{8}$$

This equation is central to the conversion of the experimentally available data of the cantilever deflection, d, and the position, z, of the piezoelectric stage to the actual separation distance, D, between surfaces.

The initial separation distance, D_O, is usually not known precisely, but it can be eliminated from the conversion considering the "molecular" contact regime between surfaces. In this "hard sphere" interaction, the separation distance D is very small, and we can set-off the value of 0 for this distance (for solid surfaces, this value is about 0.2 nm). However, for generality we describe the separation distance in the contact regime by D_C and obtain from (8:

$$D_C = d_C\left(1 + \frac{k_C}{k_B}\right) - z_C + D_O \tag{9}$$

Eliminating D_O from (8 and (9 gives:

$$D = D_C + (d - d_C)\left(1 + \frac{k_C}{k_B}\right) - (z - z_C) \tag{10}$$

This equation allows the actual separation distance to be determined from the measured variables d, d_C, z and z_C.

However, other types of deformation at the air-water interface also can be possible as schematically shown on Fig. 6. Electrostatic and hydrodynamic repulsion may cause formation of a dimple on the surface, while attractive hydrophobic forces may cause formation of a bulge and finally TPL and neck formation. In this last case the particle will additionally penetrate the air bubble depending on the hydrophobicity as explained in the previous part of this paper. Furthermore, the presence of interfacial forces may change the spring constant of the bubble which may become distance

dependant. More detailed approaches to the problem of the surface deformation accounting for the presence of interaction forces are also available (Parker and Attard, 1992; Miklavcic et al., 1995; Miklavcic, 1998; Nguyen and Stechemesser, 1998).They are difficult to apply in practical systems and do not take into account many important factors like the presence of non-DLVO interaction forces, especially hydrophobic attraction.

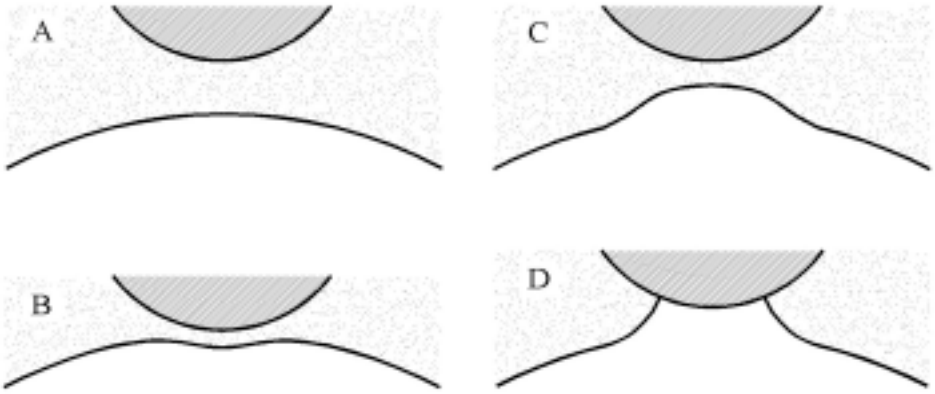

Fig.6. Schematic for the possible deformations of the bubble surface. (A) - particle far from bubble - no deformation; (B) - hydrophilic particle - dimple formation; (C) - hydrophobic particle - bulge formation; (D) - hydrophobic particle closer to the surface – formation of neck and TPL

Nevertheless, the AFM can successfully be used for the study of bubble-particle interactions. For example, the effect of particle hydrophobicity (natural, rendered by the silanization or the adsorption of surfactants) on the particle attachment can be studied (Butt, 1994; Ducker et al., 1994; Preuss and Butt, 1998a; Preuss and Butt, 1999). An example of such a study is shown on Fig. 7. It can be seen that in the case of a hydrophilic particle the water film between the particle and bubble is stable and only repulsive forces are observed, which involve at least three repulsive components: electric double layer, van der Waals and hydrodynamic forces. Hydrophobic particles jump to contact at a given distance and the TPL is formed. It can be seen that for strongly hydrophobic particle the jump-to-contact distance is much greater than that for a weakly hydrophobic particle. However it has to be noted that the separation distance is only relative here. The particles, after jump to contact, penetrate the air-water interface for a certain distance dependent on the particle hydrophobicity. Additionally, when the particle approaches, the air-water interface deforms due to the surface forces which are also dependent on particle surface chemistry. This problem cannot be resolved without measurement of real particle-bubble separation distance using an independent method (e.g. interferometry).

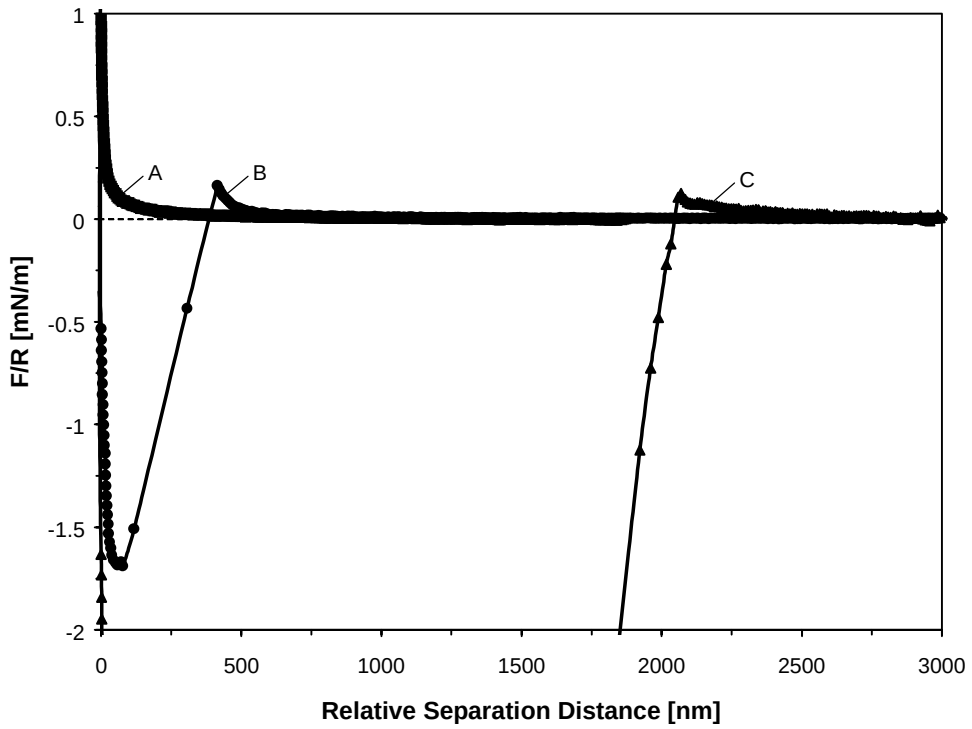

Fig. 7. Interaction forces between air bubble surface in water and spherical particles of different hydrophobicity. (A) - hydrophilic particle $\theta_R = 0^O$; (B) - slightly hydrophobic particle $\theta_R = 10^O$; (C) - strongly hydrophobic particle $\theta_R = 39^O$

HYDRODYNAMIC FORCES

Another important force which has to be considered in the flotation process is the hydrodynamic force during the bubble-particle approach. These forces were of great interest in previous studies (Pugh et al., 1994; Dai et al., 1998; Nguyen, 1999; Ralston et al., 1999; Yoon, 2000). The AFM can be used for the study of hydrodynamic interactions between a mineral particle and an air bubble.

Typically, the force measurements are carried out with a very low speed of the piezoelectric translator such that the dynamic phenomena of the system can be ignored and the static analysis of the force curve can be applied. It is interesting to note that commercially available AFM systems are capable of operating in the highly dynamic regime. Therefore, a speed of the piezoelectric translator on the order of tens to hundreds of microns per second can easily be achieved. By changing the speed of piezoelectric translator the hydrodynamic component of the interaction force between a spherical particle and a solid surface can be measured (Craig and Neto, 2001). Using

a similar approach, the dynamic interaction between a bubble and a particle, which is close to the interactions expected in the flotation of mineral particles, can also be studied.

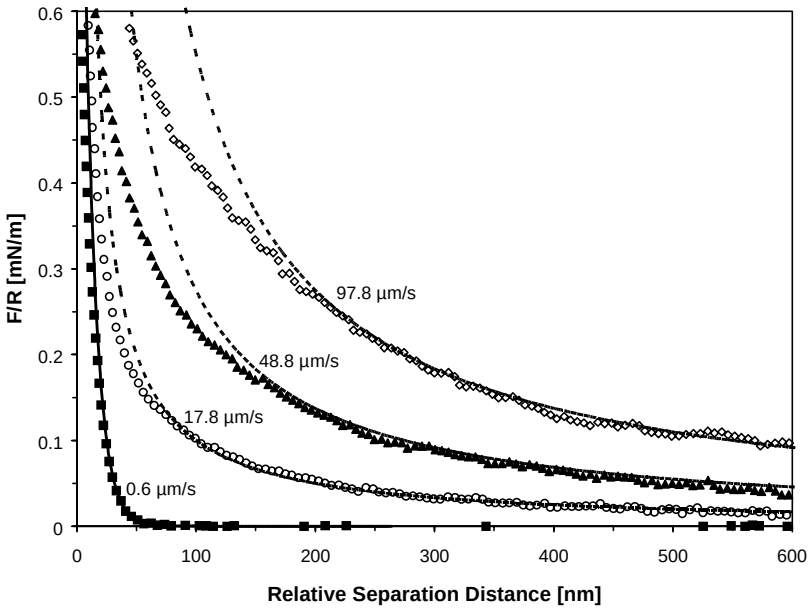

Fig. 8. Interaction force between hydrophilic glass particle and air bubble in 1×10^{-3} M KCl solution as a function of approach speed. Continuous line (at 0.6 µm/s) indicates theoretical DLVO repulsion for constant charge model ($A=-1.0\times10^{-20}$ J, Ψ_B=-15 mV, Ψ_P=-60 mV), dotted lines indicate theoretical hydrodynamic forces

The force curves recorded between hydrophilic glass particle (27 µm radius) and an air bubble in 1×10^{-3} M KCl solution are shown in Fig. 8 as a function of approach speed. Only repulsive forces were found in this system. The range and magnitude of the force increase significantly with an increase in approach speed. The experimental values were fitted to DLVO theory using the constant charge model (Israelachvili, 1991):

$$F_{DLVO} / R = \frac{4\pi\sigma_B\sigma_P}{\varepsilon\varepsilon_0\kappa} e^{-\kappa D} - \frac{A}{6D^2} \tag{11}$$

where σ_B, σ_P indicate the surface charge of bubble and particle, accordingly, calculated using the Graham equation (Israelachvili, 1991):

$$\sigma = 0.117[KCl]^{0.5} \sinh(\Psi / 51.4) \tag{12}$$

Other symbols indicate: ε – dielectric constant of medium, ε_0 – the permittivity of free space, κ – reverse Debye length, A – Hamaker constant, D – separation distance and Ψ – surface potential.

Previous work has shown that a potential for the air bubble of Ψ_B=-15 mV (Usui et al., 1981), and a surface potential for silica of Ψ_P=-60 mV (Ducker et al., 1991) can be used. A nonretarded Hamaker constant $A=-1.0\times10^{-20}$ J, calculated theoretically for silica/water/air system (Hough and White, 1980) was used in these calculations. Because of the uncertainty in the separation distance and zero separation value due to possible deformation, calculated values were shifted to correspond to those with relative zero separation distance.

The hydrodynamic force was calculated using the simplified Brenner's equation (Horn et al., 2000), which can be used when the separation distance between a sphere and the wall is much smaller than radius of the sphere:

$$F_{HYDR} / R = 6\pi\eta U \frac{R}{D} \tag{13}$$

where η is viscosity and U is the approach velocity.

It has to be noted that a very simplistic approach was used here – no deformation analysis was employed and the surfaces were treated as nondeformable and planar (in view of the fact that the diameter of the air bubble is orders of magnitude greater than the diameter of the particle). Nevertheless, the calculated results agree quite well with measured values. For higher approach speeds the hydrodynamic component of the repulsive force is predominant over the DLVO surface forces as can be concluded from the comparison with the force curve obtained for a low speed of approach (0.6 μm/s). Theoretical hydrodynamic forces, calculated using (13, show agreement with experimental data for larger separation distances, while deviate significantly at shorter distance. This may be related to the deformation of air-water interface due to the surface forces at closer separation distances.

In a similar way the hydrodynamic forces between hydrophobic particles and an air bubble can be studied. They have also repulsive character and strongly affect jump-to-contact distance and formation of TPL as it has been experimentally observed (Nguyen et al., 2002).

CONCLUSIONS

The AFM can be used as a valuable tool for investigating particle-bubble interactions in mineral processing science. Despite many limitations with respect to the theoretical analysis of experimental data, important information about the particle-bubble system can be obtained, including contact angle for a single particle, surface

forces, and hydrodynamic forces. However in order to facilitate further progress in this area, important issues regarding the geometry of the system, particularly the real separation distance due to deformation, and the existence of strong hydrophobic interactions leading to formation of the TPL have to be addressed. Limitations of commercial AFM systems as a tool for particle-bubble interaction studies should also be recognized. These limitations include: short vertical distance of the piezo translators unable in most cases to fully retract the particle from the bubble after attachment, nonlinearity of the scanner, and small range/nonlinearity of position sensitive photodetector. It was evident that the commercial AFM system is not specifically designed for the study of particle-bubble interactions, which prevents measurement of the stability of particle-bubble attachment and simple measurement of the advancing contact angle, and finally results in a higher degree of uncertainty when compared with measurements between solid surfaces. In order to fully utilize the potential of AFM for studies of particle-bubble interactions, a specially designed instrument is recommended, based on the AFM design, as described in the literature (Butt, 1994). Further improvement of such designs by including an interferometer coupled with a high speed video camera for the measurement of separation distance and surface geometry will provide for further advances in the study of particle-bubble interactions.

ACKNOWLEDGMENTS

Financial support provided by the Department of Energy, Basic Science Division Grant No. DE-FG-03-93ER14315 (J.N. and J.D.M) and the Australian Academy of Science, the Australian Research Council and the Research Management Committee of the University of Newcastle (A.V.N.) is gratefully acknowledged.

REFERENCES

ALEKSEEV V.N., 1991, *Forces acting between a bubble and solid particles in a sound field*, Akust. Zh. 37, 597-604.

ATTARD P., 2000, *Thermodynamic Analysis of Bridging Bubbles and a Quantitative Comparison with the Measured Hydrophobic Attraction*, Langmuir 16, 4455-4466.

BARTELL F.E.,OSTERHOF H.J., 1927, *Determination of the wettability of a solid by a liquid*, Ind. Eng. Chem. 19, 1277-1280.

BIGGS S.,PROUD A.D., 1997, *Forces between Silica Surfaces in Aqueous Solutions of a Weak Polyelectrolyte*, Langmuir 13, 7202-7210.

BINNIG G., QUATE C.,GERBER C., 1986, *Atomic force microscope*, Phys. Rev. Lett. 56, 930-933.

BUTT H.-J., 1994, *A technique for measuring the force between a colloidal particle in water and a bubble*, J. Colloid Interface Sci. 166, 109-117.

CHIANG K.J.P., 1983, *Electrokinetics, particle diffusion, and particle-bubble interaction in the flotation process*. In *Lehigh Univ.,Bethlehem,PA,USA. FIELD URL:, pp*. 326 pp.

CHRISTENSON H.K.,CLAESSON P.M., 1988, *Cavitation and the interaction between macroscopic hydrophobic surfaces*, Science (Washington, D. C., 1883-) 239, 390-392.

CHRISTENSON H.K.,CLAESSON P.M., 2001, *Direct measurements of the force between hydrophobic surfaces in water*, Advances in Colloid and Interface Science 91, 391-436.

CLEVELAND J.P., MANNE S., BOCEK D.,HANSMA P.K., 1993, *A nondestructive method for determining the spring constant of cantilevers for scanning force microscopy*, Rev. Sci. Instrum. 64, 403-405.

COLLINS G.L., MOTARJEMI M.,JAMESON G.J., 1978, *A method for measuring the charge on small gas bubbles*, J. Colloid Interface Sci. 63, 69-75.

CRAIG V.S.J.,NETO C., 2001, *In Situ Calibration of Colloid Probe Cantilevers in Force Microscopy: Hydrodynamic Drag on a Sphere Approaching a Wall*, Langmuir 17, 6018-6022.

DAI Z., DUKHIN S., FORNASIERO D.,RALSTON J., 1998, *The inertial hydrodynamic interaction of particles and rising bubbles with mobile surfaces*, J. Colloid Interface Sci. 197, 275-292.

DERJAGUIN B.V., RABINOVICH Y.I.,CHURAEV N.V., 1978, *Direct measurement of molecular forces*, Nature (London) 272, 313-318.

DIGGINS D.,RALSTON J., 1993, *Particle wettability by equilibrium capillary pressure measurements*, Coal Prep. (Gordon & Breach) 13, 1-19.

DRELICH J.,MILLER J.D., 2001, *Improved flotation deinking of sorted office papers by flocculation of ink particles*, Progress in Paper Recycling 11, 38-46.

DRELICH J., NALASKOWSKI J., GOSIEWSKA A., BEACH E.,MILLER J.D., 2000, *Long-range attractive forces and energy barriers in de-inking flotation: AFM studies of interactions between polyethylene and toner*, J. Adhes. Sci. Technol. 14, 1829-1843.

DRZYMALA J.,LASKOWSKI J., 1980, *Electrokinetic measurements in mineral processing*, Fizykochem. Probl. Mineralurgii, 35-45.

DUCKER W.A., SENDEN T.J.,PASHLEY R.M., 1991, *Direct measurement of colloidal forces using an atomic force microscope*, Nature (London) 353, 239-241.

DUCKER W.A., XU Z.,ISRAELACHVILI J.N., 1994, *Measurements of Hydrophobic and DLVO Forces in Bubble-Surface Interactions in Aqueous Solutions*, Langmuir 10, 3279-3289.

ECKE S., PREUSS M.,BUTT H.-J., 1999, *Microsphere tensiometry to measure advancing and receding contact angles on individual particles*, J. Adhes. Sci. Technol. 13, 1181-1191.

FIELDEN M.L., HAYES R.A.,RALSTON J., 1996, *Surface and Capillary Forces Affecting Air Bubble-Particle Interactions in Aqueous Electrolyte*, Langmuir 12, 3721-3727.

FUERSTENAU D.W.,HERRERA-URBINA R., 1989, *Mineral separation by froth flotation*, Surfactant Sci. Ser. 33, 259-320.

GRACIAA A., CREUX P., LACHAISE J.,SALAGER J.-L., 2000, *Zeta potential at an air-water surface related to the critical micelle concentration of aqueous mixed surfactant systems*, Industrial & Engineering Chemistry Research 39, 2677-2681.

HORN R.G., VINOGRADOVA O.I., MACKAY M.E.,PHAN-THIEN N., 2000, *Hydrodynamic slippage inferred from thin film drainage measurements in a solution of nonadsorbing polymer*, Journal of Chemical Physics 112, 6424-6433.

HOUGH D.B.,WHITE L.R., 1980, *The calculation of Hamaker constants from Lifshitz theory with applications to wetting phenomena*, Adv. Colloid Interface Sci. 14, 3-41.

ISRAELACHVILI J.N., 1991, *Intermolecular and Surface Forces*. (Academic Press, New York).

ISRAELACHVILI J.N.,TABOR D., 1972, *Measurement of van der Waals dispersion forces in the range 1.5 to 130 nm*, Proc. Roy. Soc. London, Ser. A 331, 19-38.

KERN W.,PUOTIENE D.A., 1970, RCA Rev. 31, 187.

LASKOWSKI J.S., YORDAN J.L.,YOON R.H., 1989, *Electrokinetic potential of microbubbles generated in aqueous solutions of weak electrolyte type surfactants*, Langmuir 5, 373-376.

LEKKI J.,LASKOWSKI J., 1976, *Dynamic interaction in particle-bubble attachment in flotation*, Colloid Interface Sci., [Proc. Int. Conf.], 50th 4, 331-345.

LINS F.F., MIDDEA A.,ADAMIAN R., 1995, *Hamaker constants of hydrophobic minerals*, Process. Hydrophobic Miner. Fine Coal, Proc. UBC-McGill Bi-Annu. Int. Symp. Fundam. Miner. Process., 1st, 61-75.

LUTTRELL G.H.,YOON R.H., 1992, *A hydrodynamic model for bubble-particle attachment*, J. Colloid Interface Sci. 154, 129-137.

MAEDA N.,SENDEN T.J., 2000, *A Method for the Calibration of Force Microscopy Cantilevers via Hydrodynamic Drag*, Langmuir 16, 9282-9286.

MIKLAVCIC S.J., 1998, *Perturbation analysis of droplet deformation under electrical double layer forces*, Phys. Rev. E: Stat. Phys., Plasmas, Fluids, Relat. Interdiscip. Top. 57, 561-568.

MIKLAVCIC S.J., HORN R.G.,BACHMANN D.J., 1995, *Colloidal Interaction between a Rigid Solid and a Fluid Drop*, Journal of Physical Chemistry 99, 16357-16364.

NALASKOWSKI J., DRELICH J., HUPKA J.,MILLER J.D., 1999a, *Preparation of hydrophobic microspheres from low-temperature melting polymeric materials*, J. Adhes. Sci. Technol. 13, 1-17.

NALASKOWSKI J., HUPKA J.,MILLER J.D., 1999b, *Influence of dissolved gas on the interaction forces between hydrophobic surfaces in water - atomic force microscopy studies*, Phys. Prob. Min. Process. 33, 129-141.

NALASKOWSKI J., VEERAMASUNENI S.,MILLER J.D., 1998, *Interaction forces in the flotation of colemanite as measured by atomic force microscopy*, Innovations Miner. Coal Process., Proc. Int. Miner. Process. Symp., 7th, 159-165.

NGUYEN A.V., 1999, *Hydrodynamics of liquid flows around air bubbles in flotation: a review*, Int. J. Miner. Process. 56, 165-205.

NGUYEN A.V.,EVANS G.M., 2002, *The Liquid Flow Force on a Particle in the Bubble-Particle Interaction in Flotation*, J. Colloid Interface Sci. 246, 100-104.

NGUYEN A.V., EVANS G.M.,SCHULZE H.J., 2001, *Prediction of van der Waals interaction in bubble-particle attachment in flotation*, Int. J. Miner. Process. 61, 155-169.

NGUYEN A.V., NALASKOWSKI J.,MILLER J.D., 2002, *The dynamic nature of contact angle on sphere measured by atomic force microscopy*, J. Colloid Interface Sci., submitted.

NGUYEN A.V.,STECHEMESSER H., 1998, *Dynamics of the impact interaction between a fine solid sphere and a plane gas-liquid interface*, Stud. Interface Sci. 6, 525-562.

ODEGAARD H., 2001, *The use of dissolved air flotation in municipal wastewater treatment*, Water Sci. Technol. 43, 75-81.

PARKER J.L.,ATTARD P., 1992, *Deformation of surfaces due to surface forces*, Journal of Physical Chemistry 96, 10398-10405.

PARKER J.L., CLAESSON P.M.,ATTARD P., 1994, *Bubbles, cavities, and the long-ranged attraction between hydrophobic surfaces*, Journal of Physical Chemistry 98, 8468-8480.

PAZHIANUR R.,YOON R.H., 1997, *Direct force measurement for a sulfide mineral flotation system*, Processing of Complex Ores: Mineral Processing and the Environment, Proceedings of the UBC-McGill Bi-Annual International Symposium on Fundamentals of Mineral Processing, 2nd, Sudbury, Ont., Aug. 17-19, 1997, 247-256.

PREUSS M.,BUTT H.-J., 1998a, *Direct Measurement of Particle-Bubble Interactions in Aqueous Electrolyte: Dependence on Surfactant*, Langmuir 14, 3164-3174.

PREUSS M.,BUTT H.-J., 1998b, *Measuring the contact angle of individual colloidal particles*, J. Colloid Interface Sci. 208, 468-477.

PREUSS M.,BUTT H.-J., 1999, *Direct measurement of forces between particles and bubbles*, Int. J. Miner. Process. 56, 99-115.

PUGH R.J., AKSOY S.,YOON R.H., 1994, *Hydrophobicity and film rupture in flotation*, Dispersion Aggregation, Proc. Eng. Found. Conf., 141-154.

RABINOVICH Y.I.,YOON R.H., 1994, *Use of Atomic Force Microscope for the Measurements of Hydrophobic Forces between Silanated Silica Plate and Glass Sphere*, Langmuir 10, 1903-1909.

RALSTON J.,DUKHIN S.S., 1999, *The interaction between particles and bubbles*, Colloids Surf., A 151, 3-14.

RALSTON J., DUKHIN S.S.,MISHCHUK N.A., 1999, *Inertial hydrodynamic particle-bubble interaction in flotation*, Int. J. Miner. Process. 56, 207-256.

RAMIREZ E.R.,JOHNSON D.L., 1980, *Wastewater flotation*. In *Can.*, ((Dravo Corp., USA). Ca), *pp*. 29 pp.

SADER J.E., LARSON I., MULVANEY P.,WHITE L.R., 1995, *Method for the calibration of atomic force microscope cantilevers*, Rev. Sci. Instrum. 66, 3789-3798.

SAULNIER P., LACHAISE J., MOREL G.,GRACIAA A., 1996, *Zeta potential of air bubbles in surfactant solutions*, J. Colloid Interface Sci. 182, 395-399.
SCHELUDKO A., TOSHEV B.V.,BOJADJIEV D.T., 1976, *Attachment of particles to a liquid surface (capillary theory of flotation)*, J. Chem. Soc., Faraday Trans. 1 72, 2815-2828.
SHEN H., PUGH R.J.,FORSSBERG E., 2002, *Floatability, selectivity and flotation separation of plastics by using a surfactant*, Colloids Surf., A 196, 63-70.
SIEBOLD A., NARDIN M., SCHULTZ J., WALLISER A.,OPPLIGER M., 2000, *Effect of dynamic contact angle on capillary rise phenomena*, Colloids Surf., A 161, 81-87.
SIEBOLD A., WALLISER A., NARDIN M., OPPLIGER M.,SCHULTZ J., 1997, *Capillary rise for thermodynamic characterization of solid particle surface*, J. Colloid Interface Sci. 186, 60-70.
SKVARLA J.,KMET S., 1993, *What is the role of hydrophilic/hydrophobic surface forces and/or polar interfacial interactions in the interaction between bubbles and minerals?*, Colloids Surf., A 79, 89-95.
SKVARLA J.V., 2001, *Hydrophobic interaction between macroscopic and microscopic surfaces. Unification using surface thermodynamics*, Advances in Colloid and Interface Science 91, 335-390.
TOIKKA G., HAYES R.A.,RALSTON J., 1998, *Surface forces between zinc sulfide and silica in aqueous electrolyte*, Colloids Surf., A 141, 3-8.
TYRRELL J.W.G.,ATTARD P., 2002, *Atomic force microscope images of nanobubbles on a hydrophobic surface and corresponding force-separation data*, Langmuir 18, 160-167.
USUI S., SASAKI H.,MATSUKAWA H., 1981, *The dependence of zeta potential on bubble size as determined by the Dorn effect*, J. Colloid Interface Sci. 81, 80-84.
YOON R.H., 1992, *Hydrodynamic and surface forces in bubble-particle interactions*, Mines Carrieres: Tech., 74-79.
YOON R.H., 2000, *The role of hydrodynamic and surface forces in bubble-particle interaction*, Int. J. Miner. Process. 58, 129-143.
YOON R.-H., FLINN D.H.,RABINOVICH Y.I., 1997, *Hydrophobic interactions between dissimilar surfaces*, J. Colloid Interface Sci. 185, 363-370.
YOON R.-H.,MAO L., 1996, *Application of extended DLVO theory, IV. Derivation of flotation rate equation from first principles*, J. Colloid Interface Sci. 181, 613-626.
YOON R.-H.,PAZHIANUR R., 1998, *Direct force measurement between hydrophobic glass sphere and covellite electrode in potassium ethyl xanthate solutions at pH 9.2*, Colloids Surf., A 144, 59-69.

Nalaskowski J., Nguyen A.V., Hupka J., Miller J.D., *Badania oddziaływań cząstka-pęcherzyk za pomocą mikroskopu sił atomowych – obecne możliwości i wyzwania*, Fizykochemiczne Problemy Mineralurgii, 36 (2002), 253-272 (w jęz. angielskim)

Badania oddziaływań pomiędzy cząstkami mineralnymi i pęcherzykami powietrza są kluczowe do zrozumienia przebiegu flotacji. Wykorzystanie mikroskopii sił atomowych (AFM) i techniki próbnika koloidalnego umożliwia pomiar takich oddziaływań. Przy użyciu AFM oddziaływania pomiędzy pojedynczą cząstką przymocowaną do dźwigni AFM i pęcherzykiem powietrza, umieszczonym na powierzchni hydrofobowej, mogą być mierzone w środowisku wodnym. Ważna jest znajomość sił występujących przed przerwaniem filmu międzyfazowego wody oraz hydrofobowość użytej cząstki jak wykazano w obecnej pracy. Zmierzono również siły hydrodynamiczne pomiędzy zbliżającym się pęcherzykiem powietrza i cząstką mineralną. Pomimo znaczących możliwości techniki próbnika koloidalnego i AFM w badaniu oddziaływań cząstka-pęcherzyk, istnieje szereg wyzwań związanych z modyfikacją konstrukcji instrumentu, procedurą pomiarową oraz analizą teoretyczną danych. Szczególnej uwagi wymaga uwzględnienie zasięgu ugięcia dźwigni AFM oraz skanera piezoelektrycznego, wyznaczanie stałej sprężystości pęcherzyka, właściwego wyboru punktu kontaktu cząstki z pęcherzykiem oraz uwzględnienie deformacji powierzchni pęcherzyka.

Physicochemical Problems of Mineral Processing, 36 (2002) 273-278
Fizykochemiczne Problemy Mineralurgii, 36 (2002) 273-278

DEXTRINS AS SELECTIVE FLOTATION DEPRESSANTS FOR SULFIDE MINERALS

Jan DRZYMALA*, Piotr TOMASIK**, Beata SYCHOWSKA**, Marek SIKORA**

Received March 15, 2002; reviewed and accepted May 15, 2002

Dextrins from thermal modification of potato starch under ammonia, hydrogen sulfide, and gluten were tested as flotation depressants of galena and chalcocite in a Hallimond cell with xanthate to make the sulfides hydrophobic. All dextrins, except prepared under hydrogen sulfide, depressed flotation of the sulfides. The cessation of flotation occurred at different doses of dextrins, usually between 2 and 20 kg per ton of the floated material. Dextrins from starches thermally modified under ammonia were found to be promising selective depressants in the studies with model (1:1) mixtures of galena and chalcocite but poor separation was achieved with copper ore containing lead minerals. The separation of galena from chalcocite form synthetic mixtures was also poor in the presence of gluten-modified dextrins.

Key words: flotation, galena, chalcocite, dextrin

INTRODUCTION

Starch is a common and most readily renewable plant polysaccharide. Recently, its non-nutritional applications evoked a considerable interest (Miller and Laskowski, 1983;. Ye et al., 1996; Raju and Forsling, 1997; Tomasik and Schilling, 1998). Roasting of starch leads to dextrins, called the British gums, properties of which can be controlled by heating condition (Tomasik et al., 1989). Due to their origin, dextrins are environmentally friendly biodegradable products. Aqueous solutions of polymeric dextrins and starches influence the surface properties of particles in water (Gaudin, 1963; Laskowki, 1969; Lin and Budrick, 1988) leading to a modification of their flotation. It is known that dextrins depress, to a different extend flotation of a number of minerals including sulfides, which are present in the Kupferschiefer Cu-Ag ore from the Lubin region in Poland. Recently, new methods of dextrinization were

*Technical University of Wroclaw (I-11), Wybrzeze Wyspianskiego 27, 50-370 Wroclaw, Poland
**University of Agriculture, Mickiewicza Ave. 21, 30-120 Krakow, Poland

developed. Dextrinization carried out under ammonia (Sychowska and Tomasik, 1997), hydrogen sulfide (Sychowska et al., 1998) and with gluten (Sychowska and Tomasik, 1996) provided series of novel dextrins. Their application for flotation of galena and chalcocite, the dominant sulfide minerals in the Polish copper ore, in the presence of xanthate as the flotation collector is described in the present study.

EXPERIMENTAL

Galena originated from a deposit of sulfide minerals in Trzebionka (Poland) and synthetic chalcocite was kindly provided by the Copper Smelting Plant in Legnica (Poland). The minerals were crushed and ground in an agate mortar shortly before flotation to avoid oxidation of sulfides. The 0.16-0.20 mm size fractions were used in the experiments. The solid particles (0.2 cm^3 that is 1.0 g of PbS or 0.7 g of Cu_2S) were suspended in 120 cm^3 of aqueous solution of depressant, then agitated for 5 minutes. The pH of the solution varied between 6.4 and 7.2. Amount of butyl xanthate subsequently added to the solution provided its final concentration of 0.0001 $kmol/m^3$. After 5 min of agitation, the suspension was transferred to the Hallimond tube and floated for 15 minutes with the airflow of 0.625 cm^3/s. Starches and dextrins were used in the test as modifying reagents. Dextrins prepared from starch modified under ammonia (N) (Sychowska and Tomasik, 1997) hydrogen sulfide (S) (Sychowska et al., 1998), and with gluten (30% w/w) (G) (Sychowska and Tomasik, 1996) were prepared according to the methods descried in the indicated sources. Roasting time and temperature used in the preparation of the dextrins tested in this study were as follows: G-9: 4h, 180^{o}C; N-1: 2h, 140^{o}C; N-8: 4h, 180^{o}C. Also unmodified potato starch (S-O) was used in our studies.

Flotation tests involving a copper ore were also carried out in a Mechanobr laboratory flotation machine, equipped with a 500 cc cell. A sample of 150 g of ore was used in the experiment. Flotation was carried out in distilled water in the presence of 75g/Mg potassium amyl xanthate, 25g/Mg α-terpineol and 600g/Mg of dextrin. The solids were introduced to water followed by dextrin, collector and finally frother. The time of agitation with the chemicals was 5, 3, and 1 minute, respectively. The pH of flotation was 8.0. Initial flotation provided a rough concentrate and tailing. The rough concentrate was cleaned in a subsequent flotation to produce a final concentrate and a semiproduct.

The copper ore was kindly supplied by the KGHM Polska Miedz, SA, Lubin (Poland).

RESULTS AND DISCUSSION

The results of flotation of chalcocite and separately galena, both with xanthate and dextrins are presented in Figs 1-2, respectively. They show that the depression of flotation of the investigated sulfides appears at a rather high, about 20 kg/ton, admixture. When either N- or G- dextrins were added, chalcocite was more sensitive to depression than galena. S-dextrins depressed neither galena nor chalcocite.

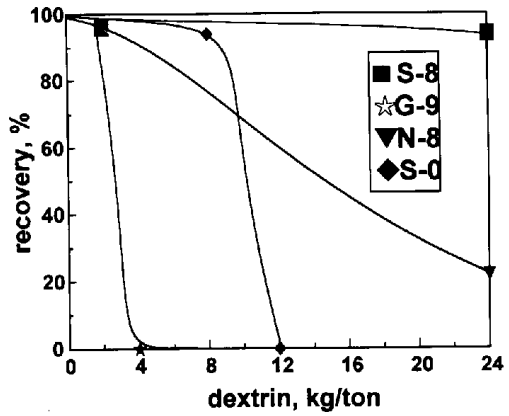

Fig. 1. Flotation of chalcocite in the presence of various dextrins (pH = 6.4-7.2)

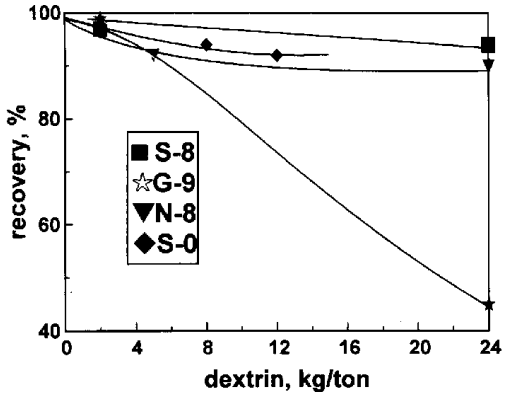

Fig. 2. Flotation of galena in the presence of various dextrins (pH = 6.4-7.2)

Dextrin G-9 and N-type dextrins were additionally tested. The results of separation of galena from chalcocite, carried out in the Hallimond tube with 1:1 (by weight) mixtures of both minerals in the presence of dextrin G-9, are shown in Figs 3. It can be seen that dextrin G-9 did not facilitate a good separation of galena and chalcocite. The difference between the recovery of chalcocite and galena never reached 100%.

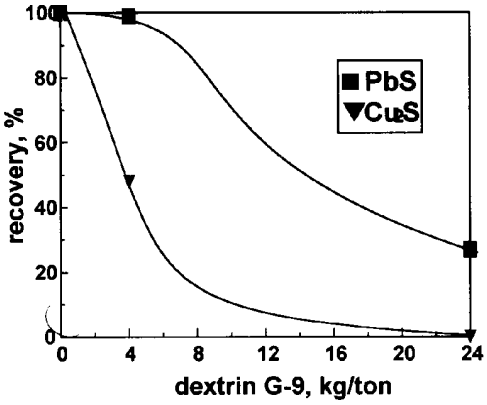

Fig. 3. Flotation of 1:1 galena - chalcocite mixtures in the presence of dextrin G-9 (pH = 7.1-7.2)

N-1 and N-8 dextrins offered promising results. The results revealed that dextrin N-8 prepared under more drastic roasting conditions provided increasing separation (Fig. 4a-b). The effect of separation of galena and chalcocite, when the 1:1 mixture of the minerals was subjected to flotation in the presence of dextrin N-8 (Fig.5), almost reached the level anticipated from the flotation tests for individual minerals.

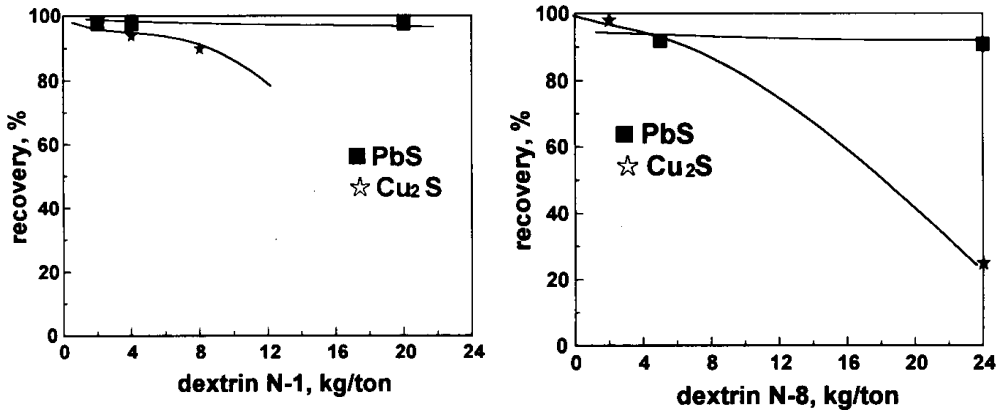

Fig. 4. Results of flotation of galena and chalcocite in the presence of dextrins N-1(a), and N-8 (b). pH = 7.1-7.2. Minerals were floated separately

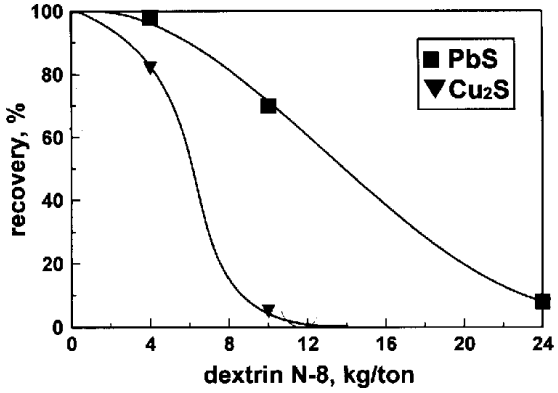

Fig. 5. Flotation of galena-chalcocite (1:1) mixture in the presence of dextrin N-8 (pH=7.1-7.2)

Dextrin N-8 was also tested with the copper ore and the results are given in Fig. 6. For comparison purpose the results of flotation of the copper ore in the presence of dextrin without modification (DBM) and flotation without any dextrin are also given in Fig. 6. It appears from Fig. 6 that the selectivity of separation of copper and lead minerals in the presence and absence of investigated dextrin is poor. Dextrin DBM does not change the selectivity of separation though it slightly depresses the flotation of sulfides in comparison to flotation without any dextrin. Dextrin N-8 has some

depressing power towards copper minerals because the reduction of flotation of copper minerals is greater than towards the lead minerals. Still greater amount of dextrin N-8 depresses flotation of sulfides in the ore almost completely.

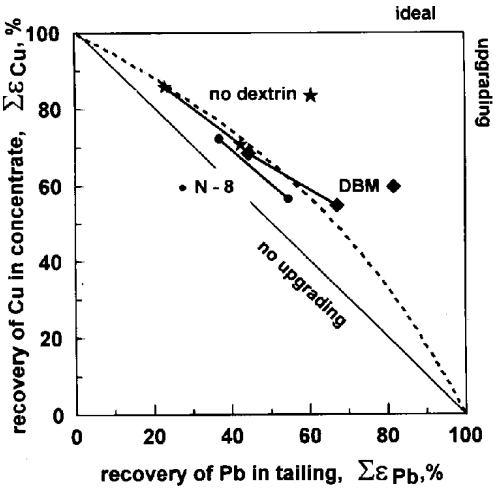

Fig.6. Result of flotation of copper and lead from copper ore in the presence of dextrin N-8 and dextrin thermolyzed in the absence of modifying chemicals (DBM). Results in the absence of dextrin are given for comparison. Dextrin concentration was 600 g/Mg, pH around 7.

According to Lekki (2002) the reason of the unequal selectivity of separation achieved for synthetic mixtures and real ore most likely results from different redox environments in the systems.

CONCLUSIONS

Ammonia, hydrogen sulfide and gluten modified dextrins are not very promising modifiers in the xanthate flotation of sulfides on a small laboratory scale experiments carried out with pure galena and chalcocite as well as with the Polish copper ore.

LITERATURE

GAUDIN, A.M., (1963), *Flotation*, Wyd. Slask, Katowice.

LEKKI, J., (2002), *Private communication*.

LASKOWKI, J., (1969), *Physical chemistry in mineral processing*, Wyd. Śląsk, Katowice, in Polish.

LI YE, LIU QI, XU SHI, (1966), *Adsorption behavior and interaction mechanism of dextrin with oxide mineral surface*, Zhongguo Youse Jinshu Xuebao, 6(3), 30-34, Chem. Abst., 126, 120354k (1997).

LIN, K.F., BUDRICK, C.L., (1988), *Polymeric Depressants, in: Reagents in Mineral Technology*, P. Somasundaran and B.M. Moudgil (editors), Surfactant Science Series, 27, 471- 483.

MILLER J.D. LASKOWSKI J.S., CHANG S.S., (1983), *Dextrin adsorption by oxidized coal*, Colloids and Surfaces, 8, 137-151.

RAJU G.B., HOLMGREN A., FORSLING W., (1997), *Adsorption of dextrin at mineral/water interface*, J. Colloid Interface Sci., 193, 215-222.

SYCHOWSKA B, TOMASIK, P., (1996), *Thermolysis of starch with gluten*, Pol. J.Food Nutr. Sci., 5, 53-60.
SYCHOWSKA B, TOMASIK, P., (1997), *Thermolysis of starch under ammonia*, Pol. J.Food Nutr. Sci., 6, 27-34.
SYCHOWSKA B, TOMASIK, P., WANG, Y., (1998*), Thermolysis of starch under hydrogen sulfide*, Pol. J.Food Nutr. Sci., 7, 23-28.
TOMASIK, P., SCHILLING, C.H., (2002), *Chemical modification of starch, Adv.*, Carbohydr. Chem, Biochem, in press.
DRZYMAŁA JAN, TOMASIK, P., WIEJAK, S., PALASINSKI, M., 1989, *The thermolysis of starch*, Adv. Carbohydr. Chem. Biochem. 47, 279-344.

Drzymala J., Tomasik P., Sychowska, B., Sikora M., *Dekstryny jako selektywne depresory dla minerałów siarczkowych,* Fizykochemiczne Problemy Mineralurgii, 36, (2002), 273-278 (w jęz. ang.)

Dekstryny, otrzymane przez termiczną modyfikację skrobi ziemniaczanej w obecności amoniaku, siarczku sodu oraz glutenu, zastosowano jako depresory ksantogenianowej flotacji galeny i chalkozynu. Pomiary przeprowadzono we flotowniku Hallimonda. Badane dekstryny, z wyjątkiem tej która była modyfikowana siarkowodorem, depresowały flotację zarówno chalkozynu jak i galeny, gdy minerały te poddawano flotacji osobno. Zanik flotacji miał miejsce przy różnych stężeniach dekstryn, ale zwykle miało to miejsce przy użycie od 2 do 20 kg na megagram flotowanego materiału. Dekstryny otrzymane przez termiczną modyfikację amoniakiem okazały się obiecującymi selektywnymi depresorami ksantogenianowej flotacji, gdy badania prowadzono z udziałem modelowych mieszanin czystych minerałów galeny i chalkozynu, ale uzyskano słabą selektywność procesu, gdy do badań użyto rudy miedzi zamierającej także minerały ołowiu. Rozdział galeny od chalkozynu zawartych w syntetycznych mieszaninach obu minerałów była słaba, gdy jako depresora użyto skrobi modyfikowanej glutenem.

Physicochemical Problems of Mineral Processing, 36 (2002) 279-288
Fizykochemiczne Problemy Mineralurgii, 36 (2002) 279-288

Wiesław WÓJCIK*, Bronisław JAŃCZUK and Robert OGONOWSKI

SILICA INTERPARTICLES ACTION IN ALKANES

Received March 5, 2002; reviewed and accepted May 15, 2002

Measurements of the destruction time of the sediment column structure of silica particles were carried out for different fractions of silica particles in alkanes from decane to hexadecane. The authors studied the correlations between the measured destruction time of the silica particles sediment column structure and the bulk properties of silica particles and alkanes, as well as the alkane-air, silica particles-air and silica particles-alkane interfacial properties. On the basis of this study linear relationships between the reciprocal of the destruction time and the average diameter of the silica particles fractions, the work of alkanes cohesion, the alkanes density and the difference between the detachment and attachment forces were found. From these relationships, the critical values of the particle diameter, the cohesion work of the alkane density and the difference between the detachment and the attachment forces were determined. It was found that for the systems, having critical values of the parameters mentioned above, the detachment force is equal to the attachment force, both resulting from gravitational and interfacial interactions, respectively. It also results from the present study that the attachment force between silica particles depends on the work of alkane cohesion and the work of silica particle adhesion to liquid, and that destruction of silica particles sediment column structure takes place as a result of interruption of the alkane film between two silica particles. The changes of the destruction time as a function of the number of carbon atoms in the molecule of alkanes occurred as a result of the decreased detachment force and the perimeter of the contact plane and increased attachment force between silica particles in alkanes.

Key words: Adhesion, silica particles, alkanes, attachment and detachment forces.

INTRODUCTION

Studies of the physical and chemical properties of silica surfaces have been carried out for nearly two centuries because it is the most widespread mineral on the Earth. The properties of silica depend on its forms which can be crystalline, as in crystalline silica particles, or amorphous, as in fused silica. Its surface can be hydrophobic when the surface chemical groups are mainly siloxane (Si-O-Si) groups, or hydrophilic

*Department of Interfacial Phenomena, Faculty of Chemistry, Maria Curie-Sklodowska University, Maria Curie-Sklodowska Sq. 3, 20-031 Lublin, Poland

when the surface possesses mainly silanol (Si-O-H) groups (Iler 1979). Therefore, according to conditions silica can reveal different surface properties which influence interparticle interactions in the dispersion system. The interactions are considered as attractive van der Waals and repulsive forces due to a layer of structured water at silica-water interface (Churaev 1999) and (Elimelech 1990). Different studies and various techniques are used to evidence these forces which can include measurements of colloidal stability (Elimelech 1990) and (Allen et al. 1970) and force measurements (Churaev 1999), (Elimelech 1990) and (Vigil et al. 1994). These forces play an important role in solid particle-liquid-solid particle interactions which influence numerous industrial processes.

The purpose of this paper is to determine the interaction forces between silica particles through liquid phase by measurements of the destruction time of the sediment silica column structure. Long chain alkanes were used as the liquid phase, which are often used as bridging liquid in all kinds of aggregation processes (Attita 1992), (Laskowski 1992), (Warren 1992) and (Sadowski 1994). The interactions among silica particles through the apolar phase will be discussed in this work.

EXPERIMENTAL

METHOD

A device for measurements of the destruction time of the sediment column structure was constructed in our laboratory (Waksmundzki et al. 1965) and (Ogonowski et al. 2001), and its schematic diagram is presented in Fig.1. The main part of the device is a glass tube (4) 0.4 m long and 3×10^{-3}m in inner diameter and a glass vessel (2) 4.5×10^{-5} m^3 in volume. The glass vessel is connected with the glass tube by a rubber plug (3) so as to move the tube up and down, and the vessel is closed by a stopper (1). The other end of the tube is closed by a silicone plastics seal (5) tightened by a screw (6).

MEASUREMENTS

The destruction time of the sediment column structure was measured for high silica purity (>99.99%) which came from naturally occurring Russian silica particles (Caucasus).The silica powder, kindly supplied from the Glassworks "Ożarów" was fractionated by screening into four narrow particle size-fractions whose average diameters were: 1.04×10^{-4}m, 1.35×10^{-4}m, 1.75×10^{-4}m and 2.25×10^{-4}m, respectively. To remove contaminations of the particles surface occurring during screening, each fraction was treated by hydrochloric acid solution (1:1) for 24 h and next the particles were washed by redistilled and deionized water till its pH and conductivity were natural. The washed silica particles were heated for 5 h at 400^0 C and the dried products were stored in hermetically closed jars. The measurements of the destruction time of the sediment silica column structure for the studied size-

fractions were carried out in long chain alkanes from decane to hexadecane. Directly before the measurement each alkane used was purified by distillation and dried by a wide-porous silica gel.

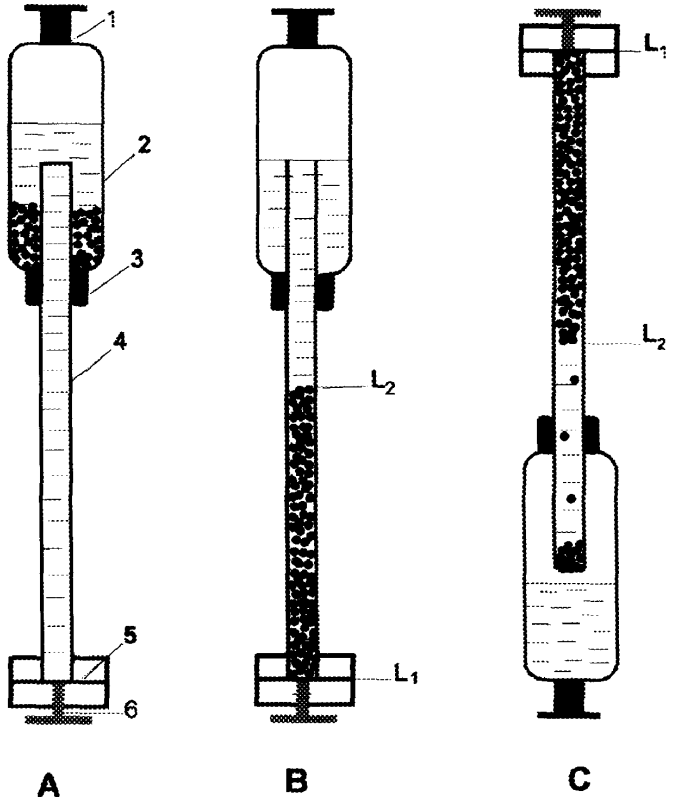

Fig. 1. A scheme of the device for destruction time measurements: (1) stopper, (2) glass vessel, (3) rubber plug, (4) glass tube, (5) silicone plastics seal and (6) screw. (A) the device, (B) formation of the sediment column, (C) destruction sediment column structure, L, and L_2 levels of the column sediments

The sediment column of silica particles was formed in the glass tube pouring 3.0×10^{-5} m^3 of the liquid in the glass vessel and adding 1.388×10^{-3} kg sample of a given fraction of silica particles. The particles falling into the tube formed a sediment column and then the tube was moved up over the level of alkane (Fig. 1B), and the column structure was established in 10 min. Next, the device was quickly inverted as shown in Fig. 1C (the lower end of the tube must be over the liquid level) and the silica particles detached from the sediment column and dropped to the end of the tube, forming a new sediment column. The destruction time of the silica sediment column structure was measured by a stop-watch, starting when the first silica particle detached from the column at the level L_2 (Fig. 1C), and stopping when the last silica particle

started to drop at the level L_1 (Fig.1 C). The measurements of the destruction time were repeated several times for each silica fraction and each liquid used. The reproducibility of the destruction time measurements was very good.

RESULTS

The measured values of the destruction time of the silica sediment column structure were expressed for the sediment column formed of 1×10^{-3}kg silica sample. The obtained results are presented as a function of the bulk properties of the components of the studied system, i.e. viscosity and density of alkanes and average diameter of the fractions of silica particles. The destruction time (*t*) of the silica column structure and reciprocal of the destruction time (*1/t*) as a functions of the viscosity and density of the alkanes are presented in Fig. 2 and 3, respectively. Curves 1,2,3 and 4 show the changes of the destruction time and the reciprocal of the destruction time of the sediment column structure of silica particles having average diameters of 1.04×10^{-4}m, 1.35×10^{-4}m, 1.75×10^{-4}m and 2.25×10^{-4}m, respectively. As can be seen the destruction time increases linearly with increasing viscosity of alkanes (Fig. 2). A similar relationship of the destruction time as a function of density is non linear and it is not presented here, but it appeared that the reciprocal of the destruction time (*1/t*) as a function of the density is linear (Fig. 3). From Fig. 2 and 3 it can be seen that the destruction time decreases with increasing size of silica particles.

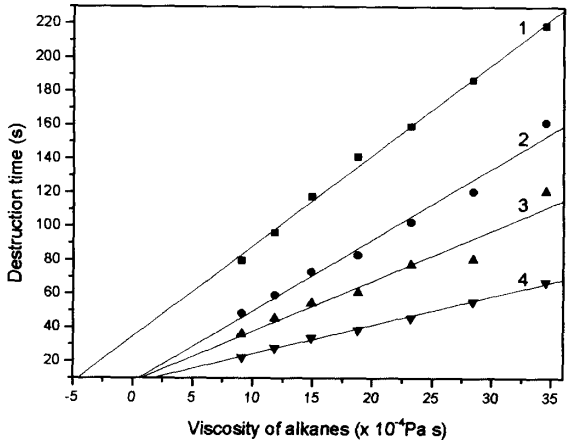

Fig. 2. Relationship between the destruction time (*t* in *s*) of the silica sediment column structure and viscosity of alkanes (from decane to hexadecane). Curves 1, 2, 3 and 4 represent the changes in *t* obtained for silica particles having the following average diameters: 1.04×10^{-4} m, 1.35×10^{-4} m, 1.75×10^{-4} m. and 2.25×10^{-4} m, respectively.

DISCUSSION

The fact suggests that the difference between detachment and attachment forces of silica particles through the alkane increased with its increasing viscosity and density, and decreased with increasing average diameter of silica particles (Fig. 2 and 3). So, for some diameters of silica particles the destruction time is infinitely long, and the particles do not detach from those in the column.

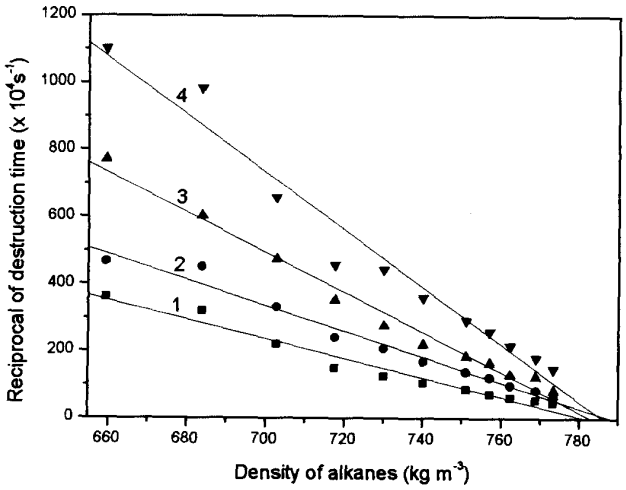

Fig. 3. Reciprocal of the destruction time ($1/t_1$ in $1/s$) as a function of the density of alkanes. Curves 1, 2, 3 and 4 represent the changes in $1/t$ obtained for silica particles having the following average diameters: 1.04×10^{-4} m, 1.35×10^{-4} m, 1.75×10^{-4} m and 2.25×10^{-4} m, respectively

The diameter of such particles is called the critical diameter (d_{cr}) (Waksmundzki et al. 1965) and (Waksmundzki 1965a) whose value can be determined from linear relationship between the reciprocal of the destruction time of the sediment column structure and average diameter of silica particles. The relationship is presented in Fig. 4. Curves from 1 to 7 were obtained for alkanes from decane to hexadecane, respectively, and they satisfy the linear equation

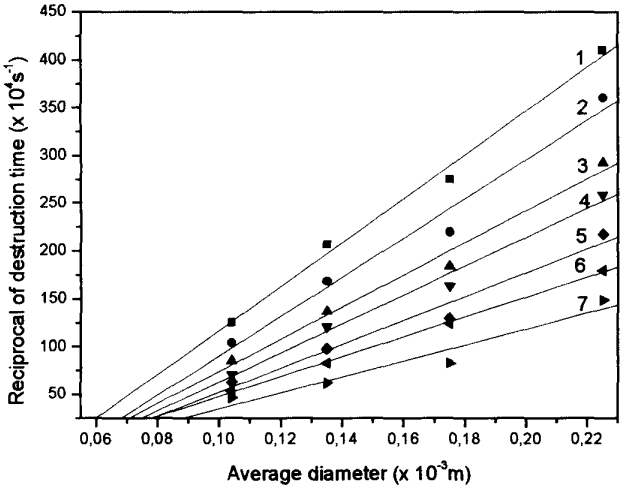

Fig. 4. Reciprocal of the destruction time ($1/t$ in $1/s$) as a function of the average diameter (d in m) of the silica particles. The t values were measured in decane (curve 1) undecane (2), dodecane (3), tridecane (4), tetradecane (5), pentadecane (6) and heksadecane (7)

$$1/t = a + bx \tag{1}$$

where t is the destruction time, a and b are the constants, x is the independent variable and in this case it is the average diameter (d) of silica particles.

The values of the critical diameter of silica particles calculated from Eq. 1 are listed in Tab. 1. As we can see, the values of the critical diameter do not depend on the number of carbon atoms in the molecule of the studied alkanes, and the average value is 5.6 x 10^{-5} m. The silica particles having a diameter ≤ d_{cr} do not detach from those of the column.

For silica particles having the critical diameter the attachment force of particles through the alkane should be equal to the detachment force, and they do not detach from those in the column. The detachment force of silica particles from those forming the sediment column in the alkane can be calculated from the following equation (Wójcik et al. 2000)

$$F_D = mg - V\rho_H g = \tfrac{1}{6}\pi d_{cr}^3 (\rho_S - \rho_H) \quad (2)$$

where m is the silica particle mass, g is the acceleration due the gravity, V is the silica particle volume, ρ_S and ρ_H are the density of silica and hydrocarbon, respectively, and d_{cr} is the average critical diameter.

Assuming that the silica particles are spherical for which d_{cr} = 5.6 x 10^{-5} m and ρ_S = 2476 kg/m^3 (Poradnik, 1974) the detachment forces (F_D) were calculated from Eq. 2. The values of F_D are listed in Tab. 1. and as we can see the detachment forces per particle decreased from 17.28 x 10^{-10} N to 16.89 x 10^{-10} N.

The F_D values (Tab. I) for the critical diameter of the silica particles depend on the density of the studied alkanes. The relationship between the reciprocal of the destruction time ($\frac{1}{t}$) and the density of alkanes (ρ) taken from literture (Janz et al. 1972) and (Wójcik et al. 2000), as it seen in Fig. 3, is linear, and the curves satisfy Eq. 1 in which the independent variable (x) is the density of alkanes (ρ).

In this case, like in the case of the average diameter of particle fractions, for an alkane in which the sediment column structure is stable, i.e. the silica particles do not detach from those in the column, its density is called critical (ρ_{cr}). The values of the critical density calculated from Eq. 1 are listed in Tab. 2 and, as can be seen, they do not depend on the average diameter of the fractions of silica particles. The average value of the critical density of alkane is 795.5 kg/m^3 (Tab. 2). It means that the sediment column of silica particles formed in the alkane of 795.5 kg/m^3 density is stable. For such alkane the detachment force calculated from Eq. 2 is 16.69 x 10^{-10} N/particle, whose value as it is seen from Tab. 1, is minimal.

The minimal value (F_{DM}) satisfies the equation (Wójcik et al. 2001) and (Ogonowski et al. 2001)

$$F_{DM} = W_{Coh.cr} \cdot L = W_{Coh.cr} \cdot 2\pi R \quad (3)$$

where F_{DM} is the minimal detachment force in alkane whose density and cohesion work of ($W_{coh.cr}$) are critical, L is the perimeter of the contact plane between two silica particles in the alkane, R is the radius of the contact plane.

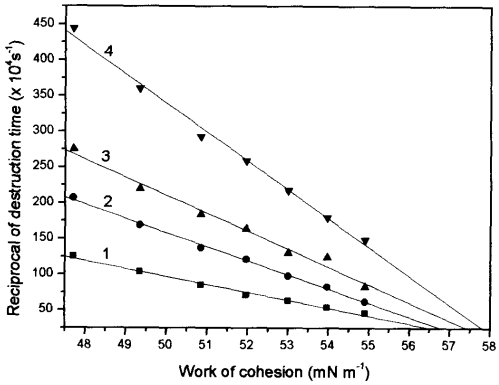

Fig. 5. Reciprocal of the destruction time ($1/t_1$ in $1/s$) as a function of the work of cohesion (W_{Coh}, in mN/m). Curves 1, 2, 3 and 4 represent the changes in $1/t$ obtained for silica particles having the following average diameters:1.04x10^{-4} m, 1.35x10^{-4} m, 1.75x10^{-4} m and 2.25x10^{-4} m, respectively

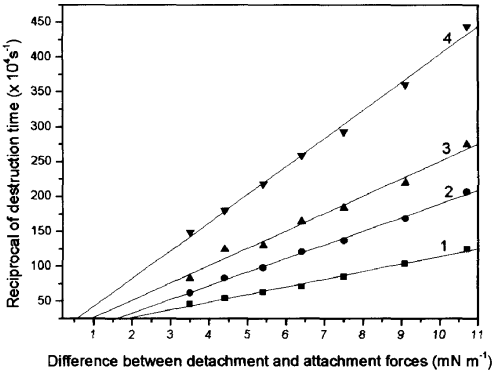

Fig. 6. Reciprocal of the destruction time ($1/t$ in $1/s$) as a function of the difference between the detachment and attachment force (ΔF in mN/m). Curves 1, 2, 3 and 4 represent the changes in $1/t$ obtained for silica particles having the following average diameters:1.04x10^{-4} m, 1.35x10^{-4} m, 1.75x10^{-4} m and 2.25x10^{-4} m, respectively.

To find the radius of the contact plane between two silica particles in n-alkane, the critical work of cohesion was determined from Fig. 5, which presents the relationship of the reciprocal of the destruction time of the silica sediment column structure as a function of the work of cohesion of alkanes (Wójcik et al. 2001). The curves in Fig.5 are linear and they satisfy Eq. 1 in which the independent variable (x) is the cohesion work of alkanes (W_{Coh}). For the studied fractions the values of the critical cohesion work of the alkane calculated from Eq. 1 are listed in Tab. II and, as it is seen, they range from 58.0 to 58.8 mN/m, and the average value is 58.4 mN/m. Using this value and the detachment force from Tab. I (F_D), the radii of the contact planes (R) between two silica particles in the studied alkanes were calculated and they are listed in Tab I. The radii of the contact planes decrease from 47.1· 10^{-10}m to 46,05· 10^{-10}m with increasing work of alkane cohesion from 47.7 to 54.9 mN/m (Tab.I). For the alkane having the critical cohesion work of 58.4mN/m the radius of the contact plane is 45.5· 10^{-10} m.

In the equilibirum conditions the attachment force between two silica particles in n-alkane is expressed in the form:

$$F_A = W_{Coh.} 2\pi R \tag{4}$$

where F_A is the attachment force, W_{Coh} is the cohesion work of alkanes.

Table 1. Values of the critical diameter of silica particles (d_{cr}) the detachment (F_D) and attachment (F_A) force, the radii (R) of the contact plane and the difference (ΔF) between the detachment and attachment force, values of the F_D, F_A, R and ΔF obtained for the critical parameters

Alkane	d_{cr}x10^{-5}m	F_Dx10^{-10} N/particle	R x10^{-10}m	F_Ax10^{-10} N/particle	ΔF mN/m
Decane	5.4	17.28	47.12	14.11	10.7
Undecane	5.6	17.19	46.87	14.52	9.1
Dodecane	5.6	17.09	46.60	14.88	7.5
Tridecane	5.8	17.04	46.46	15.16	6.4
Tetradecane	5.8	16.99	46.32	15.42	5.4
Pentadecane	5.4	16.93	46.16	15.64	4.4
Hexadecane	5.8	16.89	46.05	15.88	3.5
Average	5.6	16.69	45.5	16.69	0

Table 2. Values of average diameters of particle size-fraction (d_a), and values of the critical: density (ρ_{cr}), the work of cohesion ($W_{coh.cr}$), the difference (ΔF_{cr}) between detachment and attachment forces

d_ax10^{-4}m	ρ_{cr} kg/m^3	$W_{Coh.cr}$ in mN/m	ΔF_{cr} mN/m
1.04	797.7	58.8	-0.43
1.35	793.3	58.0	0.31
1.75	795.6	58.4	-0.05
2.25	795.5	58.4	-0.05
Average	795.5	58.4	-.055

Taking into account the radii of the contact planes from Tab. 2 and the cohesion work of alkanes from the literature (CRC Handbook 1972) and (Wójcik et al. 2000), the attachment forces were calculated from Eq. 4 and they are listed in Tab. 1. As can be seen the attachment force between two silica particles, in contrast to the detachment force, increases from 14.1 x 10^{-10} to 16.7 x 10^{-10} N/particle with increasing cohesion work of alkanes.

The detachment and attachment forces were expressed in term of mN/m, and the differences between them ($\Delta F = F_D - F_A$) were calculated and listed in Tab. 1. The relationship of the reciprocal of the destruction time as a function of the ΔF is presented in Fig. 6. As it is seen the curves in Fig 6 are linear and they satisfy Eq. 1 in which the independent variable (x) is the difference between the detachment and attachment force (ΔF). The critical values of ΔF (the destruction time is equal to infinity) calculated from Eq. 1 are listed in Tab. 2, and, as we can see, their values do not depend on the average diameters of size-fractions of silica particles, and the

average value is small but negative. It may mean that detachment of silica particles from those in the sediment column occurred by disruption of the alkane film present between silica particles. Small negative values of ΔF_{cr} suggest that the free energy of the alkane film is a little changed by the free energy of silica surfaces. Such small changes of the free energy of alkane film caused by the surface free energy of silica may result from a small difference between the surface free energy of alkane being the Lifshitz van der Waals energy and the Lifshitz van der Waals component of the surface free energy of silica.

CONCLUSION

The presented analysis and discussion of the results of the detachment experiments has clearly shown that detachment of coal particle from one another in the studied liquids occurs by disruption of the liquid film present between them. The free energy of the alkane film is a little increased by the free surface energy of silica particles.

The perimeter of the contact plane between two coal particles decreases with increasing length of the hydrocarbon chain of alkanes and alcohols. Increase of the destruction time of the sediment column structure of coal particles with increasing length of the hydrocarbon chain of the studied liquids results on the one hand from decrease of the detachment force of coal particle and from one another and on other from an increase of the attachment force between them.

REFERENCES

ALLEN L. H. and MATIJEVIC E. (1970), *Stability of colloidal silica*, J. Colloid Interface Sci., Vol. 33, No. 3, 420-429.

ATTITA Y. A. (1992), *Flocculation* in "Colloid Chemistry in Mineral Processing" (Eds. J. S. Laskowski and J. Ralston), Elsevier, Amsterdam, London, New York, Tokyo, Developments in Mineral Processing, Vol. 12, pp. 277-308.

CRC Handbook of Chemistry and Physic (1972), 80-th Edition, (Ed. D. R. Lide) CRC Press, Boca Raton, London, New York, Washington D.C, V.I, Chapter 6, pp. 3-183.

CHURAEV N. (1999), *The DLVO theory in Russian colloid science*, Adv. Colloid Interface Sci., 83, 19-32.

ELIMELECH M. (1990), *Indirect evidence for hydration forces in the deposition of polystyrene latex colloids on glass surface*, J. Chem. Soc. Faraday Trans., Vol. 86, No 9, 1623-1624.

ILER R. K. (1979), "The Chemistry of Silica", J. Wiley, New York, pp. 540-546, 628-644.

JANZ G. J. and TOMKINS R. P. T. (1972), *Physical properties of solvents*, in "Nonaqueous Electrolytes Handbook", Academic Press, New York and London, V.I Chapter 1, 10-82.

LASKOWSKI J. S. (1992), *Oil assisted particle processing* in "Colloid Chemistry in Mineral Processing", (Eds. J. S. Laskowski and J. Ralston), Elsevier, Amsterdam, London, New York, Tokyo, Developments in Mineral Processing, Vol. 12, pp. 361-394.

PORADNIK FIZYKOCHEMICZNY, (1974) Tablica właściwości związków nieorganicznych, WNT, Warszawa 1974.

OGONOWSKI R, WÓJCIK W and JAŃCZUK B. (2001), *The effect of liquids on the interaction between coal particles*, Physicochemical Problems of Mineral Processing, Vol. 35, 43-53.

SADOWSKI Z. (1994), *Hydrofobowa agregacja zawiesin minerałów węglanowych i siarczkowych.* Rozprawa habilitacyjna, Wyd. UMCS, Lublin, 5-72.
VIGIL G., Xu Z., STEINBERG S. and ISRAELACHVILI J.N., (1994), *Interactions of silica surfaces,* J. Colloid Interface Sci., Vol. 165, No.2, 367-385.
WAKSMUNDZKI A., SZYMAŃSKI E., (1965), *Niszczenie struktury słupka sedymentu jako metoda badania wielkości sił zlepiania pomiędzy ziarnami suspensji mineralnych.* Roczniki Chem. Vol. 39, No. 5,731-736.
WAKSMUNDZKI A., SZYMAŃSKI E and CHOJNACKA G. (1965a) *Czynniki wpływające na wielkość sił zlepiania ziaren mineralnych w suspensjach wodnych*, Roczniki Chem. Vol. 39, No. 5, 895-900.
WARREN L. J. (1992) *Shear flocculation,* in "Colloid Chemistry in Mineral Processing", (Eds. J. S. Laskowski and J. Ralston), Elsevier, Amsterdam, London, New York, Tokyo, Developments in Mineral Processing, Vol. 12, 309-329.
WÓJCIK W., JAŃCZUK B. and OGONOWSKI R. (2000), *Interparticle interaction between coal grains through an alkane*, J. Adhesion Sci. Technol. Vol. 14,1021-1033.
WÓJCIK W., JAŃCZUK B. and OGONOWSKI R. (2001), *Determination of the attachment and detachment forces in a coal grain/liquid/coal grain system by detachment experiments*, J. Adhesion Sci. Technol. Vol. 15, No 12, 1393-1401.

W. Wójcik, B. Jańczuk, R. Ogonowski, *Oddziaływanie między ziarnami krzemionki w alkalicznym środowisku,* Fizykochemiczne Problemy Mineralurgii, 36, 2002, 279-288 (w jęz. ang.)

W pracy przedstawiono wyniki pomiarów czasu niszczenia struktury słupka sedymentu ziaren krzemionki w węglowodorach alifatycznych od dekanu do heksadekanu. Pomiary te przeprowadzono w tzw. „rurce Waksmundzkiego" dla frakcji ziarnowych krzemionki, których średnie średnice wynoszą odpowiednio: 1,04 x 10^{-4} m, 1,35 x 10^{-4} m, 1,75 x 10^{-4} m i 2,25 x 10^{-4} m.

Uzyskane rezultaty czasu niszczenia struktury słupka sedymentu ziaren krzemionki omówione zostały w zależności od objętościowych właściwości krzemionki i alkanów, jak również w zależności od międzyfazowych właściwości. Czas niszczenia struktury słupka sedymentu rośnie liniowo tylko ze wzrostem lepkości badanych alkanów, natomiast liniowe zmiany stwierdzone zostały dla zależności odwrotności czasu niszczenia struktury w funkcji średniej średnicy ziaren krzemionki, gęstości i pracy kohezji węglowodorów. Z tych liniowych zależności wyznaczona została krytyczna średnica ziaren, krytyczna gęstość i praca kohezji. W układach, w których jeden z parametrów ma krytyczną wartość, struktura słupka sedymentu jest trwała tzn. niemożliwe jest jej zniszczenie. Wówczas siły odrywu są równe siłom zlepienia. Zakładając, że ziarna krzemionki są kulkami obliczono siły odrywu, które nieznacznie maleją ze wzrostem długości łańcucha węglowodorowego alkanów. Wykorzystując wyznaczoną krytyczną wartość pracy kohezji, która praktycznie nie zależy od wielkości ziaren krzemionki, obliczono promień płaszczyzny kontaktu pomiędzy ziarnami krzemionki. Znając wielkość promienia płaszczyzny kontaktu obliczono siły zlepienia pomiędzy ziarnami krzemionki w alkanach.

Siły zlepienia, w przeciwieństwie od siły odrywu, rosną ze wzrostem długości łańcucha węglowodorowego alkanów, w rezultacie różnica pomiędzy nimi maleje od 3,2 x 10^{-10} N/ziarno (10.7 mN/m) dla dekanu do zera dla węglowodoru o krytycznej pracy kohezji.

Na podstawie liniowych zmian odwrotności czasu niszczenia struktury słupka sedymentu krzemionki w funkcji różnicy sił odrywu i zlepienia wyznaczono krytyczną wartość tej różnicy. Niewielkie ujemne wartości krytycznej średnicy świadczą, że energia filmu węglowodorowego pomiędzy ziarnami krzemionki jest nieco zwiększona przez swobodną energię powierzchniową krzemionki.

Physicochemical Problems of Mineral Processing, 36 (2002), 289-298
Fizykochemiczne Problemy Mineralurgii, 36 (2002) 289-298

Barbara KOŁODZIEJ, Zbigniew ADAMSKI, Tomasz WŁODEK*

INVESTIGATIONS ON OBTAINING CATHODIC COBALT IN A DIAPHRAGM TYPE ELECTROLYSER

Received March 5, 2002; reviewed and accepted May 15, 2002

The investigations on cobalt electrolysis from cobalt chloride solutions while using diaphragm electrolyser have proved that: 1) Electrodeposition of cobalt should be carried out from solutions, where the pH value ranges from 5.1 to 5.3; the cathode cobalt obtained under those conditions was solid metal, bright and glossy; the current efficiency of the cathode process was 98%. 2) Three stages can be distinguished in the course of electrolytic cobalt deposition from $CoCl_2$ solutions. Stage I – slight changes in the pH value of the catholyte solutions, duration this stage depends an cobalt concentration in the solution. Cobalt obtained during this stage adheres very well to the cathode, its survace is smooth and glossy. Stage II – rapid decrease of pH in the catholyte and first hydrogen bubbles appar (pH≅3.0). Stage III – the electrolysis proceeds with a continuous but small decrease of the catholyte pH value; the cathode deposit begins to come off the ground, it is dark and full of pits;. the current efficiency of the process drops to about 90%. 3) Electrolyser modification by introducing buffer compartments that separate catholite from the anolyte makes possible to extend the stage I of electrolysis which is the most favourable stage in the whole process of cobalt deposition.

Key words:

INTRODUCTION

Cobalt is a metal correlated for years with the growth of the armaments industry and aeronautics. Over the last decade of the previous century new applications of this metal emerged. Cobalt is a component of modern aluminum – nickel alloys applied in high-reliability equipment, as well as of special-purpose corrosion resistant alloys (Curwick et al., 1980; Papp,1988; Charewicz et al., 1998). Considerable quantities of cobalt are necessary in manufacturing of cobalt-nickel batteries, compact discs, audio- and video-tapes. Cobalt is also a catalyst to numerous chemical reactions.

* Institute of Inorganic Chemistry and Metallurgy of Rare Elements, Technical University 50-370 Wrocław

The main source of metallic cobalt is electrlytic process developed in the early fifties of the last century. (Mantel, 1965; Redden and Greaves, 1992) However the knowledge of basic phenomena in the process of cathode separation of cobalt is still incomplete (Jeffrey et al., 2000). This relates in particular to the process of electrolytic separation of cobalt from chloride solutions. According to the literature reports (Chikovani 1996) certain pyrometallurgical processes can be effectively substituted in the cobalt winning technology by chloro-hydrometallurgical operations. One example is the industrial complex "Norylskij Nikiel", where leaching of nickel matte containing cobalt by hydrochloric acid was introduced. Having first removed copper and nickel from such chloride solutions, cobalt carbonate or cobalt hydroxide is precipitated, which after dissolution in sulfuric acid, produces an electrolyte solution for use in the process of cobalt cathode deposition.

Therefore the purpose of the present work is investigation of the cobalt electrowinning directly from the cobalt (II) chloride solutions in a diaphragm type electrolyser.

EXPERIMENTAL

DIAPHRAGM ELECTROLYSER

The electrolyser used in the present work is a modified version of a large scale laboratory electrolyser that was used earlier to obtain copper and nickel in the electrolytic process (Łętowski et al., 1979; Adamski et al., 1981). Cathode and anode compartments were in form of modules made of polyamide and suitably sealed. They were separated from each other by porous diaphragms of vacuum-moulded PVC. Circulation of catholyte and anolyte was forced by two peristaltic pumps. Catholyte and anolyte circulated in a closed cycle between the catholyte and anolyte tanks and the cathode and anode compartments respectively, through the inlet connections (placed under the modules) and outlet connections (in the upper part of modules). The electrolyser was powered from DC power supply type *SEL-1*. Ammeter and voltmeter type *ML-1* were used to measure the electrolyser current flow and voltage drop.

Cathodes, 85 x 85 mm, of mat sheet nickel, and lead anodes containing 7% Sb, were hung on copper bars that rested on rails connected to the DC power supply. Cathode current density was 150 A/m^2. Current efficiency of the cathode process was calculated from the mass of cobalt deposited on the cathode.

CATHOLYTE AND ANOLYTE

Catholyte was prepared of pure cobalt(II) chloride. Magnesium oxide (MgO, pure) and hydrochloric acid were used to control the acidity of the catholyte solution. The 1M sodium sulfate solution was used as the anolyte.The pH of the solutions was measured using *R-10* electrodes and a pH-meter (*Digital pH Meter PM-1)*. Catholyte volume was ranging from 750 to 900 cm^3, and the anolyte volume from 900 to 1000 cm^3. In order to effectively limit the chlorine evolution on the anode, a slight penetration of anolyte into the catholyte solution was forced in the following way:

- by using as the anolyte the 1M Na_2SO_4 with the respect to that, that its density (1.125 g/cm^3) is higher than the catholyte solution density which varied between 1.090 and 1.08 g/cm^3, depending on $CoCl_2$ concentration,
- setting mutually different flow values for circulation of anolyte and catholyte through the electrolyser compartments; the anolyte flow was 3.7 cm^3/s, and the catholyte flow was 3.0 cm^3/s.

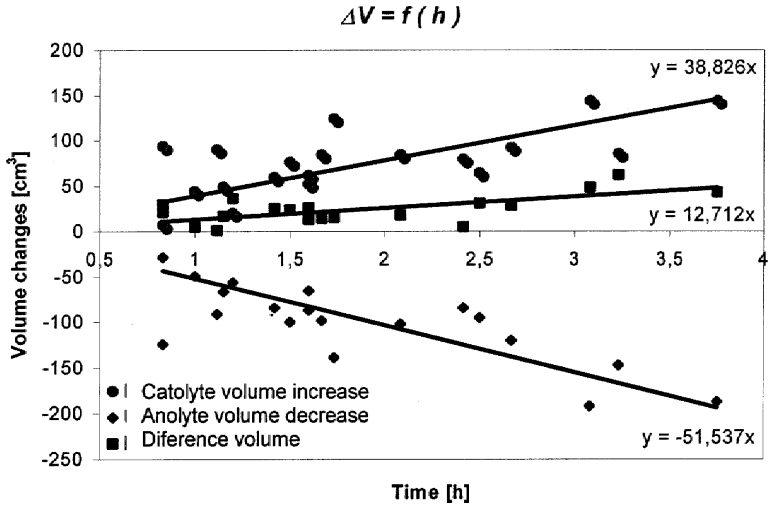

Fig. 1. atholyte and anolyte volume changes during the electrolysis process

To check the effectiveness of the above mentioned efforts, anolyte and catholyte volumes were measured before and after each electrolysis experiment. The measurements of the catholyte and anolyte volume after every one of 18 electrolysis experiments, where each of experiments took 75 to 155 minutes, showed that the catholyte volume after electrolysis was greater than that before the experiment. The diagrams of the catholyte volume increase and of the anolyte volume decrease versus time of electrolysis have been shown in Fig. 1. The constant difference of 24.6% was observed between the anolyte volume decrease and the catholyte volume increase, which is the effect of changing mass and density of the catholyte solution in the course of electrolysis. It can be concluded from the curves presented in Fig. 1, that 51.5 cm^3 (mean value) of anolyte penetrates into the catholyte within one hour.

RESULTS AND DISCUSSION

According to the Pourbaix diagram for the Co – H_2O system (Pourbaix, 1966), the reversible electrode potential for cobalt, in a solution containing cobalt ions at the concentration of 1.0 mole/dm^3 is –0.277 V. This potential in a solution at pH < 4.5 is lower than the electrochemical hydrogen ion reduction potential. Therefore the

electrolytical separation of cobalt from solutions at pH < 4.5 shall always proceed with a evaluation of hydrogen. It can be found a very narrow pH range, between 4.5 and 6.2 where the reversible electrode potential for cobalt:

$$Co^{2+} + 2e = Co \quad (1)$$

is higher then the electrochemical potential corresponding to the equilibrium of the hydrogen ion reduction to hydrogen:

$$2H^{+} + 2e = H_2 \quad (2)$$

Within the specified pH range the pure cathode cobalt is winning from solutions of its salts. Therefore there are reports in the literature that the cobalt electrolysis should be run from weak-acid or neutral solutions (Das and Subbaiah, 1984). However, the Das and Subbaiah's examinations have shown that running the electrolysis of the cobalt sulfate solution, at pH equal to 6.8, in the electrolyser where the cathode space and anode space are not separated, the pH of the bath falls abruptly to pH equal to 4 already within the first 10 minutes. After 120 minutes the pH reaches value 2. Increased electrolyte acidity is the result of reaction taking place on the anode:

$$2H_2O = O_2 + 4H^{+} + 4e \quad (3)$$

Such strong increase of the electrolyte acidity effects in significant reduction of the current efficiency of the process. According to the data obtained by Das and Subbaiah, when the pH value of the solution is 2.0, the current efficiency value reaches 86%, while the pH value lowers to 1.25, the current efficiency drops rapidly to 60%. Owind to use of a diaphragm electrolyser, it was possible to limit the acidity increase in the catholyte.

pH CHANGE IN ANOLYTE AND CATHOLYTE DURING THE ELECTROLYSIS

During the electrolysis the anolyte as well as catholyte pH was measured. The apprpriate values shown in Fig. 2 and Fig. 3. The pH values presented in Fig.2 are the mean values obtained from 10 electrolysis experiments. The anolyte pH value drops rapidly within the first 15 minutes from 5.0 to 2.5. After 1 hour in the electrolysis, the anolyte pH value is 2.1, after 2 hours – it decreases only by 0.2, and reaches 1.9.

The curves presented in Fig.3 shown how the pH values of the catholyte solution depeds on time of electrolysis, the pH value and cobalt concentration in the solution before the electrolysis (see Table 1). Inotial pH values and the cobalt concentration in electrolysed solutions have been given in Table 1.

Table 1. Initial pH value and cobalt concentration in catholyte

Number of electrolysis	pH	[Co] g/dm^3
1	5,16	51,0
2	5,16	33,0
3	5,31	29,9
4	5,53	18,6
5	5,00	40,8
6	4,97	31,0
7	4,90	21,5
8	3,40	40,8

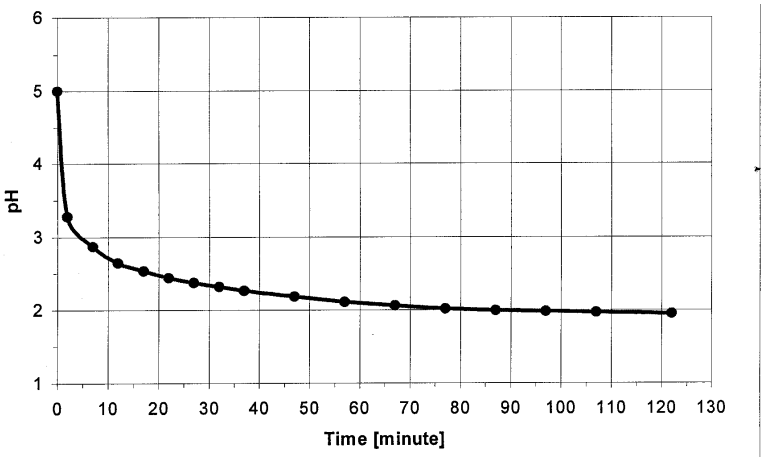

Fig. 2. Anolyte pH changes in the course of electrolysis process

Going through the results presented in Fig. 3 one can observed three cases:

1. *The pH value of the catholyte solution before electrolysis is ranged from 5.2 to 5.5.* Three stages can be distinguished on the curves showing how the pH value changes with the progress of electrolysis:
   Stage I: only slight changes in the pH value of the catholyte solution is observed,
   Stage II: rapid increase in the concentration of hydrogen ions in the catholyte solution (pH is falling); such situation will develop when the catholyte pH value during the electrolysis decreases to somewhere near 4.9.
   Stage III: small but continuous increase of the catholyte acidity.
2. *The pH value of the catholyte solution before electrolysis is ranged from 4.5 to 4.9;* stage I, does not show on the curves of pH value versus time electrolysis, in stage II the decrease of the pH value is much more extended in time compared with the stage II for the first case, stage III shows very small but continuous increase of the catholyte acidity.

3. *The pH value of the catholyte solution before electrolysis is ranged from 3.2 to 3.5;* the catholyte pH value versus time of electrolysis show a continuous, slight decrease; the stage I and II is not observed.

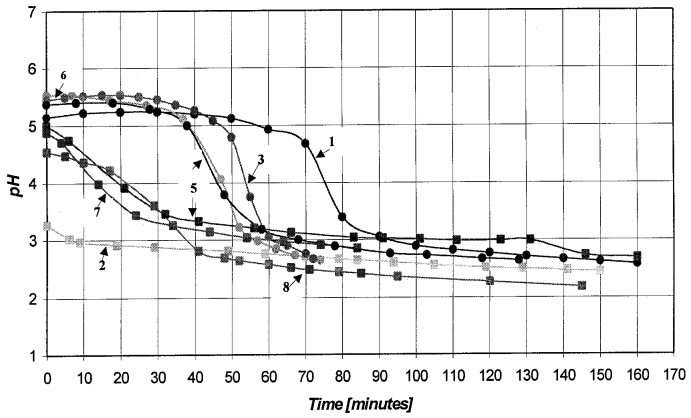

Fig. 3 .Catholyte pH changes versus time of electrolysis, initial pH value and cobalt concentration in catholyte (current density 150 A/m^2)

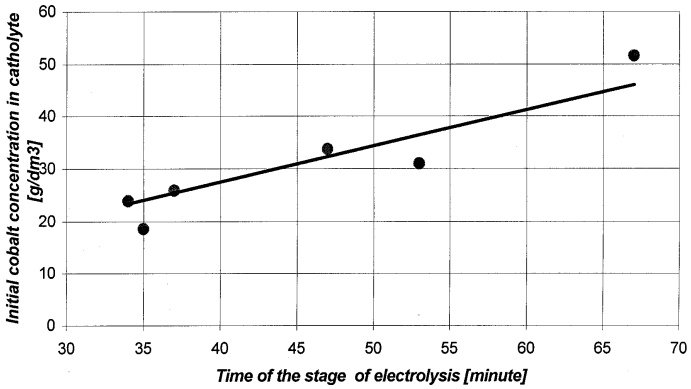

Fig. 4. Effect of initial cobalt concentration in catholyte on duration of the stage I of electrolysis (current density 150 A/m^2)

It was found that the duration of the stage I of electrolysis depends on cobalt chloride concentration in the catholyte solution. The higher initial cobalt concentration in the solution, the longer time of stage I of the electrolysis is observed. The relation has been presented in Fig.4.

HYDROGEN EVOLUTION

The first hydrogen bubbles appear on the cathode when the catholyte pH value drops to about 3.0 (stage III of the electrolysis). The starting point of the hydrogen evolution was manifested by a slight but noticeable voltage increase in the electrolyser. That phenomenon was observed in each electrolysis experiment. Relation between the voltage on the electrolyser and the duration of electrolysis, for two

selected electrolysis experiments has been presented in Fig.5. The difference between the voltage values just before, and just after the hydrogen evolution had started, was 0.1 V. The moment of hydrogen appearance depends on the duration of the stage I of the electrolysis, and thus on the pH value of and cobalt concentration in the solution before the electrolysis. The relevant relation has been shown in Fig.6.

Fig. 5. Voltage change on electrolyser versus time of electrolysis

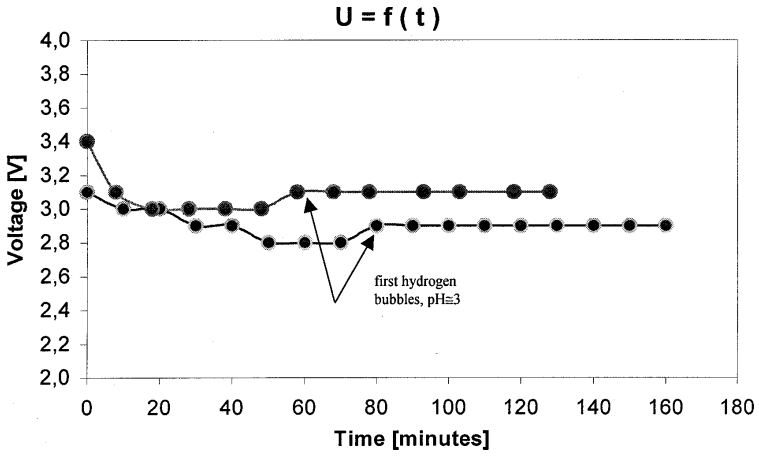

Fig. 6. Effect of the electrolysis stage I duration on the time of appearing the first hydrogen bubbles

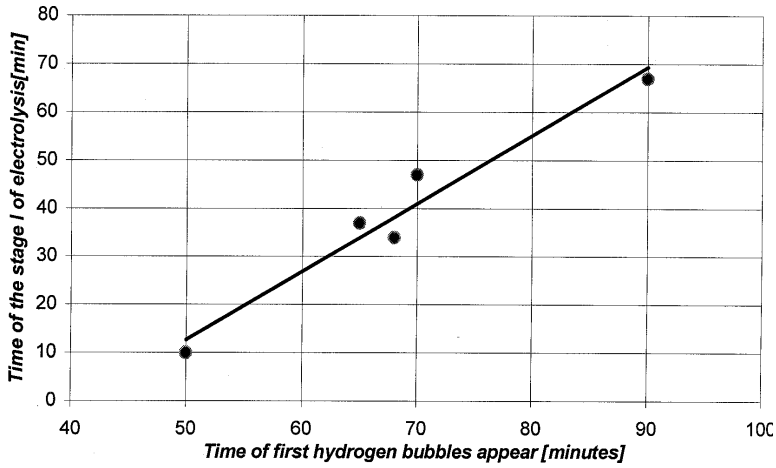

CATHOLYTE PH EFFECT ON THE CURRENT EFFICIENCY AND ON THE CATHODE COBALT QUALITY

To determine the catholyte pH effect on the current efficiency and the quality of the cathode cobalt, the diaphragm electrolysis was carried out when using a cobalt chloride solution of pH equal to 5.16 and containing 51 g of Co in 1 dm^3. Cobalt was deposited on matted nickel electrodes. The pH of the catholyte solution was monitored

in the course of electrolysis. When the pH value reached 3.0, the cathodes were removed from the solution, washed carefully and dried. They were replaced by nickel cathodes plated with a thin layer of cobalt. Duration of electrolysis before the replacement of cathodes (total time of the stage I and II) and after the replacement of cathodes (stage III) was the same, 80 minutes. Four such experiments of electrolysis were carried out. The mean current efficiency was calculated from the cathodes mass increment. The mean current efficiency corresponding to the stage I and II was 97.2%. In case of electrolysis run from the solutions of pH < 3 (the stage III), the mean current efficiency was 90.1%. Cobalt obtained during the electrolysis from $CoCl_2$ solutions of pH ranging from 5.16 to 3.0 adhered very well to the cathode. Its surface was smooth, bright and glossy. In case of electrolysis from solutions of pH less than 3.0, cracks could be seen on the cathode deposit layer, the surface of the deposit was dull, dark and full of pits. Those pits were the spots of hydrogen bubbles formation.

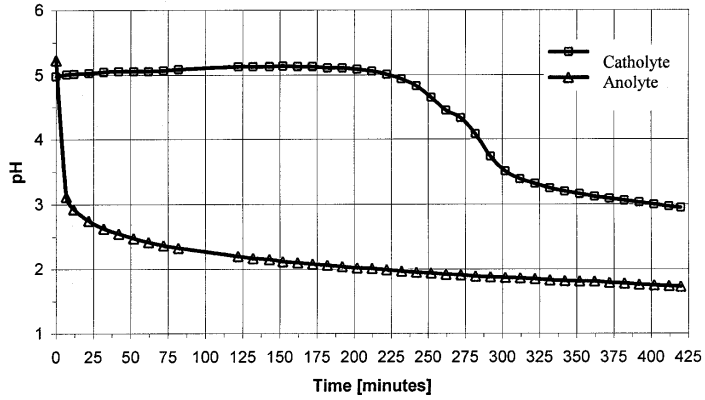

Fig. 7. pH changes in anolyte and in catholyte in the course of diaphragm electrolysis after introducing buffer compartments

DIAPHRAGM ELECTROLYSIS WHEN INTRODUCING A BUFFER COMPARTMENT

The investigations presented above indicate that obtaining the electrolytic cobalt from chloride solutions is most efficient if the initial pH of the catholyte ranges from 5.16 to 5.45, and during the electrolysis remains fixed (see Fig.3). Therefore efforts ought to be made to limit anolyte penetration into the catholyte solution, and thus to limit the catholyte acidification. It can be done by introducing buffer compartments that separate the cathode compartments from the anode ones. The buffer compartments were filled with 1M Na_2SO_4 solution. The electrolyte in the buffer compartments was maintained still. Circulation flows of anolyte as well as catholyte were the same as in case of electrolysis run without buffer compartments. The cathode current density was 150 A/m^2. Initial cobalt concentration in the catholyte solution was 59.8 g/dm^3, and the pH value of the solution was equal 5.16. The pH changes in

the catholyte and in the anolyte solutions during the electrolysis have been shown in Fig.7. The time interval of when the pH value remains constant is threefold longer as compared with the time of the stage I of electrolysis run without buffer compartments. The obtained cathode cobalt was pure metal, bright and glossy. The current efficiency of the cathode process was 98%. It needs be mentioned that the modification of the diaphragm electrolysis process by introducing buffer compartments requires further investigation on possible reduction of resistance of the total system. This parameter value decides on the consumption of energy during this process.

CONCLUSIONS

The investigations on cobalt electrolysis from cobalt chloride solutions while using diaphragm electrolyser have proved that:

1. The pH value of the catholyte solution is a critical parameter and it effects the quality of cathode cobalt and the current efficiency of the process.
2. Electrodeposition of cobalt should be carried out from solutions, where the pH value ranges from 5.1 to 5.3; the cathode cobalt obtained under those conditions was solid metal, bright and glossy; the current efficiency of the cathode process was 98%.
3. Hydrogen starts to evolve when the catholyte pH drps to about 3.0; the quality of cobalt being deposited on the cathode becomes worse, and the current efficiency decreases.
4. Three stages can be distinguished in the course of electrolytic cobalt deposition from $CoCl_2$ solutions:
   - Stage I: typical for this stage of elecrolysis are only slightly changing in the pH value of the catholyte solution as compared with the initial pH value equal 5.2÷5.5; duration of the this stage I depends on cobalt concentration in the solution; cobalt obtained during this stage of electrolysis, adheres very well to the cathode, its surface is smooth and glossy.
   - Stage II: rapid decrease of pH value in the catholyte and first hydrogen bubbles appear. Evolving hydrogen (by pH<3.0) causes a slight voltage increase on electrolyser.
   - Stage III: the electrolysis proceeds with a continuous but small decrease of the catholyte pH value; the cathode deposit begins to come off the ground, it is dark and full of pits;. the current efficiency of the process drops to about 90%.
5. Electrolyser modification by introducing buffer compartments that separate catholyte from the anolyte makes possible to extend the stage I of electrolysis which is the most favourable stage in the whole process of cobalt deposition. The experiments carried out after the buffer compartments had been implemented, the time interval of the stage I of electrolysis was threefold longer as compared with the time attained previously in the process of diaphragm electrolysis.

REFERENCES

ADAMSKI Z., CHMIELEWSKI T., ŁĘTOWSKI F., (1981*) Recovery of nickel from used catalysts,* Rudy Metale, 26, 252 – 54.

CHAREWICZ W., CHMIELEWSKI T., WALKOWIAK W., (1998), *in III Seminar of Cobalt,* May Lubin,.

CHIKOVANI A.A., (1996), *Several problems of production of non ferrous metals,* Tsvetnye Metally, 5, 69 – 70.

CURVICK L.R., PETERSON W.A., AND MAKAR H.V., (1980), *Availability of critical scrap metals containing chromium in the Unites States. Superalloys and cast hest – and corrosion – resistant alloys.* US Bur. Mines IC 8821, 51 pp.

DAS S.C., SUBBAIAH T., (1984), *Electrowinning of cobalt. I. Winning from pure cobalt sulphate bath, Hydrometallurgy*, 12, 317 – 333.

JEFFREY M.I., CHO W.L., BREUER P.L., (2000), *The effect of additives and impurities on the cobalt electrowinning process,* Minerals Eng., vol. 13, No. 12, 1231 – 1241.

ŁĘTOWSKI F., KOŁODZIEJ B., CZERNECKI M., JĘDRCZAK A., ADAMSKI Z., (1979), *New hydrometallurgical method for the processing of copper concentrates using ferric sulphate,* Hydrometallurgy, 4, 169 – 184.

MANTEL C.L., (1960), *Electrochemical Engineering*, Mc Graw – Hill Book Company, Inc.

PAPP J.F., (1988), Superalloy recycling 1976 – 1986, In: S. Reichman, D.N. Duhl, G. Maurer, S. Antolovich and C. Lund (Editors), Superalloys 1988. Metall. Soc. AIME, Warrendale, Pa., pp. 367 – 376.

POURBAIX M., (1966), *Atlas of electrochemical equilibria in aqueous solutions*, Pergamon Press.

REDDEN L.D., GREAVES J.N., (1992), *The technical and economic aspects of producing high – purity cobalt and nickel from superalloy scrap utilizing a duble – membran electrolytic cell,* Hydrometallurgy, 29, 547 – 565.

Kołodziej B., Adamski, Z., Włodek T., *Badania nad otrzymywaniem kobaltu katodowego przy zastosowaniu elektrolizera przeponowego, Fizykochemiczne Problemy Mineralurgii, 36, 289-298 (w jęz. ang.)*

Badania nad elektrolizą kobaltu z roztworów chlorku kobaltu w elektrolizerze przeponowym wykazały, że: 1) Elektrowydzielanie kobaltu należy prowadzić z roztworów, których pH wynosi od 5.1 do 5.3; otrzymany w tych warunkach kobalt katodowy był lity, jasny i błyszczący; wydajność prądowa procesu katodowego wynosiła 98%. 2) Podczas elektrolitycznego wydzielania kobaltu wyróżnić można trzy etapy. Etap I charakteryzuje się nieznacznym wzrostem pH; czas trwania tego etapu zależy od stężenia kobaltu w roztworze; wydzielony kobalt ściśle przylega do katody, jest gładki i błyszczący. Etap II to gwałtowny spadek pH katolitu i pojawienie się pierwszych pęcherzyków wodoru (pH≅3.0). Etap III – elektroliza przebiega przy ciągłym, niewielkim, zmniejszaniu się pH katolitu; kobalt katodowy zaczyna odstawać od podłoża, jest ciemny z licznymi wgłębieniami; wydajność prądowa spada i wynosi 90%. 3) Stwierdzono, że zmiana konstrukcji elektrolizera polegająca na wprowadzeniu przestrzeni buforowych, oddzielających katolit od anolitu pozwala na wydłużenie I etapu elektrolizy, który jest najkorzystniejszy dla procesu wydzielania kobaltu.

Physicochemical Problems of Mineral Processing, 36 (2002) 299-306
Fizykochemiczne Problemy Mineralurgii, 36 (2002) 299-306

Maciej KOZAK[1], Ludwik DOMKA[2], Andrzej SKRZYPCZAK[3],

ADSORPTION OF THE QUATERNANRY AMMONIUM SALTS ON BENTONITE

Received March 5, 2002; reviewed and accepted May 15, 2002

Sodium bentonite was subjected to the effect of two new homologue series of chlorides (alcoxymethyl) dimethyloctyloamonium chlorides and 3-alcoxymethyl-1-octylimidazole chlorides with the hydrophobic substituents of the same length. Morphology of the obtained modified bentonite was studied under scanning electron microscope [SEM] and the degree of adsorption of the ammonium salts was determined by two-phase titration. The results allowed an assessment of the influence of the length of the hydrophobic substituents and the site of the quaternary nitrogen atom on the adsorption of chlorides.

Key words: bentonite, surface modification, quaternary ammonium salts

INTRODUCTION

Bentonites belong to a group of clay minerals formed as a result of the process of weathering of volcanic ashes. The main component of bentonite (over 60%) is montmorillonite a representative of stratiform silicates containing some amounts of quartz, and small admixtures of illite, calcite, mica, chlorites and undecomposed grains of volcanic glass. Montmorillonite from the group of smectites is a representative of the 2:1 type stratiform silicates. It is built of packets of two tetrahedral silicate layers and an octahedral (metalohydroxyl) with adjacent margins. As a result of isomorphous replacement of clay from the octahedral layer by cations of lower valence an excessive negative charge appears on the packet surface. This negative charge is compensated by the adsorption of cations in the interpacket space.

[1] Adam Mickiewicz University, School of Physics, Poznan
[2] Center of Technology, School of Chemistry, Adam Mickiewicz University, Poznan
[3] Poznan University of Technology, School of Chemical Technology, Poznan

Therefore, the most general classification of bentonites is based on the type of cations dominant in the interpacket space – sodium, calcium or rarely magnesium (Van Olphen, 1977; Worral, 1986).

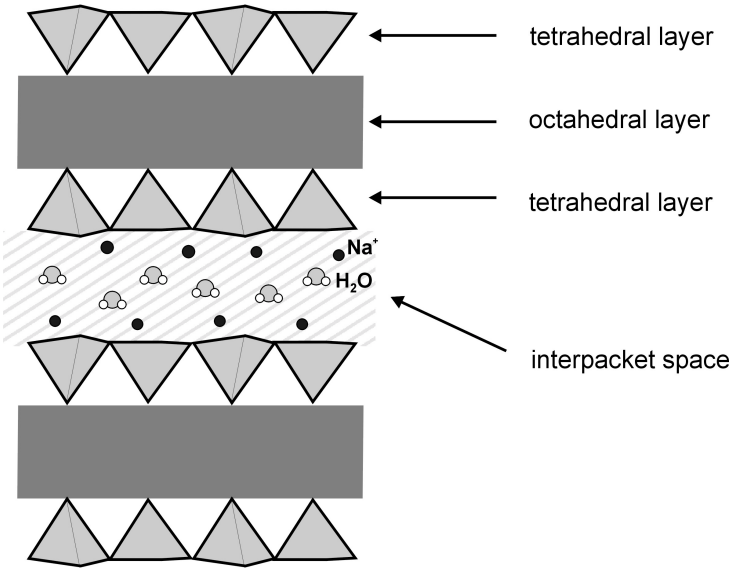

Fig. 1. Schematic representation of montmorillonite structure

The bentonites of high content of sodium montmorillonite reveal an ability to adsorb water in the interpacket space. This ability is very interesting from the point of view of technological applications. Water penetrating among the silicate layers forms layers of about 0.3 nm in thickness, consequently bentonite is capable of adsorbing the mass of water 5 times greater than its own mass. The layer of hydrated bentonite makes a compact barrier for the flow of liquid. Therefore, bentonite is often used in construction of sealing layers, geomembranes or in drilling technology. According to a similar mechanism other solvents, surfactant solutions or polymers may be adsorbed in bentonites. Investigation of this phenomenon is particularly important because of the promising possibility of application of the modified bentonite or pure montmorylonitu in polymer technology for preparation of new nanocomposite systems characterised by unique mechanical properties (LeBaron et al., 1999; Alexandre and Dubois, 2000).

This study was meant as an attempt at determination of the adsorption properties of bentonite with respect to quaternary ammonium salts. Adsorption of these compounds on the surface of silica has been well recognised (Drach et al., 1998; Esumi et al., 1996), but adsorption of quaternary ammonium salts on bentonite has not been the subject of interest of many authors. The results of this study were meant to provide information on the adsorption of the salts on the properties of the modified bentonite.

Two new homologous series of chlorides have been chosen for the study: (alcoxymethyl)dimethyloctyloammonium chlorides and 3-alcoxymethyl-1-octylimidazole chlorides with the hydrophobic substituents of the same length differing in the site of appearance of the positive charge. In the compounds of the first series the positive charge is localised at the ammonium nitrogen atom, while in the second it is delocalised on the imidazole ring. The aim of the study was to determine the influence of the hydrophobic substituents length and the site of the quaternary nitrogen atom (with positive charge) on the process of adsorption in bentonite.

MATERIALS AND METHODS

REAGENTS

Powdered bentonite was purchased at the Fisher Scientific, Great Britain. The chlorides used (alcoxymethyl)dimethyloctyloammonium and 3-alcoxymethyl-1-octylimidazole chlorides were obtained in the reaction of a proper chloromethylalkil ether with N,N-dimethyloctylamine or 1-octyloimidazole according to the procedure described by Pernak et al. (1987) and Skrzypczak et al. (1997).

Table 1. List of the compounds synthesised

No.	Compound Name	Reaction yield wt.
1	(butoxymethyl)dimethyloctylammonium chloride	95,3%
2	dimethyl(hexyloxymethyl)octylammonium chloride	92,1%
3	dimethyloctyl(octyloxymethyl)ammonium chloride	93,6%
4	(decyloxymethyl)dimethyloctylammonium chloride	90,4%
5	dimethyl(dodecyloxymethyl)octylammonium chloride	88,3%
6	3-butoxymethyl-1-octylimidazole chloride	97,5%
7	3-hexyloxymethyl-1-octylimidazole chloride	94,6%
8	1-octyl-3-oktyloxymethylimidazole chloride	86,5%
9	3-decyloxymethyl-1-octylimidazole chloride	89,9%
10	3-dodecyloxymethyl-1-octylimidazole chloride	85,7%

After synthesis, isolation and purification procedures the purity of each compound was checked by thin layer chromatography.

MODIFICATION OF THE BENTONITE SURFACE

The study was performed with the use of water solutions of the quaternary ammonium salts of the concentration of 2 g/dm^3. To portions of 20 cm^3 of a given solution of the quaternary salt the weighted portions of bentonite of 0.02g, 0.04g, 0.06g, 0.08g, 0.10g were added. The solution with a given portion of bentonite was

intensely stirred for 20 min and filtered off through a qualitative filter at a moderate rate of filtration. The precipitate was washed with three portions of distilled water, afterwards left for further analysis. The precipitate was subjected to morphological examination under a scanning electron microscope.

SCANNING ELECTRON MICROSCOPY SEM

Morphology of the samples was examined by scanning electron microscopy (SEM-515, Philips). The powdered sample, intended for the studies, was dispersed in t-butanol and, following sedimentation on a microscope holder, it was coated with gold in an ionisation chamber. The typical magnification ratio was 2,500×.

TWO-PHASE TITRATION

The filtrate was tested for the presence of the cation-active substance according to the procedure recommended by the Polish standards PN-87/C-04818. The titration was performed in a two-phase water-chloroform system by the solution of sodium dodecyl sulphate in the presence of a mixed indicator composed of a mixture of a cationic indicator (dimidiowy bromide) and an anionic indicator (disulphine blue). The anionic salt reacts with the mixed indicator forming a salt, which dissolves in chloroform giving a specific blue colour. Upon titration, sodium dodecyl sulphate added displaces the anionic indicator from the salt, which changes the colour of the chloroform layer into pink.

RESULTS AND DISCUSSION

The morphology of the unmodified bentonite is shown in Fig. 1, while Fig. 2 shows the morphology of the 0.02 g bentonite sample after adsorption of (butoxsymethyl) dimethylctylammonium chloride. A comparison of the photographs proves that the adsorption of the chloride did not cause an increase of the degree of agglomeration of bentonite particles. The sample after modification reveals some prevalence of the fraction of greater particles but also a better equalisation.

Figures 4 and 5 present the loss of ammonium and imidazole chlorides studied from the solution as a function of the bentonite concentration. The results of two-phase titration presented in Fig. 4 and 5 indicate that the adsorption of the compounds studied on bentonite is not a linear process. At the first stage, so for the weighted portion of 0.02g bentonite, a significant loss of a given quaternary salt from the solution is observed. When a multiplied portion is used the adsorption grows systematically (for almost all compounds) but usually is by one order of magnitude lower than that for the portion of 0.02g of bentonite. These data suggest that the description of the process of adsorption of the quaternary salts studied from water solutions on the surface of bentonite should take into regard the surface activity properties of these compounds.

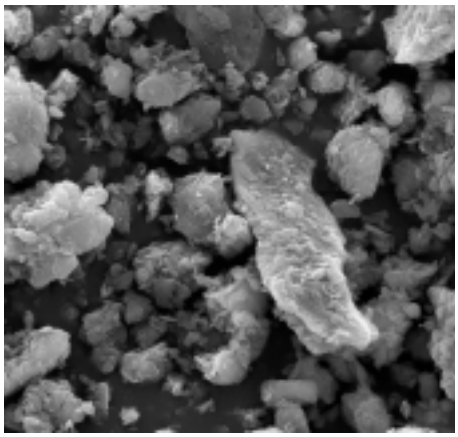

Fig. 2. Standard bentonite (SEM microphotograph, 2,500 x magnification)

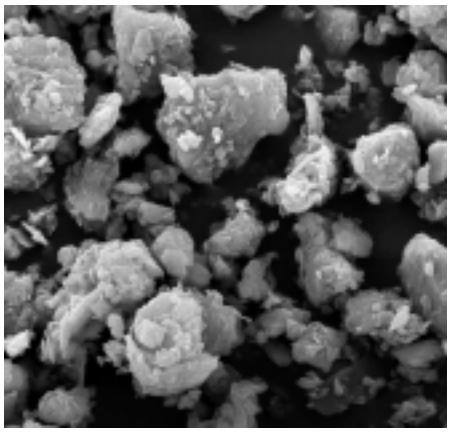

Fig. 3. Bentonite after adsorption of (butoxymethyl)dimethylctylamonium chloride (on 0.02 g bentonite) (SEM microphotograph, 2,500 x magnification)

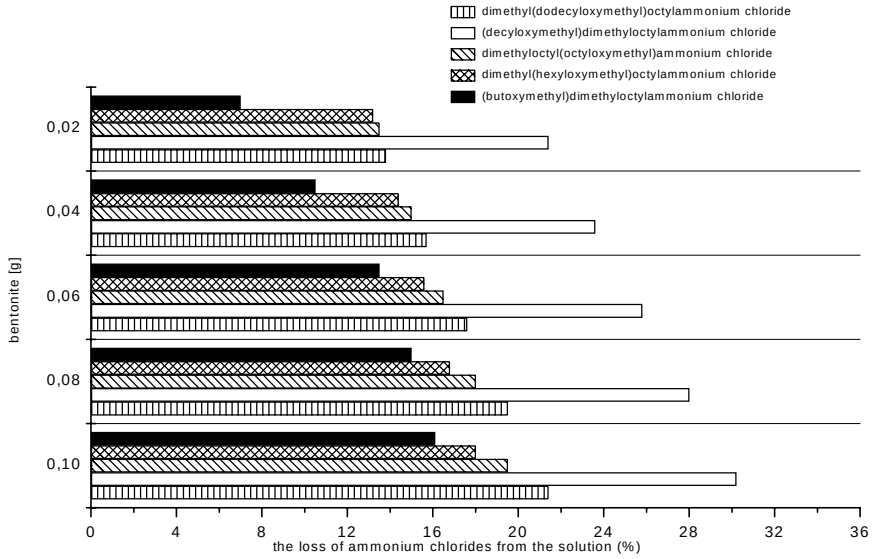

Fig. 4. The loss of ammonium chlorides from the water solution as a function of the bentonite added

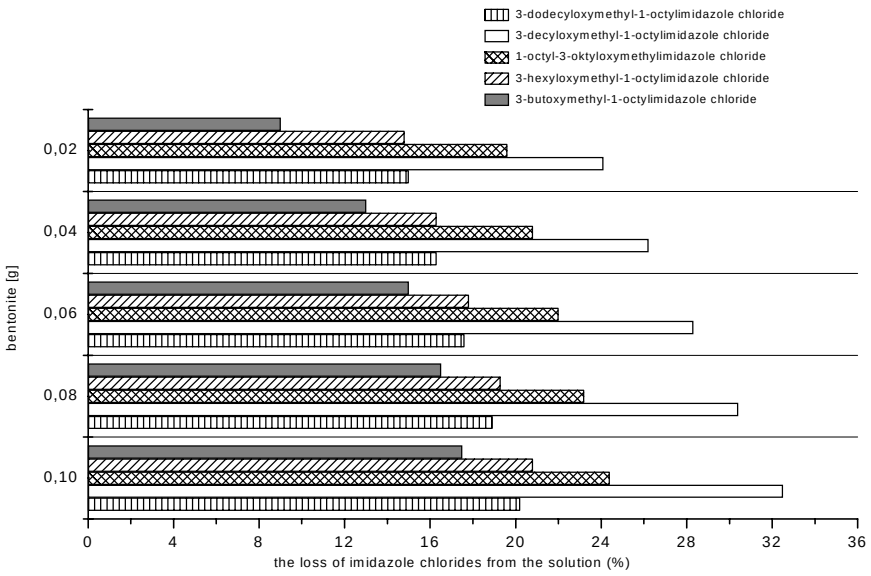

Fig. 5. The loss of imidazole chlorides from the water solution as a function of the bentonite added

Analysis of the loss of ammonium and imidazole chlorides in the solution, has shown that it becomes more pronounced with increasing length of the substituent (from butoxymethyl to decyloxymethyl). The smallest loss of the quaternary salt in the solution (relative to the weighted portion of 0.1 g of bentonite) was observed for (butoxymethyl)dimethyloctylammonium chloride (16.1 %) and 3-butoxymethyl-1-octylimidazole chloride (17 %), while the greatest for (decyloxymethyl)-dimethyloctylammonium chloride (30.2 %) and 3-decyloxymethyl-1-octylimidazole chloride (32.5 %).For the longest substituent (dodecyloxymethyl) a deviation from the above rule was noted and the values of the loss of dimethyl(dodecyloxymethyl) octylammonium chloride and 3-dodecyloxymethyl-1-octylimidazole chloride were 21.4 % and 20.2 %, respectively.

A probable mechanism of adsorption of surfactants on the surface of bentonite (Fig. 6) dependent on the surfactant concentration was proposed by Alemdar et al. (2000) for adsorption of cetyltrimethylammonium bromide (CTAB) and distearyldimethylammonium chloride (DDAC) on the surface of sodium and calcium bentonite. This mechanism (Fig. 6) involving adsorption on a single or double layer depending on the bentonite concentration, is also valid for the quaternary salts studied. A comparison of the percent loss of the chlorides from the two homologue series from water solutions as a result of adsorption on bentonite brings about the information on the effect of localisation of the positive charge on the character of the adsorption studied.

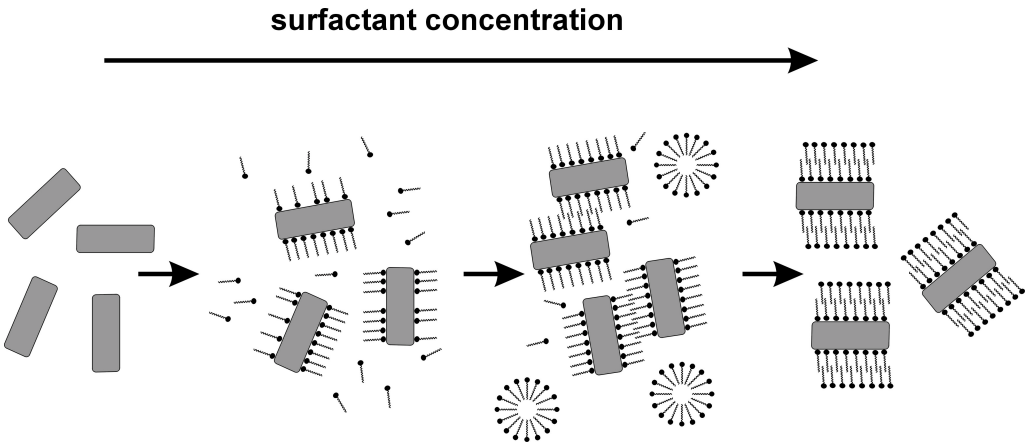

Fig. 6. Schematic representation of adsorption of cationic surfactants on bentonite as a function of surfactant concentration (after Alemdar et al. 2000)

A similar nonlinear chanracter of surfactants adsorption has also been observed by other authors in adsorption of sodium dodecylbenzene sulfonate on organophilic bentonites (Rodrıguez-Sarmiento and Pinzon-Bello, 2001) and in modification of bentonite using nonionic surfactants (Shen, 2001).

The compounds with the imidazole core in which the positive charge is localised on the imidazole ring are adsorbed to a degree by a few percent greater than those in which the positive charge is localised on a specific nitrogen atom (ammonium compounds).

ACKNOWLEDGMENT

The work was supported by intercollegiate (UAM/AE) grant. The authors would like to thanks Rectors of Adam Mickiewicz University (Poznań) as well as Poznań University of Economics for generous support.

REFERENCES

ALEMDAR A., ATICI O., GÜNGÖR N. (2000) *The influence of cationic surfactants on rheological properties of bentonite-water systems.* Materials Letters, Vol. 43, 57.

ALEXANDRE M., DUBOIS P. (2000) *Polymer-layered nanocomposites: preparation, properties and uses of a new class of materials.* Material Science and Engineering, Vol. 28, 1.

DRACH M., ŁAJTAR L., NARKIEWICZ-MICHAŁEK J., RUDZIŃSKI W., ZAJĄC J. (1998) *Adsorption of cationic surfactants on hydrophilic silica: effects of surface energetic heterogeneity*, Colloids and Surfaces, Vol. 145**,** 245.

ESUMI K., GOINO M., KOIDE Y. (1996) *Adsorption and adsolubilization by monomeric, dimeric, or trimeric quaternary ammonium surfactant at silica/water interface*, J. Coll. and Int.Sci., Vol. 183**,** 539.

LeBARON P.C., WANG Z., PINNAVAIA T.J. (1999), *Polymer-layered silicate nanocomposites: an overview.* Applied Clay Sciences Vpl 15, 11.

PERNAK J., KRYSIŃSKI J., SKRZYPCZAK A. (1987), Tenside Surfactans Detergents, Vol. 24**,** 276.

RODRIGUEZ-SARMIENTO D.C., PINZON-BELLO J.A. (2001), *Adsorption of sodium dodecylbenzene sulfonate on organophilic bentonites.* Appl. Clay Sci. Vol. 18, 173.
SKRZYPCZAK A., BRYCKI B., MIRSKA I., PERNAK J. (1997). *Synthesis and antimicrobial activities of new quats*, Eur. J. Med. Chem., Vol. 32**,** 661.
SHEN Y.H. (2001), *Preparations of organobentonite using non-ionic surfactants.* Chemosphere Vol. 44, 989.
WORRAL E. (1986), *Clays and Ceramic Raw Materials*, Elsevier, London.
VAN OLPHEN H. (1977), *Clay Colloid Chemistry*, Willey, New York.

Kozak M., Domka L., Skrzypczak A., *Adsorpcja czwartorzędowych soli amoniowych na bentonicie*, Fizykochemiczne Problemy Mineralurgii, 36, 2002, 299-306 (w jęz. ang.).

W ramach prezentowanych badań poddaliśmy bentonit sodowy działaniu dwóch nowych szeregów homologicznych chlorków (alkoksymetylo)dimetylo-oktyloamoniowych oraz chlorków 3-alkoksymetylo-1-oktyloimidazoliowych o identycznej długości analogicznych podstawników hydrofobowych. Przeprowadziliśmy analizę morfologii zmodyfikowanego bentonitu z użyciem skaningowej mikroskopii elektronowej oraz stopnia adsorpcji soli amoniowej przy pomocy miareczkowania dwufazowego. Uzyskane wyniki pozwoliły określić wpływ długości podstawników hydrofobowych oraz miejsca, gdzie występuje czwartorzędowy atom azotu, na proces adsorpcji chlorków.

Physicochemical Problems of Mineral Processing, 36 (2002) 307-316
Fizykochemiczne Problemy Mineralurgii, 36 (2002) 307-316

Teofil JESIONOWSKI* , Andrzej KRYSZTAFKIEWICZ and Aleksandra DEC**

MODIFIED, Al_2O_3 - TREATED TITANIUM WHITES AS PIGMENTS OF ACRYLIC PAINTS

Received March 15, 2002; reviewed and accepted May 15, 2002

In the studies, aluminium-oxide treated titanium white (R-001 type) was used, produced by the Chemical Works Police S.A. Surface of titanium white was modified with silane coupling agents. For the purpose 3-methacryloxypropyltrimethoxysilane (A-174), vinyltrimethoxysilane (U-611) and N-2-aminoethyl-3-aminopropyltrimethoxysilane (U-15D) were used.

The unmodified and the modified titanium whites were subjected to physicochemical analysis. Moreover, tests were conducted in order to define morphology, surface structure and particle dispersion, as affected by the type of applied modifier. The analysis involved modern investigative techniques, SEM and DLS.

The modified and the unmodified titanium whites were applied as pigments in acrylic paints. The modified TiO_2 were particularly effective in improvement of strength and utility parameters of acrylic paints.

Key words*: titanium dioxide (R-001), surface modification, silane, particle size distribution, SEM, acrylic paint*

INTRODUCTION

Titanium dioxide pigments include spherical particles of various size. The particle size range used to be 0.005 to 1.0 μm but the fraction showing sizes of 0.2 to 0.4 μm prevails (Braun, 1997). The particle size strictly determines the extent of whiteness of titanium dioxide pigments. Even if pure TiO_2 is colourless, at high dispersion it represents the most effective white pigment. Within the visible light spectrum, titanium white practically does not absorb the incident light. The light is transmitted or deflected by the crystals or reflected from the surfaces of crystal contacts (Braun et al., 1992).

* Poznan University of Technology, Institute of Chemical Technology and Engineering
Pl. M. Sklodowskiej-Curie 2, 60-965 Poznan, Poland
E-mail: Teofil.Jesionowski@put.poznan.pl, phone:+48(61)6653720, fax:+48(61)6653649
** W Lakma S.A., Frysztacka 173 St., 43-400 Cieszyn, Poland

On the surface of titanium dioxide particles the associated hydroxyl ions cause that surface of titanium white exhibits an ionic character (Buxbaun, 1993). Depending on the type of the bonds, particle surface exhibits an acidic or an alkaline character. Coating of the surface with hydroxyl groups affects several properties of the pigments, e.g., their dispersive potential, absorptive capacity, electrokinetic potential or resistance to external influences. The size and nature of the surface of TiO_2 pigment particles affect adsorption of dispersive or wetting agents, solvents and ahesives. The presence of hydroxyl groups opens potential for accomodating in the site photochemically-inducible reactions (Woodbridge, 1991).

Surface processing exerts immense effects on the character and size of pigment surface area. The most frequently applied inorganic processing with hydrated aluminium oxide and silica may even double specific surface area of titanium white (Wicks et al., 1992). Effect of silica clearly depends on the character of silica. The compact form of silica, which coats TiO_2 particles augments specific surface area of the pigment only slightly. On the other hand, the so called fluffy form (e.g., pyrogenic silica) may markedly elevate the specific surface area.

EXPERIMENTAL DETAILS

MATERIALS

Titanium dioxide (R-001) was obtained by the sulfate technology in the Chemical Works “Police” S.A. (Poland). Principal physicochemical data of the pigment are shown in Table 1. The data of Table 1 allowed us to conclude that a standard titanium white was used, of typical pH and oil absorption number.

Table 1. Principal properties of the applied titanium white

Physicochemical variable	Titanium white R-001
Density (g/cm^3)	4.1
Content of titanium dioxide (% w/w)	at least 95
-including rutile	at least 98
Content of volatile substances at 105^oC (% w/w)	max. 0.5
Content of water soluble materials (% w/w)	max. 0.5
Residue on a sieve of 45 μm. mesh (% w/w)	max. 0.02
Brightness	95.5
Shade in a white paste	7.0
Relative scattering ability	100
Ability to tone down the shade	1850
Shade in a gray paste	3.5
pH in water suspension	7.5
Oil absorption number (g/100g pigment)	21
Specific resistance of water extract (Ohm x cm)	12000
Inorganic surface treatment	Al_2O_3

3-Methacryloxypropyltrimethoxysilane (A-174), vinyltrimethoxysilane (U-611) and N-2-aminoethyl-3-aminopropyltrimethoxysilane (U-15D) produced by Witco Co. (USA) and UniSil Co. (Poland) were used as modifiers.

METHODS

Modification process

Modification of the surface of TiO_2 was carried out in a mixer. For modification, solutions of appropriate silane were prepared, while solutions of the silane coupling agents were prepared in a mixture of water and methanol (4:1 v/v). Solutions containing 0.5 weight parts of these compounds in appropriate solvents per 100 weight parts of the modified titanium dioxide were used. The amount of solutions of modifying compounds was always selected in such a way as to ensure optimum wettability of the surface of TiO_2. After mixing, the solvent was removed by evaporation and the modified powders were dried at 110^{o}C.

Examination of physicochemical properties

Following the modification, the titanium dioxide was subjected to physicochemical tests, the bulk density as well as water, dibutyl phthalate and paraffin oil absorption capacity was estimated. The end point of water absorption capacity was observed when an excess of a single drop induced an evident liquefaction of the paste being formed. The end point of dibutyl phtahalate or paraffin oil absorption capacities was registered when an excess of a single phthalate or oil drop altered abruptly the consistency of the paste which adhered to a glass plate.

Table 2. Systems of acrylic dispersion paints for studies on the application of samples of titanium dioxide

1. AKRYL LAKMA Acrylic dispersion paint, white, water soluble, for facade use	Amount (wt%)
Acrylic-styrene dispersion (acrylic-styrene polymer, 50 wt% in water)	20-25
Carbonate fillers	30-35
Titanium white R-001 unmodified or modified	15-17
Dispersing agents, wetting agents, densifiers	23-35
2. AKRYBET Acrylic dispersion paint, white, organic solvent soluble, for exterior use	Amount (wt%)
Acryl resin in a solvent (whitespirit)	20-25
Carbonate fillers	30-35
Titanium white R-001 unmodified or modified	15-17
Dispersing agents, wetting agents, densifiers	23-35

Studies on morphology and microstructure were performed in order to obtain data on dispersion, particle shape and morphology of the granules, structure of individual particles and on TiO_2 aggregation and agglomeration type. The researches were conducted using scanning electron microscopy (SEM). The observations were performed using a Phillips SEM 515 microscope.

Size distributions of TiO_2 particles were estimated using a ZetaPlus instrument (Brookhaven Instruments Inc., USA), by the dynamic light scattering method.

Application of modified titanium white

Titanium white was applied as a pigment in acrylic dispersion paints (Jesionowski et al., 2001) Two types on acrylic paints were selected, listed in Table 2. Titanium whites were introduced to paints for interior or exterior use.

RESULTS AND DISCUSSION

The conducted studies on TiO_2 surface modification using silane coupling agents aimed at altering the hydrophilic/hydrophobic character of the surface.
Basic physicochemical parameters of unmodified and the modified titanium white are presented in Table 3. Only insignificant alterations in the surface character were noted in the surface modified pigments.

Table 3. Physicochemical parameters of unmodified and modified titanium dioxide (R-001)

Bulk density (g/dm^3)	Water absorbing capacity ($cm^3/100g$)	Dibutyl phthalate absorbing capacity ($cm^3/100g$)	Paraffin oil absorbing capacity ($cm^3/100g$)
TiO_2 - unmodified			
716	150	150	200
TiO_2 + U-611			
909	100	150	250
TiO_2 + A-174			
908	100	150	250
TiO_2 + U-15D			
900	150	100	250

An increased capacity to absorb water by TiO_2 surface could be observed only after modification of the surface with U-15D aminosilane. Since surface of the so modified titanium white carries amine groups which can interact by hydrogen bonds with water molecules, the surface exhibits a slightly hydrophilic character.

The use of silane coupling agents for the modification was followed by a distinct increase in bulk densities of the titanium white samples.

Particle size distribution of the unmodified sample of titanium white, R-001, is presented in Fig.1a, while the appropriate electron micrograph of the titanium pigment sample is shown in Fig.1b.

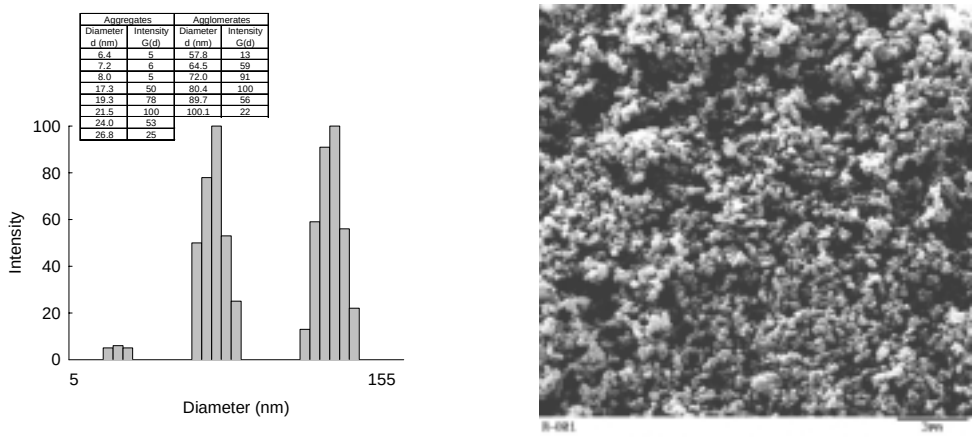

a) b)

Fig. 1. a) Multimodal particle size distribution and b) SEM of unmodified TiO_2

The particle size distribution (Fig.1a) manifested the presence of two bands, responsible for the presence of primary particles and of aggregates. One of the bands fitted the range of 6.4 to 8.0 nm and the other corresponded to the range of 17.3 to 26.8 nm (maximum intensity of 100 corresponded to the particle diameter of 21.5 nm). The third band proved that somewhat larger particles (agglomerates) were present. Size range of the latter included particles of 57.7 to 100.1 nm in diameter. Maximum intensity of 100 corresponded to agglomerates of 80.4 nm in diameter. Mean diameter of particles of this unmodified titanium white amounted to 49.7 nm and the polydispersity was 0.262. Also the respective electron microphotographs (Fig. 1b) provided an evidence for the presence of particles of a variable diameter and for the tendency to form aggregates and agglomerates. The observed dispersive and morphological properties of titanium white, R-001 resulted from coating of the pigment surface with aluminium oxide in the course of the technological process.

Titanium white modified with U-611 silane manifested quite a variable disperse character. In the particle size distribution (Fig. 2a) four bands were observed. The first band of low intensity documented the presence of very small particles (1.0-1.3 nm), the second and the third band included a broad range of diameters (3.4 to 10.4 nm). Maximum intensities for the bands were as follows: for the band of 3.4 to 5.0 nm intensity of 42 has corresponded to particles of 4.4 nm in diameter, for the band of 5.6 to 10.4 nm the intensity of 80 corresponded to the particle diameter of 8.1 nm. The most intense particle band fitted the range of 17.1-31.6 nm (maximum intensity of 100 corresponded to particles of 21.8 nm in diameter). The very clear electron microscopical pattern (Fig. 2b) pointed to the presence of isolated primary TiO_2 particles and provided an evidence for low tendency to form particle agglomerates.

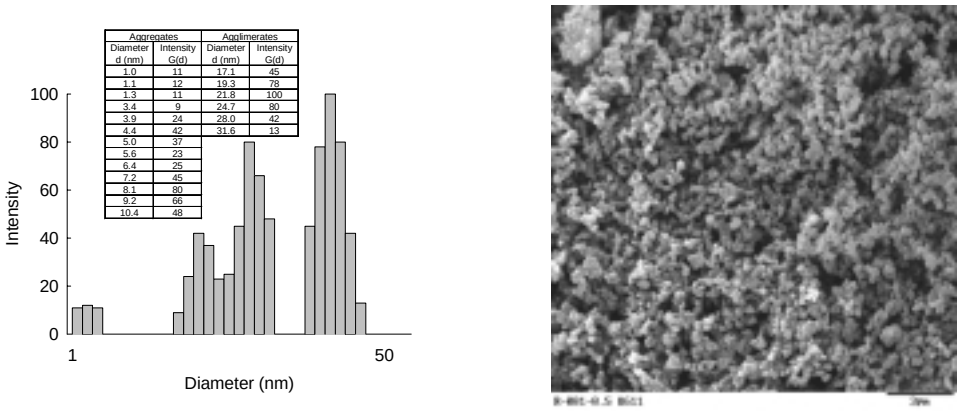

a) b)

Fig. 2. a) Multimodal particle size distribution and b) SEM of TiO_2 modified with U-611 silane

Mean diameter of particles in U-611 silane-modified titanium white reached 13.6 nm and the polydispersity amounted to 0.228.

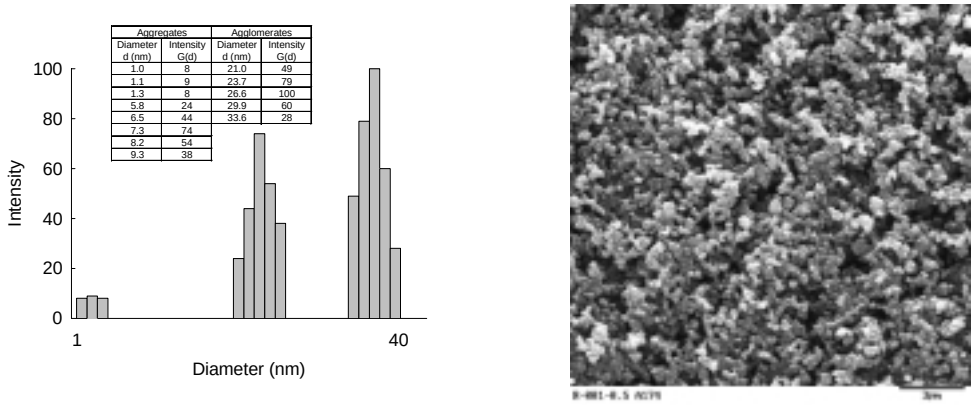

a) b)

Fig. 3. a) Multimodal particle size distribution and b) SEM of TiO_2 modified with A-174 silane

Very similar results were obtained following modification of the surface of R-001 titanium white using metacryloxypropyltrimethoxysilane, A-174. Mean particle diameter reached 17.5 nm and the polydispersity was 0.273. The particle size distribution and electron micrograph of so modified titanium white are shown in Fig. 3. Two bands were particularly intense (Fig. 3a): one within the range of 6.5-9.3 nm (maximum intensity of 74 has corresponded to particle diameter of 7.3 nm) and the other, more intense band within the range of 21.0-33.6 nm (maximum intensity of 100 corresponded to the particles of 26.6 nm in diameter).

Modification of titanium white with silane U-15D agent induced no significant changes in disperse and morphological characteristics of titanium white (Fig.4).

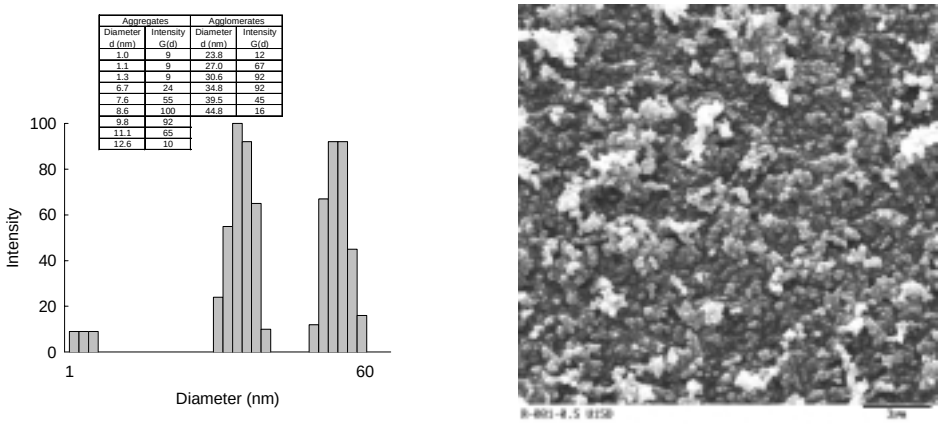

a) b)

Fig. 4. a) Multimodal particle size distribution and b) SEM of TiO_2 modified with U-15D silane

Mean particle diameter was 19.9 nm and polydispersity amounted to 0.241. The particle size distribution (Fig. 4a) included three bands.

One of the bands fitted the range of 1.0-1.3 nm and showed very low intensity (maximum intensity of 9 corresponded to particles of 1.1 nm diameter). The remaining two bands were very intense. The more intense band fitted the range of 6.7-12.6 nm (maximum intensity of 100 corresponded to particle diameter of 8.6 nm). On the other hand, the less intense band corresponded to particles diameter in the range of 23.8-44.8 nm (maximum intensity of 92 corresponded to partocle diameter of 30.6-34.8 nm). SEM photograph (Fig.4b) proved that particles of aminosilane-modified titanium white exerted the most pronounced effect on interactions between the particles.

Results of studies on the application of modified or unmodified R-001 titanium white in *ACRYL LAKMA* and *AKRYBET* facade and external paints are shown in Tables 4-5.

As shown by the presented data, all the studied paint systems fitted the required range of density and viscosity. Problems were encountered with grinding of aminosilane-modified pigments in a grindometer. Such parameters as adhesion to the sublayer, spreading capacity and quality coating were consistent with the norms and all standards.

CONCLUSIONS

- Surface modification of R-001 titanium white surface with silane coupling agents induced evident increase in their bulk densities.
- Vinyltrimethoxysilane (U-611) and 3-methacryloxypropyltrimethoxysilane (A-174) were most effective in increasing hydrophobicity of titanium white and of homogeneity of its particles.
- N-2-(aminoethyl)-3-aminopropyltrimethoxysilane (U-15D) modified TiO_2 surface exhibited hydrophilic character.
- The modified titanium white (R-001), employed in studied paint types, improved quality of the paints and, in particular, their resistance and utility parameters.

REFERENCES

BRAUN J.H., 1997, *Titanium Dioxide a Review*, J. Coatings Technol., 69, 868.

BRAUN J.H., BAIDINS A. and MARGANSKI R.F., 1992, *TiO_2 pigment technology: a review*, Progress in Organic Coatings, 20, 105.

BUXBAUM G., 1993, "Industrial Inorganic Pigments", VCH, Amsterdam.

WOODBRIDGE R., 1991, "Principle of Paint Formulation", Blackie and Son Ltd., London.

WICKS Z.W., JONES F.N. and PAPPAS S.P., 1992, "Organic Coatings: Science and Technology", John Wiley & Sons, New York.

JESIONOWSKI T., KRYSZTAFKIEWICZ A., and DEC A., 2001, *Modified titanium white – chatacteristics and application*, Physicochemical Problems of Mineral Processing, 35, 195.

ACKNOWLEDGEMENTS

This work was supported by the Polish Scientific Committee Research Grant BW No. 32/001/2002.

Jesionowsk T., Krysztafkiewicz A., Dec D., *Modyfikowane biele tytanowe obrabiane Al_2O_3 jako pigmenty farb akrylowych*, Fizykochemiczne Problemy Mineralurgii, 36, (2002) 307-316 (w jęz. ang.).

W badaniach zastosowano biel tytanową obrabianą tlenkiem glinu produkowaną przez Zakłady Chemiczne Police S.A. typu R-001. Powierzchnię bieli tytanowej modyfikowano silanowymi związkami wiążącymi. W tym celu użyto metakryloksypropylotrimetoksysilan (A-174), winylotrimetoksysilan (U-611) oraz N-2-(aminoetylo)-3-aminopropylotrimetoksysilan (U-15D).

Biel tytanową niemodyfikowaną i modyfikowaną poddano analizie fizykochemicznej. Ponadto przeprowadzono badania mające na celu określenie morfologii, budowy powierzchni i dyspersji cząstek przede wszystkim w zależności od rodzaju modyfikatora. Przy ocenie wykorzystano nowoczesne techniki badawcze – SEM i DLS.

Modyfikowane i niemodyfikowane biele tytanowe zastosowano jako pigmenty w farbach akrylowych. W szczególności modyfikowane biele tytanowe poprawiają właściwości wytrzymałościowe i użytkowe farb akrylowych.

Physicochemical Problems of Mineral Processing, 36 (2002) 317-326
Fizykochemiczne Problemy Mineralurgii, 36 (2002) 317-326

Maria Clara COSTA[*], Agnieszka. URYGA[**], Zygmunt SADOWSKI[**]

THE USE OF N,N'-DIMETHYL-N,N'-DIPHENYLMALONAMIDE FOR IRON(III) EXTRACTION

Received March 5, 2002; reviewed and accepted May 15, 2002

N,N'-dimethyl-N,N,-diphenylmalomanide (DMDPHMA) has been proposed as selective reagent for extracting iron(III) from hydrochloric acid media. The influence of hydrochloric acid concentration on the extraction of Fe^{3+} ions was studied. Iron(III) ions were completely extracted from the concentrated hydrochloric acid solution (>8 M). When the concentration of chloride ions was maintained at 12 M by LiCl addition to the aqueous phase, the yield of iron(III) was nearly 100%. The stripping of iron(III) from the loaded organic phase (1,2-dichloroethane) was achieved by simple contact with water. The possible extraction mechanism and the composition of the extracted iron(III) species have been determined by using UV, IR and NMR spectroscopic techniques. The results showed that the metal ion was extracted as $FeCl_4^-$ complex.

Key words: extraction, iron(III),N,N'-dimethylN,N'-diphenylmalonamide, UV, IR, NMR spectroscopy

INTRODUCTION

The solvent extraction method is generally applied to the concentration of valuable metal ions from leaching solution. It can be used for eliminating these ions which trouble in recovery of the valuable metals presented in aqueous solution. For instance, the leaching solution after polymetalic copper ores treating contains Cu, Ni, Co and Fe. Dissolved metals can be separated using various procedures such as: cementation, precipitation, ions exchange or solvent extraction. The selective iron(III) separation is one of the targets for the precipitation of other metal ions from leaching solution (RABAH, 2000; RODRIGUEZ DE SAN MIGUEL, et al., 2000).

During bioleaching of gold-bearing minerals, metal ions such as Fe^{3+} are accumulated in the leaching liquor. The presence of an excess of Fe^{3+} ions in leaching

[*]Universidade do Algarve, Faro, Portugal
[**]Wroclaw University of Technology, Wroclaw, Poland

solutions leads to jarosite precipitation (MARTINEZ et al., 1999; LANYN et al., 1999).

Malonamides belong to diamides that are amides with the functional group of (RCON).It has derived from malonic acid. The extractive properties of diamides, especially as extractants of multi-valent metal ions can be explained by the existence of hybrid forms of monoamides (TIAN, HUGHES, 1994, FERNANDES 1998). The chemical structure of the malonamide used in this investigation is shown in figure 1.

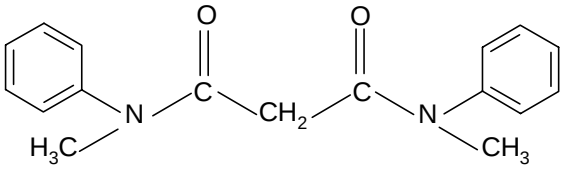

Fig. 1. General structure of DMDPHMA

The main objective of this study was to investigate the extractive features of the above structure for iron(III) extraction from hydrochloric acid solutions.

EXPERIMENTAL METHODS

REAGENTS

The extraction reagent was synthesised from the intermediate compounds: methylaniline and dimethylmalonate. These intermediate compounds were purchased from Aldrich (Germany). The malonamide was recrystallized from aqueous solution and its purity was established by both melting point and spectroscopic methods. 1,2 dichloroethane was used as organic diluent The stock solution of Fe(III) was prepared with $FeCl_3.6H_2O$. All other chemical reagents were of A.R. grade.

EXTRACTION PROCEDURE

The stock solution of the extraction reagent was prepared by dissolving appropriate weights of the compound in 12-dichloroethane. The organic phase was dichloroethane. The extraction experiments were carried out in Erlenmeyer's flask. Equal volumes of the aqueous solution containing iron(III) and organic solution were agitated for 15 min at room temperature. Both phases were placed at separatory funnels. Then, the aqueous phase was separated. Iron(III) concentration in the aqueous phases before and after the extraction process was analysed by atomic absorption spectrometry (Shimatzu AA680).

NMR, IR SPECTROSCOPY

The Infrared spectra were recorded on a MATTSON 1000 FTIR spectrometer and the Nuclear Magnetic Resonance spectra were measured on a BRUKER (300 MHz) NMR spectrometer. In the case of NMR the chemical shifts were expressed with

respect to an internal reference standard (TMS) and were δ values in *ppm*. The solvent in all cases was deuterated chloroform ($CDCl_3$), which frequency is attaining at about 77.0 – 79-0 ppm. In this study the observed for this solvent frequency was: 77.3 – 78.1 ppm.

In the present work IR spectra of the extractant molecule in different organic diluents, such as CCl_4, 1,2-dichloroethane, toluene and dichloromethane were analysed and compared. Similar spectra were obtained and that is why the results will be only presented for 1,2-dichloroethane (the diluent, which was chosen for DMDPHMA in this work).

RESULTS AND DISCUSSION

The influence of the ligand concentration on iron(III) extraction was studied using organic phases with different concentration of the extractant. The results obtained are shown in table1.

Table 1. Influence of ligand concentration on Fe^{3+} extraction

Ligand Concentration [mol/dm^3]	Initial Fe^{3+} concent. [mg/dm^3]	Final Fe^{3+} concnt. [mg/dm^3]	Fe^{3+} concent. organic faze [mg/dm^3]	Fe^{3+} extraction E [%]
0.10	582.7	1.4	581.3	99.8
0.010	582.7	7.0	575.6	98.8
0.0010	582.7	502.3	80.4	13.8

The experimental data show that Fe(III) is extracted quantitatively from the aqueous solution using 0.01 mol/dm^3 DMDPHMA dissolved in an organic phase. Experiments have also been conducted to establish the equilibrium isotherm curve (Fig. 2). The isotherm shows the dependence of the Fe^{3+} concentration in aqueous phase to the Fe^{3+} concentration in the organic phase.

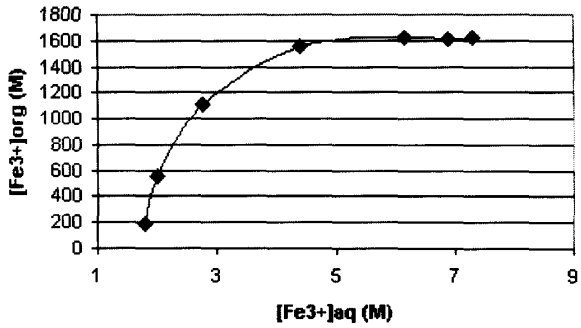

Fig. 2. The equilibrium isotherm curve

The shape of the obtained curve corresponds to the shape, which is characteristic for a ion-pair mechanism. The influence of hydrochloric acid concentration on the Fe^{3+} ions extraction was also studied using 1.0 M to 12 M range of concentration (Fig. 3).

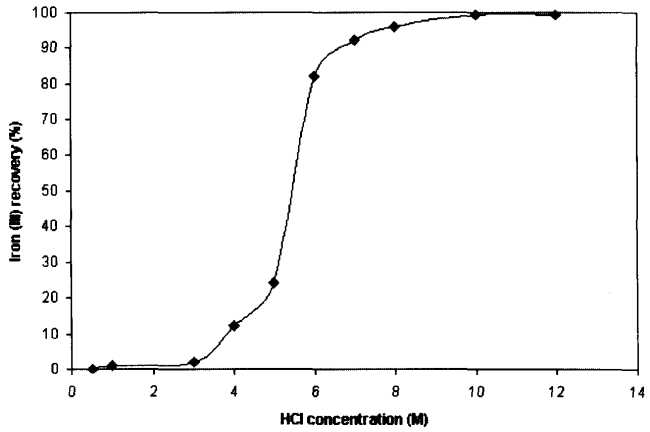

Fig. 3. Fe^{3+} ions extraction from HCl solutions

According to the obtained results it is possible to establish that the ability of DMDPHMA to extract Fe^{3+} from hydrochloric acid solutions is dependent on the acid concentration. This extraction behaviour is very close to the literature data (FERNANDES 1998; COSTA, et al. 1999, COSTA, PAIVA, 2002). The extraction of Fe^{3+} from 12 M of the total chloride concentration showed an absence of the acid concentration dependence (Table 2), when chloride concentration was achieved by LiCl addition.

Table 2. Fe^{3+} extraction from HCl solutions of 12 M of total Cl^- ions concentration

Total Cl^- conc.	12 M	12 M.	12 M	12 M	12 M
HCl conc. mol/dm^3	3	4	5	7	8
Initial Fe^{3+} conc. mg/dm^3	574.8	562.9	608.9	585.7	601.5
Final Fe^{3+} conc. mg/dm^3	5.6	5.4	5.8	8 .0	6.1
Fe^{3+} extraction E[%]	99.0	99.0	99.0	98.6	99.0

It is interesting to note that, when LiCl was replaced by sodium chloride the percentage of Fe^{3+} extraction was 20 %. According to the ion-pair formation mechanism, the lithium ion has a dimension like to a proton and is able to replace proton in the following process.

$$MAH^+Cl^-_{(org)} + Li^+_{(aq)} + FeCl_4^-{}_{(aq)} \rightarrow MaLi^+FeCl_4^-{}_{(org)} + H^+Cl^-_{(aq)}$$

When the hydrochloric acid solution was substituted by both nitric or sulphuric acid solutions, the results of Fe^{3+} extraction were unsuitable (HNO_3 8M, E[%] = 30.0; H_2SO_4 5M, E[%] = 20.0). In the case of malonamide as extractant, the possible protonation of its molecule should be taken into account, when metal extraction from concentrate acid solution is considered. Previous studies have shown that the protonation occurs on the carbonyl oxygen's rather that at the nitrogen atom (TIAN, HUGHES, 1994).

To find out, which iron(III) species are preferable extracted by DMDPHMA from hydrochloric acid media both aqueous and organic phases were analysed by UV spectroscopy. The UV spectra of the iron(III)-loaded organic phase show two peaks at 364.2 nm and 314.2 nm. (Fig. 4). According to the literature data these bands correspond to $FeCl_4^-$ species (LEVER, 1968). The peaks at about 364.0 nm and 314.0 nm were also identified in aqueous phases with chloride ion concentrations higher than 4 M. This can indicate that $FeCl_4^-$ is the predominant specie in HCl > 4 M.

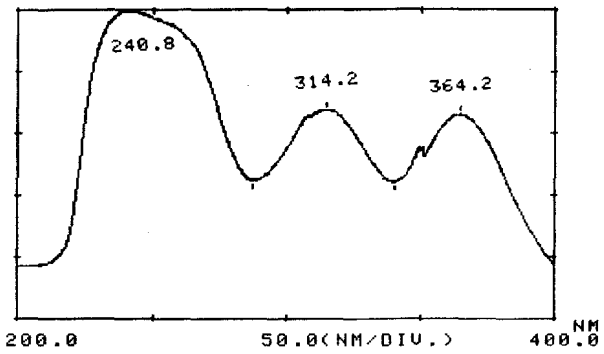

Fig 4. UV spectra of iron (III)-loaded organic phase in 1,2-dichloroethane after extraction from 8M HCl

Peaks corresponding to $FeCl_4^-$ were also observed in the spectrum of both organic and aqueous phases when the LiCl solution was used. NMR spectroscopy gives the possibility to investigate the structure of the extractant in different connections; before and after extraction. It is helpful to understand the mechanism of iron(III) extraction. NMR spectra of DMDPHMA in $CDCl_3$ are shown in Fig.5a,b.

Table 3. NMR assignments of DMDPHMA

^{1}H NMR δ(ppm)	^{13}C NMR δ(ppm)
3.01 (2H,s,a)	38.0 (2C,s,i)
3.23 (6H,s,b)	42.0 (1C,s,ii)
7.03-7.06 (4H,d,c)	128.1-130.3 (10C,m,iii)
7.28 7.38 (6H,m,d)	144.4 (2C,s,iv)
	167.7 (2C,s,v)

(s-singlet, d-doublet, t-triplet, m-multiplet)

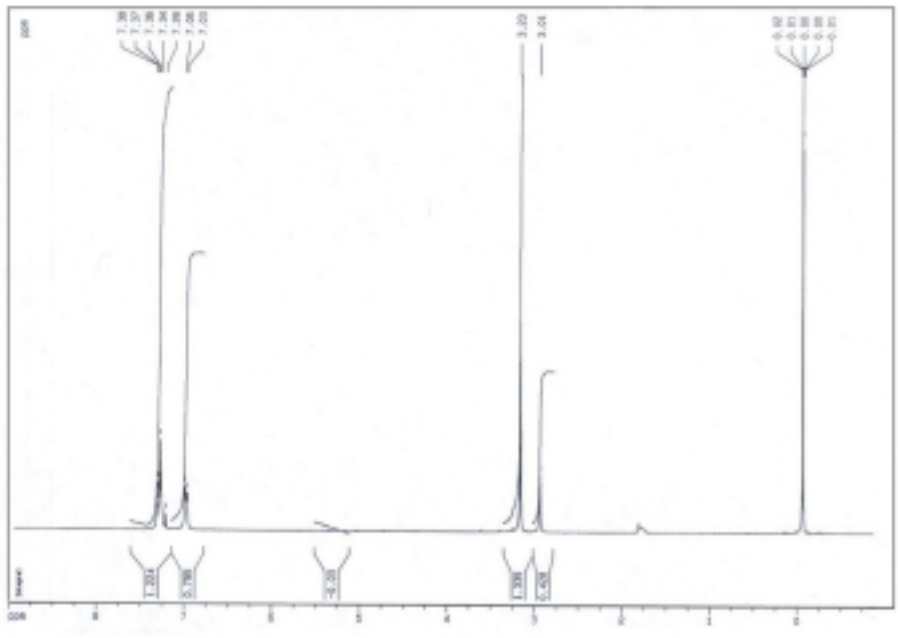

Fig. 5a. Proton NMR spectrum of DMDPHMA in $CDCl_3$ solution

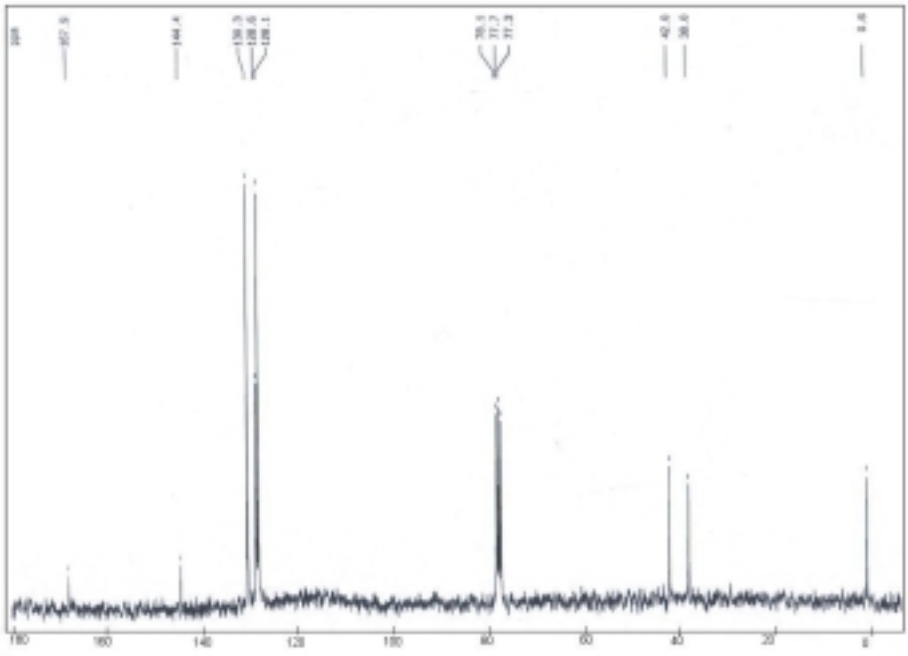

Fig.5b. Carbon NMR spectrum of DMDPHMA

Table 3 summarises the information of ^{1}H NMR and ^{13}C NMR spectra as well as NMR spectra of DMDPHMA after extraction and after contact with 8 M hydrochloric acid solution show the presence of four additional protons. This suggests that protonation occurs on both carbonyl oxygen atoms and on nitrogen atoms. According to previous IR-studies (FERNANDES, 1998), when coordination through the carbonyl oxygen occurs, a decrease in the C=O stretching band (1640 cm^{-1} in Fig. 6) intensity takes place. In the spectrum of DMDPHMA in 1,2-dichloroethane after extraction (Fig. 7), a decrease of intensity in the region of both groups (C=O and C-N) is observed. This suggests that protonation can occur on the carbonyl oxygen's and on the both nitrogen atoms.

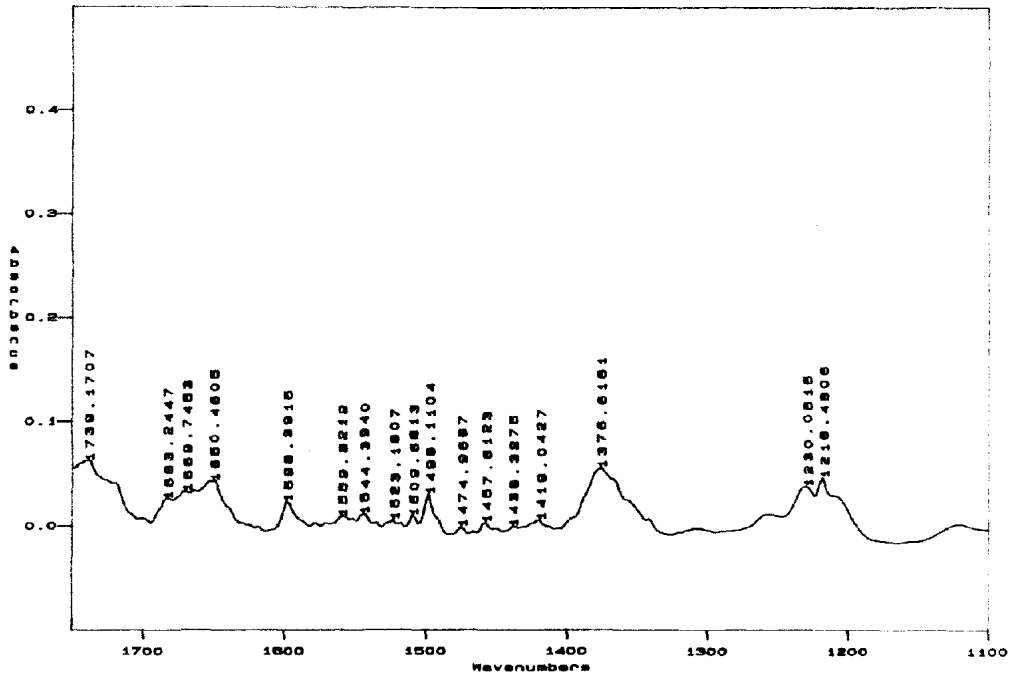

Fig. 6. IR spectra of DMDPHMA in 1, 2-dichloroethane

The titration of the aqueous phase with NaOH solution confirmed the fact that four moles of H^{+} ions were attached to one mole of DMDPHMA. The kinetic study showed that the extraction of iron(III) from aqueous phase was realised in a very short period of time. Fig 8 shows that the iron recovery dramatically increased during the first 5 minutes of the extraction experiment.

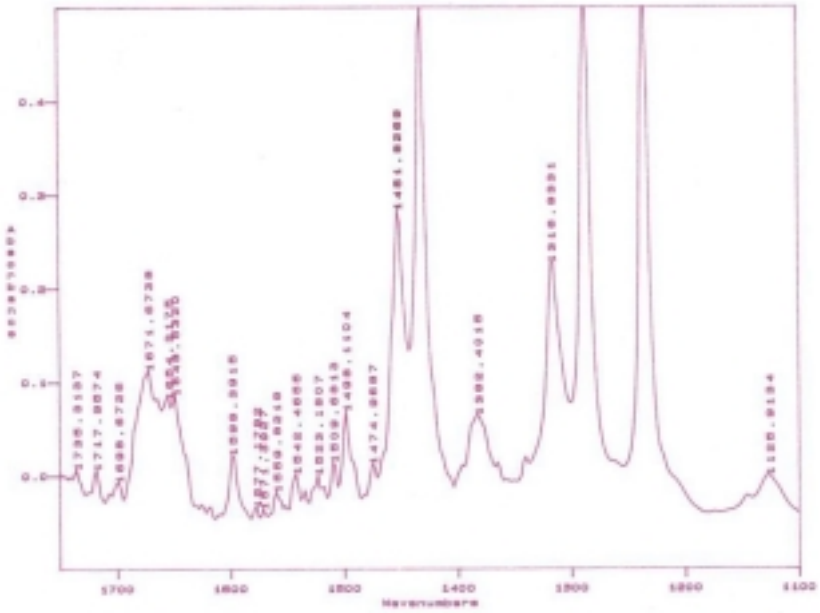

Fig. 7. IR spectra of DMDPHMA in 1, 2-dichloroethane after extraction of iron (III) from 8M HCl solution

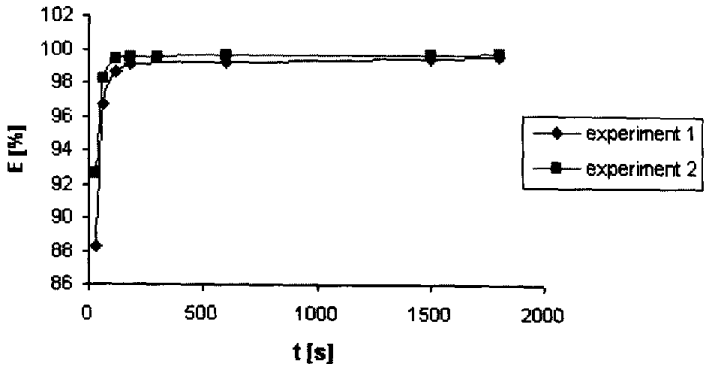

Fig. 8. Kinetic of iron (III) extraction using DMDPHMA

Further extraction experiments to test the selectivity of DMDPHMA through the presence of Cu(II), Zn(II) and Fe(II) ions in the aqueous solution were performed. No extraction of those ions was observed and in addition, their presence does not affect iron(III) extraction. In addition to the selectivity experiments stripping essays were conducted using water as the stripping agent. According to the results iron(III) can be totally stripped from the loaded organic phase with water.

The good selectivity of DMDPHMA for iron(III) is an important result considering that this metal is usually co-extracted together with zinc(II) and copper(II). It gives the better results then other extractants such as DZEHPA or TBP are used.

CONCLUSIONS

1. Iron(III) extraction depends on the extractant concentration in the organic phase, as well as on the concentration of hydrochloric acid in the aqueous phase.
2. The yield of iron(III) extraction was 100% when the chloride ions concentration was 12 M by adding LiCl to the aqueous phase.
3. UV spectroscopy studies confirmed that iron is extracted as $FeCl_4^-$.
4. NMR spectroscopy investigation proved that during extraction protonation of the extractant occurs and four protons are attached to one DMDPHMA molecule.
5. In IR spectra of DMDPHMA after contact with HCl solution (8M) and after iron (III) extraction small shifts were observed in the stretching frequency of the carbonyl group as a consequence of its protonation.
6. The rate of iron(III) extraction to the organic phase is high (3-4 minutes).
7. Good selectivity of DMDPHMA for iron(III) towards other base metal cations (Cu(II), Zn(II) and Fe(II)) is achieved.
8. Iron(III) can be easily and completely removed from the loaded organic phase by simple contact with water.
9. DMDPHMA can be an interesting alternative to commercial organophosphorous extractants.

ACKNOWLEGEMENT

The authors would like to thank SOCRATES ERASMUS European Program for the provision of scholarship to Agnieszka Uryga at Algarve University.

REFERENCES

COSTA, M.C., FERNANDES, C.E., HUDSON, M.J., IVESON P.B., (1999), *Solvent extraction of base metal cations such as iron(III) from hydrochloric acid solutions using N,N`-substitutedmalonamides*, Proc. Int. Solv. Extr. Conference, Barcelona, Spain, pp. 271-275.

COSTA M.C., PAIVA, A.P., (1999), *Solvent extraction of iron(III) from hydrochloric acid solutions using N,N`-dimethyl-N,N`-diphenylmalonamide*, Proc. Int. Solv. Extr. Conference, Cape Town, South Africa, pp. 371-376.

FERNANDES, C., (1998*), Estudo de extracção de HCl e ferro(III) pela DMDPHTDMA*, Final report of the Chemistry degree, Universidade da Madeira, Portugal.

LANYON, M.R., LWIN, T., MERRITT, R.R., (1999), The dissolution of iron in the hydrochloric acid leach of an ilmenite concentrate, Hydrometallurgy, 51, 299-323.

LEVER, A.B.P., (1968), *Inorganic Electronic Spectroscopy*, Elsevier, Amasterdam, pp.295-317.

MARTINEZ, S., SASTRE, M.A., ALGUACIL, F.J., (1999*), Solvent extraction of gold(III) by the chloride salt of the tetra amine Hostarex A 327. Estimation of the interaction coefficient between* $AuCl_4^-$ *and* H^+, Hydrometallurgy, 52, 63-70.

RABAH, M.A., (2000), *Recovery of iron and copper from spent HCl used to clean up dirty car radiators*, Hydrometallurgy, 56, 75-92.

RODRIGUEZ DE SAN MIGUEL, E., AGUILAR, J.C., RODRIGUEZ, M.T.J., DE GYVERS, J., (2000), *Solvent extraction of Ga(III), Gd(II), Fe(III), Zn(II), Cu(II) and Pb(II) with ADOGEN 364 dissolved in kerosene from 1-4 mol* dm^{-1} *HCl media*, Hydrometallurgy, 57, 151-165.

TIAN, H., HUGHES, M.A., (1994), *The mechanism of extraction of* HNO_3 *and neodymium with diamides*, Hydrometallurgy, 36, pp. 315-330.1

Costa M.C. , Uryga A., Sadowski Z., *Zastosowanie N,N'-dwumetylo-N,N'-dwufenyloamidy kwasu malonowego do ekstrakcji żelaza(III),* Fizykochemiczne Problemy Mineralurgii, 36, (2002) 317-326 (w jęz. ang.)

N,N'-dwumetylo-N,N'-dwufenyloamid kwasu malonowego został zaproponowany jako selektywny kstrahent dla ekstrakcji żelaza(III) z roztworów kwasu solnego. Badano wpływ stężenia kwasu solnego na proces ekstrakcji jonów Fe^{3+}, stwierdzając, że jony Fe^{3+} były całkowicie ekstrahowane z roztworów o wysokim stężeniu kwasu solnego (>8M). W przypadku, gdy wysokie stężenie jonów chlorkowych (12M) uzyskano przez dodanie chlorku litu (LiCl), odzysk jonów żelaza(III) był również bliski 100%. Zastosowanie innych roztworów chlorkowych (KCl,NaCl) nie przyniosło zadawalających wyników ekstrakcji. Reekstrakcje z fazy organicznej (dwuchloroetan) realizowano przy pomocy wody destlowanej. W celu wyjaśnienia mechanizmu selektywnej ekstrakcji żelaza(III) przeprowadzono badania spektrofotometryczne (UV,IR) oraz NMR. Wyniki tych badań wskazują, że odpowiedzialnym za ekstrakcję żelaza(III) jest kompleks $FeCl^-$.

Our books are available in the foolowing booksohps:
„Politechnika", Wybrzeże Wyspiańskiego 27,
50-370 Wrocław, budynek A-1 PWr, tel. (071) 320 25 34
„Tech", plac Grunwaldzki 13,
50–377 Wrocław, budynek D-1 PWr, tel. (071) 320 32 52
Orders can also be sent by post.

ISSN 0137-1282
Physicochemical Problems of Mineral Processing, 36 (2002)